Université de Montréal

Rôle des astrocytes dans la décharge rythmique neuronale du noyau sensoriel principal du trijumeau

par PHILIPPE MORQUETTE

Département de Neurosciences

Faculté de médecine

Thèse présentée à la Faculté des études supérieures
en vue de l'obtention du grade de Philosophiæ Doctor (Ph. D.)
en Neurosciences

Décembre 2015

Université de Montréal Faculté des études supérieures et postdoctorales

Thèse intitulée :

«Rôle des astrocytes dans la décharge rythmique neuronale du noyau sensoriel principal du trijumeau»

Présentée par :

PHILIPPE MORQUETTE

a été évaluée par un jury composé des personnes suivantes :

Serge Rossignol, Ph. D.

Président-rapporteur

Arlette Kolta, Ph. D.

Directeur de recherche

Richard Robitaille, Ph. D.

Co-Directeur de recherche

Roberto Araya, Ph.D.

Membre du jury

Christopher A. Del Negro, Ph.D.

Examinateur externe

Louis-Éric Trudeau, Ph. D.

Représentant du doyen de la FES

Résumé

La communication entre les neurones est fondée sur leur capacité à changer leur patron de décharge pour l'encodage de différents messages. Pour plusieurs fonctions vitales, comme la respiration et la mastication, les neurones doivent pouvoir générer des patrons d'activité répétitifs, et les groupes de neurones responsables de ces décharges rythmiques sont des générateurs de patron central (GPC). En dépit de recherches soutenues, les mécanismes précis qui sous-tendent la rythmogénèse dans les GPCs ne sont pas bien définis. Le plus souvent, la potentielle contribution des astrocytes demeure grandement inexplorée, même si ces cellules sont aujourd'hui connues pour leur implication dans la modulation synaptique neuronale.
Pour nos travaux, le noyau sensoriel principal du trijumeau (NVsnpr) a été pris comme modèle à cause de son rôle central dans les mouvements rythmiques de la mastication. Dans ce noyau, des travaux antérieurs ont montré que la décharge en bouffées rythmiques est déclenchée dans les neurones lorsque la concentration de calcium extracellulaire ($[Ca^{2+}]_e$) est artificiellement baissée. Nous fondant sur cette observation, notre première hypothèse a postulé que la baisse de la $[Ca^{2+}]_e$ pouvait survenir de façon physiologique en lien avec des stimulations sensorielles pertinentes. Deuxièmement, parce que les astrocytes ont été impliqués dans le tamponnage et l'homéostasie d'ions extracellulaires comme le K^+, nous avons postulé que ces cellules pouvaient jouer un rôle équivalent dans le contrôle de la $[Ca^{2+}]_e$.

Nos résultats montrent que les astrocytes peuvent réguler la $[Ca^{2+}]_e$ et ainsi contrôler la capacité des neurones à changer leur patron de décharge. Premièrement, en stimulant les afférences sensorielles au NVsnpr, nous avons montré que des baisses physiologiques de la $[Ca^{2+}]_e$ sont observées en parallèle à l'apparition de bouffées rythmiques neuronales. Deuxièmement, nous avons démontré que les astrocytes répondent aux mêmes stimuli qui induisent l'activité rythmique neuronale, et que leur blocage avec un chélateur de Ca^{2+} empêche les neurones de générer un patron de décharge en bouffées rythmiques. Cette habilité est rétablie en rajoutant la S100β, une protéine astrocytaire liant le Ca^{2+}, dans le milieu extracellulaire, alors que l'anticorps anti-S100β empêche l'activité rythmique. Ces résultats indiquent que les astrocytes régulent une propriété neuronale fondamentale : la capacité à changer de patron de décharge. Ainsi, les GPCs dépendraient des fonctions intégrées des astrocytes et des neurones. Ces découvertes pourraient avoir des implications transposables à

plusieurs autres circuits neuronaux dont la fonction dépend de l'induction d'activité rythmique.

Mots-clés : Mastication, Noyau sensoriel principal du trijumeau, Rythmicité, Générateur de patron central, Calcium, Astrocyte, S100β.

Abstract

Communication between neurons rests on their capacity to change their firing pattern to encode different messages. For several vital functions, such as respiration and mastication, neurons need to generate a repetitive firing pattern, and the groups of neurons responsible for these rhythmic discharges are called central pattern generator (CPG). Despite intense research in this field, the exact mechanisms underlying rhythmogenesis in CPGs are not completely defined. In most instances, the potential contribution of astrocytes is largely unexplored, even though these cells are now well known to be involved in neuronal synaptic modulation.

In our work, the trigeminal main sensory nucleus (NVsnpr) was used as a model owing to its central role in the rhythmic movement of mastication. Previous work have shown that rhythmic bursting discharge is triggered in NVsnpr neurons when extracellular calcium concentration ($[Ca^{2+}]_e$) is artificially decreased. Based on this observation, our first hypothesis postulated that the reduction of $[Ca^{2+}]_e$ could also happen physiologically in relation to relevant sensory stimulation. Secondly, because astrocytes have been involved in the buffering and the homeostasis of extracellular ions like potassium, we have postulated that these cells could also play a role in the control of $[Ca^{2+}]_e$.

The results presented in this thesis show that astrocytes can regulate $[Ca^{2+}]_e$ and thus control the ability of neurons to change their firing pattern. First, we showed that stimulation of sensory afferent fibers to the NVsnpr induced neuronal rhythmic bursting and in parallel reduction of $[Ca^{2+}]_e$. Secondly, we have demonstrated that astrocytes respond to the same sensory stimuli that induce neuronal rhythmic activity, and their blockade with a Ca^{2+} chelator prevents generation of neuronal rhythmic bursting. This ability is restored by adding S100β, an astrocytic Ca^{2+}-binding protein, to the extracellular space, while the application of an anti-S100β antibody prevents generation of rhythmic activity. These results indicate that astrocytes regulate a fundamental neuronal property: that is the capacity to change their firing pattern. Thus, CPG functions result from integrated neuronal and glial activities. These findings may have broad implications for many other neural networks whose functions depend on the generation of rhythmic activity.

Keywords : Mastication, Trigeminal main sensory nucleus, Rhythmicity, Central pattern generator, Calcium, Astrocyte, S100β.

Table des matières

Liste des tableaux

Liste des figures

CHAPITRE 1

Liste des abréviations

4-AP : 4-aminopyridine
ACM : aire corticale masticatoire
ACSF : fluide cérébro-spinal artificiel
ADP : après-dépolarisation
AHP : après-hyperpolarisation
AMPA : acide alpha-amino-3-hydroxy-5-methyl-4-isoxazolepropionique
APV : D,L-2-amino-5-phosphonovaleric acid
ATP : adénosine-5′-triphosphate
BIC : bicuculline
BK-Ca : grand courant potassique dépendant du calcium
BSA : Bas seuil d'activation
$[Ca^{2+}]_e$: concentration du calcium extracellulaire
CCDV : canaux calciques dépendants au voltage
$[Cl^-]_e$: concentration du chlore extracellulaire
DNQX : 6,7-dinitro-quinoxaline
GABA : acide gamma-aminobutyrique
GC : noyau gigantocellulaire
GPC : générateur de patron central
GFAP : *glial fibrillary acidic protein*
HRP : peroxydase du Raifort
HSA : haut seuil d'activation
I_h : courant activé par l'hyperpolarisation
I_{NaP} : courant sodique persistant
I_{NaT} : courants sodiques transitoires
IntV : région inter-trigéminale
IP_3R : récepteurs de l'inositol 1,4,5-triphosphate
$[K^+]_e$: concentration du potassium extracellulaire
mPeriV : région péri-trigéminale médiane
MPTP : 1-methyl-4-phenyl-1,2,3,6-tetrahydropyridine
$[Na^+]_e$: concentration du sodium extracellulaire
$[Na^+]_i$: concentration du sodium intracellulaire
NMA : N-methyl-D,L-aspartate
NVII : noyau facial
NVmes : noyau mésencéphalique du trijumeau
NVmot : noyau moteur du trijumeau
NVsnpr : noyau sensoriel principal du trijumeau
NVsp : noyau spinal du trijumeau
NVspc : sous-noyau caudalis du noyau spinal trigéminal
NVspi : sous-noyau interpolaris du noyau spinal trigéminal
NVspo : sous-noyau oralis du noyau spinal trigéminal
NXII : noyau hypoglosse
NMDA : N-méthyl-D,-aspartate
nPontC : noyau pontis caudalis

PCRt : formation réticulée parvocellulaire
PCRt-α : la partie latérale de la formation réticulée parvocellulaire
PGC : noyau paragigantocellulaire
PériV : région péri-trigéminale
PPSE : Potentiel postsynaptique excitateur
SON : noyau supraoptique
SK-Ca : petit courant potassique dépendant du calcium
TEA : tétraéthylamonium
TTX: tétrodotoxine
VPM : noyau ventropostéromédian du thalamus

« Dicebat Bernardus Carnotensis nos esse quasi nanos, gigantium humeris insidentes, ut possimus plura eis et remotiora videre, non utique proprii visus acumine, aut eminentia corporis, sed quia in altum subvenimur et extollimur magnitudine gigantea. »

« Nous sommes comme des nains assis sur des épaules de géants.
Si nous voyons plus de choses et plus lointaines qu'eux,
ce n'est pas à cause de la perspicacité de notre vue, ni de notre grandeur,
c'est parce que nous sommes élevés par eux. »

Livre III du Metalogicon, Jean de Salisbury

Remerciements

Tout d'abord, je tiens à exprimer ma gratitude envers ma directrice de thèse, le Dre Arlette Kolta, pour m'avoir donné l'opportunité de faire un doctorat dans son laboratoire. Votre support et mentorat rigoureux m'ont poussé à me dépasser et à viser l'excellence. Vous m'avez aussi permis d'assister à des conférences et congrès nationaux et internationaux qui ont été pour moi des occasions d'interagir avec des chercheurs de renom, ce qui a grandement contribué au développement de ma pensée scientifique.

Je tiens aussi à remercier mon co-directeur le Dr Richard Robitaille notamment pour son expertise et ses conseils judicieux qui ont grandement contribué à la réalisation de ce projet de thèse.

Je veux remercier tous mes collègues passés et présents des laboratoires du Dre. Kolta, du Dr. Robitaille et du Département de Neuroscience (anciennement département de Physiologie). Je tiens à souligner ma reconnaissance envers la Dre. Dorly Verdier pour sa rigueur et son dévouement. Dorly, tu m'as accompagné durant les hauts et les bas de mon doctorat et ceci jusqu'à la correction de cet ouvrage. Un grand merci aussi au Dre Aude Panatier pour son souci du travail bien fait allant jusqu'aux menus détails, et aussi pour sa perspicacité scientifique qui, mine de rien, a permis de définir une grande partie de ce projet. Houssam, je te remercie grandement de ton amitié. Nous avons cheminé côte à côte durant toutes ces années et sommes devenus des compagnons scientifiques.

J'aimerais aussi mentionner d'autres personnes qui ont su contribué de loin ou de près à ce projet de thèse. Il s'agit d'Aklesso, Antony, Isabelle, Raphaël, ainsi que Joanne et Danielle.

J'aimerais remercier le Réseau de recherche en santé bucco-dentaire et osseuse (RSBO) ainsi que le GRSNC pour leur soutien financier au travers de leurs bourses durant ces années.

Finalement à ma famille, je veux dire mille mercis : Tout d'abord à mes parents sans qui cette thèse n'aurait pas vu le jour ; Merci pour votre appui moral, financier, spirituel et vos encouragements inépuisables. Je remercie infiniment mes sœurs Barbara et Valérie pour leur précieux soutien. Elles ont été présentes à chaque étape de ce doctorat et ont su être un support inestimable durant ces années. Je tiens aussi à remercier Valérie F.L. pour son soutien et ses encouragements.

Préambule

En raison de leur passivité électrique, le rôle des cellules gliales a longtemps été relégué à celui de fonction secondaire de soutien dans le système nerveux central. Toutefois, au cours des deux dernières décennies, un nombre grandissant d'études démontrent que ces cellules sont non seulement sensibles à l'activité neuronale, mais qu'elles semblent également capables de la moduler. Dans le cadre de cette thèse, nous avons travaillé sur l'implication des astrocytes dans la rythmogénèse neuronale.

L'introduction de cette thèse traite tout d'abord du mouvement de la mastication qui constitue le modèle expérimental de nos travaux. Dans un deuxième temps, nous abordons les mécanismes cellulaires qui sont à la base de la rythmogénèse neuronale. Finalement, nous présenterons les astrocytes, leurs rôles dans le système nerveux central et plus précisément certaines de leurs caractéristiques qui suggèrent leur implication dans la rythmogénèse neuronale.

Le corps de la thèse démontre que l'activation des astrocytes est nécessaire à l'induction de l'activité rythmique des neurones du noyau sensoriel principal du trijumeau (NVsnpr) et décrit le mécanisme par lequel ils exercent leur effet. Ainsi, les travaux de cette thèse soutiennent l'idée qui veut que les astrocytes soient des joueurs importants dans l'encodage de l'information nerveuse.

La majorité des travaux présentés dans cette thèse ont fait l'objet d'un article dont je suis le premier auteur (Nature Neuroscience). J'ai parallèlement participé à trois articles de revue de littérature et à un commentaire d'article (voir Annexe). Par ailleurs, j'ai également participé, à titre de deuxième auteur, à une étude sur le remodelage de l'arbre dendritique de cellules ganglionnaires de la rétine après lésion axonale (Cell Death and Differenciation, *Nature publishing group*). Cette dernière étude, menée en collaboration avec le laboratoire du Dre Di Polo, ne sera toutefois pas abordée dans la présente thèse (l'article est également disponible en Annexe).

CHAPITRE 1

1. Introduction générale

L'activité électrique émanant d'un réseau neuronal reflète l'essence de sa fonction. Ce postulat, sur lequel repose l'étude des neurosciences par l'approche de l'électrophysiologie, explique pourquoi tant de recherches tentent de percer les secrets de l'encodage de l'activité électrique neuronale. Dans ce contexte, l'étude des mouvements rythmiques comme la locomotion, la respiration et la mastication présente un avantage car le lien entre la fonction et l'activité électrique nerveuse y semble être évident.

1.1 Les mouvements rythmiques

Les mouvements rythmiques sont constitués de mouvements stéréotypés qui sont répétés pendant une période de temps. Comme proposé par Grillner et Feldman (Feldman and Grillner, 1983), la base neuronale supportant tout mouvement rythmique peut être décomposée en quatre sous-structures fonctionnelles différentes; 1) Un centre supérieur contrôlant l'initiation du mouvement ainsi que son adaptation en fonction de stimuli environnementaux (par exemple : visuels ou sensoriels); 2) Un niveau d'output constitué des motoneurones qui contrôlent directement la contraction des muscles; 3) Des récepteurs sensoriels périphériques activés pendant le mouvement afin de produire un rétrocontrôle permettant l'ajustement du mouvement en cours; 4) Des réseaux neuronaux capables de produire des décharges rythmiques coordonnées de groupes de neurones (Feldman and Grillner, 1983). Ces derniers réseaux, communément appelés générateurs de patron centraux (GPC), sont situés au niveau du tronc cérébral ou de la moelle épinière, et peuvent générer un patron d'activité motrice rythmique en absence d'input sensoriel des récepteurs périphériques ou d'input des centres supérieurs. Cette dernière composante est au cœur de la recherche et de la réflexion de cette thèse.

Nous avons travaillé sur les circuits neuronaux du système trigéminal impliqués dans le mouvement de la mastication afin de mieux comprendre les mécanismes cellulaires des GPCs qui sont à la base des mouvements rythmiques.

1.2 La mastication

Comme les autres mouvements rythmiques abordés plus haut, la mastication est une fonction vitale. Elle permet de préparer et de faciliter la digestion de la nourriture en la réduisant en petits morceaux facilement ingérables.

1.2.1 Le mouvement masticatoire

La mastication est souvent considérée, à tort, comme étant un mouvement simple d'alternance d'ouverture et de fermeture de la mâchoire. En fait, ce mouvement est plus complexe et nécessite une coordination précise des muscles faciaux avec ceux de la langue afin d'assurer un bon positionnement du bol alimentaire, une bonne réduction et une ingestion sans entraves des aliments. Malgré tout, lorsque le mouvement de la mastication est abordé avec une perspective d'étude de mouvement rythmique, il est plus judicieux de le définir comme étant la fermeture et l'ouverture alternées de la mâchoire dues aux contractions alternées des muscles masticatoires.

Chez les mammifères, les muscles impliqués dans le mouvement de fermeture de la mastication sont: les muscles temporaux, masséters et ptérygoïdes médians. Le mouvement d'ouverture est quant à lui généré par les muscles digastriques antérieurs et mylohyoïdes. L'organisation de tous ces muscles est bilatérale et permet un mouvement de la mandibule sur l'axe de l'articulation temporo-mandibulaire.

1.2.2 Les périodes de la séquence masticatoire

Le modèle du lapin a souvent servi de fondement pour la description du mouvement de la mastication, car il permet d'obtenir un mouvement relativement naturel en dépit des conditions expérimentales. Dans sa revue de 1991, Lund décrit les phases de la mastication à partir du moment où la nourriture est ingérée jusqu'au moment où elle est avalée (déglutition).

Ainsi, une séquence masticatoire comprend trois périodes qui sont constituées de cycles masticatoires différents (voir figure 1-1). La première période est constituée d'une série de cycles de mouvements dits de type I. Il s'agit de cycles préparatoires avec des phases d'ouvertures et de fermetures rapides et peu de mouvements latéraux. Ces mouvements servent principalement à positionner la nourriture sur les dents arrière grâce à la langue (Lund, 1991).

Par la suite, les cycles de type II, correspondant à la seconde période, servent à réduire les aliments en de plus petits morceaux. Pour plusieurs espèces, les cycles à cette étape sont décomposables en trois phases; i) une phase d'ouverture, ii) une phase de fermeture rapide; et iii) une phase de fermeture lente (voir figure 1-1). Pendant la fermeture rapide, la mâchoire présente un mouvement latéral vers le côté en travail, expliqué par le fait qu'une grande majorité d'animaux mastiquent d'un côté de la bouche (unilatérale) (Hiiemae, 1985). La phase de fermeture lente débute ensuite, lorsque les dents commencent à écraser les aliments; il y a alors en parallèle une décélération du mouvement de fermeture. Durant cette phase, alors que la mâchoire inférieure présente un mouvement vers la ligne médiane, la nourriture est broyée entre les molaires supérieures et inférieures. Graduellement, alors que la nourriture s'affine au fil des séries de réduction, il y a une diminution de l'amplitude verticale du mouvement d'ouverture et de fermeture de la mâchoire. Cette période de réduction permet la formation du bol alimentaire par le mélange de la nourriture écrasée sous l'action de la salive (Lund, 1991). Finalement, la troisième et dernière période consiste en l'étape de prédéglutition où le bol alimentaire est placé à l'arrière de la cavité orale. Les cycles, dits de types III, de cette période comptent cinq phases: deux phases de fermeture rapide et lente, et trois phases d'ouverture. Il est intéressant de noter que la majorité des études, faisant référence à la mastication, considère en fait seulement les cycles de la période de réduction qui produisent le bol alimentaire (Lund, 1991).

Figure 1-1: Mouvements masticatoires verticaux

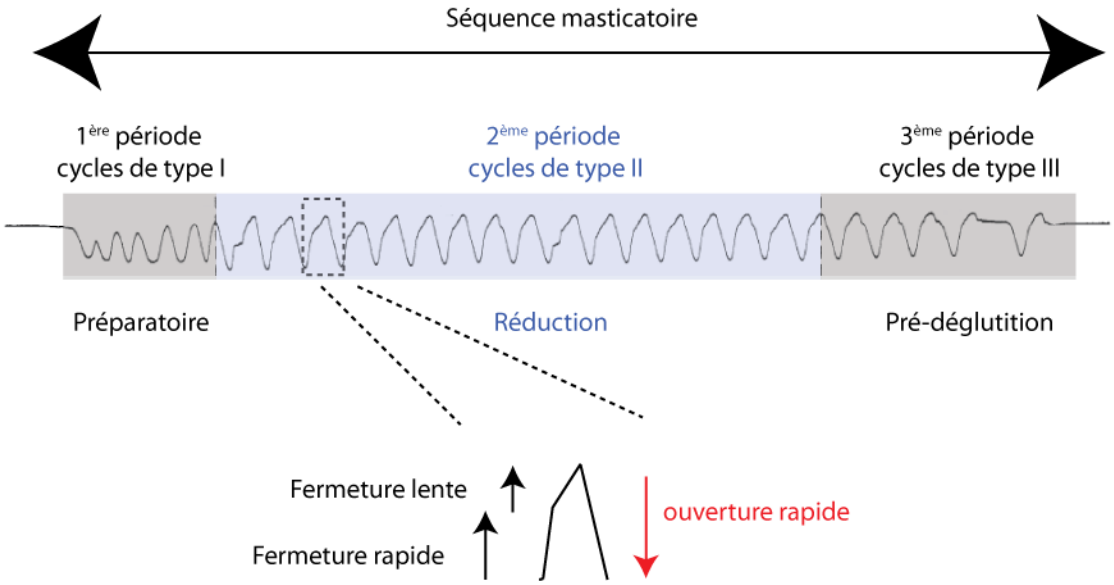

Mouvements masticatoires verticaux chez le lapin éveillé. La tête était immobilisée pendant l'enregistrement des mouvements de la mandibule avec un système de photodiodes. Un morceau de nourriture est placé dans la bouche (à gauche). La nourriture est d'abord transportée aux molaires pendant la période préparatoire (gris à gauche), mastiquée pendant la période de réduction (bleu), et finalement préparée pour la déglutition (gris à droite). La période en bleu correspond à la mastication étudiée dans la plupart des études. Figure modifiée de Schwartz et al., 1989.

1.3 Structures fonctionnelles à la base du mouvement rythmique masticatoire

Tout comme proposé par Grillner et Feldman (Feldman and Grillner, 1983), les quatre différentes structures fonctionnelles, à la base des mouvements rythmiques, sont également retrouvées pour le mouvement de la mastication (voir figure 1-2). En l'occurrence: 1) Un centre supérieur contrôlant l'initiation du mouvement et son adaptation en fonction de stimuli de l'environnement (voir section 1.3.1); 2) Un niveau d'output constitué des motoneurones qui contrôlent directement la contraction des muscles (voir section 1.3.2); 3) un rétrocontrôle permettant l'ajustement du mouvement en cours par les afférences de récepteurs sensoriels périphériques activés pendant le mouvement (voir section 1.3.3); 4) Un réseau neuronal capable de générer des décharges rythmiques et coordonnées de groupes de neurones (voir section 1.3.4).

Ces différentes composantes du système masticatoire ont déjà été étudiées et la section qui suit résume brièvement ce qui est connu à leur sujet.

Figure 1-2: Les quatre structures impliquées dans la génération du mouvement rythmique

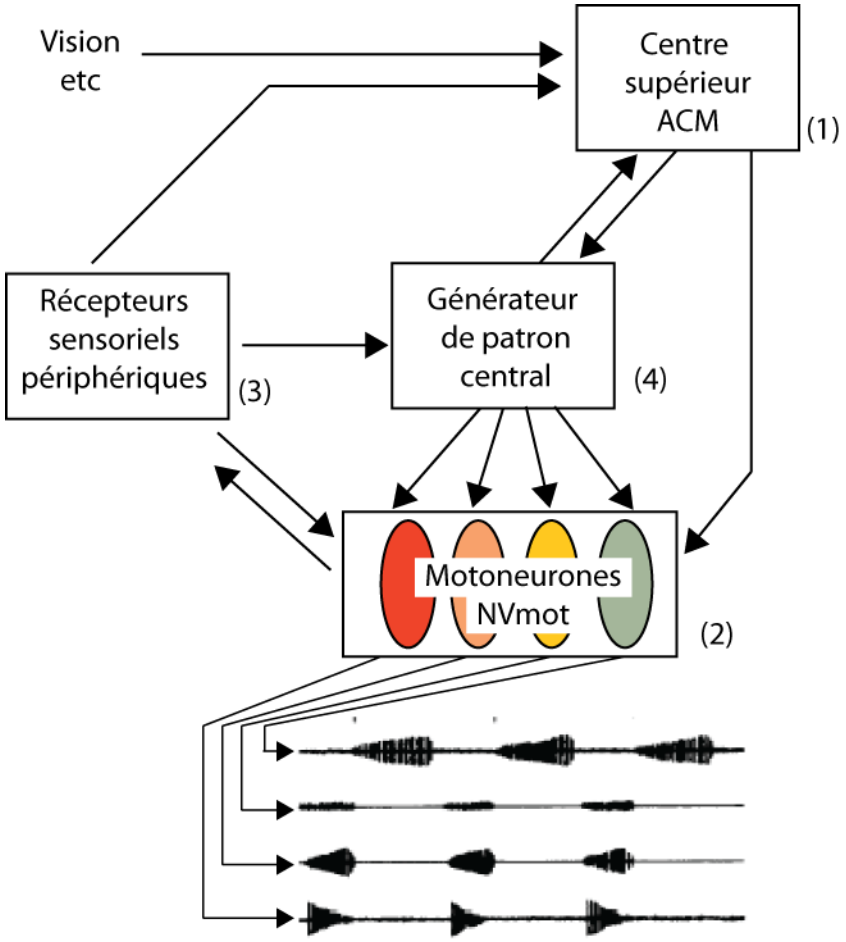

Les quatre structures impliquées dans la génération du mouvement rythmique de la mastication. 1) Un centre supérieur contrôlant l'initiation du mouvement et son adaptation en fonction de stimuli de l'environnement. Pour la mastication il s'agit de l'aire corticale masticatoire (ACM, voir section 1.3.1). 2) Un niveau d'output constitué des motoneurones qui contrôlent directement la contraction des muscles. Pour la mastication il s'agit du noyau moteur trigéminal (NVmot, voir section 1.3.2). 3) Un rétrocontrôle permettant l'ajustement du mouvement en cours par les afférences de récepteurs sensoriels périphériques activés pendant le mouvement (voir section 1.3.3). 4) Un réseau neuronal capable de générer des décharges rythmiques et coordonnées de groupes de neurones (voir section 1.3.4). Adapté de (Feldman and Grillner, 1983).

1.3.1 Un centre supérieur: Le contrôle cortical de la mastication

Les premiers travaux démontrant l'induction d'un patron moteur masticatoire par une stimulation corticale remontent à 1886 (Ferrier, 1886). Ces travaux ont été réalisés chez le lapin avec des stimulations électriques au niveau du cortex. Par la suite, ce procédé a été reproduit pour différentes espèces, dont le rat, le chat et le primate. Ceci dit, le lapin et le cochon d'Inde ont souvent été utilisés pour la recherche sur la genèse des mouvements masticatoires, car les mouvements induits par stimulation corticale sont très proches des mouvements naturels (Lund, 1991).

L'ensemble des régions corticales dont la stimulation induit une activation des muscles impliqués dans la mastication est appelé aire corticale masticatoire (ACM). Chez le cochon d'Inde et le lapin, l'ACM se situe dans le cortex moteur et sensoriel primaire, et plus précisément, dans les zones dédiées aux muscles du visage, de la mâchoire, aux lèvres et à la langue (Bremer, 1923; Goldberg and Tal, 1978; Liu et al., 1993; Lund et al., 1984; Nozaki et al., 1986a).

Dans des travaux datant de 1923, Bremer a montré que les patrons masticatoires pouvaient être modifiés en fonction du site des stimulations dans les différentes zones de l'ACM (Bremer, 1923). D'autres études ultérieures ont montré chez le lapin que l'activation de l'ACM antérieure induisait un patron associé aux mouvements observés pendant la séquence préparatoire de la mastication. L'activation de l'ACM postérieure induisait quant à elle des mouvements ressemblant à ceux observés pendant la période de réduction (Lund et al., 1984).

La mastication induite par stimulation de l'ACM nécessite des trains de stimuli de fréquences allant de 10 à 100Hz avec des durées relativement longues (supérieures à 100ms). Notons que le rythme masticatoire obtenu après ces stimulations semble être indépendant de la fréquence de stimulation. Ceci a notamment été démontré par Dellow et Lund (1971), où des fréquences allant de 20 à 200hz ne changeaient pas le rythme de la mastication. Cette même étude indiquait l'existence d'une latence relativement longue (200ms à 10s) entre le début des stimulations corticales et le début des mouvements masticatoires. Cette latence ne pouvait pas s'expliquer par le délai synaptique entre les régions corticales et les motoneurones, car des réponses apparaissent entre ces derniers avec une latence très courte (~5ms) (Lund et al., 1984).

Ces observations suggèrent que l'ACM peut induire la mastication, et aussi changer le patron masticatoire en fonction de la région qui est spécifiquement activée. Toutefois, il est intéressant de souligner 1) qu'une simple activation de l'ACM ne semble pas suffire à l'induction de la mastication, étant donné la longue latence entre le début de la stimulation et l'initiation des mouvements; et 2) que l'activité induite dans l'ACM semble être indépendante du rythme masticatoire en tant que tel, car les différentes fréquences de stimulations toniques induisent toutes des décharges rythmiques de mastication sans variation de fréquences (ou très minime). Ces observations semblent déjà suggérer la présence d'une sous structure, activée par l'ACM- qui serait le vrai centre générateur du rythme masticatoire, indépendante de la fréquence de stimulation corticale et qui nécessite un délai d'activation. L'idée d'une telle sous-structure est soutenue par l'observation de Bazett et Penfield, où les animaux décérébrés étaient quand même capables de mastiquer (Bazett and Penfield, 1922). Ainsi, le délai d'activation pourrait correspondre au temps nécessaire pour le recrutement de populations de neurones responsables de la formation d'un patron masticatoire. Cette hypothèse, qui concorde avec l'idée d'un GPC masticatoire situé dans le tronc cérébral, a été proposée et corroborée par les expériences de Dellow et Lund (1971) où le tronc cérébral isolé des animaux décérébrés et paralysés pouvait induire une activité rythmique dans les nerfs V, VII et XII semblable à celle observée pendant la mastication (Dellow and Lund, 1971).

En plus des régions corticales, la mastication peut aussi être induite par la stimulation de plusieurs centres supérieurs sous-corticaux: les ganglions de la base, l'hypothalamus latéral, et certaines parties de l'amygdale (Hashimoto et al., 1989; Kawamura and Tsukamoto, 1960; Lund and Dellow, 1973; Nakamura and Kubo, 1978; Nozaki et al., 1986b; Sumi, 1971).

1.3.2 L'output: Les motoneurones qui contrôlent les muscles de la mastication

La majorité des motoneurones qui innervent les différents muscles de la mastication sont situés dans le noyau moteur du trijumeau (NVmot). Le NVmot est constitué de deux populations fonctionnelles de motoneurones. Les premiers sont situés dans la région ventromédiane et innervent les muscles d'ouverture de la mâchoire (digastriques antérieurs et mylohyoïdes, voir section 2.1). L'autre population de motoneurones est localisée dans la partie

dorsolatérale, et innerve les muscles de fermeture de la mâchoire (muscles temporaux, masséters et ptérygoïdes médians; voir section 2.1; Mizuno et al., 1975, Limwongse and DeSantis, 1977, Sasamoto, 1979, Jacquin et al., 1983, Lynch, 1985) . Il existe également un groupe de cellules, nommé Groupe k, impliqué dans le contrôle de muscles de la mastication. Ce groupe de cellules est situé ventro-latéralement au NVmot et contient les corps cellulaires de motoneurones γ qui innervent les muscles masséters et digastriques (Donga et al., 1992; Saad et al., 1999).

Plusieurs études ont observé le patron d'activité des motoneurones durant la mastication. Elles ont montré que les motoneurones d'ouverture et de fermeture reçoivent des inputs excitateurs pendant les phases respectives d'ouverture ou de fermeture, et que seulement les motoneurones de fermeture reçoivent un input inhibiteur pendant la phase d'ouverture (Chandler and Goldberg, 1982; Inoue et al., 1994; Kubo et al., 1981; Nakamura and Kubo, 1978; Nozaki et al., 1993). En d'autres mots, ces motoneurones de fermeture ont une alternance d'inputs excitateurs et inhibiteurs pendant les phases de fermeture et d'ouverture, respectivement (Voir figure 1-3). Lors du premier mouvement d'une série masticatoire, l'inhibition des motoneurones des muscles de fermeture arrive avant l'activation du muscle digastrique. Aussi, l'inhibition peut être induite par des stimulations corticales qui sont d'intensité trop faible pour induire la décharge des motoneurones d'ouverture. De plus, il existe très peu d'évidences de collatérales des motoneurones des muscles d'ouverture vers les motoneurones antagonistes de fermeture, tout ceci indique qu'il n'y aurait pas d'inhibition réciproque entre les mouvements d'ouverture et de fermeture (Kidokoro et al., 1968; Shigenaga et al., 1988). Une explication quant à l'origine de l'inhibition est proposée à la section 1.3.4.2.

Figure 1-3: Résumé schématique de l'activité des motoneurones et des muscles masséters et digastriques pendant la mastication

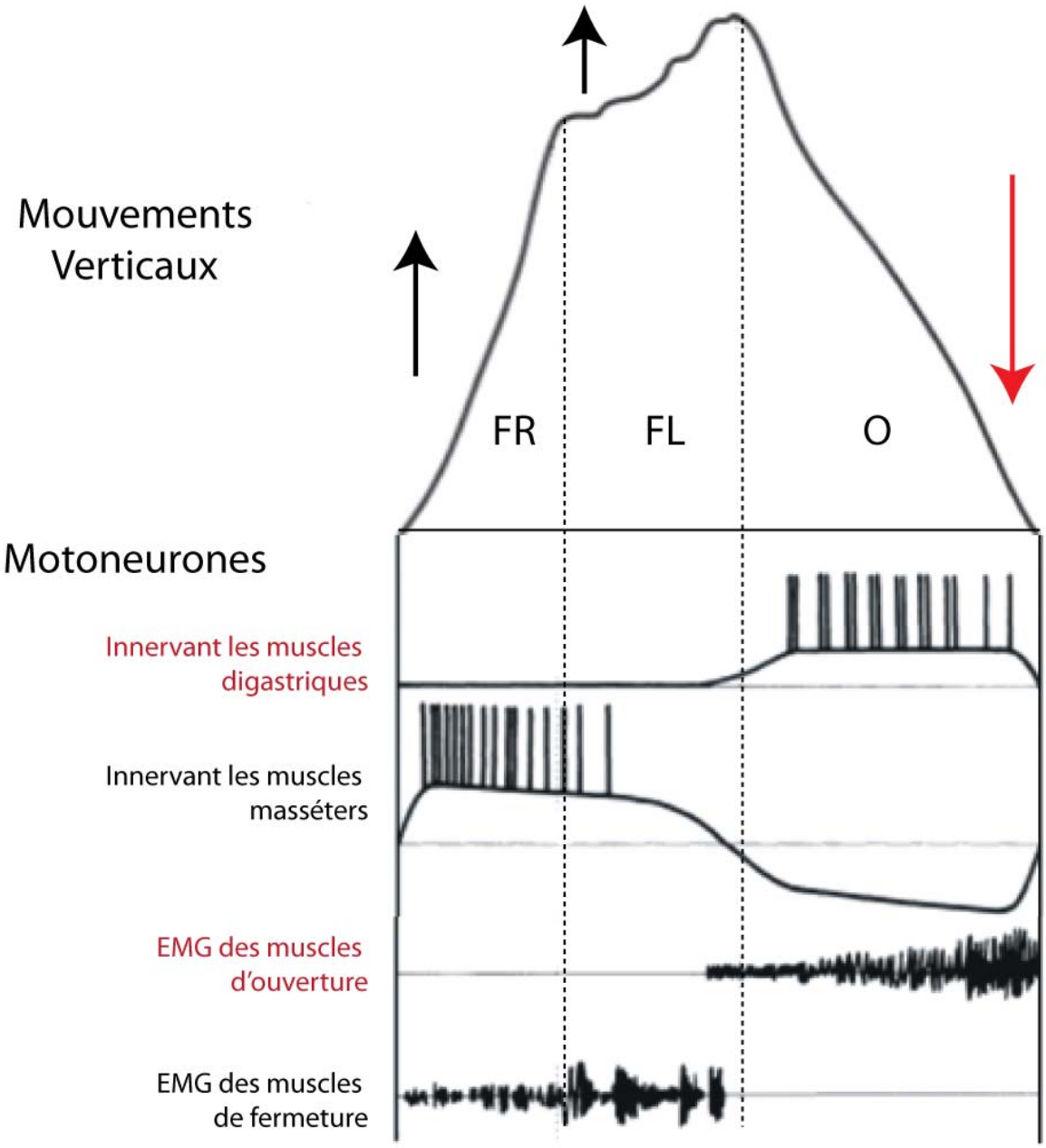

Résumé schématique de l'activité des motoneurones et des muscles masséters et digastriques pendant la mastication. La sortie du GPC masticatoire est visible par l'activité des motoneurones et dans les l'activité musculaire. Les motoneurones innervant les muscles digastriques sont au potentiel de repos durant la FR et pendant la majeure une partie de la FL. Une lente dépolarisation survient pendant l'O et ces motoneurones déchargent. De façon réciproque, les motoneurones innervant les muscles masséters sont dépolarisés pendant la FR et la FL, toutefois ils sont fortement hyperpolarisé pendant l'O. Fermeture rapide (FR), fermeture lente (FL) et ouverture (O). Modifié de Lund, 1991.

1.3.3 Rétrocontrôle de la mastication permettant l'ajustement du mouvement

Plusieurs types d'afférences trigéminales -innervant la muqueuse, les ligaments, les muscles, les dents, etc.- informent le GPC de la mastication de différents paramètres concernant la consistance et le positionnement des aliments dans la cavité orale. Il a été démontré, en conditions expérimentales artificielles, que ces inputs ne sont pas requis pour le maintien d'un mouvement rythmique de base. Toutefois, ces inputs s'avèrent essentiels quand il s'agit d'adapter le mouvement masticatoire en fonction de la consistance de la nourriture, et pour compenser la commande motrice lors de perturbations inattendues (Lund, 1991). Les afférences les plus importantes qui rapportent les caractéristiques du type de nourriture et qui permettent d'ajuster la force de fermeture de la mâchoire sont celles qui proviennent des récepteurs parodontaux et des fuseaux neuromusculaires. Les animaux ont une mastication très maladroite lorsqu'ils sont dépourvus de rétrocontrôle intraoral, à la suite de lésion des branches alvéolaire et maxillaire du nerf trigéminal éliminant ces inputs (Inoue et al., 1989).

Les corps cellulaires des mécanorécepteurs parodontaux qui innervent la racine des dents, sont situés dans le ganglion trigéminal ou dans le noyau mésencéphalique du trijumeau (NVmes; Corbin, 1940, Corbin and Harison, 1940, Jerge, 1963, Cody et al., 1972, Byers et al., 1986) . Ils sont sensibles à la force, ou à l'accélération du changement de la force qui s'applique sur la couronne des dents (Johansson and Olsson, 1976). Les expériences ont montré que ceux innervant les molaires, dont les corps cellulaires sont localisés dans le ganglion trigéminal,sont à adaptation rapide. Ils s'activent et déchargent avec de courtes bouffées au début de la phase de fermeture lente pendant la mastication (Appenteng et al., 1982; Lund, 1991). Chez le singe, les récepteurs dont les corps cellulaires sont dans le NVmes ont des fréquences de décharges qui sont proportionnelles à la force avec laquelle l'animal mord (Larson et al., 1981). Les récepteurs à adaptation lente sont surtout localisés autour des canines. Ils restent activés tout au long de la phase de fermeture lente avec une fréquence de décharge qui augmente proportionnellement à la pression exercée sur la dent. La pression générée pendant la phase de fermeture accroit la longueur de cette phase avec une augmentation de la fréquence de décharge des motoneurones de fermeture, suggérant que les

récepteurs à adaptation lente transmettent un rétrocontrôle positif au motoneurone de fermeture (Lund, 1991).

Les fuseaux neuromusculaires permettent de détecter les changements d'étirement et de tension des muscles. Toutefois, ces récepteurs sont seulement retrouvés de façon significative dans les muscles de fermeture (masséter, temporal, et le ptérygoïde médian). Ils sont de deux types: les dynamiques (primaires) et les statiques (secondaires). Les premiers déchargent à fréquence élevée avant le début de la mastication et sont activés de façon optimale pendant les cycles de type I et III de la mastication, en dépit du fait que les mouvements sont plus amples pendant les cycles de type II. Les récepteurs statiques déchargent à des fréquences moins élevées pendant la mastication. Les corps cellulaires des afférences fusoriales neuromusculaires sont localisés dans le NVmes (Cody et al., 1972; Jerge, 1963). Avec les afférences parodontales, ces dernières sont en grande partie responsables de l'encodage de l'information quant à la consistance et à la texture de la nourriture, ainsi que de l'ajustement de l'activité et la force des muscles de fermeture pendant les mouvements masticatoires. En effet, dans une série d'expériences, Morimoto et ses collaborateurs (1989) ont simulé une augmentation de la dureté de la nourriture en insérant des morceaux de plastiques de différentes grosseurs entre les molaires opposées chez le lapin. On observait alors une facilitation d'activation des muscles de fermeture qui était abolie seulement lorsque des lésions étaient faites à la fois dans le nerf trigéminal (les branches maxillaires et alvéolaires inférieures) et dans le NVmes.

Les afférences des organes tendineux de Golgi et des capsules des articulations temporo-mandibulaires peuvent aussi procurer un rétrocontrôle durant la mastication. Toutefois, les connaissances sur le rôle de ces récepteurs demeurent très limitées (Lund, 1991; Morquette et al., 2012).

Ainsi, les récepteurs parodontaux et les fuseaux neuromusculaires semblent être les principaux organes sensoriels impliqués dans le rétrocontrôle des muscles de la mâchoire (Inoue et al., 1989).

Néanmoins, il existe aussi d'autres récepteurs qui rapportent des informations importantes par rapport au bol alimentaire et à la position de la mâchoire. En effet, les récepteurs cutanés sont activés par la déformation de la peau, et exercent un rétrocontrôle pour le bon positionnement des muscles de la face et des lèvres. Les afférences en provenance des muqueuses de la cavité

orale interne permettent parallèlement un rétrocontrôle pour le bon positionnement de la langue et des muscles de la mâchoire (Johansson et al., 1988).

En plus d'assurer une bonne adaptation des mouvements de la mastication en fonction de la situation, les inputs sensoriels seraient également importants pour initier l'activation du GPC de la mastication, et pour l'initiation des changements de cycles et de phases de la mastication (Lund, 1991). En effet, il a été montré que dans des cas d'animal décérébré, la stimulation de la région oro-faciale pouvait être suffisante pour l'initiation de l'activité rythmique masticatoire (Bremer, 1923).

1.3.4 Le générateur de patron central

1.3.4.1 La mastication fictive

Dellow et Lund (1971) ont été les premiers à montrer qu'un tronc cérébral isolé pouvait générer de façon intrinsèque la décharge neuronale rythmique à la base de la mastication. Lors des stimulations centrales induisant la mastication *in vivo,* les bouffées rythmiques en phase avec les mouvements masticatoires étaient enregistrées dans les branches masséter et mylo-hyoïdien du nerf trigéminal, et du nerf/noyau hypoglosse. Leur étude était menée sur des animaux anesthésiés, décérébrés et ayant la moelle épinière sectionnée. Les afférences nerveuses étaient également sectionnées afin d'isoler leurs préparations de tous inputs somatiques. Ces chercheurs s'assuraient également que le patron de mastication rythmique qu'ils enregistraient n'était pas dû à une activation du système vasculaire ou respiratoire. Malgré ces conditions, ils étaient capables de voir une activité en bouffées rythmiques dans les nerfs qu'ils enregistraient. En absence de tout mouvement, de tels patrons de commandes motrices rythmiques et organisés sont décrits comme étant une « mastication fictive » ayant à son origine des groupes de neurones correspondant au GPC.

De façon générale, la mastication fictive a été étudiée et produite par les stimulations électriques de l'ACM ou par stimulation des récepteurs sensoriels des régions oro-faciales (voir section précédente). La comparaison des patrons d'activités électriques enregistrées dans les nerfs moteurs et dans les muscles, avant et après la paralysie des muscles, aide à déterminer l'importance du contrôle central sur les mouvements rythmiques. Cette

comparaison aide aussi à déterminer si l'activité rythmique enregistrée dans un élément dépend d'un rétrocontrôle sensoriel (Lund, 1991).

1.3.4.2 Localisation du GPC

Pour définir la localisation exacte du GPC, la stratégie plus communément utilisée consistait à repérer, au moyen d'enregistrements électrophysiologiques, différentes régions du tronc cérébral présentant une activité rythmique en condition de mastication fictive, pour ensuite évaluer comment leurs lésions affectent la rythmicité du patron enregistré. Plusieurs difficultés sont associées à cette stratégie: seuls, les enregistrements ne permettent pas de discriminer si la région en question génère le rythme ou le relaie. Les lésions, quant à elles, risquent souvent d'atteindre plusieurs régions vitales adjacentes dans le tronc cérébral affectant ainsi l'état de l'animal et la capacité d'induire la mastication fictive dans les expériences menées *in vivo*. Pour les expériences menées *in vitro* où l'activité rythmique est induite par des substances pharmacologiques, le problème vient du fait que les motoneurones peuvent être directement activés par ces substances et produire une activité oscillatoire, sans passer par l'activation d'un GPC. Malgré tout, les recherches, utilisant ces approches, ont permis au fil des années de repérer différentes régions d'intérêt dans le tronc cérébral. Afin de faciliter la compréhension du lecteur, le tronc cérébral est présenté de façon schématique dans la figure 1-4.

Précisons, avant d'aborder cette question plus en détail, que la localisation du GPC masticatoire a été compliquée d'une part, par le fait que différentes espèces d'animaux ont été utilisées pour l'étude de la rythmogénèse masticatoire, et, d'autre part, par l'utilisation de différentes nomenclatures pour les régions du tronc cérébral dans les différentes études. Ainsi, sans prétendre solutionner ce problème, mais plutôt dans le but de faciliter la compréhension de l'organisation du système à la base du rythme masticatoire, nous avons essayé de resituer les différentes régions énumérées au travers des études, en les situant par rapport au NVmot. Ce noyau a été choisi de par son excellente définition du point de vue anatomique et fonctionnel.

Figure 1-4: Localisation de différentes structures qui ont été impliquées dans la mastication et dans la rythmicité du GPC

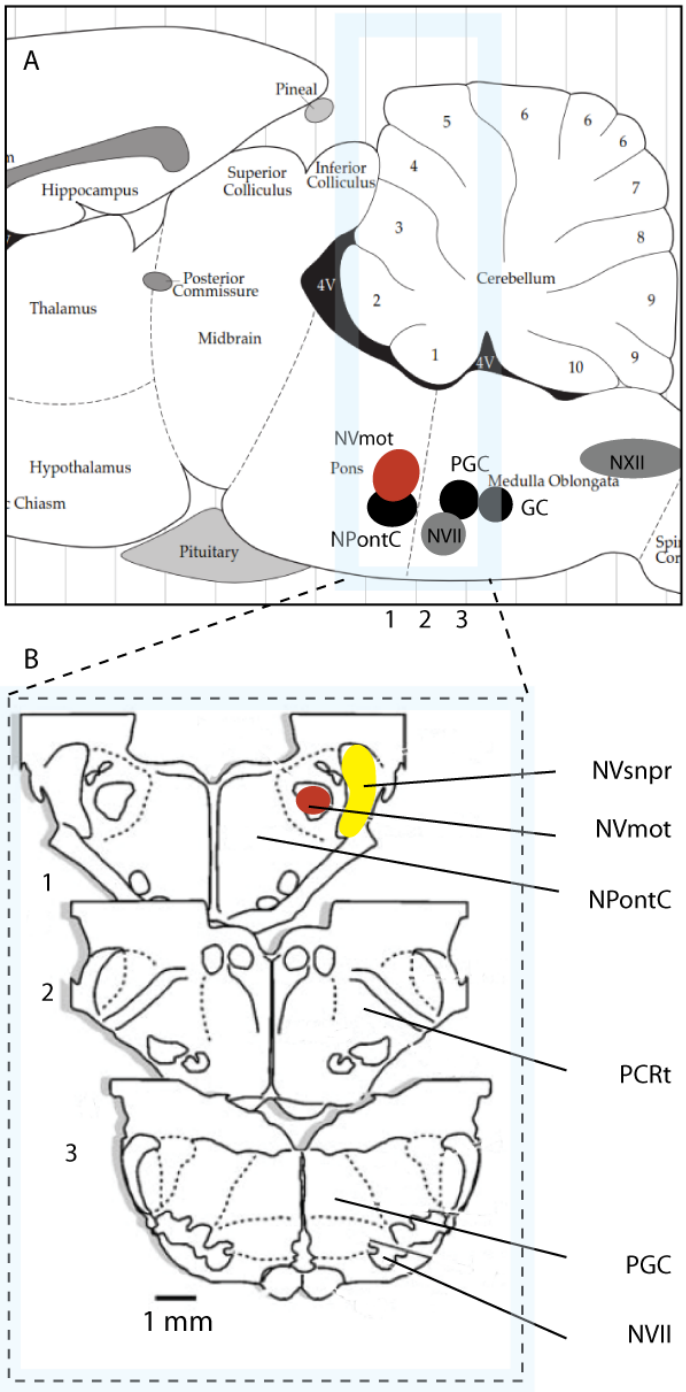

Localisation de différentes structures qui ont été impliquées dans la mastication et dans la rythmicité du GPC. Le NVmot est illustré en rouge et en jaune le NVsnpr.
A. Vue sagittale. Modifié de Paxinos et Watson 2004.
B. Coupe coronale au niveau du tronc cérébrale. NVII: noyau facial, NVmes: noyau mésencéphalique du trijumeau, NVmot: noyau moteur du trijumeau, NVsnpr: noyau trigéminal sensoriel principal, NXII: noyau hypoglosse, nPontC: noyau pontis caudalis, PCRt: formation réticulée parvocellulaire, PGC: noyau paragigantocellulaire, GC: noyau gigantocellulaire. Modifié de Westberg et Kolta 2011.

Nozaki et collaborateurs ont été les premiers à proposer un modèle de GPC de la mastication et à identifier un groupe de neurones qui pouvaient en être responsables (Nozaki et al., 1986a, b). En se fondant sur des études démontrant l'existence de connexions anatomiques entre le cortex sensorimoteur et des régions de la formation réticulée bulbaire médiane (Kuypers, 1958; Peterson et al., 1974), Nozaki et ses collègues se sont intéressés à cette dernière région, plus précisément au noyau gigantocellulaire (GC) et à la partie dorsale du noyau paragigantocellulaire (PGC). Ces régions sont situées caudalement par rapport au NVmot dans le tronc cérébral (voir figure 1-4). Dans une série d'expériences chez le cochon d'Inde, ces chercheurs ont induit la mastication fictive grâce à des stimulations électriques de l'ACM. Parallèlement, des enregistrements extracellulaires dans la formation réticulée bulbaire ont montré que les neurones dans le PGC dorsal répondaient de façon tonique en corrélation avec la stimulation répétitive de l'ACM. En revanche, une décharge en bouffées rythmiques était enregistrée au niveau des neurones de la partie dorsale du noyau GC à la suite des mêmes stimulations. L'analyse des latences des potentiels de champs induits dans le GC et dans le PGC à la suite de stimulations de l'ACM a permis aux chercheurs de postuler que le rythme masticatoire venait d'une activation monosynaptique des neurones du PGC à partir des inputs corticaux. Les neurones du PGC activaient dans un deuxième temps des neurones ayant la capacité de décharger en bouffées rythmiques dans le GC dorsal. Ces neurones du GC relayaient alors le rythme masticatoire généré directement au NVmot (voir figure 1-5). L'existence d'une projection corticale directe à la partie dorsale du PGC a été montrée par marquage rétrograde avec l'injection de HRP (Nozaki et al., 1986b), alors qu'une telle projection corticale au GC semble inexistante. De plus, ils ont confirmé que la direction de la connexion entre les deux sous-divisions de la formation réticulée médullaire médiane était du PGC vers le GC et non l'inverse. Le fait que l'inactivation de cette région (par lésions ou injections de lidocaïne) abolisse la mastication appuyait l'hypothèse stipulant l'importance de ces structures dans la genèse de la mastication. Dès lors, le PGC et GC semblaient être des structures clés du GPC de la mastication.

Figure 1-5: Schéma de l'ancien modèle du GPC de la mastication

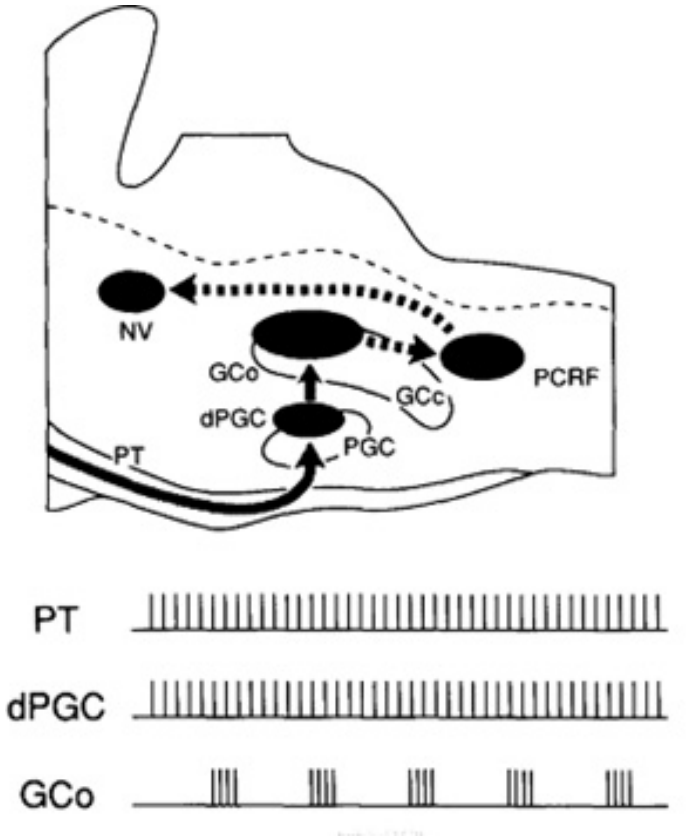

Schéma de l'ancien modèle du GPC de la mastication: On y retrouve la chaine neuronale des différentes structures neuronales impliquées à partir du tractus pyramidal (PT) jusqu'au noyau moteur trigéminal dans une vue superposée sagittale du tronc cérébral. Les flèches à trait continu représentent les activités non rythmiques alors que les flèches pointillées représentent l'activité rythmique. Notez que le rythme masticatoire est généré dans le noyau gigantocellulaire (GC). Le PCRF correspond à la formation réticulée parvocellulaire. Le PGC correspond à la partie dorsale du noyau paragigantocellulaire. Modifié de Yoshio Nakamura, Nobuo Katakura 1995.

Cependant, une faiblesse à l'hypothèse de Nozaki et ses collaborateurs (1986b) est l'absence de projections (ou du moins très peu) entre le GC et le NVmot (Landgren et al., 1986; Travers and Norgren, 1983). D'où, la proposition d'addition d'un relais dans la partie caudale de la formation réticulée parvocellulaire (PCRt) par Nozaki et ses collaborateurs (1993) et ensuite par Nakamura et Katakura (1995). Selon ce modèle revisité, le rythme était généré par les neurones du GC, mais le patron des bouffées serait généré par les interneurones prémoteurs de dernier ordre, situés dans le PCRt caudal adjacent au NXII. Cette région aussi est plus caudale que le NVmot dans le tronc cérébral (voir figure 1-4). Pour vérifier leur nouveau modèle, Nozaki et ses collaborateurs (1993) ont enregistré les neurones du PCRt pendant la mastication fictive. Ils ont montré que les interneurones prémoteurs du PCRt actifs pendant la phase d'ouverture excitaient les motoneurones d'ouverture avec en parallèle une inhibition des motoneurones de fermeture (expliquant l'inhibition observée à la figure 1-3). Toutefois, les interneurones prémoteurs du PCRt actifs pendant la phase de fermeture de la mastication fictive ont évoqué seulement des PPSEs dans les motoneurones de fermeture sans action inhibitrice sur les motoneurones d'ouverture. Cette observation a été confirmée par les données de Inoue et ses collaborateurs (Nozaki et al., 1993, Inoue et al., 1994; voir section 1.3.2 et figure 1-3). Ces données semblaient donc suggérer une importance des neurones du PCRt dans le GPC de la mastication.

Le modèle proposé par Nozaki et ses collaborateurs a toutefois été révisé par Lund (1991), car il a été démontré qu'une section du PCRt de façon rostrale au NXII n'abolit pas la mastication (Chandler and Tal, 1986). Le modèle de Nozaki et al (1986 a, b) a donc été modifié pour y ajouter une projection des neurones du GC à des neurones dotés de propriétés rythmogéniques ayant une localisation plus près du NVmot. Ces neurones ont été situés à la frontière ponto-bulbaire, dans le PCRt-α et le NVspo-γ, car une étude de Donga et Lund indiquait que ces régions contenaient des neurones rythmiquement actifs pendant la mastication fictive (Donga and Lund, 1991). Cette étude semble ainsi suggérer qu'une région beaucoup plus rostrale et à proximité du NVmot peut remplir le rôle du GPC de la mastication.

Lund (1991) a également ajouté une projection du générateur de bouffées au NVmot controlatéral par rapport au modèle initial de Nozaki. Lund s'est appuyé sur le fait que les stimulations unilatérales de l'ACM induisent une activité rythmique masticatoire bilatérale synchrone. Dans ce même contexte, une section de la ligne médiane au niveau de la médulla

permet une activité rythmique masticatoire uniquement du côté controlatéral. Toutefois, à la suite d'une telle section, les stimulations bilatérales de l'ACM induisent une activité masticatoire bilatérale asynchrone (Nozaki et al. 1991). Ces observations ont mis en évidence des GPCs indépendants de chaque côté du tronc cérébral, synchronisés par des neurones ayant des projections controlatérales (voir aussi Chandler and Tal, 1986 et Ihara et al., 2013). Une telle connexion controlatérale est également soutenue par des données électrophysiologiques qui indiquent que les neurones du PCRt-α et du NVspo-γ projettent au NVmot controlatéral (Donga and Lund, 1991; Donga et al., 1990).

Néanmoins, plusieurs études ont rapporté des éléments qui ont forcé une révision du modèle de Nozaki et de celui qui en découle, proposé par Lund. En effet, ces premiers modèles avaient assumé que les inputs du cortex masticatoire activent uniquement la formation réticulée médullaire (bulbaire) ventromédiane avec des inputs restreints aux neurones du PGC. Toutefois, plusieurs données anatomiques et électrophysiologiques montrent l'existence de projections directes entre certains sites corticaux et des neurones de 1) la formation réticulée médullaire latérale, 2) la formation réticulée pontique médiane (nPontc) et latérale (périV), et 3) les noyaux trigéminaux sensoriels principal et spinal (Donga and Lund, 1991; Enomoto et al., 1995; Inoue et al., 1992; Torvik, 1956; Yasui et al., 1985). Ainsi, toutes ces régions du tronc recevant des inputs du cortex masticatoire pourraient potentiellement jouer un rôle dans le GPC de la mastication.

Une autre indication de l'inadéquation des modèles originaux vient d'études, menées *in vitro,* suggérant une localisation du GPC dans la portion du tronc cérébral comprise entre la tringle rostrale du NVmot et le pôle rostral du NVII (Katakura N et al., 1999; Kogo et al., 1996; Kogo et al., 1998; Tanaka et al., 1999). Tanaka et ses collaborateurs ont pu le démontrer grâce à une série d'expériences sur des préparations de tronc cérébral isolé de rat (entre le Colliculus inférieur et l'Obex). Ils ont enregistré l'activité oro-motrice rythmique, induite en présence de l'acide aminé excitateur N-methyl-D,L-aspartate (NMA) et de la bicuculline (BIC, antagoniste des récepteurs inhibiteurs GABA(A)), à partir des branches du nerf trigéminal. Ces enregistrements ont été effectués en même temps qu'une série de sections transverses séquentielles (perpendiculairement à l'axe rostro-caudal) du tronc cérébral afin de déterminer la localisation de la circuiterie minimale nécessaire à la rythmogénèse trigéminale. Dans cette même étude, il a été démontré que l'activité rythmique pouvait être obtenue de façon

bilatérale, car elle était présente dans des hémisections (droite et gauche) de bloc de tronc cérébral. Ces blocs d'hémisections supportant l'activité rythmique étaient moins étendus et plus rostraux que précédemment décrits dans la littérature (Chandler and Tal, 1986; Nozaki et al., 1986a, b). Ainsi, les données de cette étude ont remis en question le rôle et la nécessité des neurones de la formation réticulée médullaire, puisque ceux-ci sont dans des régions plus caudales, et en dehors du circuit minimal nécessaire à la genèse du rythme trigéminal. En outre, l'on retrouve une mastication sévèrement compromise lorsque les souris sont génétiquement modifiées de façon à empêcher le développement normal des 3e et 5e rhombomères; ces animaux ont une réorganisation des circuits neuronaux au niveau caudal de la formation réticulée pontique (Champagnat and Fortin, 1997; Jacquin et al., 1996). Ceci suggère, encore une fois, que ces segments du tronc cérébral beaucoup plus rostraux que les régions proposées par Nozaki (Nozaki et al., 1986a, b), qui comprennent le NVmot et les régions avoisinantes, pourraient renfermer des circuits qui forment la base d'un générateur de rythmicité.

Prenant en compte toutes ces données plus récentes, un nouveau modèle du GPC de la mastication a été proposé par G. Scott et ses collaborateurs (Scott et al. 2003; voir figure 1-6, pour plus de détails). Ce dernier modèle illustre bien la restriction de la localisation du GPC aux régions plus rostrale (entre le noyau trigéminal et le NVII) comprenant essentiellement le sous-noyau oralis du noyau spinal trigéminal (NVspo), le NVmot avec les régions qui l'entourent formant la région péri-trigéminale (périV) et finalement le NVsnpr; l'on y retrouve la grande majorité des interneurones de dernier ordre projetant aux motoneurones trigéminaux et à d'autres motoneurones impliqués dans la mastication.

Plusieurs études ont démontré, à l'aide d'enregistrements unitaires, que les neurones de ces régions, particulièrement ceux de la partie dorsale au NVmot nommée supra-trigéminale (SupV), sont rythmiquement actifs pendant la mastication fictive (Inoue et al., 1994; Inoue et al., 1992). Cependant, ces études n'indiquaient pas si ces neurones génèrent le rythme de façon intrinsèque ou s'ils le relayent. Les travaux de Bourque et Kolta indiquent que les neurones à proximité de cette région dans la région PériV et ceux dans le PCRt ne semblent pas présenter de propriétés intrinsèques de décharge en bouffées, mis à part une petite proportion de neurones situés dans la partie latérale du SupV à proximité du NVsnpr (Bourque and Kolta, 2001).

Figure 1-6: Modèle du GPC de la mastication basée sur les données plus récentes.

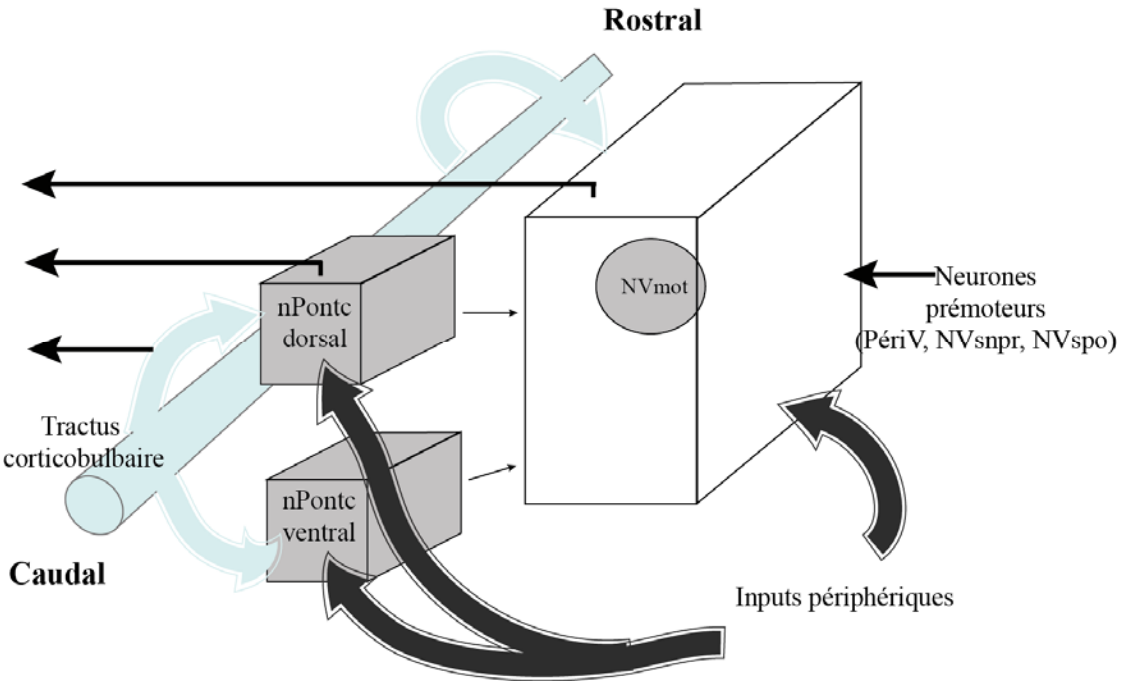

Modèle du GPC de la mastication basée sur les données plus récentes. Les différentes structures du GPC de la mastication sont situées de façon plus rostrale par rapport à l'ancien modèle. Les divisions dorsale et ventrale de la formation réticulée pontique médiane (nPontc), les régions latérales (périV), les noyaux trigéminaux sensoriels principal et spinal reçoivent tous des inputs corticaux et périphériques. Le nPontc projette vers des neurones prémoteurs qui projettent à leur tour vers le NVmot. Les flèches noires (vers la gauche) représentent les connexions commissurales. Dans ce modèle, pendant la mastication, les neurones du nPontc ventral peuvent inhiber de façon tonique d'autres parties du GPC alors que les neurones de la partie dorsale ont des effets mixtes. Il faut noter, toutefois, que ce modèle reste vague quant à la région spécifique qui serait responsable de la genèse du rythme en tant que tel. Modifié de G. Scott et al., 2003.

Dans ce contexte, la portion dorsale du NVsnpr est une région très intéressante pour la rythmogénèse trigéminale, puisque l'on y retrouve des neurones avec des capacités intrinsèques de décharges en bouffées rythmiques. De telles capacités d'autorythmicité neuronales peuvent contribuer à la rythmogénèse de comportements moteurs (Marder and Calabrese, 1996), et beaucoup de résultats accumulés au cours de la dernière quinzaine d'année indiquent l'importance du NVsnpr dans la rythmicité masticatoire. La prochaine section expose différents arguments qui révèlent l'importance du NVsnpr dans la rythmogénèse trigéminale: ce noyau pourrait constituer le cœur du GPC masticatoire.

1.3.4.3 Le NVsnpr

Le NVsnpr a particulièrement bien été localisé chez le lapin et le chat où les premiers travaux sur ce noyau ont été effectués. Chez ces espèces, Le NVsnpr se situe de 6-10 mm rostralement à l'Obex et 3,5-5,5 mm latéralement à la ligne médiane (Eisenman et al., 1963) et est bordé latéralement par le tractus trigéminal (voir figure 1-4). Le pôle rostral du NVsnpr s'aligne avec celui du NVmot et le noyau s'étend caudalement jusqu'au pôle rostral du NVII (Voir figure 1-4). Ce noyau est donc à l'intérieur de la zone critique minimale contenant les circuits de rythmicité selon l'étude de Tanaka et al (1999). Sandler et ses collaborateurs ont été les premiers à montrer qu'une grande proportion de neurones enregistrés dans ce noyau avait des propriétés intrinsèques de décharges en bouffées (Sandler et al., 1998). Cette caractéristique ne semblait pas concorder avec le rôle traditionnel associé au NVsnpr qui est celui d'un relais sensoriel de deuxième ordre vers le thalamus (Chiaia et al., 1991; Peschanski, 1984; Williams et al., 1994). En effet, il est attendu qu'un relais sensitif puisse transmettre l'information sensorielle de façon linéaire proportionnellement à l'intensité du stimulus sensoriel. Le fait est que le NVsnpr, avec des neurones déchargeant en bouffées, présente une caractéristique qui n'est pas typique d'un centre de relais sensoriel primaire (Sandler et al., 1998).

La particularité des neurones du NVsnpr de décharger en bouffées a été confirmée ultérieurement par le groupe de Kolta et Lund (Brocard et al., 2006; Tsuboi et al., 2003) et plus tard par le groupe de Chandler (Tsuruyama et al., 2013). Dans leurs études de 2003, Tsuboi et ses collaborateurs ont montré, au travers d'expériences in vivo, que les neurones dorsaux du NVsnpr déchargent rythmiquement en phase avec les motoneurones trigéminaux

pendant la mastication fictive (Tsuboi et al., 2003). Cette étude montre que près de 40% des neurones de cette région, surtout dans la partie dorsale, avaient une décharge qui était modulée lors de l'induction de la mastication fictive: 30% avec une décharge tonique et plus de 70% avec une décharge rythmique. Toutefois, tous les neurones ayant une décharge rythmique ne déchargeaient pas en phase avec le rythme moteur. Dans les faits, la majorité des neurones déchargeant en phase avec la mastication semblait recevoir des inputs des récepteurs parodontaux ou des fuseaux neuromusculaires, et les autres neurones avaient des champs récepteurs dans les régions péri-orales. Les neurones ayant une activité rythmique reliée à la mastication déchargeaient une bouffée par cycle en phase avec le mouvement d'ouverture ou celui de fermeture. Les neurones qui déchargeaient pendant la phase d'ouverture étaient distribués sur l'étendue rostro-caudale du noyau alors que ceux déchargeant pendant la phase de fermeture étaient localisés plus rostralement. L'importance du NVsnpr pour la mastication, a aussi été confirmée par l'expression augmentée de la protéine c-Fos (un marqueur fonctionnel d'activité) après des épisodes répétés de mastication fictive (Athanassiadis et al., 2005). Ainsi, ces différentes études sur l'activité neuronale retrouvée dans le NVsnpr soutiennent un rôle de ce noyau dans la rythmogénèse de la mastication.

Les afférences et les efférences du NVsnpr présentent un autre argument en faveur du rôle que peut jouer ce noyau dans le GPC. En effet, les observations montrent que les neurones du NVsnpr 1) projettent vers les noyaux moteurs V, VII et XII (Kolta et al., 2000; Li et al., 1993; Pinganaud et al., 1999; Travers and Norgren, 1983; Yoshida et al., 1998), et; 2) reçoivent des projections massives des afférences sensorielles et de l'ACM (Capra and Dessem, 1992; Yasui et al., 1985; Yoshida et al., 2009). Le NVsnpr est donc dans une position idéale pour recevoir la commande d'initiation de la mastication par l'ACM; pour générer un rythme grâce aux caractéristiques des neurones qui le constituent; pour adapter ce rythme en fonction du rétrocontrôle sensoriel; et pour transmettre une commande rythmique aux motoneurones du NVmot responsables du mouvement de la mastication (voir figure 1-2). Par ailleurs, il est intéressant de souligner que l'émergence de la mastication, qui s'établit entre la 2e et la 3e semaine postnatale, correspond à la période d'apparition de la décharge en bouffées rythmiques dans le NVsnpr au cours du développement (Brocard et al., 2006; Sandler et al., 1998; Tsuruyama et al., 2013).

Toutes ces observations suggèrent fortement que le NVsnpr pourrait constituer une composante essentielle du GPC de la mastication. Donc, les enregistrements réalisés au cours de notre étude ont été faits dans la partie dorsale de ce noyau puisque le but de notre recherche était de comprendre les mécanismes cellulaires sous-jacents à la rythmogénèse dans le circuit trigéminal responsable de la mastication.

1.4 La rythmogénèse

Dans plusieurs régions du cerveau, les neurones peuvent changer leur patron de décharge selon les conditions du moment, d'un mode que l'on appelle tonique à un mode que l'on appelle rythmique (Huh and Cho, 2013; Kadala et al., 2015; MacGregor and Leng, 2012; Mirmiran and Corner, 1982; Noda and Mikami, 1986; Sharott et al., 2012). La nécessité de telles décharges rythmiques parait beaucoup plus évidente dans le contexte des mouvements rythmiques. Ceci dit, plusieurs autres fonctions (l'attention, le sommeil, l'apprentissage et la mémoire) ou pathologies (épilepsie) découlent aussi d'activité rythmique neuronale.

La définition de ce que constitue une décharge rythmique est arbitraire et varie selon les études (voir Kadala et al., 2015 en Annexe). Dans leurs études, Kolta et collaborateurs définissent une bouffée comme étant un regroupement de plusieurs potentiels d'actions à relativement haute fréquence, surmontant un plateau de dépolarisation (pour revue voir Kadala et al., 2015). Les bouffées sont dites rythmiques lorsqu'elles se répètent avec une certaine périodicité. Par opposition, le mode tonique consiste en des décharges de potentiels d'actions unitaires. Ceux-ci peuvent être occasionnellement répétitifs, mais se produisent généralement à des fréquences beaucoup moins élevées que la décharge surmontant les plateaux dépolarisants des bouffées (Kadala et al 2015). Plusieurs études ont documenté les différents mécanismes cellulaires pouvant être impliqués dans les changements de mode de décharges neuronales. Différents modèles proposent tantôt une explication fondée sur des capacités d'autorythmicité intrinsèques de neurones unitaires, tantôt sur des systèmes de circuiteries, plus ou moins complexes, impliquant des neurones excitateurs et/ou inhibiteurs, tantôt sur une combinaison des deux. Quoi qu'il en soit, les mécanismes qui sous-tendent la transition du mode de décharge tonique vers celui en bouffées rythmiques ne sont pas complètement compris.

Dans la prochaine section, étant donné notre but d'étudier la base de la rythmogénèse des circuits trigéminaux, il est important et intéressant d'aborder au moins de façon sommaire les concepts des différents modèles de rythmogénèse qui ont été proposés au fil des années. Cela dit, nous nous attarderons plus particulièrement aux principes cellulaires de rythmogénèse qui semblent s'appliquer au NVsnpr.

1.4.1.1 Rythmicité émanant de l'organisation du circuit

Le premier modèle de CPG a été celui de « demi-centre » proposé par Graham Brown pour la locomotion (voir figure 1-7). Dans ce modèle, deux groupes de neurones sont organisés en parallèle et peuvent s'inhiber réciproquement. Il en découle l'émergence d'un patron rythmique avec l'activation en alternance de muscles extenseurs et fléchisseurs (Brown, 1911, 1914). Évidemment, une faiblesse majeure de ce modèle était qu'il ne pouvait étayer les variations de patrons observées lors de la locomotion. Par la suite un modèle de générateur de bouffées par unité (Grillner 1981), ainsi que d'autres modèles proposés par différents groupes (Kriellaars et al, 1994; Perret et Cabelguen 1980) ont été postulés. Une organisation plus complexe, en « demi-centre », sur deux niveaux, était proposée dans ces derniers modèles; le premier niveau était dédié à l'encodage/contrôle des patrons, et l'amplitude de l'activité des motoneurones; le deuxième niveau était plus précisément consacré à la génération du rythme (McCrea and Rybak, 2008; voir figure 1-7).

Figure 1-7: Illustration schématique du modèle de générateur de patron central

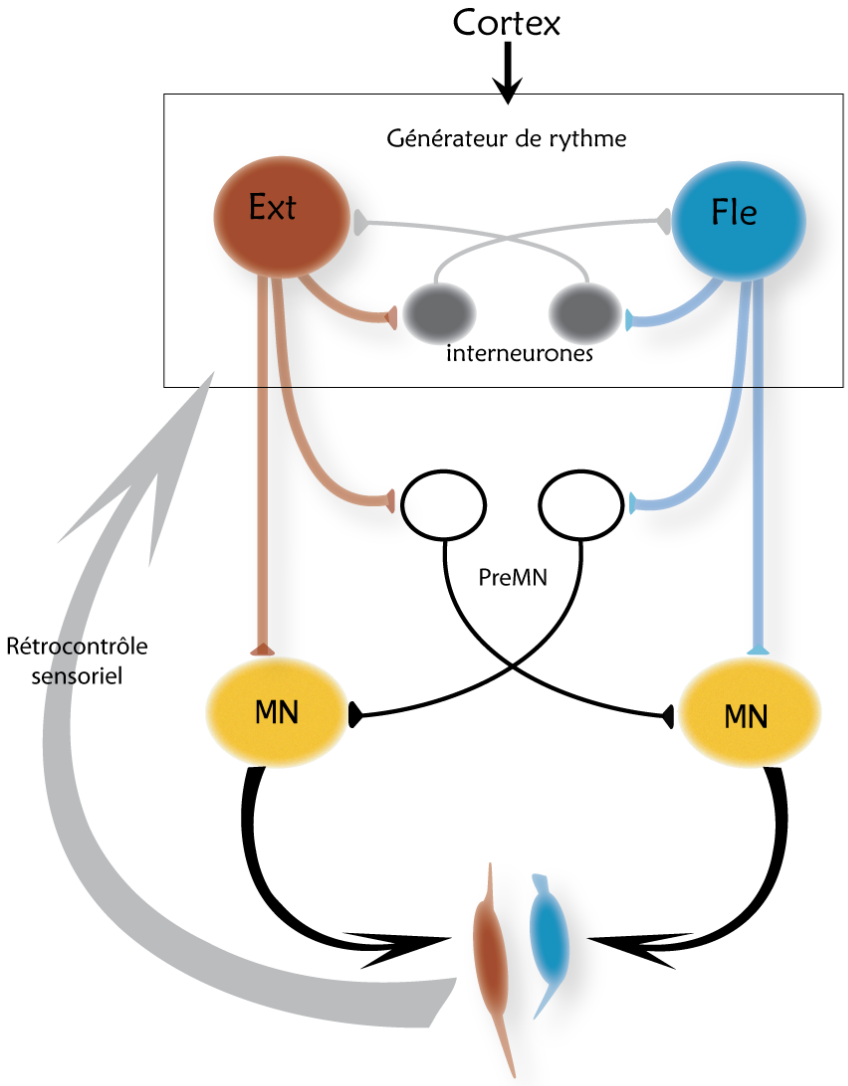

Illustration schématique du modèle de générateur de patron central des demi-centres présentant une alternance de d'activité rythmique entre les muscles fléchisseurs (Fle en bleu) et extenseurs (Ext en rouge). Les neurones fléchisseurs et extenseurs projettent aux motoneurones innervant les muscles (aussi en bleu et rouge) impliqués dans le mouvement rythmique. Dans le modèle de Graham Brown (boîte), une inhibition mutuelle via les interneurones inhibiteurs (en gris) assure l'activité alternée des deux demi-centres (fléchisseur en bleu et extenseur en rouge). La transition entre les deux demi-centres résulterait de la fatigue croissante des interneurones inhibiteurs. Dans les modèles plus récents, la circuiterie du générateur de patron central comprend deux niveaux. Le premier niveau (à l'intérieur de la boîte) génère le rythme alterné basique et le second niveau, composé des prémotoneurones, détermine l'enveloppe de la décharge en bouffées des motoneurones. Les inputs corticaux et sensoriels permettent d'initier ou de corriger le patron de décharge. Modifié de Morquette et al., 2012; en Annexe.

Pour de tels modèles, les patrons de commandes motrices rythmiques peuvent être générés par des neurones qui n'ont pas forcément des caractéristiques intrinsèques d'autorythmicité. En effet, des groupes de neurones qui s'inhibent de façon réciproque sont suffisants pour générer une activité neuronale alternée, et ainsi engendrer une commande motrice rythmique.

1.4.1.2 Rythmogénèse neuronale intrinsèque

Le fondement de l'hypothèse de « neurones *pacemaker »* est que les CPGs seraient constitués de neurones ayant des conductances voltage dépendante permettant à ces derniers de décharger en bouffées rythmiques lorsqu'isolés de tout input synaptique. Aussi, ces neurones intrinsèquement rythmiques seraient capables de transmettre leur mode de décharge à d'autres neurones « suiveurs » (Harris-Warrick, 2010). Avec un tel modèle, toute élimination ou blocage des neurones pacemakers (ou blocage des conductances qui leurs confèrent leurs caractéristiques ryhtmogène) compromet automatiquement l'ouput rythmique du GPC. Dans le contexte de la mastication, au niveau du NVsnpr dorsal, les neurones qui déchargent en bouffées rythmiques semblent justement avoir les caractéristiques pour une rythmogénèse intrinsèque. En effet, l'absence de calcium extracellulaire ne semble pas affecter la capacité de ces neurones à décharger en bouffées rythmiques. Dans une telle condition, la transmission synaptique est bloquée ou très faible, ce qui suggère que la décharge rythmique de ces neurones résulte de caractéristiques de conductances intrinsèques (Brocard et al., 2006; Tsuruyama et al., 2013). Ce phénomène de décharge rythmique, dans des conditions non propices à la transmission synaptique, a aussi été rapporté pour d'autres régions du SNC (Brocard et al., 2013; Heinemann et al., 1977; Johnson et al., 1994; Su et al., 2001; Tazerart et al., 2008). Dans une telle situation, ces neurones rythmogènes réussissent à générer une activité rythmique grâce aux caractéristiques des canaux ioniques de leur membrane.

1.4.1.3 Rythmogénèse neuronale émergente des propriétés du réseau

Avant d'aborder la prochaine section qui s'intéresse à la base ionique de la rythmogénèse neuronale, il est important de mentionner l'existence d'un troisième mécanisme de rythmogénèse neuronal. Le groupe de Feldman propose un mécanisme de « *Emergent*

Network Property » comme une alternative au mécanisme de neurones « *pacemaker* ». Ces chercheurs proposent que l'unité fondamentale d'oscillation soit formée d'ensembles de neurones avec des propriétés intrinsèques similaires ou complémentaires qui deviennent rythmiquement actifs grâce aux interactions électriques et chimiques d'inputs synaptiques (Del Negro et al., 2002b; Rekling and Feldman, 1998; Rekling et al., 2000).

Dans le GPC de la respiration, les données de l'étude de Del Negro supportent bien ce concept car l'élimination de la population de neurones *pacemaker* (réduction d'au moins 94%) ne semble pas affecter le rythme respiratoire. Ceci suggère que les bouffées rythmiques qui dépendent des conductances intrinsèques des neurones *pacemake*r ne sont pas essentielles dans la rythmogénèse de la respiration (Del Negro et al., 2002b).

1.4.2 Base ionique de la rythmogénèse

L'induction de bouffées rythmiques repose sur une séquence d'évènements qui reste similaire d'un système à l'autre, même si les types de courants ioniques impliqués peuvent être variés. Ainsi, pour induire des bouffées rythmiques, il faut premièrement, un courant entrant qui supporte un plateau dépolarisant. Deuxièmement, il faut un processus de repolarisation avec des courants sortants afin de permettre de terminer les bouffées. Finalement, il faut une force de rebond dépolarisante permettant de réactiver le processus pour en préserver la récurrence (voir figure 1-8).

1.4.2.1 Les courants dépolarisants

1.4.2.1.1 Les courants calciques

Les canaux calciques dépendants du voltage (CCDV) constituent une voie importante pour l'entrée de calcium dans les neurones. Dès lors, il n'est pas surprenant que ces canaux puissent supporter des vagues de dépolarisation à la base de bouffées rythmiques. Dans le contexte présent, deux grandes catégories de CCDV sont particulièrement importantes: les canaux à bas seuil d'activation (BSA) qui s'activent avec de petites dépolarisations. Et les canaux à haut seuil d'activation (HSA) qui s'activent lors de dépolarisations plus élevées (Weiss and Waard,

2006). Les canaux calciques à BSA sont retrouvés dans différents types de cellules, incluant les neurones. Ces canaux sont surtout composés de sous-unités de la famille des CaV3 et permettent le courant de type T (I_T). Ce dernier est responsable de la décharge en bouffée et des oscillations de basses fréquences dans le thalamus et le cervelet (Huguenard, 1996; Perez-Reyes, 2003). Au repos, les canaux calciques à BSA sont dans un état inactivé. Une hyperpolarisation membranaire est nécessaire afin de les dé-inactiver, et de les rendre activables par une faible dépolarisation. Leur activation cause une entrée massive de calcium à l'intérieur du neurone, provoquant une dépolarisation suffisamment importante pour activer un train de potentiel d'action dépendant des courants sodiques transitoires (I_{NaT}) (Aklesso et al. 2015). Le rôle de ces canaux dans les décharges en bouffées rythmiques des neurones du thalamus a été confirmé dans des expériences où les CaV3.2 et CaV3.3 ont été génétiquement éliminés « *Knock-out »*(Astori et al., 2011; Liao et al., 2011).

Les canaux calciques à HSA ont aussi été impliqués dans la décharge rythmique cellulaire. En effet, certains canaux de la famille des CaV1 sont connus pour leurs contributions au rythme électrique du tissu cardiaque atrial et des cellules chromaffines surrénales, ils pourraient aussi jouer un rôle dans la décharge rythmique de neurones dopaminergiques de la *substentia nigra* et de l'aire tegmentale ventrale (Liu et al., 2014; Putzier et al., 2009).

Le courant cationique rentrant non sélectif activé par le calcium (I_{CAN}) est activé par la mobilisation du calcium intracellulaire, et les canaux qui le supportent sont perméables aux ions potassiques, sodiques et un peu calciques (Launay et al., 2002; Ullrich et al., 2005). I_{CAN} sous-tend les longs plateaux dépolarisants (Bal and McCormick, 1993; Zhang et al., 1995) observés pendant la décharge en bouffées rythmiques de plusieurs types de cellules. L'implication de ce courant dans les bouffées a été confirmée dans des modélisations mathématiques (Rubin et al., 2009) et dans des préparations expérimentales notamment dans les neurones du noyau réticulé thalamique chez le cochon d'Inde (Bal and McCormick, 1993), les motoneurones des ganglions cardiaques du crabe (Ransdell et al., 2013), et certains neurones respiratoires du complexe pré-Bötzinger (Pace et al., 2007; Pena et al., 2004). Dans une étude récente, Chandler et ses associés ont montré que I_{CAN} semble aussi participer à l'enveloppe dépolarisante des bouffées rythmiques dans le NVsnpr (Tsuruyama et al., 2013).

Toutefois, les auteurs ont clairement montré que dans cette structure, il existe un courant sodique jouant un rôle similaire (voir ci-dessous).

1.4.2.1.2 Le courant sodique persistant

Ce courant est produit par une entrée d'ions sodium dans un neurone. Les indications de l'implication d'I_{NaP} dans la genèse de bouffées rythmiques viennent d'expériences d'enregistrement dans diverses zones telles que le complexe du pré-Bötzinger (Del Negro et al., 2002a; Del Negro et al., 2005), le NVmes (Wu et al., 2005; Wu et al., 2001), la moelle épinière (Tazerart et al., 2008), le cortex (Brumberg et al., 2000; Guatteo et al., 1996; Nishimura et al., 2001) et l'hippocampe (Jinno et al., 2003; Su et al., 2001). Dans toutes ces structures, le blocage d'I_{NaP} (avec la tétrodotoxine (TTX) ou le riluzole) empêche les décharges en bouffées rythmiques. Dans le NVsnpr, plusieurs recherches indiquent que ce courant serait responsable de l'enveloppe dépolarisante à la base des bouffées (Brocard et al., 2006; Sandler et al., 1998; Tsuruyama et al., 2013). De plus, il est intéressant de noter que ce courant fait son apparition autour de la deuxième semaine postnatale dans plusieurs régions du SNC (Alzheimer et al., 1993b; Huguenard et al., 1988). Ceci est tout à fait en adéquation avec les observations de Sandler (1998) et Brocard (2006) (voir plus haut) quant à l'apparition des décharges rythmiques dans le NVsnpr après la deuxième semaine postnatale, et l'émergence de la mastication qui se fait dans la même fenêtre temporelle (Westneat and Hall, 1992).

Plusieurs études ont cherché à caractériser I_{NaP}. À la différence des courants sodiques transitoires qui sont activés à des potentiels membranaires proches de -50 mV (Brown et al., 1994), les I_{NaP} s'activent à des potentiels entre -65 et -50 mV et atteignent leurs amplitude maximale entre -40 et -35 mV, selon la région du SNC (Brown et al., 1994; Colombo et al., 2013; Moraes et al., 2013; Tsuruyama et al., 2013). Dans une étude, Crill et ses collaborateurs indiquent qu'une partie d'I_{NaP} proviendrait d'une modification dans la cinétique d'ouverture de canaux sodiques transitoires (Alzheimer et al., 1993b). D'un autre côté, une étude sur les cellules de Purkinje semble indiquer que ce courant proviendrait de canaux sodiques complètement distincts (Vega-Saenz de Miera et al., 1997).

1.4.2.2 Les courants de terminaison de bouffées rythmiques

Dans la grande majorité des études, rapportant des décharges en bouffées récurrentes, la force hyperpolarisante qui met fin au plateau dépolarisant à la base des bouffées est médiée par des conductances potassiques sortantes. Ces conductances sont supportées par différents types de canaux potassiques qui, en s'ouvrant, permettent une sortie massive de potassium et induisent la terminaison des plateaux dépolarisants des bouffées (voir figure 1-8). Il est intéressant de noter que la diversité des canaux potassiques, avec leurs différentes caractéristiques et cinétiques d'activation, représente un moyen idéal pour moduler la durée des plateaux et la fréquence des bouffées rythmiques.

Dans le NVsnpr, Brocard et al. (2006) montrent bien l'importance des conductances potassiques. En effet, un bloqueur non spécifique des canaux potassiques (TEA) prolonge significativement les plateaux sous-jacents aux bouffées rythmiques (Brocard et al., 2006). Selon plusieurs études, les canaux potassiques impliqués dans la terminaison des bouffées rythmiques sont activés par une augmentation transitoire du calcium intracellulaire pendant les bouffées (Onimaru et al., 1997; Richter et al., 1993). Dans les neurones du NVsnpr, la chélation du calcium intracellulaire par l'addition de BAPTA dans les pipettes d'enregistrements prolonge la durée des plateaux des bouffées rythmiques. Ceci suggère que les canaux potassiques dépendants du calcium jouent un rôle dans la terminaison des bouffées rythmiques de ces neurones (Morquette et al., 2012; en Annexe). Il existe deux types de courants potassiques dépendants du calcium: les petits (SK-Ca) et les grands (BK-Ca). Dans le NVsnpr, l'utilisation de bloqueurs spécifiques aux deux types de courants, notamment la Charybdotoxine pour les BK-Ca, semble indiquer une contribution des BK-Ca dans la modulation de la durée des bouffées (Brocard et al., 2006). D'un autre côté, les canaux SK-Ca semblent être importants pour le système locomoteur, où ils seraient impliqués dans la terminaison des bouffées pendant la locomotion fictive (el Manira et al., 1994).

Dans le contexte des bouffées rythmiques supportées par I_{NAP}, la lente inactivation de ce courant peut également être impliquée dans le retour au potentiel de repos membranaire et dans la terminaison des bouffées. Ceci serait soutenu par l'activation des pompes Na^+/K^+ qui,

elles aussi, exercent une action hyperpolarisante (Ballerini et al., 1997; Darbon et al., 2003). Ces pompes seraient en fait activées par l'accumulation du sodium intracellulaire pendant les bouffées (Rubin et al., 2009). Dans le système respiratoire, d'autres mécanismes de repolarisation ont aussi été considérés dans la terminaison des bouffées: dans le complexe du pré-Bötzinger, des modèles computationnels (Smith et al., 2000) et des données expérimentales (Koizumi and Smith, 2008) suggèrent qu'un courant de fuite, principalement potassique, joue un rôle important, et est influencé par la substance P qui augmente la fréquence des bouffées rythmiques (Koizumi and Smith, 2008; Morquette et al., 2012).

1.4.2.3 Les courants de rebond

Plusieurs courants qui sous-tendent la dépolarisation, la forme et la durée des plateaux des bouffées de décharges neuronales ont été abordés. Afin d'assurer la récurrence des décharges rythmiques, il est cependant nécessaire d'avoir un courant qui permet de régénérer un prochain plateau dépolarisant, en partant de la phase d'hyperpolarisation qui termine la bouffée précédente. Le courant activé par l'hyperpolarisation (I_h) présente les caractéristiques lui permettant de jouer ce rôle: il est activé par l'hyperpolarisation à la suite du plateau d'une bouffée et il induit une rampe de dépolarisation qui conduit à la prochaine bouffée. Des chercheurs travaillant avec la salamandre ont utilisé le bloqueur spécifique de I_h, ZD 7288. En se fondant sur leurs résultats et sur d'autres études, ils sont arrivés à la conclusion que la diminution d'I_h pouvait affecter la décharge rythmique de façon significative, notamment en augmentant les périodes d'hyperpolarisation et en réduisant la fréquence de la décharge en bouffées rythmiques (Chevallier et al., 2006).

Dans le NVsnpr, les données expérimentales indiquent que les neurones expriment également le courant I_h (Brocard et al., 2006). Pour ces neurones, il pourrait représenter la force dépolarisante permettant de revenir dans la fenêtre d'activation d'$I_{NaP,}$ qui supporte la dépolarisation nécessaire aux bouffées. Il est important de noter que si dans le NVsnpr, le bloqueur ZD 7288 augmente la fréquence des bouffées rythmiques et diminue la longueur/amplitude des plateaux, il n'empêche pas les bouffées rythmiques (Brocard et al., 2006). Ainsi, dans le NVsnpr, ce courant aurait un rôle modulateur de la fréquence, sans être primordial pour le mode de décharge rythmique.

Figure 1-8: Courants ioniques supportant la décharge en bouffées répétitives

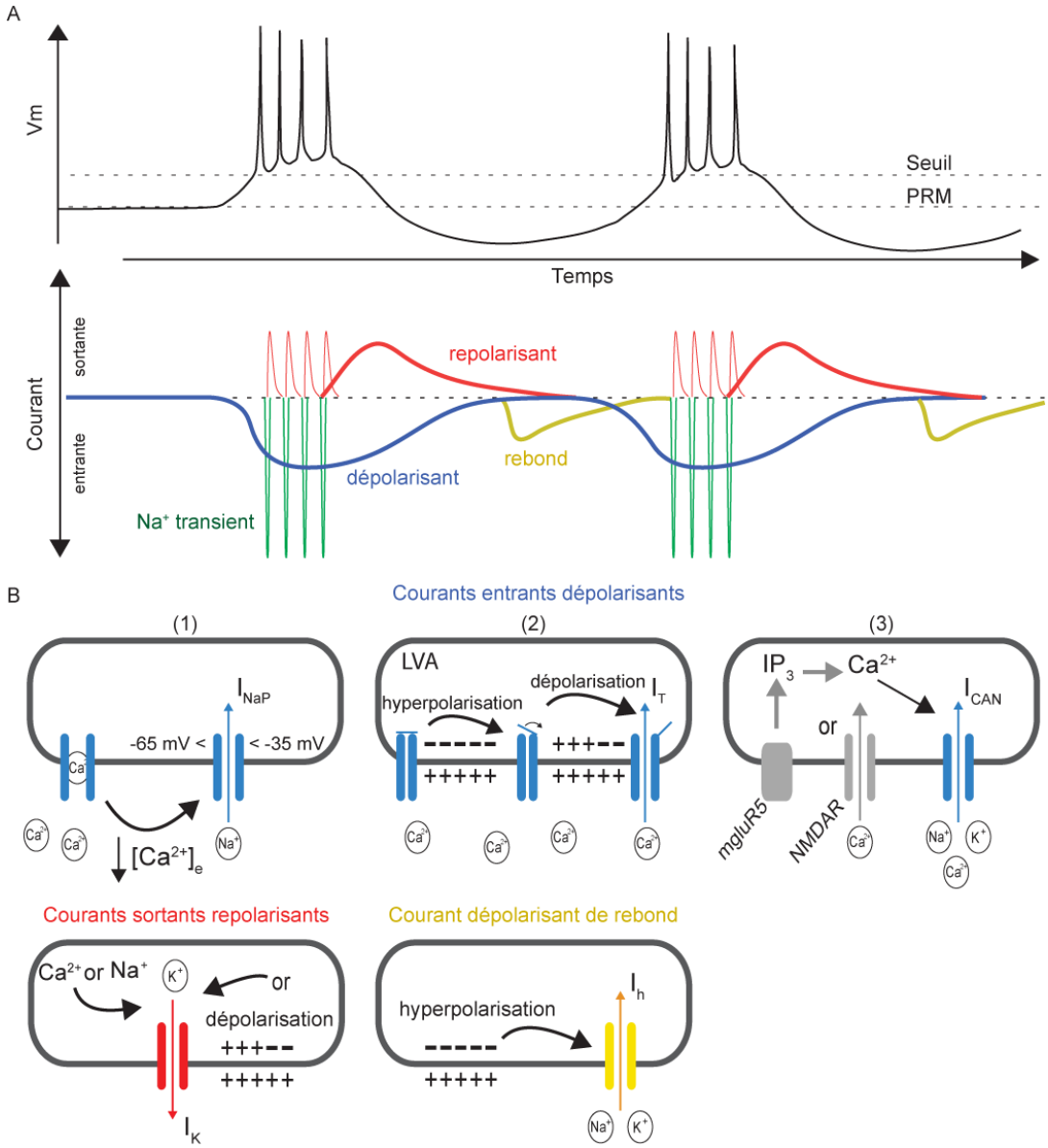

Courants ioniques supportant la décharge en bouffées répétitives. A. Représentation de deux bouffées (haut) et de la séquence d'activation des courants sous-jacents (bas). Les décharges en bouffées répétitives dépendent généralement de l'activation d'une conductance qui produit une dépolarisation soutenue ou plateau (bleu) qui amène le potentiel membranaire jusqu'au seuil d'activation des courants sodiques transitoires (vert) responsables de la génération des potentiels d'action. L'activation des canaux potassiques voltage-dépendants (rouge) repolarise la membrane après chaque potentiel d'action alors que les canaux potassiques activés par l'entrée de Ca^{2+} et de Na^+ pendant la dépolarisation et la décharge de potentiels d'action repolarisent lentement la membrane parfois au-delà du PRM. Cette hyperpolarisation membranaire active I_h permettant ainsi la régénération (jaune) du cycle en dépolarisant le potentiel membranaire jusqu'au seuil d'activation du courant responsable des plateaux dépolarisants. B. Haut: Illustration des différents canaux responsables des plateaux dépolarisants qui supportent la décharge en bouffées ainsi que leurs conditions d'activation. Bas: Illustration des canaux responsables de la repolarisation et de la terminaison des plateaux (rouge; gauche) ainsi que des canaux qui permettent la régénération du cycle par leur effet dépolarisant (jaune; droit). Adapté de Kadala et al., 2015 en Annexe.

1.4.3 Modulation de la décharge rythmique par les ions extracellulaires

Il ressort de la section précédente que les décharges rythmiques observées au niveau du NVsnpr semblent être supportées par I_{NaP} et I_{CAN}, pour la phase de dépolarisation sous-jacente aux plateaux, par les I_k, pour la phase de terminaison des bouffées (Brocard et al., 2006; Tsuruyama et al., 2013) et finalement, par un courant de type I_h pour la phase de rebond. L'amplitude de ces courants dépend des gradients de concentration de leurs ions respectifs. Il importe donc de considérer les fluctuations de concentration extracellulaire des différents ions en relation avec la rythmogénèse puisque cela aura un impact important sur les conductances identifiées.

En fait, plusieurs études, où les concentrations ioniques extracellulaires ont été mesurées dans le tissu, montrent qu'il y a des variations de ces concentrations pendant ou avant même l'apparition des décharges rythmiques (Amzica and Steriade, 2000, Amzica et al., 2002, Brocard et al., 2013; pour revue voir Kadala et al., 2015 en Annexe). Certaines de ces études semblent même indiquer une relation de cause à effet, entre la variation de la concentration extracellulaire de certains ions et le mode de décharge neuronale. Dans la section suivante, est proposé un survol rapide des principaux ions, dont la variation de concentration extracellulaire semble être associée à la décharge neuronale rythmique.

1.4.3.1 Sodium extracellulaire

Étant donné l'importance d'I_{NaP} dans la décharge rythmique de plusieurs types de neurones (voir section précédente), il parait évident qu'une variation de la concentration du Na^+, mais surtout qu'un changement du gradient de $[Na^+]_e$ vs $[Na^+]_i$, aura un effet significatif sur le mode de décharge de ces neurones. Une étude de Li et Hatton (Li and Hatton, 1996) montre, au niveau des neurones du noyau supraoptique, que la baisse de la $[Na^+]_e$ provoque une diminution ou un blocage complet des bouffées dans toutes les cellules testées.

1.4.3.2 Chlore extracellulaire

Dans les neurones Retzius de sangsue, Beck et ses collaborateurs ont montré qu'une réduction de la $[Cl^-]_e$ (≤1mM) induit une dépolarisation membranaire soutenue, et des décharges de bouffées récurrentes. Ces chercheurs indiquent que la baisse de la $[Cl^-]_e$ semble induire la décharge rythmique par le biais d'I_{NaP}, car la décharge en bouffées est bloquée par la saxitoxine (bloqueur de canaux sodiques), (Beck et al., 2001).

Dans les tranches d'hippocampe de rats, des bouffées rythmiques spontanées (Hochman et al., 1999) ou des bouffées induites par stimulation (Avoli et al., 1990) sont également observées quand la $[Cl^-]_e$ est diminuée. Ces décharges sont aussi accompagnées durant une période, d'oscillations synchrones de potentiel de champs. Cependant, une exposition prolongée à de faibles $[Cl^-]_e$ désynchronise la décharge des populations de neurones de la région du CA1. Ceci expliquerait sans doute l'effet antiépileptique du bloqueur du co-transporteur-Cl^- (furosémide) (Hochman and Schwartzkroin, 2000). Par ailleurs, il importe de noter qu'il a été montré que des bouffées rythmiques induites par la baisse de la $[Ca^{2+}]_e$, dans des tranches d'hippocampe, surviennent parallèlement à des baisses de la $[Cl^-]_e$ (Heinemann et al., 1992).

1.4.3.3 Potassium extracellulaire

Plusieurs études indiquent que les variations de la $[K^+]_e$ contribuent aux oscillations rythmiques. Entre autres, une étude de Bracci et al. (Bracci et al., 1998), a montré qu'une augmentation artificielle de la $[K^+]_e$, de 4.5mM à ~8mM, engendrait une activité rythmique locomotrice semblable à celle induite par le NMDA ou la sérotonine dans les circuits spinaux. Ils ont constaté que la fenêtre du seuil de concentration, nécessaire à l'induction du patron de décharge rythmique, était très précise (1 mM). Une fois ce seuil dépassé, la décharge rythmique repassait en mode tonique, pour ensuite finir en bloc de décharge. Une autre observation intéressante est l'effet facilitateur de la co-application, de $[K^+]_e$ infraliminaire (6 mM) avec le NMDA et la sérotonine, pour l'induction de patrons moteurs rythmiques. Des résultats similaires ont été démontrés par Jensen et Yaari (Jensen and Yaari, 1997) dans des tranches d'hippocampe de rats. Ces derniers ont rapporté l'apparition de décharges en bouffées périodiques se propageant de la région CA3 de l'hippocampe vers la région CA1,

quand les tranches étaient exposées à des $[K^+]_e$ élevés (7,5 mM) (Jensen and Yaari, 1997). Dans le contexte de la locomotion fictive, les expériences de Marchetti et al. (Marchetti et al., 2001) indiquent que le NMDA ou les stimulations électriques des racines dorsales provoquent une augmentation de la $[K^+]_e$ jusqu'à des valeurs de 6 et 8 mM; Cette étude n'indiquait pas si la $[K^+]_e$ augmentait avant ou après l'induction de l'activité locomotrice rythmique neuronale: cependant, une étude récente de Brocard et al. (2013), utilisant une technique similaire dans la moelle épinière de jeunes rats, a montré que la $[K^+]_e$ augmentait de 4mM à ~5mM avant le début de l'activité rythmique. La concentration de l'ion se stabilisait autour de 6mM au cours de la progression du rythme locomoteur. Ceci suggère qu'un changement initial de la $[K^+]_e$ pourrait aider à l'émergence de la décharge en bouffées rythmiques; l'augmentation plus tardive de l'ion pourrait être reliée, du moins en partie, à l'activité neuronale en cours (Kadala et al., 2015). Des résultats similaires, mettant en relation une augmentation de la $[K^+]_e$ et l'apparition d'activité rythmique neuronale, ont été rapportés dans la médulla ventrolatérale du chat en lien avec l'activité respiratoire centrale (Richter et al., 1978), dans la moelle épinière de lamproie en lien avec la nage fictive (Wallen et al., 1984) ainsi que dans le néocortex pendant les oscillations lentes du sommeil et les vagues d'activités épileptiques (Amzica and Steriade, 2000).

Il est probable que le potassium extracellulaire influence les bouffées rythmiques en agissant principalement sur les conductances impliquées dans la terminaison des bouffées (voir section 1.4.2.2). L'augmentation de la $[K^+]_e$, en changeant le gradient de l'ion, favorise la dépolarisation des neurones, ce qui peut contribuer à faciliter l'émergence des plateaux dépolarisants à la base des bouffées. Ce gradient aura tendance à retarder la réhyperpolarisation permettant la terminaison des bouffées. Une étude indique que l'augmentation de la $[K^+]_e$ pourrait également amplifier les courants sodiques persistants sensibles à la TTX, notamment dans les neurones pyramidaux du CA1 (Somjen and Muller, 2000). Cependant, un tel effet du $[K^+]_e$ n'a pas été corroboré par une modélisation avec des cellules Hb9 (Brocard et al., 2013). En effet, lors d'enregistrement en mode voltage-clamp de cellules Hb9, Brocard et ses collaborateurs ont mesuré I_{NaP} en relation à des variations de $[K^+]_e$. À la suite de rampes de voltage, les cellules Hb9 avaient un grand courant entrant associé à I_{NaP} car bloqué par le riluzole ou la TTX. Dans ces expériences, les augmentations de

la $[K^+]_e$, suffisantes à induire les bouffées rythmiques des cellules Hb9, n'avaient aucun effet sur l'amplitude et l'activation du I_{NaP} isolé (Brocard et al., 2013).

Finalement, une action de la $[K^+]_e$ sur l'augmentation des courants I_h a aussi été documentée par des chercheurs (Spain et al., 1987). Ce phénomène pourrait également expliquer une facilitation des bouffées rythmiques par l'élévation extracellulaire de cet ion.

1.4.3.4 Calcium extracellulaire

Tout comme le potassium, le calcium extracellulaire a des effets drastiques sur le mode de décharge de plusieurs régions du système nerveux: l'augmentation de la $[Ca^{2+}]_e$ favorise l'activation des CCDV à BSA et l'apparition éventuelle de décharge en bouffées (Formenti et al., 2001). Cependant, même si la décharge rythmique peut être induite par l'augmentation de la $[Ca^{2+}]_e$, ce mode de décharge est généralement associé à une baisse du $[Ca^{2+}]_e$. En effet, la baisse artificielle de la $[Ca^{2+}]_e$ a été associée aux bouffées rythmiques dans des préparations *in vitro* du noyau supraoptique (SON) du rat (Li and Hatton, 1996), de l'hippocampe (Su et al., 2001), des neurones respiratoires médullaires (Del Negro et al., 2002a; Johnson et al., 1994; Onimaru et al., 1995) et de la moelle épinière (Brocard et al., 2013). L'étude de Brocard (2006) a démontré le même phénomène dans la région dorsale du NVsnpr. Dans ces expériences, les tranches de tronc cérébral ont été perfusées d'un fluide cérébro-spinal artificiel (ACSF) sans calcium ajouté. Lors d'enregistrement unitaire, ceci a augmenté fortement la proportion de neurones déchargeant spontanément en bouffées rythmiques (Brocard et al., 2006). Ces données ont été corroborées par l'étude du groupe de Chandler (Tsuruyama et al., 2013). Brocard et al. (2006) ont postulé que ce mécanisme de bouffées rythmiques, décrit dans un circuit impliqué dans la mastication, pouvait être similaire pour d'autres GPCs de mouvements rythmiques (Brocard et al., 2006).

Dans un contexte plus physiologique, il est intéressant de noter que la simulation de l'activité synaptique (par la stimulation électrique ou par le NMDA) peut induire des baisses de la $[Ca^{2+}]_e$, et ces baisses précèdent l'arrivée des bouffées rythmiques (Brocard et al., 2013). De telles baisses naturelles de la $[Ca^{2+}]_e$ ont été rapportées dans des expériences *in vivo*, au niveau du néocortex lors de crises épileptiques (Heinemann et al., 1977).

Le lien entre la baisse de la $[Ca^{2+}]_e$ et l'apparition des bouffées rythmiques semble être le courant sodique persistant: l'étude de Brocard citée plus haut, montre dans le NVsnpr que les bloqueurs d'I_{NaP} (Riluzole et TTX) arrêtent la décharge rythmique induite par la perfusion du ACSF sans calcium. En fait, la déplétion de la $[Ca^{2+}]_e$ déplace l'activation d'I_{NaP} vers des potentiels plus hyperpolarisés et augmente l'amplitude d'I_{NaP} (Li and Hatton, 1996; Tazerart et al., 2008). Selon des modèles computationnels, même un petit changement du seuil d'activation d'I_{NaP} serait suffisant au passage d'une décharge tonique à une décharge en bouffées rythmiques (Brocard et al., 2013). Les travaux d'Armstrong (1999), dans l'axone géant de calmar, suggèrent que la présence du calcium extracellulaire favoriserait la fermeture des canaux sodiques en occupant les pores des canaux (Armstrong, 1999).

1.4.3.5 L'effet synergique des ions dans l'induction de bouffées rythmiques

Comme expliqué plus haut, bien que la variation sélective de la concentration de différents ions puisse avoir certains effets sur la décharge rythmique neuronale, des variations simultanées de ces ions pourraient agir de façon synergique afin de promouvoir la décharge rythmique neuronale (Kadala et al., 2015), et ce, par leur action concertée sur les différentes conductances rythmogéniques. Les travaux de Brocard (2013), démontrent l'existence d'un tel effet synergique entre la baisse de la $[Ca^{2+}]_e$ et l'augmentation du $[K^+]_e$ pour l'induction de la décharge rythmique dans le GPC de la locomotion (figure 1-9). Les auteurs rapportent que la concentration extracellulaire des deux ions commence à changer avant même qu'une activité rythmique ne soit détectée dans les racines motrices. Ainsi, les changements de concentration des ions ne seraient pas uniquement le résultat de l'activité neuronale, mais en partie la cause de la décharge rythmique. En réduisant la $[Ca^{2+}]_e$ à 0.9 mM et augmentant $[K^+]_e$ à 6 mM , pour les deux de façon artificielle, les auteurs ont confirmé l'effet de cette synergie, car cette manipulation a induit des bouffées rythmiques dans 25% des neurones enregistrés (Brocard et al., 2013). De la même façon, il a été montré que des variations d'un ion peuvent antagoniser l'effet rythmogène associé à la variation d'un autre ion: dans le pré-Bötzinger, le rythme généré, dans un ACSF ayant 3 mM K^+ et 1 mM de Ca^{2+}, est contrecarré par une faible augmentation du Ca^{2+} et est immédiatement restauré si le potassium est aussi augmenté (Panaitescu et al., 2009).

Figure 1-9: Interactions synergétiques des concentrations extracellulaires des ions

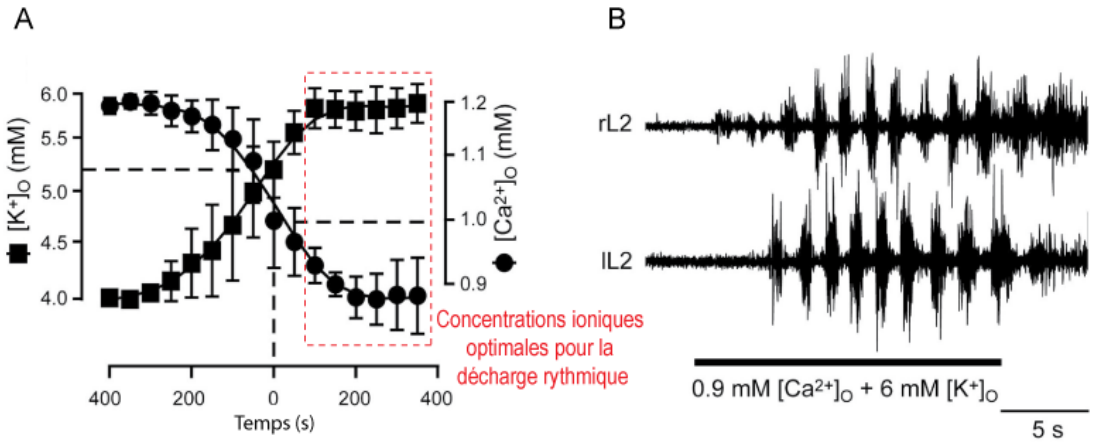

Démonstration des interactions synergétiques des concentrations extracellulaires des ions calciques et potassiques dans la rythmogenèse. A. Évolution des concentrations extracellulaires de calcium (cercles) et de potassium (carrés) avant et après l'émergence d'un épisode rythmique locomoteur. Rectangle rouge: Concentrations optimales de calcium et de potassium favorables à une activité en bouffées. Une activité rythmique apparaît autour d'une concentration de calcium de 0,9 mM et d'une concentration de potassium de 6 mM. B. Enregistrements extracellulaires dans les segments droits et gauches (dL2, gL2) de la moelle épinière du rat pendant l'application d'un médium dont la concentration extracellulaire de calcium est 0,9 mM et la concentration extracellulaire de potassium est 6 mM. Modifié de Brocard et al., 2013.

Il est indéniable que l'homéostasie des ions extracellulaires a un impact important sur la décharge neuronale. Et dans cette optique, la question qui demeure est de savoir quels mécanismes pourraient être impliqués dans la modulation de ces ions. Brocard et ses collaborateurs proposent que l'augmentation du $[K^+]_e$ reflèterait l'équilibre entre d'une part, la sortie de potassium des neurones durant leurs activités, et d'autre part, la clairance de cet ion de l'espace extracellulaire par les pompes Na^+/K^+ (Sykova, 1987) et par les cellules gliales (Jendelova and Sykova, 1991). La baisse du calcium, quant à elle, serait due principalement à une recapture de cet ion par les somas postsynaptiques et/ou les dendrites (Heinemann and Pumain, 1981). Dans le même ordre d'idée, une étude de Lian et Stringer suggère l'implication de la glie dans l'homéostasie du potassium et du calcium extracellulaire dans le cortex (Lian and Stringer, 2004). L'implication des cellules gliales dans le tamponnage et l'homéostasie du potassium extracellulaire est un phénomène bien connu et étudié par plusieurs chercheurs (voir section 1.5.3.4.3). D'un autre côté, une telle implication de la glie par rapport au calcium n'a pas été documentée. Pour s'intéresser à cette problématique, il est important de réaliser qu'il existe différents types de glies, et qu'elles n'exercent pas le même rôle dans le SNC.

1.5 Les cellules gliales

Les cellules gliales constituent la majorité des cellules du système nerveux, mais de par leur nature électriquement passive, leur rôle actif dans la modulation de l'activité synaptique neuronale a longuement été ignoré. Ceci découle de la doctrine neuronale proposée par Ramón y Cajal à la fin du 19e siècle, et prévalente encore aujourd'hui, qui avance que tout le processus d'encodage du cerveau repose sur l'activité électrique et donc sur les neurones. Cependant, grâce aux nouvelles études qui s'intéressent aux rôles des cellules gliales dans le système nerveux, cette vision « neurocentrique » est de plus en plus remise en question.

Il importe, avant d'aborder le rôle que peut jouer la glie dans l'encodage neuronal, de réaliser que le terme de cellules gliales regroupe un large éventail de cellules avec des morphologies anatomiques variées, mais surtout des fonctions complètement différentes. Il est intéressant de rapporter comment historiquement le concept de la glie est né et a évolué avant de définir les différents types cellulaires et de passer en revue leurs rôles et fonctions. Nous conclurons cette section par un résumé plus approfondi d'un type de cellules gliales particulier, les astrocytes, qui semblent être les plus susceptibles d'influencer directement l'encodage neuronal. Nous verrons que ces cellules pourraient être notamment impliquées dans l'induction de la décharge rythmique des neurones du NVsnpr.

1.5.1 Historique et évolution du concept de la glie

Dans une revue datant de 1988 Somjen, présente un historique du terme « glial». Ainsi, Rudolf Virchow (1856) est souvent crédité pour la découverte des cellules gliales. Toutefois, ce que Virchow décrivait ne correspond pas exactement à ce que nous considérons de nos jours comme étant les cellules gliales. Virchow essayait de démontrer qu'il y avait bel et bien du tissu conjonctif dans le cerveau. Étant pathologiste de formation, Virchow associait l'inflammation au tissu conjonctif et était donc persuadé de l'existence de ce genre de tissus à différents niveaux du cerveau, du moins au niveau des ventricules. Dans un tel état d'esprit, avec ses recherches il a cru trouver ce qu'il considérait comme étant ce tissu conjonctif: il a trouvé un tissu qui infiltrait le cerveau, séparant le tissu nerveux des vaisseaux sanguins, et remplissant les interstices entre les cellules nerveuses et leurs prolongements. Virchow écrit

alors: « Cette substance conjonctive forme dans le cerveau, la moelle épinière, et dans les nerfs sensoriels supérieurs une sorte de mastique[1] (neuroglie)» ([1]suivant la traduction de *Kitt* (allemand) proposé par Somjen en anglais *putty*. L'auteur note que malgré son choix de *putty*, plusieurs l'on traduit par *glue*; Virchow, 1858, Somjen, 1988) .

Le terme neuroglie a été choisi à cause des caractéristiques de cette substance qui semblaient spécifiques par rapport au tissu conjonctif retrouvé dans les autres organes. Par la suite, le nom est resté même si le concept qui lui était associé a depuis grandement changé.

Grâce à l'amélioration des techniques de microscopie, plusieurs chercheurs dont, Deiters (1865), Golgi (1885), Ramon y Cajal (1913), Del rio-Hortega (1920), ont fait une caractérisation plus complète des différents sous-types de cellules gliales révélant la diversité morphologique des cellules qui étaient regroupées sous le terme de cellules gliales (Deiters, 1865; del Río-Hortega, 1920; Golgi, 1885; Ramón y Cajal, 1913). Se fondant sur les données morphologiques et anatomiques et l'origine développementale des cellules, une nomenclature s'est développée afin de classifier diffèrent sous-types de glies (Somjen, 1988). Ensuite, grâce aux améliorations des techniques d'électrophysiologie, à l'avènement de la biologie moléculaire et de la génétique; et finalement le développement des techniques d'imagerie, la nomenclature s'est raffinée notamment en tenant compte des différents rôles physiologiques joués par ces cellules.

1.5.2 Les différents sous-types de cellules gliales

Les cellules gliales sont généralement classées en deux grandes familles: les microglies et les macroglies. Dans les macroglies on retrouve les oligodendrocytes, les cellules $NG2^{+}$ et les astrocytes. La prochaine section fera une description sommaire des principaux types de cellules gliales ainsi que les fonctions qui leur sont associées. Cette revue ne se veut pas exhaustive, mais permettra d'introduire les astrocytes qui constituent la plus grande proportion des cellules gliales, et ce sont les astrocytes qui nous intéresseront particulièrement dans le contexte des travaux de cette thèse.

1.5.2.1 La microglie

Les microglies sont souvent considérées comme les cellules immunitaires du cerveau, même si dans les faits leur fonction est beaucoup plus diversifiée. La microglie constitue de 5 à 20% de la population des cellules gliales du SNC (Streit, 2005). Il est intéressant de noter que la microglie tire son origine du mésoderme, alors que tous les autres types de cellules du cerveau, les autres types de glies et aussi les neurones, tirent leurs origines de l'ectoderme (pour revue voir Ginhoux et al., 2013). Del Rio-Hortega (1932) est le premier à avoir fait une recherche systématique sur la microglie et ses observations cytologiques restent pertinentes encore aujourd'hui. Dans le cerveau adulte les microglies sont retrouvées sous au moins trois formes différentes clairement identifiables: 1) la microglie phagocytaire correspondant aux cellules sphériques considérées comme les macrophages du cerveau; 2) les microglies au repos sous forme de cellule ramifiée; et 3) les microglies réactives, retrouvées dans différentes pathologies, mais qui ne sont pas des cellules phagocytaires (Morioka et al., 1992; Streit et al., 1988). La microglie est distribuée de façon ubiquitaire dans le cerveau normal (Lawson et al., 1990). Elle est généralement considérée comme formant le système immunitaire du cerveau et joue un rôle important dans le processus inflammatoire du SNC (pour revue voir Streit et al., 1988 et Graeber, 2010). Toutefois depuis quelques années de plus en plus d'études, se fondant principalement sur les travaux de Stevens et ses collaborateurs, démontrent un rôle important de la microglie dans l'élimination synaptique (Schafer et al., 2012; Stevens et al., 2007), processus important pour le sculptage des interconnexions entre les neurones. Ces études semblent même suggérer un rôle de la microglie dans la modulation synaptique notamment avec le concept de la synapse « *quad-partite* » (Schafer et al., 2013).

1.5.2.2 Les macroglies

L'autre groupe majeur de cellules gliales du système nerveux correspond aux macroglies. Dans le SNC cette catégorie est principalement constituée par les oligodendrocytes, les astrocytes -qui ont différents noms en fonction des régions du SNC- et les cellules $NG2^{+}$ (Halassa et al., 2007a). Ces différents types de cellules sont classifiés en fonction de leur morphologie, des contacts formés par leur prolongement cellulaire (Reichenbach, 1989), de leurs caractéristiques électrophysiologiques et de leur rôle physiologique dans le SNC.

1.5.2.2.1 Les oligodendrocytes

Les oligodendrocytes sont les cellules qui forment la gaine de myéline qui isole les axones des neurones et permettent la conduction saltatoire des potentiels d'action. Rio-Hortega (1928) est reconnu comme étant le premier à avoir montré que les oligodendrocytes ont des prolongements cellulaires. Ce dernier a alors classifié les oligodendrocytes en quatre sous types, en fonction du nombre de leurs prolongements et de la grosseur des fibres nerveuses qu'ils contactaient. Cependant, ce n'est qu'avec l'arrivée de la microscopie électronique que la relation cellulaire entre les oligodendrocytes et la gaine de myéline a pu être démontrée (Bunge, 1968; Hirano, 1968; Peters, 1964). Contrairement aux oligodendrocytes du SNC, dans le système nerveux périphérique (SNP) les cellules qui remplissent le même rôle, nommées cellules de Schwann myélinisantes, sont capables de myéliniser l'axone d'un seul neurone à la fois. Il existe aussi des cellules de Schwann non myélinisantes qui peuvent enveloppées un faisceau d'axones, ainsi que des cellules non myélinisantes présente à la jonction neuromusculaire nommées cellules de Schwann périsynaptiques (Ko and Robitaille, 2015; Mirsky et al., 2008).

1.5.2.2.2 Les cellules $NG2^+$

Les cellules $NG2^+$ expriment le protéoglycane de sulfate de chondroïtine NG2. Il s'agit de cellules progénitrices multi-potentes pouvant apparemment se différencier en oligodendrocytes, et en astrocytes (voir les revues de Butt et al., 2005 et Wigley et al., 2007). Les cellules $NG2^+$ expriment des récepteurs AMPA, et sont capables de générer une activité calcique. Ces cellules possèdent des canaux potassiques sensibles au voltage et ainsi ne sont pas passives du point de vue électrophysiologique; des études rapportent même la présence de potentiels d'actions dans des sous-populations de $NG2^+$ dans le cervelet (Karadottir et al., 2008) et dans le cortex visuel (Ge et al., 2009). Il est intéressant de préciser que ces cellules ont pendant longtemps été considérées comme un étant un sous-type d'astrocytes : les astrocytes GluR (voir la section 5.2.2.3.2 et la figure 9)

1.5.2.2.3 Les astrocytes

1.5.2.2.3.1 Marquages et structure morphologique des astrocytes

Les astrocytes tirent leur nom de leur aspect étoilé. Différents types de marquage ont été utilisés afin d'identifier de façon plus ou moins spécifique les astrocytes. L'un des marqueurs souvent utilisés est la GFAP (*glial fibrillary acid protein*). Chez le rat cette protéine est exprimée dans les astrocytes matures et joue un rôle important pour leur cytosquelette (Dahl, 1981). Toutefois, les prolongements les plus fins des astrocytes ne sont pas révélés par le marquage immunohistochimique de la GFAP. En fait l'immunomarquage par la GFAP ne révèlerait au mieux que 15% du volume total des astrocytes chez le rongeur (Oberheim et al., 2012). Des techniques plus modernes utilisent le génie génétique afin de marquer les astrocytes. Le gène de la GFAP est utilisé comme rapporteur pour exprimer des fluorophores qui révèlent alors une structure plus complète des astrocytes (Nolte et al., 2001; Zhuo et al., 1997). Une étude du groupe de Hirase indique que lors d'enregistrements intracellulaires dans le cortex cérébral et dans l'hippocampe de rats adultes, entre 70% et 80% des astrocytes étaient positifs au marquage à la GFAP, indiquant qu'une faible proportion d'astrocytes expriment peu ou pas la GFAP (Mishima and Hirase, 2010). Un autre marqueur souvent utilisé afin d'identifier les astrocytes est la protéine S100β, une protéine chélatrice de calcium principalement exprimée par les astrocytes (Van Eldik et al., 1984, Zimmer et al., 1995, Sen and Belli, 2007; voir encadré 1). Nous verrons par la suite que cette protéine S100β, pouvant être relâchée dans l'espace extracellulaire par les astrocytes, aura un rôle important dans le mécanisme de rythmogénèse que nous avons étudié.

Encadré 1 : La protéine S100β

I- Les caractéristiques de la S100β

En 1965, Moore a isolé une substance du cerveau de bovins (Moore, 1965) qui fut appelée S100 à cause de sa solubilité dans du sulfate d'ammonium saturé à 100%. Cette protéine constitue jusqu'à 0.2% du volume total des protéines solubles du cerveau et est retrouvée dans le cytosol des cellules gliales (Moore, 1965; Tabuchi et al., 1983). Par la suite, d'autres études ont démontré que la substance en question correspondait à deux polypeptides S100A1 et S100β ayant des poids moléculaires d'environs 10 kDa formant des motifs structuraux de type main EF (EF Hand) pouvant lier le Ca^{2+} (Zimmer et al., 1995). De façon générale la protéine S100β est retrouvée sous forme d'homodimères maintenus ensemble par des liaisons non covalentes (Isobe and Okuyama, 1978, 1981). Même si la protéine S100β est principalement retrouvée dans les astrocytes, des données indiquent qu'elle pourrait être exprimée dans certaines sous-populations de neurones (Ichikawa et al., 1997; Rambotti et al., 1989; Rickmann and Wolff, 1995; Yang et al., 1995a; Yang et al., 1996; Yang et al., 1995b).

Comme mentionné plus tôt, une caractéristique bien connue de la protéine S100β est sa capacité à attacher le calcium. La protéine S100β (sous la forme dimérisée) est caractérisée par deux sites de liaison au Ca^{2+} de relativement haute affinité (KD = 20 – 50 μM) et 2 sites de liaison de plus faible affinité (KD = 200 – 500 μM). Le potassium aurait tendance à diminuer l'affinité de la protéine pour le calcium, mais le zinc aurait un effet inverse sur la protéine et inhiberait aussi l'effet du potassium (Baudier et al., 1985; Markowitz et al., 2005).

II- Les rôles connus de la protéine S100β

La S100β fait partie de la superfamille des protéines S100/calmoduline/troponine C qui régulent l'activité, de façon calcium dépendante, de différentes plusieurs protéines cibles. Cette protéine jouerait notamment un rôle dans la phosphorylation de protéines. Parmi les protéines cibles de la S100β, on retrouve entre autres des protéines comme la p53, la hdm2, la hdm4, la Rsk1 et la RAGE. Ces différentes cibles illustrent bien pourquoi il est difficile de définir un rôle précis pour la protéine S100β puisque cette dernière modulerait différentes protéines impliquées dans des phénomènes divers, qui semblent même parfois être contradictoires (voir tableau I; Kira G. Hartman et al., 2013) .

Tableau I

Activité cellulaire	Protéine modulée par la S100β
Homéostasie du calcium intracellulaire	AHNAK
Régulation du cytosquelette	Caldesmon/ Calponin / CapZα GFAP/ IQGAP1 / MARCKS Src kinase / τ-protein / Tubulin
Régulation du cycle cellulaire	Hdm2 / Hdm4 / NDR
Métabolisme énergétique	Fructose 1,6 diphosphate / aldolase Phosphoglucomutase
Croissance et survie	p53

Tableau résumant différentes fonctions cellulaires qui impliquent la protéine S100β. Modifié de (Kira G. Hartman et al., 2013)

Ainsi, les réponses cellulaires induites par la S100β changeraient en fonction de plusieurs conditions incluant la concentration, le type cellulaire, et la localisation dans le système (Donato, 2001; Harpio and Einarsson, 2004).

Croissance et mort cellulaire. La présence extracellulaire de la S100β à de faibles concentrations semble promouvoir la croissance neuronale, alors que les concentrations extracellulaires élevées semblent être toxiques et induire l'apoptose neuronale (Castets et al., 1997; Harpio and Einarsson, 2004). L'addition de S100β extracellulaire aux cultures primaires de neurones corticaux promeut l'extension de neurites (Kligman and Marshak, 1985). Dans la même ligne d'idée, la S100β agit comme agent mitogène et stimule la prolifération des cellules gliales (Selinfreund et al., 1991). Il semblerait que l'effet mitogénique et neurotrophique de la S100β dépend de la forme dimérisée de la protéine (Selinfreund et al., 1991; Winningham-Major et al., 1989).

La S100β a aussi été associée à des effets qui semblent être complètement contradictoires avec ceux décrits plus tôt.
Dans un modèle de lignée cellulaire PC12, des augmentations de la $[Ca^{2+}]_i$ induit par la S100β sont associées à l'apoptose (Fano et al., 1993; Mariggio et al., 1994).

Modulation de l'activité neuronale. Il a été montré que l'application de la S100β dans les concentrations de l'ordre du pico/nano g/ml aurait un effet modulateur sur des courants potassiques, suggérant un rôle de cette protéine en tant que neuromodulateur dans les fonctions nerveuses. Entre autres, la protéine hyperpolarisait le potentiel de repos membranaire induisant en parallèle une inhibition de la décharge spontanée (Kubista et al., 1999). Dans une autre étude, la protéine S100β a été impliquée dans la modulation de la plasticité synaptique à long terme. Les souris mutantes n'exprimant pas la S100β avaient des potentialisations à long terme augmentées dans la région CA1 de l'hippocampe. Ces potentialisations étaient aussi accompagnées d'une augmentation de la mémoire spatiale dans Le labyrinthe de Morris. Encore une fois, ces résultats suggèrent que la protéine gliale S100β module l'activité et la plasticité neuronale (Nishiyama et al., 2002). Finalement, le groupe de Hirase a montré que l'application locale de la S100β augmente les oscillations gamma *in vivo*, dans les souris mutantes n'exprimant pas la protéine S100β. De plus, l'application locale de l'anticorps anti-S100β dans les souris normales atténuait les oscillations gamma. Ces résultats indiquent que la présence extracellulaire de la S100β influence l'activité neuronale (Sakatani et al., 2008).

Cela dit, avant de nous intéresser au rôle de la S100β dans notre système il est important de finir notre revue des caractéristiques des astrocytes. Nous disions donc que la S100β est fréquemment utilisée comme marqueur astrocytaire.

La sulforhodamine-101 (SR-101) est aussi souvent utilisée pour marquer les astrocytes. Son avantage est qu'elle peut être appliquée en extracellulaire dans certaines conditions et être retrouvée spécifiquement dans les astrocytes. Toutefois, les raisons de l'absorption spécifique par les astrocytes de ce marqueur demeurent inconnues (Kafitz et al., 2008; Nimmerjahn et al., 2004).

Les astrocytes ont un soma dont le diamètre fait de 7 à 9 µm d'où irradient environ quatre prolongements principaux, leurs donnant une apparence étoilée d'où ils tirent leur nom. Toutefois, la dense ramification partant des prolongements principaux confère à ces cellules un aspect spongieux (Bushong et al., 2002, Bushong et al., 2004 ; voir figure 1-10). L'ensemble formé du corps cellulaire et des prolongements qui en émergent correspond au « domaine » d'un astrocyte. De façon générale, chaque astrocyte occupe son propre domaine avec un minimum de chevauchement entre astrocytes adjacents (Bushong et al., 2002, Ogata and Kosaka, 2002, Halassa et al., 2007b; voir figure 1-10). Dans le cortex de rongeurs, le volume du domaine d'un astrocyte serait d'environ 22 000 μm^3, alors que dans l'hippocampe le volume irait jusqu'a à 66 000 μm^3. En se basant sur la densité des synapses Oberheim et coll. (2009) calculent que le domaine d'un astrocyte pourrait couvrir 20 000 à 120 000 synapses selon les régions (Oberheim et al., 2009). Le domaine astrocytaire n'est cependant pas une unité fonctionnelle uniforme. En effet, lorsqu'observé en microscopie électronique, le domaine astrocytaire révèle une nature compartimentalisée en microdomaine (Grosche et al., 1999). Par exemple, on retrouve des renflements au niveau des processus des astrocytes. Ces structures, considérées comme étant des compartiments astrocytaires, sont en étroite apposition avec les épines dendritiques : l'élément postsynaptique glutamatergique dans les neurones pyramidaux du CA1 (Panatier et al., 2011).

Figure 1-10: Morphologie et aspect spongieux d'astrocytes matures

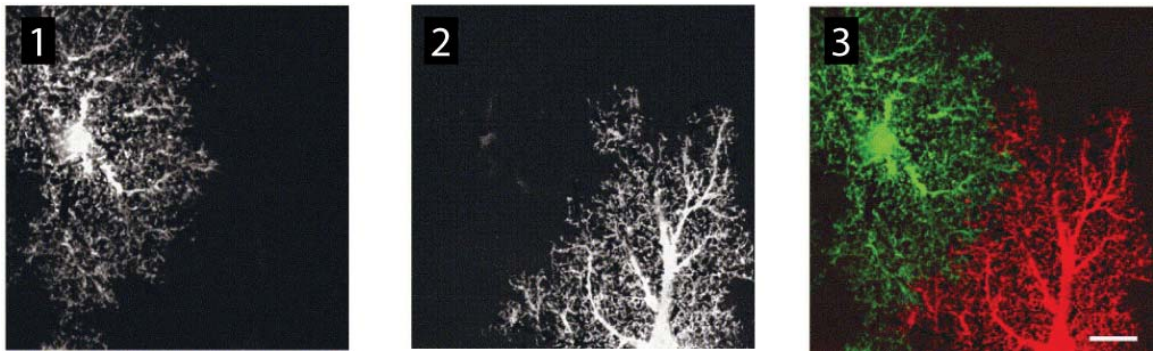

Morphologie et aspect spongieux d'astrocytes matures (1-3). La région d'interface entre les astrocytes (1) et (2) marqués respectivement par le Lucifer Yellow (vert) et l'Alexa 568 (rouge) dans l'image (3), démontre peu de superposition mis à part pour les plus fins prolongements. Ceci illustre bien le concept de domaine astrocytaire. Ces images correspondent à une projection de tranches optique sur 1 µm. Barre d'échelle : 10 µm. Modifié de Bushong et al., 2004.

1.5.2.2.3.2 Hétérogénéité des astrocytes

Le mot « astrocyte » a été utilisé pour la première fois par Michael von Lenhossek en 1893 pour décrire le grand nombre de cellules à forme étoilée observé dans les préparations histologiques de cerveau (Kettenmann and Ransom, 2005). Toutefois, une certaine hétérogénéité a été observée assez tôt dans les populations de cellules à forme étoilée. Ainsi déjà au cours de la même année, Andrienzen faisait la distinction entre les astrocytes, fibreux, de la matière blanche et ceux, dit protoplasmiques, dans la matière grise (Andriezen, 1893). Une telle classification est encore utilisée par plusieurs (Bushong et al., 2002; Oberheim et al., 2009; Szoke et al., 2006; Theodosis et al., 2008), même si de nombreuses études suggèrent une hétérogénéité des astrocytes beaucoup plus grande dans les différentes régions du SNC. À titre d'exemple, Takata et Hirase rapportent que les astrocytes localisés dans différentes couches corticales ont des activités avec des dynamiques différentes (Takata and Hirase, 2008); alors que dans l'hippocampe, les travaux de Zhou et Kimelberg (2001) et Matthias et al (2003) suggèrent la coexistence de sous-types d'astrocytes (Matthias et al., 2003; Zhou and Kimelberg, 2001). Ces études ont différencié les astrocytes en fonction de leurs propriétés électrophysiologiques et de l'expression différentielle de protéines membranaires. Il en est découlé une terminologie distinguant les astrocytes GluT (exprimant les transporteurs du glutamate GLAST et GLT-1) et GLuR (exprimant le récepteur ionotropique AMPA du glutamate). La signature électrophysiologique des astrocytes GluT est une relation courant-voltage parfaitement linéaire (figure 1-11) avec évidemment l'absence de potentiel d'action. Les astrocytes GluR sont caractérisés par des courbes I-V non linéaires résultant de la présence de forts courants sortants (figure 1-11). La résistance d'entrée des astrocytes GluR est beaucoup plus grande que celle des astrocytes GluT (figure 1-11), et les premiers ont tendance à avoir des valeurs de potentiel membranaire au repos moins hyperpolarisé que les deuxièmes; cette dernière observation est toutefois controversée (voir les études de Wallraff et al., 2004, Adermark and Lovinger, 2008) . Une autre distinction importante entre les astrocytes GluR et GluT est le niveau de couplage permettant la formation de syncytium; les premiers ne forment pas de syncytium ou en forment de très petits par rapport aux deuxièmes qui forment des syncytia significativement plus grands (Schools et al., 2006; Serrano et al., 2008). Selon une étude de Wallraff, ceci pourrait s'expliquer en partie par le fait que les astrocytes à rectification (GluR) n'expriment pas la connexine 43 (Cx43), constituante

principale des jonctions gap entre les astrocytes (Wallraff et al., 2004). Dans les faits, des analyses d'immunohistochimie indiquent que les cellules passives (GluT) expriment la GFAP alors que les cellules (GLuR) sont NG2 positives. (Grass et al., 2004; Matthias et al., 2003; Schools et al., 2003). Ainsi plusieurs considèrent que les astrocytes (GluT) passifs correspondent aux vrais astrocytes alors que les cellules GluR correspondent au $NG2^{+}$ (Nishiyama et al., 2005, Mishima and Hirase, 2010; voir section 1.5.2.2.2) .

L'ancienne définition des astrocytes basée sur l'apparence étoilée de ces cellules incluait plusieurs sous-types de cellules dans la catégorie d'astrocytes. Toutefois, selon la plus récente vision, le terme d'astrocytes s'applique uniquement aux cellules électriquement passives capables de former des syncytia en plus de : 1) tamponner le potassium extracellulaire et le glutamate; 2) exprimer la GFAP, 3) contacter les vaisseaux sanguins et les synapses des neurones (Fiacco et al., 2009). Aussi, dans les travaux présentés dans cette thèse nous référons à ce type cellulaire passif lorsque nous parlerons d'astrocytes.

Figure 1-11: Distinctions entre les astrocytes GluT et GluR

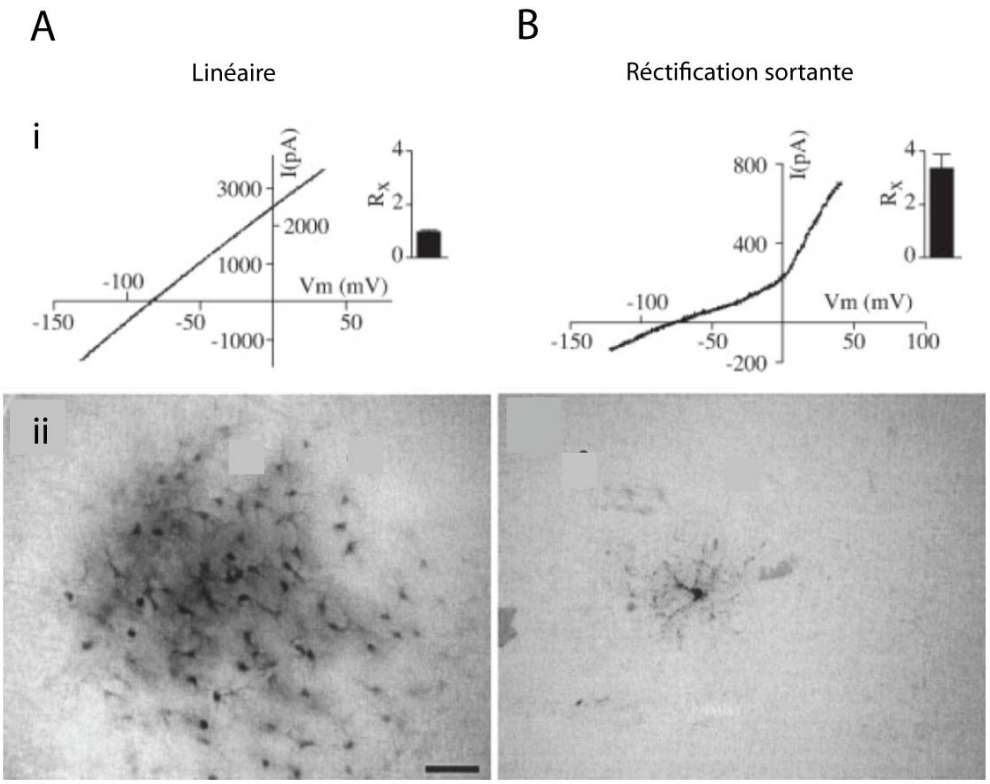

Distinctions entre les astrocytes GluT (qui correspondent à la définition moderne des astrocytes) (A) et les astrocytes GluR (B). Ces distinctions se reflètent dans la relation courant-voltage et la résistance membranaire (i) et sur l'intensité du couplage interastrocytaire (ii) (Adapté de Serrano et al.2008 et wallraff et al 2004).

1.5.2.2.3.3 Différentes fonctions des astrocytes

Les astrocytes occupent plusieurs fonctions au sein du SNC. Ils sont notamment importants pour le maintien de la barrière hématoencéphalique, le contrôle du flux sanguin, et l'approvisionnement en nutriments et le métabolisme énergétique du SNC (Belanger et al., 2011; Iadecola and Nedergaard, 2007; Mulligan and MacVicar, 2004; Pellerin and Magistretti, 1994; Simard et al., 2003; Zonta et al., 2003).

Les astrocytes sont aussi impliqués dans l'homéostasie du milieu extracellulaire du SNC avec un rôle dans la recapture de neurotransmetteurs et le contrôle de la concentration d'ions extracellulaires comme le K^+ (Araque et al., 1999; Danbolt, 2001; Kadala et al., 2015; Lian and Stringer, 2004; Mennerick and Zorumski, 1994; Newman and Reichenbach, 1996; Orkand et al., 1966; Szoke et al., 2006).

Dans un contexte plus pathologique, les astrocytes occupent une fonction dans le système immunitaire et inflammatoire du SNC, notamment avec des aptitudes de cellules macrophages et de cellules présentatrices d'antigènes, la formation de cicatrice gliale et l'apparition d'astrocytes dits « réactifs » dans différents troubles affectant le SNC (Ji et al., 2006; Wang and Bordey, 2008).

Les astrocytes ont aussi été impliqués dans la synaptogénèse, la stabilisation/raffinement des connexions synaptiques (Clarke and Barres, 2013; Eroglu and Barres, 2010; Pfrieger and Barres, 1997) et l'isolation des synapses (Bergles et al., 1999; Danbolt, 2001).

Finalement, plusieurs études montrent que les astrocytes sont également impliqués dans la modulation de l'activité synaptique par la relâche de neuromodulateurs qui activent directement des récepteurs neuronaux. Ces interactions neurones glies sont particulièrement pertinentes dans le contexte de cette thèse et sont abordées dans la section suivante.

1.5.3 Interactions neurone-glie

De plus en plus de groupes intègrent la modulation synaptique par les astrocytes dans leurs analyses de l'encodage nerveux (Araque et al., 2014; Min et al., 2012). Une multitude d'études ont démontré l'impact de l'activité astrocytaire sur des fonctions aussi variées que l'apprentissage et la mémoire (Min and Nevian, 2012); l'intégration sensori-motrice (Gourine et al., 2010; Takata et al., 2011); et même dans différentes pathologies comme l'épilepsie ou la maladie de Parkinson (Fellin et al., 2006; Martin et al., 2015).

Plusieurs mécanismes dépendants de l'activité des astrocytes peuvent influencer l'activité neuronale. Cependant, dans cette thèse nous nous concentrerons sur deux phénomènes principaux : la gliotransmission et l'homéostasie des ions extracellulaires. La gliotransmission, parce que l'importance de ce phénomène a été démontrée dans un autre GPC, celui de la respiration (Gourine et al., 2010). Et l'homéostasie des ions extracellulaires, parce que la variation d'ions extracellulaires est un phénomène important dans l'induction de la décharge rythmique neuronale dans plusieurs régions du SNC dont plusieurs GPCs y compris le NVsnpr. Toutefois, avant cela, nous présenterons des travaux qui situent anatomiquement les astrocytes dans différentes structures du SNC. Cet exercice permet de mesurer comment les astrocytes sont idéalement positionnés par rapport aux neurones pour moduler leur activité.

1.5.3.1 L'organisation morphologique des astrocytes par rapport aux synapses

L'organisation anatomique des astrocytes par rapport aux neurones dépend de la région neuronale considérée. Par exemple, 57 % des synapses du *stratum radiatum* sont en contact avec un astrocyte (Ventura and Harris, 1999). Alors que seulement 29% des synapses du cortex visuel sont associées à des astrocytes et que 67 à 94% des fibres de Purkinje sont recouvertes par des cellules de Bergmann, équivalentes aux astrocytes dans le cervelet (Grosche et al., 1999; Spacek, 1985; Xu-Friedman et al., 2001). Selon Ventura et Harris, le fait que toutes les synapses ne soient pas associées à des astrocytes pourrait s'expliquer par le fait que la glie serait associée seulement aux synapses actives libérant des neurotransmetteurs, par opposition aux synapses inactives (silencieuses).

Une panoplie d'études suggère une implication active de la glie dans le contrôle de l'activité neuronale et de la transmission synaptique. Mises ensemble, ces recherches montrent que les astrocytes sont des cellules excitables sensibles à l'activité neuronale, qu'elles peuvent en

retour moduler par la libération de substances neuroactives, nommées gliotransmetteurs (Grandes et al., 1991; Newman, 2003). En se basant sur ces avancées, Araque et ses collaborateurs ont proposé le concept de la synapse tripartite, où la glie est un partenaire actif de l'encodage nerveux au niveau de la synapse (Araque et al., 1999; voir figure 1-12) . Dans la section qui suit, nous survolerons les études et arguments qui ont permis de supporter les différents aspects de ce concept.

Figure 1-12: La synapse tripartite

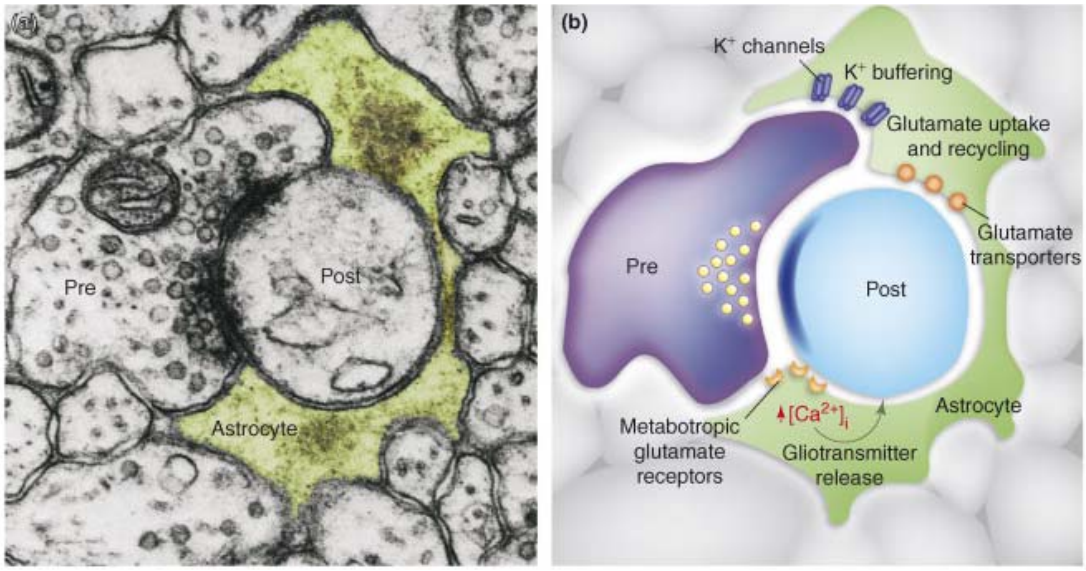

L'astrocyte, le troisième élément actif de la synapse tripartite. (a) Photographie en microscopie électronique montrant une terminaison pré- et postsynaptique (Pre et Post) enveloppée par un prolongement astrocytaire (vert) formant ainsi la synapse tripartite. (b) L'association étroite entre les prolongements astrocytaires et les composantes pré- et post-synaptiques permet la recapture des ions K^+ qui s'accumulent pendent l'activité neuronale, et aussi la recapture du glutamate par des transporteurs spécifiques. De plus, la relâche de neurotransmetteurs par la terminaison présynaptique peut activer des récepteurs astrocytaires qui à leur tour déclenchent des mécanismes permettant la relâche par les astrocytes de substances neuroactives (voir sections suivantes). Modifié de Halassa et al., 2007a.

1.5.3.2 Récepteurs astrocytaires et détection de l'activité neuronale

Les premières observations démontrant la présence de récepteurs activables par des neurotransmetteurs sur les astrocytes ont été faites dans des cultures d'astrocytes primaires, où l'application de certains agonistes induisait des cascades intracellulaires impliquant des seconds messagers (Gilman and Schrier, 1972; McCarthy and de Vellis, 1978; van Calker et al., 1980). Par la suite, le développement de différentes techniques, surtout de biologie moléculaire, notamment la réaction en chaine par polymérase (PCR) et les techniques d'immunomarquages spécifiques, a permis de confirmer la présence de récepteurs sur les astrocytes *in situ* et *in vitro* (Aoki and Pickel, 1992; Van Der Zee et al., 1993; Whitaker-Azmitia et al., 1993). Grâce aux techniques d'électrophysiologie et d'imagerie calcique, la fonctionnalité de ces récepteurs sur les astrocytes a pu être démontrée dans différents contextes impliquant une activité synaptique neuronale et une libération endogène de neurotransmetteurs (Araque et al., 2002; Porter and McCarthy, 1996). Il est maintenant bien connu que les astrocytes expriment une panoplie de récepteurs qui leur confèrent la capacité d'être activés par différents neurotransmetteurs et autres substances (pour revue voir Porter and McCarthy, 1997, Zhang and Haydon, 2005) . L'hétérogénéité des différents récepteurs exprimés par les astrocytes semble dépendre de la région du système nerveux et changerait aussi au cours du développement (Bal et al., 1994; Deecher et al., 1993; Muller et al., 1994). À titre d'exemple, le groupe de Nedergaard a montré que l'expression par les astrocytes de récepteurs métabotropiques au glutamate mGluR5 diminuait drastiquement à partir de la 3e semaine postnatale alors que celle des mGluR3 augmentait avec la maturation des souris (Sun et al., 2013).

Ainsi les recherches des dernières décennies ont montré de façon convaincante que les astrocytes peuvent détecter l'activité neuronale grâce à la présence de récepteurs spécifiques sur leur membrane.

1.5.3.2.1 Récepteurs des astrocytes.

Dans les faits, il semblerait que les astrocytes expriment des récepteurs sensibles à la plupart des neurotransmetteurs. Il serait impossible d'aborder en détail chacun de ces récepteurs dans le contexte de cette thèse. Toutefois, nous proposons une énumération non exhaustive ainsi que les références principales qui s'y rapportent. Les plus connus sont: les récepteurs

purinergiques; les récepteurs GABAa et GABAb, les récepteurs sérotoninergiques; les récepteurs muscariniques; les récepteurs histaminiques; les récepteurs opioïdes, endocannabinoïdes, adrénergiques, dopaminergiques (Pour revue voir Porter and McCarthy, 1997 et Verkhratsky, 2008) .

1.5.3.2.2 Récepteurs au glutamate des astrocytes

La présence de récepteurs NMDA sur les astrocytes a longtemps été niée. À cause du blocage par le Mg^{2+} (Mayer et al., 1984; Nowak et al., 1984), ces récepteurs sont non activables aux potentiels membranaires hyperpolarisés. Une dépolarisation jusqu'à environ −40 mV suffit à les débloquer, mais le potentiel membranaire des astrocytes avoisine les −80 mV et la forte densité de canaux K^+ qui définit ce potentiel de repos rend les dépolarisations substantielles presqu'impossibles dans ces cellules. Ainsi il était généralement accepté que d'éventuels récepteurs NMDA dans les astrocytes seraient de toute façon non fonctionnels. Malgré cela, plusieurs groupes ont progressivement rapporté des activations se faisant vraisemblablement par le biais de récepteurs NMDA dans les cultures d'astrocytes (Kondoh et al., 2001; Nishizaki et al., 1999; Puro et al., 1996). Aussi dans des expériences *in situ* l'application du NMDA induisait des réponses électriques ou calciques dans le cortex (Schipke et al., 2001), la moelle épinière (Ziak et al., 1998), des sous-populations d'astrocytes de l'hippocampe (Porter and McCarthy, 1995; Serrano et al., 2008; Steinhauser et al., 1994) et dans les cellules de Bergmann (Muller et al., 1993). Dans la même période, des ARNm spécifiques aux récepteurs NMDA et des protéines composant les sous-unités de ce récepteur ont été mis en évidence dans les astrocytes corticaux (Conti et al., 1996; Schipke et al., 2001).

Malgré toutes ces indications, l'expression de récepteurs NMDA fonctionnels dans les astrocytes a été confirmée bien après dans des expériences sur des astrocytes corticaux isolés de souris génétiquement modifiées, exprimant la protéine fluorescente verte (*green fluorescent protein*) dans les astrocytes. Ainsi, dans des astrocytes identifiés par ce marquage et isolés mécaniquement, des expériences en voltage-imposé ont été menées, et l'application de NMDA induisait des courants sensibles au MK-801, un antagoniste des récepteurs NMDA (Lalo et al., 2006).

Dans les travaux de Schipke et ses collaborateurs, la réponse NMDA intrinsèque des astrocytes a été montrée en bloquant l'activation neuronale et par le fait même les effets

indirects qui pourraient en découler. Dans cette condition, lors de l'enregistrement des astrocytes, l'application de NMDA induisait un courant avec un potentiel de renversement à 0 mV, et engendrait aussi une augmentation du calcium intracellulaire (Schipke et al., 2001). Ces données et celles du groupe de Lalo démontrent donc que les astrocytes corticaux expriment des récepteurs NMDA fonctionnels. Dans la même ligne d'idée, les travaux du groupe de Robitaille dans l'hippocampe ont montré que les astrocytes expriment aussi de tels récepteurs fonctionnels. En effet, dans leur étude, le blocage de l'activité neuronale (par la TTX) n'abolit pas les réponses électriques induites par le NMDA dans les astrocytes (Serrano et al., 2008).

Il est important de souligner une différence importante entre les récepteurs NMDA astrocytaires et les récepteurs NMDA neuronaux classiques: les récepteurs NMDA astrocytaires sont très peu sensibles (voir pas du tout) au Mg^{2+} et ils ont une relation courant-voltage linéaire. Les récepteurs NMDA des astrocytes s'activent donc aux potentiels membranaires très négatifs typiquement retrouvés dans ces cellules (Lalo et al., 2006; Schipke et al., 2001). Cela dit, l'explication de la faible sensibilité au Mg^{2+} des récepteurs NMDA astrocytaires reste inconnue.

Différents groupes ont montré que l'activation des récepteurs AMPA/kainate exprimés par les astrocytes provoque des réponses calciques astrocytaires dans les préparations en cultures et dans les tranches d'hippocampes (Burnashev et al., 1992; Glaum et al., 1990; Holzwarth et al., 1994; Muller et al., 1992; Porter and McCarthy, 1995; Seifert and Steinhauser, 1995; Shelton and McCarthy, 1999) . Selon le groupe de Steinhauser, ces réponses calciques seraient principalement dues à l'entrée de calcium à travers le canal du récepteur (Jabs et al., 1994).

Les astrocytes in situ expriment aussi des récepteurs métabotropiques du glutamate (mGluR) (Porter and McCarthy, 1995). Parmi les 8 sous-types de mGluRs, seulement les mGluR1 et mGluR5 sont associés à la libération de $[Ca^{2+}]_i$ (Pin and Duvoisin, 1995), indiquant que les réponses astrocytaires observées dans l'hippocampe suite à la perfusion d'agonistes mGluRs étaient probablement médiées par les mGluR1 et 5 (Porter and McCarthy, 1997). Toutefois, des expériences d'immunohistochimie ont surtout montré la présence des récepteurs mGluRs de type 5 dans les astrocytes de l'hippocampe et du cortex (Romano et al., 1995) et dans l'hypothalamus (van den Pol et al., 1995). De par leur proximité aux synapses glutamatergiques, les récepteurs astrocytaires mGluR5 sont idéalement positionnés pour être

activés par le glutamate libéré au niveau synaptique (Porter and McCarthy, 1997). D'ailleurs, Panatier et al. 2011, ont décrit un mécanisme d'activation des processus astrocytaires qui dépendait d'une telle activation des récepteurs mGluR5 (Panatier et al., 2011). Les récepteurs mGluRs astrocytaires associés à l'activation des phospholipase C sont probablement de type mGluR5 (Porter and McCarthy, 1997), plusieurs études ont aussi rapporté la présence de mGluR3 sur les astrocytes (Sun et al., 2013). Ces derniers récepteurs seraient associés à l'inhibition d'adénylate cyclase.

1.5.3.3 Activités calciques des astrocytes

Le fait que les astrocytes soient des cellules actives, en dépit de leurs incapacité à générer des potentiels d'action, a été démontré pour la première fois par l'observation de réponses calciques intracellulaires à la suite d'applications de glutamate sur des astrocytes en culture (Cornell-Bell et al., 1990). Qui plus est, les vagues de propagation des réponses calciques d'un astrocyte à l'autre suggéraient une communication intercellulaire. Cette idée fut confirmée au courant de l'année suivante lors d'expériences où les astrocytes étaient stimulés mécaniquement (Charles et al., 1991).

Plusieurs groupes ont fait des expériences démontrant la persistance des réponses calciques astrocytaires même en absence de calcium extracellulaire (Jensen and Chiu, 1991). Dans les faits, la plupart des réponses calciques astrocytaires dépendent de la libération du calcium par les réserves intracellulaires du réticulum endoplasmique via l'activation de récepteurs à l'inositol 1,4,5-triphosphate (IP_3R). La recapture du calcium se fait ensuite par le biais de Ca^{2+}-ATPases spécifiques (Simpson and Russell, 1997). Même si la plupart des réponses calciques astrocytaires semblent dépendre du phénomène décrit plus haut, il reste que les astrocytes possèdent également différents canaux membranaires perméables au calcium. À ce sujet, certaines études ont décrit des réponses qui proviendraient de l'entrée du calcium extracellulaire (voir figure 1-13).

Figure 1-13: Source de l'augmentation de la $[Ca^{2+}]_i$ astrocytaire

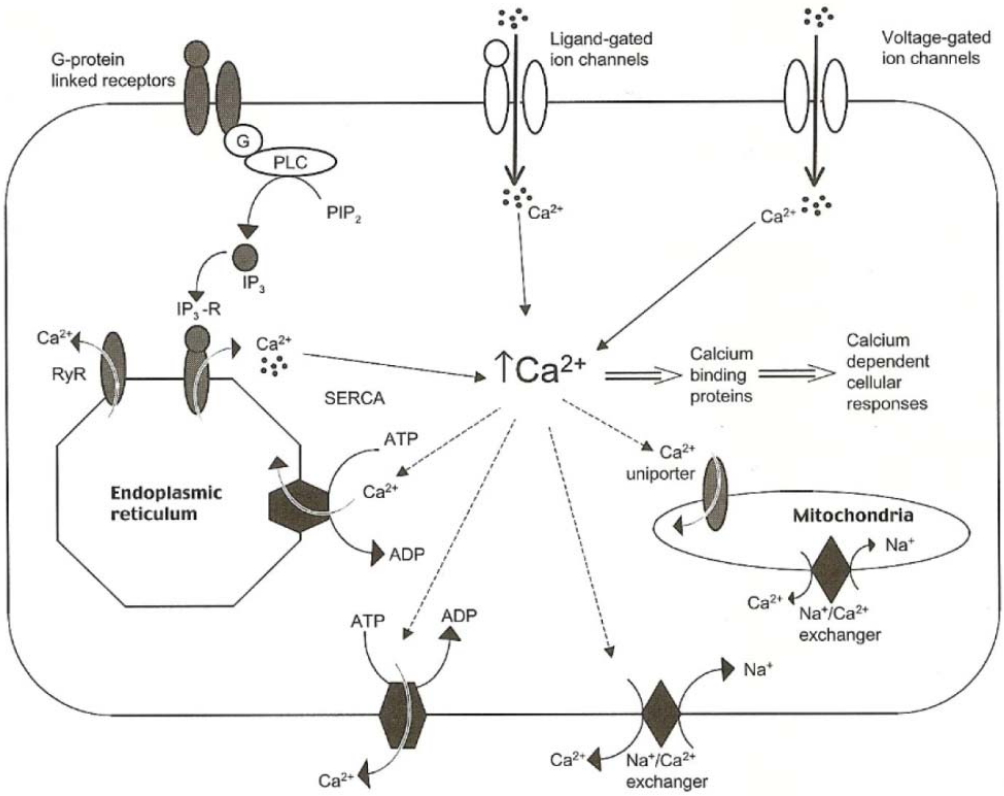

Source de l'augmentation de la $[Ca^{2+}]_i$ astrocytaire. La majorité des études montrent que l'élévation du Ca^{2+} cytosolique est la conséquence de la libération de Ca^{2+} par les stores internes (Réticulum endoplasmique) de manière dépendante à l'IP3 suite à l'activation de récepteurs couplés aux protéines G. Toutefois, plusieurs autres voies de signalisation ont étés décrites et pourraient être à l'origine des élévations du Ca^{2+}, modifié de (Cotrina and Nedergaard, 2005).

1.5.3.4 Modulation de l'activité neuronale par les astrocytes

Les prochaines sections sont un bref survol, premièrement, des phénomènes qui dépendent de la gliotransmission, et, deuxièmement, des mécanismes de modulation neuronale qui dépendent de l'homéostasie des ions extracellulaires. D'ailleurs, nous le verrons plus tard, la gliotransmission peut être intrinsèquement reliée à l'homéostasie de certains ions extracellulaires.

1.5.3.4.1 Les astrocytes influencent l'activité neuronale par la gliotransmission

Les premiers travaux montrant une influence des astrocytes sur l'activité neuronale datent de 1994 et ont été faits par Nedergaard et par le groupe de Haydon. En utilisant différentes techniques, ces chercheurs ont démontré qu'une activation spécifique des astrocytes pouvait induire des réponses dans les neurones (Nedergaard, 1994; Parpura et al., 1994). Depuis, plusieurs groupes ont continué l'étude de la signalisation des astrocytes aux neurones en évoluant des préparations en culture pour se rendre à des expériences in vivo.

Les travaux de différents laboratoires ont montré que les astrocytes participaient à la transmission synaptique en relâchant des gliotransmetteurs incluant le glutamate, l'ATP, l'adénosine, et la D-serine. La plupart des études s'intéressant à l'impact de l'activité des astrocytes sur l'activité neuronale l'ont fait en étudiant les potentiels postsynaptiques excitateurs (PPSE) ou inhibiteurs (PPSI). Il s'agissait de montrer une modification de la fréquence ou de l'amplitude de ces potentiels (ou des courants induisant ces potentiels), à la suite d'une activation sélective des astrocytes (voir tableau II). Entre autres, il a été démontré que les réponses calciques astrocytaires étaient à la fois suffisantes et nécessaires pour moduler la libération vésiculaire spontanée et influencer les fréquences des courants miniatures postsynaptiques excitateurs et inhibiteurs (Araque et al., 1998b). Les expériences de ces chercheurs ont souvent utilisé la stratégie consistant à introduire du BAPTA dans les astrocytes afin de bloquer leurs activités calcium dépendantes et d'en évaluer la conséquence sur la modulation neuronale. Ceci a permis, entre autres, de suggérer que la libération du glutamate par les astrocytes dépendait d'une machinerie vésiculaire qui dépend d'une élévation calcique intracellulaire (Araque et al., 1998a; Araque et al., 1998b; Bezzi et al., 1998; Innocenti et al., 2000; Kang et al., 1998; Parpura and Haydon, 2000) et de protéines

SNARE sensibles aux toxines botulique et tétanique (Araque et al., 2000; Hepp et al., 1999; Maienschein et al., 1999; Parpura et al., 1995; Pasti et al., 2001).

Tableau II. Effets des gliotransmetteurs dans différentes régions du système nerveux.

Région du système nerveux	Effet neuromodulateur
Glutamate	
Hippocampe	Dépression des courants postsynaptiques inhibiteurs et excitateurs évoqués
Hippocampe	Augmentation de la fréquence des miniatures postsynaptiques
Hippocampe	Augmentation de la fréquence des courants miniatures inhibiteurs
Hippocampe	Augmentation de la fréquence des courants spontanés excitateurs
Hippocampe	Augmentation de la fréquence des courants spontanés inhibiteurs
Hippocampe	Courants entrants postsynaptiques lents
Hippocampe	Augmentation de l'excitabilité neuronale
Hippocampe	Dépression hétérosynaptique
Hippocampe	Modulation de la DLT
Hippocampe	Modulation de la PLT
Hippocampe	Potentialisation synaptique
Hippocampe	Modulation des potentiels d'action
Hippocampe	Modulation de l'activité de synapses uniques
Hippocampe	Régulation de la cinétique des courants miniatures excitateurs évoqués
Cortex	Courants entrants postsynaptiques lents
Cortex	Modulation de la DLT
Thalamus ventro-basal	Courants entrants postsynaptiques lents
Corne dorsale de la moelle épinière	Courants entrants postsynaptiques lents
Noyau médial du corps trapézoïde	Courants entrants postsynaptiques lents
ATP/Adénosine	
Hippocampe	Dépression hétérosynaptique
Hippocampe	Modulation de la PLT
Hippocampe	Dépression de l'activité synaptique basale
Hippocampe	Régulation de la neurotransmission à l'état basal
Hippocampe	Dépression de l'activité excitatrice évoquée
Cortex	Modulation de l'activité de synapses uniques
Cortex	Régulation des oscillations corticales lentes
Cervelet	Dépression de l'activité spontanée excitatrice

Rétine	Activité neuronale induite par la lumière
Rétine	Dépression de l'activité excitatrice induite par la lumière
Nucleus accumbens	Courants entrants postsynaptiques lents
Noyau paraventriculaire de l'hypothalamus	Augmentation de l'amplitude des courants excitateurs
Jonction neuromusculaire	Potentialisation et dépression persistante
Medulla oblongata	Activation des neurones chémorécepteurs
D-Serine	
Hippocampe	Modulation de la PLT
Cortex	Modulation de la PLT/DLT
Rétine	Potentialisation de la transmission NMDARs
Noyau supraoptique de l'hypothalamus	Modulation de la PLT/DLT
Amygdale	Modulation des NMDARs
Amygdale	Augmentation de la plasticité homéosynaptique
TNF	
Hippocampe	Insertion de récepteurs AMPA
Hippocampe	Augmentation de la plasticité homéosynaptique
GABA	
Hippocampe	Courants sortants postsynaptiques lents
Cervelet	Courants toniques
Bulbe olfactif	Courants sortants postsynaptiques lents
Gliotransmetteurs inconnu	
Cortex	Régulation de l'état d'éveil cortical
Jonction neuromusculaire	Dépression synaptique
Jonction neuromusculaire	Potentialisation synaptique

*Tableau modifié de Araque et al., 2014

Comme discuté à la section 1.5.3.3, une des sources principales des réponses calciques astrocytaires provient des stores sensibles à IP_3. Ainsi, Fiacco et McCarthy ont utilisé la photolyse d'IP_3-encagé afin d'activer les astrocytes de façon spécifique et montré que cela induisait une augmentation transitoire de la fréquence des courants postsynaptiques excitateurs (CPSE) dans les tranches d'hippocampe (Fiacco and McCarthy, 2004). Le groupe de McCarthy a ensuite présenté des résultats qui semblaient contredire toutes ces données en montrant que dans les souris génétiquement modifiées pour bloquer l'expression des récepteurs à l'IP_3R (IP_3R_2), et donc présumément l'activité calcique des astrocytes, la transmission synaptique et la plasticité ne semblaient pas être affectées (Agulhon et al., 2010). Ces données ont ravivé la controverse quant à l'importance de l'activité calcique des astrocytes dans la modulation de l'activité neuronale. Toutefois une publication récente du groupe de Khakh montre que, chez les souris IP_3R_2 K-O les astrocytes préservent des réponses dans des microdomaines de leurs prolongements, ce qui pourrait expliquer les données de l'étude de McCarthy (Srinivasan et al., 2015).

La mesure de l'efficacité de la transmission synaptique (*synaptic failures*) a aussi été utilisée est pour montrer l'influence des astrocytes sur la transmission synaptique. Ces expériences sont toutefois plus difficiles, car elles impliquent des enregistrements en double patch (pré et post synaptique), ou des stimulations minimales. Quoi qu'il en soit, les données montrent que l'activité calcique des astrocytes peut diminuer le nombre d'échecs de 10 à 30% (Jourdain et al., 2007).

Un autre effet de l'activation des astrocytes sur les neurones est l'activation de récepteurs NMDA extra synaptiques entrainant l'apparition de courants excitateurs lents dans les neurones (en anglais : *slow inward currents* SIC) (Fellin et al., 2004; Navarrete and Araque, 2008). Plusieurs chercheurs ont étudié ces effets qui dépendent d'une libération de glutamate par les astrocytes.

1.5.3.4.2 Impact de la gliotransmission au niveau systémique

Dans le système respiratoire, Gourine et ses collaborateurs ont démontré l'importance de l'activité des astrocytes du noyau retro-trapézoïde et de la gliotransmition. Dans leurs expériences, les astrocytes répondaient aux baisses physiologiques de pH par des élévations calciques intracellulaires et par la sécrétion subséquente d'adénosine-5′-triphosphate (ATP);

cette sécrétion d'ATP répandait l'excitation calcique astrocytaire a d'autres astrocytes, par la suite activait une population spécifique de neurones et finissait par induire une augmentation de la fréquence respiratoire. Ils ont montré de façon élégante que l'induction de réponse calcique astrocytaire, par stimulation optogénétique d'astrocytes qui expriment la channelrhodopsin-2, activait une population de neurones via un mécanisme dépendant de l'ATP; ces derniers déclenchaient alors une forte réponse respiratoire in vivo (Gourine et al., 2010). Cette étude a été la première à démontrer clairement l'implication de l'activité gliale dans un GPC.

Il est intéressant de mentionner que dans le contexte de la locomotion fictive, dans la moelle de rats nouveau-nés, des chercheurs ont montré que les acides aminés les plus rythmogènes, dont l'homocystéine, étaient principalement retrouvés dans la glie. Ces observations avaient même poussé ces chercheurs, déjà à l'époque, à faire l'hypothèse que la glie était impliquée dans la modulation de l'activité neuronale (Houssaini et al. 1993, Grandes et al.1991).

1.5.3.4.3 Les astrocytes influencent l'activité neuronale en contrôlant la $[K^+]_e$

Un autre rôle bien connu des astrocytes est le contrôle et l'homéostasie des ions extracellulaires, et plus spécifiquement l'homéostasie de la $[K^+]_e$ (pour revue voir (Kadala et al., 2015). Déjà en 1966, Orkand et ses collaborateurs ont proposé le concept du tamponnage spatial du potassium par les astrocytes comme éléments stabilisateurs des concentrations extracellulaires de cet ion (Orkand et al., 1966). Selon ce concept, le potassium accumulé dans l'espace extracellulaire, pendant l'activité neuronale, est « pompé » par les astrocytes avoisinants. Il s'en suit une redistribution de l'ion, au travers des jonctions GAP dans le syncytium des astrocytes, vers les régions où les concentrations de l'ion sont plus basses (Scemes and Spray, 2012; Schnell et al., 2011). Aussi, l'élévation de la $[K^+]_e$ augmente le couplage par les jonctions GAP des astrocytes (De Pina-Benabou et al., 2001), ce qui semble appuyer cette théorie. À cause de la grande perméabilité de la membrane des astrocytes au potassium, la régulation de la $[K^+]_e$ se fait principalement de façon passive. Cependant, selon D'Ambrosio et ses collaborateurs (D'Ambrosio et al., 2002), la régulation de la $[K^+]_e$ se fait aussi bien par les canaux Kir que par des pompes Na^+-K^+-ATPase. Dans la même ligne de pensée, il est important de noter deux autres mécanismes dépendants des astrocytes qui peuvent influencer la $[K^+]_e$: 1) les aquaporines-4 (AQP4) qui permettent des flux d'eau au

travers des membranes des astrocytes et qui sont responsables du changement de volume des astrocytes et la compression de l'espace extracellulaire observée lors d'activités neuronales intenses (Nagelhus et al., 2004), et 2) les cotransporteurs Na^+-K^+-$2Cl^-$ qui peuvent aussi aider à contrecarrer l'augmentation de la $[K^+]_e$ (Tas et al., 1987).

Des travaux récents ont montré que les astrocytes sont également impliqués dans le contrôle actif de la $[K^+]_e$ au repos. En effet, Wang et ses collaborateurs ont montré que les réponses calciques, d'astrocytes dans l'hippocampe, provoquent une recapture rapide de potassium extracellulaire accompagné d'une diminution transitoire de la $[K^+]_e$ (Wang et al., 2012). Selon cette étude l'effet sur les neurones était une diminution de la fréquence des PPSEs au niveau de base, en parallèle à une augmentation de la fiabilité synaptique. Ceci revenant à dire que l'activité calcique des astrocytes augmente le ratio du signal /bruit de l'activité neuronale (Haydon and Nedergaard, 2015).

En résumé, nous avons vu que les astrocytes sont capables de détecter l'activité neuronale dans différents contextes dans le SNC. Aussi, nous avons vu que ces cellules semblent pouvoir moduler directement l'activité neuronale par la sécrétion de gliotransmetteurs, mais aussi par le contrôle de l'homéostasie d'ions extracellulaires. C'est donc dans ce contexte que nous avons décidé d'intégrer et d'étudier le rôle potentiel des astrocytes dans notre recherche s'intéressant aux mécanismes cellulaires à la base de la rythmogénèse des neurones du NVsnpr.

1.6 Objectifs et buts de la thèse.

Notre étude ne s'est pas penché sur l'homéostasie du potassium extracellulaire mais plutôt sur celle du calcium extracellulaire pour la raison suivante: dans les préparations *in vitro* de tronc cérébral, la baisse artificielle de la $[Ca^{2+}]_e$ provoque une augmentation drastique de la proportion de neurones du NVsnpr qui déchargent en bouffées rythmiques. Les plateaux de dépolarisation sous-jacents à ces bouffées augmentent en durée et en amplitude avec la baisse du calcium extracellulaire et ils sont bloqués par la TTX (Brocard et al., 2006). Ces observations suggèrent que la $[Ca^{2+}]_e$ régule le mode de décharge des neurones du NVsnpr en modulant l'amplitude des courants I_{NaP} (Brocard et al., 2006).

Le NVsnpr reçoit des inputs massifs de régions corticales et d'afférences sensorielles, en particulier de ceux importants pour l'ajustement du patron des mouvements de la mastication. Même si les deux types d'inputs atteignent le NVsnpr à très courte latence (~5ms), il est habituellement nécessaire d'avoir des stimulations répétitives de durée relativement longue (>100ms) de l'ACM ou des nerfs sensoriels avant d'induire la mastication *in vivo* (Dellow and Lund, 1971; Lund et al., 1984). En utilisant de tels stimuli, une autre étude de notre laboratoire a montré que l'activité en bouffées rythmiques des neurones du NVsnpr pouvait être induite sans baisser la $[Ca^{2+}]_e$ artificiellement (Bernier et al., 2010).

Cela dit, les activités neuronales intenses et soutenues ont souvent été associées à des baisses de $[Ca^{2+}]_e$ (Amzica et al., 2002; Nicholson et al., 1978; Pumain and Heinemann, 1985; Pumain et al., 1983; Somjen, 1980): ces baisses de $[Ca^{2+}]_e$ peuvent atteindre des concentration de 0,8 mM dans le cortex cérébral du chat lors de stimulations répétitives locales (Nicholson et al., 1978), et dans le néocortex de rats lors d'applications locales de glutamate (Pumain and Heinemann, 1985). De plus, plusieurs études indiquent que les bouffées neuronales sont accompagnées de baisses importantes de $[Ca^{2+}]_e$ dans différentes régions du SNC (Benninger et al., 1980; Brocard et al., 2013; Heinemann et al., 1990).

Figure 1-14: Schéma conceptuel de l'objectif et des buts de la thèse

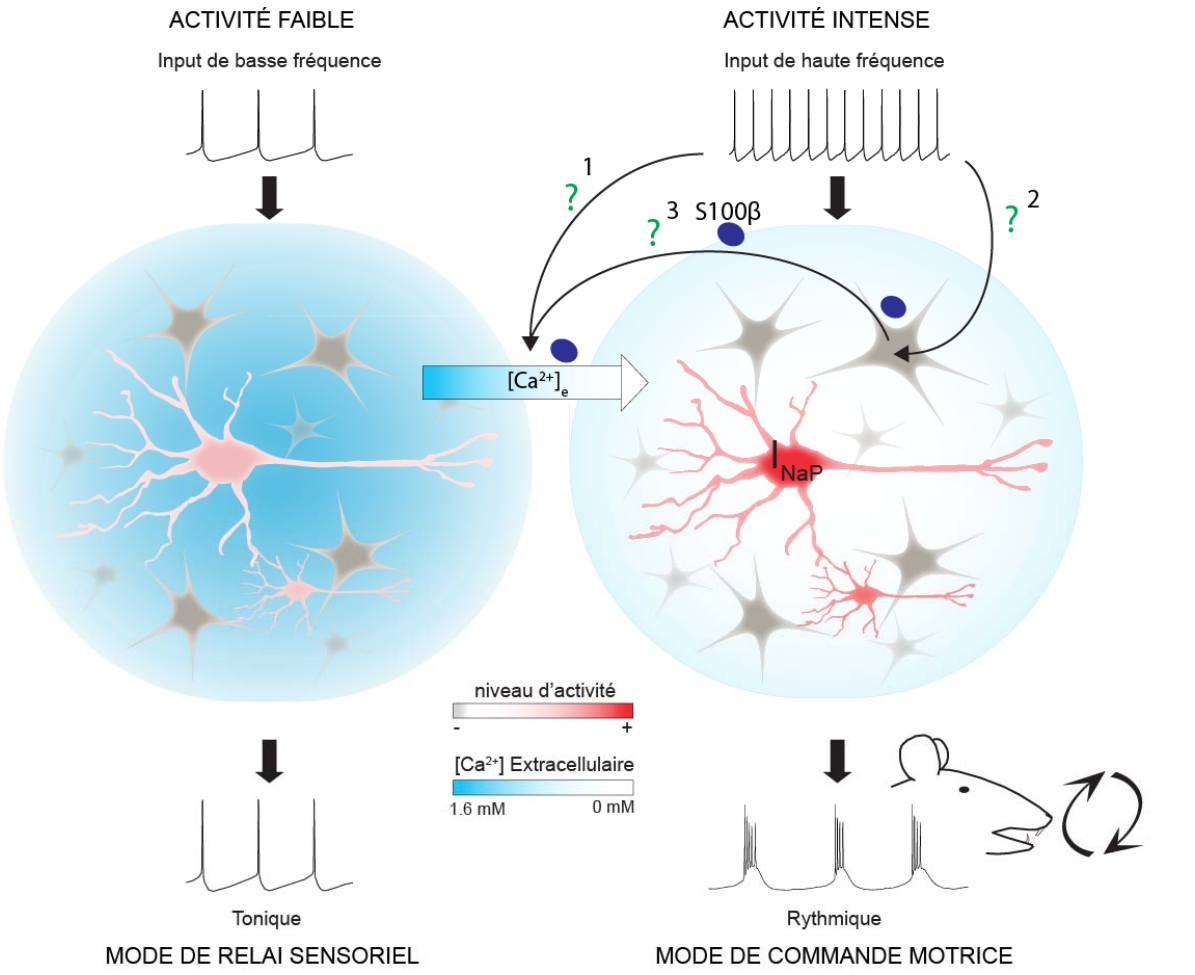

Schéma conceptuel de l'objectif et des buts de la thèse. Notre hypothèse de travail postule que : (1) l'activation soutenue de l'aire corticale masticatoire ou des afférences sensorielles trigéminales est suffisante pour diminuer la $[Ca^{2+}]_e$. Le mécanisme sous-jacent à la baisse de calcium extracellulaire dépendrait (2) de la capacité des astrocytes à détecter et à être activés par l'input sensoriel qui déclenche l'activité rythmique, (3) cette activation des astrocytes du NVsnpr serait impliquée dans le mécanisme qui permet la baisse de la $[Ca^{2+}]_e$. Nous proposons que le mécanisme en question est la relâche dans l'espace extracellulaire de la protéine chélatrice de calcium S100β par les astrocytes. Cette situation déclencherait alors la décharge rythmique des neurones du NVsnpr par l'activation des courants I_{NaP}. Cette rythmicité est alors transmise aux motoneurones du noyau moteur du trijumeau associés à la mastication.

Ces observations ont donc défini le premier but de cette thèse : déterminer si des baisses de $[Ca^{2+}]_e$ physiologiques accompagnent les bouffées rythmiques neuronales induites par des stimuli physiologiques. Il s'agissait, dans un premier temps, de vérifier que le mécanisme d'induction des bouffées rythmiques par la baisse du calcium extracellulaire pouvait être un phénomène physiologique.

Le deuxième but de nos travaux a été d'étudier les mécanismes qui pourraient être à l'origine d'une baisse physiologique du calcium extracellulaire. Nous avons considéré la possibilité que les astrocytes soient impliqués dans le contrôle des concentrations de calcium extracellulaire et donc par ricochet dans le mode de décharge des neurones du NVsnpr. Cette idée s'appuie sur 1) les données de la littérature discutées plus tôt, qui indiquent que les astrocytes sont impliqués dans la modulation de l'activité neuronale, mais aussi sur 2) les études qui montrent que les astrocytes sont impliqués dans l'homéostasie d'un autre ion extracellulaire, le potassium. Pour nous, ce deuxième point était une indication que les astrocytes pourraient potentiellement jouer un rôle similaire dans le contrôle du calcium extracellulaire.

Pour ce deuxième but, nous avons défini qu'il fallait étudier trois points importants : 1) Déterminer si les astrocytes du NVsnpr sont activés par les stimuli qui déclenchent la décharge rythmique des neurones du NVsnpr. 2) Déterminer l'impact du blocage de l'activation des astrocytes sur la capacité subséquente des neurones à décharger de façon rythmique. Et finalement, 3) identifier les mécanismes par lesquels les astrocytes pourraient engendrer une diminution de la $[Ca^{2+}]_e$ (voir figure 1-14). Nous avons envisagé deux mécanismes simples qui pouvaient permettre aux astrocytes de baisser la $[Ca^{2+}]_e$ soit : 1) la recapture du calcium extracellulaire par des canaux calciques sur la membrane des astrocytes, ou 2) la libération dans l'espace extracellulaire, par les astrocytes, d'une substance pouvant « chélater » le calcium extracellulaire et ainsi faire baisser la $[Ca^{2+}]_e$. De prime abord, il faut avouer que cette deuxième possibilité semble un tant soit peu inusitée, il est maintenant intéressant de se rappeler les caractéristiques de la protéine S100β vues à l'encadré 1. En effet, cette protéine est spécifique aux astrocytes, elle peut lier le calcium et finalement les astrocytes peuvent la sécréter. Ainsi pour ces différentes raisons, nous avons décidé de tester l'hypothèse que la S100β serait la protéine clé du mécanisme impliquant les astrocytes dans la baisse du $[Ca^{2+}]_e$ et

par ricochet l'induction de la décharge en bouffées rythmiques des neurones du NVsnpr (voir figure 1-14). Une grande partie de l'étude a donc été consacrée à tester la validité de cette hypothèse.

Afin d'étudier l'activité neuronale, les principales techniques utilisées ont été celles d'enregistrements de *patch clamp* en mode cellules entières ainsi que des techniques d'enregistrements extracellulaires. Les $[Ca^{2+}]_e$ ont été étudiées à l'aide d'enregistrements avec des électrodes ions sensibles. L'activité des astrocytes a été mesurée électriquement et par les techniques d'imagerie calcique.

La suite de cette thèse est organisée en deux parties : la première présente les résultats de nos travaux de recherche publiée dans la revue *Nature Neuroscience*. Et la deuxième présente une discussion générale qui aborde les résultats que nous avons obtenus au cours de cette étude ainsi que leurs implications dans un contexte plus large.

CHAPITRE 2

2. Résultats

Ce chapitre comporte la publication suivante :

Philippe Morquette, Dorly Verdier, Aklesso Kadala, James Féthière, Antony G Philippe, Richard Robitaille and Arlette Kolta. ***An astrocyte-dependent mechanism for neuronal rhythmogenesis.*** Nature Neuroscience 18, 844–854; 04 May 2015.

2.1 Abstract

Communication between neurons rests on their capacity to change their firing pattern to encode different messages. For several vital functions, such as respiration and mastication, neurons need to generate a rhythmic firing pattern. Here we show in the rat trigeminal sensori-motor circuit for mastication that this ability depends on regulation of the extracellular Ca^{2+} concentration ($[Ca^{2+}]_e$) by astrocytes. In this circuit, astrocytes respond to sensory stimuli that induce neuronal rhythmic activity, and their blockade with a Ca^{2+} chelator prevents neurons from generating a rhythmic bursting pattern. This ability is restored by adding S100β, an astrocytic Ca^{2+}-binding protein, to the extracellular space, while application of an anti-S100β antibody prevents generation of rhythmic activity. These results indicate that astrocytes regulate a fundamental neuronal property: the capacity to change firing pattern. These findings may have broad implications for many other neural networks whose functions depend on the generation of rhythmic activity.

2.2 Introduction

The pattern of activity that emerges from a neuronal network defines the essence of its function. Many fundamental nervous functions, including attention, learning and memory, and control of sleep/wake cycle, result from rhythmic or oscillatory activities in neuronal networks. Obvious examples of such functions are rhythmic movements such as walking, breathing and chewing, which are generated by networks referred to as central pattern generators (CPGs) (Dellow and Lund, 1971, Grillner, 1975, Smith et al., 1991). These networks generate a rhythmic motor activity that is continuously adjusted by sensory feedback to produce a movement pattern that is adapted to the prevailing conditions. Despite intense research in this field, the exact mechanisms underlying generation of this rhythmic activity and its adaptation by sensory inputs remain elusive. Some studies point to intrinsic pacemaker properties, while others emphasize synaptic connections (Harris-Warrick, 2010). In a few models, rhythmic network properties emerge from the combination of intrinsic properties and synaptic connections, but the mechanism underlying their interaction is ill-defined (Del Negro et al., 2010). In most instances, the potential contribution of astrocytes, the most abundant type of cell in the brain, is largely ignored. Only in respiration has it been shown that astrocytes contribute, by detecting pH changes in the blood and modulating neuronal firing in response (Gourine et al., 2010, Okada et al., 2012).

Several ionic conductances endow neurons with rhythmogenic abilities. I_{NaP}, a persistent voltage-dependent sodium current, is one such conductance that has been shown to underlie rhythmogenesis in the cortex, the hippocampus and several brainstem and spinal CPG systems. Rhythmogenic neurons of the trigeminal circuit involved in mastication and of the spinal locomotor CPG have I_{NaP}-mediated rhythmic bursting properties that are enhanced when the extracellular Ca^{2+} concentration ($[Ca^{2+}]_e$) diminishes (Brocard et al., 2006, Tazerart et al., 2008). Here we propose that this Ca^{2+} dependency forms the basis of the mechanism that enables synaptic inputs of sensory afferents to interact with intrinsic bursting properties and determines the neuronal ability to change firing pattern. We found that, in the dorsal part of the trigeminal main sensory nucleus (NVsnpr), where rhythmogenic neurons are found, stimulation of sensory fibers that project to the nucleus activated astrocytes. In turn, astrocytes regulated the external Ca^{2+} to trigger bursting by releasing a Ca^{2+} binding protein, S100β.

Specific inactivation of astrocytes prevented neuronal bursting, which could be rescued only by addition of S100β; conversely, bursting could not be produced when S100β was blocked. These results will help understand the mechanisms leading to rhythmic firing and may have widespread implications for normal functions relying on rhythmogenesis, as well as abnormal rhythmic firing observed in several pathologies, such as Parkinson disease or epilepsy, where astrocytes are known to contribute.

2.3 Results

2.3.1 Burst-inducing stimuli decrease external calcium

We showed in previous work that rhythmic bursting could be elicited in NVsnpr neurons by artificially reducing the Ca^{2+} concentration of the perfusing medium (Brocard et al., 2006). Decreases of $[Ca^{2+}]_e$ have been reported to occur during intense or sustained neuronal activity (Massimini and Amzica, 2001) or during pharmacologically induced locomotor-like activities in isolated neonatal rodent spinal cords (Brocard et al., 2013), but it is unknown whether they occur in the trigeminal system and if they can be elicited by more physiological stimuli. We first tested the effects of electrical stimulation of the trigeminal tract on $[Ca^{2+}]_e$ and on neuronal firing. The trigeminal tract contains fibers of sensory afferents that project to NVsnpr. Ion-sensitive electrodes were used to monitor $[Ca^{2+}]_e$ following repetitive stimulation of the tract at 40 Hz, a frequency close to the sensory afferents' natural firing frequency during mastication (Trulsson and Johansson, 2002). To avoid possible washout of small external Ca^{2+} changes that could result from the rapid perfusion in a submerged preparation chamber, we conducted these experiments in a Haas-type interface chamber, where preparations were maintained at the interface between a warm, humidified atmosphere of O_2/CO_2 and a perfusing artificial cerebrospinal fluid (aCSF) containing 1.6 mM Ca^{2+} (Fig. 1a). However, only extracellular recordings can be conducted in this condition. In 14 of 22 cells, repetitive stimulation of the trigeminal tract produced long-lasting (≥30 min) decreases of $[Ca^{2+}]_e$ in dorsal NVsnpr (average drop: 1.1 ± 0.1 mM; Fig. 1b), while in the remaining 8 cases, no changes could be detected. In 9 of those 14 cases, $[Ca^{2+}]_e$ dropped below 0.4 mM (average drop of 1.3 ± 0.1 mM), and in all of these 9 cases, the firing pattern of neurons recorded

extracellularly near the Ca^{2+}-sensitive electrode changed from tonic to rhythmic bursting (Fig. 1c,d). In the remaining 5 cases, the Ca^{2+} drop was of smaller amplitude (0.7 ± 0.1 mM) and no changes were observed on firing patterns of adjacent cells recorded. Firing patterns considered as rhythmic bursting and as tonic firing are illustrated in Supplementary Figure 1 and the criteria used to distinguish them are described in Online Methods. Bursting occurred at an average frequency of 8.56 Hz ± 1.02 (Supplementary Table 1), well within the frequency range of bursts observed by electromyography in the jaw muscles of freely chewing rats (5–11 Hz, with a mean of 8.5 Hz; Westneat and Hall, 1992).

Figure 2-1 : Sensory fibers stimulation and local NMDA application lead to $[Ca^{2+}]_e$ decreases and I_{NaP}-dependent neuronal bursting.

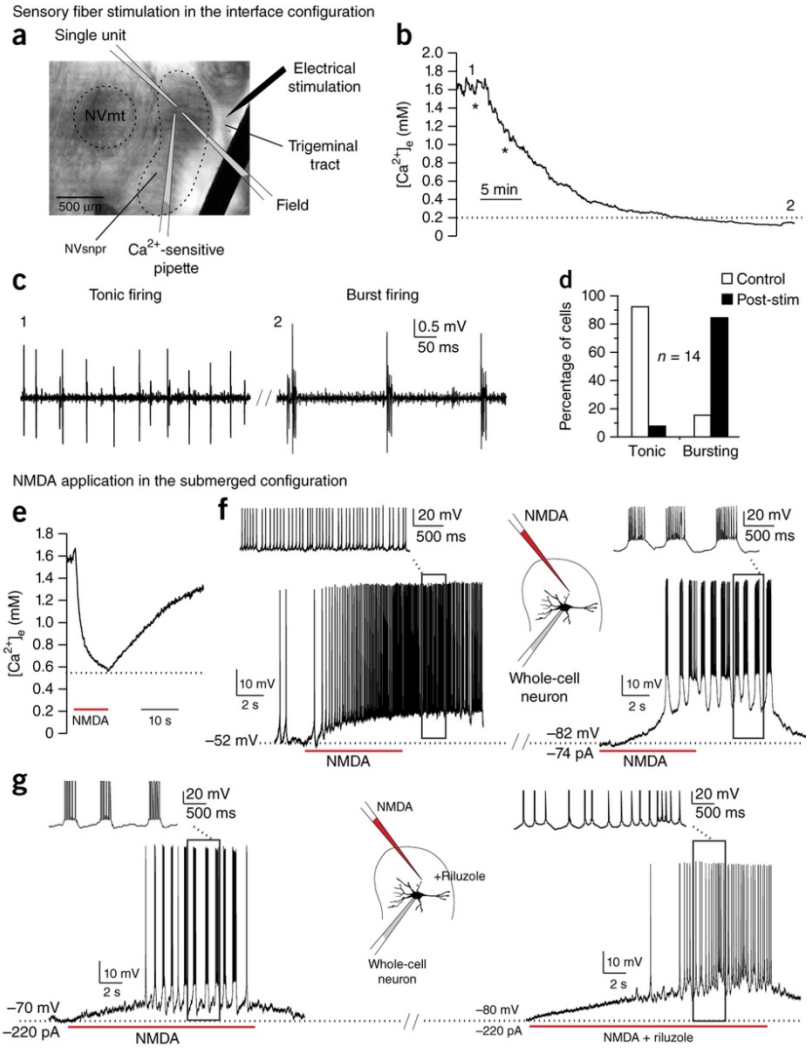

(a) Stimulating and recording electrodes arrangement used in the interface chamber superimposed on a brainstem slice photomicrograph. NVmt, trigeminal motor nucleus. (b) Electrical stimulation (*, 1-s trains at 40 Hz) of sensory fibers in the trigeminal tract caused a long-lasting decrease in $[Ca^{2+}]_e$ (n = 14 of 22 recording locations in 18 slices from 14 rats). (c) Example of a neuron with a firing pattern that was tonic before stimulation (1) and became rhythmically bursting (2) when $[Ca^{2+}]_e$ dropped to under 0.3 mM (dotted line in b). (d) Firing pattern prevalence before (control) and after stimulation (post-stim) of the tract (see also Supplementary Fig. 1). (e) In submerged preparations, local application of NMDA (1 mM) also caused a decrease in $[Ca^{2+}]_e$ (n = 8 applications in 2 slices from 2 rats). (f) Left, at resting membrane potential, such applications produced a large depolarization and an increase in firing frequency, but no bursting (see inset) (1 mM: n = 5 cells in 3 slices from 3 rats; 2 mM: n = 3 cells in 3 slices from 1 rat). Right, rhythmic bursting (inset) was induced if the neuron was hyperpolarized by current injection before the application. (g) Rhythmic bursting induced by local application of NMDA (1 mM; left) was prevented when a blocker of I_{NaP} channels, riluzole (20 µM), was added to the bath (right). In this condition, NMDA no longer induced bursting, but was still strongly depolarizing and excitatory (n = 3 cells in 3 slices from 3 rats).

We then sought a robust stimulus to induce bursting and $[Ca^{2+}]_e$ decreases in submerged preparations, in order to conduct whole-cell recordings and Ca^{2+} imaging. In a previous study we had shown that rhythmic bursting elicited in NVsnpr neurons following stimulation of sensory afferents is blocked by an antagonist of NMDA receptors, DL-2-amino-5-phosphonopentanoic acid (APV), suggesting that these receptors are involved in burst induction (Bernier et al., 2010). Hence, we assessed in both interface and submerged slice preparations whether $[Ca^{2+}]_e$ and neuronal firing pattern would be altered by local applications of NMDA (1–2 mM). In interface preparations (n = 12 cells in 12 slices from 12 animals), local NMDA application elicited rhythmic bursting at frequencies (7.43 ± 1.2 Hz) close to those of rhythmic bursting elicited by stimulation of sensory afferents (Supplementary Table 1). In submerged preparations, similar NMDA applications produced $[Ca^{2+}]_e$ decreases (0.89 ± 0.11 mM; n = 8) (Fig. 1e) of shorter duration than those elicited by stimulation of sensory fibers in the interface chamber (23.69 ± 4.58 s). When applied near a neuron held at its resting membrane potential, NMDA caused a long-lasting depolarization and induced firing, but the firing pattern remained tonic (n = 5 of 5 at 2 mM and 3 of 3 at 1 mM) (Fig. 1f). Rhythmic bursting (Supplementary Table 1) occurred only if the neurons were hyperpolarized before NMDA application (n = 37 at 2 mM, n = 54 at 1 mM in slices from 74 animals) (Fig. 1f) and showed the same voltage dependency as I_{NaP}-mediated events (namely, between −65 mV and −50 mV) (Crill, 1996) (Supplementary Table 1). Further, this NMDA-induced bursting was abolished by two I_{NaP} blockers, TTX (1 μM; n = 5 cells in 5 slices from 5 animals; data not shown) and riluzole (20 μM; n = 3; Fig. 1g).

2.3.2 I_{NaP}-mediated bursting is modulated by $[Ca^{2+}]_e$ but not $[Ca^{2+}]_i$

The above results suggest that bursting is associated with decreases in $[Ca^{2+}]_e$, but do not discriminate between the extracellular $[Ca^{2+}]$ or the potential subsequent fluctuation of intracellular $[Ca^{2+}]$ as the factor that promotes bursting. Under control conditions, when using a physiological [Ca2+]e (1.6 mM) (Jones and Keep, 1988) in the perfusing medium, most neurons had a tonic firing pattern when activated with intracellular current injections or when firing spontaneously. Their firing pattern switched to rhythmic bursting when the perfusing medium was changed to a Ca^{2+}-free aCSF (n = 12; Fig. 2a and Supplementary Table 1) even

though no changes were observed in their resting membrane potential (−53 ± 1 mV in 1.6 mM Ca^{2+} aCSF versus −54 ± 2 mV in Ca^{2+}-free aCSF; paired t-test; P = 0.364; n = 12) and in their input resistance (276 ± 55 MΩ in controls versus 267 ± 51 MΩ in Ca^{2+}-free aCSF; paired t-test; P = 0.81; n = 10). Even more confined Ca^{2+} reductions of shorter duration induced by local extracellular application of the Ca^{2+} chelator BAPTA (5–35 mM) near the recorded neurons induced rhythmic bursting (n = 13 of 13; Fig. 2b). In contrast, depletion of neuronal intracellular Ca^{2+} ($[Ca^{2+}]_i$) by addition of BAPTA (10–35 mM) to the solution used in the recording electrode did not induce bursting in neurons firing tonically under physiological $[Ca^{2+}]_e$ (n = 11) (Fig. 2c) and did not prevent NMDA-induced bursting (n = 3 of 3) (Fig. 2c). As with NMDA, bursts induced by local applications of extracellular BAPTA were I_{NaP}-dependent, as they were abolished by riluzole (n = 5 of 6; Fig. 2d).

Figure 2-2 : Reduction of extracellular Ca^{2+} leads to I_{NaP} dependent bursting independently of effects on intracellular Ca^{2+}.

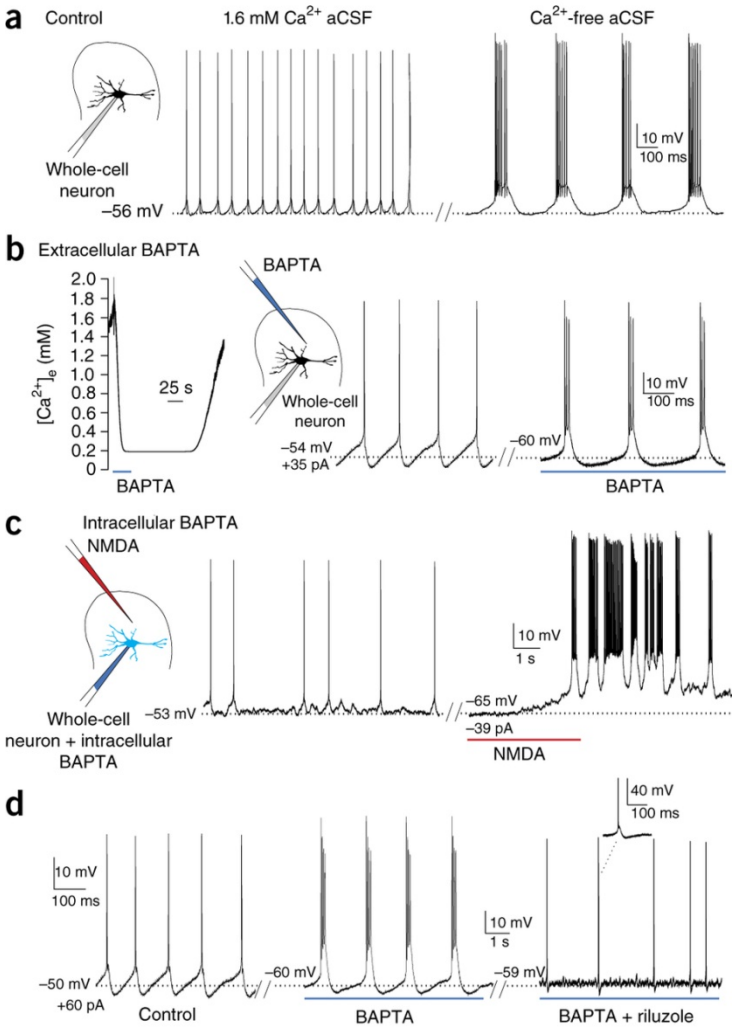

Reduction of extracellular Ca^{2+} leads to I_{NaP} dependent bursting independently of effects on intracellular Ca^{2+}. (a) The tonic firing pattern of NVsnpr neurons recorded under physiological $[Ca^{2+}]_e$ (1.6 mM; left) switches to burst firing when the perfusing medium is replaced by a Ca^{2+}-free medium (n = 12 cells in 10 slices from 10 rats). (b) Local extracellular application of BAPTA (10 mM; submerged preparation) produced a large but transient decrease of $[Ca^{2+}]_e$ (left) and induced rhythmic bursting (right) in an adjacent NVsnpr neuron that was firing tonically (middle) before the application (n = 13 cells in 9 slices from 9 rats). (c) The switch is not due to lack of intracellular Ca^{2+}, because chelation of neuronal intracellular Ca^{2+} by adding BAPTA (35 mM) to the recording pipette solution did not induce rhythmic bursting in a neuron firing tonically under physiological $[Ca^{2+}]_e$ (1.6 mM; left, n = 11 cells in 11 slices from 7 rats) and did not prevent NMDA-induced recurrent bursting in the same neuron (right, n = 3 cells in 3 slices from 3 rats). (d) Local extracellular application of BAPTA (10 mM) near a tonically firing NVsnpr neuron (left) induced rhythmic bursting (middle) under control conditions, but not in presence of riluzole (20 μM; right) in the bath. In the presence of riluzole, BAPTA had an effect on the spike after hyperpolarization, but little effect on the firing pattern (n = 5 of 6 cells in 6 slices from 5 rats).

Low $[Ca^{2+}]_e$ has been reported to enhance I_{NaP} (Li and Hatton, 1996, Su et al., 2001, Brocard et al., 2006, Brocard et al., 2013). To ensure that this is the case here, we performed a series of voltage clamp experiments in a modified aCSF (see Online Methods) to pharmacologically block Ca^{2+} and K^+ conductances and isolate Na+ currents. A slow voltage ramp (18 mV/s, 5 s) was used to activate I_{NaP} without activating fast sodium currents. In 11 dorsal NVsnpr neurons tested, the slow voltage-clamp command produced an inward sodium current (Supplementary Fig. 2a). Local application of extracellular BAPTA (10 mM) during the ramp protocol (n = 6) increased the peak of this inward current (Supplementary Fig. 2b) by 58 ± 13%. Peak currents were obtained at −44.7 ± 1.3 mV under control conditions and at −48.5 ± 1.7 mV with BAPTA, a shift of 8%. This inward current was blocked with bath application of riluzole (20 μM; n = 4 cells in 4 slices from 3 rats) or TTX (1–2 μM; n = 2 cells in 2 slices from 1 animal). We subtracted the trace obtained with a blocker (riluzole or TTX) from the trace obtained under control conditions or the trace obtained with BAPTA to isolate the I_{NaP} current observed in control conditions and in presence of BAPTA, respectively (Supplementary Fig. 2c). The characteristics of this isolated I_{NaP} current were obtained with the fitting of a single Boltzmann function to the normalized (to gmax) conductance-voltage data (Supplementary Fig. 2d). Taken together, these results strongly suggest that extracellular decrease of $[Ca^{2+}]$ promotes bursting and enhances I_{NaP} currents.

A recent report showed that decreasing $[Ca^{2+}]_e$ alters neuronal discharge through an astrocytic ATP-dependent mechanism (Torres et al., 2012). To verify whether bursting induced by decreases in Ca^{2+} somehow involve ATP release and purinergic receptors, we assessed the effects of bath-applied suramine, a broad-spectrum antagonist of purinergic receptors (50 μM for >1 h). We found no effects on bursting induced by application of extracellular BAPTA (10 mM) in 5 of 5 cells (Supplementary Fig. 3).

2.3.3 Astrocytes respond to burst-inducing stimuli

Since regulation of extracellular ions is a key mechanism by which astrocytes affect neuronal functions (Wang et al., 2012), we hypothesized that astrocytes may influence neuronal bursting by regulating $[Ca^{2+}]_e$. In this case, they should respond to the two stimuli (NMDA and sensory stimulation) that induce $[Ca^{2+}]_e$ decreases and neuronal bursting. We identified astrocytes by specific loading of sulforhodamine 101 (SR101; 1 μM in the bath) and their lack

of active membrane properties (Fig. 3a). Using simultaneous whole-cell patch recordings and Ca^{2+} imaging, we observed that local NMDA (1 mM) applications produced large increases of intracellular Ca^{2+} (143.2 ± 28.8% ΔF/F0) accompanied by depolarizations (6.6 ± 1.2 mV; n = 5 astrocytes; Fig. 3b) under current clamp conditions. Consistently, repetitive stimulation (40–60 Hz; n = 5) of the glutamatergic (Lazarov, 2002) sensory fibers also depolarized NVsnpr astrocytes (Fig. 3b). Addition of TTX (1 μM) to the perfusing medium had little effect on the amplitude of the NMDA-induced membrane depolarization in astrocytes (Fig. 3c,e; n = 9 of 9), while addition of a mix of drugs blocking AMPA receptors, sodium channels, calcium channels and glutamate uptake (CNQX 10 μM, TTX 1 μM, cadmium 100 μM and L-trans-pyrollidine-2,4-dicarboxylic acid (PDC) 50 μM) reduced the NMDA-induced response by 53% on average (Fig. 3d,e; n = 5) and abolished (n = 2) or greatly reduced (by 93%; n = 1) synaptic responses to electrical stimulation of the sensory fibers (Fig. 3d,e). The remaining response to NMDA with the mix of blockers present presumably resulted from isolated NMDA-evoked current. To further test whether NVsnpr astrocytes express functional NMDA receptors, the NMDA receptor antagonist MK-801 (2 mM) was added to the internal recording solution. In 11 astrocytes recorded in this condition, NMDA applied locally elicited no response in 8 of the cells and a small depolarization in the 3 remaining cells. These depolarizations occurred only in the first minutes after initiating recording and disappeared after a few minutes of diffusion of MK-801 (Fig. 3f), while responses to local application of glutamate (1 mM), used as a control to test viability of the recorded cells, persisted in all 11 cells (Fig. 3f). These results clearly demonstrate that NMDA-induced activation of astrocytes does not depend on neuronal transmission and is at least partially mediated by direct activation of astrocytic NMDA receptors.

Figure 2-3: NVsnpr astrocytes have functional NMDA receptors and are activated by stimuli that cause $[Ca^{2+}]_e$ decreases and elicit neuronal rhythmic bursting.

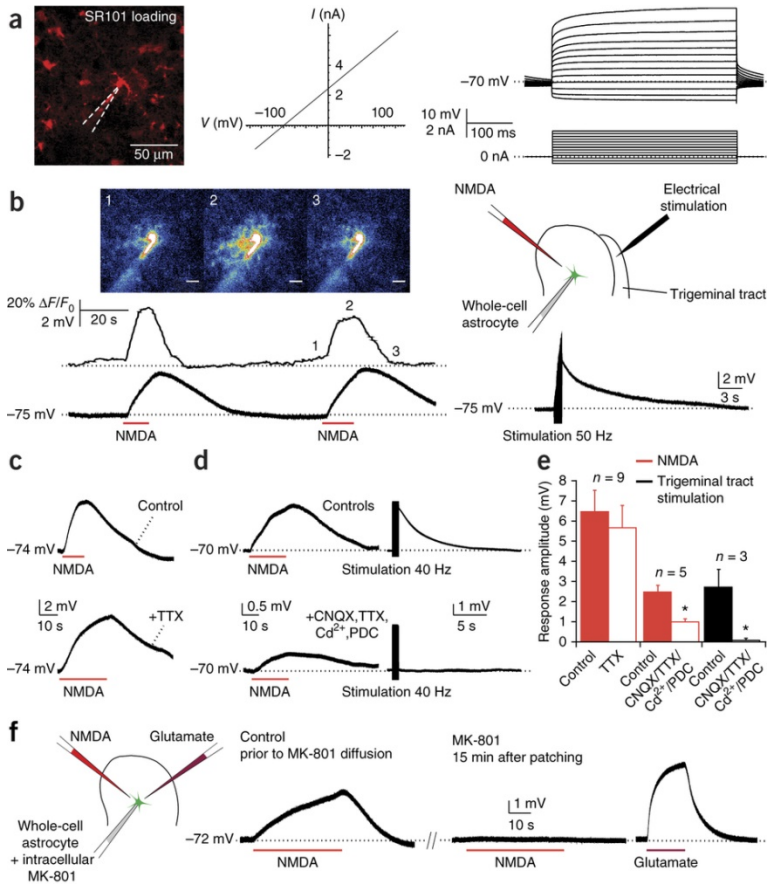

NVsnpr astrocytes have functional NMDA receptors and are activated by stimuli that cause $[Ca^{2+}]_e$ decreases and elicit neuronal rhythmic bursting. (a) Astrocytes were identified on the basis of their typical linear passive characteristics when imposing a depolarizing ramp from −130 mV to 110 mV in voltage clamp mode (middle) and the lack of action potentials in current clamp mode (right). In some experiments (left), the specific marker SR101 (red) was also used. (b) Repeated local NMDA applications induced reproducible Ca^{2+} responses (left: top and middle, fluo-4; 100 µM) and concomitant membrane depolarizations (bottom left) (n = 5 astrocytes in 5 slices from 4 rats), while 50 Hz stimulation of the trigeminal tract induced membrane depolarizations of astrocytes (bottom right, n = 5 cells in slices from 5 rats). Scale bars, 10 µm. (c) Depolarizations induced by local applications of NMDA under control conditions (top) and in presence of TTX (bottom) (1 µM) (n = 9 of 9 cells in 9 slices from 6 rats). (d) Depolarizations induced by local applications of NMDA (left, n = 5 cells in 5 slices from 5 rats) and stimulation of sensory afferents at 40 Hz (right, n = 3 cells in 3 slices from 2 rats) under control conditions (top) and in presence of a mix of drugs (bottom) blocking AMPA receptors (CNQX, 10 µM), glutamate uptake (PDC, 50 µM), Ca^{2+} channels (Cd^{2+}, 100 µM) and Na^{+} channels (TTX, 1 µM). (e) Histograms show the effects of the different blockers on the amplitude of the depolarizations elicited by NMDA (paired t-test; P = 0.002) or sensory fibers stimulation (paired t-test; P = 0.043). *P < 0.05. (f) Local applications of NMDA (1 mM) caused membrane depolarization in an astrocyte immediately after entering the cell with a pipette filled with the NMDA receptor antagonist MK-801 (left), but no longer did so after 15 min of diffusion of MK-801 (middle), while glutamate (1 mM), which was used to ensure viability of the cell, still elicited a robust response after 15 min of diffusion (right) (n = 11 cells in 9 slices from 6 rats).

2.3.4 Inactivation of astrocytes prevents neuronal bursting

Astrocytes are coupled through gap junctions and form syncytia, as shown by dye diffusion (Fig. 4a). Hence a Ca^{2+}-chelating agent introduced in one astrocyte by a patch pipette will diffuse to neighboring astrocytes (Serrano et al., 2006) and prevent astrocytic activity resulting from changes in cytosolic Ca^{2+}. Under control conditions, local application of NMDA induced widespread Ca^{2+} responses in cells loaded with a membrane-permeant Ca^{2+} indicator that were also positively labeled as astrocytes with SR101 (Fig. 4b). However, BAPTA introduced in a single astrocyte prevented Ca2+-dependent astrocytic activation of nearby astrocytes that were presumably coupled (Fig. 4c). Indeed, throughout 8 experiments with NMDA application per experiment, a total of 26 cells showed an intracellular Ca^{2+} increase in response to NMDA. Patching a single astrocyte in each experiment with a BAPTA-loaded electrode (20–35 mM) resulted in a loss of >75% of the original response to NMDA in 23 of the 26 cells.

Figure 2-4: NVsnpr astrocytes are coupled and can be inactivated by introduction of BAPTA to the syncytium.

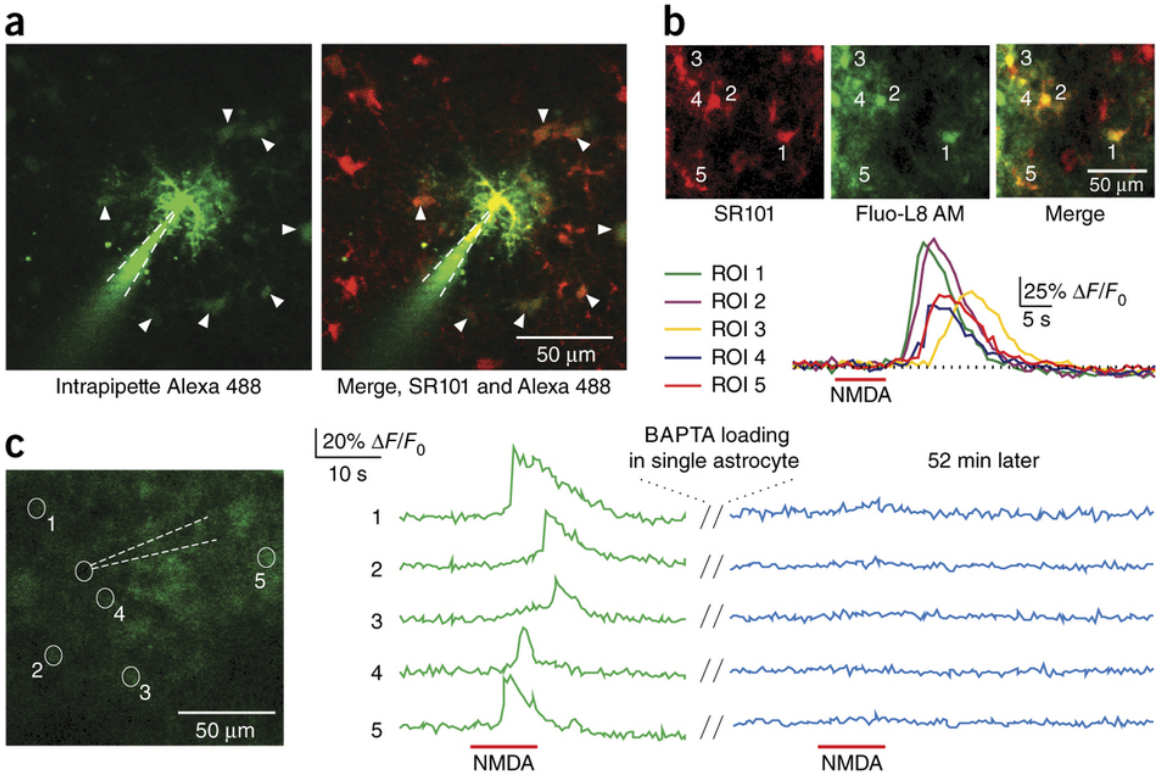

NVsnpr astrocytes are coupled and can be inactivated by introduction of BAPTA to the syncytium. (a) Coupling between astrocytes is revealed by diffusion of the tracer Alexa 488 (green; 100 µM) added to the internal solution of an electrode used to patch a single astrocyte and spreading to neighboring astrocytes (arrowheads) preloaded with SR101 (red) (double-labeled cells, right). (b) Single local NMDA application elicited Ca^{2+} responses in several astrocytes, as shown by the colocalization (merge) of the membrane-permeant indicator fluo-L8 AM (green) with SR101 (red) in the top panel. Bottom, Ca^{2+} responses in different astrocytes defined in regions of interest (ROI). (c) After incubation with fluo-L8 AM, several cells (circles and numbers, left) responded to a single NMDA application (green traces). Ca^{2+} responses to NMDA application were blocked in all cells after patching a single astrocyte with a BAPTA-filled (20 mM) pipette (blue traces). Mean intracellular Ca^{2+} increase before BAPTA, ΔF/F0 51.3 ± 4%; after BAPTA, 14.2 ± 3%; n = 26 cells, paired t-test; P = 1.082 × 10−7.

To test whether inactivation of the astrocytic syncytium interferes with neuronal bursting, we performed dual recordings of a neuron and an adjacent astrocyte and assessed the neuronal bursting ability when BAPTA was added in the electrode used to record from the astrocyte. In 19 such pairs, local application of NMDA in the first few minutes of recording depolarized both the astrocyte and the neuron and led to rhythmic bursting if the neuron had been hyperpolarized before the application (Fig. 5a,b). By contrast, in 16 of the 19 pairs, NMDA still depolarized neurons and astrocytes after diffusion of BAPTA in the syncytium but could no longer elicit rhythmic bursting (Fig. 5a–c), even when further hyperpolarization was imposed on the neuron. In the 3 remaining cases, NMDA applications still elicited bursting even after BAPTA diffusion in the syncytium. This apparent lack of effect may result from impaired network integrity in the slice preparation. It is noteworthy that repeated NMDA applications caused reproducible bursting in neurons and Ca^{2+} increases in astrocytes recorded under control conditions over extended periods of time (Fig. 5d). In 3 more pairs in which either a second neuron, another type of glial cell or a distant astrocyte was inadvertently patched and dialyzed with BAPTA, NMDA-induced neuronal bursting persisted even after up to 90 min of BAPTA diffusion. In 4 more paired recordings, dialysis of the astrocytes with a much lower concentration of BAPTA (0.1 mM) did not alter neuronal bursting for over 60 min (Supplementary Fig. 4a).

Figure 2-5: Inactivation of the astrocytic syncytium by diffusion of BAPTA impedes neuronal bursting.

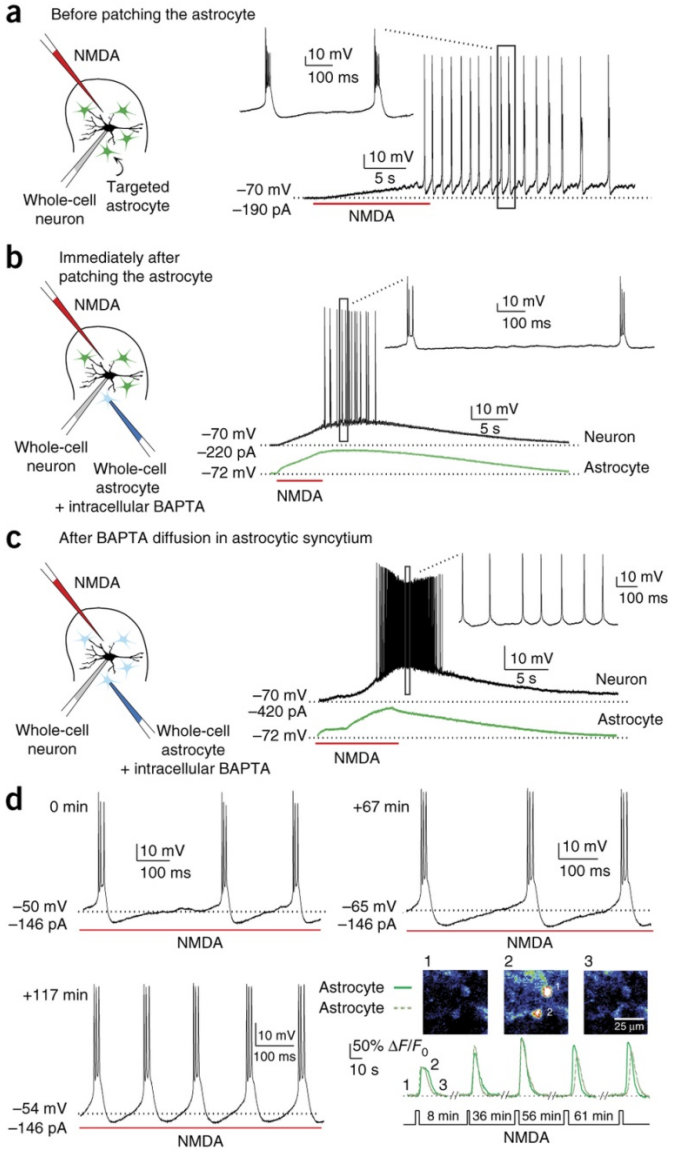

Inactivation of the astrocytic syncytium by diffusion of BAPTA impedes neuronal bursting. (a) Local NMDA application induced burst firing in an NVsnpr neuron before recording of an adjacent astrocyte with a BAPTA-filled pipette (20 mM). (b) NMDA applied immediately (<3 min) after entering the astrocyte with a BAPTA-filled electrode still elicited burst firing in the NVsnpr neuron (top), with a concomitant depolarization of the recorded astrocyte (green trace, bottom). (c) After diffusion of BAPTA in the astrocytic syncytium (>30 min), NMDA failed to elicit bursting, despite maintaining a depolarizing effect on the recorded neuron and astrocyte (n = 16 of 19 pairs in 19 slices from 19 rats). (d) In control conditions, rhythmic bursting could be elicited repetitively by NMDA applications in NVsnpr neurons recorded over long periods of time (here, 117 min). Similarly, calcium responses could be induced consistently in fluo-L8 AM–loaded astrocytes with repeated NMDA applications over long periods of time (bottom right). Calcium responses are shown in pseudocolor.

Knowing that astrocytes are important for bursting and that reduction of $[Ca^{2+}]_e$ facilitates I_{NaP}-mediated bursting, we postulated that artificially reducing $[Ca^{2+}]_e$ should occlude the effect of BAPTA diffusion in the astrocytic syncytium. Indeed, in 3 pairs recorded in Ca^{2+}-free aCSF, neuronal bursting persisted after letting BAPTA (20 mM) diffuse in the astrocytic syncytium for more than 1 h (Supplementary Fig. 4b).

2.3.5 S100β induces bursting, reduces $[Ca^{2+}]_e$ and enhances I_{NaP}

We next investigated the mechanisms by which astrocytes could alter $[Ca^{2+}]_e$. The astrocytic protein S100β is a prime candidate owing to its glial specificity, its established Ca^{2+}-binding properties and its secretion by astrocytes (Ciccarelli et al., 1999, Sakatani et al., 2008). As expected, immunostaining with an antibody directed against S100β revealed numerous immunoreactive astrocytes in dorsal NVsnpr (Supplementary Fig. 5; n = 2 animals). To assess the effects of this protein, we first synthesized it using a recombinant approach and tested its binding to Ca^{2+} with isothermal titration calorimetry (ITC). A clear endothermic binding of calcium to this S100β was observed with an apparent dissociation constant (Kd) of 25 µM and a stoichiometry of two calcium molecules for each molecule of protein, indicating that the synthesized S100β adopts its calcium-bound form (Supplementary Fig. 6a).

To test the effects of S100β on neuronal firing and on $[Ca^{2+}]_e$, we suspended the synthesized protein in a 20 mM HEPES buffer containing 140 mM NaCl and applied it locally at 129 µM in the submerged recording chamber and 50 µM in the interface chamber. In this initial set of experiments, the buffer used to suspend S100β was devoid of Ca^{2+} to prevent saturation of the protein and preserve its Ca^{2+}-binding ability. Consistent with this ability, we found that S100β applied locally in submerged preparations (bathed in aCSF containing 1.6 mM Ca^{2+}) caused large decreases in $[Ca^{2+}]_e$ as measured with ion-sensitive electrodes (reduction of 1.0 ± 0.1 mM, n = 15, Fig. 6a,b). As with BAPTA and NMDA, local extracellular applications of S100β caused neurons recorded in both interface and submerged chambers to change their firing pattern from tonic to rhythmic bursting (n = 62 of 76; Fig. 6a). Dual recordings of intracellular activity and $[Ca^{2+}]_e$ with ion-sensitive electrodes revealed that the transition from tonic to bursting firing appeared gradually and paralleled the Ca^{2+} decrease (Fig. 6a,b, n = 5). Doublet firing (shown in Supplementary Fig. 1 and described in Online Methods) appeared,

intermingled with single spikes, at a $[Ca^{2+}]_e$ of 0.9 ± 0.27 mM. At higher concentrations, only tonic firing (single spikes) was observed, and at a $[Ca^{2+}]_e$ of 0.69 ± 0.19 mM, only doublets were observed. Bursts (plateaus with three or more spikes) mingled with doublets appeared at a $[Ca^{2+}]_e$ of 0.54 ± 0.16 mM, and only bursts were seen at a $[Ca^{2+}]_e$ of 0.4 ± 0.13 mM and less. Notably, the frequency of the S100β-induced bursting was similar to that of bursting obtained following sensory fibers stimulation when tested in the interface chamber (7.47 ± 0.54 Hz versus 8.56 ± 1.03 Hz, respectively), as well as to that of NMDA-induced bursting when tested in submerged preparations (3.54 ± 0.53 versus 3.48 ± 0.71 for S100β versus NMDA, respectively; Supplementary Table 1).

Figure 2-6: The astrocytic Ca^{2+} binding protein S100β causes $[Ca^{2+}]_e$ decreases and induces I_{NaP}-dependent bursting.

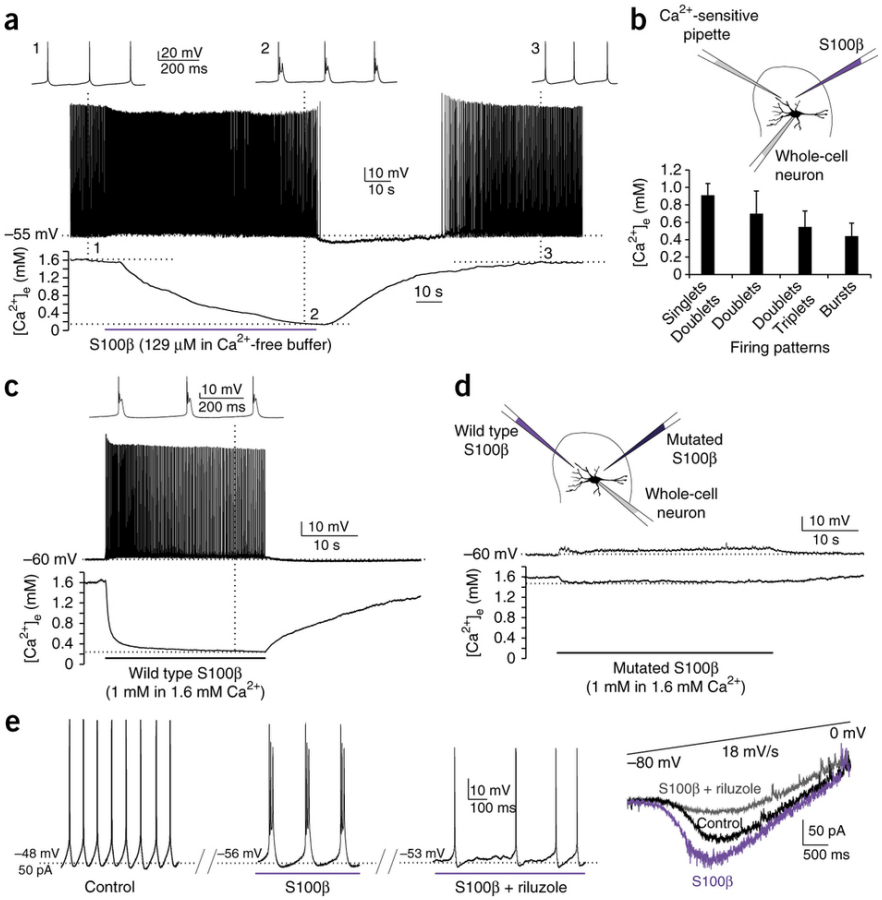

The astrocytic Ca^{2+} binding protein S100β causes $[Ca^{2+}]_e$ decreases and induces I_{NaP}-dependent bursting. (a) Local application of S100β (129 μM in Ca^{2+}-free buffer) near an NVsnpr neuron (left) in a submerged preparation causes a transient decreases of $[Ca^{2+}]_e$ (n = 15 $[Ca^{2+}]e$ recording locations in 8 slices from 8 rats) and rhythmic bursting in an adjacent neuron (n = 62 of 76 cells in 66 slices from 57 rats). Insets (1, 2 and 3) show the firing pattern of the neuron on a larger time scale at the corresponding times on the $[Ca^{2+}]_e$ trace. (b) Histograms showing changes in firing pattern with $[Ca^{2+}]_e$ (n = 5 cells in 5 slices from 5 rats). (c) Similar effects on firing (n = 10 of 10 cells) and $[Ca^{2+}]_e$ (n = 8 recording locations) were elicited by local application of a wild-type S100β suspended in a solution containing 1.6 mM Ca^{2+}, but only if the concentration of the protein was raised to 1 mM to avoid its saturation (4 slices from 4 rats). (d) Local application of a recombinant S100β (1 mM in a buffer containing 1.6 mM Ca^{2+}) with two residues mutated to prevent Ca^{2+} binding had no effect on firing and caused only marginal changes in $[Ca^{2+}]_e$ (n = 7 cells and 7 adjacent $[Ca^{2+}]_e$ recording locations in 2 slices from 2 rats). (e) The S100β-induced bursting (middle) was abolished in the presence of the I_{NaP} blocker riluzole (20 μM, right, n = 11 of 14 cells in 14 slices from 11 rats). Left, voltage clamp recordings of a pharmacologically isolated inward current induced by a voltage ramp from −80 to 0 mV (top trace). The inward current elicited under control conditions (black) was increased by local application of S100β (purple; n = 7 cells in 7 slices from 5 rats; control, 88 ± 26 pA versus S100β, 135 ± 41 pA; paired t-test; P = 0.021) and blocked by riluzole (20 μM; gray, n = 3 cells in 3 slices from 2 rats).

S100β can have multiple effects, but the above results suggest that it promotes neuronal bursting by lowering $[Ca^{2+}]_e$. A series of experiments was undertaken to verify this and to determine whether the Ca^{2+}-free solution in which it was suspended had any effects on its own. First, local applications of the Ca^{2+}-free buffer alone caused a small decrease of $[Ca^{2+}]_e$ (0.55 ± 0.09 mM; n = 6; Supplementary Fig. 7a), but it did not alter the neuronal firing pattern in extracellular recordings in the interface chamber (n = 11; Supplementary Fig. 7b) and in intracellular recordings in the submerged configuration (n = 3; Supplementary Fig. 7c). Second, saturating the Ca^{2+}-binding activity of S100β by increasing to 2.6 mM the $[Ca^{2+}]$ in the circulating aCSF prevented induction of bursting by local applications of the protein suspended in Ca^{2+}-free solution (n = 4; Supplementary Fig. 7d). Similarly, S100β suspended in a buffer containing 1.6 mM Ca^{2+} had no effects on firing at the concentration used throughout the study (129 μM; n = 5; Supplementary Fig. 7e), and, as expected, the buffer alone containing 1.6 mM Ca^{2+} had no effect by itself on neuronal firing (n = 3 in 2 slices from 2 rats) and on $[Ca^{2+}]_e$ (n = 4 in 2 slices from 2 rats; data not shown). However, raising the concentration of the protein to 1 mM to overcome its saturation in the Ca^{2+}-containing buffer restored its effects on neuronal firing and on $[Ca^{2+}]_e$. Local applications of this solution containing 1 mM of S100β suspended in a buffer containing 1.6 mM $[Ca^{2+}]$ induced bursting in all 10 cells tested in the submerged configuration (Supplementary Fig. 7e) and caused large decreases in $[Ca^{2+}]_e$ (reduction of 1.27 ± 0.05 mM, n = 8 applications; Fig. 6c). Finally, to ensure that these effects of S100β could be attributed to its Ca^{2+}-binding ability, we tested the effects of an S100β protein with two mutated residues that obliterated its Ca^{2+} binding (Markowitz et al., 2005). Local applications of a solution containing 1 mM of this mutated protein suspended in a 20 mM HEPES buffer containing 140 mM NaCl and 1.6 mM $CaCl_2$, had no effect on the neuronal firing pattern of the 7 cells recorded in the submerged configuration and caused only a marginal decrease of $[Ca^{2+}]_e$ (0.15 ± 0.02 mM; n = 7; Fig. 6d). These data provide very strong evidence that the effects of S100β on neuronal firing pattern result from its ability to bind Ca^{2+} and to decrease $[Ca^{2+}]_e$, which in turn enhances I_{NaP} and favors bursting. In all of the following experiments, S100β was used at the lower concentration (129 μM) in the submerged chamber and was suspended in the Ca^{2+}-free buffer.

We used riluzole to ascertain that the S100β-induced bursting involved I_{NaP}. Blockade of I_{NaP} channels with riluzole indeed prevented bursting induced by local application of S100β (Fig. 6e; n = 7 of 10 and 4 of 4 in interface and submerged preparations, respectively). In 3 cases, riluzole did not block the S100β-induced bursting, probably because of ineffective drug perfusion in the brain tissue, as these instances occurred only in the interface recording conditions.

To further assess whether the burst-inducing action of S100β could result from a modulation of I_{NaP}, we examined its effects on the pharmacologically isolated I_{NaP} current in voltage clamp experiments. As was the case for extracellular BAPTA, locally applied S100β (129 μM) significantly increased the peak amplitude of the isolated $I_{NaP,}$ by 55 ± 11% (n = 7; Fig. 6e and Supplementary Fig. 2b), and shifted the potential at which it occurred by 4%, or 2 mV (−44.7 ± 1.3 mV for controls versus −46.6 ± 1.9 mV for S100β). Again, the inward current induced by S100β was blocked with bath application of riluzole (20 μM; n = 3) or TTX (1–2 μM; n = 2 cells in 2 slices from 2 rats). The characteristics of this current assessed by fitting a Boltzmann function gave values between those obtained in controls and those obtained under BAPTA (Supplementary Fig. 2d).

If changes in neuronal firing and $[Ca^{2+}]_e$ induced by NMDA and sensory fibers stimulation depend on S100β, and if S100β release is downstream of NMDA and/or other glutamatergic receptors activation, then blocking Ca^{2+} responses in astrocytes with BAPTA should prevent NMDA-induced but not S100β-induced bursting. Indeed, in paired recordings of neurons and adjacent astrocytes with BAPTA in the electrode used for the astrocyte, either local applications of NMDA or of S100β induced rhythmic bursting in the first few minutes (Fig. 7a). NMDA-induced bursting was gradually blocked by diffusion of BAPTA in the astrocytic syncytium, whereas S100β-induced bursting persisted unaltered for as long as the cell was recorded (20–80 min after blockade of NMDA-induced bursting, n = 5 of 5; Fig. 7b).

Figure 2-7: S100β-induced bursting persists after inactivation of the astrocytic syncytium with BAPTA.

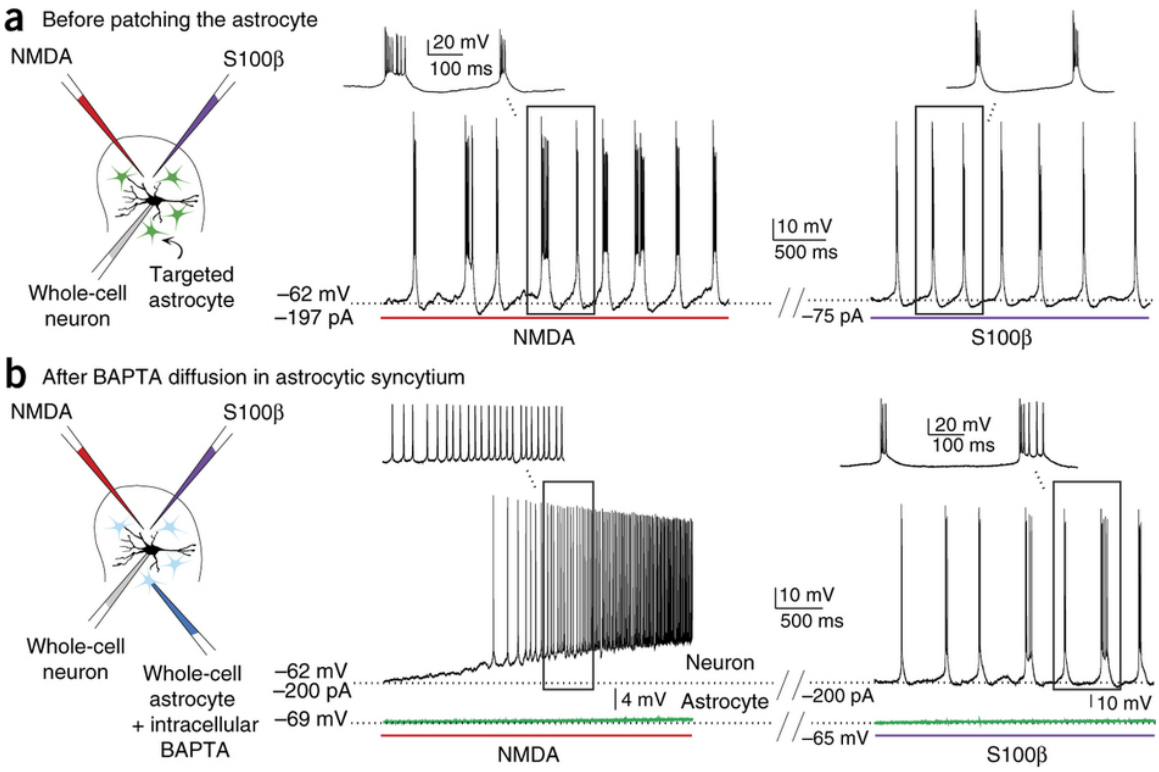

S100β-induced bursting persists after inactivation of the astrocytic syncytium with BAPTA. (a) Exogenously applied NMDA and S100β both induced burst firing in an NVsnpr neuron before dialysis of an adjacent astrocyte with BAPTA. (b) After BAPTA diffusion in the astrocytic syncytium, NMDA applied to the same neuron had a clear excitatory effect but no longer elicited rhythmic bursting (left), whereas S100β could still induce bursting (right) (n = 5 of 5 pairs in 5 slices from 5 rats).

2.3.6 Blockade of S100β prevents bursting induced by sensory fiber stimulation or NMDA

The above data suggest that S100β can still elicit bursting after inactivation of the astrocytic syncytium but do not prove that S100β is required for bursting. We therefore tested whether blocking extracellular S100β activity with a local application of an S100β-subunit monoclonal antibody (40–80 μg/ml)24 would prevent bursting induced by NMDA applications or sensory fiber stimulation. To insure that the antibody did interfere with the Ca^{2+}-binding ability of S100β, we used ITC. Indeed, no difference in the generated heat was observed when Ca^{2+} was added to S100β in the presence of the anti-S100β monoclonal antibody, indicating that binding of the antibody to S100β inhibited calcium binding (Supplementary Fig. 6b). In 4 of 4 slices examined in the interface chamber, pretreatment with this antibody before stimulation of the sensory fibers prevented neuronal bursting and $[Ca^{2+}]_e$ decreases measured with ion-sensitive electrodes (Fig. 8a). In 2 other cases, similar pretreatment with a nonspecific antibody (donkey anti–sheep IgG) did not prevent the Ca^{2+} decrease, nor the accompanying neuronal bursting (Fig. 8b) induced by sensory fibers stimulation. In 9 of 11 cells recorded in submerged slices, rhythmic bursting induced by NMDA was totally (n = 7; Fig. 8c) or partially (n = 2) blocked by treatment with the anti-S100β antibody. In the 2 cases considered partially blocked, NMDA applications elicited a few irregular bursts with a much shorter duration when compared to those elicited before application of the antibody. Use of the nonspecific antibody did not prevent bursting induced by NMDA in 5 of 5 cases (Fig. 8d). These data strongly suggest that sensory fibers stimulation and NMDA-induced neuronal bursting depend on the presence of S100β in the extracellular space and its capacity to bind Ca^{2+}.

Figure 2-8: The presence of S100β in the extracellular space is required for bursting to occur in NVsnpr.

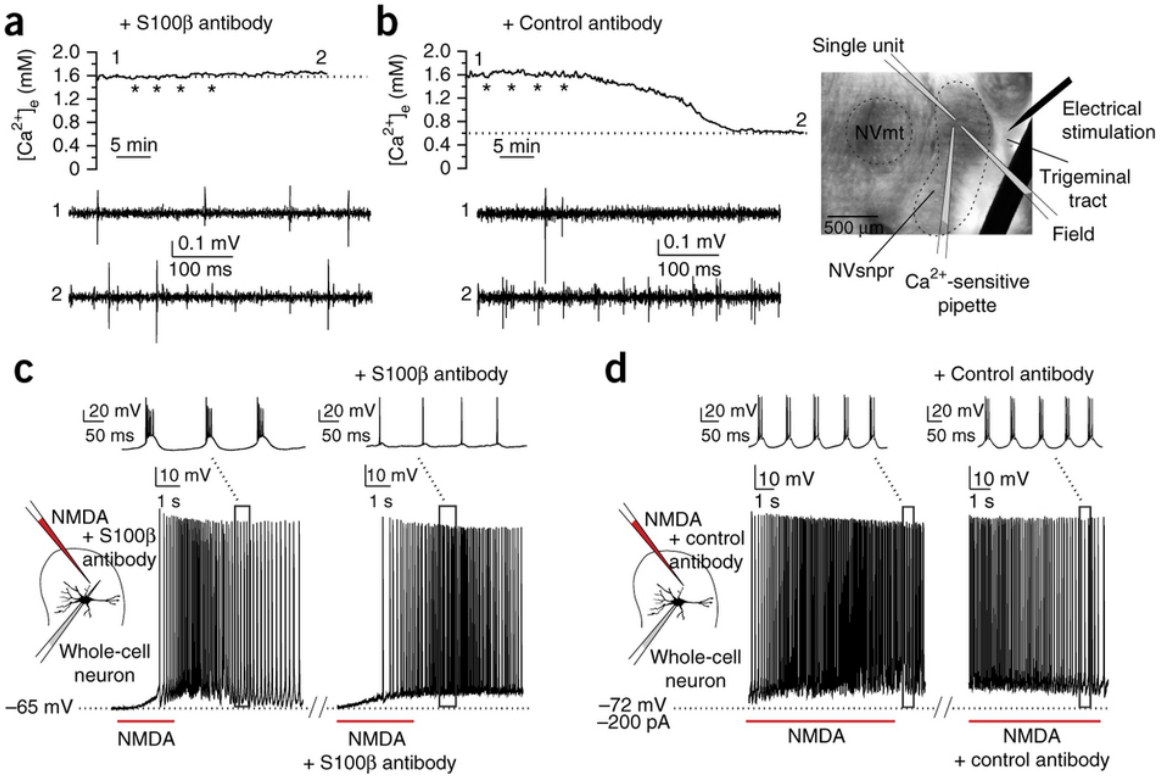

The presence of S100β in the extracellular space is required for bursting to occur in NVsnpr. (a) Inhibiting extracellular endogenous S100β activity with S100β antibody prevented the $[Ca^{2+}]_e$ decrease (top) following repetitive electrical stimulation (4 trains (*); 40 Hz, 1 s) of the trigeminal tract (n = 4 cells and 4 adjacent $[Ca^{2+}]_e$ recording locations in 4 slices from 3 rats). Bottom: in the same preparation, the tonic firing pattern of a spontaneously active neuron (1), recorded near the Ca^{2+}-sensitive electrode, was unaltered by the stimulation in presence of the antibody (2). 1 and 2 are recordings of the neuronal activity at times corresponding to 1 and 2 on the $[Ca^{2+}]$ record above. (b) Local application of an unrelated antibody (directed against sheep IgG) did not prevent the $[Ca^{2+}]_e$ decrease (top) and switch to burst firing (bottom) induced by repetitive stimulation of the trigeminal tract (*, 1-s trains at 40 Hz) (n = 2 cells and 2 adjacent $[Ca^{2+}]_e$ recording locations in 2 slices from 2 rats). (c) Similarly, in an NVsnpr neuron, NMDA-induced burst firing (left) was blocked by local application of anti-S100β antibody (40 µg/ml), resulting in tonic increase of firing without bursting (right) (n = 11 cells in 11 slices from 10 rats). (d) NMDA-induced rhythmic bursting (left) was unaltered by local application of the antibody against sheep IgG (n = 5 of 5 cells in 5 slices from 4 rats).

2.4 Discussion

The results presented here uncover a new mechanism for rhythmogenesis that depends on proper functioning of the astrocytes. The key element of this mechanism is regulation of I_{NaP}, the ionic conductance driving neuronal rhythmic burst firing, by decreases of $[Ca^{2+}]_e$. Changes in $[Ca^{2+}]_e$ follow stimulation of afferent inputs to NVsnpr neurons and result from activation of astrocytes and presumed subsequent release of the Ca^{2+}-binding protein S100β, which is required for bursting and $[Ca^{2+}]_e$ decreases to occur.

2.4.1 Physiological induction of $[Ca^{2+}]_e$ decreases and their implications for I_{NaP}-mediated bursting

Given the widespread importance of calcium signaling in numerous intracellular processes, studies have focused mainly on its regulation in the intracellular compartment. However, the imposition of artificial fluctuations in $[Ca^{2+}]_e$ in a variety of preparations have revealed marked effects of this ion on neuronal excitability. In an attempt to determine whether large changes in $[Ca^{2+}]_e$ can be expected to occur in the brain, Egelman and Montague (Egelman and Montague, 1999), using a computational approach, concluded that large external Ca^{2+} fluctuations, leading to up to 100% depletion in many cases, must occur. Indeed, reductions in $[Ca^{2+}]_e$ have been reported to occur in parallel with $[K^+]_e$ increases during intense neuronal activity associated with seizures (Massimini and Amzica, 2001) or spreading depression (Lian and Stringer, 2004), or with activity induced by massive electrical or pharmacological activation of the locomotor CPG (Brocard et al., 2013) or electrical stimulation of the cerebellar cortex (Nicholson et al., 1977). The $[Ca^{2+}]_e$ decreases reported in the above studies range between 0.1 mM and 0.7 mM and are of smaller magnitude than those reported here following stimulation of the trigeminal tract at a frequency close to the natural firing frequency of intra-oral afferents during mastication (Trulsson and Johansson, 2002). The difference in the measured $[Ca^{2+}]_e$ drops may result from various factors, including the age of the animal, the baseline $[Ca^{2+}]_e$ used and the positioning of the ion-sensitive electrode in relation to the location where the $[Ca^{2+}]_e$ drops occur.

How $[Ca^{2+}]_e$ drops affect bursting is not exactly known. Ca^{2+}-free perfusate has often been used to assess the role of synaptic transmission in various functions, and in many preparations this procedure leads to the appearance of spontaneous burst discharges (Jefferys and Haas, 1982, Del Negro et al., 2002). Although a link between this bursting and I_{NaP} had been described in supraoptic neurons (Li and Hatton, 1996) and in hippocampus (Su et al., 2001), it was established in CPGs only recently by us in the masticatory system (Brocard et al., 2006) and later by others in the locomotor CPG (Tazerart et al., 2008, Brocard et al., 2013). This link is also likely to exist in at least part of the respiratory CPG, as low-Ca^{2+} perfusate is routinely used to obtain spontaneous bursting in *in vitro* preparations, including those of the pre-Bötzinger complex, where I_{NaP} is responsible for intrinsic bursting (Del Negro et al., 2002). However, the fact that I_{NaP}-mediated bursting is facilitated under low-Ca^{2+} conditions does not preclude the possibility that it may occur under physiological Ca^{2+} conditions as well. Indeed, our data from the sensory fiber stimulation suggest that neuronal activity can also produce Ca^{2+} decreases and I_{NaP} dependent bursting.

The interaction between Ca^{2+} and I_{NaP} is not fully understood, but work in the squid giant axon suggests that Ca^{2+} can occupy the pore of the sodium channel to favor its closing. In the absence of Ca^{2+}, closing slows or does not occur. The voltage sensitivity of closing kinetics also change with Ca^{2+} concentration and seem to depend in part on the ability of Ca^{2+} to enter and block the channels as voltage is driven negative[31]. This may partly explain why hyperpolarization was required to induce bursting when using NMDA. On one hand, hyperpolarization was required to keep the cells membrane potential within the I_{NaP} activation range by counteracting the depolarization induced by NMDA. On the other, it may have helped relieve the Ca^{2+} block of the Na^+ channel. In neurons of the supraoptic nucleus, removal of external Ca^{2+} shifts the I_{NaP} activation threshold by ~13 mV towards more hyperpolarized potentials (Li and Hatton, 1996), while in Hb9 neurons of the locomotor CPG, every 0.1 mM decrease of Ca^{2+} shifts the I_{NaP} activation threshold and half-activation voltage by ~1 mV towards more hyperpolarized potentials; in both cases, I_{NaP} amplitude increases substantially (Brocard et al., 2013). This is in line with our data, wherein local applications of BAPTA and S100β, which both decrease $[Ca^{2+}]_e$, shifted the activation and half-activation voltage of I_{NaP} towards more hyperpolarized potentials. According to predictions based on a

computational model of Hb9 cells, a slight shift of I_{NaP} activation would suffice to cause tonically firing neurons to burst rhythmically (Brocard et al., 2013). Here we found that bursting did not occur as long as $[Ca^{2+}]_e$ did not drop beneath 0.4 mM. Brocard *et al*. (Brocard et al., 2013) were able to induce bursting in the locomotor CPG at a $[Ca^{2+}]_e$ of 0.9 mM, but only if $[K^+]$ was artificially raised to 6 mM. However, I_{NaP} currents were not upregulated by the increase of $[K^+]_e$. As suggested by Brocard *et al*. (Brocard et al., 2013) and previous work from Rybak *et al*. (Rybak et al., 2003), the facilitation seen with increased $[K^+]_e$ probably results from a change in the potassium equilibrium potential (E_K) that diminishes or suppresses a delayed-rectifier potassium current. Also, we cannot discard regional or age-related differences in I_{NaP} characteristics. Indeed, the mean peak amplitude that we observed was larger and occurred at more hyperpolarized potentials than those previously reported in NVsnpr neurons of younger animals (postnatal days 8–12) (Tsuruyama et al., 2013).

2.4.2 Function of astrocytes in regulating $[Ca^{2+}]_e$

Our data suggest that, in addition to activating NVsnpr neurons, stimulation of sensory afferents at a frequency close to their natural firing frequency (Trulsson and Johansson, 2002) also activates astrocytes. Astrocytes have been shown to detect neurotransmitters release induced by basal (Panatier et al., 2011) as well as intense neuronal activity (Pasti et al., 1997) and to respond by releasing gliotransmitters, modulating neuronal activity in return. Here we show that NVsnpr astrocytes have functional NMDA receptors that enable them to respond to the glutamate released by afferent fibers. Astrocytes in other brain regions have also been reported to have functional NMDA receptors (Lee et al., 2010). Locally applied NMDA may act on neuronal NMDA receptors and/or on these astrocytic NMDA receptors, causing release of other factors that may mediate burst induction. Rhythmic bursting induced by NMDA has traditionally been ascribed to the biphasic current-voltage (*I-V*) relationship of the current mediated by neuronal NMDA receptors (Sigvardt et al., 1985, Kim and Chandler, 1995). However, although we cannot rule out involvement of all neuronal NMDA receptors, our observations suggest that NMDA receptors of the recorded neuron itself are unlikely to play a significant role, as neuronal NMDA receptors are normally blocked in hyperpolarized states and are mostly permeable to Ca^{2+}. The findings that hyperpolarization was required for burst

induction and that the NMDA-induced bursting was insensitive to intraneuronal diffusion of BAPTA suggest that NMDA receptors located elsewhere than on the recorded neuron are likely to be involved in the observed bursting.

We postulate that activation of astrocytes through their NMDA receptors and/or other glutamatergic receptors leads to $[Ca^{2+}]_e$ decreases because (i) the astrocytic syncytium must be functional and (ii) $[Ca^{2+}]_e$ must decrease for bursting to occur. Modulation of $[Ca^{2+}]_e$ by astrocytes has often been postulated, but never demonstrated. The fact that exogenous applications of a Ca^{2+}-binding protein released by astrocytes, S100β (Ciccarelli et al., 1999, Sakatani et al., 2008), decreased Ca^{2+} and induced bursting even after inactivation of the astrocytic syncytium with BAPTA is a clear indication, but not proof, that astrocytes act by releasing S100β. However, the fact that blockade of this protein with a specific antibody prevents $[Ca^{2+}]_e$ decreases and bursting induced with sensory fibers stimulation and NMDA applications is strong evidence that S100β is required for bursting to occur. Furthermore, the secretion of S100β from astrocytes has been reported to be stimulated by glutamate receptors activation as well as by intracellular calcium increase (Donato et al., 2009), two conditions that are met in our experiments.

Surprisingly, despite its well-established Ca^{2+}-binding property, previous studies that have focused on S100β extracellular actions have not addressed a possible regulatory function of local extracellular Ca^{2+} concentration. Intracellularly, S100β carries out many regulatory activities through Ca^{2+}-dependent interactions with the cytoskeleton and with several cytoplasmic proteins involved in cell differentiation, proliferation and survival (for review, see Donato et al., 2009). Once released in the extracellular compartment, S100β carries out many actions via activation of RAGE (receptor for advanced glycation end products, Donato et al., 2009). We cannot rule out the possibility that these other effects of S100β are important, but we can affirm that its effects on extracellular Ca^{2+} are required for bursting. Indeed, S100β loses its ability to alter neuronal firing once mutated at its Ca^{2+}-binding sites, and inactivation of astrocytes with BAPTA in the Ca^{2+}-free condition did not alter bursting. This latter finding also suggests that no other gliotransmitters that may be released from astrocytes in a Ca^{2+}-dependent manner are required for bursting. In particular, our data argue strongly that ATP, a

well-known gliotransmitter, is not likely to be involved owing to the lack of effect on neuronal bursting of suramine, a broad antagonist of purinergic receptors.

2.4.3 Functional significance: switch of neuronal function in territories defined by glial syncytia

On the basis of these results, we propose a model whereby sustained synaptic inputs to NVsnpr arriving at a physiologically relevant frequency (40–60 Hz) initiate rhythmogenesis by activating both neurons and astrocytes (Supplementary Fig. 8). Sporadic or low-frequency firing of the inputs is insufficient to activate the astrocytes. Under this condition, the circuit operates in a conventional sensory relay mode wherein the output is linearly related to the input (Supplementary Fig. 8). With more sustained activity at higher frequency, astrocytes are activated, couple to form a syncytium and release S100β. The extent of the syncytium would define a territory (Supplementary Fig. 8) within which the confined neurons will be exposed to the same decrease in $[Ca^{2+}]_e$ and, therefore, have the same conditions of activation or inactivation of I_{NaP} channels. The terminals of inputs to NVsnpr are highly organized (Capra and Dessem, 1992) and are likely to activate adjacent neurons and astrocytes. Firing of these inputs could therefore act as a common trigger to initiate rhythmic activity in a given population of neurons, which will be synchronized because they are surrounded by the same astrocytic syncytium. The population of rhythmogenic neurons could vary constantly and in an adaptive manner according to the pattern of incoming inputs. Notably, NVsnpr neurons also receive glutamatergic projections from the cortical masticatory area, known to be important for initiation of the movements and the first few cycles of a masticatory sequence (Yamamura et al., 2002). Stimulation of this area elicits mastication *in vivo*, but only when trains of stimuli are delivered at frequencies between 20 and 100 Hz and optimally around 40–50 Hz (Lund and Dellow, 1971). Thus, NVsnpr neurons could be considered an interface converting sensory and/or cortical inputs into rhythmic motor commands when astrocytes are activated by increased or coincident activity of these inputs. A similar role was assigned to the lamprey reticulospinal cells receiving sensory inputs from the trigeminal system (Di Prisco et al., 1997). This dual function of NVsnpr neurons is in line with their projections to the thalamus (sensory relay mode) and to brainstem motor neurons and premotor interneurons, on one hand,

and with their two firing modes on the other. Interestingly, the bursting frequency of NVsnpr neurons reported during fictive mastication in rabbit (~3 Hz) (Tsuboi et al., 2003) corresponds to the chewing frequency in that species. Similarly, the frequency of bursting elicited here in the interface chamber, whether by sensory stimulation, NMDA or S100β, corresponds to the chewing frequency observed *in vivo* in rats (Westneat and Hall, 1992). In submerged preparations, the bursting frequency was slower, but this probably results from differences in temperature between the two recording conditions (room temperature for submerged versus 30–32 °C for interface).

2.4.4 Implications for health and pathology

Astrocytes have many important functions, including at least one in a rhythmic circuit, the respiratory CPG, where they alter the inspiratory rhythm by releasing ATP (Gourine et al., 2010) in response to a change in pH. However, in this case, the mechanism involved is pH dependent and seems specific to the ventral brainstem respiratory area (Kasymov et al., 2013), whereas the mechanism of action reported here may be of a much broader relevance given the widespread distribution of both S100β and I_{NaP} (refs. (Li and Hatton, 1996, Su et al., 2001, Del Negro et al., 2002, Brocard et al., 2006, Tazerart et al., 2008, Harris-Warrick, 2010, Brocard et al., 2013).

Regulation of I_{NaP}-mediated bursting by astrocytes may help explain the appearance of bursting in normal and pathological conditions, such as epileptic seizures, where astrocytes are overactivated (Gomez-Gonzalo et al., 2010). Generation and propagation of seizures are generally attributed to spread of activity in excitatory feedback circuits. However, surprisingly, *in situ* measurements with ion-selective electrodes show that during seizures, $[Ca^{2+}]_e$ drops to levels incompatible with chemical synaptic transmission (Pumain et al., 1985). Our results may help explain this paradoxical finding and could explain how bursting activity is maintained in the absence of chemical synaptic transmission. These findings could help develop new targets and strategies for the treatment of these conditions.

2.5 Methods

2.5.1 Brainstem slice preparations.

All procedures abided by the Canadian Institutes of Health Research rules and were approved by the University of Montreal Animal Care and Use Committee. Experiments were conducted on 15- to 21-day-old Sprague-Dawley rats anesthetized with isoflurane (Pharmaceutical Partners of Canada Inc., Richmond Hill, Ontario, Canada) before decapitation. Their brain was quickly removed from the cranium and dipped in an ice-cold sucrose-based solution consisting of (in mM) 3 KCl, 1.25 KH_2PO_4, 4 $MgSO_4$, 26 $NaHCO_3$, 10 dextrose, 0.2 $CaCl_2$, 219 sucrose bubbled with a mix of 95% O_2 and 5% CO_2, pH 7.3–7.4, 300–320 mosmol/kg. Transverse slices (300–400 μm thick) of the trigeminal main sensory nucleus (NVsnpr) were prepared in the same medium with a vibratome (Leica, model VT 100S). Slices were then stored and allowed to rest for an hour in a holding chamber filled with artificial cerebrospinal fluid (aCSF) at room temperature (95% O_2 + 5% CO_2). The aCSF consisted of (in mM) 124 NaCl, 3 KCl, 1.25 KH_2PO_4, 1.3 $MgSO_4$, 26 $NaHCO_3$, 10 dextrose and 1.6 $CaCl_2$, pH 7.3–7.4, 290–300 mosmol/kg. This composition of aCSF was used in all experiments throughout the study, except in experiments conducted to isolate I_{NaP} in voltage clamp (see below) and experiments where the $CaCl_2$ was either increased to 2.6 mM or omitted and replaced by $MgCl_2$ (1.6 mM). The experiments where such manipulations of the $[Ca^{2+}]$ were used are noted in the Results.

2.5.2 Electrophysiological recordings.

Interface configuration. For experiments done in the interface chamber configuration, 400-μm-thick slices were kept at 30–32 °C at the interface between a warm humidified atmosphere of 95% O_2/5% CO_2 and aCSF. NVsnpr was identified under 4× magnification and extracellular field potential recording electrodes as well as calcium-sensitive electrodes (see details below) were placed in the dorsal part of the nucleus and connected through their own amplifiers to a Micro 1401 mk II acquisition unit (Cambridge Electronic Design, Cambridge, UK). All electrodes, except for the calcium-sensitive one, were filled with NaCl (0.5 M). An Isostim stimulator (model A320; WPI, Sarasota, FL, USA) and tungsten (unipolar) or

nichrome (bipolar) electrodes were used to electrically stimulate (40–60 Hz) the sensory fibers in the trigeminal tract projecting to NVsnpr.

Submerged configuration. Whole cell experiments and calcium imaging recordings were conducted at room temperature in an immersion chamber using slices 300–350 μm thick. Neurons and astrocytes were visualized with an infrared-sensitive CCD camera and displayed on a video monitor. The camera was mounted on an Olympus FluoView FV 1000 confocal microscope equipped with a 40× water-immersion objective. Whole-cell recordings were performed in the current clamp mode or in the voltage clamp mode (see below) using a computer-controlled Multiclamp 700A amplifier and a Digidata 1322A digitizer (Axon Instruments, Downingtown, PA, USA). The apparatus was equipped with two headstages, allowing recordings of pairs of cells. Patch pipettes were pulled from borosilicate glass capillaries (1.5 mm OD, 1.12 mm ID; World Precision Instruments, Sarasota, FL) on a Sutter P-97 puller (Sutter Instruments, Novato, CA). Electrodes for neuronal recordings (resistance 7–10 MΩ) were filled with (in mM) 140 potassium gluconate, 5 NaCl, 2 $MgCl_2$, 10 HEPES, 0.5 EGTA, 2 Tris ATP salt, 0.4 Tris GTP salt, pH 7.2–7.3, 280–300 mosmol/kg. After the establishment of a gigaseal, the pipette resistance and capacitance were compensated electronically. Neurons were monitored throughout experiments to assess their viability and were discarded when action potentials did not overshoot 0 mV or when the resting membrane potential was depolarized (≥ –45 mV). Electrodes for astrocyte recordings (resistance 5–7 MΩ) were filled with (in mM) 125 KCH_3SO_4, 10 HEPES, 4 $MgCl_2$, 4 ATP, 0.4 GTP, 10 disodium creatine phosphate and 0.1 Alexa Fluor 488, pH 7.2–7.3, 295–300 mosmol/kg. For imaging experiments in single astrocytes, the Ca^{2+} indicator fluo-4 (100 μM) (Invitrogen) was added to the internal solution and Alexa Fluor 488 was omitted. Astrocytes were identified on the basis of their small size (~10 μm) and characteristic morphology of a round soma surrounded by many processes. In some experiments, sulforhodamine 101 (SR101, 1 μM) was used as a specific marker of astrocytes following the procedure of Kafitz *et al*. (Kafitz et al., 2008). Astrocytes were also systematically characterized by performing a whole-cell current–voltage profile with a ramp voltage command from −130 to 110 mV (586 ms duration) and also injection of step current to confirm their characteristic passive membrane. Astrocytes with resting membrane potentials more depolarized than −60 mV were rejected. In some

experiments, (1,2-bis(o-aminophenoxy)ethane-*N*,*N*,*N*′,*N*′-tetraacetic acid (BAPTA) tetrapotassium salt, 0.1 or 10–35 mM) was added to the internal solution and KCH_3SO_4 or potassium gluconate concentration was adjusted accordingly to maintain potassium ion concentration.

Voltage-clamp experiments. Whole-cell voltage clamp recordings were conducted in presence of several blockers to assess the effects Ca^{2+}, extracellular BAPTA and S100β on pharmacologically isolated Na^+ currents. The modified aCSF used contained (in mM) 131 NaCl, 10 HEPES, 3 KCl, 10 glucose, 2 $CaCl_2$, 2 $MgCl_2$, 10 tetraethylammonium chloride, 10 CsCl, 1 4-aminopyridine and 0.3 $CdCl_2$. The electrodes were filled with a solution containing (in mM) 130 CsF, 9 NaCl, 10 HEPES, 10 EGTA, 1 $MgCl_2$, 3 K_2-ATP, and 1 Na-GTP. The pH and the osmolality were adjusted to 7.2–7.3 and 280–290 mosmol/kg respectively. All current traces were leak subtracted and I_{NaP} current was revealed by subtraction of the currents remaining in riluzole or TTX.

2.5.3 Calcium-sensitive electrodes.

Electrodes were made of borosilicate glass pretreated with dimethylchlorosilane and dried at 120 °C for 2 h. The tip of the pipette was filled with calcium ionophore I cocktail A (Sigma-Aldrich, St. Louis, Missouri, USA). The rest of the electrode was filled with $CaCl_2$ (2 M). Before recordings, the electrode was calibrated with aCSF solutions containing increasing concentrations of calcium (0, 0.4, 0.8, 1.2, 1.6 and 2 mM) and the potential jump for each concentration was recorded. The calibration curve obtained from these data was best fitted with a logarithmic function. Only electrodes exhibiting a potential jump higher than 20 mV (mean = 26.96 ± 1.82 mV, n = 13) per decade (that is, between concentrations 0.2 and 2 mM) were kept for our experiments.

2.5.4 Ca^{2+} imaging.

Confocal imaging was performed using an Olympus FluoView FV 1000 confocal microscope equipped with a 40× water-immersion lens (Olympus, 0.80 N.A.). The 559-nm diode laser line was used to excite SR101 and the emitted fluorescence was detected through a band-pass filter (570–640 nm). Ca^{2+} indicators (fluo-4, fluo4-AM or fluo8L-AM) and Alexa Fluor 488 were

excited with an argon laser line (488 nm) and emission was detected through a band-pass filter (500–545 nm). For Ca^{2+} imaging in single cells, the Ca^{2+} indicator fluo-4 (100 μM, Invitrogen, Grand Island, NY, USA) was added to the internal solution of the recorded cell, while for Ca^{2+} imaging in a population of cells, the slices were incubated for 45–60 min with the cell-permeant Ca^{2+} indicators fluo4-AM (20 μM, Invitrogen, Grand Island, NY, USA) or fluo8L-AM (20 μM, AAT Bioquest, Inc, Sunnyvale, CA, USA) and 0.5% dimethylsulfoxide at room temperature in oxygenated aCSF. Slices were allowed to rest for 30 min before sequence acquisition. Images were acquired at 0.429 s per frame. Offline analysis of sequences was performed with ImageJ software (NIH, USA). Fluorescence intensity was determined on each individual cell by measuring the average pixel values in defined regions of interest (ROIs) on each frame of the sequence. ROIs were placed either on the somata (for AM loading) or on the processes (intra-loading experiment). Changes in fluorescence (ΔF), are presented as relative changes in fluorescence intensity from baseline and expressed as $(\%\Delta F/F_0) = [(F - F_0)/F_0] \times 100$, F_0 being the fluorescence baseline. Because responses were collected over extended periods of time and after repeated NMDA applications, only robust changes of more than 25% were included in the analysis.

2.5.5 Drugs.

The following drugs were locally applied near the recorded cells using positive pressure pulses (Picospritzer III) to one or two pipettes: *N*-methyl-D-aspartate (NMDA, 1–2 mM), BAPTA tetrasodium salt (10 mM), glutamate (1 mM). In some experiments, MK-801 (2 mM) and BAPTA tetrapotassium salt (0.1, 10–35 mM) were added to the internal solution of the recording electrode. The following drugs were bath applied: tetrodotoxin (TTX, 1–2 μM), riluzole (20 μM), suramine (50 μM), CNQX (10 μM), cadmium (100 μM), and L-*trans*-pyrollidine-2,4-dicarboxylic acid (PDC) (50 μM). Compounds were purchased from Sigma-Aldrich (Oakville, Ontario, Canada), Tocris Bioscience (Ellisville, Missouri, USA) and Invitrogen (Grand Island, New York, USA).

Antibodies used to pretreat the tissue in some experiments were applied with a large-tip pipette that was lowered to the surface of the tissue near the neuronal and ion-sensitive recording electrodes. The antibody containing pipette was left there to leak for 10–15 min

before testing the effects of the antibody. Sometimes a small pressure was applied to eject the antibody from the pipette. Two antibodies were tested: anti-S100β antibody (40 µg/ml, sodium azide salt (140 µM); Sigma- Aldrich, S2532) or nonspecific donkey anti-sheep antibody (120 µg/ml, sodium azide salt (312 µM); Invitrogen–Molecular Probes, A11015).

S100β was synthesized at the Recombinant Proteins and Antibodies Facility of the Institute for Research in Immunology and Cancer of the University of Montreal. A cDNA corresponding to mouse S100β (*S100b*) was subcloned in a pETM14 expression vector harboring an N-terminal hexahistidine tag and a prescission cleavage site. The resulting vector was used to transform BL21*E. coli* cells for protein expression in Terrific Broth medium supplemented with 1% glucose and 50 µg/ml kanamycin. Cells were grown at 37 °C with vigorous shaking. When the culture reached an OD_{600} of 0.8, the temperature was reduced to 18 °C and expression was induced with 0.5 mM IPTG for 16 h. Cells were then harvested by centrifugation and resuspended in lysis buffer (Tris-HCl 50 mM, pH 8, NaCl 500 mM, BME 5 mM, PMSF 1 mM and one tablet per 100 ml of complete EDTA-free protease inhibitors (Roche Diagnostics). After two cycles of freeze-thaw, cells were sonicated and centrifuged for 1 h at 45,000*g*. Recombinant protein in the supernatant was purified by metal affinity chromatography on a POROS-MC20 perfusion chromatography column (with Ni^{2+}as the chelating metal), pre-equilibrated in Tris-HCl 50 mM, pH 8, NaCl 500 mM, BME 5 mM, PMSF 1 mM and EDTA-free protease inhibitor tablet. After extensive washing of the column, bound proteins were eluted with a gradient of imidazole (0–500 mM) in Tris-HCl, 50 mM, pH 8, and NaCl 150 mM. Fractions were analyzed by SDS-PAGE, and positive ones were pooled and further purified on a preparative-scale high-resolution Superdex-200 gel filtration column equilibrated in HEPES, 20 mM, pH 7.4, NaCl 150 mM, BME 5 mM and protease inhibitors. Fractions containing recombinant S100β were pooled and concentrated by ultrafiltration on Amicon Ultra YM-30 membranes to a concentration of 14.0 mg/ml, supplemented with glycerol to a final concentration of 50%, aliquoted and flash frozen in liquid nitrogen before storing at −80 °C. Before use, aliquots of the protein were thawed and microdialyzed overnight using a dialysis device to eliminate the glycerol (Float-A-Lyzer, Spectra/Por) floating in a 20 mM HEPES buffer containing 140 mM of NaCl at pH 7.4. The protein was then reconcentrated using centrifugal filter units (Amicon Ultra). The same buffer (20 mM HEPES containing 140

mM NaCl but no Ca^{2+}) was used to suspend S100β and adjust S100β concentration to either 129 μM for local application in the submerged chamber or 50 μM for local application in the interface chamber. In a second set of experiments, 1.6 mM $CaCl_2$ was added to the buffer used to suspend S100β and the protein was tested at two concentrations in this buffer (129 μM and 1 mM).

The mutated S100β protein was obtained from D. Weber from the Center for Biomolecular Therapeutics, University of Maryland School of Medicine. It was synthesized using similar methods as above, but had two mutated residues, E31A and E72A, in both the pseudo- and typical EF-hand domains. This mutated protein was characterized using nuclear magnetic resonance (NMR), stopped-flow kinetics and thermodynamic binding methods (isothermal titration calorimetry) and shown to have very weak, if any, binding to Ca^{2+}, even at concentrations greater than 20 mM (Markowitz et al., 2005). The mutated protein was also suspended in a 20 mM HEPES buffer containing 140 mM NaCl and 1.6 mM $CaCl_2$, and locally applied at a concentration of 1 mM.

2.5.6 Isothermal titration calorimetry.

The apparent dissociation constant (K_d) for calcium binding to recombinant S100β and the effect of anti-S100β monoclonal antibody on calcium binding of S100β was measured by isothermal titration calorimetry (ITC) at 20 °C using a Microcal ITC-200 microcalorimeter (GE Healthcare). The recombinant protein was dialyzed extensively against 20 mM HEPES, pH 7.4, containing 20 mM NaCl, and $CaCl_2$ was added to 2 mM in the resulting dialysis buffer. S100β at a concentration of 25 μM in the reservoir was titrated with 16 injections of 2.5 μl of the 2 mM $CaCl_2$ solution. To verify the effect of antibody binding on S100β calcium binding capacity, a preformed complex of 25 μM S100β and 50 μM monoclonal S100β antibody was dialyzed against the same buffer and titrated with 2 mM $CaCl_2$. The resulting thermograms for both experiments were analyzed with the ORIGIN 7 software.

2.5.7 Analysis of firing patterns.

Firing patterns were characterized as tonic or rhythmic bursting discharge. Tonic discharge typically consisted of low-frequency single spikes separated by regular but relatively long

intervals (interspike intervals: ISI of 150–300 ms; Supplementary Fig. 1). In intracellular recordings these intervals appeared as afterhyperpolarizations. In transition between tonic and burst firing, the afterhyperpolarization gradually reverted into an afterdepolarization which often gave rise to a second spike (Supplementary Fig. 1, middle panel) at a very short ISI. Although these doublets resembled burst firing, we used more stringent criteria for the latter by defining bursts as clusters of at least three action potentials occurring at high frequency (>130 Hz) followed by a long silent period. In intracellular records, bursts appeared as depolarizing plateaus over-ridden by at least three actions potentials. The period separating the beginning of two consecutive plateaus was used to calculate the inter-burst frequency in intracellular recordings, whereas in extracellular recordings, the period separating the first spike of two consecutive bursts was used for this measure. Bursting frequency was calculated only in neurons that displayed a stable rhythmic discharge for more than five cycles. In both types of recording, the ISI of action potentials within a burst was used to calculate the intra-burst frequency.

2.5.8 Immunohistochemistry.

Standard immunocytochemical procedures as reported in Panatier *et al*. (2011)(Panatier et al., 2011) were used for immunostainings of S100β in NVsnpr.

2.5.9 Statistics.

Data are presented as mean ± s.e.m. throughout the text. No statistical methods were used to predetermine sample sizes, but our sample sizes are similar to those generally employed in the field. Since there was no a priori treatment of the animals, no procedures were used for blinding or randomization. Parametric tests were used when data was distributed normally according to the Kolmogorov-Smirnov test. In that case, between groups comparisons were performed with ANOVAs and, for pairwise comparisons, paired *t*-tests, independent *t*-tests or Tukey's tests were used. Otherwise, non-parametric tests were used. Groups were compared with Kruskal-Wallis and Dunn's post test for multiple comparisons, while Mann-Whitney test was used for pairwise comparisons. Probabilities of α-type errors of <0.05 were considered to be significant.

2.6 Supplementary Text and Figures

Supplementary Figure 1

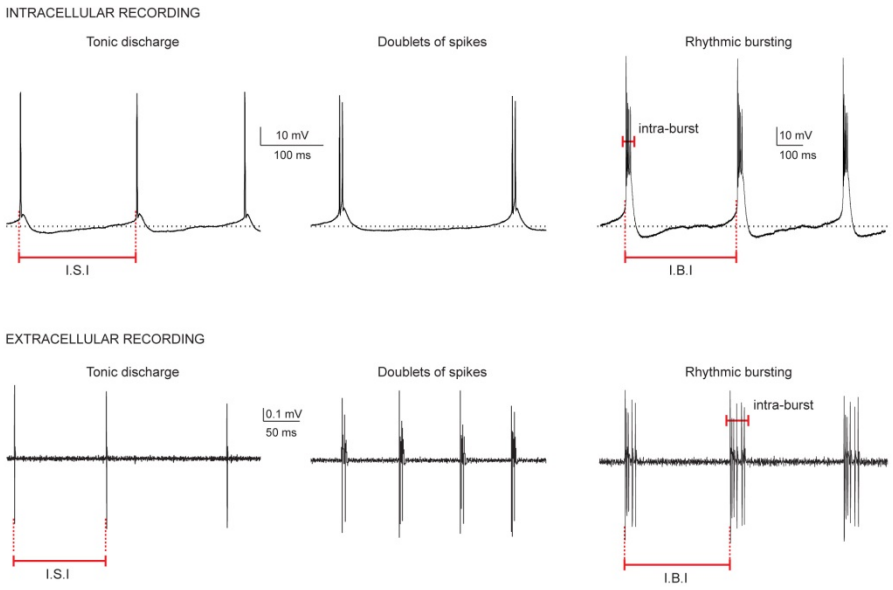

Distinction between different firing patterns. Examples of whole cell recordings (top) and extracellular recordings (bottom) showing the regular low-frequency firing referred to as tonic firing (left) and the rhythmic bursting firing (right). Bursts are clusters of at least 3 spikes occurring at high frequency separated by silent periods. In whole cell rhythmic records, these spikes appeared on top of depolarizing plateaus. Doublets of spikes (middle), where an ADP following the first spike supports a second spike, are often recorded in transition between these two types of firing patterns. ISI = interspike interval; IBI = interburst interval.

Supplementary Figure 2

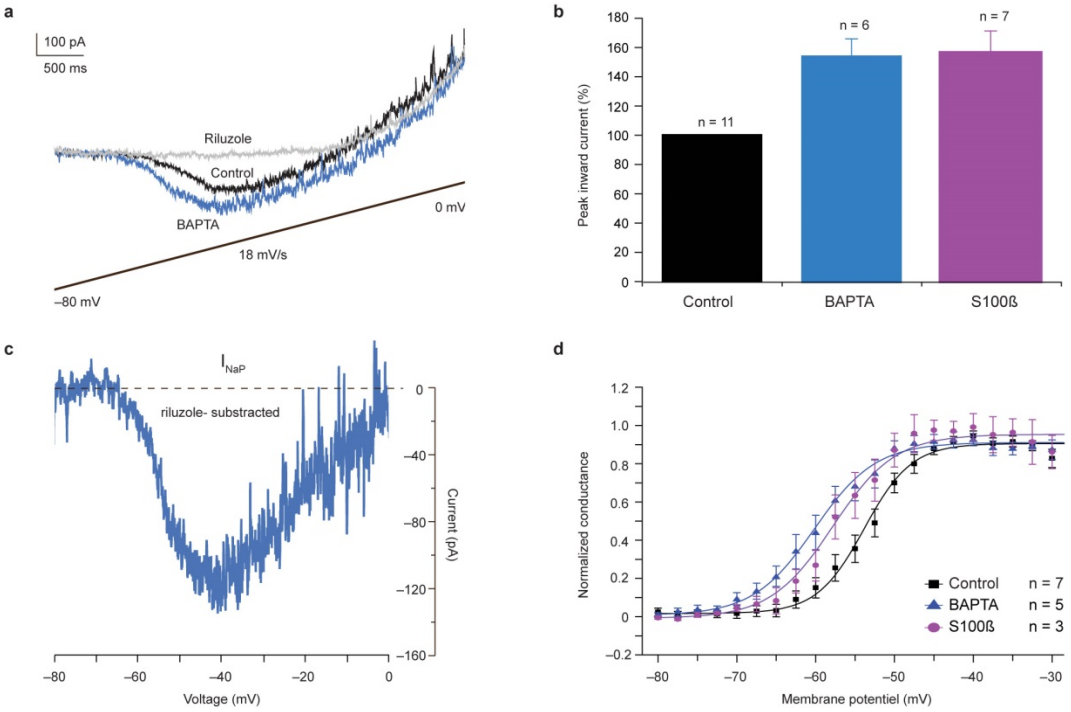

Modulation of the pharmacologically-isolated I_{NaP} by local applications of substances that reduce $[Ca^{2+}]_e$. (**a**) The inward current induced by voltage ramps from –80 to 0 mV (lower trace), after leak subtraction, under control conditions (black) is enhanced during local application of BAPTA (10 mM) (blue, *n* = 6 cells in 4 slices from 4 rats, control: 126.69 ± 40 pA vs BAPTA: 188 ± 54 pA, paired *t*-test; *P* = 0.021) and blocked by riluzole (20 µM) (grey, *n* = 4 cells in 4 slices from 3 rats). (**b**) The histograms illustrate the amplitude of the peak inward current during local application of BAPTA (*n* = 6 cells in 4 slices from 4 rats) and S100β (*n* = 7 cells in 5 slices from 5 rats) normalized to the control (*n* = 11 cells in 7 slices from 7 rats). (**c**) Pharmacologically-isolated trace of I_{NaP} obtained after subtracting the trace obtained with BAPTA and riluzole from the trace obtained with BAPTA alone (same cell as in (**a**)). (**d**) Voltage-dependency of I_{NaP} activation under control conditions (black) and during BAPTA (blue) and S100β (purple) application. I_{NaP} was normalized to the maximal value and fitted with a single Boltzmann function. Controls: $V_{1/2}$max = –53.8 ± 0.4 mV, slope factor of the fitted curve k = 7.4. BAPTA: $V_{1/2}$max = –60.2 ± 0.5 mV and k = 5.8. S100β: $V_{1/2}$max = –57.8 ± 0.7 mV and k = 6.1. Conductance was calculated with $G = I / (V - E_{rev})$. E_{rev} = –65 mV, based on the concentration of extracellular and intracellular pipette solutions.

Supplementary Figure 3

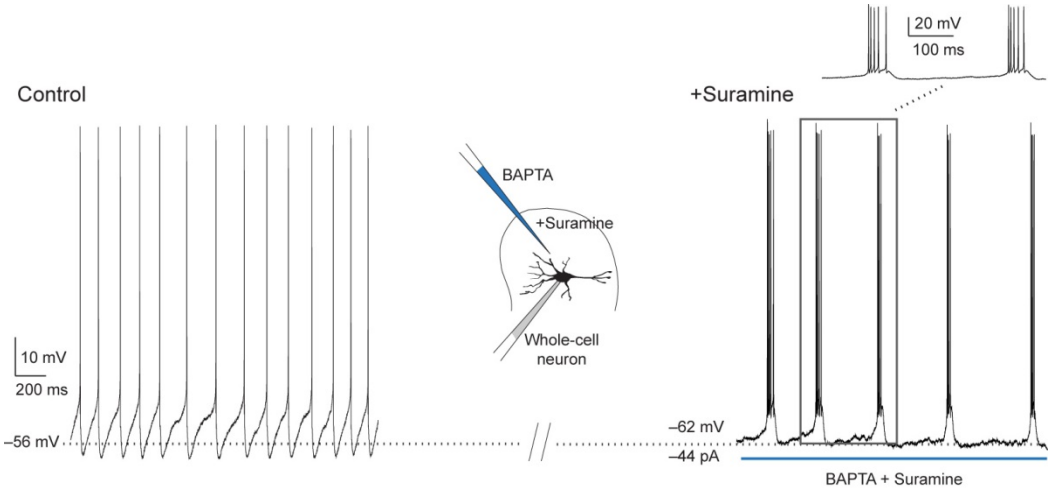

Neuronal NVsnpr bursting does not depend on a purinergic mechanism. A tonically firing NVsnpr neuron (left) displayed rhythmic bursting after local extracellular application of BAPTA (10 mM; right) in presence of bath-applied Suramine (50 µM, n = 5/5 cells in 3 slices from 1 rat), a purinergic receptors antagonist, indicating that NVsnpr neuronal bursting does not depend on a purinergic mechanism triggered by the $[Ca^{2+}]_e$ decrease.

Supplementary Figure 4

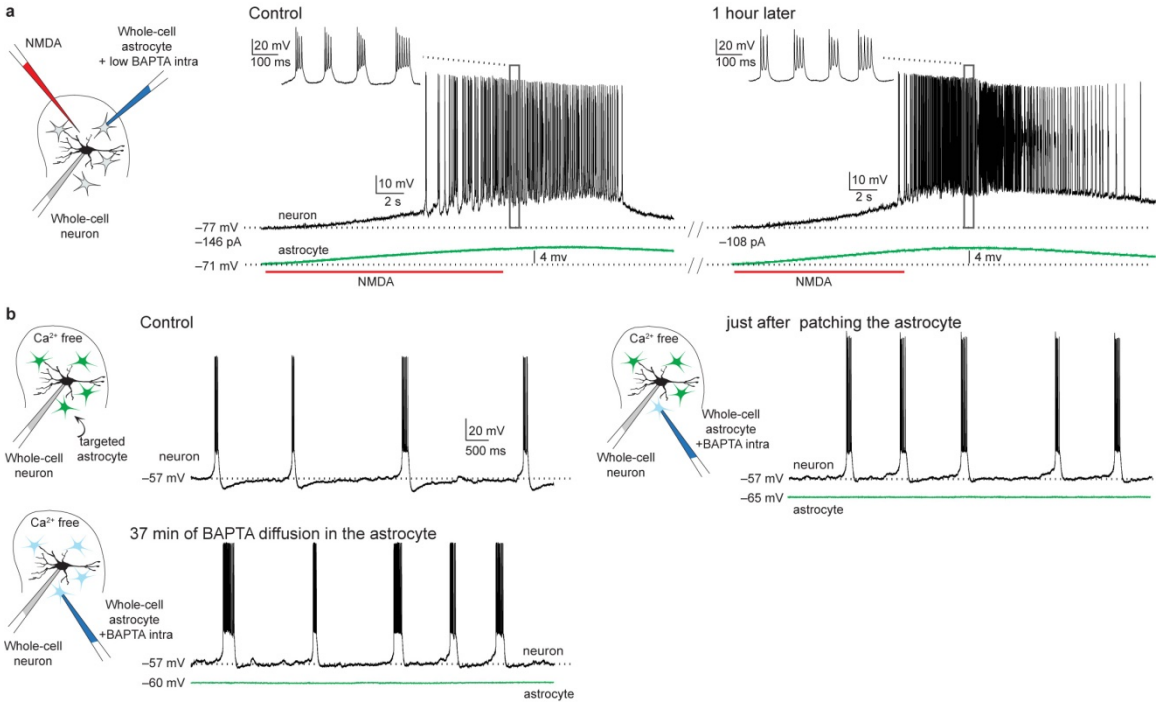

The effects of diffusion of intracellular BAPTA in the astrocytic syncytium depend on the concentration of BAPTA used and are occluded in Ca^{2+}-free aCSF. (**a**) Dialysis of an astrocyte with a low concentration of BAPTA (0.1 mM) does not prevent bursting in the adjacent neuron, even after one hour (n = 4/4 pairs in 4 slices from 4 rats). (**b**) Spontaneous rhythmic bursting of an NVsnpr neuron recorded in Ca^{2+}-free aCSF (top left) persisted after dialysis of an adjacent astrocyte (green trace) with BAPTA (20 mM, bottom left, n = 3 pairs in 3 slices from 3 rats) consistent with an astrocytic regulation of neuronal bursting by decreasing $[Ca^{2+}]_e$.

Supplementary Figure 5

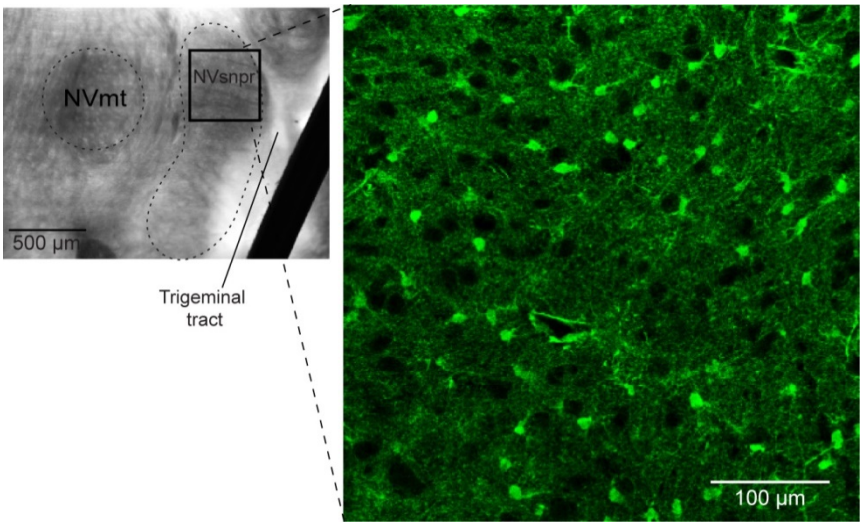

Immunostaining of S100β in dorsal NVsnpr. The dorsal part of NVsnpr (box in the image on left) contains a large number of immunoreactive astrocytes when an antibody against S100β is used.

Supplementary Figure 6

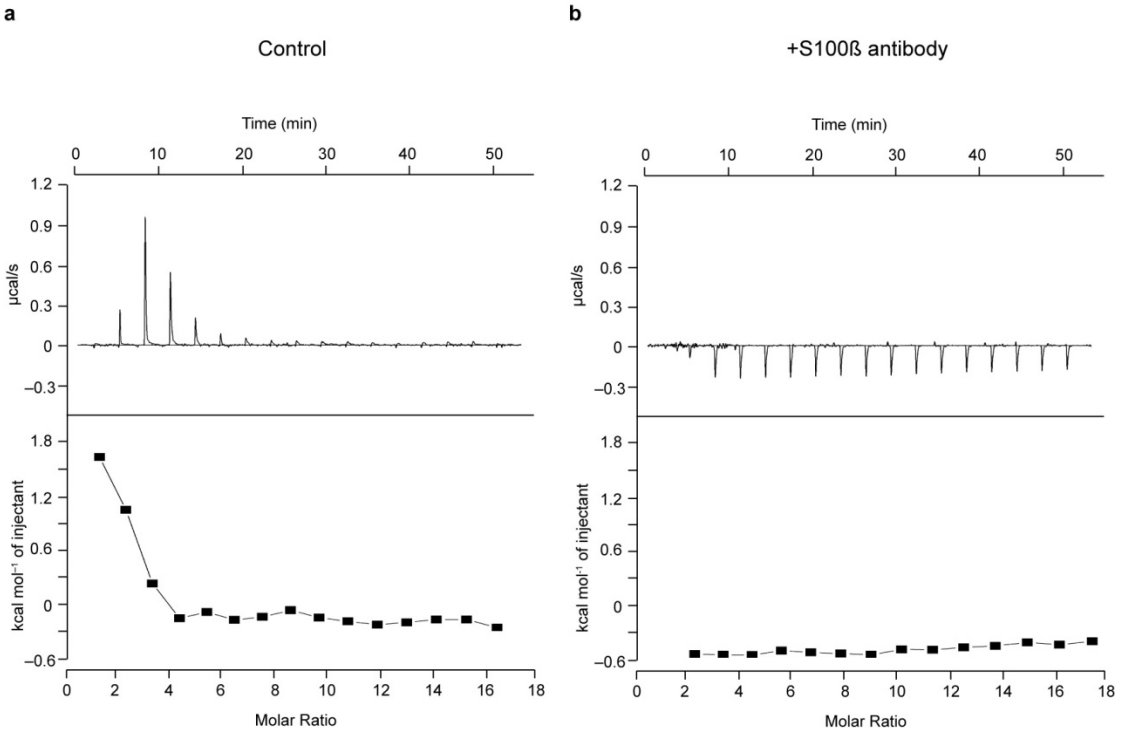

Binding of Ca^{2+} to S100β is prevented in presence of an antibody. Isothermal titration calorimetry data for the titration of S100β with Ca^{2+} in the absence (**a**) or the presence (**b**) of an anti-S100β antibody. Top panel: raw thermogram of S100β titrated with $CaCl_2$ at 20°C. Bottom panel: Integrated heats of the raw data from the top panel.

Supplementary Figure 7

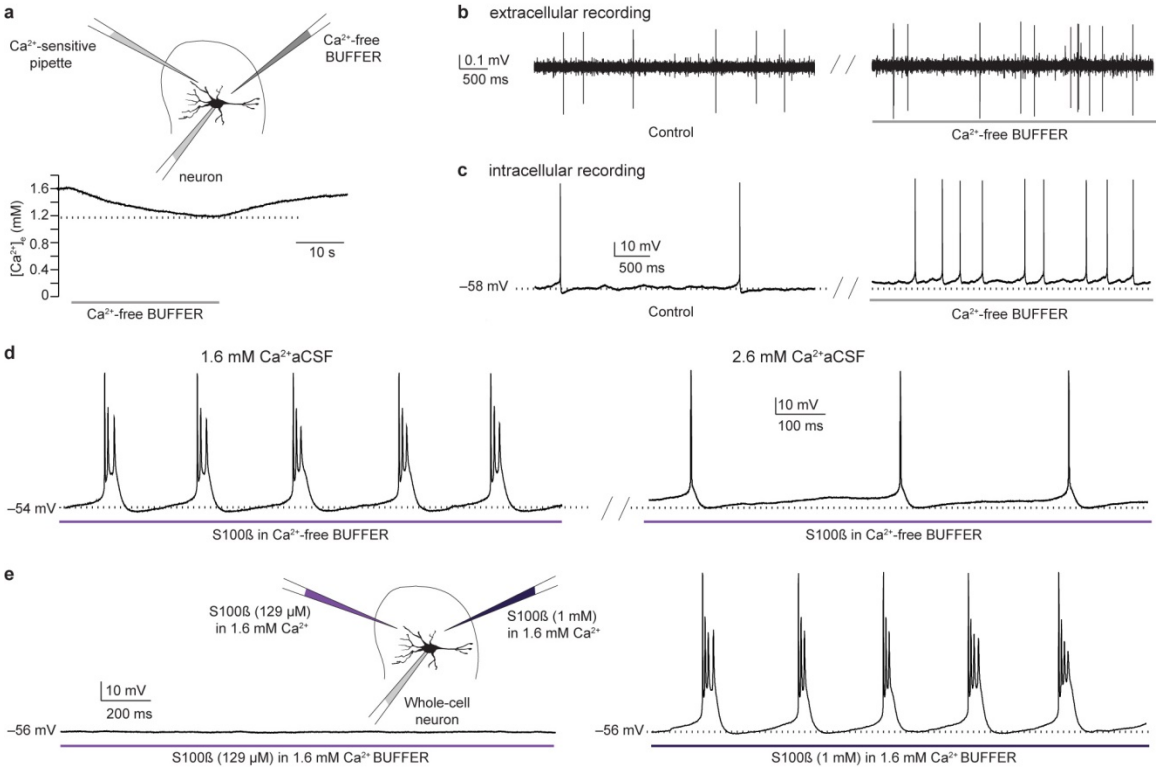

Effects of S100ß depend on its ability to reduce the extracellular calcium. (**a**) Local application of the Ca^{2+}-free buffer used to dilute S100ß induces a small decrease of $[Ca^{2+}]_e$ (n = 6 recording sites in 6 slices from 3 rats), but does not cause bursting in NVsnpr neurons, in neither the interface ((**b**) extracellular recording; right trace, n = 11 cells in 11 slices from 6 rats) or the submerged configuration ((**c**) intracellular recording; right trace, n = 3 cells in 3 slices from 2 rats). (**d**) Local application of S100ß diluted in the Ca^{2+}-free buffer elicits neuronal bursting (left trace) in a cell from a preparation submerged in normal aCSF (with 1.6 mM Ca^{2+}), but not after raising the $[Ca^{2+}]_e$ in the aCSF to 2.6 mM (n = 4 cells in 4 slices from 3 rats). (**e**) Local application of S100ß diluted in a buffer containing 1.6 mM Ca^{2+} can still elicit bursting, when its concentration is increased to1 mM (right trace (n = 10 cells in 4 slices from 4 rats) to prevent its saturation, but not at the concentration of 129 µM; left trace (n = 5 cells in 3 slices from 3 rats).

Supplementary Figure 8

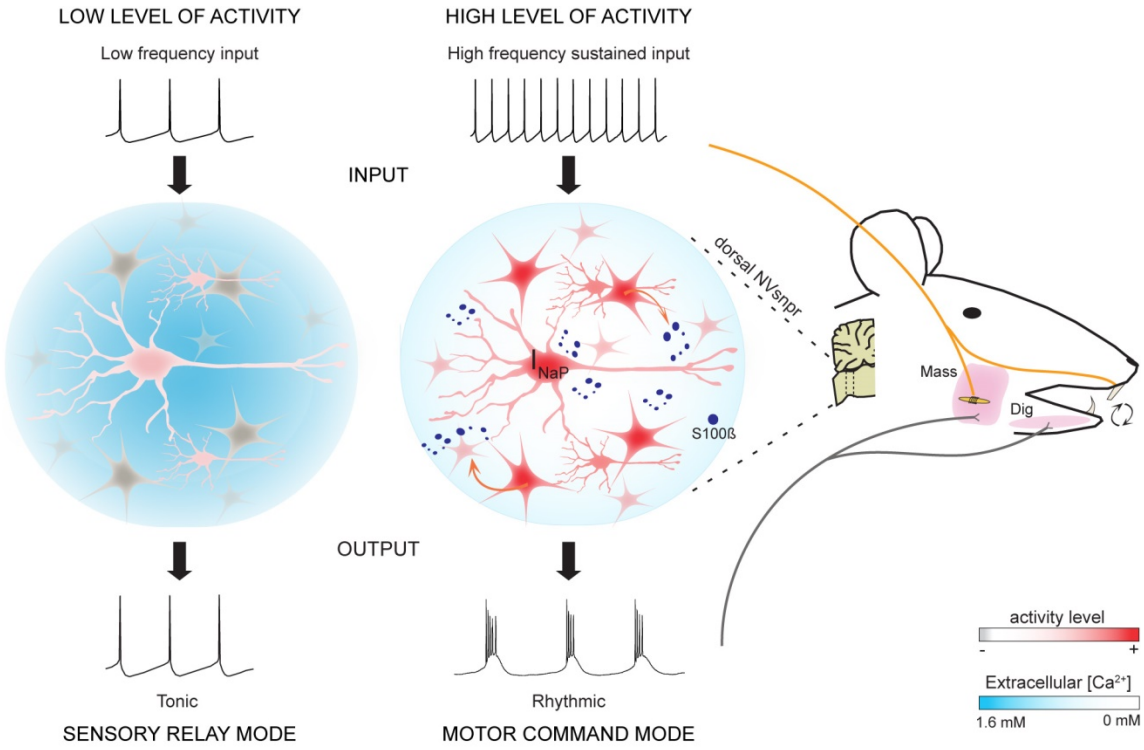

Model of the sequence of events leading to rhythmogenesis. Left: Low sensory activity level are insufficient to activate astrocytes and lower $[Ca^{2+}]_e$, thus preventing activation of I_{NaP} and neuronal bursting. In this condition, NVsnpr neurons work in a sensory relay mode with their tonic output faithfully relaying their tonic input. Right: With food intake and intraoral stimulation, sensory inputs from the periodontal ligament and the jaw muscle spindles increase their activity level and signal the need for rhythmic mastication. This increased activity activates astrocytes and leads to release of the Ca^{2+}-binding protein S100β and subsequent decrease of $[Ca^{2+}]_e$. This in turn will activate I_{NaP} and elicit rhythmic bursting in NVsnpr neurons. The generated bursting frequency and pattern, reflecting the pattern of sensory inputs will then be transmitted to jaw closing and opening motoneuronal pools (masseter (mass) and digastric (dig), respectively).

Supplementary Table 1: Characteristics of burst firing.

	Interface configuration			Submerged configuration		
	Electrical stim	**NMDA**	**S100β**	**Ca^{2+}-free**	**NMDA**	**S100β**
Inter-burst frequency (Hz)	8.56±1.03 (n=9)	7.43±1.20 (n=12)	7.47±0.54 (n=31)	2.77±0.76 (n=14)	3.48±0.71 (n=57)	3.54±0.53 (n=33)
Intra-burst frequency (Hz)	217.56±13.41 (n=9)	214.83±24.14 (n=12)	286.87±17.71 (n=31)	152.88±15.72 (n=12)	172.44±9.78 (n=52)	217.97±13.27* (n=30)
Frequency of tonic discharge (Hz)	5.99±2.32 (n=9)	5.12±0.17 (n=10)	3.33±0.77 (n=22)	6.42±1.26 (n=10)	6.06±0.74 (n=35)	5.52±0.74 (n=17)
Vm burst (mV)	-	-	-	-55.83±1.35 (n=14)	-60.66±0.78* (n=57)	-58.27±0.97 (n=33)

Bursting frequency differed systematically between the submerged and the interface configurations (Mann-Whitney test*; P* = < 1E-10), even when bursting was induced by the same substance. However, bursting obtained in each configuration with different drugs or procedures did not differ in frequency. For each condition, control tonic firing was obtained in 1.6mM Ca^{2+} prior to the experimental condition. Some cells were silent at rest, discharged irregularly or had ripples instead of spikes on their plateaus. These were not included in the data analysis above. In all conditions, for the two configurations, the intra-burst frequency differed markedly from the frequency of tonic firing (Mann-Whitney test*; P* = < 1E-10). In the submerged configuration, the intra-burst frequency obtained with S100β was significantly higher than with NMDA (*n* = 12 cells in 10 slices from 10 rats) and Ca^{2+}- free aCSF (Tukey's test $P = 0.02$*; *P* < 0.05). The potentials at which bursts first appeared (Vm burst) varied slightly across conditions, but differed significantly only between NMDA and Ca^{2+}-free aCSF (Tukey's test $P = 0.016$*; *P* < 0.05).

2.7 References

Armstrong, CM, (1999) Distinguishing surface effects of calcium ion from pore-occupancy effects in Na+ channels. Proc. Natl. Acad. Sci. USA 96, 4158-4163

Bernier AP, Arsenault I, Lund JP, Kolta A (2010) Effect of the stimulation of sensory inputs on the firing of neurons of the trigeminal main sensory nucleus in the rat. J Neurophysiol 103:915-923.

Brocard F, Shevtsova NA, Bouhadfane M, Tazerart S, Heinemann U, Rybak IA, Vinay L (2013) Activity-dependent changes in extracellular Ca2+ and K+ reveal pacemakers in the spinal locomotor-related network. Neuron 77:1047-1054.

Brocard F, Verdier D, Arsenault I, Lund JP, Kolta A (2006) Emergence of intrinsic bursting in trigeminal sensory neurons parallels the acquisition of mastication in weanling rats. J Neurophysiol 96:2410-2424.

Capra NF, Dessem D (1992) Central connections of trigeminal primary afferent neurons: topographical and functional considerations. Crit Rev Oral Biol Med 4:1-52.

Ciccarelli R, Di Iorio P, Bruno V, Battaglia G, D'Alimonte I, D'Onofrio M, Nicoletti F, Caciagli F (1999) Activation of A(1) adenosine or mGlu3 metabotropic glutamate receptors enhances the release of nerve growth factor and S-100beta protein from cultured astrocytes. Glia 27:275-281.

Crill WE (1996) Persistent sodium current in mammalian central neurons. Annual review of physiology 58:349-362.

Del Negro CA, Hayes JA, Pace RW, Brush BR, Teruyama R, Feldman JL (2010) Synaptically activated burst-generating conductances may underlie a group-pacemaker mechanism for respiratory rhythm generation in mammals. Progress in brain research 187:111-136.

Del Negro CA, Morgado-Valle C, Feldman JL (2002) Respiratory rhythm: an emergent network property? Neuron 34:821-830.

Dellow PG, Lund JP (1971) Evidence for central timing of rhythmical mastication. J Physiol 215:1-13.

Di Prisco GV, Pearlstein E, Robitaille R, Dubuc R (1997) Role of sensory-evoked NMDA plateau potentials in the initiation of locomotion. Science 278:1122-1125.

Donato R, Sorci G, Riuzzi F, Arcuri C, Bianchi R, Brozzi F, Tubaro C, Giambanco I (2009) S100B's double life: intracellular regulator and extracellular signal. Biochim Biophys Acta 1793:1008-1022.

Egelman DM, Montague PR (1999) Calcium dynamics in the extracellular space of mammalian neural tissue. Biophysical journal 76:1856-1867.

Gomez-Gonzalo M, Losi G, Chiavegato A, Zonta M, Cammarota M, Brondi M, Vetri F, Uva L, Pozzan T, de Curtis M, Ratto GM, Carmignoto G (2010) An excitatory loop with astrocytes contributes to drive neurons to seizure threshold. PLoS Biol 8:e1000352.

Gourine AV, Kasymov V, Marina N, Tang F, Figueiredo MF, Lane S, Teschemacher AG, Spyer KM, Deisseroth K, Kasparov S (2010) Astrocytes control breathing through pH-dependent release of ATP. Science 329:571-575.

Grillner S (1975) Locomotion in vertebrates: central mechanisms and reflex interaction. Physiological reviews 55:247-304.

Harris-Warrick RM (2010) General principles of rhythmogenesis in central pattern generator networks. Progress in brain research 187:213-222.

Jefferys JG, Haas HL (1982) Synchronized bursting of CA1 hippocampal pyramidal cells in the absence of synaptic transmission. Nature 300:448-450.
Jones HC, Keep RF (1988) Brain fluid calcium concentration and response to acute hypercalcaemia during development in the rat. J Physiol 402:579-593.
Kafitz KW, Meier SD, Stephan J, Rose CR (2008) Developmental profile and properties of sulforhodamine 101--Labeled glial cells in acute brain slices of rat hippocampus. J Neurosci Methods 169:84-92.
Kasymov V, Larina O, Castaldo C, Marina N, Patrushev M, Kasparov S, Gourine AV (2013) Differential sensitivity of brainstem versus cortical astrocytes to changes in pH reveals functional regional specialization of astroglia. The Journal of neuroscience 33:435-441.
Kim YI, Chandler SH (1995) NMDA-induced burst discharge in guinea pig trigeminal motoneurons in vitro. J Neurophysiol 74:334-346.
Lazarov NE (2002) Comparative analysis of the chemical neuroanatomy of the mammalian trigeminal ganglion and mesencephalic trigeminal nucleus. Prog Neurobiol 66:19-59.
Lee MC, Ting KK, Adams S, Brew BJ, Chung R, Guillemin GJ (2010) Characterisation of the expression of NMDA receptors in human astrocytes. PloS one 5:e14123.
Li Z, Hatton GI (1996) Oscillatory bursting of phasically firing rat supraoptic neurones in low-Ca2+ medium: Na+ influx, cytosolic Ca2+ and gap junctions. J Physiol 496 (Pt 2):379-394.
Lian XY, Stringer JL (2004) Astrocytes contribute to regulation of extracellular calcium and potassium in the rat cerebral cortex during spreading depression. Brain research 1012:177-184.
Lund JP, Dellow PG (1971) The influence of interactive stimuli on rhythmical masticatory movements in rabbits. Arch Oral Biol 16:215-223.
Markowitz J, Rustandi RR, Varney KM, Wilder PT, Udan R, Wu SL, Horrocks WD, Weber DJ (2005) Calcium-binding properties of wild-type and EF-hand mutants of S100B in the presence and absence of a peptide derived from the C-terminal negative regulatory domain of p53. Biochemistry 44:7305-7314.
Massimini M, Amzica F (2001) Extracellular calcium fluctuations and intracellular potentials in the cortex during the slow sleep oscillation. J Neurophysiol 85:1346-1350.
Nicholson C, Bruggencate GT, Steinberg R, Stockle H (1977) Calcium modulation in brain extracellular microenvironment demonstrated with ion-selective micropipette. Proc Natl Acad Sci U S A 74:1287-1290.
Okada Y, Sasaki T, Oku Y, Takahashi N, Seki M, Ujita S, Tanaka KF, Matsuki N, Ikegaya Y (2012) Preinspiratory calcium rise in putative pre-Botzinger complex astrocytes. J Physiol 590:4933-4944.
Panatier A, Vallee J, Haber M, Murai KK, Lacaille JC, Robitaille R (2011) Astrocytes are endogenous regulators of basal transmission at central synapses. Cell 146:785-798.
Pasti L, Volterra A, Pozzan T, Carmignoto G (1997) Intracellular calcium oscillations in astrocytes: a highly plastic, bidirectional form of communication between neurons and astrocytes in situ. The Journal of neuroscience 17:7817-7830.
Pumain R, Menini C, Heinemann U, Louvel J, Silva-Barrat C (1985) Chemical synaptic transmission is not necessary for epileptic seizures to persist in the baboon Papio papio. Exp Neurol 89:250-258.

Rybak IA, Shevtsova NA, St-John WM, Paton JF, Pierrefiche O (2003) Endogenous rhythm generation in the pre-Botzinger complex and ionic currents: modelling and in vitro studies. The European journal of neuroscience 18:239-257.

Sakatani S, Seto-Ohshima A, Shinohara Y, Yamamoto Y, Yamamoto H, Itohara S, Hirase H (2008) Neural-activity-dependent release of S100B from astrocytes enhances kainate-induced gamma oscillations in vivo. The Journal of neuroscience 28:10928-10936.

Serrano A, Haddjeri N, Lacaille JC, Robitaille R (2006) GABAergic network activation of glial cells underlies hippocampal heterosynaptic depression. The Journal of neuroscience 26:5370-5382.

Sigvardt KA, Grillner S, Wallen P, Van Dongen PA (1985) Activation of NMDA receptors elicits fictive locomotion and bistable membrane properties in the lamprey spinal cord. Brain research 336:390-395.

Smith JC, Ellenberger HH, Ballanyi K, Richter DW, Feldman JL (1991) Pre-Botzinger complex: a brainstem region that may generate respiratory rhythm in mammals. Science 254:726-729.

Su H, Alroy G, Kirson ED, Yaari Y (2001) Extracellular calcium modulates persistent sodium current-dependent burst-firing in hippocampal pyramidal neurons. The Journal of neuroscience 21:4173-4182.

Tazerart S, Vinay L, Brocard F (2008) The persistent sodium current generates pacemaker activities in the central pattern generator for locomotion and regulates the locomotor rhythm. The Journal of neuroscience 28:8577-8589.

Torres A, Wang F, Xu Q, Fujita T, Dobrowolski R, Willecke K, Takano T, Nedergaard M (2012) Extracellular Ca(2)(+) acts as a mediator of communication from neurons to glia. Sci Signal 5:ra8.

Trulsson M, Johansson RS (2002) Orofacial mechanoreceptors in humans: encoding characteristics and responses during natural orofacial behaviors. Behav Brain Res 135:27-33.

Tsuboi A, Kolta A, Chen CC, Lund JP (2003) Neurons of the trigeminal main sensory nucleus participate in the generation of rhythmic motor patterns. The European journal of neuroscience 17:229-238.

Tsuruyama K, Hsiao CF, Chandler SH (2013) Participation of a persistent sodium current and calcium-activated nonspecific cationic current to burst generation in trigeminal principal sensory neurons. J Neurophysiol 110:1903-1914.

Wang F, Smith NA, Xu Q, Fujita T, Baba A, Matsuda T, Takano T, Bekar L, Nedergaard M (2012) Astrocytes modulate neural network activity by Ca(2)+-dependent uptake of extracellular K+. Sci Signal 5:ra26.

Westneat MW, Hall WG (1992) Ontogeny of feeding motor patterns in infant rats: an electromyographic analysis of suckling and chewing. Behavioral neuroscience 106:539-554.

Yamamura K, Narita N, Yao D, Martin RE, Masuda Y, Sessle BJ (2002) Effects of reversible bilateral inactivation of face primary motor cortex on mastication and swallowing. Brain research 944:40-55.

CHAPITRE 3

3. Discussion générale

Les travaux de cette thèse contribuent à l'avancement des connaissances en neurosciences en confirmant le rôle de la glie dans l'encodage nerveux, et surtout en décrivant un mécanisme complètement inédit d'interaction neurone/glie, centré sur la protéine gliale S100β. Dans les circuits trigéminaux impliquant les neurones du NVsnpr, la rythmogénèse neuronale dépend de l'activité intégrée de deux réseaux de cellules : les neurones et les astrocytes. L'élément clé de cette rythmogénèse est l'augmentation du courant I_{NaP}, le courant qui sous-tend les bouffées rythmiques neuronales, par la baisse de la concentration de la $[Ca^{2+}]_e$ contrôlée par les astrocytes. Nos résultats démontrent que les changements de calcium extracellulaire sont subséquents aux stimulations des inputs afférents au NVsnpr, et qu'ils sont probablement dus à l'activation des astrocytes puisqu'ils dépendent de la relâche d'une protéine astrocytaire la S100β. Cette protéine chélatrice de calcium est nécessaire à la baisse de $[Ca^{2+}]_e$ et à l'induction de la décharge en bouffées rythmiques des neurones. Ces résultats nous mènent à proposer le modèle présenté dans la figure 3-1 selon lequel la rythmogénèse serait initié par une augmentation de l'input afférent au NVsnpr. Cette augmentation peut refléter l'activation des afférences sensorielles fusoriales ou parodontales lors de la prise de nourriture, ou aussi l'activation des projections corticales de l'ACM pour signaler le besoin de débuter la mastication. Cette augmentation d'excitation active les astrocytes et mène à la relâche de la protéine S100β, et à la baisse subséquente de la $[Ca^{2+}]_e$. Ceci entraine l'activation des courants I_{NaP} et l'induction du mode de décharge en bouffées rythmiques des neurones du NVsnpr. Le patron et la fréquence de décharge des bouffées rythmiques induites, modulées par l'intensité de l'activité des inputs sensoriels, seront alors retransmis aux motoneurones contrôlant les muscles d'ouverture et de fermeture de la mastication.

Figure 3-1: Schéma conceptuel de la discussion

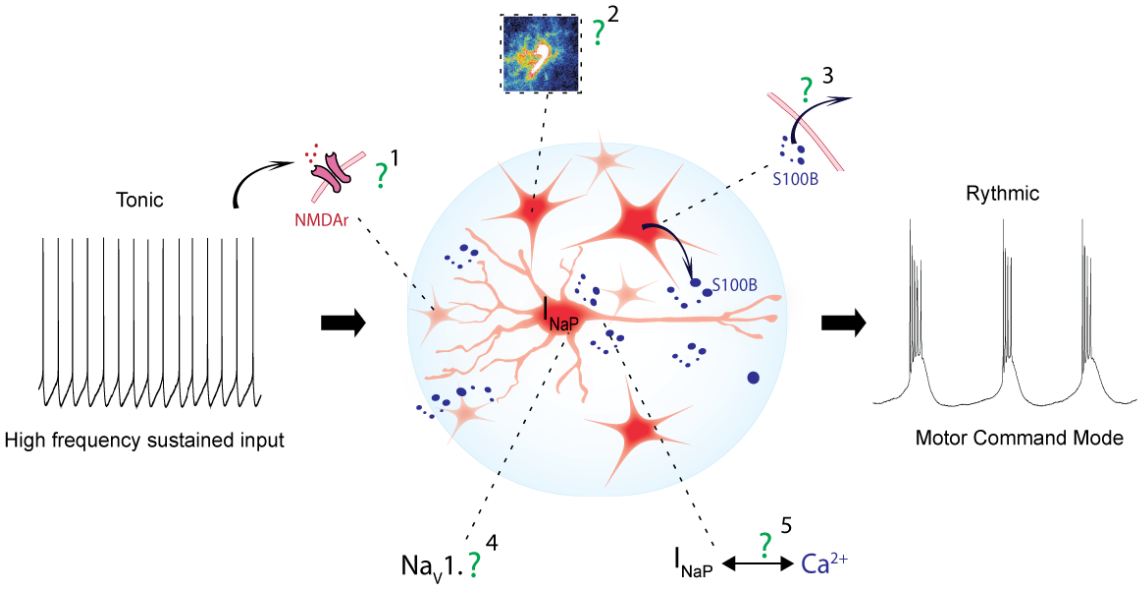

Schéma illustrant la démarche suivie dans la discussion. Schéma présentant les différentes questions soulevées par nos travaux. 1-La détection de l'input glutamatergique (sensoriel ou cortical) par les astrocytes. 2- La signification du signal calcique astrocytaire. 3- la relâche de S100β. 4- Les canaux sodiques sous-jacents aux courants sodiques persistants. 5- La modulation du courant I_{NaP} par le calcium extracellulaire.

Toutefois certains points de ce modèle restent à confirmer ou soulèvent des questions. Ces points numérotés de 1 à 5 dans la figure 3-1 seront discutés à la lumière de nos résultats et des études de différents groupes. Dans les prochaines sections nous aborderons: 1) la détection du signal glutamatergique (sensoriel ou cortical) par les astrocytes et 2) les réponses calciques qui en découlent; 3) la relâche de S100β; 4) les canaux sodiques sous-jacents aux courants sodiques persistants; et 5) l'effet de la baisse de calcium sur ces courants. Ce faisant, nous envisagerons différents scénarios pouvant constituer des pistes de recherches pour la suite de cette étude d'une façon plus intégrée par rapport à la mastication. Finalement, nous verrons dans quelles mesures nos résultats et les concepts qui en découlent pourraient s'appliquer à d'autres situations physiologiques et pathologiques.

3.1 Détection de l'input glutamatergique par les astrocytes

Les résultats de nos expériences ont clairement montré que l'activation des astrocytes est une condition sine qua non à l'induction de la décharge rythmique des neurones du NVsnpr. Du même coup, ces expériences indiquent que l'activation des astrocytes est en amont de l'induction de l'activité rythmique neuronale dans le NVsnpr. Dès lors, il paraissait logique que les astrocytes puissent détecter l'input qui déclenche l'activation de ce mode de décharge. Tout comme les fibres corticales, les fibres des afférences sensorielles qui déclenchent l'activité rythmique neuronale dans le NVsnpr sont glutamatergiques (Bernier et al., 2010). La présence sur les astrocytes de récepteurs glutamatergiques de types métabotrope (mGluR3 et 5) ou ionotrope est bien connue (voir section 1.5.3.2.2 au chapitre 1), et des données préliminaires de notre laboratoire indiquent que les astrocytes du NVsnpr ont des récepteurs mGluR3 et 5. Ceci dit, à cause de l'importance des récepteurs NMDA dans la rythmogénèse de ce noyau (Bernier et al., 2010), nous avons considéré la possibilité que les astrocytes en soient pourvus et nous avons concentré nos travaux sur ces derniers récepteurs, même si dans la littérature la présence de récepteurs NMDA fonctionnels sur les astrocytes reste controversée (voir section 1.5.3.2.2 au chapitre 1).

Nos résultats ont permis de montrer une activation directe des astrocytes par des récepteurs NMDA. Ceux-ci ont été mis en évidence par les expériences en courant imposé (*current clamp*) avec le MK-801 dans les astrocytes. Cependant, à cause de la controverse sur la

fonctionnalité de récepteurs NMDA sur les astrocytes, des expériences en mode *voltage clamp* ont également été menées afin d'investiguer les variations des courants évoqués par le NMDA à différents potentiels dans les astrocytes. Cela dit, la qualité des enregistrements d'astrocytes en voltage imposé (*voltage clamp*) est mauvaise parce que 1) la résistance membranaire (Rm) de ces cellules est trop faible par rapport à celle de la pipette d'enregistrement, ce qui rend les commandes de voltage imprécises (Berger et al., 1991; Ma et al., 2014; Steinhauser et al., 1992), et 2) à cause des variations de Rm des astrocytes dues à l'augmentation ou la diminution du couplage de ces cellules (McKhann et al., 1997). Ainsi, à cause des réserves énumérées ci-dessus, les résultats de la série d'expériences en *voltage clamp* dans les astrocytes, discutés ci-après, ont été exclus de la publication reliée à cette thèse.

Dans ces enregistrements, nous avons mesuré la réponse membranaire d'astrocytes à une série de créneaux (pulses) hyperpolarisants et dépolarisants. Les courbes courant-voltage (IV) obtenues avant l'application de NMDA ont ensuite été soustraites des courbes obtenues après 30 secondes d'application de NMDA pour estimer la courbe IV des courants induits par le NMDA. Ces derniers courants ont été enregistrés en condition contrôle en présence et en absence de la carbénoxolone (CBX, 20 µM), bloqueur de jonctions GAP (les cellules enregistrées en présence et en absence de CBX montraient des réponses similaires au NMDA, et ont donc été regroupées) ou avec le MK-801 dans les pipettes d'enregistrements sans CBX. Toutes les courbes obtenues étaient linéaires (typiques des astrocytes) même en présence du NMDA, corroborant les résultats rapportés par d'autres études (Schipke et al., 2001). Dans les conditions contrôle, le NMDA induisait une dépolarisation qui était associée à une augmentation de conductance. Toutes les cellules enregistrées avec le MK-801 dans le milieu interne montraient des courbes IV presque identiques avant et après l'application de NMDA. Ceci démontre que les réponses observées dans les astrocytes dépendent principalement de l'activation de récepteurs NMDA spécifiques aux astrocytes. Ceci confirme donc les résultats de notre étude démontrant que les astrocytes du NVsnpr possèdent des récepteurs NMDA fonctionnels (voir Annexe).

Dans notre étude nous avons évalué l'activation des astrocytes par leurs dépolarisations, mais aussi par leurs activités calciques. Néanmoins, les expériences démontrant une activation directe des astrocytes par le NMDA ont seulement évalué la composante électrique de leur activation. Par cette approche, nous voulions montrer que les réponses n'étaient pas dues à

l'accumulation de K^+ extracellulaire (causé par l'activité en bouffées neuronales), mais aussi qu'il s'agissait bien de réponses dues à des courants NMDA astrocytaires. Il aurait été intéressant d'évaluer aussi la réponse calcique des astrocytes dans des conditions de blocage de l'activité neuronale (TTX) ou en présence de MK-801 intracellulaire. Dans l'étude de Serrano (2006), les auteurs indiquent que la réponse calcique des astrocytes est grandement diminuée dans les tranches d'hippocampe sous TTX, sans que l'activité ne soit abolie: cela implique qu'au moins une partie de cette réponse NMDA est directe.

Nos données indiquent que l'activité calcique et les réponses de dépolarisations des astrocytes ne vont pas nécessairement de pair. En effet, bien que le BAPTA intracellulaire bloque les réponses calciques des astrocytes, il est intéressant de constater que les dépolarisations ne semblent pas être affectées par cette manipulation (voir Figure 5 au chapitre 2). Cette même observation a été faite dans les astrocytes d'hippocampe de souris (Serrano et al., 2008) et suggèrent que l'activité électrique est indépendante de l'activité calcique, même si ces deux réponses ont été observées en parallèle dans toutes les expériences contrôles où les deux phénomènes ont été mesurés (voir figure 3 au chapitre 2). Le fait que l'activité électrique puisse être indépendante pourrait suggérer la présence de mécanismes astrocytaires qui ne nécessitent pas une activité calcique des astrocytes. Par exemple, les dépolarisations des astrocytes et le changement du potentiel d'équilibre du K^+, pourraient avoir un effet direct sur le tamponnage du K^+ extracellulaire.

3.2 L'activité des astrocytes : la signification des réponses calciques

À cause des récepteurs NMDA et mGluRs sur leurs membranes, les astrocytes du NVsnpr sont en position idéale pour détecter le signal sensoriel qui dicte le changement du mode de décharge neuronale de tonique à rythmique. L'application de NMDA qui mime une activité neuronale intense (requise pour la baisse de calcium extracellulaire et l'induction des bouffées rythmiques) active ces cellules. De plus, sans la réponse calcique qui découle de cette détection, le phénomène de rythmicité neuronal est bloqué. Ceci implique que le signal calcique des astrocytes reflète un certain niveau de décodage et de traitement de l'input

sensoriel par ces cellules afin de provoquer en retour un effet qui déclenche la décharge en bouffées des neurones avoisinants. Autrement dit, le signal calcique des astrocytes représente, dans ce contexte, un niveau de traitement d'information neuronale. Dans la même ligne d'idée, l'étude de Todd et de ses collaborateurs (2010) montre que les homologues des astrocytes dans le système nerveux périphérique, les cellules de Schwann périsynaptiques, sont capables 1) de détecter différents patrons d'activité d'inputs synaptiques (soutenue vs en bouffée); 2) d'avoir des réponses calciques avec des signatures distinctes en fonction des différents patrons (réponse phasique vs réponse longue oscillatoire); et 3) de moduler l'activité synaptique en retour (potentialisations vs dépressions) (Todd et al., 2010). Dans notre étude, nous n'avons considéré que la présence ou l'absence des réponses calciques des astrocytes en les étudiant au niveau du corps cellulaire ou au niveau des prolongements principaux de ces cellules. Dans toutes les données que nous avons recueillies, l'activité calcique au niveau de ces sous-structures consistait en une réponse lente non oscillatoire. Toutefois, il serait intéressant à l'avenir d'étudier plus en profondeur les caractéristiques détaillées de ce signal calcique qui pourrait révéler un encodage beaucoup plus gradé et fin notamment au niveau des plus petits prolongements astrocytaires. Par exemple, une étude de Panatier et ses collaborateurs indique que les astrocytes sont capables d'avoir des réponses calciques rapides (de l'ordre des millisecondes) qui restent localisées au niveau de leurs plus fins prolongements (Panatier et al., 2011), alors que dans notre étude, où nous avons observé les réponses calciques aux niveaux des somas et des prolongements principaux, les réponses étaient plus lentes (de l'ordre des secondes). La différence entre ces deux types de réponse s'explique sans doute, en partie, par l'intensité des stimuli utilisés pour activer les astrocytes. En effet dans l'étude de Panatier il s'agissait de stimulations minimales, alors que nous appliquions le NMDA localement de façon à simuler une activité intense. Quoiqu'il en soit, ces résultats pris ensemble montrent clairement la capacité des astrocytes à détecter des types d'inputs différents, mais plus encore, ils montrent leurs capacités à y répondre différemment pour produire une modulation neuronale adaptée. Ce concept a bien été discuté récemment par Araque et ses collaborateurs (Araque et al., 2014).

Déjà en 1992, Smith avait émis l'hypothèse fort intéressante selon laquelle les réseaux d'astrocytes pourraient influencer l'encodage d'informations des réseaux neuronaux à partir de

leurs activités calciques voir la figure 3-2 (Smith, 1992). Nos résultats semblent supporter ce concept, car dans notre étude le signal calcique astrocytaire mène à un changement drastique de la décharge des neurones. Autrement dit, dans le NVsnpr, les astrocytes déterminent, grâce à leurs activités calciques, le mode de décharge neuronale. Il va sans dire que cette capacité des astrocytes à décoder l'information neuronale, et à former un code basé sur le signal calcique représente un champ très intéressant qu'il faudrait explorer plus en profondeur.

Figure 3-2

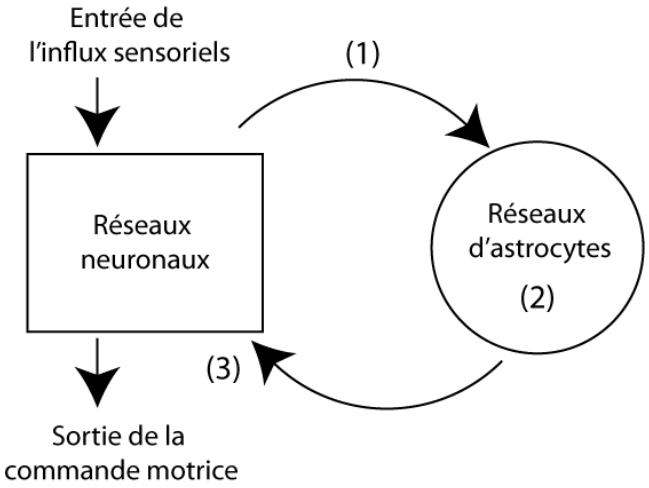

Représentation schématique de la manière dont les réseaux neuronaux et astrocytaires pourraient interagir pour traiter l'information (encodée en tant que patron d'activité neuronale) qui entre ou sort du système nerveux central.

1) Les vagues calciques astrocytaires sont initiées en réponse à l'activité des réseaux neuronaux 2-Les vagues calciques se propagent activement dans les réseaux astrocytaires. 3- Les vagues calciques astrocytaires rétroagissent sur l'activité des réseaux neuronaux. Adapté de (Smith, 1992).

3.3 La gliotransmission: la libération de la S100β

Des études antérieures ont révélé la possibilité d'une libération de S100β dépendante d'une activation des récepteurs au glutamate mGluR3 ou à l'adénosine A1 (Ciccarelli et al., 1999; Sakatani et al., 2008). Nos résultats indiquent que la réponse calcique des astrocytes est en amont de la libération de S100β puisqu'après la diffusion du BAPTA intracellulaire dans ces cellules l'application de S100β exogène est suffisante pour induire les bouffées rythmiques neuronales. Cela dit, la gliotransmission (et la libération de S100β) demeure un phénomène mal compris. Il existe diverses voies pour la libération de neuromodulateurs par les astrocytes. Plusieurs études démontrent des mécanismes qui dépendraient du calcium intracellulaire (Araque et al., 2000; Montana et al., 2006; Perea and Araque, 2005, 2007) par le biais d'exocytose vésiculaire ou lysosomale (pour revue voir (Perea et al., 2009)). Le phénomène que nous avons étudié est bloqué par le BAPTA intracellulaire ce qui suggère que ces voies dépendantes du calcium seraient impliquées, d'autant plus qu'une étude précédente a montré que le S100β est relâché à la suite d'élévation de calcium intracellulaire (Davey et al., 2001). Des mécanismes de secrétions alternatifs incluant les hémicanaux connexines/pannexines ont aussi été proposés (pour revue voir (Parpura et al., 2004). Toutefois, dans leur étude de 2008 Sakatani et ses collaborateurs excluent l'implication des connexines 43 dans la libération de S100β, car le poids moléculaire de cette protéine indique qu'elle ne pourrait pas passer via d'aussi petites structures (Sakatani et al., 2008).

Quoi qu'il en soit, la libération de S100β par les astrocytes est indéniable (Sakatani et al., 2008; Shashoua et al., 1984; Van Eldik and Zimmer, 1987). Il reste à déterminer si le S100β est sécrété en quantité suffisante pour diminuer la $[Ca^{2+}]_e$, avoir un effet sur I_{NaP} et induire la décharge rythmique neuronale. Le blocage de la baisse du calcium extracellulaire et des bouffées rythmiques neuronales par l'anticorps spécifique au S100β indique que la concentration libérée de façon endogène est suffisante. Aussi, le fait que le BAPTA doive diffuser dans le syncytium astrocytaire avant de pouvoir bloquer la décharge rythmique neuronale suggère que la formation de syncytium par les astrocytes est importante, et pourrait refléter le fait que plusieurs astrocytes participent à la libération de la S100β augmentant ainsi la quantité de protéine disponible pour la sécrétion.

De plus, les astrocytes n'ont pas nécessairement besoin de sécréter une quantité importante de la protéine chélatrice pour induire la décharge rythmique neuronale provoquée par la baisse de la $[Ca^{2+}]_e$ puisqu'à la synapse l'espace extracellulaire est très restreint, et un changement de quelques ions suffit à constituer une variation importante en termes de concentration. Ce concept a bien été modélisé par Smith SJ. (1992), qui suggère que des variations minimes de calcium extracellulaire au niveau d'une fente synaptique peuvent correspondre à des diminutions importantes en termes de concentration et avoir un effet majeur sur les phénomènes qui dépendent de cette concentration (Rusakov and Fine, 2003; Smith, 1992).

Nous verrons à la section 3.4.1 de la discussion que les canaux sodiques contenant la sous-unité α de type 1.6 ($Na_V1.6$) permettent des courants persistants souvent sous-jacents aux bouffées rythmiques des neurones. Certaines études indiquent que la distribution de ces canaux sur la membrane des neurones est non uniforme, et qu'on en retrouverait une plus grande concentration sur les segments initiaux des axones (Akin et al., 2015; Boiko et al., 2003; Hu et al., 2009; Osorio et al., 2010). Si tel est le cas pour les neurones du NVsnpr, une libération localisée et en quantité relativement moins importante de la S100β pourrait être envisagée. En effet, de fortes baisses de calcium juste au niveau de ces zones précises pourraient induire l'apparition des courants I_{NaP} et induire les bouffées rythmiques neuronales (voir figure 3-3).

De plus, la diminution de la $[Ca^{2+}]_e$ par le S100β n'exclut pas la possibilité que d'autres mécanismes puissent participer ou amplifier le phénomène. Les conditions nécessaires à l'activation des astrocytes, c'est-à-dire des activations soutenues des afférences sensorielles (stimulation répétitive à 40Hz), sont aussi propices à la mise en place de phénomènes pouvant avoir une influence sur la $[Ca^{2+}]_e$. Comme par exemple l'entrée de calcium dans les neurones suite à l'activation de canaux récepteurs ou l'activation de canaux calciques (Heinemann and Pumain, 1981), ou encore l'entrée de calcium dans les cellules gliales suite à l'activation des canaux calciques dépendants du voltages sur la membrane de ces cellules (MacVicar, 1984). En condition contrôle, nos résultats n'excluent pas que des mécanismes similaires puissent s'additionner à celui de la S100β pour amplifier la baisse de la $[Ca^{2+}]_e$. Cependant, nos expériences démontrent que, à eux seuls, ces phénomènes ne sont pas suffisants pour baisser le

calcium extracellulaire de façon significative, car le blocage de l'action de la S100β endogène suffit à empêcher la baisse de la $[Ca^{2+}]_e$ et la décharge en bouffées rythmiques des neurones induites tant par la stimulation des afférences que par une application locale de NMDA (voir figure 8 au chapitre 2).

3.3.1 Un nouveau concept d'interaction neurone-glie : Une gliotransmission non conventionnelle.

Nos résultats confirment l'implication des astrocytes dans la modulation de l'encodage de l'information neuronale. Toutefois, le mécanisme que nous avons décrit ne correspond pas tout à fait au concept de gliotransmission et de la synapse tripartite qui sont à la base des interactions neurone-glie décrites dans la majorité des études (voir figure 3-3). En effet, d'une part la synapse tripartite implique que les astrocytes détectent et modulent l'activité neuronale principalement au niveau synaptique, d'autre part la gliotransmission « classique » implique un effet des gliotransmetteurs sur des récepteurs qui peuvent aussi être activés par les neurotransmetteurs relâchés par les neurones. Le mécanisme que nous avons décrit est assez différent. Bien que l'activation des astrocytes se fasse probablement au niveau des synapses glutamatergiques tripartites qui reçoivent les afférences des fibres sensorielles périphériques, la modulation en retour exercé pas les astrocytes ne se fait vraisemblablement pas localement (aux synapses) et ne nécessite pas l'activation d'un récepteur sur les neurones. Dans notre cas, nous décrivons une gliotransmission (la libération de S100β) qui exerce son effet neuromodulateur par le contrôle de l'homéostasie du calcium extracellulaire et non par l'activation d'un récepteur. En effet, la protéine mutée (ne pouvant pas lier le calcium) n'affecte pas la $[Ca^{2+}]_e$ et ne peut pas induire les bouffées rythmiques neuronales (voir figure 6 au chapitre 2). Ceci suggère donc que les effets la S100β dans notre étude dépendent de la baisse du calcium et non d'une interaction de la protéine avec d'autres récepteurs ou protéines neuronales ou astrocytaires (voir encadré 1 au chapitre 1). L'interaction neurone-glie que nous décrivons peut donc paraitre inusitée en intégrant de façon surprenante la libération d'une substance par les astrocytes (donc une sorte de gliotransmetteur) à l'homéostasie d'un ion extracellulaire (voir figure 3-3). De plus, notre modèle suggèrent une détection/activation des astrocytes se faisant à un niveau (probablement synaptique) avec une modulation se faisant de

façon distante autour des zones neuronales qui renferment les canaux sodiques sensibles à la baisse de la $[Ca^{2+}]_e$. Nos résultats amènent donc une toute nouvelle dimension au concept de l'interaction neurone-glie.

Figure 3-3: Schématisation conceptuelle d'une interaction neurone-glie basée sur une gliotransmission non conventionnelle.

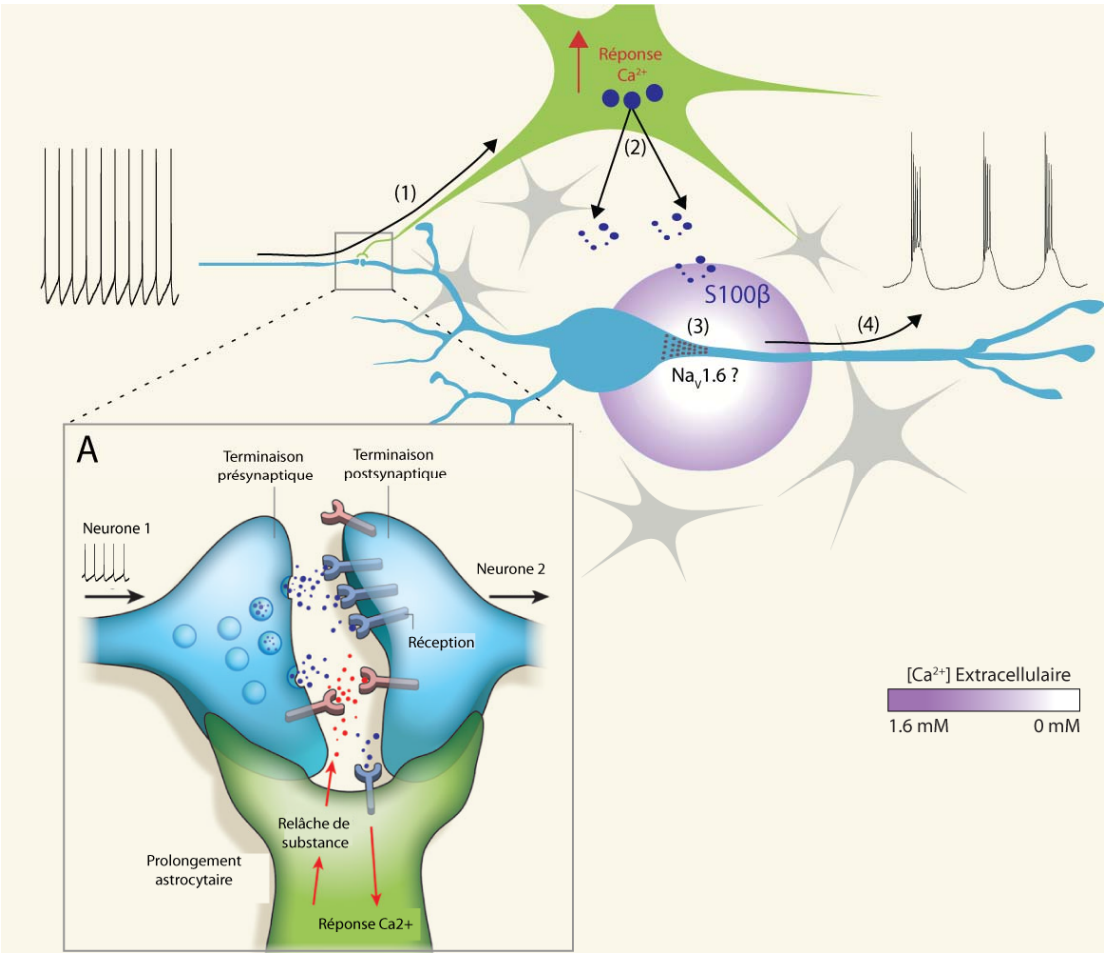

Schématisation conceptuelle d'une interaction neurone-glie basée sur une gliotransmission non conventionnelle. (A) Élargissement d'une synapse tripartite « classique »: plusieurs des récepteurs exprimés par les neurones le sont aussi par les astrocytes. Lors de la libération des neurotransmetteurs dans la fente synaptique par les terminaisons présynaptiques neuronales, les récepteurs astrocytaires sont activés, induisent une réponse calcique dans les astrocytes et la relâche de différentes substances actives (comme le glutamate, l'ATP, la D-serine) qui modulent en retour la réponse des neurones postsynaptique aux neurotransmetteurs. Modifié de Allen et Barres, 2009. (1) Notre étude indique que les astrocytes détectent l'input des afférences trigéminale par des récepteurs NMDA sur leur membrane, et rien n'indique que cette détection ne se fait pas au niveau des synapses recevant l'input des afférences trigéminales (comme dans l'encadré). Toutefois, la modulation des neurones (en retour de l'activation des astrocytes) ne se fait pas par l'activation de récepteurs sur les neurones. (2) En effet, la protéine S100β n'exerce pas son effet sur un récepteur neuronal, mais par la baisse de la $[Ca^{2+}]_e$. De plus nos résultats indiquent que la baisse de la $[Ca^{2+}]_e$ ne reste pas confinée au niveau de la synapse tripartite, mais qu'elle s'étend aux zones neuronales contenant les canaux sodiques qui sont sous-jacents aux courants I_{NaP}. (3) Hypothèse: comme proposé dans la section 3.3, les segments initiaux des axones des neurones pourraient contenir les canaux sodiques qui sont sous-jacents aux courants I_{NaP}, et dès lors une sécrétion plus localisée de la S100β dans cette zone spécifique serait suffisante pour induire (4) les bouffées rythmiques neuronales. Une autre possibilité serait que plusieurs astrocytes d'un syncytium (autres astrocytes en gris) « déversent » plus de S100β qui pourrait alors « clamper » la $[Ca^{2+}]e$ à un niveau bas dans une zone plus étendue.

3.4 La décharge en bouffées rythmiques des neurones.

3.4.1 Les canaux sodiques sous-jacents au courant sodique persistant

Les canaux sodiques dépendants du voltage sont composés d'une large sous-unité α qui est associée à d'autres protéines. Ils forment en général des hétérodimères ou hétérotrimères de 1 sous-unité α et de 1 ou 2 sous-unités β. Au total, neuf sous-unités α distinctes ont été clonées chez les mammifères ($Na_V1.1$-1.9) (Goldin et al., 2000). Les sous-unités α sont formées d'une répétition de 4 domaines (I à IV) contenant chacun six segments transmembranaires (S1 à S6). Le segment S4 est hautement conservé et constitue le senseur de voltage. La sous-unité α constitue la partie principale du canal et est fonctionnelle même sans la présence de sous-unités β. L'association des sous-unités α aux sous-unités β permet la formation de complexes avec des caractéristiques d'activation variées, et permet une distribution et une localisation différentielle des canaux sur la membrane des cellules (Aman et al., 2009). La diversité des courants sodiques dépend en partie de la composition en sous-unités, en occurrence α et β, des canaux sodiques. Il existe 4 sous-unités β (β1, 2, 3 et 4). Plusieurs études indiquent que la sous-unité β1 serait impliquée dans l'inactivation rapide des canaux sodiques et dans la diminution des courants persistants. D'un autre côté, les sous-unités β2, 3, et 4 faciliteraient dans différentes conditions la persistance des courants (Aman et al., 2009).

Toutefois, l'identité des canaux sodiques sous-jacents aux courants I_{NaP} reste mal définie. Il semble que les canaux contenant les sous-unités α $Na_V1.4$ ou $Na_V1.5$ n'expriment presque pas de courant I_{NaP} (Mantegazza et al., 2005). D'un autre côté, plusieurs travaux indiquent que les canaux contenant la sous-unité α $Na_V1.6$ sont fortement exprimés dans différents neurones où les courants I_{NaP} sont prépondérants (Maurice et al., 2001; Mercer et al., 2007; Osorio et al., 2010) dont les neurones du NVmes (Enomoto et al., 2007). Cela dit, dans les neurones pyramidaux du CA1 où les $Na_V1.6$ ont été génétiquement éliminés, les courants I_{NaP} sont seulement diminués de 40% (Royeck et al., 2008), suggérant que d'autres sous-unités pourraient sous-tendre ces courants (Carter et al., 2012). En fait, il semblerait que les sous-unités $Na_V1.1$, 1.2, 1.6, 1.8 et 1.9 semblent toutes avoir une forte capacité à former des canaux capables d'engendrer des courants I_{NaP} (Enomoto et al., 2007; Mantegazza et al., 2005; Ptak et al., 2005; Rush et al., 2005). Cependant, seules les sous-unités $Na_V1.1$, 1.2, et 1.6 sont

retrouvées dans le système nerveux central, tandis que les 1.8 et 1.9 sont restreintes au système nerveux périphérique (Yu and Catterall, 2003). Dans le contexte de nos recherches, l'étude de l'expression des sous-unités $Na_V1.1$, 1.2, et 1.6 dans le NVsnpr pourrait permettre de préciser l'origine des courants I_{NaP} à la base des bouffées rythmiques. À cet égard, il serait intéressant de tester la 4,9 anhydro TTX, toxine dérivée de la TTX, qui bloque sélectivement les canaux $Na_V1.6$ et les courants I_{NaP} qui en dépendent (Hargus et al., 2013; Rosker et al., 2007).

Carter et ses collaborateurs (Carter et al., 2012) suggèrent que les courants I_{NaP} pourraient provenir des mêmes canaux qui sont à l'origine des courants sodiques transitoires (I_{NaT}) sous-jacents aux potentiels d'action: dans leur modélisation, ils montrent, du moins pour les neurones pyramidaux de l'aire CA1, que sans changer les caractéristiques des canaux sodiques, ils peuvent induire des courants sodiques persistants. En effet, les auteurs proposent que ces courants persistants reflètent des propriétés d'ouverture (*gating*), à des potentiels hyperpolarisés sous-laminaires, de canaux sodiques « standard »: les mêmes canaux qui en cas de dépolarisation supra-laminaires provoqueraient des potentiels d'action classiques. Les auteurs n'excluent pas la possibilité que ces courants I_{NaP} puissent être augmentés par d'autres mécanismes plus spécifiques, par exemple: des modes d'ouverture particuliers durant lesquels les canaux resteraient en conformation ouverts plus longtemps (Alzheimer et al., 1993a). De telles spécialisations seraient plus couramment retrouvées dans les neurones ayant des courants persistants plus proéminents (Magistretti and Alonso, 2002; Magistretti et al., 1999) et pourraient peut-être se retrouver pour les courants I_{NaP} du NVsnpr. Dans cette même ligne de pensée, le groupe de Crill avait déjà proposé que les courants I_{NaT} et I_{NaP} proviennent de flux dans les mêmes canaux. Dans le cas des I_{NaP}, il s'agirait de canaux sodiques qui perdent leurs caractéristiques d'inactivation de façon intermittente (Brown et al., 1994).

Les protéines kinases C (PKC) ont aussi été impliquées dans la modulation des canaux sodiques et l'induction des courants I_{NaP} (Brown et al., 1994). L'action de ces kinases ralentirait l'inactivation des courants sodiques macroscopiques et en parallèle réduirait les pics de ces courants (Astman et al., 1998; Cantrell et al., 1996). Le ralentissement de l'inactivation pourrait mener à des courants $I_{NaP,}$ cependant une amplitude diminuée des pics ne correspond pas à la signature du courant I_{NaP} que nous avons observé et qui est décrite par plusieurs groupes (Brocard et al., 2010; Brown et al., 1994; Tazerart et al., 2007; Tsuruyama et al.,

2013). D'ailleurs, une étude a montré que l'activation des PKCs bloquerait les décharges en bouffées (dépendante de I_{NaP}) dans les neurones de l'hippocampe (Alroy et al., 1999). Il semble donc judicieux d'exclure un rôle des PKCs dans l'induction de courants I_{NaP} dans le NVsnpr.

De nombreuses études montrent une grande sensibilité des canaux sodiques aux protéases qui par leur action peuvent influencer les propriétés d'inactivation de ces canaux (Iwata et al., 2004; Kraner et al., 1989; Zwerling et al., 1991). Par exemple, en conditions pathologiques comme dans les lésions axonales in vitro (von Reyn et al., 2012), les calpaïnes sont connues pour leur capacité à cliver des segments spécifiques des Na_V qui seraient importants dans la désactivation de ces canaux. En modifiant la structure de ces canaux, ces protéases pourraient permettre l'apparition de courants sodiques avec une persistance plus importante. Dans la même ligne d'idée, un lien entre la calpaïne et l'augmentation d'I_{NaP} a déjà été observé au niveau du système cardiaque (Undrovinas et al., 2013).
En conclusion, différents mécanismes semblent être en mesure de modifier la structure ou les propriétés d'ouverture des Na_V, et pourraient être à l'origine des courants I_{NaP}. De plus, ceci expliquerait la difficulté qui semble inhérente à définir de façon exacte l'origine de ces courants et le type des canaux impliqués.

3.4.2 Effet de la baisse de calcium sur I_{NaP}?

Nos expériences montrent un effet robuste de la baisse de calcium sur I_{NaP} et ces données sont en adéquation totale avec plusieurs études (Brocard et al., 2013; Brocard et al., 2006; Tazerart et al., 2007; Tazerart et al., 2008; Tsuruyama et al., 2013). Néanmoins, les mécanismes qui expliquent un tel effet de la baisse du calcium restent mal connus, et n'ont pas été étudiés durant nos travaux. Nous avons proposé l'explication avancée par Armstrong qui soutient que les ions calciques pourraient bloquer les pores des canaux sodiques et ainsi favoriser leur fermeture (voir la discussion de l'article (Armstrong, 1999).

Une autre théorie souvent avancée pour expliquer l'effet du calcium sur les propriétés d'ouverture des canaux ioniques en général est celle de « charge de surface ». Elle s'appuie sur l'idée que les champs électriques locaux, créés par les charges des ions divalents à la surface des membranes, peuvent biaiser les détecteurs de voltage des canaux qui sont dans ces

membranes. Par exemple, en présence de Ca^{2+} extracellulaire, des charges positives s'accumulent sur la surface extracellulaire des membranes et biaisent les détecteurs de voltage leur indiquant alors une « fausse » hyperpolarisation. Par contre, en absence de Ca^{2+} extracellulaire, ces mêmes détecteurs seraient biaisés pour capter une dépolarisation (Hille, 2001). Ce phénomène n'explique pas la persistance des courants, mais il pourrait expliquer le déplacement de la courbe d'activation du courant I_{NaP} vers des potentiels plus hyperpolarisés lorsque la $[Ca^{2+}]_e$ est diminuée (voir figure supplémentaire 2 de l'article). Toutefois cette explication ne semble pas pouvoir s'appliquer à nos expériences puisque lorsque le Ca^{2+} était omis du ACSF, un autre ion divalent (le Mg^{2+}) était rajouté afin de compenser l'effet de charges de surface. Cette même procédure a aussi été faite par d'autres groupes qui ont étudié l'effet de la baisse de calcium sur le courant I_{NaP} (Su et al., 2001; Tazerart et al., 2007; Tazerart et al., 2008; Tsuruyama et al., 2013).

L'étude d'Armstrong (1999), démontre la différence de l'effet de charge de surface et l'effet d'occupation des pores par le calcium. En utilisant la saxitoxine (STX), une toxine qui occupe l'entrée extérieure des pores des canaux sodiques, ce chercheur a mesuré le courant d'ouverture (*gating current*) généré par le mouvement du segment transmembranaire S4 des canaux sodiques. En présence de STX, les variations de $[Ca^{2+}]_e$ ont peu d'effet sur le *gating current*, ce qui indique que le phénomène « charges de surfaces » n'est pas important pour l'ouverture des canaux sodiques. D'un autre coté, en absence de STX, un effet beaucoup plus important du calcium peut être observé sur le *gating current*. Ceci indique que la modulation par le calcium est due à l'entrée de l'ion dans les pores des canaux sodiques; le blocage qui en résulte serait alors réversible par la diminution du calcium extracellulaire (Armstrong, 1999).

3.5 Implications de nos résultats

3.5.1 Implications fonctionnelles au niveau du NVsnpr

Notre étude décrit un mécanisme robuste permettant un changement du mode de décharge des neurones du NVsnpr. Un point important que nous n'avons cependant pas étudié est celui de la synchronisation. Dans un GPC, il est important qu'il y ait une synchronisation entre les neurones qui contrôlent une même population de motoneurones (MNs). Le fait que les

astrocytes forment des syncytia soulève la possibilité intéressante que ces cellules puissent définir des domaines fonctionnels. Par exemple dans le cortex somatosensoriel associé aux vibrisses, les astrocytes forment des réseaux qui délimitent les barils (Houades et al., 2008) indiquant une organisation définissant des limites fonctionnelles. Avec une telle organisation, la sécrétion de S100β pourrait créer un environnement extracellulaire dépourvu de calcium pour plusieurs neurones qui sont incorporés dans un même syncytium. Ces neurones « baignant » dans un environnement extracellulaire uniforme, par l'action des astrocytes, rentreraient alors dans le même mode de décharge en bouffées rythmiques alors que les inputs sensoriels pourraient synchroniser les phases de ces décharges rythmiques. Il est intéressant de noter que ces inputs arrivent au NVsnpr de façon très organisée et contactent des cellules adjacentes les unes aux autres. Une suite logique de ce projet, déjà amorcée à notre laboratoire, est d'examiner la synchronisation des neurones à l'intérieur d'un même syncytium.

Plusieurs études ont montré qu'il existe des projections entre le NVsnpr et le NVmot (voir section 1.3.4.3 au chapitre 1). Comme nous l'avons vu plus tôt, le NVsnpr pourrait constituer une partie essentielle du GPC de la mastication. Toutefois à ce jour, aucune étude n'a montré de façon directe que le rythme induit dans le NVsnpr pouvait être transmis aux MNs du NVmot qui contrôlent les muscles de la mastication. Une autre suite logique à notre projet serait d'examiner l'activité des MNs du NVmot suite à l'activation des neurones du NVsnpr.

Enfin, bien que notre étude ne se soit pas directement penchée sur la question, dans le contexte d'une activité rythmique qui sous-tend l'activité masticatoire, un point important est de savoir comment le mécanisme de rythmicité peut être arrêté après avoir été enclenché. Le modèle que nous avons proposé repose sur l'apparition d'un courant sodique persistant dépendant du voltage qui s'active avec la baisse de la concentration du calcium extracellulaire. Nous pensons que plusieurs mécanismes pourraient permettre un arrêt de l'activité rythmique:

1) Un premier mécanisme pourrait reposer sur la recapture ou la dégradation du S100β dans l'espace extracellulaire, permettant un retour de la $[Ca^{2+}]_e$, une diminution du courant sodique persistant, et donc un arrêt des bouffées rythmiques. Cette hypothèse semble moins plausible puisque nos données en interface montrent qu'à la suite de stimulations électriques, le calcium extracellulaire semble diminuer pour une durée qui dépasserait, en toute vraisemblance, la

durée d'un vrai cycle masticatoire (voir figure 2-1 b). Ceci pourrait être une indication que l'arrêt du mode de décharge en bouffées rythmiques ne dépend pas uniquement ou directement de la $[Ca^{2+}]_e$.

2) Un autre mécanisme de terminaison des bouffées pourrait reposer sur le caractère intrinsèque de dépendance au voltage du courant sodique persistant. En effet, ce courant s'active entre -65 et -50mV (voir section 1.4.2.1.2). D'ailleurs, ce phénomène est bien visible dans la figure 1 de l'article, où un neurone non-hyperpolarisé ne peut décharger en bouffées rythmiques. Ainsi, durant un cycle masticatoire, un input sensoriel continu qui produit une dépolarisation graduelle des neurones finira par les amener en dehors de la fenêtre d'activation du I_{NaP}, et, par le fait même, terminera la séquence masticatoire en dépit de l'activation des astrocytes et de la baisse de calcium extracellulaire. Il est intéressant de noter que ce même mécanisme pourrait expliquer l'arrêt brusque de la mastication lorsque l'on mord par surprise dans une olive non dénoyautée; le fort stimulus sensoriel provoqué par le noyau dur pourrait être à l'origine d'une dépolarisation trop importante des neurones et ainsi causer un arrêt du générateur des mouvements rythmiques. Une terminaison des bouffées rythmiques par ce mécanisme pourrait à la fois arrêter les séquences masticatoires normales ou même offrir un mécanisme protecteur lorsque la mastication doit être interrompue de façon abrupte à cause d'un imprévu détecté par les récepteurs parodontaux.

3) Finalement, nous pensons que des afférences inhibitrices pourraient jouer un rôle important pour l'arrêt de la rythmicité notamment dans un contexte qui impliquerait un blocage volontaire et brusque du mouvement masticatoire. Du point de vue fonctionnel, une telle inhibition pourrait être tout aussi efficace si elle se fait directement sur les neurones qui produisent le rythme, au niveau du NVsnpr, ou sur les neurones du NVmot qui contrôlent directement les mouvements masticatoires.

Cela dit, ces différentes hypothèses n'ont pas été abordées par nos travaux et il est clair que l'étude des mécanismes responsables de l'arrêt des décharges rythmiques pourrait constituer une autre avenue intéressante pour la suite de notre projet.

3.5.2 Implications physiologiques dans le SNC

Un rôle des courants I_{NaP} a aussi été démontré dans les circuits neuronaux des GPCs de la respiration et de la locomotion (Brocard et al., 2013; Brocard et al., 2010; Del Negro et al., 2005; Ryczko et al., 2010; Tazerart et al., 2007; Tazerart et al., 2008; Zhong et al., 2007). Dans le contexte de la locomotion, l'étude de Brocard et de ses collaborateurs (2013) a clairement démontré que les décharges rythmiques (qui dépendent des courants I_{NaP}) pouvaient être induites artificiellement par des changements spécifiques de la $[Ca^{2+}]_e$ et $[K^+]_e$ (voir la figure 9 au chapitre 1). Encore plus intéressant, ces auteurs ont observé que lorsqu'une activité de type locomotrice était évoquée de façon «physiologique», il y avait dans les régions qui correspondent au GPC de la locomotion une diminution du $[Ca^{2+}]_e$ et une augmentation du $[K^+]_e$ (Brocard et al., 2013; Brocard et al., 2010). Il est bien connu que l'activité neuronale soutenue augmente la $[K^+]_e$, alors que les mécanismes à l'origine de la diminution du $[Ca^{2+}]_e$ restent inconnus. Selon les auteurs, il s'agirait d'une recapture du calcium par les somas et dendrites neuronaux, mais rien n'empêche de penser que les astrocytes de la moelle épinière soient également impliqués. En effet, par la libération de S100β, les astrocytes de la moelle épinière pourraient baisser la $[Ca^{2+}]_e$ dans ces circuits locomoteurs et jouer le même rôle que nous avons décrit dans le NVsnpr.

Considérant l'ubiquité de la S100β dans le SNC et le fait que la baisse de la $[Ca^{2+}]_e$ induit l'apparition de décharge en bouffées dans différentes populations de neurones du SNC selon plusieurs études; (Brocard et al., 2006; Heinemann et al., 1977; Johnson et al., 1994; Su et al., 2001; Tazerart et al., 2008), nous pensons que le mécanisme décrit dans le NVsnpr pourrait être retrouvé à différents niveaux du SNC, et être à la base de plusieurs fonctions physiologiques. Outre les circuits impliqués dans des mouvements rythmiques comme la mastication, la respiration et la locomotion, l'activité rythmique neuronale a aussi été observée dans plusieurs régions du système nerveux où le lien avec des comportements rythmiques n'est pas évident. Ainsi, les décharges de types oscillatoires ont été associées à des processus cognitifs (Luu et al., 2004), au transfert d'informations entre des régions du cerveau (Rubino et al., 2006), à l'apprentissage et la mémoire (Sederberg et al., 2007), au sommeil et à l'éveil (Destexhe et al., 1999), ou encore à la coordination motrice (Kuhn et al., 2004; Lee, 2003).

Dès lors, dans ces différents contextes, le mécanisme que nous avons décrit pourrait imposer l'étude du rôle des astrocytes dans l'encodage de phénomènes cognitifs plus complexes.

3.5.3 Implications pathologiques

L'altération des concentrations de la S100β dans le sérum ou le fluide cérébro-spinal est associée à un grand nombre de pathologies qui affectent le SNC (pour revue voir Yardan et al., 2011) . Ainsi, dans plusieurs neuropathologies incluant la maladie d'Alzheimer, l'Épilepsie, la Schizophrénie, la maladie de Parkinson et le Syndrome de Down des augmentations du niveau d'expression de la S100β sont observées (Griffin et al., 1989; Muramatsu et al., 2003; Rothermundt et al., 2004; Schmitt et al., 2005). Par exemple, dans le modèle de la maladie de Parkinson induite par le MPTP (1-methyl-4-phenyl-1,2,3,6-tetrahydropyridine), l'expression de la S100β par les astrocytes est significativement augmentée par le MPTP dans le striatum et dans la substance noire (Muramatsu et al., 2003).

Le syndrome de Down représente un cas particulier intéressant. En effet, le gène qui code l'expression de la S100β est situé dans la région du chromosome 21 associé au syndrome de Down, et la surexpression de la S100β dans cette maladie, du fait de la trisomie de ce chromosome, est associée à plusieurs troubles neurologiques liés à cette maladie (Allore et al., 1988; Griffin et al., 1998; Griffin et al., 1989). Aussi, en lien avec nos résultats, il est très intéressant de noter que les sujets qui souffrent du syndrome de Down ont des mouvements masticatoires mal coordonnés, et ils souffrent souvent aussi de dyskinésie oro-faciale notamment avec des mouvements masticatoires invasifs (Dinan and Golden, 1990; Faulks et al., 2008; Gisel et al., 1984; Hennequin et al., 2005). Bien que plusieurs raisons puissent expliquer ces difficultés, à la lumière de notre étude, on pourrait postuler que cette affectation motrice de la mastication à un lien direct avec le déséquilibre des taux de S100β extracellulaire et la modulation des courants I_{NaP} dans le NVsnpr.

La sclérose latérale amyotrophique (SLA) est également une maladie intéressante du point de vue de nos travaux pour trois raisons principales. 1) Plusieurs données indiquent que le développement de cette pathologie est associé à l'apparition de spasticité musculaire qui dépendrait de la présence de courant I_{NaP} dans les MNs. Par exemple, des études ont montré que dans les souris mutantes S0D1, un modèle de la SLA, l'amplitude des courants I_{NaP} est

augmentée dans les MNs de la moelle épinière (Kuo et al., 2004; Kuo et al., 2005; Pieri et al., 2003). De plus, le riluzole, substance connue pour sa capacité à bloquer les courants I_{NaP} (Urbani and Belluzzi, 2000), est un médicament utilisé pour la SLA suggérant d'autant plus l'implication de ces courants dans cette maladie (Bensimon et al., 1994). 2) Dans un autre ordre d'idée, l'équipe de YANG a montré que l'activité des astrocytes influençait le développement de la SLA dans le modèle de souris SOD1G93A. Cette étude indique qu'un dysfonctionnement cellulaire des astrocytes amplifie leurs réponses calciques et la gliotransmission qui en découle. Ces chercheurs ont montré que dans ce même contexte, le blocage de la gliotransmission retardait l'évolution de la maladie (Kawamata et al., 2014). 3) À ce jour, il n'y a pas eu beaucoup d'études liant la S100β et la SLA, à part une étude chez l'humain indiquant que l'expression de la S100β est augmentée dans les astrocytes de la moelle épinière de patients atteints de SLA (Migheli et al., 1999) et une autre étude indiquant que les niveaux de S100β sont diminués dans le sérum des patients souffrant de la SLA (Otto et al., 1998). Il est clair que d'autres recherches sur l'expression de la S100β dans la SLA sont nécessaires pour clarifier ces résultats qui semblent à priori contradictoires. Quoi qu'il en soit, il est clair que la SLA semble impliquer : 1) une amplification de courants I_{NaP}, 2) une activité calcique des astrocytes et 3) un débalancement des taux de S100β. Dès lors, le mécanisme que nous avons décrit pourrait peut-être expliquer certains aspects de la physiopathologie de la SLA.

De façon générale, la dégénérescence neuronale est un des phénomènes notables de plusieurs maladies associées à la surexpression de la S100β. À la vue de nos résultats il serait envisageable que l'accumulation extracellulaire de la S100β puisse diminuer la $[Ca^{2+}]_e$, augmenter l'activité de canaux sodiques et induire un effet d'excitotoxicité (Carter, 1998; Carter et al., 2000). Les changements de $[Ca^{2+}]_e$ peuvent aussi avoir d'autres effets qui ne dépendent pas d'une modulation des canaux Na^+. Par exemple, il est bien connu que la déplétion du Ca^{2+}extracellulaire diminue ou bloque la transmission synaptique. Aussi, certains transporteurs membranaires comme le Ca^{2+}-ATPase et l'échangeur Na^+/Ca^+ seront potentiellement affectés par les changements de gradients dus aux variations de la $[Ca^{2+}]_e$ (Strehler and Zacharias, 2001). De tels phénomènes pourraient certainement être impliqués dans des conditions pathologiques qui dépendent d'une baisse de la $[Ca^{2+}]_e$ par la libération de la S100β. Finalement, il est important de rappeler (voir encadré 1 au Chapitre 1) que la

protéine S100β, outre sa capacité d'attacher le Ca^{2+}, agit sur plusieurs protéines impliquées dans diverses fonctions cellulaires incluant des protéines comme la p53 impliquée dans l'apoptose cellulaire. Dès lors, on ne peut pas exclure que ces autres fonctions de la S100β jouent un rôle important dans les neuropathologies ayant une expression augmentée de la protéine.

La maladie ayant peut-être le plus de points en commun avec le mécanisme décrit par nos travaux est l'épilepsie. Les décharges neuronales observées pendant les crises épileptiques sont très similaires à celles enregistrées dans le NVsnpr pendant l'activité rythmique. Aussi, les courants I_{NaP} ainsi que les canaux $Na_V1.6$ seraient impliqués dans cette maladie (Hargus et al., 2013; Makinson et al., 2014). De plus, des études rapportent que la $[Ca^{2+}]_e$ diminue de façon significative dans différentes régions du SNC pendant l'activité épileptique (Heinemann et al., 1977; Pumain et al., 1983; Pumain et al., 1985). En fait ces études indiquent que la $[Ca^{2+}]_e$ chute à un niveau tel que la transmission synaptique serait abolie. Nos données pourraient alors expliquer le fait paradoxal que l'activité nerveuse excessive et rythmique continue à se propager même en absence de transmission synaptique. Finalement, les concentrations de S100β mesurées dans les cerveaux de sujets épileptiques sont beaucoup plus élevées, et plusieurs éléments indiquent que les astrocytes pourraient jouer un rôle prépondérant dans cette pathologie (Coulter and Steinhauser, 2015; Steinhauser et al., 2015).

3.6 Conclusion

Notre étude démontre que les astrocytes peuvent diminuer la concentration du calcium extracellulaire en sécrétant la protéine S100β. Ce faisant, ils contrôlent activement le mode de décharge des neurones avoisinants, les faisant passer d'un mode tonique à un mode rythmique. Ainsi, dans le domaine des neurosciences, cette étude contribue à l'avancement des connaissances non seulement en confirmant le rôle de la glie dans l'encodage nerveux, mais surtout en décrivant un mécanisme complètement inédit d'interaction neurone-glie faisant appelle à une gliotransmission qui implique non pas l'activation d'un récepteur, mais la modulation de la concentration d'un ion extracellulaire. Outre une compréhension plus complète de la base cellulaire de la rythmogénèse dans le système trigéminal, le mécanisme présenté dans cette thèse, possiblement applicable à d'autres GPCs, a le potentiel de mener à

de nouvelles cibles thérapeutiques puisque la protéine S100β semble être impliquée dans plusieurs pathologies du SNC. Dès lors, il sera intéressant à l'avenir d'examiner l'importance de cette protéine et de l'activité des astrocytes dans d'autres GPC.

Bibliographie

Adermark, L., and Lovinger, D.M. (2008). Electrophysiological properties and gap junction coupling of striatal astrocytes. Neurochem Int 52, 1365-1372.
Agulhon, C., Fiacco, T.A., and McCarthy, K.D. (2010). Hippocampal short- and long-term plasticity are not modulated by astrocyte Ca2+ signaling. Science 327, 1250-1254.
Akin, E.J., Sole, L., Dib-Hajj, S.D., Waxman, S.G., and Tamkun, M.M. (2015). Preferential targeting of Nav1.6 voltage-gated Na+ Channels to the axon initial segment during development. PLoS One 10, e0124397.
Allen, N.J., and Barres, B.A. (2009). Neuroscience: Glia - more than just brain glue. Nature 457, 675-677.
Allore, R., O'Hanlon, D., Price, R., Neilson, K., Willard, H.F., Cox, D.R., Marks, A., and Dunn, R.J. (1988). Gene encoding the beta subunit of S100 protein is on chromosome 21: implications for Down syndrome. Science 239, 1311-1313.
Alroy, G., Su, H., and Yaari, Y. (1999). Protein kinase C mediates muscarinic block of intrinsic bursting in rat hippocampal neurons. J Physiol 518, 71-79.
Alzheimer, C., Schwindt, P.C., and Crill, W.E. (1993a). Modal gating of Na+ channels as a mechanism of persistent Na+ current in pyramidal neurons from rat and cat sensorimotor cortex. J Neurosci 13, 660-673.
Alzheimer, C., Schwindt, P.C., and Crill, W.E. (1993b). Postnatal development of a persistent Na+ current in pyramidal neurons from rat sensorimotor cortex. J Neurophysiol 69, 290-292.
Aman, T.K., Grieco-Calub, T.M., Chen, C., Rusconi, R., Slat, E.A., Isom, L.L., and Raman, I.M. (2009). Regulation of persistent Na current by interactions between beta subunits of voltage-gated Na channels. J Neurosci 29, 2027-2042.
Amzica, F., Massimini, M., and Manfridi, A. (2002). Spatial buffering during slow and paroxysmal sleep oscillations in cortical networks of glial cells in vivo. J Neurosci 22, 1042-1053.
Amzica, F., and Steriade, M. (2000). Neuronal and glial membrane potentials during sleep and paroxysmal oscillations in the neocortex. J Neurosci 20, 6648-6665.
Andriezen, W.L. (1893). The Neuroglia Elements in the Human Brain. Br Med J 2, 227-230.
Aoki, C., and Pickel, V.M. (1992). C-terminal tail of beta-adrenergic receptors: immunocytochemical localization within astrocytes and their relation to catecholaminergic neurons in N. tractus solitarii and area postrema. Brain Res 571, 35-49.
Appenteng, K., Lund, J.P., and Seguin, J.J. (1982). Intraoral mechanoreceptor activity during jaw movement in the anesthetized rabbit. J Neurophysiol 48, 27-37.
Araque, A., Carmignoto, G., Haydon, P.G., Oliet, S.H., Robitaille, R., and Volterra, A. (2014). Gliotransmitters travel in time and space. Neuron 81, 728-739.
Araque, A., Li, N., Doyle, R.T., and Haydon, P.G. (2000). SNARE protein-dependent glutamate release from astrocytes. J Neurosci 20, 666-673.
Araque, A., Martin, E.D., Perea, G., Arellano, J.I., and Buno, W. (2002). Synaptically released acetylcholine evokes Ca2+ elevations in astrocytes in hippocampal slices. J Neurosci 22, 2443-2450.

Araque, A., Parpura, V., Sanzgiri, R.P., and Haydon, P.G. (1998a). Glutamate-dependent astrocyte modulation of synaptic transmission between cultured hippocampal neurons. Eur J Neurosci 10, 2129-2142.
Araque, A., Parpura, V., Sanzgiri, R.P., and Haydon, P.G. (1999). Tripartite synapses: glia, the unacknowledged partner. Trends Neurosci 22, 208-215.
Araque, A., Sanzgiri, R.P., Parpura, V., and Haydon, P.G. (1998b). Calcium elevation in astrocytes causes an NMDA receptor-dependent increase in the frequency of miniature synaptic currents in cultured hippocampal neurons. J Neurosci 18, 6822-6829.
Armstrong, C.M. (1999). Distinguishing surface effects of calcium ion from pore-occupancy effects in Na+ channels. Proc Natl Acad Sci U S A 96, 4158-4163.
Astman, N., Gutnick, M.J., and Fleidervish, I.A. (1998). Activation of protein kinase C increases neuronal excitability by regulating persistent Na+ current in mouse neocortical slices. J Neurophysiol 80, 1547-1551.
Astori, S., Wimmer, R.D., Prosser, H.M., Corti, C., Corsi, M., Liaudet, N., Volterra, A., Franken, P., Adelman, J.P., and Luthi, A. (2011). The Ca(V)3.3 calcium channel is the major sleep spindle pacemaker in thalamus. Proc Natl Acad Sci U S A 108, 13823-13828.
Athanassiadis, T. (2009). Neural circuits engaged in mastication and orofacial nociception
Athanassiadis, T., Olsson, K.A., Kolta, A., and Westberg, K.G. (2005). Identification of c-Fos immunoreactive brainstem neurons activated during fictive mastication in the rabbit. Exp Brain Res 165, 478-489.
Avoli, M., Drapeau, C., Perreault, P., Louvel, J., and Pumain, R. (1990). Epileptiform activity induced by low chloride medium in the CA1 subfield of the hippocampal slice. J Neurophysiol 64, 1747-1757.
Bal, A., Bachelot, T., Savasta, M., Manier, M., Verna, J.M., Benabid, A.L., and Feuerstein, C. (1994). Evidence for dopamine D2 receptor mRNA expression by striatal astrocytes in culture: in situ hybridization and polymerase chain reaction studies. Brain Res Mol Brain Res 23, 204-212.
Bal, T., and McCormick, D.A. (1993). Mechanisms of oscillatory activity in guinea-pig nucleus reticularis thalami in vitro: a mammalian pacemaker. J Physiol 468, 669-691.
Ballerini, L., Bracci, E., and Nistri, A. (1997). Pharmacological block of the electrogenic sodium pump disrupts rhythmic bursting induced by strychnine and bicuculline in the neonatal rat spinal cord. J Neurophysiol 77, 17-23.
Baudier, J., Labourdette, G., and Gerard, D. (1985). Rat brain S100b protein: purification, characterization, and ion binding properties. A comparison with bovine S100b protein. J Neurochem 44, 76-84.
Bazett, H.C., and Penfield, W.G. (1922). A study of the Sherrington decerebrate animal in the chronic as well as acute condition. Brain 45, 185.
Beck, A., Lohr, C., Nett, W., and Deitmer, J.W. (2001). Bursting activity in leech Retzius neurons induced by low external chloride. Pflugers Arch 442, 263-272.
Belanger, M., Allaman, I., and Magistretti, P.J. (2011). Brain energy metabolism: focus on astrocyte-neuron metabolic cooperation. Cell Metab 14, 724-738.
Benninger, C., Kadis, J., and Prince, D.A. (1980). Extracellular calcium and potassium changes in hippocampal slices. Brain Res 187, 165-182.
Bensimon, G., Lacomblez, L., and Meininger, V. (1994). A controlled trial of riluzole in amyotrophic lateral sclerosis. ALS/Riluzole Study Group. N Engl J Med 330, 585-591.

Berger, T., Schnitzer, J., and Kettenmann, H. (1991). Developmental changes in the membrane current pattern, K+ buffer capacity, and morphology of glial cells in the corpus callosum slice. J Neurosci 11, 3008-3024.
Bergles, D.E., Diamond, J.S., and Jahr, C.E. (1999). Clearance of glutamate inside the synapse and beyond. Curr Opin Neurobiol 9, 293-298.
Bernier, A.P., Arsenault, I., Lund, J.P., and Kolta, A. (2010). Effect of the stimulation of sensory inputs on the firing of neurons of the trigeminal main sensory nucleus in the rat. J Neurophysiol 103, 915-923.
Bezzi, P., Carmignoto, G., Pasti, L., Vesce, S., Rossi, D., Rizzini, B.L., Pozzan, T., and Volterra, A. (1998). Prostaglandins stimulate calcium-dependent glutamate release in astrocytes. Nature 391, 281-285.
Boiko, T., Van Wart, A., Caldwell, J.H., Levinson, S.R., Trimmer, J.S., and Matthews, G. (2003). Functional specialization of the axon initial segment by isoform-specific sodium channel targeting. J Neurosci 23, 2306-2313.
Bourque, M.J., and Kolta, A. (2001). Properties and interconnections of trigeminal interneurons of the lateral pontine reticular formation in the rat. J Neurophysiol 86, 2583-2596.
Bracci, E., Beato, M., and Nistri, A. (1998). Extracellular K+ induces locomotor-like patterns in the rat spinal cord in vitro: comparison with NMDA or 5-HT induced activity. J Neurophysiol 79, 2643-2652.
Bremer, F. (1923). Physiologie nerveuse de la mastication chez le chat et le lapin. Reponses masticatrices corticales et centre corticale du gout. Archives Internationales de Physiologie 21, 308-358.
Brocard, F., Shevtsova, N.A., Bouhadfane, M., Tazerart, S., Heinemann, U., Rybak, I.A., and Vinay, L. (2013). Activity-dependent changes in extracellular Ca2+ and K+ reveal pacemakers in the spinal locomotor-related network. Neuron 77, 1047-1054.
Brocard, F., Tazerart, S., and Vinay, L. (2010). Do pacemakers drive the central pattern generator for locomotion in mammals? Neuroscientist 16, 139-155.
Brocard, F., Verdier, D., Arsenault, I., Lund, J.P., and Kolta, A. (2006). Emergence of intrinsic bursting in trigeminal sensory neurons parallels the acquisition of mastication in weanling rats. J Neurophysiol 96, 2410-2424.
Brown, A.M., Schwindt, P.C., and Crill, W.E. (1994). Different voltage dependence of transient and persistent Na+ currents is compatible with modal-gating hypothesis for sodium channels. J Neurophysiol 71, 2562-2565.
Brown, T.G. (1911). The intrinsic factors in the act of progression in the mammal. Proc R Soc Lond B Biol Sci 84, 308-319.
Brown, T.G. (1914). On the nature of the fundamental activity of the nervous centres; together with an analysis of the conditioning of rhythmic activity in progression, and a theory of the evolution of function in the nervous system. J Physiol 48, 18-46.
Brumberg, J.C., Nowak, L.G., and McCormick, D.A. (2000). Ionic mechanisms underlying repetitive high-frequency burst firing in supragranular cortical neurons. J Neurosci 20, 4829-4843.
Bunge, R.P. (1968). Glial cells and the central myelin sheath. Physiol Rev 48, 197-251.
Burnashev, N., Khodorova, A., Jonas, P., Helm, P.J., Wisden, W., Monyer, H., Seeburg, P.H., and Sakmann, B. (1992). Calcium-permeable AMPA-kainate receptors in fusiform cerebellar glial cells. Science 256, 1566-1570.

Bushong, E.A., Martone, M.E., and Ellisman, M.H. (2004). Maturation of astrocyte morphology and the establishment of astrocyte domains during postnatal hippocampal development. Int J Dev Neurosci 22, 73-86.
Bushong, E.A., Martone, M.E., Jones, Y.Z., and Ellisman, M.H. (2002). Protoplasmic astrocytes in CA1 stratum radiatum occupy separate anatomical domains. J Neurosci 22, 183-192.
Byers, M.R., O'Connor, T.A., Martin, R.F., and Dong, W.K. (1986). Mesencephalic trigeminal sensory neurons of cat: axon pathways and structure of mechanoreceptive endings in periodontal ligament. J Comp Neurol 250, 181-191.
Cantrell, A.R., Ma, J.Y., Scheuer, T., and Catterall, W.A. (1996). Muscarinic modulation of sodium current by activation of protein kinase C in rat hippocampal neurons. Neuron 16, 1019-1026.
Capra, N.F., and Dessem, D. (1992). Central connections of trigeminal primary afferent neurons: topographical and functional considerations. Crit Rev Oral Biol Med 4, 1-52.
Carter, A.J. (1998). The importance of voltage-dependent sodium channels in cerebral ischaemia. Amino Acids 14, 159-169.
Carter, A.J., Grauert, M., Pschorn, U., Bechtel, W.D., Bartmann-Lindholm, C., Qu, Y., Scheuer, T., Catterall, W.A., and Weiser, T. (2000). Potent blockade of sodium channels and protection of brain tissue from ischemia by BIII 890 CL. Proc Natl Acad Sci U S A 97, 4944-4949.
Carter, B.C., Giessel, A.J., Sabatini, B.L., and Bean, B.P. (2012). Transient sodium current at subthreshold voltages: activation by EPSP waveforms. Neuron 75, 1081-1093.
Castets, F., Griffin, W.S., Marks, A., and Van Eldik, L.J. (1997). Transcriptional regulation of the human S100 beta gene. Brain Res Mol Brain Res 46, 208-216.
Champagnat, J., and Fortin, G. (1997). Primordial respiratory-like rhythm generation in the vertebrate embryo. Trends Neurosci 20, 119-124.
Chandler, S.H., and Goldberg, L.J. (1982). Intracellular analysis of synaptic mechanisms controlling spontaneous and cortically induced rhythmical jaw movements in the guinea pig. J Neurophysiol 48, 126-138.
Chandler, S.H., and Tal, M. (1986). The effects of brain stem transections on the neuronal networks responsible for rhythmical jaw muscle activity in the guinea pig. J Neurosci 6, 1831-1842.
Charles, A.C., Merrill, J.E., Dirksen, E.R., and Sanderson, M.J. (1991). Intercellular signaling in glial cells: calcium waves and oscillations in response to mechanical stimulation and glutamate. Neuron 6, 983-992.
Chevallier, S., Nagy, F., and Cabelguen, J.M. (2006). Cholinergic control of excitability of spinal motoneurones in the salamander. J Physiol 570, 525-540.
Chiaia, N.L., Rhoades, R.W., Bennett-Clarke, C.A., Fish, S.E., and Killackey, H.P. (1991). Thalamic processing of vibrissal information in the rat. I. Afferent input to the medial ventral posterior and posterior nuclei. J Comp Neurol 314, 201-216.
Ciccarelli, R., Di Iorio, P., Bruno, V., Battaglia, G., D'Alimonte, I., D'Onofrio, M., Nicoletti, F., and Caciagli, F. (1999). Activation of A(1) adenosine or mGlu3 metabotropic glutamate receptors enhances the release of nerve growth factor and S-100beta protein from cultured astrocytes. Glia 27, 275-281.
Clarke, L.E., and Barres, B.A. (2013). Emerging roles of astrocytes in neural circuit development. Nat Rev Neurosci 14, 311-321.

Cody, F.W., Lee, R.W., and Taylor, A. (1972). A functional analysis of the components of the mesencephalic nucleus of the fifth nerve in the cat. J Physiol 226, 249-261.
Colombo, E., Franceschetti, S., Avanzini, G., and Mantegazza, M. (2013). Phenytoin inhibits the persistent sodium current in neocortical neurons by modifying its inactivation properties. PLoS One 8, e55329.
Conti, F., DeBiasi, S., Minelli, A., and Melone, M. (1996). Expression of NR1 and NR2A/B subunits of the NMDA receptor in cortical astrocytes. Glia 17, 254-258.
Corbin, K.B. (1940). Observations on the peripheral distribution of fibers arising in the mesencephalic nucleus of the fifth cranial nerve. The Journal of Comparative Neurology 73, 153-177.
Corbin, K.B., and Harison, F. (1940). Function of the mesencephalic root of the fifth cranial nerve. . J Neurophysiol 423-435. .
Cornell-Bell, A.H., Finkbeiner, S.M., Cooper, M.S., and Smith, S.J. (1990). Glutamate induces calcium waves in cultured astrocytes: long-range glial signaling. Science 247, 470-473.
Cotrina, M.L., and Nedergaard, M. (2005). Intracellular calcium control mechanisms in glia. In Neuroglia (Oxford University Press), pp. 229-250.
Coulter, D.A., and Steinhauser, C. (2015). Role of astrocytes in epilepsy. Cold Spring Harb Perspect Med 5, a022434.
D'Ambrosio, R., Gordon, D.S., and Winn, H.R. (2002). Differential role of KIR channel and Na(+)/K(+)-pump in the regulation of extracellular K(+) in rat hippocampus. J Neurophysiol 87, 87-102.
Dahl, D. (1981). The vimentin-GFA protein transition in rat neuroglia cytoskeleton occurs at the time of myelination. J Neurosci Res 6, 741-748.
Danbolt, N.C. (2001). Glutamate uptake. Prog Neurobiol 65, 1-105.
Darbon, P., Tscherter, A., Yvon, C., and Streit, J. (2003). Role of the electrogenic Na/K pump in disinhibition-induced bursting in cultured spinal networks. J Neurophysiol 90, 3119-3129.
Davey, G.E., Murmann, P., and Heizmann, C.W. (2001). Intracellular Ca2+ and Zn2+ levels regulate the alternative cell density-dependent secretion of S100B in human glioblastoma cells. J Biol Chem 276, 30819-30826.
De Pina-Benabou, M.H., Srinivas, M., Spray, D.C., and Scemes, E. (2001). Calmodulin kinase pathway mediates the K+-induced increase in Gap junctional communication between mouse spinal cord astrocytes. J Neurosci 21, 6635-6643.
Deecher, D.C., Wilcox, B.D., Dave, V., Rossman, P.A., and Kimelberg, H.K. (1993). Detection of 5-hydroxytryptamine2 receptors by radioligand binding, northern blot analysis, and Ca2+ responses in rat primary astrocyte cultures. J Neurosci Res 35, 246-256.
Deiters, O. (1865). Untersuchungen über Gehirn und Rückenmark des Menschen und der Säugethiere. Vieweg.
Del Negro, C.A., Koshiya, N., Butera, R.J., Jr., and Smith, J.C. (2002a). Persistent sodium current, membrane properties and bursting behavior of pre-botzinger complex inspiratory neurons in vitro. J Neurophysiol 88, 2242-2250.
Del Negro, C.A., Morgado-Valle, C., and Feldman, J.L. (2002b). Respiratory rhythm: an emergent network property? Neuron 34, 821-830.
Del Negro, C.A., Morgado-Valle, C., Hayes, J.A., Mackay, D.D., Pace, R.W., Crowder, E.A., and Feldman, J.L. (2005). Sodium and calcium current-mediated pacemaker neurons and respiratory rhythm generation. J Neurosci 25, 446-453.

del Río-Hortega, P. (1920). La microglia y su transformación en células en basoncito y cuerpos gránulo-adiposos. Trab. Lab. Invest. Biol. Madrid 18, 37-82.
Dellow, P.G., and Lund, J.P. (1971). Evidence for central timing of rhythmical mastication. J Physiol 215, 1-13.
Destexhe, A., Contreras, D., and Steriade, M. (1999). Spatiotemporal analysis of local field potentials and unit discharges in cat cerebral cortex during natural wake and sleep states. J Neurosci 19, 4595-4608.
Dinan, T.G., and Golden, T. (1990). Orofacial dyskinesia in Down's syndrome. Br J Psychiatry 157, 131-132.
Donato, R. (2001). S100: a multigenic family of calcium-modulated proteins of the EF-hand type with intracellular and extracellular functional roles. Int J Biochem Cell Biol 33, 637-668.
Donga, R., Dubuc, R., Kolta, A., and Lund, J.P. (1992). Evidence that the masticatory muscles receive a direct innervation from cell group k in the rabbit. Neuroscience 49, 951-961.
Donga, R., and Lund, J.P. (1991). Discharge patterns of trigeminal commissural last-order interneurons during fictive mastication in the rabbit. J Neurophysiol 66, 1564-1578.
Donga, R., Lund, J.P., and Veilleux, D. (1990). An electrophysiological study of trigeminal commissural interneurons in the anaesthetized rabbit. Brain Res 515, 351-354.
Eisenman, J., Landgren, S., and Novin, D. (1963). Functional Organization in the Main Sensory Trigeminal Nucleus and in the Rostral Subdivision of the Nucleus of the Spinal Trigeminal Tract in the Cat. Acta Physiol Scand Suppl, SUPPL214:211-244.
el Manira, A., Tegner, J., and Grillner, S. (1994). Calcium-dependent potassium channels play a critical role for burst termination in the locomotor network in lamprey. J Neurophysiol 72, 1852-1861.
Enomoto, A., Han, J.M., Hsiao, C.F., and Chandler, S.H. (2007). Sodium currents in mesencephalic trigeminal neurons from Nav1.6 null mice. J Neurophysiol 98, 710-719.
Enomoto, S., Kohase, H., and Nakamura, Y. (1995). Dual brain stem projection from the cortical masticatory area in guinea-pig. Neuroreport 6, 1573-1577.
Eroglu, C., and Barres, B.A. (2010). Regulation of synaptic connectivity by glia. Nature 468, 223-231.
Fano, G., Mariggio, M.A., Angelella, P., Nicoletti, I., Antonica, A., Fulle, S., and Calissano, P. (1993). The S-100 protein causes an increase of intracellular calcium and death of PC12 cells. Neuroscience 53, 919-925.
Faulks, D., Collado, V., Mazille, M.N., Veyrune, J.L., and Hennequin, M. (2008). Masticatory dysfunction in persons with Down's syndrome. Part 1: aetiology and incidence. J Oral Rehabil 35, 854-862.
Feldman, J.L., and Grillner, S. (1983). Control of vertebrate respiration and locomotion: a brief account. Physiologist 26, 310-316.
Fellin, T., Gomez-Gonzalo, M., Gobbo, S., Carmignoto, G., and Haydon, P.G. (2006). Astrocytic glutamate is not necessary for the generation of epileptiform neuronal activity in hippocampal slices. J Neurosci 26, 9312-9322.
Fellin, T., Pascual, O., Gobbo, S., Pozzan, T., Haydon, P.G., and Carmignoto, G. (2004). Neuronal synchrony mediated by astrocytic glutamate through activation of extrasynaptic NMDA receptors. Neuron 43, 729-743.
Ferrier, D. (1886). The Function of the Brain (Londre).
Fiacco, T.A., Agulhon, C., and McCarthy, K.D. (2009). Sorting out astrocyte physiology from pharmacology. Annu Rev Pharmacol Toxicol 49, 151-174.

Fiacco, T.A., and McCarthy, K.D. (2004). Intracellular astrocyte calcium waves in situ increase the frequency of spontaneous AMPA receptor currents in CA1 pyramidal neurons. J Neurosci 24, 722-732.
Formenti, A., De Simoni, A., Arrigoni, E., and Martina, M. (2001). Changes in extracellular Ca2+ can affect the pattern of discharge in rat thalamic neurons. J Physiol 535, 33-45.
Ge, W.P., Zhou, W., Luo, Q., Jan, L.Y., and Jan, Y.N. (2009). Dividing glial cells maintain differentiated properties including complex morphology and functional synapses. Proc Natl Acad Sci U S A 106, 328-333.
Gilman, A.G., and Schrier, B.K. (1972). Adenosine cyclic 3',5'-monophosphate in fetal rat brain cell cultures. I. Effect of catecholamines. Mol Pharmacol 8, 410-416.
Gisel, E.G., Lange, L.J., and Niman, C.W. (1984). Chewing cycles in 4- and 5-year-old Down's syndrome children: a comparison of eating efficacy with normals. Am J Occup Ther 38, 666-670.
Glaum, S.R., Holzwarth, J.A., and Miller, R.J. (1990). Glutamate receptors activate Ca2+ mobilization and Ca2+ influx into astrocytes. Proc Natl Acad Sci U S A 87, 3454-3458.
Goldberg, L.J., and Tal, M. (1978). Intracellular recording in trigeminal motoneurons of the anesthetized guinea pig during rhythmic jaw movements. Exp Neurol 58, 102-110.
Goldin, A.L., Barchi, R.L., Caldwell, J.H., Hofmann, F., Howe, J.R., Hunter, J.C., Kallen, R.G., Mandel, G., Meisler, M.H., Netter, Y.B.*, et al.* (2000). Nomenclature of voltage-gated sodium channels. Neuron 28, 365-368.
Golgi, C. (1885). Sulla fina anatomia degli organi centrali del sistema nervoso. 214

Gourine, A.V., Kasymov, V., Marina, N., Tang, F., Figueiredo, M.F., Lane, S., Teschemacher, A.G., Spyer, K.M., Deisseroth, K., and Kasparov, S. (2010). Astrocytes control breathing through pH-dependent release of ATP. Science 329, 571-575.
Grandes, P., Kq, K.Q.D., Morino, P., Cuenod, M., and Streit, P. (1991). Homocysteate, an Excitatory Transmitter Candidate Localized in Glia. Eur J Neurosci 3, 1370-1373.
Grass, D., Pawlowski, P.G., Hirrlinger, J., Papadopoulos, N., Richter, D.W., Kirchhoff, F., and Hulsmann, S. (2004). Diversity of functional astroglial properties in the respiratory network. J Neurosci 24, 1358-1365.
Griffin, W.S., Sheng, J.G., McKenzie, J.E., Royston, M.C., Gentleman, S.M., Brumback, R.A., Cork, L.C., Del Bigio, M.R., Roberts, G.W., and Mrak, R.E. (1998). Life-long overexpression of S100beta in Down's syndrome: implications for Alzheimer pathogenesis. Neurobiol Aging 19, 401-405.
Griffin, W.S., Stanley, L.C., Ling, C., White, L., MacLeod, V., Perrot, L.J., White, C.L., 3rd, and Araoz, C. (1989). Brain interleukin 1 and S-100 immunoreactivity are elevated in Down syndrome and Alzheimer disease. Proc Natl Acad Sci U S A 86, 7611-7615.
Grosche, J., Matyash, V., Moller, T., Verkhratsky, A., Reichenbach, A., and Kettenmann, H. (1999). Microdomains for neuron-glia interaction: parallel fiber signaling to Bergmann glial cells. Nat Neurosci 2, 139-143.
Guatteo, E., Franceschetti, S., Bacci, A., Avanzini, G., and Wanke, E. (1996). A TTX-sensitive conductance underlying burst firing in isolated pyramidal neurons from rat neocortex. Brain Res 741, 1-12.
Halassa, M.M., Fellin, T., and Haydon, P.G. (2007a). The tripartite synapse: roles for gliotransmission in health and disease. Trends Mol Med 13, 54-63.

Halassa, M.M., Fellin, T., Takano, H., Dong, J.H., and Haydon, P.G. (2007b). Synaptic islands defined by the territory of a single astrocyte. J Neurosci 27, 6473-6477.
Hargus, N.J., Nigam, A., Bertram, E.H., 3rd, and Patel, M.K. (2013). Evidence for a role of Nav1.6 in facilitating increases in neuronal hyperexcitability during epileptogenesis. J Neurophysiol 110, 1144-1157.
Harpio, R., and Einarsson, R. (2004). S100 proteins as cancer biomarkers with focus on S100B in malignant melanoma. Clin Biochem 37, 512-518.
Harris-Warrick, R.M. (2010). General principles of rhythmogenesis in central pattern generator networks. Prog Brain Res 187, 213-222.
Hashimoto, N., Katayama, T., Ishiwata, Y., and Nakamura, Y. (1989). Induction of rhythmic jaw movements by stimulation of the mesencephalic reticular formation in the guinea pig. J Neurosci 9, 2887-2901.
Haydon, P.G., and Nedergaard, M. (2015). How do astrocytes participate in neural plasticity? Cold Spring Harb Perspect Biol 7, a020438.
Heinemann, U., Albrecht, D., Kohr, G., Rausche, G., Stabel, J., and Wisskirchen, T. (1992). Low-Ca(2+)-induced epileptiform activity in rat hippocampal slices. Epilepsy Res Suppl 8, 147-155.
Heinemann, U., Lux, H.D., and Gutnick, M.J. (1977). Extracellular free calcium and potassium during paroxsmal activity in the cerebral cortex of the cat. Exp Brain Res 27, 237-243.
Heinemann, U., and Pumain, R. (1981). Effects of tetrodotoxin on changes in extracellular free calcium induced by repetitive electrical stimulation and iontophoretic application of excitatory amino acids in the sensorimotor cortex of cats. Neurosci Lett 21, 87-91.
Heinemann, U., Stabel, J., and Rausche, G. (1990). Activity-dependent ionic changes and neuronal plasticity in rat hippocampus. Prog Brain Res 83, 197-214.
Hennequin, M., Allison, P.J., Faulks, D., Orliaguet, T., and Feine, J. (2005). Chewing indicators between adults with Down syndrome and controls. J Dent Res 84, 1057-1061.
Hepp, R., Perraut, M., Chasserot-Golaz, S., Galli, T., Aunis, D., Langley, K., and Grant, N.J. (1999). Cultured glial cells express the SNAP-25 analogue SNAP-23. Glia 27, 181-187.
Hiiemae, K.M.a.C., A. W. (1985). Mastication, food transport, and swallowing, in Functional Vertebrate Morphology (harvard univ. press. cambridge, ma.).
Hille, B. (2001). Modification of Gating in Voltage-Sensitive Channels. In Ion Channels of Excitable Membranes (Sinauer Associates, Inc).
Hirano, A. (1968). A confirmation of the oligodendroglial origin of myelin in the adult rat. J Cell Biol 38, 637-640.
Hochman, D.W., D'Ambrosio, R., Janigro, D., and Schwartzkroin, P.A. (1999). Extracellular chloride and the maintenance of spontaneous epileptiform activity in rat hippocampal slices. J Neurophysiol 81, 49-59.
Hochman, D.W., and Schwartzkroin, P.A. (2000). Chloride-cotransport blockade desynchronizes neuronal discharge in the "epileptic" hippocampal slice. J Neurophysiol 83, 406-417.
Holzwarth, J.A., Gibbons, S.J., Brorson, J.R., Philipson, L.H., and Miller, R.J. (1994). Glutamate receptor agonists stimulate diverse calcium responses in different types of cultured rat cortical glial cells. J Neurosci 14, 1879-1891.
Houades, V., Koulakoff, A., Ezan, P., Seif, I., and Giaume, C. (2008). Gap junction-mediated astrocytic networks in the mouse barrel cortex. J Neurosci 28, 5207-5217.

Houssaini, Y.S., Cazalets, J.R., Martini, F., and Clarac, F. (1993). Induction of fictive locomotion by sulphur-containing amino acids in an in vitro newborn rat preparation. Eur J Neurosci 5, 1226-1232.
Hu, W., Tian, C., Li, T., Yang, M., Hou, H., and Shu, Y. (2009). Distinct contributions of Na(v)1.6 and Na(v)1.2 in action potential initiation and backpropagation. Nat Neurosci 12, 996-1002.
Huguenard, J.R. (1996). Low-threshold calcium currents in central nervous system neurons. Annu Rev Physiol 58, 329-348.
Huguenard, J.R., Hamill, O.P., and Prince, D.A. (1988). Developmental changes in Na+ conductances in rat neocortical neurons: appearance of a slowly inactivating component. J Neurophysiol 59, 778-795.
Huh, Y., and Cho, J. (2013). Discrete pattern of burst stimulation in the ventrobasal thalamus for anti-nociception. PLoS One 8, e67655.
Iadecola, C., and Nedergaard, M. (2007). Glial regulation of the cerebral microvasculature. Nat Neurosci 10, 1369-1376.
Ichikawa, H., Jacobowitz, D.M., and Sugimoto, T. (1997). S100 protein-immunoreactive primary sensory neurons in the trigeminal and dorsal root ganglia of the rat. Brain Res 748, 253-257.
Innocenti, B., Parpura, V., and Haydon, P.G. (2000). Imaging extracellular waves of glutamate during calcium signaling in cultured astrocytes. J Neurosci 20, 1800-1808.
Inoue, T., Chandler, S.H., and Goldberg, L.J. (1994). Neuropharmacological mechanisms underlying rhythmical discharge in trigeminal interneurons during fictive mastication. J Neurophysiol 71, 2061-2073.
Inoue, T., Kato, T., Masuda, Y., Nakamura, T., Kawamura, Y., and Morimoto, T. (1989). Modifications of masticatory behavior after trigeminal deafferentation in the rabbit. Exp Brain Res 74, 579-591.
Inoue, T., Masuda, Y., Nagashima, T., Yoshikawa, K., and Morimoto, T. (1992). Properties of rhythmically active reticular neurons around the trigeminal motor nucleus during fictive mastication in the rat. Neurosci Res 14, 275-294.
Isobe, T., and Okuyama, T. (1978). The amino-acid sequence of S-100 protein (PAP I-b protein) and its relation to the calcium-binding proteins. Eur J Biochem 89, 379-388.
Isobe, T., and Okuyama, T. (1981). The amino-acid sequence of the alpha subunit in bovine brain S-100a protein. Eur J Biochem 116, 79-86.
Iwata, A., Stys, P.K., Wolf, J.A., Chen, X.H., Taylor, A.G., Meaney, D.F., and Smith, D.H. (2004). Traumatic axonal injury induces proteolytic cleavage of the voltage-gated sodium channels modulated by tetrodotoxin and protease inhibitors. J Neurosci 24, 4605-4613.
Jabs, R., Kirchhoff, F., Kettenmann, H., and Steinhauser, C. (1994). Kainate activates Ca(2+)-permeable glutamate receptors and blocks voltage-gated K+ currents in glial cells of mouse hippocampal slices. Pflugers Arch 426, 310-319.
Jacquin, M.F., Rhoades, R.W., Enfiejian, H.L., and Egger, M.D. (1983). Organization and morphology of masticatory neurons in the rat: a retrograde HRP study. J Comp Neurol 218, 239-256.
Jacquin, T.D., Borday, V., Schneider-Maunoury, S., Topilko, P., Ghilini, G., Kato, F., Charnay, P., and Champagnat, J. (1996). Reorganization of pontine rhythmogenic neuronal networks in Krox-20 knockout mice. Neuron 17, 747-758.

Jendelova, P., and Sykova, E. (1991). Role of glia in K+ and pH homeostasis in the neonatal rat spinal cord. Glia 4, 56-63.
Jensen, A.M., and Chiu, S.Y. (1991). Differential intracellular calcium responses to glutamate in type 1 and type 2 cultured brain astrocytes. J Neurosci 11, 1674-1684.
Jensen, M.S., and Yaari, Y. (1997). Role of intrinsic burst firing, potassium accumulation, and electrical coupling in the elevated potassium model of hippocampal epilepsy. J Neurophysiol 77, 1224-1233.
Jerge, C. (1963). Organization and function of the trigeminal mesencephalic nucleus. J Neurophysiol 26, 379-392.
Ji, R.R., Kawasaki, Y., Zhuang, Z.Y., Wen, Y.R., and Decosterd, I. (2006). Possible role of spinal astrocytes in maintaining chronic pain sensitization: review of current evidence with focus on bFGF/JNK pathway. Neuron Glia Biol 2, 259-269.
Jinno, S., Ishizuka, S., and Kosaka, T. (2003). Ionic currents underlying rhythmic bursting of ventral mossy cells in the developing mouse dentate gyrus. Eur J Neurosci 17, 1338-1354.
Johansson, R.S., and Olsson, K.A. (1976). Microelectrode recordings from human oral mechanoreceptors. Brain Res 118, 307-311.
Johansson, R.S., Trulsson, M., Olsson, K.A., and Abbs, J.H. (1988). Mechanoreceptive afferent activity in the infraorbital nerve in man during speech and chewing movements. Exp Brain Res 72, 209-214.
Johnson, S.M., Smith, J.C., Funk, G.D., and Feldman, J.L. (1994). Pacemaker behavior of respiratory neurons in medullary slices from neonatal rat. J Neurophysiol 72, 2598-2608.
Jourdain, P., Bergersen, L.H., Bhaukaurally, K., Bezzi, P., Santello, M., Domercq, M., Matute, C., Tonello, F., Gundersen, V., and Volterra, A. (2007). Glutamate exocytosis from astrocytes controls synaptic strength. Nat Neurosci 10, 331-339.
Kadala, A., Verdier, D., Morquette, P., and Kolta, A. (2015). Ion Homeostasis in Rhythmogenesis: The Interplay Between Neurons and Astroglia. Physiology (Bethesda) 30, 371-388.
Kafitz, K.W., Meier, S.D., Stephan, J., and Rose, C.R. (2008). Developmental profile and properties of sulforhodamine 101--Labeled glial cells in acute brain slices of rat hippocampus. J Neurosci Methods 169, 84-92.
Kang, J., Jiang, L., Goldman, S.A., and Nedergaard, M. (1998). Astrocyte-mediated potentiation of inhibitory synaptic transmission. Nat Neurosci 1, 683-692.
Karadottir, R., Hamilton, N.B., Bakiri, Y., and Attwell, D. (2008). Spiking and nonspiking classes of oligodendrocyte precursor glia in CNS white matter. Nat Neurosci 11, 450-456.
Katakura N, Nakajima M, and Y, N. (1999). Ontogenetic analysis of brainstem mechanisms of ingestive activities in vitro. In: Neurobiology of mastication-from molecular to systems approach. (Amsterdam. Elsevier Science).
Kawamata, H., Ng, S.K., Diaz, N., Burstein, S., Morel, L., Osgood, A., Sider, B., Higashimori, H., Haydon, P.G., Manfredi, G., and Yang, Y. (2014). Abnormal intracellular calcium signaling and SNARE-dependent exocytosis contributes to SOD1G93A astrocyte-mediated toxicity in amyotrophic lateral sclerosis. J Neurosci 34, 2331-2348.
Kawamura, Y., and Tsukamoto, S. (1960). Neural descending pathways from the cortical jaw motor area and amygdaloid nucleus to jaw muscles. Jpn J Physiol 10, 489-498.
Kettenmann, H., and Ransom, B.R. (2005). The concept of neuroglia: a historical perspective. In Neuroglia (Oxford University Press), pp. 1-16.

Kidokoro, Y., Kubota, K., Shuto, S., and Sumino, R. (1968). Reflex organization of cat masticatory muscles. J Neurophysiol 31, 695-708.
Kira G. Hartman, Paul T. Wilder, Kristen Varney, Alexander D. Jr. MacKerell, Andrew Coop, Danna Zimmer, Lapidus, R., and Weber, D.J. (2013). Inhibiting S100B in Malignant Melanoma. In Melanoma - From Early Detection to Treatment, D.H.D. (Ed.), ed.
Kligman, D., and Marshak, D.R. (1985). Purification and characterization of a neurite extension factor from bovine brain. Proc Natl Acad Sci U S A 82, 7136-7139.
Ko, C.P., and Robitaille, R. (2015). Perisynaptic Schwann Cells at the Neuromuscular Synapse: Adaptable, Multitasking Glial Cells. Cold Spring Harb Perspect Biol 7, a020503.
Kogo, M., Funk, G.D., and Chandler, S.H. (1996). Rhythmical oral-motor activity recorded in an in vitro brainstem preparation. Somatosens Mot Res 13, 39-48.
Kogo, M., Tanaka, S., Chandler, S.H., and Matsuya, T. (1998). Examination of the relationships between jaw opener and closer rhythmical muscle activity in an in vitro brainstem jaw-attached preparation. Somatosens Mot Res 15, 200-210.
Koizumi, H., and Smith, J.C. (2008). Persistent Na+ and K+-dominated leak currents contribute to respiratory rhythm generation in the pre-Botzinger complex in vitro. J Neurosci 28, 1773-1785.
Kolta, A., Westberg, K.G., and Lund, J.P. (2000). Identification of brainstem interneurons projecting to the trigeminal motor nucleus and adjacent structures in the rabbit. J Chem Neuroanat 19, 175-195.
Kondoh, T., Nishizaki, T., Aihara, H., and Tamaki, N. (2001). NMDA-responsible, APV-insensitive receptor in cultured human astrocytes. Life Sci 68, 1761-1767.
Kraner, S., Yang, J., and Barchi, R. (1989). Structural inferences for the native skeletal muscle sodium channel as derived from patterns of endogenous proteolysis. J Biol Chem 264, 13273-13280.
Kubista, H., Donato, R., and Hermann, A. (1999). S100 calcium binding protein affects neuronal electrical discharge activity by modulation of potassium currents. Neuroscience 90, 493-508.
Kubo, Y., Enomoto, S., and Nakamura, Y. (1981). Synaptic basis of orbital cortically induced rhythmical masticatory activity of trigeminal motoneurons in immobilized cats. Brain Res 230, 97-110.
Kuhn, A.A., Williams, D., Kupsch, A., Limousin, P., Hariz, M., Schneider, G.H., Yarrow, K., and Brown, P. (2004). Event-related beta desynchronization in human subthalamic nucleus correlates with motor performance. Brain 127, 735-746.
Kuo, J.J., Schonewille, M., Siddique, T., Schults, A.N., Fu, R., Bar, P.R., Anelli, R., Heckman, C.J., and Kroese, A.B. (2004). Hyperexcitability of cultured spinal motoneurons from presymptomatic ALS mice. J Neurophysiol 91, 571-575.
Kuo, J.J., Siddique, T., Fu, R., and Heckman, C.J. (2005). Increased persistent Na(+) current and its effect on excitability in motoneurones cultured from mutant SOD1 mice. J Physiol 563, 843-854.
Kuypers, H.G. (1958). An anatomical analysis of cortico-bulbar connexions to the pons and lower brain stem in the cat. J Anat 92, 198-218.
Lalo, U., Pankratov, Y., Kirchhoff, F., North, R.A., and Verkhratsky, A. (2006). NMDA receptors mediate neuron-to-glia signaling in mouse cortical astrocytes. J Neurosci 26, 2673-2683.

Landgren, S., Olsson, K.A., and Westberg, K.G. (1986). Bulbar neurones with axonal projections to the trigeminal motor nucleus in the cat. Exp Brain Res 65, 98-111.
Larson, C.R., Smith, A., and Luschei, E.S. (1981). Discharge characteristics and stretch sensitivity of jaw muscle afferents in the monkey during controlled isometric bites. J Neurophysiol 46, 130-142.
Launay, P., Fleig, A., Perraud, A.L., Scharenberg, A.M., Penner, R., and Kinet, J.P. (2002). TRPM4 is a Ca2+-activated nonselective cation channel mediating cell membrane depolarization. Cell 109, 397-407.
Lawson, L.J., Perry, V.H., Dri, P., and Gordon, S. (1990). Heterogeneity in the distribution and morphology of microglia in the normal adult mouse brain. Neuroscience 39, 151-170.
Lee, D. (2003). Coherent oscillations in neuronal activity of the supplementary motor area during a visuomotor task. J Neurosci 23, 6798-6809.
Li, Y.Q., Takada, M., and Mizuno, N. (1993). Identification of premotor interneurons which project bilaterally to the trigeminal motor, facial or hypoglossal nuclei: a fluorescent retrograde double-labeling study in the rat. Brain Res 611, 160-164.
Li, Z., and Hatton, G.I. (1996). Oscillatory bursting of phasically firing rat supraoptic neurones in low-Ca2+ medium: Na+ influx, cytosolic Ca2+ and gap junctions. J Physiol 496 (Pt 2), 379-394.
Lian, X.Y., and Stringer, J.L. (2004). Astrocytes contribute to regulation of extracellular calcium and potassium in the rat cerebral cortex during spreading depression. Brain Res 1012, 177-184.
Liao, Y.F., Tsai, M.L., Chen, C.C., and Yen, C.T. (2011). Involvement of the Cav3.2 T-type calcium channel in thalamic neuron discharge patterns. Mol Pain 7, 43.
Limwongse, V., and DeSantis, M. (1977). Cell body locations and axonal pathways of neurons innervating muscles of mastication in the rat. Am J Anat 149, 477-488.
Liu, Y., Harding, M., Pittman, A., Dore, J., Striessnig, J., Rajadhyaksha, A., and Chen, X. (2014). Cav1.2 and Cav1.3 L-type calcium channels regulate dopaminergic firing activity in the mouse ventral tegmental area. J Neurophysiol 112, 1119-1130.
Liu, Z.J., Masuda, Y., Inoue, T., Fuchihata, H., Sumida, A., Takada, K., and Morimoto, T. (1993). Coordination of cortically induced rhythmic jaw and tongue movements in the rabbit. J Neurophysiol 69, 569-584.
Lund, J.P. (1991). Mastication and its control by the brain stem. Crit Rev Oral Biol Med 2, 33-64.
Lund, J.P., and Dellow, P.G. (1973). Rhythmical masticatory activity of hypoglossal motoneurons responding to an oral stimulus. Exp Neurol 40, 243-246.
Lund, J.P., Sasamoto, K., Murakami, T., and Olsson, K.A. (1984). Analysis of rhythmical jaw movements produced by electrical stimulation of motor-sensory cortex of rabbits. J Neurophysiol 52, 1014-1029.
Luu, P., Tucker, D.M., and Makeig, S. (2004). Frontal midline theta and the error-related negativity: neurophysiological mechanisms of action regulation. Clin Neurophysiol 115, 1821-1835.
Lynch, R. (1985). A qualitative investigation of the topographical representation of masticatory muscles within the motor trigeminal nucleus of the rat: a horseradish peroxidase study. Brain Res 327, 354-358.
Ma, B., Xu, G., Wang, W., Enyeart, J.J., and Zhou, M. (2014). Dual patch voltage clamp study of low membrane resistance astrocytes in situ. Mol Brain 7, 18.

MacGregor, D.J., and Leng, G. (2012). Phasic firing in vasopressin cells: understanding its functional significance through computational models. PLoS Comput Biol 8, e1002740.
MacVicar, B.A. (1984). Voltage-dependent calcium channels in glial cells. Science 226, 1345-1347.
Magistretti, J., and Alonso, A. (2002). Fine gating properties of channels responsible for persistent sodium current generation in entorhinal cortex neurons. J Gen Physiol 120, 855-873.
Magistretti, J., Ragsdale, D.S., and Alonso, A. (1999). High conductance sustained single-channel activity responsible for the low-threshold persistent Na(+) current in entorhinal cortex neurons. J Neurosci 19, 7334-7341.
Maienschein, V., Marxen, M., Volknandt, W., and Zimmermann, H. (1999). A plethora of presynaptic proteins associated with ATP-storing organelles in cultured astrocytes. Glia 26, 233-244.
Makinson, C.D., Tanaka, B.S., Lamar, T., Goldin, A.L., and Escayg, A. (2014). Role of the hippocampus in Nav1.6 (Scn8a) mediated seizure resistance. Neurobiol Dis 68, 16-25.
Mantegazza, M., Yu, F.H., Powell, A.J., Clare, J.J., Catterall, W.A., and Scheuer, T. (2005). Molecular determinants for modulation of persistent sodium current by G-protein betagamma subunits. J Neurosci 25, 3341-3349.
Marchetti, C., Beato, M., and Nistri, A. (2001). Evidence for increased extracellular K(+) as an important mechanism for dorsal root induced alternating rhythmic activity in the neonatal rat spinal cord in vitro. Neurosci Lett 304, 77-80.
Marder, E., and Calabrese, R.L. (1996). Principles of rhythmic motor pattern generation. Physiol Rev 76, 687-717.
Mariggio, M.A., Fulle, S., Calissano, P., Nicoletti, I., and Fano, G. (1994). The brain protein S-100ab induces apoptosis in PC12 cells. Neuroscience 60, 29-35.
Markowitz, J., Mackerell, A.D., Jr., Carrier, F., Charpentier, T.H., and Weber, D.J. (2005). Design of Inhibitors for S100B. Curr Top Med Chem 5, 1093-1108.
Martin, R., Bajo-Graneras, R., Moratalla, R., Perea, G., and Araque, A. (2015). GLIAL CELL SIGNALING. Circuit-specific signaling in astrocyte-neuron networks in basal ganglia pathways. Science 349, 730-734.
Matthias, K., Kirchhoff, F., Seifert, G., Huttmann, K., Matyash, M., Kettenmann, H., and Steinhauser, C. (2003). Segregated expression of AMPA-type glutamate receptors and glutamate transporters defines distinct astrocyte populations in the mouse hippocampus. J Neurosci 23, 1750-1758.
Maurice, N., Tkatch, T., Meisler, M., Sprunger, L.K., and Surmeier, D.J. (2001). D1/D5 dopamine receptor activation differentially modulates rapidly inactivating and persistent sodium currents in prefrontal cortex pyramidal neurons. J Neurosci 21, 2268-2277.
Mayer, M.L., Westbrook, G.L., and Guthrie, P.B. (1984). Voltage-dependent block by Mg2+ of NMDA responses in spinal cord neurones. Nature 309, 261-263.
McCarthy, K.D., and de Vellis, J. (1978). Alpah-adrenergic receptor modulation of beta-adrenergic, adenosine and prostaglandin E1 increased adenosine 3':5'-cyclic monophosphate levels in primary cultures of glia. J Cyclic Nucleotide Res 4, 15-26.
McCrea, D.A., and Rybak, I.A. (2008). Organization of mammalian locomotor rhythm and pattern generation. Brain Res Rev 57, 134-146.
McKhann, G.M., 2nd, D'Ambrosio, R., and Janigro, D. (1997). Heterogeneity of astrocyte resting membrane potentials and intercellular coupling revealed by whole-cell and gramicidin-

perforated patch recordings from cultured neocortical and hippocampal slice astrocytes. J Neurosci 17, 6850-6863.
Mennerick, S., and Zorumski, C.F. (1994). Glial contributions to excitatory neurotransmission in cultured hippocampal cells. Nature 368, 59-62.
Mercer, J.N., Chan, C.S., Tkatch, T., Held, J., and Surmeier, D.J. (2007). Nav1.6 sodium channels are critical to pacemaking and fast spiking in globus pallidus neurons. J Neurosci 27, 13552-13566.
Migheli, A., Cordera, S., Bendotti, C., Atzori, C., Piva, R., and Schiffer, D. (1999). S-100beta protein is upregulated in astrocytes and motor neurons in the spinal cord of patients with amyotrophic lateral sclerosis. Neurosci Lett 261, 25-28.
Milani, D., Facci, L., Guidolin, D., Leon, A., and Skaper, S.D. (1989). Activation of polyphosphoinositide metabolism as a signal-transducing system coupled to excitatory amino acid receptors in astroglial cells. Glia 2, 161-169.
Min, R., and Nevian, T. (2012). Astrocyte signaling controls spike timing-dependent depression at neocortical synapses. Nat Neurosci 15, 746-753.
Min, R., Santello, M., and Nevian, T. (2012). The computational power of astrocyte mediated synaptic plasticity. Front Comput Neurosci 6, 93.
Mirmiran, M., and Corner, M. (1982). Neuronal discharge patterns in the occipital cortex of developing rats during active and quiet sleep. Brain Res 255, 37-48.
Mirsky, R., Woodhoo, A., Parkinson, D.B., Arthur-Farraj, P., Bhaskaran, A., and Jessen, K.R. (2008). Novel signals controlling embryonic Schwann cell development, myelination and dedifferentiation. J Peripher Nerv Syst 13, 122-135.
Mishima, T., and Hirase, H. (2010). In vivo intracellular recording suggests that gray matter astrocytes in mature cerebral cortex and hippocampus are electrophysiologically homogeneous. J Neurosci 30, 3093-3100.
Mizuno, N., Konishi, A., and Sato, M. (1975). Localization of masticatory motoneurons in the cat and rat by means of retrograde axonal transport of horseradish peroxidase. J Comp Neurol 164, 105-115.
Montana, V., Malarkey, E.B., Verderio, C., Matteoli, M., and Parpura, V. (2006). Vesicular transmitter release from astrocytes. Glia 54, 700-715.
Moore, B.W. (1965). A soluble protein characteristic of the nervous system. Biochem Biophys Res Commun 19, 739-744.
Moraes, D.J., da Silva, M.P., Bonagamba, L.G., Mecawi, A.S., Zoccal, D.B., Antunes-Rodrigues, J., Varanda, W.A., and Machado, B.H. (2013). Electrophysiological properties of rostral ventrolateral medulla presympathetic neurons modulated by the respiratory network in rats. J Neurosci 33, 19223-19237.
Morioka, T., Baba, T., Black, K.L., and Streit, W.J. (1992). Response of microglial cells to experimental rat glioma. Glia 6, 75-79.
Morquette, P., Lavoie, R., Fhima, M.D., Lamoureux, X., Verdier, D., and Kolta, A. (2012). Generation of the masticatory central pattern and its modulation by sensory feedback. Prog Neurobiol 96, 340-355.
Muller, T., Fritschy, J.M., Grosche, J., Pratt, G.D., Mohler, H., and Kettenmann, H. (1994). Developmental regulation of voltage-gated K+ channel and GABAA receptor expression in Bergmann glial cells. J Neurosci 14, 2503-2514.
Muller, T., Grosche, J., Ohlemeyer, C., and Kettenmann, H. (1993). NMDA-activated currents in Bergmann glial cells. Neuroreport 4, 671-674.

Muller, T., Moller, T., Berger, T., Schnitzer, J., and Kettenmann, H. (1992). Calcium entry through kainate receptors and resulting potassium-channel blockade in Bergmann glial cells. Science 256, 1563-1566.
Mulligan, S.J., and MacVicar, B.A. (2004). Calcium transients in astrocyte endfeet cause cerebrovascular constrictions. Nature 431, 195-199.
Muramatsu, Y., Kurosaki, R., Watanabe, H., Michimata, M., Matsubara, M., Imai, Y., and Araki, T. (2003). Expression of S-100 protein is related to neuronal damage in MPTP-treated mice. Glia 42, 307-313.
Nagelhus, E.A., Mathiisen, T.M., and Ottersen, O.P. (2004). Aquaporin-4 in the central nervous system: cellular and subcellular distribution and coexpression with KIR4.1. Neuroscience 129, 905-913.
Nakamura, Y., and Katakura, N. (1995). Generation of masticatory rhythm in the brainstem. Neurosci Res 23, 1-19.
Nakamura, Y., and Kubo, Y. (1978). Masticatory rhythm in intracellular potential of trigeminal motoneurons induced by stimulation of orbital cortex and amygdala in cats. Brain Res 148, 504-509.
Navarrete, M., and Araque, A. (2008). Endocannabinoids mediate neuron-astrocyte communication. Neuron 57, 883-893.
Nedergaard, M. (1994). Direct signaling from astrocytes to neurons in cultures of mammalian brain cells. Science 263, 1768-1771.
Newman, E., and Reichenbach, A. (1996). The Muller cell: a functional element of the retina. Trends Neurosci 19, 307-312.
Newman, E.A. (2003). New roles for astrocytes: regulation of synaptic transmission. Trends Neurosci 26, 536-542.
Nicholson, C., ten Bruggencate, G., Stockle, H., and Steinberg, R. (1978). Calcium and potassium changes in extracellular microenvironment of cat cerebellar cortex. J Neurophysiol 41, 1026-1039.
Nimmerjahn, A., Kirchhoff, F., Kerr, J.N., and Helmchen, F. (2004). Sulforhodamine 101 as a specific marker of astroglia in the neocortex in vivo. Nat Methods 1, 31-37.
Nishimura, Y., Asahi, M., Saitoh, K., Kitagawa, H., Kumazawa, Y., Itoh, K., Lin, M., Akamine, T., Shibuya, H., Asahara, T., and Yamamoto, T. (2001). Ionic mechanisms underlying burst firing of layer III sensorimotor cortical neurons of the cat: an in vitro slice study. J Neurophysiol 86, 771-781.
Nishiyama, A., Yang, Z., and Butt, A. (2005). Astrocytes and NG2-glia: what's in a name? J Anat 207, 687-693.
Nishiyama, H., Knopfel, T., Endo, S., and Itohara, S. (2002). Glial protein S100B modulates long-term neuronal synaptic plasticity. Proc Natl Acad Sci U S A 99, 4037-4042.
Nishizaki, T., Matsuoka, T., Nomura, T., Kondoh, T., Tamaki, N., and Okada, Y. (1999). Store Ca2+ depletion enhances NMDA responses in cultured human astrocytes. Biochem Biophys Res Commun 259, 661-664.
Noda, H., and Mikami, A. (1986). Discharges of neurons in the dorsal paraflocculus of monkeys during eye movements and visual stimulation. J Neurophysiol 56, 1129-1146.
Nolte, C., Matyash, M., Pivneva, T., Schipke, C.G., Ohlemeyer, C., Hanisch, U.K., Kirchhoff, F., and Kettenmann, H. (2001). GFAP promoter-controlled EGFP-expressing transgenic mice: a tool to visualize astrocytes and astrogliosis in living brain tissue. Glia 33, 72-86.

Nowak, L., Bregestovski, P., Ascher, P., Herbet, A., and Prochiantz, A. (1984). Magnesium gates glutamate-activated channels in mouse central neurones. Nature 307, 462-465.
Nozaki, S., Iriki, A., and Nakamura, Y. (1986a). Localization of central rhythm generator involved in cortically induced rhythmical masticatory jaw-opening movement in the guinea pig. J Neurophysiol 55, 806-825.
Nozaki, S., Iriki, A., and Nakamura, Y. (1986b). Role of corticobulbar projection neurons in cortically induced rhythmical masticatory jaw-opening movement in the guinea pig. J Neurophysiol 55, 826-845.
Nozaki, S., Iriki, A., and Nakamura, Y. (1993). Trigeminal premotor neurons in the bulbar parvocellular reticular formation participating in induction of rhythmical activity of trigeminal motoneurons by repetitive stimulation of the cerebral cortex in the guinea pig. J Neurophysiol 69, 595-608.
Oberheim, N.A., Goldman, S.A., and Nedergaard, M. (2012). Heterogeneity of astrocytic form and function. Methods Mol Biol 814, 23-45.
Oberheim, N.A., Takano, T., Han, X., He, W., Lin, J.H., Wang, F., Xu, Q., Wyatt, J.D., Pilcher, W., Ojemann, J.G.*, et al.* (2009). Uniquely hominid features of adult human astrocytes. J Neurosci 29, 3276-3287.
Ogata, K., and Kosaka, T. (2002). Structural and quantitative analysis of astrocytes in the mouse hippocampus. Neuroscience 113, 221-233.
Onimaru, H., Arata, A., and Homma, I. (1995). Intrinsic burst generation of preinspiratory neurons in the medulla of brainstem-spinal cord preparations isolated from newborn rats. Exp Brain Res 106, 57-68.
Onimaru, H., Arata, A., and Homma, I. (1997). Neuronal mechanisms of respiratory rhythm generation: an approach using in vitro preparation. Jpn J Physiol 47, 385-403.
Orkand, R.K., Nicholls, J.G., and Kuffler, S.W. (1966). Effect of nerve impulses on the membrane potential of glial cells in the central nervous system of amphibia. J Neurophysiol 29, 788-806.
Osorio, N., Cathala, L., Meisler, M.H., Crest, M., Magistretti, J., and Delmas, P. (2010). Persistent Nav1.6 current at axon initial segments tunes spike timing of cerebellar granule cells. J Physiol 588, 651-670.
Otto, M., Bahn, E., Wiltfang, J., Boekhoff, I., and Beuche, W. (1998). Decrease of S100 beta protein in serum of patients with amyotrophic lateral sclerosis. Neurosci Lett 240, 171-173.
Pace, R.W., Mackay, D.D., Feldman, J.L., and Del Negro, C.A. (2007). Inspiratory bursts in the preBotzinger complex depend on a calcium-activated non-specific cation current linked to glutamate receptors in neonatal mice. J Physiol 582, 113-125.
Panaitescu, B., Ruangkittisakul, A., and Ballanyi, K. (2009). Silencing by raised extracellular Ca2+ of pre-Botzinger complex neurons in newborn rat brainstem slices without change of membrane potential or input resistance. Neurosci Lett 456, 25-29.
Panatier, A., Vallee, J., Haber, M., Murai, K.K., Lacaille, J.C., and Robitaille, R. (2011). Astrocytes are endogenous regulators of basal transmission at central synapses. Cell 146, 785-798.
Parpura, V., Basarsky, T.A., Liu, F., Jeftinija, K., Jeftinija, S., and Haydon, P.G. (1994). Glutamate-mediated astrocyte-neuron signalling. Nature 369, 744-747.
Parpura, V., and Haydon, P.G. (2000). Physiological astrocytic calcium levels stimulate glutamate release to modulate adjacent neurons. Proc Natl Acad Sci U S A 97, 8629-8634.

Parpura, V., Liu, F., Brethorst, S., Jeftinija, K., Jeftinija, S., and Haydon, P.G. (1995). Alpha-latrotoxin stimulates glutamate release from cortical astrocytes in cell culture. FEBS Lett 360, 266-270.
Parpura, V., Scemes, E., and Spray, D.C. (2004). Mechanisms of glutamate release from astrocytes: gap junction "hemichannels", purinergic receptors and exocytotic release. Neurochem Int 45, 259-264.
Pasti, L., Zonta, M., Pozzan, T., Vicini, S., and Carmignoto, G. (2001). Cytosolic calcium oscillations in astrocytes may regulate exocytotic release of glutamate. J Neurosci 21, 477-484.
Paxinos, G., and Watson, C. (2005). The Rat Brain in Stereotaxic Coordinates (Elsevier Academic).
Pellerin, L., and Magistretti, P.J. (1994). Glutamate uptake into astrocytes stimulates aerobic glycolysis: a mechanism coupling neuronal activity to glucose utilization. Proc Natl Acad Sci U S A 91, 10625-10629.
Pena, F., Parkis, M.A., Tryba, A.K., and Ramirez, J.M. (2004). Differential contribution of pacemaker properties to the generation of respiratory rhythms during normoxia and hypoxia. Neuron 43, 105-117.
Perea, G., and Araque, A. (2005). Glial calcium signaling and neuron-glia communication. Cell Calcium 38, 375-382.
Perea, G., and Araque, A. (2007). Astrocytes potentiate transmitter release at single hippocampal synapses. Science 317, 1083-1086.
Perea, G., Navarrete, M., and Araque, A. (2009). Tripartite synapses: astrocytes process and control synaptic information. Trends Neurosci 32, 421-431.
Perez-Reyes, E. (2003). Molecular physiology of low-voltage-activated t-type calcium channels. Physiol Rev 83, 117-161.
Peschanski, M. (1984). Trigeminal afferents to the diencephalon in the rat. Neuroscience 12, 465-487.
Peters, A. (1964). Observations on the Connexions between Myelin Sheaths and Glial Cells in the Optic Nerves of Young Rats. J Anat 98, 125-134.
Peterson, B.W., Anderson, M.E., and Filion, M. (1974). Responses of ponto-medullary reticular neurons to cortical, tectal and cutaneous stimuli. Exp Brain Res 21, 19-44.
Pfrieger, F.W., and Barres, B.A. (1997). Synaptic efficacy enhanced by glial cells in vitro. Science 277, 1684-1687.
Pieri, M., Albo, F., Gaetti, C., Spalloni, A., Bengtson, C.P., Longone, P., Cavalcanti, S., and Zona, C. (2003). Altered excitability of motor neurons in a transgenic mouse model of familial amyotrophic lateral sclerosis. Neurosci Lett 351, 153-156.
Pin, J.P., and Duvoisin, R. (1995). The metabotropic glutamate receptors: structure and functions. Neuropharmacology 34, 1-26.
Pinganaud, G., Bernat, I., Buisseret, P., and Buisseret-Delmas, C. (1999). Trigeminal projections to hypoglossal and facial motor nuclei in the rat. J Comp Neurol 415, 91-104.
Porter, J.T., and McCarthy, K.D. (1995). GFAP-positive hippocampal astrocytes in situ respond to glutamatergic neuroligands with increases in [Ca2+]i. Glia 13, 101-112.
Porter, J.T., and McCarthy, K.D. (1996). Hippocampal astrocytes in situ respond to glutamate released from synaptic terminals. J Neurosci 16, 5073-5081.
Porter, J.T., and McCarthy, K.D. (1997). Astrocytic neurotransmitter receptors in situ and in vivo. Prog Neurobiol 51, 439-455.

Ptak, K., Zummo, G.G., Alheid, G.F., Tkatch, T., Surmeier, D.J., and McCrimmon, D.R. (2005). Sodium currents in medullary neurons isolated from the pre-Botzinger complex region. J Neurosci 25, 5159-5170.
Pumain, R., and Heinemann, U. (1985). Stimulus- and amino acid-induced calcium and potassium changes in rat neocortex. J Neurophysiol 53, 1-16.
Pumain, R., Kurcewicz, I., and Louvel, J. (1983). Fast extracellular calcium transients: involvement in epileptic processes. Science 222, 177-179.
Pumain, R., Menini, C., Heinemann, U., Louvel, J., and Silva-Barrat, C. (1985). Chemical synaptic transmission is not necessary for epileptic seizures to persist in the baboon Papio papio. Exp Neurol 89, 250-258.
Puro, D.G., Yuan, J.P., and Sucher, N.J. (1996). Activation of NMDA receptor-channels in human retinal Muller glial cells inhibits inward-rectifying potassium currents. Vis Neurosci 13, 319-326.
Putzier, I., Kullmann, P.H., Horn, J.P., and Levitan, E.S. (2009). Cav1.3 channel voltage dependence, not Ca2+ selectivity, drives pacemaker activity and amplifies bursts in nigral dopamine neurons. J Neurosci 29, 15414-15419.
Rambotti, M.G., Saccardi, C., Spreca, A., Aisa, M.C., Giambanco, I., and Donato, R. (1989). Immunocytochemical localization of S-100 beta beta protein in olfactory and supporting cells of lamb olfactory epithelium. J Histochem Cytochem 37, 1825-1833.
Ramón y Cajal, S. (1913). Contribucion al conocimento de la neurogli del cerebro humano. Trab. Lab. Invest. Biol. Univ. Madrid. 11, . 255-315
Ransdell, J.L., Temporal, S., West, N.L., Leyrer, M.L., and Schulz, D.J. (2013). Characterization of inward currents and channels underlying burst activity in motoneurons of crab cardiac ganglion. J Neurophysiol 110, 42-54.
Reichenbach, A. (1989). Attempt to classify glial cells by means of their process specialization using the rabbit retinal Muller cell as an example of cytotopographic specialization of glial cells. Glia 2, 250-259.
Rekling, J.C., and Feldman, J.L. (1998). PreBotzinger complex and pacemaker neurons: hypothesized site and kernel for respiratory rhythm generation. Annu Rev Physiol 60, 385-405.
Rekling, J.C., Shao, X.M., and Feldman, J.L. (2000). Electrical coupling and excitatory synaptic transmission between rhythmogenic respiratory neurons in the preBotzinger complex. J Neurosci 20, RC113.
Richter, D.W., Camerer, H., and Sonnhof, U. (1978). Changes in extracellular potassium during the spontaneous activity of medullary respiratory neurones. Pflugers Arch 376, 139-149.
Richter, D.W., Champagnat, J., Jacquin, T., and Benacka, R. (1993). Calcium currents and calcium-dependent potassium currents in mammalian medullary respiratory neurones. J Physiol 470, 23-33.
Rickmann, M., and Wolff, J.R. (1995). S100 protein expression in subpopulations of neurons of rat brain. Neuroscience 67, 977-991.
Romano, C., Sesma, M.A., McDonald, C.T., O'Malley, K., Van den Pol, A.N., and Olney, J.W. (1995). Distribution of metabotropic glutamate receptor mGluR5 immunoreactivity in rat brain. J Comp Neurol 355, 455-469.

Rosker, C., Lohberger, B., Hofer, D., Steinecker, B., Quasthoff, S., and Schreibmayer, W. (2007). The TTX metabolite 4,9-anhydro-TTX is a highly specific blocker of the Na(v1.6) voltage-dependent sodium channel. Am J Physiol Cell Physiol 293, C783-789.
Rothermundt, M., Ponath, G., Glaser, T., Hetzel, G., and Arolt, V. (2004). S100B serum levels and long-term improvement of negative symptoms in patients with schizophrenia. Neuropsychopharmacology 29, 1004-1011.
Royeck, M., Horstmann, M.T., Remy, S., Reitze, M., Yaari, Y., and Beck, H. (2008). Role of axonal NaV1.6 sodium channels in action potential initiation of CA1 pyramidal neurons. J Neurophysiol 100, 2361-2380.
Rubin, J.E., Hayes, J.A., Mendenhall, J.L., and Del Negro, C.A. (2009). Calcium-activated nonspecific cation current and synaptic depression promote network-dependent burst oscillations. Proc Natl Acad Sci U S A 106, 2939-2944.
Rubino, D., Robbins, K.A., and Hatsopoulos, N.G. (2006). Propagating waves mediate information transfer in the motor cortex. Nat Neurosci 9, 1549-1557.
Rusakov, D.A., and Fine, A. (2003). Extracellular Ca2+ depletion contributes to fast activity-dependent modulation of synaptic transmission in the brain. Neuron 37, 287-297.
Rush, A.M., Dib-Hajj, S.D., and Waxman, S.G. (2005). Electrophysiological properties of two axonal sodium channels, Nav1.2 and Nav1.6, expressed in mouse spinal sensory neurones. J Physiol 564, 803-815.
Ryczko, D., Charrier, V., Ijspeert, A., and Cabelguen, J.M. (2010). Segmental oscillators in axial motor circuits of the salamander: distribution and bursting mechanisms. J Neurophysiol 104, 2677-2692.
Saad, M., Dubuc, R., Westberg, K.G., and Lund, J.P. (1999). Distribution of cholinergic neurons in cell group K of the rabbit brainstem. Neuroscience 88, 927-937.
Sakatani, S., Seto-Ohshima, A., Shinohara, Y., Yamamoto, Y., Yamamoto, H., Itohara, S., and Hirase, H. (2008). Neural-activity-dependent release of S100B from astrocytes enhances kainate-induced gamma oscillations in vivo. J Neurosci 28, 10928-10936.
Sandler, V.M., Puil, E., and Schwarz, D.W. (1998). Intrinsic response properties of bursting neurons in the nucleus principalis trigemini of the gerbil. Neuroscience 83, 891-904.
Sasamoto, K. (1979). Motor nuclear representation of masticatory muscles in the rat. Jpn J Physiol 29, 739-747.
Scemes, E., and Spray, D.C. (2012). Extracellular K(+) and astrocyte signaling via connexin and pannexin channels. Neurochem Res 37, 2310-2316.
Schafer, D.P., Lehrman, E.K., Kautzman, A.G., Koyama, R., Mardinly, A.R., Yamasaki, R., Ransohoff, R.M., Greenberg, M.E., Barres, B.A., and Stevens, B. (2012). Microglia sculpt postnatal neural circuits in an activity and complement-dependent manner. Neuron 74, 691-705.
Schafer, D.P., Lehrman, E.K., and Stevens, B. (2013). The "quad-partite" synapse: microglia-synapse interactions in the developing and mature CNS. Glia 61, 24-36.
Schipke, C.G., Ohlemeyer, C., Matyash, M., Nolte, C., Kettenmann, H., and Kirchhoff, F. (2001). Astrocytes of the mouse neocortex express functional N-methyl-D-aspartate receptors. FASEB J 15, 1270-1272.
Schmitt, A., Bertsch, T., Henning, U., Tost, H., Klimke, A., Henn, F.A., and Falkai, P. (2005). Increased serum S100B in elderly, chronic schizophrenic patients: negative correlation with deficit symptoms. Schizophr Res 80, 305-313.

Schnell, C., Fresemann, J., and Hulsmann, S. (2011). Determinants of functional coupling between astrocytes and respiratory neurons in the pre-Botzinger complex. PLoS One 6, e26309.
Schools, G.P., Zhou, M., and Kimelberg, H.K. (2003). Electrophysiologically "complex" glial cells freshly isolated from the hippocampus are immunopositive for the chondroitin sulfate proteoglycan NG2. J Neurosci Res 73, 765-777.
Schools, G.P., Zhou, M., and Kimelberg, H.K. (2006). Development of gap junctions in hippocampal astrocytes: evidence that whole cell electrophysiological phenotype is an intrinsic property of the individual cell. J Neurophysiol 96, 1383-1392.
Schwartz, G., Enomoto, S., Valiquette, C., and Lund, J.P. (1989). Mastication in the rabbit: a description of movement and muscle activity. J Neurophysiol 62, 273-287.
Scott, G., Westberg, K.G., Vrentzos, N., Kolta, A., and Lund, J.P. (2003). Effect of lidocaine and NMDA injections into the medial pontobulbar reticular formation on mastication evoked by cortical stimulation in anaesthetized rabbits. Eur J Neurosci 17, 2156-2162.
Sederberg, P.B., Schulze-Bonhage, A., Madsen, J.R., Bromfield, E.B., McCarthy, D.C., Brandt, A., Tully, M.S., and Kahana, M.J. (2007). Hippocampal and neocortical gamma oscillations predict memory formation in humans. Cereb Cortex 17, 1190-1196.
Seifert, G., and Steinhauser, C. (1995). Glial cells in the mouse hippocampus express AMPA receptors with an intermediate Ca2+ permeability. Eur J Neurosci 7, 1872-1881.
Selinfreund, R.H., Barger, S.W., Pledger, W.J., and Van Eldik, L.J. (1991). Neurotrophic protein S100 beta stimulates glial cell proliferation. Proc Natl Acad Sci U S A 88, 3554-3558.
Serrano, A., Robitaille, R., and Lacaille, J.C. (2008). Differential NMDA-dependent activation of glial cells in mouse hippocampus. Glia 56, 1648-1663.
Shao, Y., and McCarthy, K.D. (1995). Receptor-mediated calcium signals in astroglia: multiple receptors, common stores and all-or-nothing responses. Cell Calcium 17, 187-196.
Sharott, A., Doig, N.M., Mallet, N., and Magill, P.J. (2012). Relationships between the firing of identified striatal interneurons and spontaneous and driven cortical activities in vivo. J Neurosci 32, 13221-13236.
Shashoua, V.E., Hesse, G.W., and Moore, B.W. (1984). Proteins of the brain extracellular fluid: evidence for release of S-100 protein. J Neurochem 42, 1536-1541.
Shelton, M.K., and McCarthy, K.D. (1999). Mature hippocampal astrocytes exhibit functional metabotropic and ionotropic glutamate receptors in situ. Glia 26, 1-11.
Shigenaga, Y., Yoshida, A., Tsuru, K., Mitsuhiro, Y., Otani, K., and Cao, C.Q. (1988). Physiological and morphological characteristics of cat masticatory motoneurons--intracellular injection of HRP. Brain Res 461, 238-256.
Simard, M., Arcuino, G., Takano, T., Liu, Q.S., and Nedergaard, M. (2003). Signaling at the gliovascular interface. J Neurosci 23, 9254-9262.
Simpson, P.B., and Russell, J.T. (1997). Role of sarcoplasmic/endoplasmic-reticulum Ca2+-ATPases in mediating Ca2+ waves and local Ca2+-release microdomains in cultured glia. Biochem J 325 (Pt 1), 239-247.
Smith, J.C., Butera, R.J., Koshiya, N., Del Negro, C., Wilson, C.G., and Johnson, S.M. (2000). Respiratory rhythm generation in neonatal and adult mammals: the hybrid pacemaker-network model. Respir Physiol 122, 131-147.
Smith, S.J. (1992). Do astrocytes process neural information? Prog Brain Res 94, 119-136.
Somjen, G.G. (1980). Stimulus-evoked and seizure-related responses of extracellular calcium activity in spinal cord compared to those in cerebral cortex. J Neurophysiol 44, 617-632.

Somjen, G.G. (1988). Nervenkitt: notes on the history of the concept of neuroglia. Glia 1, 2-9.
Somjen, G.G., and Muller, M. (2000). Potassium-induced enhancement of persistent inward current in hippocampal neurons in isolation and in tissue slices. Brain Res 885, 102-110.
Spacek, J. (1985). Three-dimensional analysis of dendritic spines. III. Glial sheath. Anat Embryol (Berl) 171, 245-252.
Spain, W.J., Schwindt, P.C., and Crill, W.E. (1987). Anomalous rectification in neurons from cat sensorimotor cortex in vitro. J Neurophysiol 57, 1555-1576.
Srinivasan, R., Huang, B.S., Venugopal, S., Johnston, A.D., Chai, H., Zeng, H., Golshani, P., and Khakh, B.S. (2015). Ca(2+) signaling in astrocytes from Ip3r2(-/-) mice in brain slices and during startle responses in vivo. Nat Neurosci 18, 708-717.
Steinhauser, C., Berger, T., Frotscher, M., and Kettenmann, H. (1992). Heterogeneity in the Membrane Current Pattern of Identified Glial Cells in the Hippocampal Slice. Eur J Neurosci 4, 472-484.
Steinhauser, C., Grunnet, M., and Carmignoto, G. (2015). Crucial role of astrocytes in temporal lobe epilepsy. Neuroscience.
Steinhauser, C., Jabs, R., and Kettenmann, H. (1994). Properties of GABA and glutamate responses in identified glial cells of the mouse hippocampal slice. Hippocampus 4, 19-35.
Stevens, B., Allen, N.J., Vazquez, L.E., Howell, G.R., Christopherson, K.S., Nouri, N., Micheva, K.D., Mehalow, A.K., Huberman, A.D., Stafford, B.*, et al.* (2007). The classical complement cascade mediates CNS synapse elimination. Cell 131, 1164-1178.
Strehler, E.E., and Zacharias, D.A. (2001). Role of alternative splicing in generating isoform diversity among plasma membrane calcium pumps. Physiol Rev 81, 21-50.
Streit, W.J. (2005). Microglial cells. In Neuroglia (Oxford University Press), p. 60.
Streit, W.J., Graeber, M.B., and Kreutzberg, G.W. (1988). Functional plasticity of microglia: a review. Glia 1, 301-307.
Su, H., Alroy, G., Kirson, E.D., and Yaari, Y. (2001). Extracellular calcium modulates persistent sodium current-dependent burst-firing in hippocampal pyramidal neurons. J Neurosci 21, 4173-4182.
Sumi, T. (1971). Modification of cortically evoked rhythmic chewing and swallowing from midbrain and pons. Jpn J Physiol 21, 489-506.
Sun, W., McConnell, E., Pare, J.F., Xu, Q., Chen, M., Peng, W., Lovatt, D., Han, X., Smith, Y., and Nedergaard, M. (2013). Glutamate-dependent neuroglial calcium signaling differs between young and adult brain. Science 339, 197-200.
Sykova, E. (1987). Modulation of spinal cord transmission by changes in extracellular K+ activity and extracellular volume. Can J Physiol Pharmacol 65, 1058-1066.
Szoke, K., Hartel, K., Grass, D., Hirrlinger, P.G., Hirrlinger, J., and Hulsmann, S. (2006). Glycine transporter 1 expression in the ventral respiratory group is restricted to protoplasmic astrocytes. Brain Res 1119, 182-189.
Tabuchi, K., Ohnishi, R., Furuta, T., and Nishimoto, A. (1983). Immunohistochemical localization of S-100 protein in human cerebral and cerebellar cortices. Experientia 39, 335-337.
Takata, N., and Hirase, H. (2008). Cortical layer 1 and layer 2/3 astrocytes exhibit distinct calcium dynamics in vivo. PLoS One 3, e2525.
Takata, N., Mishima, T., Hisatsune, C., Nagai, T., Ebisui, E., Mikoshiba, K., and Hirase, H. (2011). Astrocyte calcium signaling transforms cholinergic modulation to cortical plasticity in vivo. J Neurosci 31, 18155-18165.

Tanaka, S., Kogo, M., Chandler, S.H., and Matsuya, T. (1999). Localization of oral-motor rhythmogenic circuits in the isolated rat brainstem preparation. Brain Res 821, 190-199.
Tas, P.W., Massa, P.T., Kress, H.G., and Koschel, K. (1987). Characterization of an Na+/K+/Cl- co-transport in primary cultures of rat astrocytes. Biochim Biophys Acta 903, 411-416.
Tazerart, S., Viemari, J.C., Darbon, P., Vinay, L., and Brocard, F. (2007). Contribution of persistent sodium current to locomotor pattern generation in neonatal rats. J Neurophysiol 98, 613-628.
Tazerart, S., Vinay, L., and Brocard, F. (2008). The persistent sodium current generates pacemaker activities in the central pattern generator for locomotion and regulates the locomotor rhythm. J Neurosci 28, 8577-8589.
Theodosis, D.T., Poulain, D.A., and Oliet, S.H. (2008). Activity-dependent structural and functional plasticity of astrocyte-neuron interactions. Physiol Rev 88, 983-1008.
Todd, K.J., Darabid, H., and Robitaille, R. (2010). Perisynaptic glia discriminate patterns of motor nerve activity and influence plasticity at the neuromuscular junction. J Neurosci 30, 11870-11882.
Torvik, A. (1956). Afferent connections to the sensory trigeminal nuclei, the nucleus of the solitary tract and adjacent structures; an experimental study in the rat. J Comp Neurol 106, 51-141.
Travers, J.B., and Norgren, R. (1983). Afferent projections to the oral motor nuclei in the rat. J Comp Neurol 220, 280-298.
Tsuboi, A., Kolta, A., Chen, C.C., and Lund, J.P. (2003). Neurons of the trigeminal main sensory nucleus participate in the generation of rhythmic motor patterns. Eur J Neurosci 17, 229-238.
Tsuruyama, K., Hsiao, C.F., and Chandler, S.H. (2013). Participation of a persistent sodium current and calcium-activated nonspecific cationic current to burst generation in trigeminal principal sensory neurons. J Neurophysiol 110, 1903-1914.
Ullrich, N.D., Voets, T., Prenen, J., Vennekens, R., Talavera, K., Droogmans, G., and Nilius, B. (2005). Comparison of functional properties of the Ca2+-activated cation channels TRPM4 and TRPM5 from mice. Cell Calcium 37, 267-278.
Undrovinas, A., Maltsev, V.A., and Sabbah, H.N. (2013). Calpain inhibition reduces amplitude and accelerates decay of the late sodium current in ventricular myocytes from dogs with chronic heart failure. PLoS One 8, e54436.
Urbani, A., and Belluzzi, O. (2000). Riluzole inhibits the persistent sodium current in mammalian CNS neurons. Eur J Neurosci 12, 3567-3574.
van Calker, D., Muller, M., and Hamprecht, B. (1980). Regulation by secretin, vasoactive intestinal peptide, and somatostatin of cyclic AMP accumulation in cultured brain cells. Proc Natl Acad Sci U S A 77, 6907-6911.
van den Pol, A.N., Romano, C., and Ghosh, P. (1995). Metabotropic glutamate receptor mGluR5 subcellular distribution and developmental expression in hypothalamus. J Comp Neurol 362, 134-150.
Van Der Zee, E.A., De Jong, G.I., Strosberg, A.D., and Luiten, P.G. (1993). Muscarinic acetylcholine receptor-expression in astrocytes in the cortex of young and aged rats. Glia 8, 42-50.
Van Eldik, L.J., and Zimmer, D.B. (1987). Secretion of S-100 from rat C6 glioma cells. Brain Res 436, 367-370.

Vega-Saenz de Miera, E.C., Rudy, B., Sugimori, M., and Llinas, R. (1997). Molecular characterization of the sodium channel subunits expressed in mammalian cerebellar Purkinje cells. Proc Natl Acad Sci U S A 94, 7059-7064.
Ventura, R., and Harris, K.M. (1999). Three-dimensional relationships between hippocampal synapses and astrocytes. J Neurosci 19, 6897-6906.
Verkhratsky, A. (2008). Neurotransmitter Receptors in Astrocytes In Astrocytes in (Patho)Physiology of the Nervous System (Springer Science).
Virchow, R. (1858). Die Cellularpathologie in ihrer Begründung auf physiologische und pathologische Gewebelehre.
von Reyn, C.R., Mott, R.E., Siman, R., Smith, D.H., and Meaney, D.F. (2012). Mechanisms of calpain mediated proteolysis of voltage gated sodium channel alpha-subunits following in vitro dynamic stretch injury. J Neurochem 121, 793-805.
Wallen, P., Grafe, P., and Grillner, S. (1984). Phasic variations of extracellular potassium during fictive swimming in the lamprey spinal cord in vitro. Acta Physiol Scand 120, 457-463.
Wallraff, A., Odermatt, B., Willecke, K., and Steinhauser, C. (2004). Distinct types of astroglial cells in the hippocampus differ in gap junction coupling. Glia 48, 36-43.
Wang, D.D., and Bordey, A. (2008). The astrocyte odyssey. Prog Neurobiol 86, 342-367.
Wang, F., Smith, N.A., Xu, Q., Fujita, T., Baba, A., Matsuda, T., Takano, T., Bekar, L., and Nedergaard, M. (2012). Astrocytes modulate neural network activity by Ca(2)+-dependent uptake of extracellular K+. Sci Signal 5, ra26.
Weiss, N., and Waard, M.D. (2006). Les canaux calciques dépendants du voltage au coeur de la douleur. médecine sciences 22, 396-404.
Westneat, M.W., and Hall, W.G. (1992). Ontogeny of feeding motor patterns in infant rats: an electromyographic analysis of suckling and chewing. Behav Neurosci 106, 539-554.
Whitaker-Azmitia, P.M., Clarke, C., and Azmitia, E.C. (1993). Localization of 5-HT1A receptors to astroglial cells in adult rats: implications for neuronal-glial interactions and psychoactive drug mechanism of action. Synapse 14, 201-205.
Williams, M.N., Zahm, D.S., and Jacquin, M.F. (1994). Differential foci and synaptic organization of the principal and spinal trigeminal projections to the thalamus in the rat. Eur J Neurosci 6, 429-453.
Winningham-Major, F., Staecker, J.L., Barger, S.W., Coats, S., and Van Eldik, L.J. (1989). Neurite extension and neuronal survival activities of recombinant S100 beta proteins that differ in the content and position of cysteine residues. J Cell Biol 109, 3063-3071.
Wu, N., Enomoto, A., Tanaka, S., Hsiao, C.F., Nykamp, D.Q., Izhikevich, E., and Chandler, S.H. (2005). Persistent sodium currents in mesencephalic v neurons participate in burst generation and control of membrane excitability. J Neurophysiol 93, 2710-2722.
Wu, N., Hsiao, C.F., and Chandler, S.H. (2001). Membrane resonance and subthreshold membrane oscillations in mesencephalic V neurons: participants in burst generation. J Neurosci 21, 3729-3739.
Xu-Friedman, M.A., Harris, K.M., and Regehr, W.G. (2001). Three-dimensional comparison of ultrastructural characteristics at depressing and facilitating synapses onto cerebellar Purkinje cells. J Neurosci 21, 6666-6672.
Yang, Q., Hamberger, A., Hyden, H., Wang, S., Stigbrand, T., and Haglid, K.G. (1995a). S-100 beta has a neuronal localisation in the rat hindbrain revealed by an antigen retrieval method. Brain Res 696, 49-61.

Yang, Q., Hamberger, A., Khatibi, N., Stigbrand, T., and Haglid, K.G. (1996). Presence of S-100 beta in cholinergic neurones of the rat hindbrain. Neuroreport 7, 3093-3099.
Yang, Q., Hou, X., Hamberger, A., Wang, S., Dahlstrom, A., and Haglid, K.G. (1995b). S-100 beta immunoreactivity in neurones of the rat peripheral sensory ganglia. Neuroreport 6, 2005-2009.
Yardan, T., Erenler, A.K., Baydin, A., Aydin, K., and Cokluk, C. (2011). Usefulness of S100B protein in neurological disorders. J Pak Med Assoc 61, 276-281.
Yasui, Y., Itoh, K., Mitani, A., Takada, M., and Mizuno, N. (1985). Cerebral cortical projections to the reticular regions around the trigeminal motor nucleus in the cat. J Comp Neurol 241, 348-356.
Yoshida, A., Hiraga, T., Moritani, M., Chen, K., Takatsuki, Y., Hirose, Y., Bae, Y.C., and Shigenaga, Y. (1998). Morphologic characteristics of physiologically defined neurons in the cat trigeminal nucleus principalis. J Comp Neurol 401, 308-328.
Yoshida, A., Taki, I., Chang, Z., Iida, C., Haque, T., Tomita, A., Seki, S., Yamamoto, S., Masuda, Y., Moritani, M., and Shigenaga, Y. (2009). Corticofugal projections to trigeminal motoneurons innervating antagonistic jaw muscles in rats as demonstrated by anterograde and retrograde tract tracing. J Comp Neurol 514, 368-386.
Yu, F.H., and Catterall, W.A. (2003). Overview of the voltage-gated sodium channel family. Genome Biol 4, 207.
Zhang, B., Wootton, J.F., and Harris-Warrick, R.M. (1995). Calcium-dependent plateau potentials in a crab stomatogastric ganglion motor neuron. II. Calcium-activated slow inward current. J Neurophysiol 74, 1938-1946.
Zhang, Q., and Haydon, P.G. (2005). Roles for gliotransmission in the nervous system. J Neural Transm (Vienna) 112, 121-125.
Zhong, G., Masino, M.A., and Harris-Warrick, R.M. (2007). Persistent sodium currents participate in fictive locomotion generation in neonatal mouse spinal cord. J Neurosci 27, 4507-4518.
Zhou, M., and Kimelberg, H.K. (2001). Freshly isolated hippocampal CA1 astrocytes comprise two populations differing in glutamate transporter and AMPA receptor expression. J Neurosci 21, 7901-7908.
Zhuo, L., Sun, B., Zhang, C.L., Fine, A., Chiu, S.Y., and Messing, A. (1997). Live astrocytes visualized by green fluorescent protein in transgenic mice. Dev Biol 187, 36-42.
Ziak, D., Chvatal, A., and Sykova, E. (1998). Glutamate-, kainate- and NMDA-evoked membrane currents in identified glial cells in rat spinal cord slice. Physiol Res 47, 365-375.
Zimmer, D.B., Cornwall, E.H., Landar, A., and Song, W. (1995). The S100 protein family: history, function, and expression. Brain Res Bull 37, 417-429.
Zonta, M., Angulo, M.C., Gobbo, S., Rosengarten, B., Hossmann, K.A., Pozzan, T., and Carmignoto, G. (2003). Neuron-to-astrocyte signaling is central to the dynamic control of brain microcirculation. Nat Neurosci 6, 43-50.
Zwerling, S.J., Cohen, S.A., and Barchi, R.L. (1991). Analysis of protease-sensitive regions in the skeletal muscle sodium channel in vitro and implications for channel tertiary structure. J Biol Chem 266, 4574-4580.

Annexe

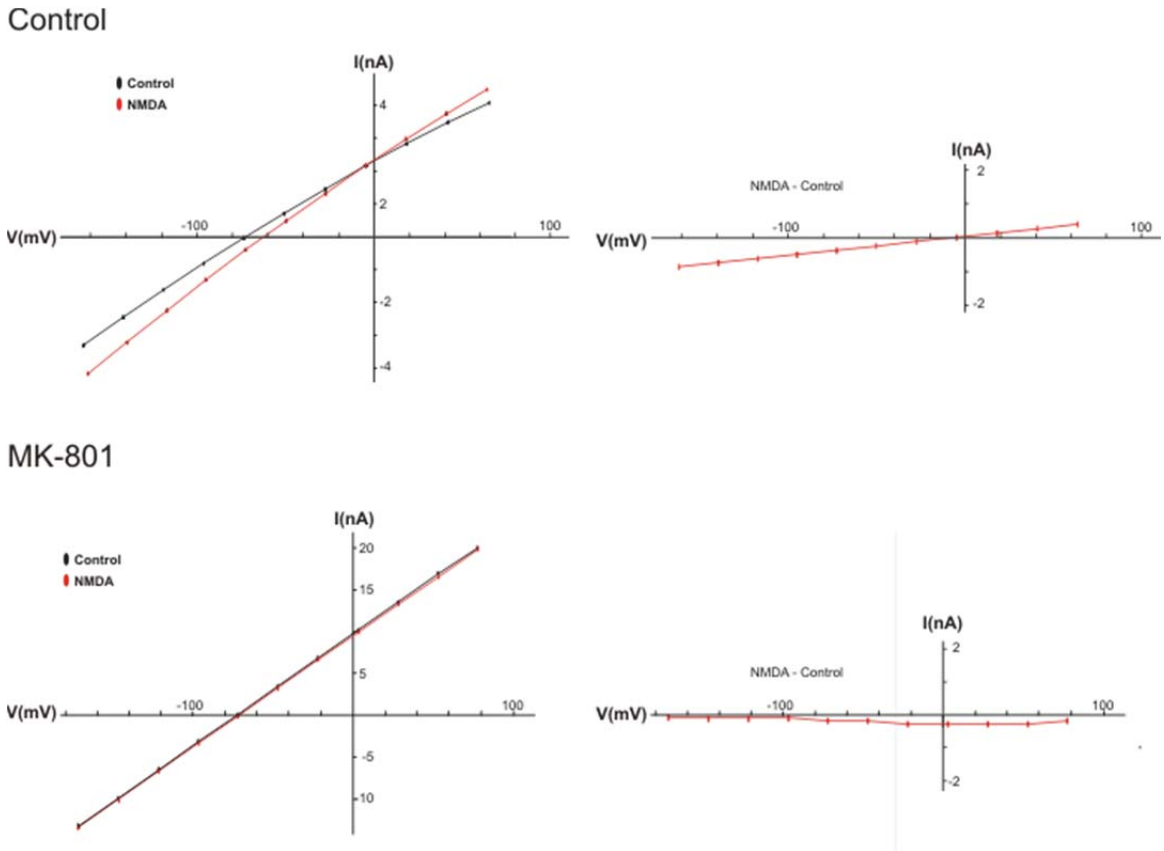

Activation de courants NMDA dans les astrocytes. Courbes IV en *voltage clamp* d'astrocytes en présence ou non de NMDA. Mesure de la réponse membranaire d'astrocytes à une série de créneaux (pulses) hyperpolarisants et dépolarisants (paliers de 25mV, durée de 100ms) de -170 mV à +80mV avant l'application de NMDA et après 30 secondes d'application de NMDA (pour laisser le temps aux membranes d'atteindre un plateau).

En condition contrôle (n=8): en haut, à gauche, l'application de NMDA induit une dépolarisation (8.1±0.9mV) qui était associée dans 6 cas sur 8 à une diminution de la résistance (augmentation de la conductance) visible par les courbes IV (diminution de résistance de 17.1±4.7%). Cette conductance augmentée serait due à l'ouverture de récepteurs canaux NMDA. Pour ces 6 cellules, le courant NMDA était entrant aux potentiels plus hyperpolarisés et sortant aux potentiels plus dépolarisés. Cependant, le potentiel de renversement variait d'une cellule à l'autre (moyenne de -22 mV). À droite: courbe résultante de la soustraction de la courbe NMDA à la courbe contrôle. La courbe représente alors le courant induit par l'application du NMDA.

En présence de MK-801(n=7): En bas, à gauche, l'application de NMDA n'a pratiquement aucun effet sur la pente (changement moyen de la résistance membranaire de 1±0.9%). La courbe après l'application du NMDA était parfois décalée par rapport celle sans NMDA, mais elles restaient parallèles entre elles. Ce léger décalage vers la droite reflète une légère dépolarisation qui persiste et qui serait probablement due à une accumulation de K^+ extracellulaire en raison de la longue application de NMDA durant ce protocole. À droite: courbe résultante de la soustraction de la courbe NMDA à la courbe contrôle.

Progress in Neurobiology 96 (2012) 340–355

Contents lists available at SciVerse ScienceDirect

Progress in Neurobiology

journal homepage: www.elsevier.com/locate/pneurobio

Generation of the masticatory central pattern and its modulation by sensory feedback

Philippe Morquette, Raphaël Lavoie, Mitch-David Fhima, Xavier Lamoureux, Dorly Verdier, Arlette Kolta *

Groupe de Recherche sur le Système Nerveux Central du FRSQ, Université de Montréal and Faculté de médecine dentaire, Université de Montréal, Canada

ARTICLE INFO

Article history:
Received 6 September 2011
Received in revised form 16 January 2012
Accepted 24 January 2012
Available online 9 February 2012
This review is dedicated to the memory of James P. Lund (1942–2009) whose tremendous contribution to the field will remain a monument.

Keywords:
Trigeminal system
Intrinsic bursting
Rhythmogenesis currents
I_{NaP}
CPG model
Development of mastication

ABSTRACT

The basic pattern of rhythmic jaw movements produced during mastication is generated by a neuronal network located in the brainstem and referred to as the masticatory central pattern generator (CPG). This network composed of neurons mostly associated to the trigeminal system is found between the rostral borders of the trigeminal motor nucleus and facial nucleus. This review summarizes current knowledge on the anatomical organization, the development, the connectivity and the cellular properties of these trigeminal circuits in relation to mastication. Emphasis is put on a population of rhythmogenic neurons in the dorsal part of the trigeminal sensory nucleus. These neurons have intrinsic bursting capabilities, supported by a persistent Na^+ current (I_{NaP}), which are enhanced when the extracellular concentration of Ca^{2+} diminishes. Presented evidence suggest that the Ca^{2+} dependency of this current combined with its voltage-dependency could provide a mechanism for cortical and sensory afferent inputs to the nucleus to interact with the rhythmogenic properties of its neurons to adjust and adapt the rhythmic output. Astrocytes are postulated to contribute to this process by modulating the extracellular Ca^{2+} concentration and a model is proposed to explain how functional microdomains defined by the boundaries of astrocytic syncitia may form under the influence of incoming inputs.

Contents

Abbreviations: AD, antidromic; ADP, afterdepolarization; AHP, afterhyperpolarization; BK-Ca, big Ca^{2+}-dependent K^+ conductance; CMA, cortical masticatory area; CPG, central pattern generator; Dig, digastric; Ext, extensors; FC, fast closing; Fle, flexors; I_{CaN}, calcium activated non-selective current; I_h, hyperpolarization activated current; I_M, Kv7/KCNQ/M channel mediated current; I_{NaP}, persistent sodium current; IntV, intertrigeminal area; JuxtV, juxtatrigeminal area; M1, primary motor cortex; Mass, masseter; MSAs, muscle spindle afferents; NMDA, N-methyl-D,L-aspartate; NVII, facial nucleus; NVmes, mesencephalic trigeminal nucleus; NVmot, motor trigeminal nucleus; NVsnpr, trigeminal main (or principal) sensory nucleus; NVspo, trigeminal spinal nucleus, oral subdivision; NVspi, trigeminal spinal nucleus, interpolar subdivision; NVspc, trigeminal spinal nucleus, caudal subdivision; NXII, hypoglossal nucleus; O, opening; PAD, primary afferent depolarization; PCRt, parvocellular reticular formation; PeriV, peritrigeminal area; r, rhombomeres; RA, rapidly adapting; RMP, resting membrane potential; RTN, retrotrapezoid nucleus; S1, primary sensory cortex; SA, slowly adapting; SC, slow closing; SK-Ca, small Ca^{2+}-dependent K^+ conductance; SupV, supratrigeminal area.

* Corresponding author at: Pavillon Paul Desmarais, Université de Montréal, C.P. 6128, succursale Centre-ville, Montréal (Qc), H3C 3J7 Canada. Tel.: +1 514 343 7112.
E-mail address: [redacted]

0301-0082/$ – see front matter © 2012 Elsevier Ltd. All rights reserved.
doi:10.1016/j.pneurobio.2012.01.011

1. Introduction

Like many rhythmical movements, mastication is a vital function. It prepares food for digestion by breaking it down into pieces that can be swallowed. Masticatory deficiencies lead to poor digestion and inadequate dietary selection which in turn are associated to a number of cardiovascular, physical and cognitive problems. In addition to this obvious function, masticatory movements have also been associated to a number of other functions including mood control and learning and memory. Although, seemingly simple, the rhythmic orofacial movements produced during mastication require coordination of several jaw, facial and tongue muscles. As in other cyclic vital functions (*e.g.* respiration and locomotion), the basic rhythmic activity of these muscles is determined by a neuronal network referred to as central pattern generator (CPG). By definition, CPGs are capable of producing such rhythmic network activity even in absence of rhythmic inputs from descending or sensory afferents. That is not to say that these inputs do not play an important role in shaping the motor output. The masticatory CPG is located in the brainstem and involves mostly neurons in the vicinity of the trigeminal system. Although this has been known since the early 1970s, the precise organization of the trigeminal circuits that are involved and the basic mechanisms governing interactions between the cellular components remain largely unknown. Here, we will first describe the anatomical organization of these circuits, their inputs and outputs, and the factors controlling their development. We will then review recent findings on the cellular mechanisms governing rhythm generation and network operations in different contexts.

2. Anatomical organization of the trigeminal complex

Innervation of the orofacial area and masticatory muscles is insured by the Vth, VIIth, IXth and XIIth cranial nerves. The most important of these for chewing is the trigeminal nerve with its associated sensory, motor and premotor nuclei. Most of trigeminal primary sensory afferents have their cell bodies located in the trigeminal ganglion. Only those innervating jaw closing muscle spindles and about half of the mechanoreceptors innervating the periodontal ligaments are located centrally in the mesencephalic trigeminal nucleus (NVmes; green nucleus in Fig. 1). Recent studies using the retrograde tracer wheat germ agglutinin-HRP injections into extraocular muscles suggest that it also contains a small number of extraocular muscle spindles afferents (Wang and May, 2008). This nucleus formed by a thin column of cells running along the 4th ventricle begins in the mesencephalon, bends slightly laterally and enlarges in its caudal part in the pons (Paxinos and Watson, 2004). Ventral to its caudal end is the motor nucleus (NVmot) containing the cell bodies of motoneurons innervating the jaw muscles with those innervating the jaw closing muscles being dorsal and rostral (blue nucleus in Fig. 1) to those innervating jaw opening muscles (fuschia subdivision in Fig. 1). Immediately surrounding the NVmot is the peritrigeminal area (PeriV) which contains last-order interneurons and which is also often referred to as the borderzone or Regio h (Meessen and Olzewski, 1949). A chain of sensory nuclei composed of the trigeminal principal nucleus (NVsnpr) followed by the trigeminal spinal nucleus (NVsp) runs lateral to PeriV from the midpons to the second cervical vertebra (C-2) and is delimited laterally by the trigeminal tract (Capra and Dessem, 1992; Sessle, 2006) containing the central axonal branches of trigeminal sensory afferents entering the brainstem through the sensory root of the Vth nerve.

2.1. Sensory components

2.1.1. The mesencephalic trigeminal nucleus

Not only is the NVmes unique by its central location, but also by the fact that the cell bodies of the primary afferents that it contains receive synapses, many of which have been shown to be functional (Verdier et al., 2004; Yokomizo et al., 2005). These central inputs arise from many regions of the CNS but also from neighbouring NVmes cells via gap junctions and via collaterals making axo-dentritic and axo-somatic contacts between them (Luo and Dessem, 1996; Paik et al., 2005). Inputs from other regions of the CNS include projections from the hypothalamic magnocellular nucleus, the medial amygdaloid nucleus, the raphe nuclei, the ventral tegmental area, the substantia nigra, the locus coeruleus, the prefrontal cortex and other trigeminal neurons in NVsnpr, NVmot, NVsp, and PeriV (Buisseret-Delmas et al., 1997; Copray et al., 1990; Iida et al., 2010; Lazarov et al., 2011; Li et al., 2000; Rokx et al., 1986; Takahashi et al., 2010). Most NVmes neurons make monosynaptic contacts with motoneurons in NVmot, but they are not restricted to this nucleus and project to many other areas via their collaterals. Those outputs reach the cerebellum, the nucleus ambiguus, the NVsnpr, all three divisions of NVsp, all subdivisions of PeriV, and the hypoglossal nucleus (NXII) (Rokx et al., 1986; Shigenaga et al., 1988, 1989a; Zhang et al., 2005, 2001).

2.1.2. The main sensory nucleus

The NVsnpr receives massive inputs from trigeminal primary afferents innervating the mechanoreceptors from the muscles, skin, teeth, mucosa, and hair of the orofacial region and temporomandibular joint (Capra and Dessem, 1992). Projections of these afferents are somatotopically organized and form an inverted somatotopic facial representation with inputs from the mandible dorsally and those from the maxillary ventrally. NVsnpr neurons also receive monosynaptic projections from the trigeminal interneurons in NVmot, PeriV, and nucleus Pontis Caudalis (Bourque and Kolta, 2001; Kolta et al., 2000). Studies using anterograde and retrograde tracers have also shown that NVsnpr receives cortical inputs from the primary somatosensory cortex (S1), the primary motor cortex (M1) and the cortical masticatory area (CMA) which overlap the jaw, face and tongue representations of M1, completely in lower mammals and partially in humans and other primates (Yasui et al., 1985; Yoshida et al., 2009).

NVsnpr is traditionally considered as a second-order sensory relay to the thalamus (Martin, 2003). Its principal neurons that receive somesthesic information from the face decussate and ascend to the ventro-posterior medial nucleus of the thalamus in the lemniscal pathway (Arsenault and Zhang, 2006), while those relaying proprioceptive information from the oral cavity ascend in the dorsal trigeminothalamic tract without crossing (Carpenter,

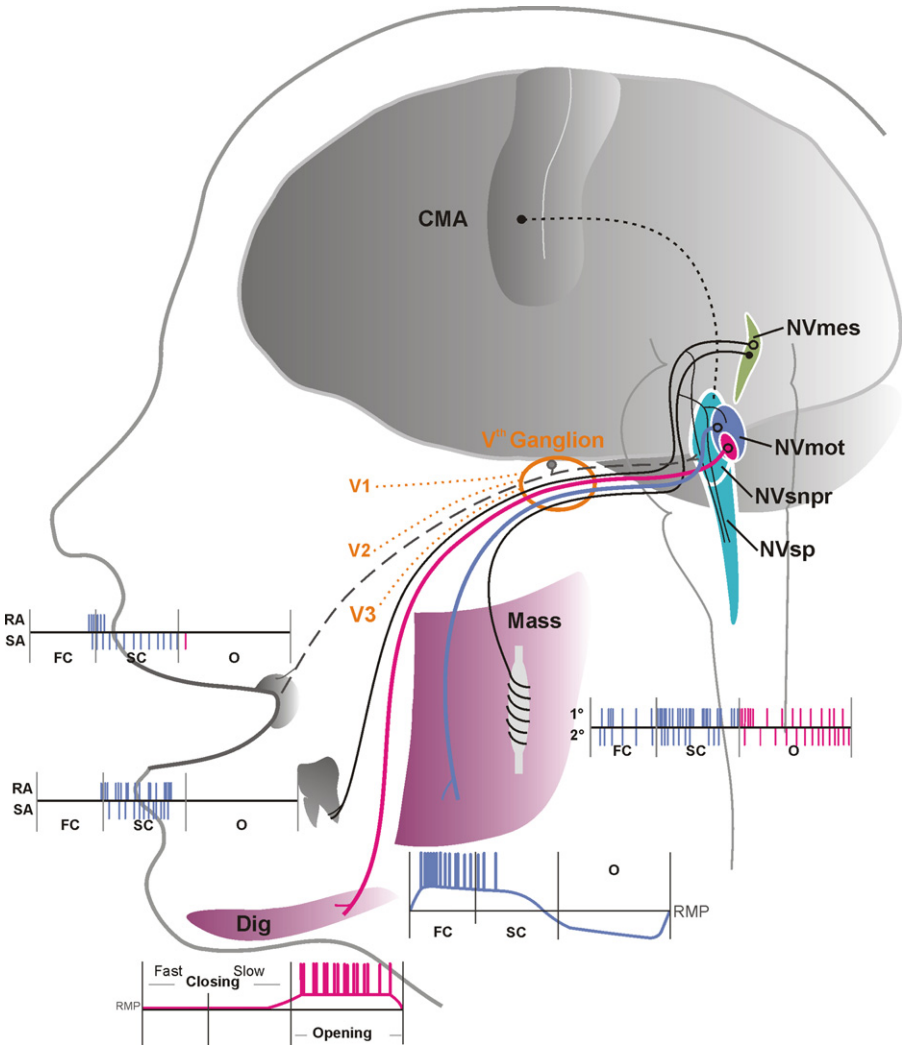

Fig. 1. Schematic representation of the trigeminal nerve branches and of the brainstem nuclei involved in orofacial movements and their connections. The trigeminal primary afferents innervating intra- and peri-oral sensory receptors (dashed line) have their cell body in the Vth ganglion, while those innervating jaw muscle spindles (solid black line innervating spindle) are located in the brainstem in the mesencephalic trigeminal nucleus (NVmes) which also contains part of the periodontal afferents innervating the teeth. The firing pattern of each type of afferents during the masticatory cycle is represented near the receptor in the periphery. Blue lines are action potentials in the jaw closing phase which is divided in fast closing (FC) and slow closing (SC). Pink lines are action potentials occurring during opening (O). Rapidly adapting (RA) units firing pattern is illustrated above the black line, whereas slowly adapting (SA) units firing pattern is illustrated below. Solid pink and blue lines are axons of motoneurons emerging from the jaw opening pool innervating digastric muscle (Dig) and the jaw closing pool innervating masseter muscle (Mass) respectively. Digastric motoneurons are silent during closing and depolarized and fire during opening (pink trace under the digastrics muscle). Masseter motoneurons are also depolarized and fire during closure, but are in addition hyperpolarized during opening (blue trace near masseter muscle). Lateral to the motor nucleus (NVmot in blue and pink) runs the sensory complex (cyan nuclei) composed of the main sensory nucleus (NVsnpr) and the spinal nucleus (NVsp) which both receive massive inputs from primary afferents and from higher brain areas including the cortical masticatory area (CMA).

1957). Other NVsnpr neurons have local brainstem projections reaching NVmot, PeriV, NVmes, the facial nucleus (NVII), NXII and the cerebellum (Athanassiadis et al., 2005; Li et al., 2005; Yatim et al., 1996; Yoshida et al., 1998).

2.1.3. The spinal nucleus

The spinal nucleus is a long nucleus subdivided into three compartments: oralis (NVspo), interpolaris (NVspi), and caudalis (NVspc). The most rostral of these subdivisions, NVspo, consists mostly of premotor neurons extending from the caudal pole of NVmot to the caudal pole of NVII. This subnucleus has two distinct topographic divisions: one medial where intra-oral structures are represented and one more lateral where vibrissae and posterior facial structures are represented (Eisenman et al., 1963; Westberg and Olsson, 1991). Mechanoreceptive inputs are from NVmes, the vibrissae, the oral-cavity structures and the anterior face while nocifensive inputs are from the teeth (Eisenman et al., 1963; Luo et al., 1995b; Park et al., 2001; Shigenaga et al., 1986b, 1989b). Like NVsnpr, NVspo receives cortical inputs from the CMA, M1 and S1 (Chang et al., 2009; Yasui et al., 1985; Yoshida et al., 2009), and sends projections to the thalamus, the cerebellum, the cervical cord, the NVmes, and PeriV interneurons which synapse in NVmot (Devoize et al., 2010; Guy et al., 2005; Westberg et al., 1998; Yatim et al., 1996; Zhang, 1998).

The NVspi is located between the NVspc and the NVspo. It extends from the caudal pole of NVII to the obex and receives inputs from the auriculotemporal nerve, the vibrissae, the ophthalmic and maxillary structures and from NVmes muscle-spindle afferents (Capra and Dessem, 1992; Jacquin et al., 1983; Luo et al., 1995a; Shigenaga et al., 1986a). The majority (75%) of these inputs is from low-threshold mechanoreceptive Aβ fibres, but a small percentage is from nociceptive fibres (Hayashi et al., 1984). As the other sensory nuclei, NVspi receives inputs from the cortical masticatory area (Yasui et al., 1985) and projects to the thalamus via the para-lemniscal pathway (Williams et al., 1994) and to the cerebellum and the cervical cord (Hayashi et al., 1984;

Yatim et al., 1996). Together NVspo and NVspi are thought to play a determinant role in the organization of trigeminal reflexes and in the transmission of sensory information to the cerebellum (Martin, 2003).

NVspc, the most caudal part of NVsp, extends from the obex to C2 (Capra and Dessem, 1992) and receives mostly inputs from small calibre myelinated (Aδ) and unmyelinated (C) fibres, relaying nociceptive and temperature information from orofacial structures (Dubner et al., 1978). It also receives collaterals from NVmes periodontal and jaw-muscle spindle afferents (Luo et al., 1995a). NVspc neurons project to the contralateral thalamus, the cerebellum, and reticular interneurons projecting to the different subnuclei of NVsp and cranio-facial motor nuclei (Capra and Dessem, 1992; Yatim et al., 1996). The three subdivisions are interconnected ipsilaterally and also receive inputs from NVsnpr (Hockfield and Gobel, 1982; Jacquin et al., 1990; Yoshida et al., 1994).

2.2. Motor components

A small group of cells named cell group K dispersed between NVmot and NVII contains some of the somata of γ-motoneurons innervating jaw closing muscles. Besides these cells, all other motoneurons supplying the muscles of mastication, except those innervating the posterior digastric belly, are found in NVmot which also contains motoneurons of accessory muscles in the middle ear (the tensor veli palatini and the tymphani), and a small population of interneurons (Hiiemae, 1967; McDavid et al., 2006, 2008; Ramirez et al., 2007). Inputs to NVmot arise from other trigeminal nuclei including NVmes, NVsnpr, NVspo, PeriV, and local interneurons within NVmot (Athanassiadis et al., 2005; Bourque and Kolta, 2001; Capra and Wax, 1989; Donga and Lund, 1991; Nakamura et al., 2008; Westberg et al., 1998, 2001; Yamamoto et al., 1989). Except for NVmes, all of these projections to NVmot are bilateral. Trigeminal motoneurons also receive monoaminergic modulatory inputs from different regions including the raphe nuclei, the subcoeruleus, the parabrachial nucleus, the Kolliker Fuse and cell groups A4 and A5 (Fort et al., 1990; Grzanna et al., 1987; Vornov and Sutin, 1983).

2.3. Premotor interneurons

The reticular borderzone surrounding NVmot, to which we refer as PeriV, is divided into four areas: the supratrigeminal area (SupV) dorsal to NVmot, the intertrigeminal area (IntV) between NVmot and NVsnpr, the juxtatrigeminal area (JuxtV) medial to NVmot and the parvocellular reticular formation (PCRt) located ventrally to NVmot which extends caudally down to the level of NXII (Bourque and Kolta, 2001; Capra and Dessem, 1992; Landgren et al., 1986; Olsson et al., 1986). These nuclei not only receive inputs from intra- and peri-oral structures and from the cortical masticatory area, but also have reciprocal connections between themselves, with interneurons in NVmot, in nucleus Pontis Caudalis and in NVsnpr (Athanassiadis et al., 2005; Bourque and Kolta, 2001; Dal Bo et al., 2005; Kolta et al., 2000; Luo et al., 1991; Nakamura et al., 2008; Nomura and Mizuno, 1985; Shigenaga et al., 1989b; Yasui et al., 1985; Yoshida et al., 1998).

3. Development of the masticatory circuitry

3.1. Genetic factors

The nuclei described above all participate to some extent to the masticatory circuitry. During development, these nuclei expand from the 2nd to the 5th rhombomeres. In all vertebrates, early development of the hindbrain and segmentation into distinct rhombomeres (r) is under the influence of the Hox genes (Fraser et al., 1990; Kiecker and Lumsden, 2005; Lumsden, 1990; Lumsden and Keynes, 1989; Oury et al., 2006). Hoxa2 is expressed all along the hindbrain, except in r1, and only weakly in r2, where it is the only Hox gene present. Its level of expression increases in r3 and r5 where Hoxb2 is also highly expressed. Oury et al. (2006) showed that the gradient of Hoxa2 expression is crucial for the correct wiring of NVsnpr, probably through a control of the expression of Eph4A and Eph7A in r3 and r5.

Prior to the compartmentalization of the hindbrain, the level of expression of Hoxa2 and Hoxb2 in r3 and r5 is controlled by the zinc finger genes, Krox-10 and Krox-20 which are essential to the formation of odd numbered rhombomeres (Gilardi et al., 1991; Maconochie et al., 2001; Nonchev et al., 1996a,b). In Krox-20 null mice, r3 and r5 are first generated but the emerging neurons share an even numbered phenotype. This results in cell loss, disappearance of 2 rhombomeres from the hindbrain (Schneider-Maunoury et al., 1993; Voiculescu et al., 2001) and death at birth due to severe respiratory and ingestion deficits (Jacquin et al., 1996).

Other factors that control expression of Hox genes in rostral rhombomeres and patterning of trigeminal neurons include the fibroblast growth factor 8 (Irving and Mason, 2000) and the Drg11 homeodomain transcription factor, the expression of which is essential for the survival of neurons in the trigeminal ganglion, NVsnpr and NVmes (Ding et al., 2003; Jacquin et al., 2008; Wang et al., 2007). The LIM homeodomain transcription factor Lmx1b is also expressed in NVsnpr and acts as a positive regulator in Drg11 expression (Dai et al., 2008; Qian et al., 2002; Xiang et al., 2010).

Trigeminal ganglion progenitors assemble partly from derivatives of the ophthalmic and maxilomandibular placodes and from neural crest cells migrating from the rostral rhombomere level, at E8–9 in mouse (Ayer-Le Lievre and Le Douarin, 1982; Kiecker and Lumsden, 2005; Pierce, 1973). Guided by the expression of Hoxa2 in r2 neuroepithelium (Oury et al., 2006), central processes from the trigeminal ganglion penetrate into the brainstem at the r2 level, by E10 in mouse and E12 in rats (Erzurumlu and Killackey, 1983; Lumsden and Keynes, 1989).

In mice, the first central trigeminal cells to be generated are those of NVmes at E8–11 (Stainier and Gilbert, 1990). Fibres from these cells grow towards their targets and reach the myoblast and the spindle at E1 and the perodontium about 10 days later, after birth (Widmer et al., 1998). For decades NVmes cells were thought to derive from the neural crest, but as discussed by De et al. (2005), several evidences now challenge this view. NVsnpr neurons are postmitotic derivatives from r2 and r3 (Oury et al., 2006) and appear at around E10 in mice (Ding et al., 2003) and E12 in rats (Miller and Muller, 1989), just before entrance of trigeminal ganglia afferents into the brainstem (al-Ghoul and Miller, 1993). Appearance of small neurons precedes emergence of large ones (Miller and Muller, 1989) and neurons migrate continuously from the medial to the lateral border of the nucleus (al-Ghoul and Miller, 1993), until E15. The inverted facial representation in NVsnpr, is governed by cue signals of rhombomeric origin (Oury et al., 2006). Cells from the dorsal half, derived mostly from r2, receive input only from lower-jaw and lips afferents of the mandibular nerve, while those of the ventral half, derived from r3 solely receive somatosensory afference from the maxillary nerve.

Trigeminal motoneurons appear as soon as E9 in mice and extend from r1 to r3 (Pierce, 1973). They form a columnar organization that is particularly distinctive by E13.5 (Widmer et al., 1998). Within those columns, motoneurons innervating the same muscle are clustered, with the digastric and hyomandibular being isolated caudally, in r3 (Turman, 2007). The trigeminal motor root exits the brainstem through r2 and the motor axon can be detected in the periphery at E11 (Widmer et al., 1998). By then the masticatory muscles are in development. Neuromuscular

junctions appear in the masseter and digastric muscles at around E15–16 (Turman, 2007; Widmer et al., 1998).

3.2. Ontogenesis of mastication

The first feeding associated movements appear *in utero*, in a sequence preserved across all mammals and at a time correlated to the species neuromuscular developmental rate (Narayanan et al., 1971). The first movements to appear are those of jaw-opening, followed by active jaw-closing and tongue movements, and later by swallowing. Suckling stabilizes shortly after birth and is used until emergence of reduction masticatory movements (Herring, 1985; Langenbach et al., 2001). This moment which corresponds to P12 and P13, in rats and rabbits respectively (Langenbach et al., 1992; Westneat and Hall, 1992), but occurs *in utero* in guinea pigs (Teaford and Walker, 1983) is shortly preceded by appearance of molars.

It is unclear at present when and how the networks responsible for sucking and chewing differ from each other. Do they depend on the same network which undergoes substantial changes of connectivity and intrinsic properties during maturation, or on different networks or again on the same network but driven by different oscillators depending on age? There is evidence supporting each of these alternatives. For instances, Nakamura's group has shown that suckling can be induced by stimulation of a cortical area located just rostral to the cortical masticatory area (CMA). Neurons of both cortical areas projected to the dorsal part of the contralateral paragigantocellular reticular nucleus. This led Nakamura's group to postulate that transition from suckling to chewing could result from a shift of the cortical projection area from suckling cortical area to the CMA (Iriki et al., 1988).

On the basis of the similarities of electromyographic recordings of the two motor patterns, Westneat and Hall (1992) and Langenbach et al. (1992) suggested that the neuronal substrate supporting mastication could be only an evolution of the one supporting suckling. Mastication and suckling both involve jaw opening and closing and clearly, many motoneurons are active during the two behaviours. However, during mastication, the force used to breakdown food is generated by jaw-closing muscles, while the power stroke for suction is provided mainly by jaw opening muscles (Colley and Creamer, 1958). Another important difference lies in the peristaltic motion of the tongue observed during the extraction phase of nutritive suckling (Ardran et al., 1958; Langenbach et al., 2001) and involving hypoglossal motoneurons (Lau, 2006).

Interestingly, in the days preceding the first masticatory movements in rats, the expression of KCC2 (a co-transporter K^+/Cl^-) increases in the Vth and XIIth motoneurons (Rivera et al., 1999) causing GABA and glycine to change from having a depolarizing to a hyperpolarizing effect (Ben-Ari, 2002). This suggests that the same CPG could produce opposite motor patterns with maturation.

Regular trigeminal rhythms are detected in rat brainstem en bloc preparations as early as E18 (Ishihama et al., 2003), but sensory experience at birth seems necessary to optimize pattern formation and brain development (Jean, 1990; Mistry and Hamdy, 2008), suggesting that changes in connectivity also occur. These rhythms are very similar to those recorded from trigeminal (V), facial (VII) and hypoglossal (XII) motoneurons in the same brainstem preparations taken from neonatal rats when the glutamate agonist N-methyl-D,L-aspartate (NMDA) is added to the bath (Enomoto et al., 2002; Katakura et al., 1995; Kogo et al., 1996, 1998; Koizumi et al., 2002; Tanaka et al., 1999). This activity, assumed to reflect suckling, is maintained in isolated sections of the brainstem containing either the V, the VII or the XII motor nuclei (Nakamura et al., 2004), as in the left and right halves of the trigeminal section (Tanaka et al., 1999), suggesting that each set of motoneurons may be driven by local neurons able to generate a rhythmic input. However, the caudal pair seems to inhibit the Vth pair (Tanaka et al., 1999). This also argues for a change of connectivity with age.

However, other observations also suggest that important changes in intrinsic properties occur. For instance, the sub-unit composition and the calcium permeability of the NMDA receptors change importantly in NVmes and NVmot as mastication emerges (Ishihama and Turman, 2006; Turman, 2007). Our previous work has also shown that in a population of neurons postulated to form the rhythmogenic core of the CPG at the level of NVmot, intrinsic properties responsible for rhythmogenecity (see below) emerge between P10 and P12, and stabilize by P-16–18 (Brocard et al., 2006).

The adult masticatory pattern is established at different ages in different species. The pattern of movements produced in a masticatory sequence varies considerably between species, but also between individual subjects within the same species and even between cycles in the same individual because of changes in food properties (Lund, 1991). In rabbits, where detailed descriptions have been made, a masticatory sequence is composed of a preparatory series where Type I cycles are observed, a reduction series where Type II cycles are observed, and a pre-swallowing series where Type III cycles are observed. In the preparatory series, which is relatively short lasting, the food is moved to the posterior teeth by the tongue. Type I cycles have only an opening phase and a fast closing phase and show very little lateral movement. Chewing and breakdown of the food really occur in the reduction series which is the longest in duration. Type II cycles have an opening (O), a fast-closing (FC) and a slow-closing (SC) phase (Lund, 1991). The actual food breakdown occurs during SC which is also referred to as the power stroke. Type III cycles prepare the crushed food bolus for swallowing and are composed of five phases: two during closure (FC and SC) and three during opening (two rapid opening phases, O1 and O3, separated by a pause, O2). Type II and Type III cycles have a significantly larger lateral component.

4. Cortical and sensory inputs to the central pattern generator

Although mastication is often considered to be stereotyped, there is a great deal of variability from cycle to cycle. Dellow and Lund (1971) have shown long ago that the basic pattern could be generated by the brainstem alone in a decerebrate paralysed animal. However, this variability of the movement envelope that occurs in physiological conditions can only be explained if one assumes that the brainstem circuits responsible for generating the basic rhythmic activity are subjected to some sort of feedback. Many subcortical areas are known to influence mastication and/or to project to the trigeminal complex. These areas include the amygdala, the hypothalamus, the anterior pretectal nucleus, the red nucleus, the periaqueductal grey, the raphe nuclei, the cerebellum and various parts of the basal ganglia (nucleus accumbens, subthalamic nucleus, and substantia nigra, pars reticulata) (Fornal et al., 1996; Hatanaka et al., 2000; Inagaki et al., 1987; Krettek and Price, 1978; Lazarov et al., 2011; Nakamura and Kubo, 1978; Takeuchi et al., 1988; Yoshida and Precht, 1971).

However, the following sections will focus mostly on feedback provided by sensory and cortical inputs.

4.1. Cortical inputs

Orofacial muscles engage in several behaviours, many of which demand complex refined control of musculature like during speech for instance. The jaw, tongue and facial muscles are represented

individually in several cortical areas including the primary motor cortex (M1) and the primary somatosensory area (SI). It is thus not surprising that several cortical areas exert descending influences on brainstem and other subcortical regions projecting to the brainstem. Ferrier was the first to show in 1886, that stimulation of a circumscribed cortical area elicits jaw movements. This area, identified as the cortical masticatory area (CMA), was further investigated by Bremer (1923) and much later by Lund et al. (1984) who showed that there was a kinesiotopic representation of the movement within this region. In the rabbit, stimulation of the most anterior part of the CMA, elicits a masticatory pattern corresponding to the first phase of mastication (Type I), while stimulation of the posterolateral part elicits Type II pattern. After constant stimulation this pattern becomes a Type III. In humans and other primates, the CMA partially overlaps lateral M1, but in lower mammals, it completely overlaps the jaw, face and tongue representations of M1. Intracortical microstimulation of other cortical areas including the face primary motor cortex (MI) (Murray and Sessle, 1992), primary somatosensory area (SI), premotor cortex, supplementary motor area, insula and anterior cingulate gyrus also evoke orofacial movements, but only repetitive stimulation of the CMA can elicit rhythmic jaw movements. Ablation or cooling of face M1 or CMA does not prevent mastication from occurring, but does cause difficulty in initiating mastication and increases total masticatory time (Enomoto et al., 1987; Yamamura et al., 2002). This is due in part to a loss of ability to coordinate food manipulation before and during chewing, and in transporting the food bolus towards the pharynx for swallowing.

Stimulation of the orofacial CMA in humans induces an excitatory bilateral activation of the jaw-muscles through corticobulbar projections to the brainstem reticular formation and bilaterally to the pons in the vicinity of the trigeminal motor nuclei (Nordstrom, 2007). Clearly, S1, M1 and CMA project to the trigeminal sensory complex and parvocellular reticular formation directly (Chang et al., 2009; Yoshida et al., 2009) but it is unclear whether direct projections to trigeminal motoneurons also exist (Hatanaka et al., 2005).

Cortical input to the motoneuron pools implies voluntary control over the muscles of mastication, specifically important for the fine control of voluntary bite force (Nordstrom, 2007). Single motor unit recordings (Nordstrom, 2007) and conduction velocity measurements based on optimal stimulation frequency and interstimulus interval (Cruccu et al., 1989) suggest that some of the corticobulbar fibres project monosynaptically onto the motoneurons. Similar direct corticomotoneuronal cells have been involved in the fractionation of finger muscles in the monkey (Bennett and Lemon, 1996). The putative direct corticomotoneuronal projections to masseter motoneurons arise from the contralateral CMA, whereas inputs to digastric motoneurons are bilateral indicating independent control of the jaw-closing muscles on each side only (Widmalm et al., 1988). Others have suggested that very few, if any, cortical projections input the trigeminal motor nucleus directly (Hatanaka et al., 2005). With the use of anterograde tracers injected into the jaw-movement-related areas, Hatanaka et al. (2005) suggested that cortical neurons reach premotor areas directly or indirectly before synapsing with V motoneuron pools. The direct pathway leads cortical inputs to premotor regions in the vicinity of NVmot, principally the supratrigeminal nucleus (SupV). The indirect pathway enters the basal ganglia at the striatum and exit via the globus pallidus and substantia nigra pars reticulata, towards the premotor nuclei. Most efferent fibres from basal ganglia are GABAergic (Yoshida and Precht, 1971), and this suggests inhibitory input from the indirect pathway into the premotor region, and excitatory synapses from the direct pathway.

Whether contributing to a direct or an indirect pathway, most cortical neurons recorded in various areas that are related to mastication seem to rely on sensory cues that they receive from orofacial afferent inputs prior to movement, or during movement, to anticipate and/or correct the movement (Lund and Lamarre, 1974; Sessle et al., 2005).

4.2. Sensory inputs

Under artificial experimental conditions, sensory inputs are not absolutely required to generate the basic masticatory movements that are produced by activation of the masticatory CPG. However, they are essential to adapt the movements to the hardness of the food and to compensate for unexpected perturbations (Grillner, 1981; Rossignol et al., 1988). Moreover, their excitatory drive is also probably needed to activate the CPG or to initiate phase transitions in the cycle (Rossignol et al., 1988). Various trigeminal afferent inputs provide sensory feedback to the masticatory CPG. The most important inputs to provide feedback on food hardness and adjust bite force are probably those of periodontal receptors and muscle spindle afferents, but others also give important feedback about other characteristics of the food bolus and position of the jaw. The firing frequency of hair afferents for instance is modulated throughout the masticatory cycle and is proportional to the velocity of movement in every direction (Appenteng et al., 1982). Activation of theses afferents is caused by the stretching of the skin area overlapping their receptive fields. Sensitivity to movement is greatest around the corners of the mouth, an area highly prone to skin distortion during jaw-movement (Lund, 1991). In contrast, very few skin afferents are activated during mastication. The responses to movement were recorded from receptors with fields concentrated at the corners of the mouth (Appenteng et al., 1982). No clear relation between firing frequency and velocity or amplitude of movement is apparent but it seems that skin afferent discharge is restricted to the jaw-closing phase (Appenteng et al., 1982). Mucosal afferents also exhibit phase dependency similarly to skin afferents, but in their case, responses are elicited only upon mechanical stimulation of their receptive field. Since cutaneous receptors are activated by deformation of the skin, they provide feedback on proper positioning of facial muscle and lips while mucosal afferents within the oral cavity signal location of the food bolus within the mouth for proper positioning of tongue and jaw muscles (Johansson et al., 1988). The firing patterns of different types of afferents according to the phase of the cycle are illustrated in Fig. 1.

As stated above, feedback from periodontal receptors and muscle spindles seems more important than that of cutaneous receptors in the control of jaw muscle (Inoue et al., 1989). Animals deprived of intraoral afferents through lesions of the inferior alveolar and maxillary nerve branches can still chew, but the contribution of these inputs becomes apparent as their mastication appears clumsy (Morimoto et al., 1989). Periodontal mechanoreceptors innervating the ligament around the roots of the teeth have their cell bodies in both the Gasserian ganglion and the Trigeminal Mesencephalic nucleus (NVmes). Those in the Gasserian ganglion are active during mastication when using the molar teeth and display a short burst of activity at the start of the slow closing (SC) phase (Appenteng et al., 1982; Lund, 1991). They are sensitive to the force or rate of change of force applied to the crown of the tooth (Johansson and Olsson, 1976). Those in NVmes are activated upon voluntary biting using the incisor teeth. They remain active throughout the power stroke (SC) and see their firing frequencies increase every time food causes the pressure on the teeth to increase (Lund, 1991). In absence of movement, they assist opening through a jaw opening reflex like the one elicited by tapping on the teeth. However, during mastication they provide

positive feedback to jaw closing motoneurons because heavy pressures generated during the JC phase of mastication cause the JC phase to lengthen, and JC motoneurons to fire at higher frequency.

In humans, most periodontal afferents encode force amplitude with a hyperbolic relation since they have a high tendency to saturate (Trulsson and Johansson, 1994). They are highly sensitive at forces beneath 1 N, but have a poor dynamic sensitivity at stronger chewing forces. They can respond to forces applied in different directions but have higher firing rates for preferred directions (Trulsson and Johansson, 1994). Together, populations of periodontal afferents provide information about which teeth are loaded and the direction of forces applied to individual teeth. Thus, it is assumed that information provided by periodontal afferents is more useful for food manipulations than to provide powerful contraction of jaw muscles (Trulsson and Johansson, 2002). Forces used to hold food between teeth are greater, more variable and increase at a slower pace when needed to split food in humans with reduced periodontal tissue (Johansson et al., 2006).

Muscle spindles which are sensitive to change in muscle length and tension are found in significant number only in jaw closing muscles (masseter, temporalis, and medial pterygoid) and are of two types: dynamic (primaries) and static (secondaries). The former fire at high frequency before the start of mastication and are maximally active during Type I and Type III cycle even though maximal amplitude of movement occurs during Type II, while the latter fire at a lower frequency at different times of the cycle (see Fig. 1). Both fire when stretched during the jaw opening phase, but the γ-motoneurons drive causes the strongest firing to occur in the JC phase (Lund, 1991; Masuda et al., 1997). All muscle spindle afferents have their cell bodies in NVmes. These afferents, together with periodontal receptors, are mostly responsible for encoding information on food consistency and for adjusting the activity and force of jaw-closing muscles during the movement; the harder the food, the greater the positive feedback to JC motoneurons through these afferents. In an experiment of Morimoto et al. (1989), increasing food hardness was simulated by insertion of plastic strips of increasing size between opposing molars in the rabbit. This caused a facilitation of JC muscles that persisted after individual lesions of either the trigeminal branches (maxillary and inferior alveolar) or the NVmes, but that was almost completely abolished when both inputs were removed. Similar results from Lavigne et al. (1987) indicated that both spindle and periodontal afferents inputs control activity of jaw-closing muscle during the power phase.

Other types of afferents that may provide feedback during mastication are those innervating Golgi tendon organs and the temporomandibular joint capsule, but only limited information exists regarding their potential role. The former are free nerve endings in the tendon capsule and are sensitive to changes in muscle tension. The mechanoreceptors innervating the joint capsule (Boyd, 1954; Skoglund, 1956) presumably encode joint position, displacement and velocity when the mandible moves, more specifically during the jaw opening phase of the masticatory cycle (Tsuboi et al., 2009).

However, there is evidence that if the sensory drive from this various kinds of receptors is needed to adapt and correct movements, CPGs do not always roughly use it as it comes, but in some occasions, subject it to some sort of control and modulation. One common strategy used by CPGs to achieve this is through the mechanism of primary afferent depolarization (PAD) of the central terminals by GABA. This mechanism allows control of sensory transmission at specific synapses without affecting all the postsynaptic targets of sensory afferents. GABA is depolarizing in primary afferents because the chloride equilibrium potential is more depolarized (∼−30 mV) than their resting membrane potential due to the lack of the chloride transporter KCC2 (Kanaka et al., 2001). Nonetheless, PADs translate into inhibition of synaptic transmission because it reduces transmitter release at the terminal where it is occurring. If PAD is strong enough, it can initiate action potentials in the central axon that propagate antidromically and can even reach the peripheral axon. PADs and phasic bursts of antidromic (AD) potentials had been reported to occur during several forms of fictive rhythmical movements such as respiration (Ritcher et al., 1986), locomotion (Dubuc et al., 1985; Gossard, 1996; Gossard et al., 1989), mastication (Kurasawa et al., 1988) and scratching (Bayev and Kostyuk, 1981), suggesting that these result from the active control of sensory terminals by CPGs.

We have already shown that bursts of AD action potentials occur in the central axons of jaw closing muscle spindle afferents (MSAs) during fictive mastication (Westberg et al., 2000). However, modulation of jaw closing MSAs appears to be more complex than this (see Fig. 2). These afferents are peculiar because their somata, as already stated, are centrally located in NVmes, coupled through gap junctions and receive synaptic inputs (inputs 1 in Fig. 2). In addition, these cells have resonant properties that produce high frequency oscillations near their resting membrane potential which sometimes lead to rhythmic bursting during depolarization (Pedroarena et al., 1999; Wu et al., 2001). In an earlier study in which we investigated the synaptic inputs to those cells by stimulating neighbouring areas, we showed that somata of primary afferents have synaptic excitatory responses that caused firing, even those mediated by GABAa receptors (Verdier et al., 2004). In addition, the inputs increased the amplitude of the fast oscillations for several cycles and reset the oscillatory rhythm, which will cause afferents receiving the same synaptic inputs to fire synchronously (Verdier et al., 2004). This, combined with the fact that many of these afferents are coupled either to another afferent or to dendrites of multipolar interneurons (see Verdier et al., 2004) indicates that firing may be sustained and synchronous in sub-populations of NVmes neurons, which may be important during rapid biting and during the mastication of very hard or though foods.

However, it is not clear whether all axonal branches are invaded by spikes generated at the soma. A few years ago, we found that the cell bodies and the central terminals of jaw closing MSAs express different patterns of modulation during fictive mastication. Both the somata and the terminals show a phasic inhibition during the jaw opening phase of the masticatory cycle, but during the jaw closing phase only the central terminals show a phasic excitation resulting from the addition of AD spikes (inputs 3 and red spikes in Fig. 2). These AD spikes propagate to other branches of the central axon and invade them orthodromically (Westberg et al., 2000), but rarely reach the soma, suggesting that an active mechanism is regulating action potential propagation into the different compartments of the axonal tree. We have shown that GABAergic axons contact the axonal trunk of these afferents (inputs 2 in Fig. 2), and that GABA applied to the trunk can block propagation of AD potentials (Verdier et al., 2003). We also showed that stimulation of local trigeminal neurons in PeriV and NVsnpr causes a similar GABAa receptor-mediated blockade of AD action potentials. These findings suggest that these primary afferents could be compartmentalized as has been shown in invertebrates before. We propose that these mechanisms enable part of the axon to act as an interneuron (by conveying the AD spikes to other postsynaptic targets) while another part of the neuron continues acting as a primary afferent conveying sensory information from the periphery through orthodromic spikes.

5. Pattern and rhythm generation

5.1. Elements of the rhythm generator

The above mentioned transections studies in the "en bloc" brainstem preparations of neonate rats clearly show that a bloc

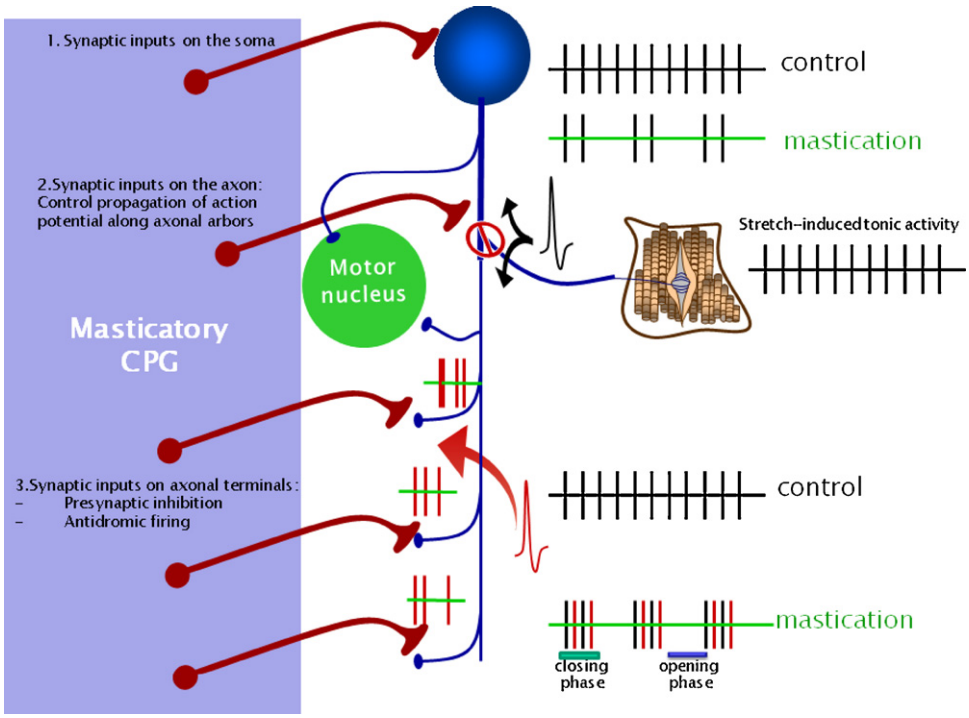

Fig. 2. Functional model of jaw closing muscle spindle afferent. (1) Synaptic inputs on the soma are responsible for the phasic inhibition of the orthodromic spikes (black bars) seen in the jaw opening phase of the masticatory cycle and also seen in the activity recorded near the central terminals. The central terminals (bottom traces) also show a phasic excitation in the jaw closing phase. This excitation is thought to reflect spikes generated from primary afferent deoplarizations (PADs) occurring at the terminals and propagated antidromically (red bars). These PADs are presumably induced by presynatic GABAergic synapses on the terminals (3). The antidromic spikes elicited at the terminals sometimes reach rostral branches but never reach the somatic compartment. GABAergic synapses (2) on the main axonal trunk cause failure of the antidromic spikes, but may not be enough to block propagation of orthodromic spikes.

extending from the rostral pole of NVmot to the rostral pole of NVII can still produce rhythmic activity in the trigeminal nerves upon addition of NMDA to the bath (Kogo et al., 1996; Tanaka et al., 1999). We have examined the intrinsic properties and connectivity of neurons comprised within this region and identified only one population of neurons with intrinsic properties capable of producing rhythmic bursting. This population of neurons forms the antero-dorsal part of NVsnpr and extends to the area just medial to the nucleus (SupV) which is cytoarchitecturally identical. These neurons fire rhythmically during fictive mastication and receive mostly inputs from intra-oral receptors (periodontal and spindle afferents) that provide crucial feedback to adjust the movement parameters (Tsuboi et al., 2003). Other neurons from the areas medial (PeriV and nucleus Pontis Caudalis) and caudal (NVspo) to NVsnpr, also fire rhythmically *in vivo* during fictive mastication (Donga and Lund, 1991; Inoue et al., 1992; Westberg et al., 1998, 2001), but except for those of NVspo which have not been examined yet, intracellular electrophysiological investigation of these neurons *in vitro* have failed to reveal intrinsic bursting properties, but showed instead robust interconnections and transmission between all divisions of PeriV (Bourque and Kolta, 2001). These connections may be important to insure a rapid and reliable distribution among premotor neurons of rhythmic inputs received from another population such as the one in NVsnpr.

The intrinsic bursting abilities of NVsnpr neurons appear around P12, in parallel with the first masticatory movements. Under normal conditions, the number of NVsnpr bursting neurons increases gradually during the 2nd postanatal week, when the transition from suckling to mastication occurs, and passes from around 5% to nearly 50% between P12 and P17 (Bernier et al., 2010; Brocard et al., 2006). The median bursting frequency (6.25 Hz; Bernier et al., 2010) coincides with the frequency range of natural mastication (6–8 Hz) and bursting is maintained and even enhanced under conditions that reduce synaptic transmission (removal of Ca^{2+} from the perfusing medium), confirming that they result from an intrinsic property.

5.2. Ionic mechanisms underlying the burst pattern

The pacemaker characteristics of NVsnpr neurons were first noticed by Sandler et al. (1998) in the gerbil. Intrinsic bursting usually involves a mechanism that provides a depolarizing driving force to induce a depolarization plateau, and a hyperpolarizing mechanism to terminate it (Harris-Warrick, 2010). Multiple ionic mechanisms can be responsible for plateau potentials and many of these involve Ca^{2+} entry into the cell either through a ionotropic receptor such as the NMDA receptor or through specific or non-specific channels such as low-threshold voltage gated Ca^{2+} channels or the calcium activated non-selective current (I_{CAN}) respectively (Chen et al., 2005; Zhang et al., 1995). Low-threshold Ca^{2+}-currents are crucial for thalamic bursting (Luthi and McCormick, 1999), whereas bursting in a subpopulation of pre-Bötzinger neurons relies on I_{CAN} (Pace et al., 2007) and can be abolished with intracellular BAPTA or blockers of these channels, like flufenamic acid. However, bursting in NVsnpr neurons is unlikely to be based on Ca^{2+} currents since it persists and is even enhanced after removal of Ca^{2+} from the perfusing medium; even if divalent ions concentration is maintained constant (Brocard et al., 2006). Further, non-bursting neurons in physiological calcium concentration start to burst when BAPTA is applied at their proximity showing that even very localized drops in extracellular calcium concentration are enough to promote bursting (Fig. 3A). Moreover, recent evidence from our laboratory indicates that neither intracellular BAPTA (see Fig. 3B) nor FFA affect the bursting ability of NVsnpr neurons. Brocard et al. (2006) clearly established that the driving force for the plateau potential supporting bursting

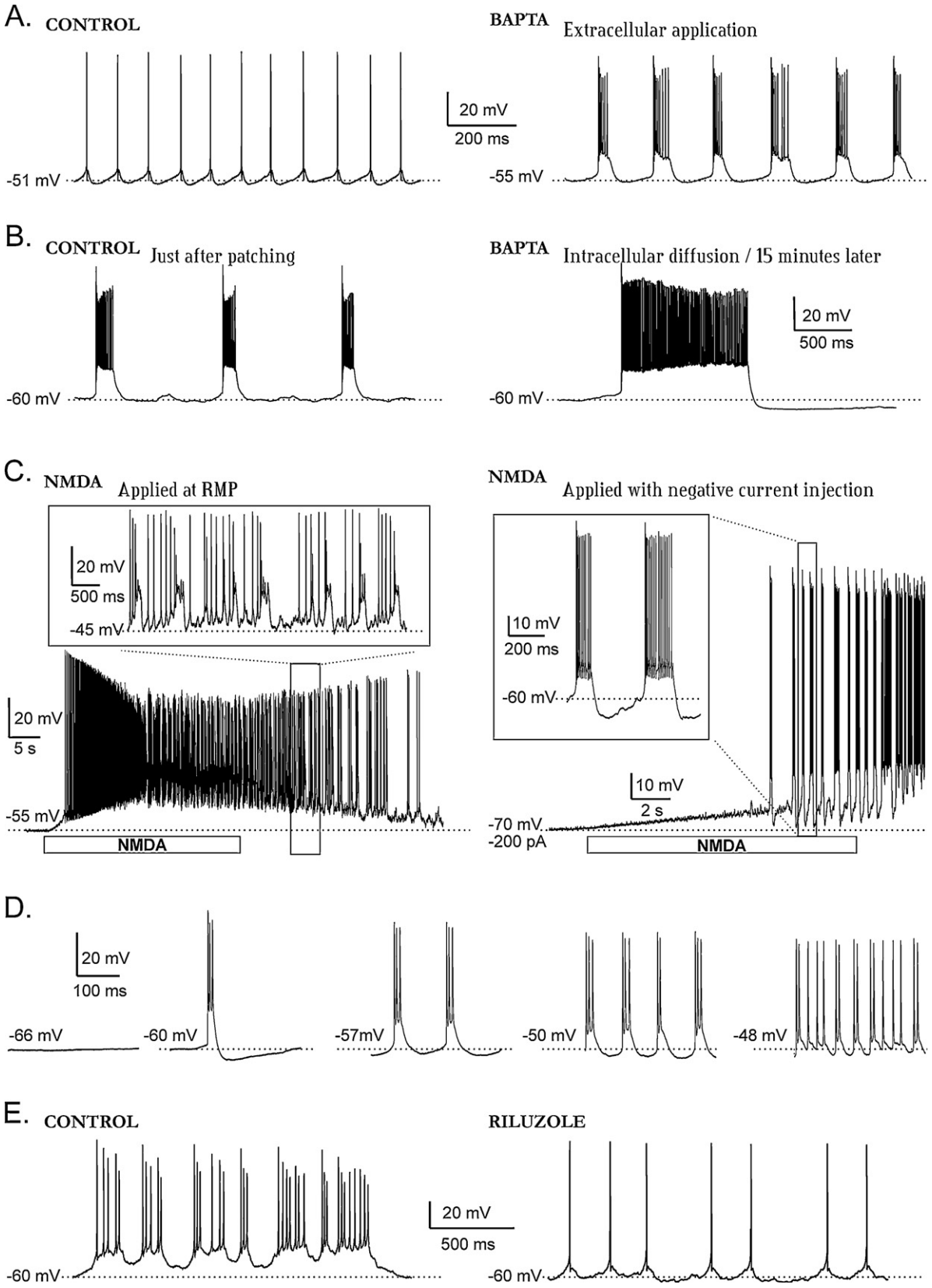

Fig. 3. Ionic mechanisms underlying bursting in NVsnpr neurons. (A) Puff-applied BAPTA causing small localized variations in extracellular Ca^{2+} concentration induces bursting (right trace) in an otherwise tonically firing neuron (left trace). (B) Chelation of intracellular Ca^{2+} with BAPTA in the internal solution does not prevent bursting but prolongs the underlying plateau, suggesting a role for Ca^{2+} dependent K^+ currents in burst termination. (C) Locally applied NMDA induces rhythmic bursting (right panel) in NVsnpr neurons only when prior hyperpolarizing current is applied to presumably counteract the strong depolarization induced by NMDA and maintain the membrane within I_{NaP} activation range. When applied at resting membrane potential (RMP; left trace), NMDA induces a disorganized tonic firing pattern with intercalated plateaux. (D) Voltage-dependency of bursting in Ca^{2+} free aCSF. Plateau-supported bursting occurs in a narrow range of membrane potentials, corresponding to I_{NaP} activation range and extending roughly from −60 mV to −50 mV. (E) Riluzole, a blocker of I_{NaP}, abolishes (right) bursting induced by local NMDA application (left) without altering the cells ability to fire action potentials indicating that the NMDA-induced bursting relies on I_{NaP}.

in NVsnpr neurons relies entirely on a sodium conductance that can be blocked by TTX or riluzole suggesting it is most probably a sodium persistent current (I_{NaP}) (Urbani and Belluzzi, 2000; Wu et al., 2005). This current is also responsible for bursting in many other CNS areas, including the pre-Bötzinger complex (Del Negro et al., 2002; Koizumi and Smith, 2008) contributing to the respiratory rhythm and neurons of the spinal cord crucial for the locomotor rhythm, to name a few (Tazerart et al., 2007; Zhong et al., 2007). The voltage dependency of the plateau (roughly between −60 mV and −50 mV) corresponds to I_{NaP} activation range (Brocard et al., 2006; Crill, 1996), and the developmental profile (appearance in the second postnatal week) is in agreement with previous report with that regard in other areas (Alzheimer et al., 1993; Huguenard et al., 1988). However, an interesting new finding was that the amplitude and duration of this plateau was inversely related to the external Ca^{2+} concentration (Brocard et al., 2006). This relationship between $[Ca^{2+}]_e$ and I_{NaP} that have also been described in spinal interneurons (Tazerart et al., 2008) and other CNS areas (Azouz et al., 1996; Li and Hatton, 1996; Su et al., 2001) is not very surprising since Ca^{2+} decreases have been shown to increase cells excitability and conductance of many ionic channels (Frankenhaeuser and Hodgkin, 1957; Hille, 2001; Nicholls et al., 2001). However, the promotion of bursting by the extracellular reduction of Ca^{2+} may also result from an effect on several K^+ channels that may play a role in burst termination (see below) or that may counteract I_{NaP} for burst initiation. For instances, in CA1 pyramidal neurons, where the spike ADP and bursting are primarily I_{NaP}-driven (Azouz et al., 1996), blocking M channels (Kv7/KCNQ family) facilitates the ADP and ultimately leads to spontaneous bursting (Yue and Yaari, 2004). These effects, which resemble those observed in NVsnpr neurons and in hippocampal neurons when decreasing the extracellular Ca^{2+}, could result from a down-regulation of the Kv7/KCNQ/M channel mediated current, since potentiating this current prevents bursting induced in CA1 pyramidal neurons by a Ca^{2+}-free perfusion (Gu et al., 2005). The M current is modulated by a large array of receptor types, many of which induce intracellular Ca^{2+} variations. Small increases of intracellular Ca^{2+} have been reported to increase I_M, whereas large increases seem to have the opposite effect. Removal of extracellular Ca^{2+} has also been reported to have opposite effects on the M current (see Marrion, 1997 for review). Another current that has been shown to contribute importantly to pacemaking properties is the hyperpolarization activated current (I_h). This conductance, often triggered by the hyperpolarization following the plateau phase of a burst, gives rise to a depolarizing ramp that leads to the next burst. NVsnpr neurons do express an I_h current that could contribute to bursting by helping neurons get in the activation range of I_{NAP} in order to generate a subsequent burst. However, ZD 7288, a specific I_h blocker, does not prevent bursting induced in Ca^{2+}-free ACSF, but increases the burst frequency and decreases the plateau duration and amplitude. In contrast, blockade of I_h in the salamander, significantly slows bursting frequency of spinal neurons during fictive locomotion (Chevallier et al., 2006).

5.2.1. Mechanisms of burst termination

In most documented instances of recurrent bursting, the hyperpolarization terminating the plateau underlying the burst firing is mediated by a K^+ conductance. This is also probably the case of NVsnpr neurons since TEA, a non-specific K^+ channels blocker, does not prevent bursting in calcium free ACSF but prolongs significantly the burst-underlying plateau (Brocard et al., 2006). Most often, the K^+ channels involved in burst termination are activated by the transient Ca^{2+} rise that occurs during the burst (Onimaru et al., 1997; Richter et al., 1993). In NVsnpr neurons, as with TEA, intracellular Ca^{2+} chelation by addition of BAPTA in the recording electrode prolongs the burst duration and underlying plateau suggesting that Ca^{2+}-dependent K^+ currents may play a role in burst termination. Ca^{2+}-dependent K^+ current is generally of two types, small (SK-Ca) or big (BK-Ca) and are often responsible for the two phases (fast and slow) of the afterhyperpolarization (AHP) when present. In NVsnpr neurons, gradual reduction of the extracellular Ca^{2+} decreases the AHP and favours appearance of an afterdepolarization (ADP) instead. The reversal of the AHP in an ADP is reproduced by charybdotoxin, a specific blocker of BK_{Ca}, whereas apamin a specific blocker of SK_{Ca} channels did not have a significant effect on burst shape, despite having a clear effect on the AHP (Brocard et al., 2006) and in contrast with the locomotor system where SK channels have been shown to play a role in bursting termination during fictive locomotion (el Manira et al., 1994).

As discussed by others before (Del Negro et al., 2002; Ellerkmann et al., 2001), the slow inactivation of I_{NAP} may also facilitate the return to resting membrane potential by activating the electrogenic Na^+/K^+ pump which has a hyperpolarizing action (Ballerini et al., 1997; Darbon et al., 2003). This current is activated with the accumulation of Na^+ that occurs during the burst (Rubin et al., 2009). In the respiratory system, other repolarizing mechanisms are also considered to contribute to burst termination. In the pre-Bötzinger complex, both computational (Smith et al., 2000) and experimental (Koizumi and Smith, 2008) data suggest that the potassium dominated leak current plays an important role and that substance P, which increases burst frequency acts by modulating this current (Koizumi and Smith, 2008).

6. Network operation

We have now reviewed existing knowledge regarding inputs and outputs of the CPG and intrinsic properties of at least some of its rhythm generating neurons. However, we are still far from fully understanding how all of this is brought together to generate an adapted behaviour. How are the sensory and/or cortical inputs integrated to the intrinsic properties of the rhythmogenic neurons? How are the rhythmogenic neurons synchronized? Is the same population of rhythmogenic neurons active for all patterns or are different populations involved depending on the pattern? How is the generated rhythmic activity organized and transmitted to antagonistic motoneurons? As with many other complex CPG systems, only tentative answers can be provided to some of these questions at present and mostly through models.

The first CPG model was that of the "half centre" proposed by Graham Brown for the locomotor CPG (box in Fig. 4). In this model, two groups of spinal neurons organized in parallel inhibited each other reciprocally so that a rhythmic pattern is induced with the alternating activation of extensor and flexor muscles (Brown, 1911, 1914). However, this model does not account for the variability of patterns observed during locomotion.

Later a unit burst generator model was proposed by Grillner (1981) and more recent models are based on two level half-centre models (Kriellaars et al., 1994; Perret and Cabelguen, 1980). These introduce the idea that while a first level of processing controls the pattern and amplitude of motoneuronal activity, a second level (see Fig. 4) generates the rhythm *per se* (McCrea and Rybak, 2008). Individual neurons in these models do not need to have intrinsic pacemaker characteristics necessarily and the rhythm emerges from synaptic interactions. On the contrary, in other proposed models, the rhythmic output of the CPG relies on intrinsic pacemaker properties of a group of cells that drives other components of the CPG. Until recently, both modes (pacemaker neurons *vs* network properties) were viewed as being mutually exclusive. However, this view is increasingly being challenged.

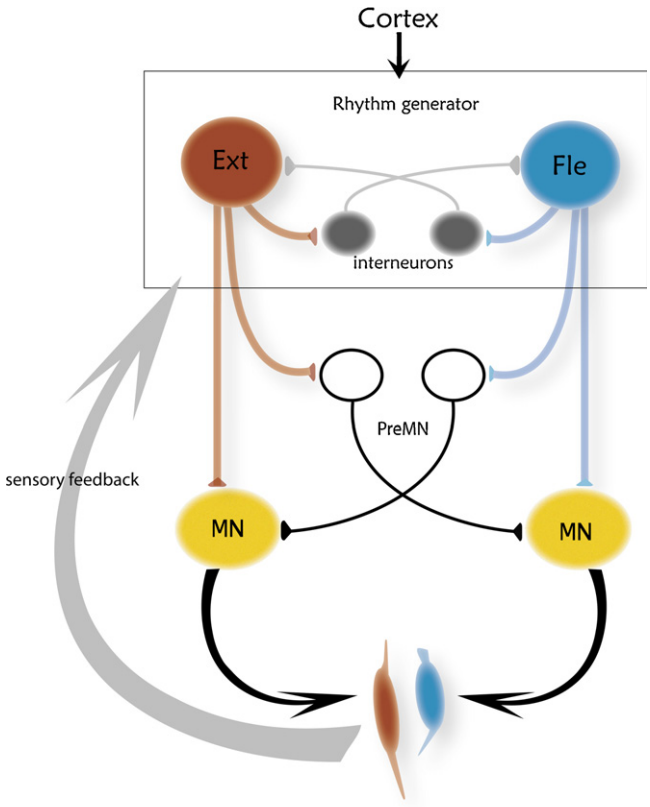

Fig. 4. Schematic illustration of half-centre models that produce alternating rhythmic activity between flexors (Fle in blue) and extensors (Ext in red). Flexor and extensor neurons have projection to motoneurons innervating muscle (also in blue and red) implicated in the rhythmic movement. In Graham Brown's model (box), mutual inhibition through inhibitory interneurons (in grey) insures alternating activity between two half centres (flexor in blue and extensor in red). Developing fatigue in the inhibitory neurons would be responsible for the switch between the two half-centres. In later models, the CPG circuitry is divided into two levels: a first one (within the box) that generates the basic alternating rhythm and a second one composed of premotoneurons that determine the envelope of the motoneuronal burst pattern. Cortical and sensory inputs are useful to trigger or correct the pattern.

As rightly pointed out by Harris-Warrick (2010) in a recent review, rhythmogenic ionic currents (such as I_{NaP}, I_{CAN}, and I_h) have been described in all CPG networks, but their expression is modulated and controlled by synaptic connections. Interactions of the two allow emergence of new network properties because these currents enable synaptic currents elicited by classical rapid neurotransmitters (such as GABA and glutamate) to trigger non-linear dynamics. In the respiratory system, for instance, Del Negro and colleagues (Del Negro et al., 2010; Rubin et al., 2009) have shown how synaptic drive can initiate the burst-generating I_{CAN} current at the beginning of each burst in a subpopulation of neurons. They have coined the term "group pacemaker" for this "emergent network property".

In neurons where bursting relies on I_{NaP}, a similar modulation must occur because of the voltage and external Ca^{2+}-dependency of this current which allows for a graded modulation of bursting in function of the afferent input. We propose that this mechanism enables sensory feedback to modify and adjust the rhythmic output pattern.

Cortical and sensory inputs to NVsnpr are glutamatergic and hence, play a crucial role in determining the membrane potential. Weak activation of these inputs will be insufficient to bring the membrane potential within I_{NaP} activation range and induce only tonic firing at a frequency linearly related to the induced depolarization. A larger amount of inputs would be more efficient to bring the cells membrane potential within I_{NaP} activation range and induce bursting, whereas a much larger amount of inputs would depolarize the cell above I_{NaP} activation range and revert firing to tonic. This is supported by the observation that low frequency stimulation (<1 Hz) of the sensory fibres projecting to NVsnpr induces only short lasting inhibition or excitation of tonic firing in NVsnpr neurons, whereas high frequency stimulation induces bursting in about 30% of these neurons (Bernier et al., 2010). Interestingly, the optimal stimulation frequency was between 40 and 60 Hz, which corresponds to the optimal stimulation frequency of the cortical masticatory area to induce mastication and to the natural firing frequency of the periodontal inputs projecting to NVsnpr (Trulsson, 2007; Trulsson and Johansson, 2002). Bursting induced by high frequency stimulation of the sensory tract is sensitive to APV, indicating that NMDA receptors may play a role in burst induction. However, when NMDA is directly applied to NVsnpr neurons, bursting can be induced only if hyperpolarizing current is injected concomitantly (Fig. 3C), supporting the idea that depolarization at levels above I_{NaP} activation range prevents bursting (Fig. 3D). This NMDA induced bursting is blocked by riluzole (Fig. 3E), indicating that it is mediated by I_{NaP}.

High frequency stimulation is important to sufficiently depolarize the cells, but may also play a determinant role in altering the extracellular Ca^{2+} concentration. Several studies have shown that extracellular calcium fluctuates dramatically with neuronal activity under both pathological and physiological conditions (Amzica et al., 2002; Nicholson et al., 1978; Somjen, 1980) and there are evidence that as little as activation of a single fibre could cause a transient depletion of calcium in the synaptic cleft (Rusakov and Fine, 2003). However, the mechanisms responsible for this Ca^{2+} drop are unknown.

The role of glial cells in maintaining extracellular ionic homeostasis is well established. An increasing body of evidence shows that glial cells express ionic channels and receptors that are sensitive to transmitters and modulators released from neurons. In turn, they have been shown to regulate neuronal activity in many physiological and pathological conditions (*e.g.* in epilepsy) and to play a determinant role in processes such as learning and memory, sleep and nociception. We therefore raised the possibility that glial cells could play an active role in determining the firing pattern of NVsnpr neurons by modulating the extracellular Ca^{2+} concentration (Kolta et al., 2010). Synaptic elements are wrapped in glial processes (Auld and Robitaille, 2003; Grosche et al., 2002, 1999; Salpeter, 1987) which can regulate the concentration of several ions (K^+ and Ca^{2+} among others) in the extracellular space and/or release a number of factors (Volterra and Meldolesi, 2005) (such as glutamate, D serine, and ATP) that can alter neuronal firing.

Recent publications suggest that glial cells may also play a role in other CPG systems. It has been proposed that astrocytes are needed to buffer excess of extracellular glutamate and potassium in the respiratory system (Grass et al., 2004). A recent study also suggests that glial cells may modulate the inspiratory rhythm generating network by releasing ATP (Huxtable et al., 2010). More specifically, Gourine et al. (2010) have shown that the astrocytes located within the ventral surface of the medulla oblongata (VS astrocytes) act as sensors for physiological pH decrease and respond to it through an intracellular calcium elevation and a subsequent ATP release. This ATP release elicits a calcium wave activation of the chemosensitive retrotrapezoid nucleus (RTN) astrocytes leading to an increased activity of RTN neurons (pH sensitive neurons) responsible for a boost of the respiratory rhythm in order to re-establish normal blood pH. They have done elegant experiments using an optogenetic *in vivo* approach in order to activate specifically VS astrocytes and showed that their activation constitutes a key element to drive the rhythm of respiration recorded from the phrenic nerve in both hypocampic

apnoea and normally breathing animals. In both cases, MRS2179, an ATP receptors antagonist, blocked the effects of the stimulation of VS astrocytes. This study provides strong evidence for an active role of astrocytes in neuronal processing involved in rhythm generation.

In the masticatory CPG, we first tested whether NVsnpr glial cells respond to stimuli that efficiently elicit bursting in this nucleus and found that both NMDA local application as well as high frequency stimulation of the sensory tract depolarized astrocytes and raised their intracellular Ca^{2+}. More interestingly, these stimuli increased coupling between astrocytes and the syncitia formed in this manner remained confined within the border of NVsnpr indicating that astrocytic syncitia could define domains within which the extracellular ionic conditions could be uniform. Primary afferent projections to NVsnpr are topographically organized and tend to contact adjacent neurons in NVsnpr. If neighbouring astrocytes receive the same inputs, than it is possible that coupling between them becomes a mean of synchronizing neurons encompassed in their syncitium. While the glial syncitium could determine the extracellular Ca^{2+} concentration within confined boundaries and hence modulate I_{NaP}, the afferent input could serve as the common depolarizing trigger. In this case a population comprised within the syncitium and linked by a common input could burst synchronously. Under different conditions, where a different population of sensory or cortical inputs would be active, then a different population of NVsnpr neurons would become rhythmogenic. These different populations would presumably drive distinct populations of motoneurons and premotor interneurons. In such a model the rythmogenic population responsible for generating the final pattern would be changing constantly depending on the sensory and/or cortical feedback and astrocytic syncitia could help defining the boundaries of functional domains linking neurons receiving common inputs. This hypothetical model illustrated in Fig. 5 is far from complete at this stage. Nonetheless, it considers factors that have been largely ignored until now and paves the way to new investigations. The proposed mechanisms could help understand how sensory feedback interacts with rythmogenic properties to constantly adapt the motor output.

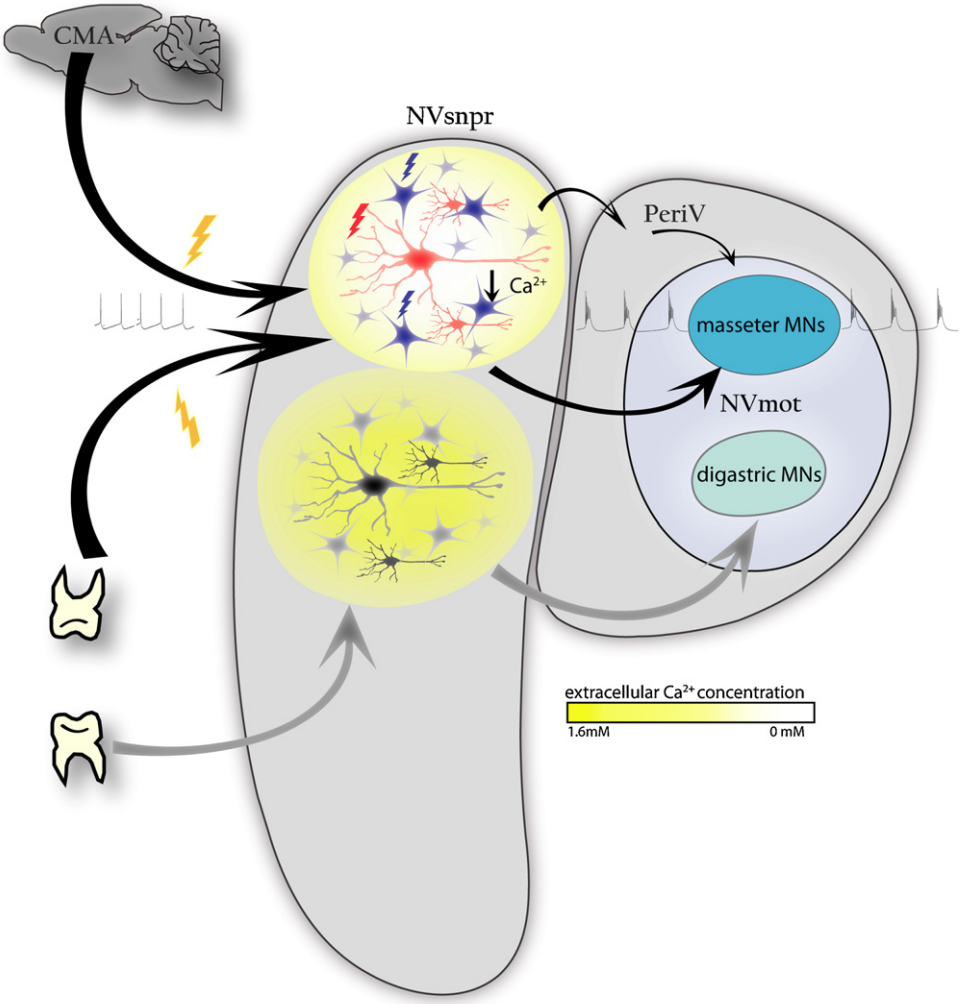

Fig. 5. Model of the masticatory CPG. Populations of neurons in the dorsal half of the NVsnpr would be functionally segregated in domains (yellow circles) defined by the boundaries of astrocytic syncitia. Adjacent neurons (cells in red and black) and astrocytes (cells in blue and grey) within these domains receive roughly the same topographically organized sensory and cortical inputs. In domains receiving weak afferent input (lower circle), I_{NaP} is poorly activated because of insufficient neuronal depolarization, on the one hand, and of insufficient astrocytic activation, on the other. In domains receiving greater inputs or maybe coincident inputs from the cortex and the sensory fibres, a more efficient astrocytic activation would decrease the extracellular Ca^{2+} and favour activation of I_{NaP}. This condition combined with the common incoming input would synchronize the population of neurons encompassed within the astrocytic syncitium and momentarily turn this population into the rhythm generator driving premotoneurons or motoneurons directly. The population driving the rhythm could constantly change depending on cortical inputs and sensory feedback. The bursting pattern and frequency of this population could be adjusted by sensory feedback, since sensory fibres provide depolarizing inputs that would determine the membrane potential of the bursting neurons, until depolarization exceeds I_{NaP} activity range reverting firing to a tonic pattern.

Much of the past 40 years has been devoted at describing the anatomical and functional organization of trigeminal circuits thought to participate in mastication. The earlier studies documented the connectivity and firing patterns of different components of these circuits. Later with development of *in vitro* preparations that facilitated use of intracellular recording techniques, the task of examining the intrinsic properties of these neurons could be tackled. In the masticatory system as in most other CPG system, we are only beginning to integrate the knowledge gained at the cellular and at the network level to achieve more realistic models rather than opposing models based on only cellular properties or connectivity.

Acknowledgements

This work was supported by Grants from the Canadian Institutes of Health Research and an infrastructure grant from the Fonds de la Recherche en Santé du Québec.

References

al-Ghoul, W.M., Miller, M.W., 1993. Orderly migration of neurons to the principal sensory nucleus of the trigeminal nerve of the rat. J. Comp. Neurol. 330, 464–475.

Alzheimer, C., Schwindt, P.C., Crill, W.E., 1993. Postnatal development of a persistent Na^+ current in pyramidal neurons from rat sensorimotor cortex. J. Neurophysiol. 69, 290–292.

Amzica, F., Massimini, M., Manfridi, A., 2002. Spatial buffering during slow and paroxysmal sleep oscillations in cortical networks of glial cells in vivo. J. Neurosci. 22, 1042–1053.

Appenteng, K., Lund, J.P., Seguin, J.J., 1982. Behavior of cutaneous mechanoreceptors recorded in mandibular division of Gasserian ganglion of the rabbit during movements of lower jaw. J. Neurophysiol. 47, 151–166.

Ardran, G.M., Kemp, F.H., Lind, J., 1958. A cineradiographic study of bottle feeding. Br. J. Radiol. 31, 11–22.

Arsenault, D., Zhang, Z.W., 2006. Developmental remodelling of the lemniscal synapse in the ventral basal thalamus of the mouse. J. Physiol. 573, 121–132.

Athanassiadis, T., Westberg, K.G., Olsson, K.A., Kolta, A., 2005. Physiological characterization, localization and synaptic inputs of bursting and nonbursting neurons in the trigeminal principal sensory nucleus of the rat. Eur. J. Neurosci. 22, 3099–3110.

Auld, D.S., Robitaille, R., 2003. Glial cells and neurotransmission: an inclusive view of synaptic function. Neuron 40, 389–400.

Ayer-Le Lievre, C.S., Le Douarin, N.M., 1982. The early development of cranial sensory ganglia and the potentialities of their component cells studied in quail–chick chimeras. Dev. Biol. 94, 291–310.

Azouz, R., Jensen, M.S., Yaari, Y., 1996. Ionic basis of spike after-depolarization and burst generation in adult rat hippocampal CA1 pyramidal cells. J. Physiol. 492 (Pt 1), 211–223.

Ballerini, L., Bracci, E., Nistri, A., 1997. Pharmacological block of the electrogenic sodium pump disrupts rhythmic bursting induced by strychnine and bicuculline in the neonatal rat spinal cord. J. Neurophysiol. 77, 17–23.

Bayev, K.V., Kostyuk, P.G., 1981. Primary afferent depolarization evoked by the activity of spinal scratching generator. Neuroscience 6, 205–215.

Ben-Ari, Y., 2002. Excitatory actions of gaba during development: the nature of the nurture. Nat. Rev. Neurosci. 3, 728–739.

Bennett, K.M., Lemon, R.N., 1996. Corticomotoneuronal contribution to the fractionation of muscle activity during precision grip in the monkey. J. Neurophysiol. 75, 1826–1842.

Bernier, A.P., Arsenault, I., Lund, J.P., Kolta, A., 2010. Effect of the stimulation of sensory inputs on the firing of neurons of the trigeminal main sensory nucleus in the rat. J. Neurophysiol. 103, 915–923.

Bourque, M.J., Kolta, A., 2001. Properties and interconnections of trigeminal interneurons of the lateral pontine reticular formation in the rat. J. Neurophysiol. 86, 2583–2596.

Boyd, I.A., 1954. The histological structure of the receptors in the knee-joint of the cat correlated with their physiological response. J. Physiol. 124, 476–488.

Bremer, F., 1923. Physiologie nerveuse de la mastication chez le chat et le lapin. Arch. Int. Physiol. 21, 308–352.

Brocard, F., Verdier, D., Arsenault, I., Lund, J.P., Kolta, A., 2006. Emergence of intrinsic bursting in trigeminal sensory neurons parallels the acquisition of mastication in weanling rats. J. Neurophysiol. 96, 2410–2424.

Brown, T., 1911. The intrinsic factors in the act of progression in the mammal. Proc. R. Soc. Lond. B Biol. Sci. 84, 308–319.

Brown, T.G., 1914. On the nature of the fundamental activity of the nervous centres: together with an analysis of the conditioning of rhythmic activity in progression, and a theory of the evolution of function in the nervous system. J. Physiol. 48, 18–46.

Buisseret-Delmas, C., Pinganaud, G., Compoint, C., Buisseret, P., 1997. Projection from trigeminal nuclei to neurons of the mesencephalic trigeminal nucleus in rat. Neurosci. Lett. 229, 189–192.

Capra, N.F., Dessem, D., 1992. Central connections of trigeminal primary afferent neurons: topographical and functional considerations. Crit. Rev. Oral Biol. Med. 4, 1–52.

Capra, N.F., Wax, T.D., 1989. Distribution and central projections of primary afferent neurons that innervate the masseter muscle and mandibular periodontium: a double-label study. J. Comp. Neurol. 279, 341–352.

Carpenter, M.B., 1957. The dorsal trigeminal tract in the rhesus monkey. J. Anat. 91, 82–90.

Chang, Z., Haque, T., Iida, C., Seki, S., Sato, F., Kato, T., Uchino, K., Ono, T., Nakamura, M., Bae, Y.C., Yoshida, A., 2009. Distribution of premotoneurons for jaw-closing and jaw-opening motor nucleus receiving contacts from axon terminals of primary somatosensory cortical neurons in rats. Brain Res. 1275, 43–53.

Chen, S., Yue, C., Yaari, Y., 2005. A transitional period of Ca^{2+}-dependent spike afterdepolarization and bursting in developing rat CA1 pyramidal cells. J. Physiol. 567, 79–93.

Chevallier, S., Nagy, F., Cabelguen, J.M., 2006. Cholinergic control of excitability of spinal motoneurones in the salamander. J. Physiol. 570, 525–540.

Colley, J.R., Creamer, B., 1958. Sucking and swallowing in infants. Br. Med. J. 2, 422–423.

Copray, J.C., Liem, R.S., Ter Horst, G.J., van Willigen, J.D., 1990. Dopaminergic afferents to the mesencephalic trigeminal nucleus of the rat: a light and electron microscope immunocytochemistry study. Brain Res. 514, 343–348.

Crill, W.E., 1996. Persistent sodium current in mammalian central neurons. Annu. Rev. Physiol. 58, 349–362.

Cruccu, G., Berardelli, A., Inghilleri, M., Manfredi, M., 1989. Functional organization of the trigeminal motor system in man. A neurophysiological study. Brain 112 (Pt 5), 1333–1350.

Dai, J.X., Hu, Z.L., Shi, M., Guo, C., Ding, Y.Q., 2008. Postnatal ontogeny of the transcription factor Lmx1b in the mouse central nervous system. J. Comp. Neurol. 509, 341–355.

Dal Bo, G., Lund, J.P., Verdier, D., Kolta, A., 2005. Inputs to nucleus pontis caudalis from adjacent trigeminal areas. Eur. J. Neurosci. 22, 1987–1996.

Darbon, P., Tscherter, A., Yvon, C., Streit, J., 2003. Role of the electrogenic Na/K pump in disinhibition-induced bursting in cultured spinal networks. J. Neurophysiol. 90, 3119–3129.

De, S., Nguyen, A.Q., Shuler, C.F., Turman Jr., J.E., 2005. Mesencephalic trigeminal nucleus development is dependent on Krox-20 expression. Dev. Neurosci. 27, 49–58.

Del Negro, C.A., Hayes, J.A., Pace, R.W., Brush, B.R., Teruyama, R., Feldman, J.L., 2010. Synaptically activated burst-generating conductances may underlie a group-pacemaker mechanism for respiratory rhythm generation in mammals. Prog. Brain Res. 187, 111–136.

Del Negro, C.A., Koshiya, N., Butera Jr., R.J., Smith, J.C., 2002. Persistent sodium current, membrane properties and bursting behavior of pre-Botzinger complex inspiratory neurons in vitro. J. Neurophysiol. 88, 2242–2250.

Dellow, P.G., Lund, J.P., 1971. Evidence for central timing of rhythmical mastication. J. Physiol. 215, 1–13.

Devoize, L., Domejean, S., Melin, C., Raboisson, P., Artola, A., Dallel, R., 2010. Organization of projections from the spinal trigeminal subnucleus oralis to the spinal cord in the rat: a neuroanatomical substrate for reciprocal orofacial–cervical interactions. Brain Res. 1343, 75–82.

Ding, Y.Q., Yin, J., Xu, H.M., Jacquin, M.F., Chen, Z.F., 2003. Formation of whisker-related principal sensory nucleus-based lemniscal pathway requires a paired homeodomain transcription factor, Drg11. J. Neurosci. 23, 7246–7254.

Donga, R., Lund, J.P., 1991. Discharge patterns of trigeminal commissural last-order interneurons during fictive mastication in the rabbit. J. Neurophysiol. 66, 1564–1578.

Dubner, R., Sessle, B.J., Storey, A.T., 1978. Jaw, facial, and tongue reflexes. In: The Neural Basis of Oral and Facial Function, Plenum Press, New York, pp. 246–310.

Dubuc, R., Cabelguen, J.M., Rossignol, S., 1985. Rhythmic antidromic discharges of single primary afferents recorded in cut dorsal root filaments during locomotion in the cat. Brain Res. 359, 375–378.

Eisenman, J., Landgren, S., Novin, D., 1963. Functional organization in the main sensory trigeminal nucleus and in the rostral subdivision of the nucleus of the spinal trigeminal tract in the cat. Acta Physiol. Scand. (Suppl.) 214, 1–44.

el Manira, A., Tegner, J., Grillner, S., 1994. Calcium-dependent potassium channels play a critical role for burst termination in the locomotor network in lamprey. J. Neurophysiol. 72, 1852–1861.

Ellerkmann, R.K., Riazanski, V., Elger, C.E., Urban, B.W., Beck, H., 2001. Slow recovery from inactivation regulates the availability of voltage-dependent Na(+) channels in hippocampal granule cells, hilar neurons and basket cells. J. Physiol. 532, 385–397.

Enomoto, A., Kogo, M., Koizumi, H., Ishihama, K., Yamanishi, T., 2002. Localization of premotoneurons for an NMDA-induced repetitive rhythmical activity to TMNs. Neuroreport 13, 2303–2307.

Enomoto, S., Schwartz, G., Lund, J.P., 1987. The effects of cortical ablation on mastication in the rabbit. Neurosci. Lett. 82, 162–166.

Erzurumlu, R.S., Killackey, H.P., 1983. Development of order in the rat trigeminal system. J. Comp. Neurol. 213, 365–380.

Ferrier, D., 1886. The Function of the Brain. G.P. Putnam's Sons, New York.

Fornal, C.A., Metzler, C.W., Marrosu, F., Ribiero-do-Valle, L.E., Jacobs, B.L., 1996. A subgroup of dorsal raphe serotonergic neurons in the cat is strongly activated during oral–buccal movements. Brain Res. 716, 123–133.

Fort, P., Luppi, P.H., Sakai, K., Salvert, D., Jouvet, M., 1990. Nuclei of origin of monoaminergic, peptidergic, and cholinergic afferents to the cat trigeminal motor nucleus: a double-labeling study with cholera-toxin as a retrograde tracer. J. Comp. Neurol. 301, 262–275.
Frankenhaeuser, B., Hodgkin, A.L., 1957. The action of calcium on the electrical properties of squid axons. J. Physiol. 137, 218–244.
Fraser, S., Keynes, R., Lumsden, A., 1990. Segmentation in the chick embryo hindbrain is defined by cell lineage restrictions. Nature 344, 431–435.
Gilardi, P., Schneider-Maunoury, S., Charnay, P., 1991. Krox-20: a candidate gene for the regulation of pattern formation in the hindbrain. Biochimie 73, 85–91.
Gossard, J.P., 1996. Control of transmission in muscle group IA afferents during fictive locomotion in the cat. J. Neurophysiol. 76, 4104–4112.
Gossard, J.P., Cabelguen, J.M., Rossignol, S., 1989. Intra-axonal recordings of cutaneous primary afferents during fictive locomotion in the cat. J. Neurophysiol. 62, 1177–1188.
Gourine, A.V., Kasymov, V., Marina, N., Tang, F., Figueiredo, M.F., Lane, S., Teschemacher, A.G., Spyer, K.M., Deisseroth, K., Kasparov, S., 2010. Astrocytes control breathing through pH-dependent release of ATP. Science 329, 571–575.
Grass, D., Pawlowski, P.G., Hirrlinger, J., Papadopoulos, N., Richter, D.W., Kirchhoff, F., Hulsmann, S., 2004. Diversity of functional astroglial properties in the respiratory network. J. Neurosci. 24, 1358–1365.
Grillner, S., 1981. Control of locomotion in bipeds, tetrapods, and fish. In: Brookhart, M., Mountcastle, V.B. (Eds.), Handbook of Physiology, Section I: The Nervous System, vol. 2. Williams and Wilkins, Baltimore.
Grosche, J., Kettenmann, H., Reichenbach, A., 2002. Bergmann glial cells form distinct morphological structures to interact with cerebellar neurons. J. Neurosci. Res. 68, 138–149.
Grosche, J., Matyash, V., Moller, T., Verkhratsky, A., Reichenbach, A., Kettenmann, H., 1999. Microdomains for neuron–glia interaction: parallel fiber signaling to Bergmann glial cells. Nat. Neurosci. 2, 139–143.
Grzanna, R., Chee, W.K., Akeyson, E.W., 1987. Noradrenergic projections to brainstem nuclei: evidence for differential projections from noradrenergic subgroups. J. Comp. Neurol. 263, 76–91.
Gu, N., Vervaeke, K., Hu, H., Storm, J.F., 2005. Kv7/KCNQ/M and HCN/h, but not KCa2/SK channels, contribute to the somatic medium after-hyperpolarization and excitability control in CA1 hippocampal pyramidal cells. J. Physiol. 566, 689–715.
Guy, N., Chalus, M., Dallel, R., Voisin, D.L., 2005. Both oral and caudal parts of the spinal trigeminal nucleus project to the somatosensory thalamus in the rat. Eur. J. Neurosci. 21, 741–754.
Harris-Warrick, R.M., 2010. General principles of rhythmogenesis in central pattern generator networks. Prog. Brain Res. 187, 213–222.
Hatanaka, N., Tokuno, H., Nambu, A., Inoue, T., Takada, M., 2005. Input–output organization of jaw movement-related areas in monkey frontal cortex. J. Comp. Neurol. 492, 401–425.
Hatanaka, N., Tokuno, H., Nambu, A., Takada, M., 2000. Direct projections from the magnocellular division of the basal nucleus of the amygdala to the principal part of the cortical masticatory area in the macaque monkey. Brain Res. 854, 220–223.
Hayashi, H., Sumino, R., Sessle, B.J., 1984. Functional organization of trigeminal subnucleus interpolaris: nociceptive and innocuous afferent inputs, projections to thalamus, cerebellum, and spinal cord, and descending modulation from periaqueductal gray. J. Neurophysiol. 51, 890–905.
Herring, S.W., 1985. The ontogeny of mammalian mastication. Am. Zool. 25, 339–349.
Hiiemae, K.M., 1967. Masticatory function in the mammals. J. Dent. Res. 46, 883–893.
Hille, B., 2001. Ion Channels of Excitable Membranes. Sinauer Associates, Inc., Sunderland, MA.
Hockfield, S., Gobel, S., 1982. An anatomical demonstration of projections to the medullary dorsal horn (trigeminal nucleus caudalis) from rostral trigeminal nuclei and the contralateral caudal medulla. Brain Res. 252, 203–211.
Huguenard, J.R., Hamill, O.P., Prince, D.A., 1988. Developmental changes in Na^+ conductances in rat neocortical neurons: appearance of a slowly inactivating component. J. Neurophysiol. 59, 778–795.
Huxtable, A.G., Zwicker, J.D., Alvares, T.S., Ruangkittisakul, A., Fang, X., Hahn, L.B., Posse de Chaves, E., Baker, G.B., Ballanyi, K., Funk, G.D., 2010. Glia contribute to the purinergic modulation of inspiratory rhythm-generating networks. J. Neurosci. 30, 3947–3958.
Iida, C., Oka, A., Moritani, M., Kato, T., Haque, T., Sato, F., Nakamura, M., Uchino, K., Seki, S., Bae, Y.C., Takada, K., Yoshida, A., 2010. Corticofugal direct projections to primary afferent neurons in the trigeminal mesencephalic nucleus of rats. Neuroscience 169, 1739–1757.
Inagaki, N., Yamatodani, A., Shinoda, K., Shiotani, Y., Tohyama, M., Watanabe, T., Wada, H., 1987. The histaminergic innervation of the mesencephalic nucleus of the trigeminal nerve in rat brain: a light and electron microscopical study. Brain Res. 418, 388–391.
Inoue, T., Kato, T., Masuda, Y., Nakamura, T., Kawamura, Y., Morimoto, T., 1989. Modifications of masticatory behavior after trigeminal deafferentation in the rabbit. Exp. Brain Res. 74, 579–591.
Inoue, T., Masuda, Y., Nagashima, T., Yoshikawa, K., Morimoto, T., 1992. Properties of rhythmically active reticular neurons around the trigeminal motor nucleus during fictive mastication in the rat. Neurosci. Res. 14, 275–294.
Iriki, A., Nozaki, S., Nakamura, Y., 1988. Feeding behavior in mammals: corticobulbar projection is reorganized during conversion from sucking to chewing. Brain Res. Dev. Brain Res. 44, 189–196.
Irving, C., Mason, I., 2000. Signalling by FGF8 from the isthmus patterns anterior hindbrain and establishes the anterior limit of Hox gene expression. Development 127, 177–186.
Ishihama, K., Kogo, M., Koizumi, H., Nomura, K., Tanaka, S., Yamanishi, T., Enomoto, A., 2003. Oral-motor patterns of rhythmic trigeminal activity generated in fetal rat brainstem in vitro. Brain Res. Dev. Brain Res. 145, 163–166.
Ishihama, K., Turman Jr., J.E., 2006. NR3 protein expression in trigeminal neurons during postnatal development. Brain Res. 1095, 12–16.
Jacquin, M.F., Arends, J.J., Xiang, C., Shapiro, L.A., Ribak, C.E., Chen, Z.F., 2008. In DRG11 knock-out mice, trigeminal cell death is extensive and does not account for failed brainstem patterning. J. Neurosci. 28, 3577–3585.
Jacquin, M.F., Chiaia, N.L., Haring, J.H., Rhoades, R.W., 1990. Intersubnuclear connections within the rat trigeminal brainstem complex. Somatosens. Mot. Res. 7, 399–420.
Jacquin, M.F., Rhoades, R.W., Enfiejian, H.L., Egger, M.D., 1983. Organization and morphology of masticatory neurons in the rat: a retrograde HRP study. J. Comp. Neurol. 218, 239–256.
Jacquin, T.D., Borday, V., Schneider-Maunoury, S., Topilko, P., Ghilini, G., Kato, F., Charnay, P., Champagnat, J., 1996. Reorganization of pontine rhythmogenic neuronal networks in Krox-20 knockout mice. Neuron 17, 747–758.
Jean, A., 1990. Brainstem control of swallowing: localization and organization of the central pattern generator for swallowing. In: Taylor, A. (Ed.), Neurophysiology of the Jaws and Teeth. MacMillan, London, pp. 294–321.
Johansson, A.S., Svensson, K.G., Trulsson, M., 2006. Impaired masticatory behavior in subjects with reduced periodontal tissue support. J. Periodontol. 77, 1491–1497.
Johansson, R.S., Olsson, K.A., 1976. Microelectrode recordings from human oral mechanoreceptors. Brain Res. 118, 307–311.
Johansson, R.S., Trulsson, M., Olsson, K.A., Abbs, J.H., 1988. Mechanoreceptive afferent activity in the infraorbital nerve in man during speech and chewing movements. Exp. Brain Res. 72, 209–214.
Kanaka, C., Ohno, K., Okabe, A., Kuriyama, K., Itoh, T., Fukuda, A., Sato, K., 2001. The differential expression patterns of messenger RNAs encoding K–Cl cotransporters (KCC1,2) and Na–K–2Cl cotransporter (NKCC1) in the rat nervous system. Neuroscience 104, 933–946.
Katakura, N., Jia, L., Nakamura, Y., 1995. NMDA-induced rhythmical activity in XII nerve of isolated CNS from newborn rats. Neuroreport 6, 601–604.
Kiecker, C., Lumsden, A., 2005. Compartments and their boundaries in vertebrate brain development. Nat. Rev. Neurosci. 6, 553–564.
Kogo, M., Funk, G.D., Chandler, S.H., 1996. Rhythmical oral-motor activity recorded in an in vitro brainstem preparation. Somatosens. Mot. Res. 13, 39–48.
Kogo, M., Tanaka, S., Chandler, S.H., Matsuya, T., 1998. Examination of the relationships between jaw opener and closer rhythmical muscle activity in an in vitro brainstem jaw-attached preparation. Somatosens. Mot. Res. 15, 200–210.
Koizumi, H., Ishihama, K., Nomura, K., Yamanishi, T., Kogo, M., Matsuya, T., 2002. Differential discharge patterns of rhythmical activity in trigeminal motoneurons during fictive mastication and respiration in vitro. Brain Res. Bull. 58, 129–133.
Koizumi, H., Smith, J.C., 2008. Persistent Na^+ and K^+-dominated leak currents contribute to respiratory rhythm generation in the pre-Botzinger complex in vitro. J. Neurosci. 28, 1773–1785.
Kolta, A., Morquette, P., Lavoie, R., Arsenault, I., Verdier, D., 2010. Modulation of rhythmogenic properties of trigeminal neurons contributing to the masticatory CPG. Prog. Brain Res. 187, 137–148.
Kolta, A., Westberg, K.G., Lund, J.P., 2000. Identification of brainstem interneurons projecting to the trigeminal motor nucleus and adjacent structures in the rabbit. J. Chem. Neuroanat. 19, 175–195.
Krettek, J.E., Price, J.L., 1978. Amygdaloid projections to subcortical structures within the basal forebrain and brainstem in the rat and cat. J. Comp. Neurol. 178, 225–254.
Kriellaars, D.J., Brownstone, R.M., Noga, B.R., Jordan, L.M., 1994. Mechanical entrainment of fictive locomotion in the decerebrate cat. J. Neurophysiol. 71, 2074–2086.
Kurasawa, I., Hirose, Y., Sunada, T., Nakamura, Y., 1988. Phase-linked modulation of excitability of presynaptic terminals of low-threshold afferent fibers in the inferior alveolar nerve during cortically induced fictive mastication in the guinea pig. Brain Res. 446, 113–120.
Landgren, S., Olsson, K.A., Westberg, K.G., 1986. Bulbar neurones with axonal projections to the trigeminal motor nucleus in the cat. Exp. Brain Res. 65, 98–111.
Langenbach, G.E., Brugman, P., Weijs, W.A., 1992. Preweaning feeding mechanisms in the rabbit. J. Dev. Physiol. 18, 253–261.
Langenbach, G.E., Weijs, W.A., Brugman, P., van Eijden, T.M., 2001. A longitudinal electromyographic study of the postnatal maturation of mastication in the rabbit. Arch. Oral Biol. 46, 811–820.
Lau, C., 2006. Oral feeding in the preterm infant. NeoReviews 7, 19–27.
Lavigne, G., Kim, J.S., Valiquette, C., Lund, J.P., 1987. Evidence that periodontal pressoreceptors provide positive feedback to jaw closing muscles during mastication. J. Neurophysiol. 58, 342–358.
Lazarov, N.E., Usunoff, K.G., Schmitt, O., Itzev, D.E., Rolfs, A., Wree, A., 2011. Amygdalotrigeminal projection in the rat: an anterograde tracing study. Ann. Anat. 193, 118–126.
Li, J., Xiong, K.H., Li, Y.Q., Kaneko, T., Mizuno, N., 2000. Serotonergic innervation of mesencephalic trigeminal nucleus neurons: a light and electron microscopic study in the rat. Neurosci. Res. 37, 127–140.

Li, J.L., Wu, S.X., Tomioka, R., Okamoto, K., Nakamura, K., Kaneko, T., Mizuno, N., 2005. Efferent and afferent connections of GABAergic neurons in the supratrigeminal and the intertrigeminal regions. An immunohistochemical tract-tracing study in the GAD67-GFP knock-in mouse. Neurosci. Res. 51, 81–91.
Li, Z., Hatton, G.I., 1996. Oscillatory bursting of phasically firing rat supraoptic neurones in low-Ca^{2+} medium: Na^+ influx, cytosolic Ca^{2+} and gap junctions. J. Physiol. 496 (Pt 2), 379–394.
Lumsden, A., 1990. The cellular basis of segmentation in the developing hindbrain. Trends Neurosci. 13, 329–335.
Lumsden, A., Keynes, R., 1989. Segmental patterns of neuronal development in the chick hindbrain. Nature 337, 424–428.
Lund, J.P., 1991. Mastication and its control by the brain stem. Crit. Rev. Oral Biol. Med. 2, 33–64.
Lund, J.P., Lamarre, Y., 1974. Activity of neurons in the lower precentral cortex during voluntary and rhythmical jaw movements in the monkey. Exp. Brain Res. 19, 282–299.
Lund, J.P., Sasamoto, K., Murakami, T., Olsson, K.A., 1984. Analysis of rhythmical jaw movements produced by electrical stimulation of motor-sensory cortex of rabbits. J. Neurophysiol. 52, 1014–1029.
Luo, P., Dessem, D., 1996. Morphological evidence for recurrent jaw-muscle spindle afferent feedback within the mesencephalic trigeminal nucleus. Brain Res. 710, 260–264.
Luo, P., Wong, R., Dessem, D., 1995a. Projection of jaw-muscle spindle afferents to the caudal brainstem in rats demonstrated using intracellular biotinamide. J. Comp. Neurol. 358, 63–78.
Luo, P., Wong, R., Dessem, D., 1995b. Ultrastructural basis for synaptic transmission between jaw-muscle spindle afferents and trigeminothalamic neurons in the rostral trigeminal sensory nuclei of the rat. J. Comp. Neurol. 363, 109–128.
Luo, P.F., Wang, B.R., Peng, Z.Z., Li, J.S., 1991. Morphological characteristics and terminating patterns of masseteric neurons of the mesencephalic trigeminal nucleus in the rat: an intracellular horseradish peroxidase labeling study. J. Comp. Neurol. 303, 286–299.
Luthi, A., McCormick, D.A., 1999. Ca(2+)-mediated up-regulation of Ih in the thalamus. How cell-intrinsic ionic currents may shape network activity. Ann. N.Y. Acad. Sci. 868, 765–769.
Maconochie, M.K., Nonchev, S., Manzanares, M., Marshall, H., Krumlauf, R., 2001. Differences in Krox20-dependent regulation of Hoxa2 and Hoxb2 during hindbrain development. Dev. Biol. 233, 468–481.
Marrion, N., 1997. Control of M-current. Annu. Rev. Physiol. 59, 483–504.
Martin, J.H., 2003. Cranial nerves and the trigeminal and viscerosensory systems. In: Neuroanatomy: Text and Atlas, McGraw-Hill, pp. 135–160.
Masuda, Y., Morimoto, T., Hidaka, O., Kato, T., Matsuo, R., Inoue, T., Kobayashi, M., Taylor, A., 1997. Modulation of jaw muscle spindle discharge during mastication in the rabbit. J. Neurophysiol. 77, 2227–2231.
McCrea, D.A., Rybak, I.A., 2008. Organization of mammalian locomotor rhythm and pattern generation. Brain Res. Rev. 57, 134–146.
McDavid, S., Lund, J.P., Auclair, F., Kolta, A., 2006. Morphological and immunohistochemical characterization of interneurons within the rat trigeminal motor nucleus. Neuroscience 139, 1049–1059.
McDavid, S., Verdier, D., Lund, J.P., Kolta, A., 2008. Electrical properties of interneurons found within the trigeminal motor nucleus. Eur. J. Neurosci. 28, 1136–1145.
Meessen, H., Olzewski, J., 1949. Cytoarchitekton-ischer atlas des rautenhirns des kaninchens. Karger, Basel.
Miller, M.W., Muller, S.J., 1989. Structure and histogenesis of the principal sensory nucleus of the trigeminal nerve: effects of prenatal exposure to ethanol. J. Comp. Neurol. 282, 570–580.
Mistry, S., Hamdy, S., 2008. Neural control of feeding and swallowing. Phys. Med. Rehabil. Clin. N. Am. 19, 709–710.
Morimoto, T., Inoue, T., Masuda, Y., Nagashima, T., 1989. Sensory components facilitating jaw-closing muscle activities in the rabbit. Exp. Brain Res. 76, 424–440.
Murray, G.M., Sessle, B.J., 1992. Functional properties of single neurons in the face primary motor cortex of the primate. II. Relations with trained orofacial motor behavior. J. Neurophysiol. 67, 759–774.
Nakamura, S., Inoue, T., Nakajima, K., Moritani, M., Nakayama, K., Tokita, K., Yoshida, A., Maki, K., 2008. Synaptic transmission from the supratrigeminal region to jaw-closing and jaw-opening motoneurons in developing rats. J. Neurophysiol. 100, 1885–1896.
Nakamura, Y., Katakura, N., Nakajima, M., Liu, J., 2004. Rhythm generation for food-ingestive movements. Prog. Brain Res. 143, 97–103.
Nakamura, Y., Kubo, Y., 1978. Masticatory rhythm in intracellular potential of trigeminal motoneurons induced by stimulation of orbital cortex and amygdala in cats. Brain Res. 148, 504–509.
Narayanan, C.H., Fox, M.W., Hamburger, V., 1971. Prenatal development of spontaneous and evoked activity in the rat (*Rattus norvegicus albinus*). Behaviour 40, 100–134.
Nicholls, J.G., Martin, A.R., Wallace, B.G., Fuchs, P.A., 2001. From Neuron to Brain. Sinauer Associates, Inc., Sunderland, MA.
Nicholson, C., ten Bruggencate, G., Stockle, H., Steinberg, R., 1978. Calcium and potassium changes in extracellular microenvironment of cat cerebellar cortex. J. Neurophysiol. 41, 1026–1039.
Nomura, S., Mizuno, N., 1985. Differential distribution of cell bodies and central axons of mesencephalic trigeminal nucleus neurons supplying the jaw-closing muscles and periodontal tissue: a transganglionic tracer study in the cat. Brain Res. 359, 311–319.
Nonchev, S., Maconochie, M., Vesque, C., Aparicio, S., Ariza-McNaughton, L., Manzanares, M., Maruthainar, K., Kuroiwa, A., Brenner, S., Charnay, P., Krumlauf, R., 1996a. The conserved role of Krox-20 in directing Hox gene expression during vertebrate hindbrain segmentation. Proc. Natl. Acad. Sci. U.S.A. 93, 9339–9345.
Nonchev, S., Vesque, C., Maconochie, M., Seitanidou, T., Ariza-McNaughton, L., Frain, M., Marshall, H., Sham, M.H., Krumlauf, R., Charnay, P., 1996b. Segmental expression of Hoxa-2 in the hindbrain is directly regulated by Krox-20. Development 122, 543–554.
Nordstrom, M.A., 2007. Insights into the bilateral cortical control of human masticatory muscles revealed by transcranial magnetic stimulation. Arch. Oral Biol. 52, 338–342.
Olsson, K.A., Landgren, S., Westberg, K.G., 1986. Location of, and peripheral convergence on, the interneuron in the disynaptic path from the coronal gyrus of the cerebral cortex to the trigeminal motoneurons in the cat. Exp. Brain Res. 65, 83–97.
Onimaru, H., Arata, A., Homma, I., 1997. Neuronal mechanisms of respiratory rhythm generation: an approach using in vitro preparation. Jpn. J. Physiol. 47, 385–403.
Oury, F., Murakami, Y., Renaud, J.S., Pasqualetti, M., Charnay, P., Ren, S.Y., Rijli, F.M., 2006. Hoxa2- and rhombomere-dependent development of the mouse facial somatosensory map. Science 313, 1408–1413.
Pace, R.W., Mackay, D.D., Feldman, J.L., Del Negro, C.A., 2007. Inspiratory bursts in the preBotzinger complex depend on a calcium-activated non-specific cation current linked to glutamate receptors in neonatal mice. J. Physiol. 582, 113–125.
Paik, S.K., Kwak, M.K., Ahn, D.K., Kim, Y.K., Kim, D.S., Moon, C., Moritani, M., Yoshida, A., Bae, Y.C., 2005. Ultrastructure of jaw muscle spindle afferents within the rat trigeminal mesencephalic nucleus. Neuroreport 16, 1561–1564.
Park, S.J., Chiang, C.Y., Hu, J.W., Sessle, B.J., 2001. Neuroplasticity induced by tooth pulp stimulation in trigeminal subnucleus oralis involves NMDA receptor mechanisms. J. Neurophysiol. 85, 1836–1846.
Paxinos, G., Watson, C., 2004. The Rat Brain in Stereotaxic Coordinates. Elsevier.
Pedroarena, C.M., Pose, I.E., Yamuy, J., Chase, M.H., Morales, F.R., 1999. Oscillatory membrane potential activity in the soma of a primary afferent neuron. J. Neurophysiol. 82, 1465–1476.
Perret, C., Cabelguen, J.M., 1980. Main characteristics of the hindlimb locomotor cycle in the decorticate cat with special reference to bifunctional muscles. Brain Res. 187, 333–352.
Pierce, E.T., 1973. Time of origin of neurons in the brain stem of the mouse. Prog. Brain Res. 40, 53–65.
Qian, Y., Shirasawa, S., Chen, C.L., Cheng, L., Ma, Q., 2002. Proper development of relay somatic sensory neurons and D2/D4 interneurons requires homeobox genes Rnx/Tlx-3 and Tlx-1. Genes Dev. 16, 1220–1233.
Ramirez, L.M., Ballesteros, L.E., Sandoval, G.P., 2007. Tensor tympani muscle: strange chewing muscle. Med. Oral Patol. Oral Cir. Bucal. 12, E96–E100.
Richter, D.W., Champagnat, J., Jacquin, T., Benacka, R., 1993. Calcium currents and calcium-dependent potassium currents in mammalian medullary respiratory neurones. J. Physiol. 470, 23–33.
Ritcher, D.W., Champagnat, J., Mifflin, S., 1986. Membrane properties involved in respiratory rhythm generation. In: Von Euler, C., Lagercrantz, H. (Eds.), Neurobiology of the Control of Breathing. Raven Press, New York, pp. 141–147.
Rivera, C., Voipio, J., Payne, J.A., Ruusuvuori, E., Lahtinen, H., Lamsa, K., Pirvola, U., Saarma, M., Kaila, K., 1999. The K^+/Cl^- co-transporter KCC2 renders GABA hyperpolarizing during neuronal maturation. Nature 397, 251–255.
Rokx, J.T., Juch, P.J., van Willigen, J.D., 1986. Arrangement and connections of mesencephalic trigeminal neurons in the rat. Acta Anat. (Basel) 127, 7–15.
Rossignol, S., Lund, J.P., Drew, T., 1988. The role of sensory inputs in regulating patterns of rhythmical movements in higher vertebrates. A comparison between locomotion, respiration, and mastication. In: Cohen, A., Rossignol, S., Grillner, S. (Eds.), Neural Control of Rhythmic Movements in Vertebrates. John Wiley & Sons, New York, pp. 201–283.
Rubin, J.E., Hayes, J.A., Mendenhall, J.L., Del Negro, C.A., 2009. Calcium-activated nonspecific cation current and synaptic depression promote network-dependent burst oscillations. Proc. Natl. Acad. Sci. U.S.A. 106, 2939–2944.
Rusakov, D.A., Fine, A., 2003. Extracellular Ca^{2+} depletion contributes to fast activity-dependent modulation of synaptic transmission in the brain. Neuron 37, 287–297.
Salpeter, M., 1987. Vertebrate neuromuscular junctions: morphology, molecular organization, and functional consequences. In: Salpeter, M. (Ed.), The Vertebrate Neuromuscular Junction. Alan R. Liss. Inc., New York, pp. 1–54.
Sandler, V.M., Puil, E., Schwarz, D.W., 1998. Intrinsic response properties of bursting neurons in the nucleus principalis trigemini of the gerbil. Neuroscience 83, 891–904.
Schneider-Maunoury, S., Topilko, P., Seitandou, T., Levi, G., Cohen-Tannoudji, M., Pournin, S., Babinet, C., Charnay, P., 1993. Disruption of Krox-20 results in alteration of rhombomeres 3 and 5 in the developing hindbrain. Cell 75, 1199–1214.
Sessle, B.J., 2006. Mechanisms of oral somatosensory and motor functions and their clinical correlates. J. Oral Rehabil. 33, 243–261.
Sessle, B.J., Yao, D., Nishiura, H., Yoshino, K., Lee, J.C., Martin, R.E., Murray, G.M., 2005. Properties and plasticity of the primate somatosensory and motor cortex related to orofacial sensorimotor function. Clin. Exp. Pharmacol. Physiol. 32, 109–114.
Shigenaga, Y., Doe, K., Suemune, S., Mitsuhiro, Y., Tsuru, K., Otani, K., Shirana, Y., Hosoi, M., Yoshida, A., Kagawa, K., 1989a. Physiological and morphological characteristics of periodontal mesencephalic trigeminal neurons in the cat—intra-axonal staining with HRP. Brain Res. 505, 91–110.

Shigenaga, Y., Nishimura, M., Suemune, S., Nishimori, T., Doe, K., Tsuru, H., 1989b. Somatotopic organization of tooth pulp primary afferent neurons in the cat. Brain Res. 477, 66–89.
Shigenaga, Y., Okamoto, T., Nishimori, T., Suemune, S., Nasution, I.D., Chen, I.C., Tsuru, K., Yoshida, A., Tabuchi, K., Hosoi, M., 1986a. Oral and facial representation in the trigeminal principal and rostral spinal nuclei of the cat. J. Comp. Neurol. 244, 1–18.
Shigenaga, Y., Sera, M., Nishimori, T., Suemune, S., Nishimura, M., Yoshida, A., Tsuru, K., 1988. The central projection of masticatory afferent fibers to the trigeminal sensory nuclear complex and upper cervical spinal cord. J. Comp. Neurol. 268, 489–507.
Shigenaga, Y., Suemune, S., Nishimura, M., Nishimori, T., Sato, H., Ishidori, H., Yoshida, A., Tsuru, K., Tsuiki, Y., Dateoka, Y., et al., 1986b. Topographic representation of lower and upper teeth within the trigeminal sensory nuclei of adult cat as demonstrated by the transganglionic transport of horseradish peroxidase. J. Comp. Neurol. 251, 299–316.
Skoglund, S., 1956. Anatomical and physiological studies of knee joint innervation in the cat. Acta Physiol. Scand. Suppl. 36, 1–101.
Smith, J.C., Butera, R.J., Koshiya, N., Del Negro, C., Wilson, C.G., Johnson, S.M., 2000. Respiratory rhythm generation in neonatal and adult mammals: the hybrid pacemaker-network model. Respir. Physiol. 122, 131–147.
Somjen, G.G., 1980. Stimulus-evoked and seizure-related responses of extracellular calcium activity in spinal cord compared to those in cerebral cortex. J. Neurophysiol. 44, 617–632.
Stainier, D.Y., Gilbert, W., 1990. Pioneer neurons in the mouse trigeminal sensory system. Proc. Natl. Acad. Sci. U.S.A. 87, 923–927.
Su, H., Alroy, G., Kirson, E.D., Yaari, Y., 2001. Extracellular calcium modulates persistent sodium current-dependent burst-firing in hippocampal pyramidal neurons. J. Neurosci. 21, 4173–4182.
Takahashi, T., Shirasu, M., Shirasu, M., Kubo, K.Y., Onozuka, M., Sato, S., Itoh, K., Nakamura, H., 2010. The locus coeruleus projects to the mesencephalic trigeminal nucleus in rats. Neurosci. Res. 68, 103–106.
Takeuchi, Y., Satoda, T., Matsushima, R., 1988. Amygdaloid projections to commissural interneurons for masticatory motoneurons. Brain Res. Bull. 21, 123–127.
Tanaka, S., Kogo, M., Chandler, S.H., Matsuya, T., 1999. Localization of oral-motor rhythmogenic circuits in the isolated rat brainstem preparation. Brain Res. 821, 190–199.
Tazerart, S., Viemari, J.C., Darbon, P., Vinay, L., Brocard, F., 2007. Contribution of persistent sodium current to locomotor pattern generation in neonatal rats. J. Neurophysiol. 98, 613–628.
Tazerart, S., Vinay, L., Brocard, F., 2008. The persistent sodium current generates pacemaker activities in the central pattern generator for locomotion and regulates the locomotor rhythm. J. Neurosci. 28, 8577–8589.
Teaford, M.F., Walker, A., 1983. Dental microwear in adult and still-born guinea pigs (*Cavia porcellus*). Arch. Oral Biol. 28, 1077–1081.
Trulsson, M., 2007. Force encoding by human periodontal mechanoreceptors during mastication. Arch. Oral Biol. 52, 357–360.
Trulsson, M., Johansson, R.S., 1994. Encoding of amplitude and rate of forces applied to the teeth by human periodontal mechanoreceptive afferents. J. Neurophysiol. 72, 1734–1744.
Trulsson, M., Johansson, R.S., 2002. Orofacial mechanoreceptors in humans: encoding characteristics and responses during natural orofacial behaviors. Behav. Brain Res. 135, 27–33.
Tsuboi, A., Kolta, A., Chen, C.C., Lund, J.P., 2003. Neurons of the trigeminal main sensory nucleus participate in the generation of rhythmic motor patterns. Eur. J. Neurosci. 17, 229–238.
Tsuboi, A., Takafuji, Y., Itoh, S., Nagata, K., Tabata, T., Watanabe, M., 2009. Response properties of trigeminal ganglion mechanosensitive neurons innervating the temporomandibular joint of the rabbit. Exp. Brain Res. 199, 107–116.
Turman Jr., J.E., 2007. The development of mastication in rodents: from neurons to behaviors. Arch. Oral Biol. 52, 313–316.
Urbani, A., Belluzzi, O., 2000. Riluzole inhibits the persistent sodium current in mammalian CNS neurons. Eur. J. Neurosci. 12, 3567–3574.
Verdier, D., Lund, J.P., Kolta, A., 2003. GABAergic control of action potential propagation along axonal branches of mammalian sensory neurons. J. Neurosci. 23, 2002–2007.
Verdier, D., Lund, J.P., Kolta, A., 2004. Synaptic inputs to trigeminal primary afferent neurons cause firing and modulate intrinsic oscillatory activity. J. Neurophysiol. 92, 2444–2455.
Voiculescu, O., Taillebourg, E., Pujades, C., Kress, C., Buart, S., Charnay, P., Schneider-Maunoury, S., 2001. Hindbrain patterning: Krox20 couples segmentation and specification of regional identity. Development 128, 4967–4978.
Volterra, A., Meldolesi, J., 2005. Astrocytes, from brain glue to communication elements: the revolution continues. Nat. Rev. Neurosci. 6, 626–640.
Vornov, J.J., Sutin, J., 1983. Brainstem projections to the normal and noradrenergically hyperinnervated trigeminal motor nucleus. J. Comp. Neurol. 214, 198–208.
Wang, C.Z., Shi, M., Yang, L.L., Yang, R.Q., Luo, Z.G., Jacquin, M.F., Chen, Z.F., Ding, Y.Q., 2007. Development of the mesencephalic trigeminal nucleus requires a paired homeodomain transcription factor, Drg11. Mol. Cell. Neurosci. 35, 368–376.
Wang, N., May, P.J., 2008. Peripheral muscle targets and central projections of the mesencephalic trigeminal nucleus in macaque monkeys. Anat. Rec. (Hoboken.) 291, 974–987.
Westberg, K., Clavelou, P., Sandstrom, G., Lund, J.P., 1998. Evidence that trigeminal brainstem interneurons form subpopulations to produce different forms of mastication in the rabbit. J. Neurosci. 18, 6466–6479.
Westberg, K.G., Kolta, A., Clavelou, P., Sandstrom, G., Lund, J.P., 2000. Evidence for functional compartmentalization of trigeminal muscle spindle afferents during fictive mastication in the rabbit. Eur. J. Neurosci. 12, 1145–1154.
Westberg, K.G., Olsson, K.A., 1991. Integration in trigeminal premotor interneurones in the cat. 1. Functional characteristics of neurones in the subnucleus-gamma of the oral nucleus of the spinal trigeminal tract. Exp. Brain Res. 84, 102–114.
Westberg, K.G., Scott, G., Olsson, K.A., Lund, J.P., 2001. Discharge patterns of neurons in the medial pontobulbar reticular formation during fictive mastication in the rabbit. Eur. J. Neurosci. 14, 1709–1718.
Westneat, M.W., Hall, W.G., 1992. Ontogeny of feeding motor patterns in infant rats: an electromyographic analysis of suckling and chewing. Behav. Neurosci. 106, 539–554.
Widmalm, S.E., Lillie, J.H., Ash Jr., M.M., 1988. Anatomical and electromyographic studies of the digastric muscle. J. Oral Rehabil. 15, 3–21.
Widmer, C.G., Morris-Wiman, J.A., Calhoun, J.C., 1998. Development of trigeminal mesencephalic and motor nuclei in relation to masseter muscle innervation in mice. Brain Res. Dev. Brain Res. 108, 1–11.
Williams, M.N., Zahm, D.S., Jacquin, M.F., 1994. Differential foci and synaptic organization of the principal and spinal trigeminal projections to the thalamus in the rat. Eur. J. Neurosci. 6, 429–453.
Wu, N., Enomoto, A., Tanaka, S., Hsiao, C.F., Nykamp, D.Q., Izhikevich, E., Chandler, S.H., 2005. Persistent sodium currents in mesencephalic v neurons participate in burst generation and control of membrane excitability. J. Neurophysiol. 93, 2710–2722.
Wu, N., Hsiao, C.F., Chandler, S.H., 2001. Membrane resonance and subthreshold membrane oscillations in mesencephalic V neurons: participants in burst generation. J. Neurosci. 21, 3729–3739.
Xiang, C., Zhang, K.H., Yin, J., Arends, J.J., Erzurumlu, R.S., Jacquin, M.F., Chen, Z.F., 2010. The transcription factor, Lmx1b, is necessary for the development of the principal trigeminal nucleus-based lemniscal pathway. Mol. Cell. Neurosci. 44, 394–403.
Yamamoto, T., Matsuo, R., Kiyomitsu, Y., Kitamura, R., 1989. Sensory and motor responses of trigeminal and reticular neurons during ingestive behavior in rats. Exp. Brain Res. 76, 386–400.
Yamamura, K., Narita, N., Yao, D., Martin, R.E., Masuda, Y., Sessle, B.J., 2002. Effects of reversible bilateral inactivation of face primary motor cortex on mastication and swallowing. Brain Res. 944, 40–55.
Yasui, Y., Itoh, K., Mitani, A., Takada, M., Mizuno, N., 1985. Cerebral cortical projections to the reticular regions around the trigeminal motor nucleus in the cat. J. Comp. Neurol. 241, 348–356.
Yatim, N., Billig, I., Compoint, C., Buisseret, P., Buisseret-Delmas, C., 1996. Trigeminocerebellar and trigemino-olivary projections in rats. Neurosci. Res. 25, 267–283.
Yokomizo, Y., Murai, Y., Tanaka, E., Inokuchi, H., Kusukawa, J., Higashi, H., 2005. Excitatory GABAergic synaptic potentials in the mesencephalic trigeminal nucleus of adult rat in vitro. Neurosci. Res. 51, 463–474.
Yoshida, A., Hiraga, T., Moritani, M., Chen, K., Takatsuki, Y., Hirose, Y., Bae, Y.C., Shigenaga, Y., 1998. Morphologic characteristics of physiologically defined neurons in the cat trigeminal nucleus principalis. J. Comp. Neurol. 401, 308–328.
Yoshida, A., Taki, I., Chang, Z., Iida, C., Haque, T., Tomita, A., Seki, S., Yamamoto, S., Masuda, Y., Moritani, M., Shigenaga, Y., 2009. Corticofugal projections to trigeminal motoneurons innervating antagonistic jaw muscles in rats as demonstrated by anterograde and retrograde tract tracing. J. Comp. Neurol. 514, 368–386.
Yoshida, A., Yasuda, K., Dostrovsky, J.O., Bae, Y.C., Takemura, M., Shigenaga, Y., Sessle, B.J., 1994. Two major types of premotoneurons in the feline trigeminal nucleus oralis as demonstrated by intracellular staining with horseradish peroxidase. J. Comp. Neurol. 347, 495–514.
Yoshida, M., Precht, W., 1971. Monosynaptic inhibition of neurons of the substantia nigra by caudato-nigral fibers. Brain Res. 32, 225–228.
Yue, C., Yaari, Y., 2004. KCNQ/M channels control spike afterdepolarization and burst generation in hippocampal neurons. J. Neurosci. 24, 4614–4624.
Zhang, B., Wootton, J.F., Harris-Warrick, R.M., 1995. Calcium-dependent plateau potentials in a crab stomatogastric ganglion motor neuron. II. Calcium-activated slow inward current. J. Neurophysiol. 74, 1938–1946.
Zhang, J., Luo, P., Pendlebury, W.W., 2001. Light and electron microscopic observations of a direct projection from mesencephalic trigeminal nucleus neurons to hypoglossal motoneurons in the rat. Brain Res. 917, 67–80.
Zhang, J., Yang, R., Pendlebery, W., Luo, P., 2005. Monosynaptic circuitry of trigeminal proprioceptive afferents coordinating jaw movement with visceral and laryngeal activities in rats. Neuroscience 135, 497–505.
Zhang, J.D., 1998. Projections from dorsomedial part of the subnucleus oralis to the mesencephalic trigeminal neurons innervating the masseter muscle—a PHA-L and HRP double labeling study in the rat. J. Hirnforsch. 39, 55–64.
Zhong, G., Masino, M.A., Harris-Warrick, R.M., 2007. Persistent sodium currents participate in fictive locomotion generation in neonatal mouse spinal cord. J. Neurosci. 27, 4507–4518.

PHYSIOLOGY 30: 371–388, 2015; doi:10.1152/physiol.00023.2014

Ion Homeostasis in Rhythmogenesis: The Interplay Between Neurons and Astroglia

Aklesso Kadala,[1] Dorly Verdier,[1] Philippe Morquette,[1] and Arlette Kolta[1,2]

[1]*Département de Neurosciences and Groupe de Recherche sur le Système Nerveux Central, Université de Montréal, Montréal, Québec, Canada; and* [2]*Faculté de Médecine Dentaire and Réseau de Recherche en Santé Bucco-dentaire et Osseuse du Fonds de Recherche Québec-Santé, Université de Montréal, Montréal, Québec, Canada*

Proper function of all excitable cells depends on ion homeostasis. Nowhere is this more critical than in the brain where the extracellular concentration of some ions determines neurons' firing pattern and ability to encode information. Several neuronal functions depend on the ability of neurons to change their firing pattern to a rhythmic bursting pattern, whereas, in some circuits, rhythmic firing is, on the contrary, associated to pathologies like epilepsy or Parkinson's disease. In this review, we focus on the four main ions known to fluctuate during rhythmic firing: calcium, potassium, sodium, and chloride. We discuss the synergistic interactions between these elements to promote an oscillatory activity. We also review evidence supporting an important role for astrocytes in the homeostasis of each of these ions and describe mechanisms by which astrocytes may regulate neuronal firing by altering their extracellular concentrations. A particular emphasis is put on the mechanisms underlying rhythmogenesis in the circuit forming the central pattern generator (CPG) for mastication and other CPG systems. Finally, we discuss how an impairment in the ability of glial cells to maintain such homeostasis may result in pathologies like epilepsy and Parkinson's disease.

Proper neuronal function depends critically on the ability of neurons to encode information by changing their firing pattern. Whether a neuron unfailingly transmits spike trains or generates an oscillatory burst firing in response to a given incoming input will bestow different encodings to the conveyed information and result in totally distinct output signals that have different functional incidence. In several brain areas, neurons have been shown to display a function-related dual mode of firing, alternating between a single spike firing mode and a rhythmic burst pattern (67, 92, 98, 111, 139). The role and necessity of such rhythmic neuronal discharges is obvious for some functions such as repetitive movements like mastication, locomotion, or breathing. Indeed, for rhythmic movements to occur, repetitive motor output commands are required to produce the appropriate rhythmic contractions of the skeletal muscles involved in their execution. This implies a need for coordinated discharges by the central pattern generators (CPGs) to initiate and maintain the rhythmic output of motoneurons. Nevertheless, rhythmic activities are also observed in several areas of the brain where their function is not clearly related to a rhythmic behavior but rather to functions such as the binding of sensory features in perception (51, 93), cognitive processing (91), information transfer between brain areas (131), learning and memory (138), sleep and consciousness (38), or motor coordination (79, 84). In fact, neuronal oscillatory activity appears to be an ubiquitous phenomenon in the brain, with wide-ranging functions that occur along with normal brain processing (for review, see Ref. 159).

The mechanisms underlying the transition from single spike firing to rhythmic bursting are not fully understood yet. However, considering the critical importance of ion homeostasis for an optimal neural function, an obvious way to impact on the neuronal firing properties would be to modulate the ionic concentration in the extracellular compartment. Indeed, in several studies where the ions concentrations were measured directly in the tissue, variations in extracellular ion concentrations occurred before or simultaneously with rhythmic neuronal discharges (3, 4, 19). Moreover, artificially decreasing the concentration of extracellular calcium triggers rhythmic firing in masticatory and locomotor central pattern generator neurons (20, 149).

Astrocytes have been shown to modulate neuronal activity by a variety of mechanisms, but one of their most well established functions is to maintain ion homeostasis. Moreover, astrocytes are well positioned in terms of their structural organization relative to neurons to monitor the extracellular space content. Thus here we review the evidence suggesting that astrocytes may play a determinant role in setting the firing mode of adjacent neurons through regulation of the extracellular ionic concentrations.

In the upcoming sections, we will discuss how the concentration of different ion species evolves during rhythmic oscillations. This review will put a special emphasis on potassium and calcium, which are the most considered ions in studies interested in the generation and maintenance of rhythmic oscillations. Evidence supporting a role for glial cells in the generation of rhythmic firing in both healthy and pathological conditions will also be discussed.

Rhythmic Oscillations

Rhythmogenesis

Rhythmogenesis is the cellular process by which a rhythmic mode of firing or burst is generated at the cellular level. For the sake of clarity, we define bursts as recurrent clusters of action potentials occurring at short interspike intervals overriding a plateau-like depolarization and separated by relatively short periods of repolarization (see FIGURE 1A). Consequently, the main characteristic of the bursting pattern is its marked periodicity by contrast to the tonic spiking mode, which consists in the firing of single action potentials that may be occasional or repetitive but lack the apparent recurrent on/off phasic features and often occur at lower frequencies than the firing overriding the plateaus that compose the bursts. Rhythmic clustering of neuronal discharge is sometimes also named neural oscillations and, under this terminology, refers as well to the oscillatory activity of individual neurons or to the large-scale brain oscillations that result from recurrent activity in groups of neurons. These large-scale brain oscillations can be detected locally with field potential recordings or measured outside the scalp by electroencephalograms (EEGs) and are more evocative of the state or degree of firing synchronicity in and between groups of neurons throughout the brain. This supposes that these oscillations, in some situations, may arise from a window of specific spatio-temporal configurations of the spiking activity of individual neurons within a group without an absolute requirement for rhythmic bursting in activity of single cells. Nevertheless, numerous studies have established irrefutable links between the large-scale brain oscillations and membrane potential fluctuations or rhythmic clustering of action potentials firing in individual neurons (78, 144). This suggests that, in many cases, these large-scale brain oscillations may depend on the generation of a rhythmic firing pattern at the cellular level. In fact, it has been postulated that bursting neurons might serve as pacemaker in network oscillations (29). Consequently, in this review, we will discuss and use the term rhythmogenesis to refer both to the generation of rhythmic patterns of action potentials at the cellular level and to the generation of the large-scale brain oscillations.

Ionic Basis of Rhythmogenesis

The precise mechanisms leading to rhythmogenesis vary from one network to another and depend on an intricate interplay between synaptic and intrinsic properties in neuron populations. Many theories have been proposed to explain the generation of oscillatory activity, including synaptic interactions and feedback connections within and between neuronal populations and their contribution to different known frequency bands (159). However, in this review, we will focus on intrinsic neuronal properties that rely on ionic conductances to generate rhythmic firing.

Some of these conductances constitute the driving forces that initiate the burst firing, whereas others determine the plateau duration and bursting frequency or are part of the regenerative feature that characterizes this mode of firing (57). The persistent sodium current (I_{NaP}) is one of the most common currents that drives bursting. Unlike the transient sodium current, which appears at membrane potentials close to −50 mV (21), I_{NaP} becomes apparent at membrane potentials between −65 and −50 mV, and peaks at membrane potentials between −40 and −35 mV, depending on the structure considered (21, 28, 100, 152). Some of the persistent current originates from the same pool of channels as the transient sodium current but with different gating modes (2), and in some other cases, as in the cerebellar Purkinje cells (156), it results from distinctive pools of channels. The massive entry of sodium ions into the cells causing the persistent sodium current supports depolarizing plateaus that are crucial for rhythmic bursting in some neurons. Evidence supporting a role for I_{NaP} in the generation of bursts came from computational simulations (68, 132) and experimental recordings from the pre-Bötzinger complex (PBC) (36, 37), the main sensory nucleus of the trigeminal nerve (20, 152), the spinal cord (149), the cortex (23, 54, 110), or the hippocampus (72, 146). In these experiments, blockade of I_{NaP} prevented burst firing. I_{NaP} also contributes to large-scale oscillations like those

in the rat's visual cortex, where its blockade significantly reduces the frequency of fast gamma oscillations (113).

Other drivers of burst firing include the low-threshold voltage-activated calcium channels (LVA) and the calcium-activated non-selective cationic channels (driving I_{CAN}). The LVA calcium channels are found in a wide range of cell types, including neurons and muscle fibers, and are generally activated by small voltage changes (6, 12) near the resting potentials of the membrane they are embedded in. The LVA calcium channels (mainly formed by the CaV3 family) mediate the T-current (I_T) responsible for the low-threshold calcium spikes responsible for burst firing and low-frequency oscillations in the thalamus and the cerebellum (for review, see Refs. 66, 120). At rest, the LVA calcium channels are in an inactivated state and require membrane hyperpolarization to be de-inactivated, allowing their subsequent activation upon membrane depolarization. Activation of the LVA calcium channels by a subsequent depolarization causes a massive entry of calcium ions into the cell that generates sufficient depolarization to reach threshold and drive a train of Na^+-dependent action potentials. Whole-cell and extracellular recordings in the thalamus of mice knocked out for CaV3.2 and CaV3.3 clearly show the role that these channels play in regard to rhythmic bursting activity. In these experiments, periodic bursts were absent or significantly reduced in thalamic neurons for CaV3.3 KO mice (7), and simultaneously reduced and increased in the reticular and ventroposterior thalamic neurons, respectively, for mice devoid of CaV3.2 (88). The tonic discharges were unchanged (7). CaV1.3 calcium channels, members of the CaV1 family, could also contribute to burst firing. These channels, which are part of the L-type calcium channels, have been classified as high-voltage-activated (HVA) calcium channels, although they display, in reality, a very low voltage of activation (around −55 mV) (162). They are mostly known to contribute to pacemaking in cardiac atrial tissue and adrenal chromaffin cells but may also play a role in neuronal bursting activity (89, 122).

The channels driving I_{CAN} are activated by the mobilization of intracellular calcium. These channels are seemingly part of the transient receptor potential (TRPM) family, which includes TRPM4 and TRPM5. They are mainly permeable to potassium and sodium but very little to calcium (83, 154). I_{CAN} is responsible for prolonged plateaus (10, 164) seen during rhythmic bursting in several types of cells, although they have no inherent voltage dependency. The contribution of these channels to bursting was confirmed with mathematical models (130), and in many experimental preparations including the reticular thalamic neurons in the guinea-pig (10), the hypothalamic magnocellular neurosecretory cells in the rat (50), the motoneurons of the crab cardiac ganglion (123), the motoneurons of the crab stomatogastric ganglion (164), the main sensory nucleus of the trigeminal nerve (152), and a subset of respiratory neurons in the PBC (116, 119) in which rhythmic firing is abolished by a blocker of I_{CAN} (flufenamic acid) but not by a blocker of I_{NaP} (riluzole) (37, 119). Similar results were reported from investigations in dopaminergic neurons of mice substantia nigra pars compacta (102).

Different types of potassium currents also contribute to bursting activities, mostly by affecting the plateau duration and the bursting frequency. A Na^+-activated potassium current [$I_{K(Na)}$] contributes to the generation of the afterhyperpolarization potential and the maintenance of rhythmic bursts in rat neocortical neurons (48). It was also suggested that Ca^{2+}-dependent potassium currents [$I_{K(Ca)}$] and a muscarine-inhibited M current (I_M) mediated by activation of the Kv7 channels may modulate the firing frequency and contribute to the burst termination in lamprey's spinal cord neurons and rat CA1 pyramidal cells (44, 53). Blocking or opening the small-conductance potassium channels (SK) with apamin or 1-ethyl-2-benzimidazolinone (1-EBIO), respectively, resulted in modulation of the bursting activity in the dopaminergic neurons of the substantia nigra of rats (71).

Finally, other currents, carried by mixed ionic charges, are sometimes at play and contribute mostly to the regenerative feature of this firing mode. As an example, the electrogenic sodium/potassium pump (Na^+-K^+-ATPase) may hyperpolarize neurons and lead to activation of I_h, a cationic current activated by hyperpolarization, which may provide the depolarizing rebound required to reactivate the driving forces for the next burst of action potentials (32). I_h is often revealed by the occurrence of a depolarizing sag in response to increasing hyperpolarization. This current, carried by sodium and potassium ions, has been associated to pacemaker properties in a number of neurons (for examples and review, see Refs. 27, 90, 126).

Sequence of Events Leading to Bursts

How these various conductances interact to promote rhythmogenesis may differ from one area of the brain to another, or even within one brain structure from neuron to neuron. Even at the single-cell level, subcellular localization of different ionic channels in different cell compartments may lead to plural bursts driving modes, as it has been proposed in Purkinje cells that showed two kinds of burst firings with distinctive waveforms; a

somatically generated burst firing driven by activation of sodium persistent channels present on the soma and a dendritically generated burst firing driven by activation of LVC channels that could be found on the dendrites (47).

However, the generation of bursts presents a common sequential scheme that requires *1*) a depolarizing current to produce the plateau potential, *2*) the intervention of a repolarizing process to terminate the burst, and *3*) the need for a depolarizing rebound to reactivate the driving force for the next burst (see FIGURE 1A).

Many models have been proposed to summarize the interplay of conductances leading to the generation of a bursting activity in neurons, and this interplay is merely dependent on the set of channels that are comprised in the cell membrane. In masticatory, respiratory, and locomotor CPGs, the

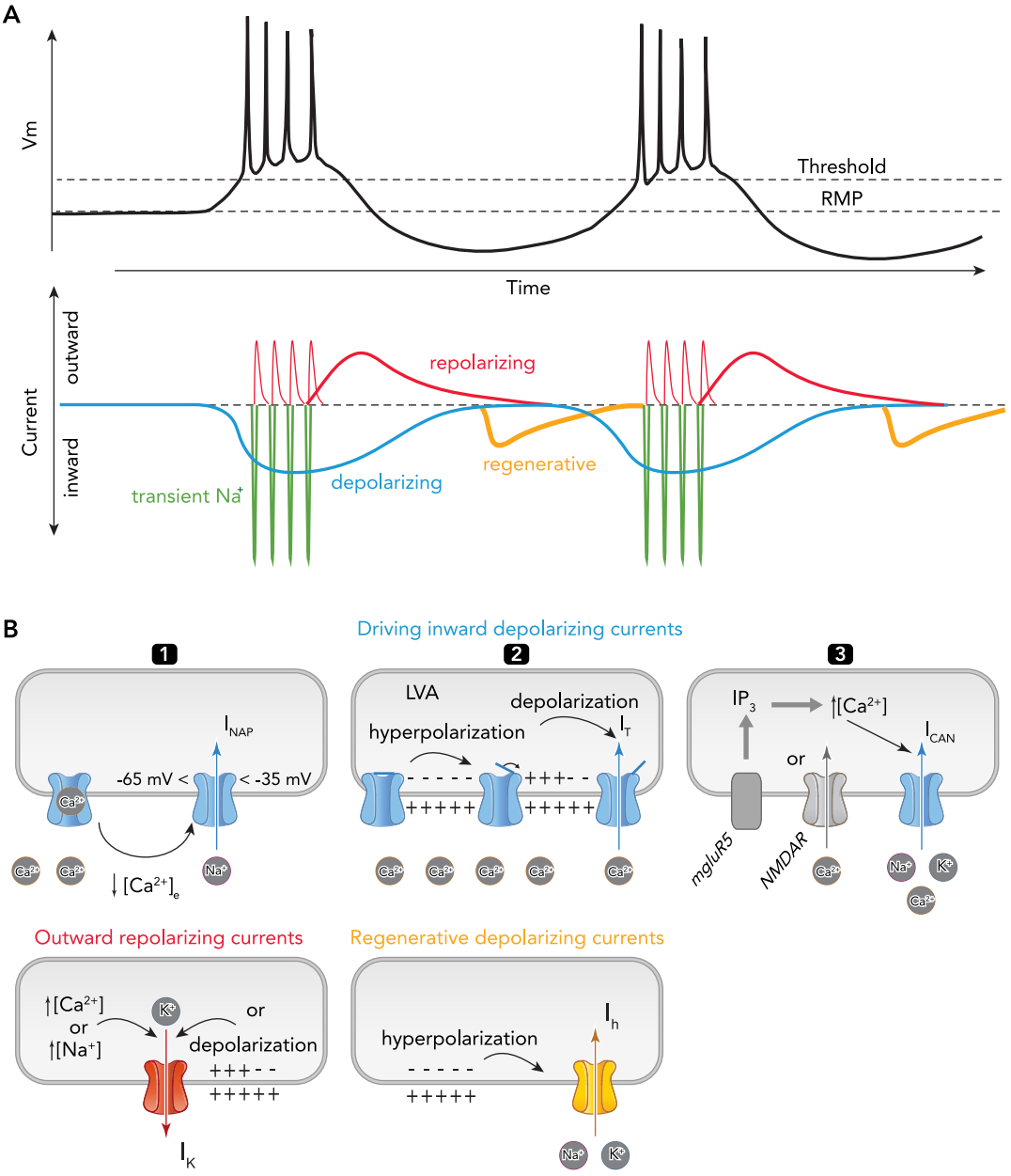

FIGURE 1. **Ionic currents underlying repetitive bursting**
A: representation of two bursts (*top*) and the sequence of activation of the underlying ionic currents (*bottom*). Repetitive bursting generally relies on activation of a conductance that produces a sustained depolarization or plateau (blue) and "drives" the membrane potential from the resting level (RMP) to the threshold for activation of transient sodium currents (dark green) responsible for action potentials. Voltage-gated potassium channels (red) repolarize the membrane after each of these action potentials, whereas other potassium channels activated by Ca^{2+} and Na^{+} entering the cell during depolarization and firing slowly repolarize the membrane often to a level below RMP. In many instances, the hyperpolarization triggers activation of I_h, which enables regeneration (yellow) of the cycle by depolarizing the membrane potential and allowing for reactivation of the driving current. *B*: *top*: different channels responsible for driving the depolarizing plateaus supporting bursting and the conditions required for their activation. *Bottom*: channels required for repolarization and burst termination (red; *left*) and for regenerating the depolarizing drive (yellow: *right*).

observation that the depolarization before bursting activity occurs at membrane potential close to the potential of activation of I_{NaP} and the fact that bursts are abolished upon application of riluzole prompted I_{NaP} as the primary driver of the neuronal bursts (see FIGURE 1B1) (20, 36, 149, 152). Since I_{NaP} is voltage-dependent, the depolarization brought up by its activation would eventually cause its inactivation. In these cells, repolarization and burst termination can be triggered by activation of $I_{K(Na)}$ and/or $I_{K(Ca)}$, which contribute to the burst termination in the rat main sensory trigeminal nucleus (20) as they do in the lamprey spinal cord (44). Voltage-gated potassium channels are also present in the lamprey spinal cord, and their blockade induces an increase in burst frequency (61), making them good candidates for the modulation of the burst cessation. Activation of all these potassium channels would lead to membrane hyperpolarization, which in turn would activate I_h in cells carrying this channel, thus providing for a regenerative drive. In ferret's thalamo-cortical neurons (90) and rat's hippocampal CA3 region (27), blockade of I_h with ZD 7288 abolished both the afterdepolarization and the progressive rebound depolarization and resulted in suppression of the oscillatory activity in these neurons.

In thalamo-cortical neurons, the sequence of events leading to bursting (FIGURE 1B2) is thought to begin with a hyperpolarization that releases LVA calcium channels from their inactivated state, making them available for activation upon depolarization, which may result from activation of I_h by the prior hyperpolarization and which would also trigger firing through the recruitment of sodium and high-voltage-activated calcium channels. The latter eventually activates calcium-dependent potassium channels and voltage-gated potassium channels, which repolarize the plasma membrane and hyperpolarize it to a level sufficient to activate I_h and drive a new boost of depolarization, leading to a renewed activation of calcium conductances (46). In this example, low-voltage-activated calcium channels are clearly the primary driver of the events leading to bursting.

As to bursts driven by I_{CAN} (FIGURE 1B3), Pace and colleagues (116) proposed two different mechanisms. The first one involves metabotropic mGluR5 receptors, which would initiate a process leading to the release of calcium from the intracellular stores through IP_3 receptors. The released calcium would then activate I_{CAN} channels. The second hypothesis involves calcium entry through NMDA receptors. Both mechanisms imply that a synaptic input would activate these channels. No indication was given as to the burst termination; however, like in the lamprey spinal cord, potassium conductances may play that role (44, 61).

Astrocytes are Involved in Ions Homeostasis and Rhythmogenesis

The most studied ions with regard to neuronal excitability and which concentrations are under strict regulation in the brain are potassium, calcium, sodium, and chloride. Potassium concentration is higher in the neuronal intracellular compartment than in the extracellular space (130 mM vs. 2.7-3.5 mM, respectively) (76), whereas the opposite is true for sodium (extracellular and intracellular concentrations are ~145 and 8–15 mM, respectively) (129). Calcium shows the highest difference with an intracellular "resting" concentration of ~100 nM and an extracellular concentration of 1–2 mM (35, 59, 109, 145). The extracellular chloride concentration ($[Cl^-]_e$) is ~120 mM (77), whereas chloride intracellular concentration is between 5 and 20 mM, and is maintained by several molecular elements, including the cation-chloride cotransporters (NKCCs for example) and Cl-HCO_3 exchangers (49, 118).

At rest or relatively low activity levels, neuronal ion pumps and transporters counteract any major ion movements and contribute to maintain the cell membrane at a relatively stable potential as well as the ionic gradient concentrations between the intra- and extracellular compartments. However, with higher activity levels, ionic concentration changes occur in both the intra- and extracellular compartments, and additional mechanisms may be required to restore homeostasis. Evidence suggests that astrocytes may play a major role in controlling the extracellular concentration of some ions.

Potassium

Astrocytes and potassium homeostasis. During neuronal discharge, activation of the voltage-gated potassium channels causes potassium ions to flow toward the extracellular space. The extracellular potassium concentration ($[K^+]_e$) can increase up to a ceiling level of ~12 mM (40) in physiological conditions. Astrocytes are responsible for bringing $[K^+]_e$ back to resting values after an activity-driven increase. In 1966, Orkand et al. (115) introduced the concept of spatial buffering as a possible way of balancing $[K^+]_e$. They proposed that the potassium accumulated during neuronal activity is taken up by neighboring astrocytes and redistributed through the syncytium to less concentrated areas. This is done mainly through the activation of gap junctions (136, 161). Indeed, it has been shown that gap-junctional coupling between astrocytes is increased by elevations in $[K^+]_e$ (34, 45), providing an anatomical support to this theory. Glial cells express several voltage-dependent potassium channels [inward rectifier (Kir); delayed rectifier

(K_d); transient A-type (K_A); Ca^{2+}-activated (K_{Ca})] (for review, see Refs. 11, 25). However, the potassium channel that is predominantly responsible for the high potassium permeability and the maintenance of glial resting membrane potential (RMP) close to the equilibrium potential of potassium (E_K) is Kir, mostly the Kir4.1 channel. Because of the high permeability of glial membrane to potassium, this regulation of $[K^+]_e$ is done mainly by a passive mechanism. However, in some cases, especially when there is an entry of sodium in the glia, an active process that relies on the action of glial Na^+-K^+-ATPase may be at play. In fact, according to D'Ambrosio et al. (31), both Kir channels and the Na^+-K^+ pump participate in the regulation of $[K^+]_e$. Their findings suggest that neuronal and glial Na^+-K^+ pumps may be involved in the setting of baseline $[K^+]_e$ levels and its recovery

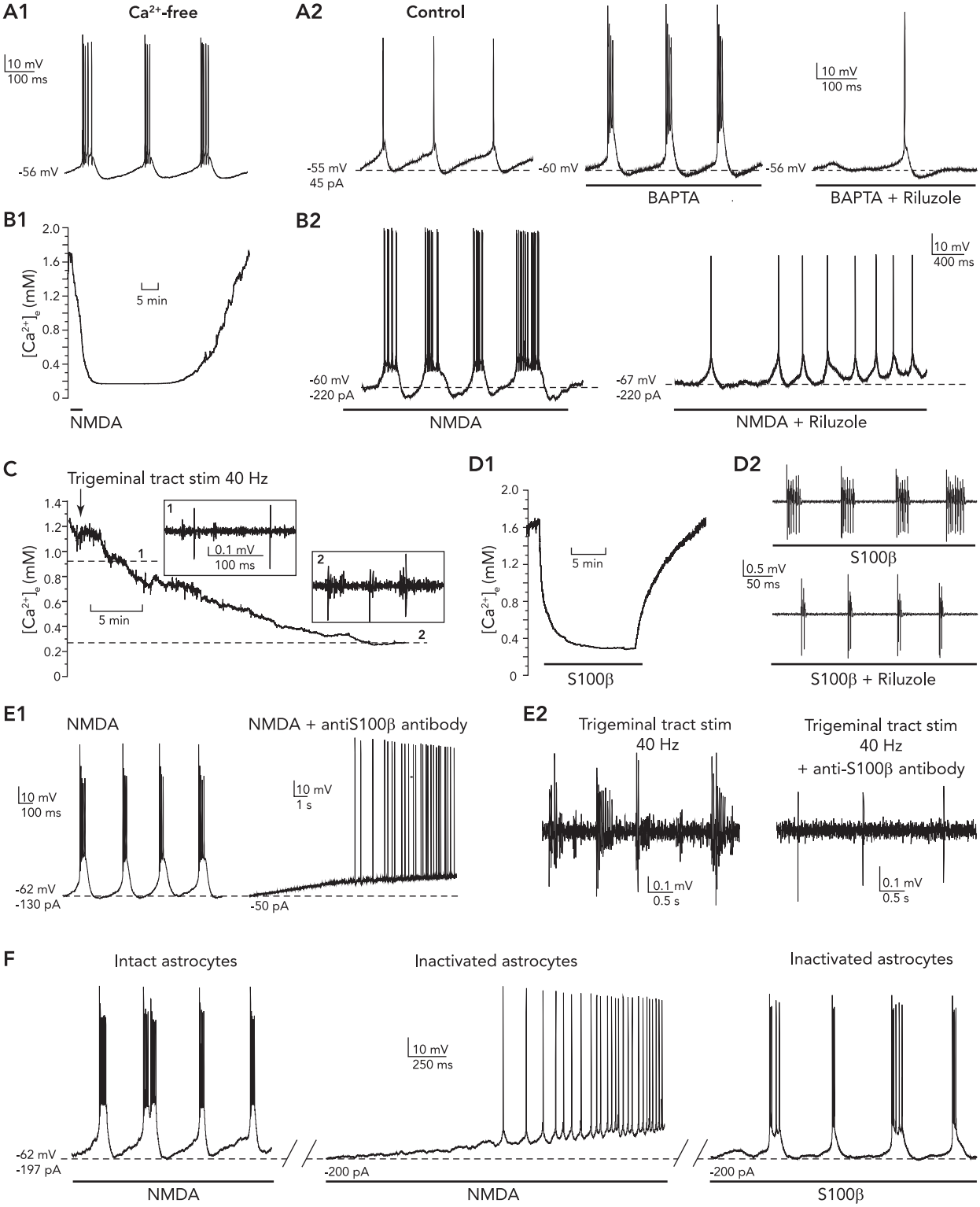

rate during sustained high-frequency firing. Glial Kir channels would also be involved in the regulation of baseline $[K^+]_e$ but might not affect the rate of potassium clearance during neuronal firing. Closely linked to the Kir4.1 channels are the aquaporins-4 (AQP4): membranous channels that allow water flux through the membrane of astrocytes and are responsible for the volume changes observed in astrocytes as well as the shrinkage of the extracellular space associated with intense neuronal activity (105). Finally, another player that helps to actively counteract the increase of $[K^+]_e$ is the Na^+-K^+-$2Cl^-$ co-transporter (60, 148).

Extracellular potassium fluctuates with burst firing. Potassium contributes to the generation of rhythmic oscillations. Indeed, using neonatal rat spinal cord in vitro preparation, Bracci et al. (18) showed that artificially rising $[K^+]_e$ from a control value of 4.5 mM to over a threshold of ~8 mM leads to sustained activation of the spinal locomotor network similar to the locomotor rhythm typically induced by serotonine and NMDA. Interestingly, they found that the suprathreshold concentration range required to elicit such sustained rhythmic motor pattern was very narrow (~1 mM), and when rhythmic activity was elicited with further increases (>2 mM over threshold), it was present only transiently before switching to tonic firing, then into block. Another interesting point is the facilitative effect they reported of co-applying subthreshold concentration of NMDA and serotonine that allows occurrence of rhythmic motor pattern with subthreshold (6 mM) $[K^+]_e$. Similar results were found in a study carried out by Jensen and Yaari (70) on rat hippocampal slices. The authors reported occurrence of periodic bursting in the CA3 region that spread to the CA1 when the slices were exposed to a saline with elevated potassium (7.5 mM). In a more physiological context, Marchetti et al. (96) reported that $[K^+]_e$, as estimated with ion-sensitive electrode recordings, increases to up to 8 and 6 mM in the spinal cord of rats during fictive locomotion induced by electrical stimulation and NMDA, respectively. In this study, the authors did not indicate whether the increases in $[K^+]_e$ occurred before or after the appearance of fictive locomotion, but in a more recent study, Brocard et al. (19), using ion-sensitive electrode recordings in neonate rat spinal cord, showed that potassium increases from a resting value of 4 mM to ~5 mM before the onset of locomotion-like activity induced pharmacologically (with application of NMA and serotonin) or with electrical stimulation of afferent sensory inputs and further to over 6 mM as the locomotor rhythm progresses. This evidence suggests that, at least, the early changes in $[K^+]_e$ can help the emergence of the rhythmic pattern since they appear before any detected rhythmic activity from the ventral roots, whereas the later $[K^+]_e$ increases could be partly consequential to the ongoing neuronal activity since they seem to be related to the increase in burst amplitude. Three of the studies mentioned above were performed on the same preparation (spinal cord, in vitro); in the study of Bracci et al., $[K^+]_e$ was artificially controlled, whereas in the other two the values of $[K^+]_e$ reported were obtained in more physiological conditions. However, the three studies reported similar values of $[K^+]_e$ correlated to occurrence of rhythmic activity. Extracellular potassium increases were also observed in the lamprey spinal cord during fictive swimming (158). The authors reported a two-component $[K^+]_e$ increase, consisting of phasic increases of $[K^+]_e$ of ~0.2 mM linked to the ventral root discharges on the ipsilateral side surimposed on a slow elevation (varying between 0.08 and 0.40 mM) of the baseline level of $[K^+]_e$ that parallels the initiation of ventral root burst activity. The authors did not clearly state whether the onset of the slow elevation precedes that of the detected rhythmic activity, but their observation that the general form of the $[K^+]_e$ curve closely resembles that of the bursts on the ipsilateral side suggests that the phasic $[K^+]_e$ increases may be a consequence of neuronal activity. Similar results have been reported in the cat ventrolateral medulla in parallel with central respiratory activity in the phrenic nerve (125).

FIGURE 2. **Involvement of astrocytes in the generation of bursts in the masticatory CPG**
A1: neurons of the trigeminal main sensory nucleus (NVsnpr) display a bursting pattern in calcium-free medium. *A2*: in control conditions, NVsnpr neurons fire tonically (*left*). Bath application of BAPTA causes one such neuron to burst (*middle*), and I_{NaP} channel blocker riluzole prevents the BAPTA-induced bursting in this neuron (*right*). *B1*: local application of NMDA leads to a significant decrease in extracellular calcium. *B2*: NMDA-induced bursting in a NVsnpr neuron recorded in whole-cell configuration (*left*) is blocked by bath application of Riluzole (*right*). *C*: electrical stimulation of the sensory trigeminal tract at 40 Hz also induces calcium depletion in the extracellular medium and bursts as seen in an extracellular recording of a NVsnpr neuron. *Inset 1* shows a tonic discharge before calcium drops. *Inset 2* shows a burst activity when extracellular calcium level is below 0.3 mM. *D1*: the astrocytic protein S100β causes extracellular calcium to diminish. *D2*: a NVsnpr neuron discharges rhythmically in presence of S100β (*top*), and S100β-induced bursts are blocked by Riluzole (*bottom*). *E1*: in whole-cell recordings, NMDA causes bursting (*left*) but not in presence of an antibody specifically directed against S100β (*right*). E2: in extracellular recordings, electrical stimulation of the sensory trigeminal tract at 40 Hz elicits bursting in control conditions (*left*) but not in presence of an anti-S100β antibody (*right*). *F*: in whole-cell recordings, NMDA induced rhythmic bursting under control conditions (*left*) but only tonic firing after inactivating a neighboring astrocyte with intracellular dialysis of BAPTA (*middle*). Bursting was restored with an external application of S100β (*right*).

In this case, $[K^+]_e$ started to rise before the discharge of action potentials; thus the authors proposed that the efflux of potassium was produced as a consequence of synaptic transmission. Finally, local transients (between 1 and 2 mM) in $[K^+]_e$ were also seen during cortical slow sleep oscillations and spike-wave seizures (4).

Extracellular potassium likely interacts with the conductances that shape the bursts. Indeed, low concentrations of TEA or increased $[K^+]_e$ have been shown to prolong burst duration and to increase oscillation amplitude in the supraoptic nucleus of rats (86) probably by preventing burst termination. A computational model of Hb9 cells suggests that increase in $[K^+]_e$ does not upregulate I_{NaP} in locomotor CPG circuits (19). However, recordings from CA1 pyramidal neurons in hippocampal slices revealed a TTX-sensitive persistent inward current in these neurons that was reversibly enhanced when $[K^+]_e$ was raised (141). It has also been shown that elevated $[K^+]_e$ increases the conductance of the channels mediating I_h (143).

Evidence for spatial buffering of potassium during bursting. Is there any evidence that the astrocyte-driven spatial buffering of potassium takes place along with rhythmic firing in physiological conditions? Working on brain stem slice preparations of neonatal rats, Schnell et al. (137) reported periodic fluctuations of the membrane current of astrocytes occurring in phase with the rhythmic discharges of PBC neurons. Blockade of Kir channels with barium (Ba^{2+}) decreased the amplitude of the periodic membrane current fluctuations by >50%, suggesting that these currents partially reflect the periodic uptake of the elevated extracellular potassium around the astrocytes with each fired burst. Such potassium buffering seems to occur along with large-scale oscillations as well. In the cerebral cortex of anesthetized cats, a periodic increase in intraglial K^+ concentrations ($[K^+]_i$) occurs simultaneously to the depolarizing phase of the slow oscillations (3).

Impairment of spatial buffering may be involved in pathologies like epilepsy. Epilepsy is characterized by periodic seizures resulting from abnormal neuronal hyperexcitability and high synchronicity. Epileptiform activity is generally initiated in restricted areas of the brain but can spread to other parts (8, 106, 121, 151). It has been known for more than four decades that extracellular potassium increases during epileptogenesis (99), and much evidence suggests a role for astrocytes in $[K^+]_e$ regulation in this pathology. For instance, a study by Kivi et al. (75) suggests an impairment of potassium buffering in hippocampal CA1 slices from epileptic rats. Indeed, an application of Ba^{2+} did not affect the level of extracellular potassium in epileptic slices with Ammon' Horn sclerosis. In sclerotic tissues, astrocytes show lower densities of Kir channels (62). Beside Kir channels, many investigations also suggest that astrocyte-expressed aquaporins may play a significant part since they are responsible for the water flow and therefore volume changes in the extracellular space and ultimately the $[K^+]_e$. Indeed, epilepsy has been associated with abnormal expression of aquaporin AQP4 in mice hippocampus (85) and human cortex (97).

Calcium

Astrocytes and calcium homeostasis. Neuronal activity is associated with a decrease of the extracellular concentration of $[Ca^{2+}]_e$ that occurs in parallel to the rise in $[Ca^{2+}]_i$ due to calcium influx into the cells through voltage- and ligand-gated ion channels. Contrary to potassium, much less is known about the role of glia in the regulation of $[Ca^{2+}]_e$. It is, however, known that, in many brain areas, astrocytes possess voltage-gated calcium channels (25, 82) and express calcium sensors (24). Furthermore, direct evidence shows that astrocytes can effectively sense the level of calcium in the extracellular compartment. Indeed, Zanotti and Charles (163) have shown that astrocytes exposed to low $[Ca^{2+}]_e$ respond with increases in $[Ca^{2+}]_i$ that propagate intercellularly as Ca^{2+} waves. This is consistent with the observation that decreased $[Ca^{2+}]_e$ promotes the opening of hemichannels that mediate electrical coupling of neurons and glial cells (150). This low calcium-mediated intracellular calcium rise, however, relies on a release of calcium from intracellular stores since it is inhibited by thapsigargin (163). There is evidence that the astrocytic Ca^{2+} waves modulate the firing frequency of ganglion cells in dissected eyecup retina neurons (108). Lian and Stringer (87) have shown that, during induced spreading depression in the rat cortex, the $[Ca^{2+}]_e$ remained low for a longer time-lapse than normal and that the shape of the recovery curve was altered when astrocytes activity was artificially inhibited with fluorocitrate (FC) and fluoroacetate (FA). Indeed, under control conditions, the $[Ca^{2+}]_e$ recovery curve presents a phase of transient overshoot indicative of an active extrusion of calcium from cells in an amount greater than that which had moved into the cells. The overshoot phase was lacking with the use of FC/FA, suggesting that the failure of astrocytes to actively extrude calcium may account for the longer time required to restore the level of extracellular calcium.

Extracellular calcium fluctuates with burst firing. The extracellular concentration of calcium also seems to be a determinant for bursting in a number of brain areas. Although increases in $[Ca^{2+}]_e$ can lead to bursting as shown by Formenti

et al. (46) in rat thalamic neurons, bursting is most often associated with decreases of $[Ca^{2+}]_e$. In vivo, bursting in the neocortex during seizures is associated with decreases in $[Ca^{2+}]_e$ that occur before the onset of phasic activity (59). In vitro, artificial reduction of $[Ca^{2+}]_e$ has been associated with neuronal bursting in preparations of the rat supraoptic nucleus (86), hippocampus (146), medullary respiratory neurons (36, 73, 114), spinal neurons (19), and neurons of the trigeminal main sensory nucleus (NVsnpr) (FIGURE 2A1) (20, 101, 152). In most of these studies, the medium used was calcium free. In the trigeminal main sensory nucleus, even locally restricted changes induced by extracellular application of the Ca^{2+} chelator BAPTA convert tonic firing into rhythmic bursting (FIGURE 2A2). More interestingly, stimuli like NMDA (locally applied) or stimulation of sensory inputs to the nucleus, which efficiently elicit bursting in these neurons (FIGURE 2, B2, C, AND E2) are also associated with a decrease in $[Ca^{2+}]_e$ (close to 0.89 and 1.1 mM, respectively) (FIGURE 2, B1 AND C). In the spinal cord, Brocard et al. (19) reported 1.03 mM as the extracellular Ca^{2+} concentration below which they observed locomotor-like activity when they electrically stimulated the ventral funiculus, whereas in the main sensory trigeminal nucleus the $[Ca^{2+}]_e$ needed to drop beneath 0.4 mM for rhythmic activity to appear (101). These differences may reflect differences in age, structure, or electrode placement between these two studies. In neurons of the trigeminal main sensory nucleus, bursting elicited by NMDA or BAPTA applications is driven by I_{NaP} (FIGURE 2A2 AND 2B2). Depletion of extracellular calcium shifts the *I*-V curve of I_{NaP} toward more hyperpolarized potentials (86, 101, 149), and from predictions based on a computational model of Hb9 cells, it appears that a slight shift of I_{NaP} activation suffices to switch the neuron firing pattern from tonic to rhythmic bursting (19). The work by Armstrong (5) in the squid giant axon suggests that Ca^{2+} may favor closing of the channel by occupying its pore. In its absence, closing slows considerably or does not occur. This effect of calcium may also help understand the voltage dependency of the activation range of I_{NaP} since the ability of calcium to enter the pore and block it is reduced as voltage is driven negative.

Unlike sodium-persistent channels, activation of LVA Ca^{2+} channels is promoted with rises in $[Ca^{2+}]_e$. This effect may result from the fact that these channels are activated at more hyperpolarized potentials. Increases of $[Ca^{2+}]_e$ hyperpolarize thalamic neurons and shift the conductance-voltage relationship of their LVA Ca^{2+} channels to the right (46). The hyperpolarization, which may result from a masking of the negative fixed charges on the membrane surface by the calcium ions facilitates activation of the LVA channels, whereas the increased Ca^{2+} driving force favors appearance of low-threshold Ca^{2+} spikes and eventually bursting.

Astrocyte-mediated extracellular calcium depletions during bursting. Although often postulated, direct evidence of astrocytic regulation of extracellular calcium were only recently obtained. We recently showed that an astrocytic protein, S100β, reduces $[Ca^{2+}]_e$ (FIGURE 2D1) and induces I_{NaP}-driven bursting in neurons of the trigeminal main sensory nucleus (FIGURE 2D2) (101). Protein S100β was proven to be released from astrocytes (155) after elevation of cytosolic Ca^{2+} (33), but the exact mechanisms underlying its release or secretion have not been deciphered yet. Some studies (26, 134) suggested that these mechanisms may involve the activation of glutamate mGluR3 and/or A1 adenosine receptors, whereas others (134) have ruled out involvement of Cx43 hemichannels. S100β exerts many actions, one of which is calcium chelation (94, 95). In support of this role, we have observed that blockade of endogenous S100β with application of an antibody directed against it prevents bursting and Ca^{2+} decreases induced in the trigeminal sensory nucleus with NMDA or sensory fibers stimulation (FIGURE 2, E1 AND E2; Ref. 101). These findings strongly suggest a prominent role for astrocytes in rhythmogenesis. This is further supported by the finding that preventing activation of astrocytes with intracellular dialysis of BAPTA in one of several connected astrocytes led to cessation of NMDA-induced bursting (FIGURE 2F; Ref. 101) in adjacent neurons. Bursting blocked by this procedure could be restored by exogenous application of S100β (FIGURE 2F, RIGHT; Ref. 101). Thus we propose that in the trigeminal main sensory nucleus, which is postulated to form part of the core of the masticatory CPG, rhythmic activity results from activation of astrocytes by incoming sensory glutamatergic inputs (101), leading to release of S100β, which in turn binds extracellular calcium, causing a decrease in $[Ca^{2+}]_e$ and a consequent shift in I_{NaP} activation curve, which facilitates bursting (see FIGURE 4). This study constitutes the first demonstration that directly links astrocytic S100β to neuronal firing pattern in individual cells (101). However, other evidence suggests that S100β can also play a role in large-scale oscillations. In two studies using S100β knockout mice, no significant differences were found in the spontaneous oscillations detected in the hippocampus and the neocortex compared with wild-type mice (133, 134). However, these oscillations diverged during kainate-induced seizures. Under these conditions, there was a significant increase in the amplitude of gamma waves (133, 134) that was correlated with increased level of extracellular S100β in the wild-type mice

(134), suggesting that S100β may contribute to gamma oscillations in the hippocampus. Gamma oscillations are high-frequency waves (30–80 Hz) associated with attentive behavioral states that can be found in the neocortex and the hippocampus. Evidence of S100β implication in these rhythmic events support our data showing an important role for S100β in rhythmogenesis in the masticatory GPG.

Several other findings link changes in astrocytic functions to dysregulation of extracellular calcium and brain pathologies. In kainate-induced epilepsy in rats, for instance, immunocytochemical investigations have shown an upregulation of L-type voltage-gated calcium channel α2 subunit in astrocytes surrounding the lesion (160). No significant changes were reported in neurons. In the hippocampi of patients who suffered from temporal lobe epilepsy associated with Ammon's horn sclerosis, astrocytes were also strongly immunoreactive for α1c subunits (42). Some of the voltage-gated calcium channels have a relatively high threshold of activation, and, given the very negative membrane potential of healthy astrocytes, it is unlikely that they can be depolarized enough to activate these channels. Nevertheless, it has been shown using brain slices or cultures that astrocytes from human sclerotic epileptogenic hippocampal seizure foci display more depolarized membrane potential (around −55 mV) compared with astrocytes from nonsclerotic tissue (around −75 to −80 mV) (112) and express higher TTX-sensitive Na^+ channel density, allowing them to generate action potential-like responses with membrane depolarization (17, 112). In these conditions, one should expect such upregulations of L-type voltage-gated calcium channel subunits to lead to an increased flow of calcium into astrocytes, potentially causing a decrease in $[Ca^{2+}]_e$. Parkinson's disease may be another example of pathology that results from an inefficient regulation of calcium levels in the extracellular space. Symptoms of Parkinson's disease include neuronal death and excessive synchronicity of beta waves in the cortex and in the basal ganglia (22, 56, 153). Glial cells play a significant role in the ontogenesis of that disease (55). In a mouse model of MPTP (1-methyl-4-phenyl-1,2,3,6-tetrahydropyridine)-induced Parkinson's disease, the number of S100β-positive astrocytes increases in the striatum and the substantia nigra immediately after treatment with MPTP but declines after 7 days (104). Increases in the levels of S100β were also reported in midbrain slices and cerebrospinal fluid of patients who suffered from Parkinson's disease (135). S100β is a calcium-binding protein (94, 95), and it is possible that its transitory accumulation in the extracellular space leads to a chelation of calcium. A precursor sign of Parkinson's disease could then be a transient decrease of calcium in the extracellular space.

Sodium

Astrocytes and sodium homeostasis. As neurons fire, there is a decrease in the extracellular sodium concentration ($[Na^+]_e$) due to influx of sodium ions into the cells through voltage- and ligand-gated ion channels (41). Indeed, in a study carried out on hippocampal slices, Karus et al. (74) reported that, during bursts, the neuronal intracellular concentration of sodium ($[Na^+]_i$) increases to up to 22 mM from a resting baseline value of ~14 mM and recovers to around baseline level between bursts. Intraneuronal concentrations of sodium need to be tightly controlled to maintain cell integrity and excitability and also because extrusion of sodium ions by the Na^+-K^+-ATPase is an energy-expensive process. How do astrocytes participate in sodium homeostasis? Astrocytes express voltage-gated Na^+ channels (for a review about sodium homeostasis and signaling in astrocytes, see Ref. 128), which allows for a small but steady influx of Na^+ ions to ensure the maintenance of cytoplasmic Na^+ at concentrations required for proper functioning of the glial Na^+-K^+ pump (142). Moreover, sodium signaling concomitant with neuronal activity has been shown to occur in astrocytes. Indeed, combining somatic whole-cell patch-clamp recordings with quantitative sodium imaging with the sodium-sensitive fluorescent indicator dye (sodium-binding benzofuran isophthalate), Bennay et al. (15) showed that short bursts of synaptic activity resulted in glial sodium signals of up to 9 mM in cellular branches of cerebellar Bergmann glial cells. These sodium increases persisted for tens of seconds. Sodium may also build up in astrocytes following excitatory neuronal activity because of the glial glutamate transporter, which carries three Na^+ ions with each glutamate molecule (80). In cultures of cortical astrocytes, uptake of glutamate produces intercellular sodium waves that occur in parallel with calcium waves following stimulation of a single astrocyte. Sodium underlying these waves has to come from the extracellular space since it could not be released from the intracellular stores as with calcium. Thus, at sites of intense activity, the consequent lowering of extracellular sodium could weaken the drive for this ion toward the neuronal intracellular compartment. Other than the glutamate transporter, the glial Na^+-K^+ pump, which is involved in $[K^+]_e$ homeostasis, can also greatly impact neuronal sodium homeostasis. Indeed, blocking astrocyte metabolism during basal activity using sodium-fluoroacetate results in an increase of baseline intracellular sodium of ~4 mM in hippocampal neurons and by ~12 mM in astrocytes (74). The authors attribute

the larger increase in astrocytes to the weakening of the glial Na^+-K^+-ATPase. Under conditions of increased network activity, blocking of astrocyte metabolism increases even more the baseline intracellular sodium in both cells types but also produces a nearly fivefold prolongation of individual epileptiform bursts and similar increase in the number of population spikes per burst (74). The authors proposed that the increased neuronal excitability results, in part, from reduced glutamate uptake due to reduced activity of the glutamate transporter that greatly depends on the transmembrane sodium gradient in astrocytes, which in turn depends on the activity of the Na^+-K^+-ATPase. Furthermore, since the glial Na^+-K^+-ATPase is also involved in the clearance of extracellular potassium following intense neuronal activity, its weakening reduces potassium intake, thus increasing neuronal excitability. No measurements of extracellular sodium have been made in parallel in this study; however, this evidence of astrocyte involvement in the control of neuronal $[Na^+]_i$ suggests that, even indirectly, by achieving other basic cellular functions, astrocytes may participate in the homeostasis of extracellular sodium.

Extracellular sodium and bursting. Studies addressing the direct role of sodium ions in bursting are relatively scarce. Many of the studies addressed the involvement of sodium channels rather than the role of the ionic sodium gradient per se. One study by Li and Hatton (86) carried out on the magnocellular neurons of the hypothalamic supraoptic nucleus (SON) showed that both $[Na^+]_e$ and $[Na^+]_i$ are determinants for the low calcium-mediated burst firing observed in a subpopulation of these neurons. They examined the effect of reducing the extracellular sodium and reported that this treatment abolished or reduced bursting in all tested cells. Finally, even though no study has formally measured the changes in extracellular sodium during rhythmic activities, $[Na^+]_e$ is likely to decrease because of all the voltage- and ligand-activated channels allowing movements of Na^+ ions from the extracellular space toward the intracellular compartment. However, the question remains as to the extent of sodium depletion and how such decreases may influence other conductances involved in bursting.

Evidence for synchronized sodium signaling in astrocytes somata during bursting. In the study cited above, Karus et al. (74) showed that, during neuronal recurrent bursting, astrocytes showed an increase of ~2.9 mM in $[Na^+]_i$ that occurred in parallel with the transient $[Na^+]_i$ increase seen in neurons. In ~30% of the astrocytes, this increase was followed by an undershoot below baseline. The increases of astrocytic $[Na^+]_i$ observed during neuronal bursts were accompanied by recurring membrane depolarizations of ~10 mV and were paralleled by recurring transient increases of $[K^+]_e$ of up to 2 mM. Between bursts, the astrocytic $[Na^+]_i$ recovered to resting baseline values. Using several pharmacological tools, the authors concluded that sodium signals in astrocytes result from dual contribution of two opposing mechanisms: an influx of sodium ions caused by the sodium-dependent glutamate uptake and an efflux of sodium ions brought out by the elevated $[K^+]_e$-induced activation of the Na^+-K^+-ATPase.

Chloride

The movements of chloride ions in response to neuronal activation are more complex than the other ions (41). Probably, since it is the main permeable anion, chloride ion movements are partly determined by balancing measures in relation to

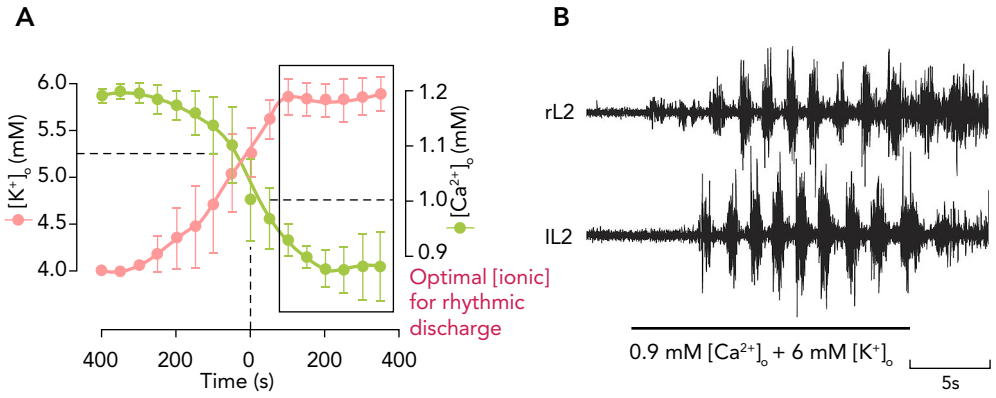

FIGURE 3. **Example of synergistic interactions between potassium and calcium in rhythmogenesis**
A: evolution of extracellular concentration of calcium (green) and potassium (pink) before and after the onset (at 0 ms) of a locomotor-like bursting episode. Optimal concentrations of calcium and potassium for a bursting activity are emphasized by the rectangle. A rhythmic activity appears at concentrations of calcium and potassium close to 0.9 and 6 mM, respectively. *B*: extracellular recordings in the right and left L2 segments (rL2 and lL2) of rat spinal cord along with application of 0.9 mM $[Ca^{2+}]_e$ and 6 mM $[K^+]_e$. **Figure** was modified from Ref. 19 with permission.

fluctuations of the cation gradient concentration. Dietzel et al. (41) reported that, during stimulus-induced self-sustained afterdischarges (SAD) in neurons of the sensorimotor cortex of cats, $[Cl^-]_e$ always showed an average increase of 7 mM (when measured at a depth of 1 mm), often preceded by an initial small decrease. They observed that the maximum increase appears to coincide with the end of the ictal period.

Astrocytes and chloride homeostasis. Chloride channels exist in astrocytes and include volume-sensitive chloride channels (157). The latter participate

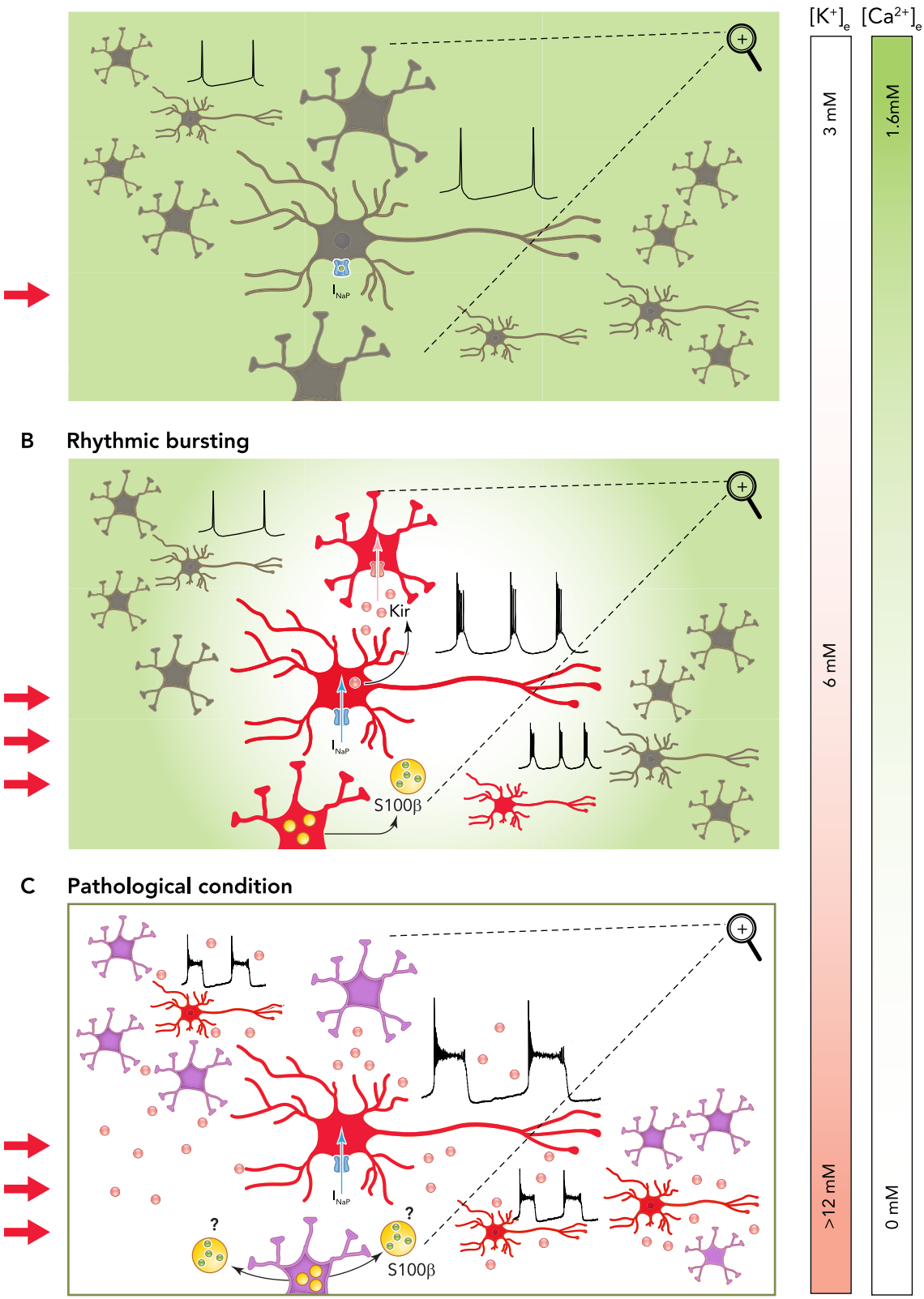

in ion homeostasis mainly through the process of astrocyte swelling (30). By swelling, astrocytes change their volume and thereby control the concentration of several ions in both the intra- and extracellular space. In addition to potassium-mediated machinery, which intervenes in astrocyte swelling (39, 107), an inward rectifier chloride current (14, 81) and Na^+-K^+-Cl^- cotransporter are also activated (69). The participation of chloride channels to astrocytic volume change might result from their association with actin proteins, which form the cytoskeleton (157). Bikson and collaborators (16) tested the effect of DNDS (4,4′-dinitrostilbene-2,2′-disulfonic acid), a glial Cl^- channel blocker (103), on the duration of low calcium-mediated bursts in rat pyramidal CA1 cells and found that high concentration of DNDS caused a 6- to 10-fold increase in burst duration, suggesting that glial uptake of chloride ions contributes to the burst termination.

Extracellular chloride and bursting. Working on the leech's Retzius neurons, Beck and colleagues found that decreasing $[Cl^-]_e$ (≤1 mM) induces a sustained membrane depolarization and recurrent bursting activity that were accompanied by recurrent rises in intracellular Ca^{2+}, which oscillated in synchrony with the bursts. Using a chloride-free and calcium-free medium, they determined that the intracellular calcium rises were presumably due to Ca^{2+} influx through voltage-dependent Ca^{2+} channels, since they could no longer be seen in this medium. Moreover, the bursting activity was not affected by depletion of intracellular calcium but was inhibited by saxitoxin, a sodium channel blocker, suggesting that it relies on I_{NaP} (13). In rat hippocampal slices, spontaneous (63) or stimulus-evoked (9) bursting discharges also developed when the $[Cl^-]_e$ was decreased. These cellular discharges were accompanied for a time with synchronous oscillations in the field potential. However, longer exposure to low chloride medium desynchronized the firing activity of neuronal populations in the CA1 region of hippocampal slices, which may explain the anti-epileptic effect of chloride-cotransport blockade by furosemide (64). Reciprocally, it has been shown that calcium-free mediated bursting occurs concomitantly with large decreases in $[Cl^-]_e$ (58).

Synergistic Interactions and Rhythmogenesis

Changes in the ionic gradient concentration of the main ions that regulate brain activity exert tremendous effects on neuronal excitability and are determinant of the neuronal firing mode. By their concerted actions on the rhythmogenic conductances, they may act in synergy to promote rhythmogenesis. Indeed, Brocard et al. (19) reported that such a synergistic effect exists between the $[Ca^{2+}]_e$ reduction and the $[K^+]_e$ increase for burst generation in the locomotor CPG (FIGURE 3). The authors stated that both $[Ca^{2+}]_e$ and $[K^+]_e$ concurrently changed before any rhythmic activity was detected from ventral roots, suggesting that these changes are not just a consequence of the neuronal activity but are part of the cause for the rhythmic pattern observed. They confirmed this synergistic interaction by artificially manipulating both ion concentrations while recording neuronal activity and reported that concomitant reduction of $[Ca^{2+}]_e$ to 0.9 mM and increase of $[K^+]_e$ to 6 mM (the same values reported with physiologically induced changes in concentration for both ions) elicited bursts in 25% of the recorded neurons. A similar interaction between both ion concentrations reported this time as a "Ca^{2+}/K^+ antagonism" is also encountered in mice rhythmogenic inspiratory active pre-Bötzinger complex (117). The authors indeed showed that the rhythm generated in 3 mM K^+ and 1 mM Ca^{2+} is depressed following a modest rise of Ca^{2+} and restored when K^+ is subsequently raised. Ultimately, they proposed that the optimal window to obtain long-term stable slice rhythm would be 0.75–1 mM for calcium and 4–6 mM for potassium, which seems to be in accordance with the values obtained for either ion in more physiological conditions (4, 19, 96, 125).

How do all of the elements converge to allow the emergence of an oscillatory activity? From the reports examined here, it seems that the starting point is the increased firing that causes an elevation of extracellular potassium. According to Hounsgaard and Nicholson (65), an individual burst is initiated when intense neuronal firing results in a local increase in $[K^+]_e$ that would in turn depolarize neighboring neurons. Increased activity

FIGURE 4. **A general model for rhythmogenesis in CPGs**
A: under resting conditions, glutamatergic inputs are low (red arrow), astrocytes (gray) are at resting activity levels, $[Ca^{2+}]_e$ (green) is elevated, and $[K^+]_e$ (pink) is low. The I_{NaP} channels are obstructed by calcium (green dot), and neurons fire tonically. *B*: as the glutamatergic inputs increase, $[K^+]_e$ (pink dots) rises, and astrocytes get activated (red), release S100β (yellow), and initiate spatial buffering through Kir channels. Protein S100β chelates calcium and causes $[Ca^{2+}]_e$ to drop. As a consequence, I_{NaP} channels are freed and drive bursting in neurons (red). The bursting population is limited to the extent of coupled astrocytes forming a syncytium. *C*: under pathological conditions, astrocytes (purple) fail to initiate spatial buffering in the presence of intense neuronal activity, leading to an accumulation of potassium and a spread of excitation and depolarization block among neurons. The level of S100β in the extracellular space may increase and further lead to neuronal hyperexcitability by decreasing $[Ca^{2+}]_e$.

of these neighboring neurons would boost the $[K^+]_e$ to a further extent. This increased activity and $[K^+]_e$ would directly activate the astrocytes and cause them to start the spatial buffering of potassium to prevent local build-up of extracellular K^+ that would cause a depolarizing block and cessation of cell activity. Spread of K^+ will be limited only to astrocytes that are coupled. Thus gap-junctional coupling between astrocytes may provide a means to limit spreading of activity to a specific neuronal population as well as an explanation for the observed synergistic interaction between ions. As already stated, extracellular accumulation of K^+ increases gap-junctional coupling between astrocytes. Interestingly, Scemes and Spray (136) found that this increase in dye-coupling long outlasted the exposure to elevated potassium, suggesting that the effect of potassium on coupling may be indirect. Indeed, the elevated extracellular K^+ causes astrocytic membrane depolarization and leads to the influx of Ca^{2+} through L-type voltage-activated Ca^{2+} channels (34, 43, 147), promoting increases in $[Ca^{2+}]_i$. Blocking the influx of calcium with the L-type calcium channel blocker nifedipine or potentiating this influx with Bay-K-8644 prevented and potentiated, respectively, the K^+-induced increase in coupling (34). At last, they provide evidence that the K^+-induced increased coupling relies on the activation of a CaM kinase by the intracellular calcium rise since it can be prevented by the calmodulin antagonist calmidazolium and by the inhibitor of CaM kinases KN-93. The authors hypothesized that the increased coupling might result from an increased number of active channels within gap-junction plaques. However, only very large increases of extracellular potassium (50 mM), much larger than those observed even with intense neuronal activity of 8–12 mM (140), yielded an elevation of $[Ca^{2+}]_i$ in astrocytes, suggesting that voltage-gated Ca^{2+} influx would be unique to pathological conditions associated with deregulations of $[K^+]_e$. However, the accumulation of sodium in astrocytes during intense excitatory discharge may also cause a calcium entry by reversing the function of the sodium/calcium exchanger (52, 124, 127) and consequently lead to an extracellular decrease of Ca^{2+}. Other mechanisms may also account for the decreased calcium level in the extracellular compartment that occurs in conjunction with rhythmic firing. Astrocytes have a wide array of ionotropic and metabotropic receptors (25), the activation of which leads to intracellular rises of calcium, and glutamate-induced calcium waves in astrocytes have been commonly reported (1). As described above, data from our laboratory suggest that glutamatergic activation of astrocytes may also cause release of the protein S100β from astrocytes, leading to extracellular calcium depletion, subsequent I_{NaP} activation, and burst firing (101). FIGURE 4 summarizes how astrocytes may participate in emergence and synchronization of rhythmic firing in NVsnpr neurons. The proposed model rests on the fact that NVsnpr astrocytes are activated by glutamatergic afferent inputs to this nucleus, but only if they reach a sufficient level of activity. At high activity level, glutamate or K^+ released from these inputs activate astrocytes and cause release of S100β. The extent of neurons exposed to the released S100β will depend on the extent of coupled astrocytes. Among these neurons, only those having I_{NaP} will change their firing. In young rats (P8-12), only 38% of the dorsal NVsnpr neurons perfused with a calcium-free medium showed bursts firing, and bursting and non-bursting cells displayed distinct morphological characteristics and significantly different input resistance and membrane capacitance (152). However, using older rats (P16), Brocard et al. showed that 85% of dorsal NVsnpr neurons had intrinsic bursting properties in calcium-free medium and that bursting relied on I_{NaP} in all tested cells (20). We postulate that the extent of the active network would likely be determined by the population of cells (neurons and astrocytes) that share the same input, and since the primary afferent inputs are somatotopically organized, only functionally related cells would share the same input. Eventually, cessation of primary afferent activation would stop the network activation or excessive stimulation would depolarize the neurons beyond the range of I_{NaP} activation.

Conclusions

The classic concept in which brain function relied exclusively on neuron-to-neuron communication was shattered by evidence in which glial cells switched from the role of brain glue to active information processors expressing a large spectrum of ion channels and receptors. This review recounts the progress made in understanding the prominent role that glial cells play in the generation and maintenance of rhythmic oscillations. Glial cells have proven to be essential partners in coordinating the numerous elements participating in rhythmogenesis through a cross-talk with surrounding neurons. The control of extracellular concentration of ions necessary for rhythmic activities to occur clearly depicts that dialogue. ■

This work was supported by grants from the Canadian Institutes for Health Research and the Network for Oral and Bone Health Research (RSBO), and we are grateful to the Groupe de Recherche sur le Système Nerveux Central (GRSNC) for infrastructural support.

No conflicts of interest, financial or otherwise, are declared by the author(s).

Author contributions: A. Kadala and A. Kolta drafted manuscript; A. Kadala, D.V., P.M., and A. Kolta edited and revised manuscript; A. Kadala, D.V., P.M., and A. Kolta approved final version of manuscript; D.V. and P.M. prepared figures.

References

1. Agulhon C, Petravicz J, McMullen AB, Sweger EJ, Minton SK, Taves SR, Casper KB, Fiacco TA, McCarthy KD. What is the role of astrocyte calcium in neurophysiology? *Neuron* 59: 932–946, 2008.
2. Alzheimer C, Schwindt PC, Crill WE. Modal gating of Na^+ channels as a mechanism of persistent Na^+ current in pyramidal neurons from rat and cat sensorimotor cortex. *J Neurosci* 13: 660–673, 1993.
3. Amzica F, Massimini M, Manfridi A. Spatial buffering during slow and paroxysmal sleep oscillations in cortical networks of glial cells in vivo. *J Neurosci* 22: 1042–1053, 2002.
4. Amzica F, Steriade M. Neuronal and glial membrane potentials during sleep and paroxysmal oscillations in the neocortex. *J Neurosci* 20: 6648–6665, 2000.
5. Armstrong CM. Distinguishing surface effects of calcium ion from pore-occupancy effects in Na^+ channels. *Proc Natl Acad Sci USA* 96: 4158–4163, 1999.
6. Armstrong CM, Matteson DR. Two distinct populations of calcium channels in a clonal line of pituitary cells. *Science* 227: 65–67, 1985.
7. Astori S, Wimmer RD, Prosser HM, Corti C, Corsi M, Liaudet N, Volterra A, Franken P, Adelman JP, Luthi A. The Ca(V)3.3 calcium channel is the major sleep spindle pacemaker in thalamus. *Proc Natl Acad Sci USA* 108: 13823–13828, 2011.
8. Avoli M, D'Antuono M, Louvel J, Kohling R, Biagini G, Pumain R, D'Arcangelo G, Tancredi V. Network and pharmacological mechanisms leading to epileptiform synchronization in the limbic system in vitro. *Prog Neurobiol* 68: 167–207, 2002.
9. Avoli M, Drapeau C, Perreault P, Louvel J, Pumain R. Epileptiform activity induced by low chloride medium in the CA1 subfield of the hippocampal slice. *J Neurophysiol* 64: 1747–1757, 1990.
10. Bal T, McCormick DA. Mechanisms of oscillatory activity in guinea-pig nucleus reticularis thalami in vitro: a mammalian pacemaker. *J Physiol* 468: 669–691, 1993.
11. Barres BA, Chun LL, Corey DP. Ion channels in vertebrate glia. *Ann Rev Neurosci* 13: 441–474, 1990.
12. Bean BP. Two kinds of calcium channels in canine atrial cells. Differences in kinetics, selectivity, and pharmacology. *J Gen Physiol* 86: 1–30, 1985.
13. Beck A, Lohr C, Nett W, Deitmer JW. Bursting activity in leech Retzius neurons induced by low external chloride. *Pflügers Arch* 442: 263–272, 2001.
14. Benesova J, Rusnakova V, Honsa P, Pivonkova H, Dzamba D, Kubista M, Anderova M. Distinct expression/function of potassium and chloride channels contributes to the diverse volume regulation in cortical astrocytes of GFAP/EGFP mice. *PLos One* 7: e29725, 2012.
15. Bennay M, Langer J, Meier SD, Kafitz KW, Rose CR. Sodium signals in cerebellar Purkinje neurons and Bergmann glial cells evoked by glutamatergic synaptic transmission. *Glia* 56: 1138–1149, 2008.
16. Bikson M, Ghai RS, Baraban SC, Durand DM. Modulation of burst frequency, duration, and amplitude in the zero-Ca^{2+} model of epileptiform activity. *J Neurophysiol* 82: 2262–2270, 1999.
17. Bordey A, Sontheimer H. Properties of human glial cells associated with epileptic seizure foci. *Epilepsy Res* 32: 286–303, 1998.
18. Bracci E, Beato M, Nistri A. Extracellular K^+ induces locomotor-like patterns in the rat spinal cord in vitro: comparison with NMDA or 5-HT induced activity. *J Neurophysiol* 79: 2643–2652, 1998.
19. Brocard F, Shevtsova NA, Bouhadfane M, Tazerart S, Heinemann U, Rybak IA, Vinay L. Activity-dependent changes in extracellular Ca^{2+} and K^+ reveal pacemakers in the spinal locomotor-related network. *Neuron* 77: 1047–1054, 2013.
20. Brocard F, Verdier D, Arsenault I, Lund JP, Kolta A. Emergence of intrinsic bursting in trigeminal sensory neurons parallels the acquisition of mastication in weanling rats. *J Neurophysiol* 96: 2410–2424, 2006.
21. Brown AM, Schwindt PC, Crill WE. Different voltage dependence of transient and persistent Na^+ currents is compatible with modal-gating hypothesis for sodium channels. *J Neurophysiol* 71: 2562–2565, 1994.
22. Brown P. Abnormal oscillatory synchronisation in the motor system leads to impaired movement. *Curr Opin Neurobiol* 17: 656–664, 2007.
23. Brumberg JC, Nowak LG, McCormick DA. Ionic mechanisms underlying repetitive high-frequency burst firing in supragranular cortical neurons. *J Neurosci* 20: 4829–4843, 2000.
24. Chattopadhyay N, Evliyaoglu C, Heese O, Carroll R, Sanders J, Black P, Brown EM. Regulation of secretion of PTHrP by Ca^{2+}-sensing receptor in human astrocytes, astrocytomas, and meningiomas. *Am J Physiol Cell Physiol* 279: C691–C699, 2000.
25. Christensen RK, Petersen AV, Perrier JF. How do glial cells contribute to motor control? *Curr Pharmaceutical Design* 19: 4385–4399, 2013.
26. Ciccarelli R, Di Iorio P, Bruno V, Battaglia G, D'Alimonte I, D'Onofrio M, Nicoletti F, Caciagli F. Activation of A(1) adenosine or mGlu3 metabotropic glutamate receptors enhances the release of nerve growth factor and S-100beta protein from cultured astrocytes. *Glia* 27: 275–281, 1999.
27. Cobb SR, Larkman PM, Bulters DO, Oliver L, Gill CH, Davies CH. Activation of Ih is necessary for patterning of mGluR and mAChR induced network activity in the hippocampal CA3 region. *Neuropharmacology* 44: 293–303, 2003.
28. Colombo E, Franceschetti S, Avanzini G, Mantegazza M. Phenytoin inhibits the persistent sodium current in neocortical neurons by modifying its inactivation properties. *PLos One* 8: e55329, 2013.
29. Coombes S, Bressloff PC. *Bursting: The Genesis of Rhythm in the Nervous System*. Hackensack, NJ: World Scientific, 2005, p. 401.
30. Crepel V, Panenka W, Kelly ME, MacVicar BA. Mitogen-activated protein and tyrosine kinases in the activation of astrocyte volume-activated chloride current. *J Neurosci* 18: 1196–1206, 1998.
31. D'Ambrosio R, Gordon DS, Winn HR. Differential role of KIR channel and Na^+/K^+-pump in the regulation of extracellular K^+ in rat hippocampus. *J Neurophysiol* 87: 87–102, 2002.
32. Darbon P, Tscherter A, Yvon C, Streit J. Role of the electrogenic Na/K pump in disinhibition-induced bursting in cultured spinal networks. *J Neurophysiol* 90: 3119–3129, 2003.
33. Davey GE, Murmann P, Heizmann CW. Intracellular Ca^{2+} and Zn^{2+} levels regulate the alternative cell density-dependent secretion of S100B in human glioblastoma cells. *J Biol Chem* 276: 30819–30826, 2001.
34. De Pina-Benabou MH, Srinivas M, Spray DC, Scemes E. Calmodulin kinase pathway mediates the K^+-induced increase in Gap junctional communication between mouse spinal cord astrocytes. *J Neurosci* 21: 6635–6643, 2001.
35. Deitmer JW, Verkhratsky AJ, Lohr C. Calcium signalling in glial cells. *Cell Calcium* 24: 405–416, 1998.
36. Del Negro CA, Koshiya N, Butera RJ Jr, Smith JC. Persistent sodium current, membrane properties and bursting behavior of pre-Botzinger complex inspiratory neurons in vitro. *J Neurophysiol* 88: 2242–2250, 2002.
37. Del Negro CA, Morgado-Valle C, Hayes JA, Mackay DD, Pace RW, Crowder EA, Feldman JL. Sodium and calcium current-mediated pacemaker neurons and respiratory rhythm generation. *J Neurosci* 25: 446–453, 2005.
38. Destexhe A, Contreras D, Steriade M. Spatiotemporal analysis of local field potentials and unit discharges in cat cerebral cortex during natural wake and sleep states. *J Neurosci* 19: 4595–4608, 1999.
39. Dibaj P, Kaiser M, Hirrlinger J, Kirchhoff F. Neusch Kir4 C.1. channels regulate swelling of astroglial processes in experimental spinal cord edema. *J Neurochem* 103: 2620–2628, 2007.

40. Dietzel I, Heinemann U. Dynamic variations of the brain cell microenvironment in relation to neuronal hyperactivity. *Ann NY Acad Sci* 481: 72–86, 1986.

41. Dietzel I, Heinemann U, Hofmeier G, Lux HD. Stimulus-induced changes in extracellular Na^+ and Cl^- concentration in relation to changes in the size of the extracellular space. *Exp Brain Res* 46: 73–84, 1982.

42. Djamshidian A, Grassl R, Seltenhammer M, Czech T, Baumgartner C, Schmidbauer M, Ulrich W, Zimprich F. Altered expression of voltage-dependent calcium channel alpha(1) subunits in temporal lobe epilepsy with Ammon's horn sclerosis. *Neuroscience* 111: 57–69, 2002.

43. Duffy S, MacVicar BA. In vitro ischemia promotes calcium influx and intracellular calcium release in hippocampal astrocytes. *J Neurosci* 16: 71–81, 1996.

44. el Manira A, Tegner J, Grillner S. Calcium-dependent potassium channels play a critical role for burst termination in the locomotor network in lamprey. *J Neurophysiol* 72: 1852–1861, 1994.

45. Enkvist MO, McCarthy KD. Astroglial gap junction communication is increased by treatment with either glutamate or high K^+ concentration. *J Neurochem* 62: 489–495, 1994.

46. Formenti A, De Simoni A, Arrigoni E, Martina M. Changes in extracellular Ca^{2+} can affect the pattern of discharge in rat thalamic neurons. *J Physiol* 535: 33–45, 2001.

47. Forrest MD. Mathematical model of bursting in dissociated purkinje neurons. *PLos One* 8: e68765, 2013.

48. Franceschetti S, Lavazza T, Curia G, Aracri P, Panzica F, Sancini G, Avanzini G, Magistretti J. Na^+-activated K^+ current contributes to postexcitatory hyperpolarization in neocortical intrinsically bursting neurons. *J Neurophysiol* 89: 2101–2111, 2003.

49. Gamba G. Molecular physiology and pathophysiology of electroneutral cation-chloride cotransporters. *Physiol Rev* 85: 423–493, 2005.

50. Ghamari-Langroudi M, Bourque CW. Flufenamic acid blocks depolarizing afterpotentials and phasic firing in rat supraoptic neurones. *J Physiol* 545: 537–542, 2002.

51. Ghazanfar AA, Chandrasekaran C, Logothetis NK. Interactions between the superior temporal sulcus and auditory cortex mediate dynamic face/voice integration in rhesus monkeys. *J Neurosci* 28: 4457–4469, 2008.

52. Goldman WF, Yarowsky PJ, Juhaszova M, Krueger BK, Blaustein MP. Sodium/calcium exchange in rat cortical astrocytes. *J Neurosci* 14: 5834–5843, 1994.

53. Golomb D, Yue C, Yaari Y. Contribution of persistent Na+ current and M-type K^+ current to somatic bursting in CA1 pyramidal cells: combined experimental and modeling study. *J Neurophysiol* 96: 1912–1926, 2006.

54. Guatteo E, Franceschetti S, Bacci A, Avanzini G, Wanke E. A TTX-sensitive conductance underlying burst firing in isolated pyramidal neurons from rat neocortex. *Brain Res* 741: 1–12, 1996.

55. Halliday GM, Stevens CH. Glia: initiators and progressors of pathology in Parkinson's disease. *Movement Disorders* 26: 6–17, 2011.

56. Hammond C, Bergman H, Brown P. Pathological synchronization in Parkinson's disease: networks, models and treatments. *Trends Neurosci* 30: 357–364, 2007.

57. Harris-Warrick RM. General principles of rhythmogenesis in central pattern generator networks. *Prog Brain Res* 187: 213–222, 2010.

58. Heinemann U, Albrecht D, Kohr G, Rausche G, Stabel J, Wisskirchen T. Low-Ca^{2+}-induced epileptiform activity in rat hippocampal slices. *Epilepsy Res* Suppl 8: 147–155, 1992.

59. Heinemann U, Lux HD, Gutnick MJ. Extracellular free calcium and potassium during paroxsmal activity in the cerebral cortex of the cat. *Exp Brain Res* 27: 237–243, 1977.

60. Hertz L, Chen Y, Spatz M. Involvement of non-neuronal brain cells in AVP-mediated regulation of water space at the cellular, organ, and whole-body level. *J Neurosci Res* 62: 480–490, 2000.

61. Hess D, El Manira A. Characterization of a high-voltage-activated IA current with a role in spike timing and locomotor pattern generation. *Proc Natl Acad Sci USA* 98: 5276–5281, 2001.

62. Hinterkeuser S, Schroder W, Hager G, Seifert G, Blumcke I, Elger CE, Schramm J, Steinhauser C. Astrocytes in the hippocampus of patients with temporal lobe epilepsy display changes in potassium conductances. *Eur J Neurosci* 12: 2087–2096, 2000.

63. Hochman DW, D'Ambrosio R, Janigro D, Schwartzkroin PA. Extracellular chloride and the maintenance of spontaneous epileptiform activity in rat hippocampal slices. *J Neurophysiol* 81: 49–59, 1999.

64. Hochman DW, Schwartzkroin PA. Chloride-cotransport blockade desynchronizes neuronal discharge in the "epileptic" hippocampal slice. *J Neurophysiol* 83: 406–417, 2000.

65. Hounsgaard J, Nicholson C. Potassium accumulation around individual purkinje cells in cerebellar slices from the guinea-pig. *J Physiol* 340: 359–388, 1983.

66. Huguenard JR. Low-threshold calcium currents in central nervous system neurons. *Ann Rev Physiol* 58: 329–348, 1996.

67. Huh Y, Cho J. Discrete pattern of burst stimulation in the ventrobasal thalamus for anti-nociception. *PLos One* 8: e67655, 2013.

68. Jasinski PE, Molkov YI, Shevtsova NA, Smith JC, Rybak IA. Sodium and calcium mechanisms of rhythmic bursting in excitatory neural networks of the pre-Botzinger complex: a computational modelling study. *Eur J Neurosci* 37: 212–230, 2013.

69. Jayakumar AR, Norenberg MD. The Na-K-Cl Cotransporter in astrocyte swelling. *Metab Brain Dis* 25: 31–38, 2010.

70. Jensen MS, Yaari Y. Role of intrinsic burst firing, potassium accumulation, and electrical coupling in the elevated potassium model of hippocampal epilepsy. *J Neurophysiol* 77: 1224–1233, 1997.

71. Ji H, Shepard PD. SK Ca^{2+}-activated K^+ channel ligands alter the firing pattern of dopamine-containing neurons in vivo. *Neuroscience* 140: 623–633, 2006.

72. Jinno S, Ishizuka S, Kosaka T. Ionic currents underlying rhythmic bursting of ventral mossy cells in the developing mouse dentate gyrus. *Eur J Neurosci* 17: 1338–1354, 2003.

73. Johnson SM, Smith JC, Funk GD, Feldman JL. Pacemaker behavior of respiratory neurons in medullary slices from neonatal rat. *J Neurophysiol* 72: 2598–2608, 1994.

74. Karus C, Mondragao MA, Ziemens D, Rose CR. Astrocytes restrict discharge duration and neuronal sodium loads during recurrent network activity. *Glia* 63: 936–957, 2015.

75. Kivi A, Lehmann TN, Kovacs R, Eilers A, Jauch R, Meencke HJ, von Deimling A, Heinemann U, Gabriel S. Effects of barium on stimulus-induced rises of $[K^+]_o$ in human epileptic non-sclerotic and sclerotic hippocampal area CA1. *Eur J Neurosci* 12: 2039–2048, 2000.

76. Kofuji P, Newman EA. Potassium buffering in the central nervous system. *Neuroscience* 129: 1045–1056, 2004.

77. Kroeger D, Tamburri A, Amzica F, Sik A. Activity-dependent layer-specific changes in the extracellular chloride concentration and chloride driving force in the rat hippocampus. *J Neurophysiol* 103: 1905–1914, 2010.

78. Kuhn AA, Trottenberg T, Kivi A, Kupsch A, Schneider GH, Brown P. The relationship between local field potential and neuronal discharge in the subthalamic nucleus of patients with Parkinson's disease. *Exp Neurol* 194: 212–220, 2005.

79. Kuhn AA, Williams D, Kupsch A, Limousin P, Hariz M, Schneider GH, Yarrow K, Brown P. Event-related beta desynchronization in human subthalamic nucleus correlates with motor performance. *Brain* 127: 735–746, 2004.

80. Langer J, Rose CR. Synaptically induced sodium signals in hippocampal astrocytes in situ. *J Physiol* 587: 5859–5877, 2009.

81. Lascola CD, Kraig RP. Whole-cell chloride currents in rat astrocytes accompany changes in cell morphology. *J Neurosci* 16: 2532–2545, 1996.

82. Latour I, Hamid J, Beedle AM, Zamponi GW, Macvicar BA. Expression of voltage-gated Ca^{2+} channel subtypes in cultured astrocytes. *Glia* 41: 347–353, 2003.

83. Launay P, Fleig A, Perraud AL, Scharenberg AM, Penner R, Kinet JP. TRPM4 is a Ca^{2+}-activated nonselective cation channel mediating cell membrane depolarization. *Cell* 109: 397–407, 2002.

84. Lee D. Coherent oscillations in neuronal activity of the supplementary motor area during a visuomotor task. *J Neurosci* 23: 6798–6809, 2003.

85. Lee DJ, Hsu MS, Seldin MM, Arellano JL, Binder DK. Decreased expression of the glial water channel aquaporin-4 in the intrahippocampal kainic acid model of epileptogenesis. *Exp Neurol* 235: 246–255, 2012.

86. Li Z, Hatton GI. Oscillatory bursting of phasically firing rat supraoptic neurones in low-Ca^{2+} medium: Na^+ influx, cytosolic Ca^{2+} and gap junctions. *J Physiol* 496: 379–394, 1996.

87. Lian XY, Stringer JL. Astrocytes contribute to regulation of extracellular calcium and potassium in the rat cerebral cortex during spreading depression. *Brain Res* 1012: 177–184, 2004.

88. Liao YF, Tsai ML, Chen CC, Yen CT. Involvement of the CaV3.2 T-type calcium channel in thalamic neuron discharge patterns. *Mol Pain* 7: 43, 2011.

89. Liu Y, Harding M, Pittman A, Dore J, Striessnig J, Rajadhyaksha A, Chen X. CaV1.2 CaV1.3 L-type calcium channels regulate dopaminergic firing activity in the mouse ventral tegmental area. *J Neurophysiol* 112: 1119–1130, 2014.

90. Luthi A, Bal T, McCormick DA. Periodicity of thalamic spindle waves is abolished by ZD7288,a blocker of Ih. *J Neurophysiol* 79: 3284–3289, 1998.

91. Luu P, Tucker DM, Makeig S. Frontal midline theta and the error-related negativity: neurophysiological mechanisms of action regulation. *Clin Neurophysiol* 115: 1821–1835, 2004.

92. MacGregor DJ, Leng G. Phasic firing in vasopressin cells: understanding its functional significance through computational models. *PLoS Comp Biol* 8: e1002740, 2012.

93. Maier JX, Neuhoff JG, Logothetis NK, Ghazanfar AA. Multisensory integration of looming signals by rhesus monkeys. *Neuron* 43: 177–181, 2004.

94. Mani RS, Boyes BE, Kay CM. Physicochemical and optical studies on calcium- and potassium-induced conformational changes in bovine brain S-100b protein. *Biochemistry* 21: 2607–2612, 1982.

95. Mani RS, Shelling JG, Sykes BD, Kay CM. Spectral studies on the calcium binding properties of bovine brain S-100b protein. *Biochemistry* 22: 1734–1740, 1983.

96. Marchetti C, Beato M, Nistri A. Evidence for increased extracellular K^+ as an important mechanism for dorsal root induced alternating rhythmic activity in the neonatal rat spinal cord in vitro. *Neurosci Lett* 304: 77–80, 2001.

97. Medici V, Frassoni C, Tassi L, Spreafico R, Garbelli R. Aquaporin 4 expression in control and epileptic human cerebral cortex. *Brain Res* 1367: 330–339, 2011.

98. Mirmiran M, Corner M. Neuronal discharge patterns in the occipital cortex of developing rats during active and quiet sleep. *Brain Res* 255: 37–48, 1982.

99. Moody WJ, Futamachi KJ, Prince DA. Extracellular potassium activity during epileptogenesis. *Exp Neurol* 42: 248–263, 1974.

100. Moraes DJ, da Silva MP, Bonagamba LG, Mecawi AS, Zoccal DB, Antunes-Rodrigues J, Varanda WA, Machado BH. Electrophysiological properties of rostral ventrolateral medulla presympathetic neurons modulated by the respiratory network in rats. *J Neurosci* 33: 19223–19237, 2013.

101. Morquette P, Verdier D, Kadala A, Fethiere J, Philippe AG, Robitaille R, Kolta A. An astrocyte-dependent mechanism for neuronal rhythmogenesis. *Nat Neurosci* 18: 844–854, 2015.

102. Mrejeru A, Wei A, Ramirez JM. Calcium-activated non-selective cation currents are involved in generation of tonic and bursting activity in dopamine neurons of the substantia nigra pars compacta. *J Physiol* 589: 2497–2514, 2011.

103. Muller M, Schlue WR. Macroscopic and single-channel chloride currents in neuropile glial cells of the leech central nervous system. *Brain Res* 781: 307–319, 1998.

104. Muramatsu Y, Kurosaki R, Watanabe H, Michimata M, Matsubara M, Imai Y, Araki T. Expression of S-100 protein is related to neuronal damage in MPTP-treated mice. *Glia* 42: 307–313, 2003.

105. Nagelhus EA, Mathiisen TM, Ottersen OP. Aquaporin-4 in the central nervous system: cellular and subcellular distribution and coexpression with KIR4.1. *Neuroscience* 129: 905–913, 2004.

106. Neckelmann D, Amzica F, Steriade M. Spike-wave complexes and fast components of cortically generated seizures. III. Synchronizing mechanisms. *J Neurophysiol* 80: 1480–1494, 1998.

107. Neprasova H, Anderova M, Petrik D, Vargova L, Kubinova S, Chvatal A, Sykova E. High extracellular K^+ evokes changes in voltage-dependent K^+ and Na^+ currents and volume regulation in astrocytes. *Pflügers Arch* 453: 839–849, 2007.

108. Newman EA, Zahs KR. Modulation of neuronal activity by glial cells in the retina. *J Neurosci* 18: 4022–4028, 1998.

109. Nicholson C, Bruggencate GT, Steinberg R, Stockle H. Calcium modulation in brain extracellular microenvironment demonstrated with ion-selective micropipette. *Proc Natl Acad Sci USA* 74: 1287–1290, 1977.

110. Nishimura Y, Asahi M, Saitoh K, Kitagawa H, Kumazawa Y, Itoh K, Lin M, Akamine T, Shibuya H, Asahara T, Yamamoto T. Ionic mechanisms underlying burst firing of layer III sensorimotor cortical neurons of the cat: an in vitro slice study. *J Neurophysiol* 86: 771–781, 2001.

111. Noda H, Mikami A. Discharges of neurons in the dorsal parafloccullus of monkeys during eye movements and visual stimulation. *J Neurophysiol* 56: 1129–1146, 1986.

112. O'Connor ER, Sontheimer H, Spencer DD, de Lanerolle NC. Astrocytes from human hippocampal epileptogenic foci exhibit action potential-like responses. *Epilepsia* 39: 347–354, 1998.

113. Oke OO, Magony A, Anver H, Ward PD, Jiruska P, Jefferys JG, Vreugdenhil M. High-frequency gamma oscillations coexist with low-frequency gamma oscillations in the rat visual cortex in vitro. *Eur J Neurosci* 31: 1435–1445, 2010.

114. Onimaru H, Arata A, Homma I. Intrinsic burst generation of preinspiratory neurons in the medulla of brainstem-spinal cord preparations isolated from newborn rats. *Exp Brain Res* 106: 57–68, 1995.

115. Orkand RK, Nicholls JG, Kuffler SW. Effect of nerve impulses on the membrane potential of glial cells in the central nervous system of amphibia. *J Neurophysiol* 29: 788–806, 1966.

116. Pace RW, Mackay DD, Feldman JL, Del Negro CA. Inspiratory bursts in the preBotzinger complex depend on a calcium-activated non-specific cation current linked to glutamate receptors in neonatal mice. *J Physiol* 582: 113–125, 2007.

117. Panaitescu B, Ruangkittisakul A, Ballanyi K. Silencing by raised extracellular Ca^{2+} of pre-Botzinger complex neurons in newborn rat brainstem slices without change of membrane potential or input resistance. *Neurosci Lett* 456: 25–29, 2009.

118. Payne JA, Rivera C, Voipio J, Kaila K. Cation-chloride co-transporters in neuronal communication, development and trauma. *Trends Neurosci* 26: 199–206, 2003.

119. Pena F, Parkis MA, Tryba AK, Ramirez JM. Differential contribution of pacemaker properties to the generation of respiratory rhythms during normoxia and hypoxia. *Neuron* 43: 105–117, 2004.

120. Perez-Reyes E. Molecular physiology of low-voltage-activated t-type calcium channels. *Physiol Rev* 83: 117–161, 2003.

121. Pinto DJ, Patrick SL, Huang WC, Connors BW. Initiation, propagation, and termination of epileptiform activity in rodent neocortex in vitro involve distinct mechanisms. *J Neurosci* 25: 8131–8140, 2005.

122. Putzier I, Kullmann PH, Horn JP, Levitan ES. CaV1.3 channel voltage dependence, not Ca^{2+} selectivity, drives pacemaker activity and amplifies bursts in nigral dopamine neurons. *J Neurosci* 29: 15414–15419, 2009.

123. Ransdell JL, Temporal S, West NL, Leyrer ML, Schulz DJ. Characterization of inward currents and channels underlying burst activity in motoneurons of crab cardiac ganglion. *J Neurophysiol* 110: 42–54, 2013.

124. Reyes RC, Verkhratsky A, Parpura V. Plasmalemmal Na^+/Ca^{2+} exchanger modulates Ca^{2+}-dependent exocytotic release of glutamate from rat cortical astrocytes. *ASN Neuro* 4: 2012.

125. Richter DW, Camerer H, Sonnhof U. Changes in extracellular potassium during the spontaneous activity of medullary respiratory neurones. *Pflügers Arch* 376: 139–149, 1978.

126. Robinson RB, Siegelbaum SA. Hyperpolarization-activated cation currents: from molecules to physiological function. *Ann Rev Physiol* 65: 453–480, 2003.

127. Rojas H, Ramos M, Benaim G, Caputo C, DiPolo R. The activity of the Na^+/Ca^{2+} exchanger largely modulates the $Ca^{2+}{}_i$ signal induced by hypo-osmotic stress in rat cerebellar astrocytes. The effect of osmolarity on exchange activity. *J Physiol Sci* 58: 277–279, 2008.

128. Rose CR, Karus C. Two sides of the same coin: sodium homeostasis and signaling in astrocytes under physiological and pathophysiological conditions. *Glia* 61: 1191–1205, 2013.

129. Rose CR, Ransom BR. Regulation of intracellular sodium in cultured rat hippocampal neurones. *J Physiol* 499: 573–587, 1997.

130. Rubin JE, Hayes JA, Mendenhall JL, Del Negro CA. Calcium-activated nonspecific cation current and synaptic depression promote network-dependent burst oscillations. *Proc Natl Acad Sci USA* 106: 2939–2944, 2009.

131. Rubino D, Robbins KA, Hatsopoulos NG. Propagating waves mediate information transfer in the motor cortex. *Nat Neurosci* 9: 1549–1557, 2006.

132. Rybak IA, Shevtsova NA, St-John WM, Paton JF, Pierrefiche O. Endogenous rhythm generation in the pre-Botzinger complex and ionic currents: modelling and in vitro studies. *Eur J Neurosci* 18: 239–257, 2003.

133. Sakatani S, Seto-Ohshima A, Itohara S, Hirase H. Impact of S100B on local field potential patterns in anesthetized and kainic acid-induced seizure conditions in vivo. *Eur J Neurosci* 25: 1144–1154, 2007.

134. Sakatani S, Seto-Ohshima A, Shinohara Y, Yamamoto Y, Yamamoto H, Itohara S, Hirase H. Neural-activity-dependent release of S100B from astrocytes enhances kainate-induced gamma oscillations in vivo. *J Neurosci* 28: 10928–10936, 2008.

135. Sathe K, Maetzler W, Lang JD, Mounsey RB, Fleckenstein C, Martin HL, Schulte C, Mustafa S, Synofzik M, Vukovic Z, Itohara S, Berg D, Teismann P. S100B is increased in Parkinson's disease and ablation protects against MPTP-induced toxicity through the RAGE and TNF-alpha pathway. *Brain* 135: 3336–3347, 2012.

136. Scemes E, Spray DC. Extracellular K^+ and astrocyte signaling via connexin and pannexin channels. *Neurochem Res* 37: 2310–2316, 2012.

137. Schnell C, Fresemann J, Hulsmann S. Determinants of functional coupling between astrocytes and respiratory neurons in the pre-Botzinger complex. *PLos One* 6: e26309, 2011.

138. Sederberg PB, Schulze-Bonhage A, Madsen JR, Bromfield EB, McCarthy DC, Brandt A, Tully MS, Kahana MJ. Hippocampal and neocortical gamma oscillations predict memory formation in humans. *Cereb Cortex* 17: 1190–1196, 2007.

139. Sharott A, Doig NM, Mallet N, Magill PJ. Relationships between the firing of identified striatal interneurons and spontaneous and driven cortical activities in vivo. *J Neurosci* 32: 13221–13236, 2012.

140. Somjen GG. Extracellular potassium in the mammalian central nervous system. *Ann Rev Physiol* 41: 159–177, 1979.

141. Somjen GG, Muller M. Potassium-induced enhancement of persistent inward current in hippocampal neurons in isolation and in tissue slices. *Brain Res* 885: 102–110, 2000.

142. Sontheimer H. Voltage-dependent ion channels in glial cells. *Glia* 11: 156–172, 1994.

143. Spain WJ, Schwindt PC, Crill WE. Anomalous rectification in neurons from cat sensorimotor cortex in vitro. *J Neurophysiol* 57: 1555–1576, 1987.

144. Steriade M, Nunez A, Amzica F. Intracellular analysis of relations between the slow (<1 Hz) neocortical oscillation and other sleep rhythms of the electroencephalogram. *J Neurosci* 13: 3266–3283, 1993.

145. Stockle H, Ten Bruggencate G. Fluctuation of extracellular potassium and calcium in the cerebellar cortex related to climbing fiber activity. *Neuroscience* 5: 893–901, 1980.

146. Su H, Alroy G, Kirson ED, Yaari Y. Extracellular calcium modulates persistent sodium current-dependent burst-firing in hippocampal pyramidal neurons. *J Neurosci* 21: 4173–4182, 2001.

147. Subbarao KV, Stolzenburg JU, Hertz L. Pharmacological characteristics of potassium-induced, glycogenolysis in astrocytes. *Neurosci Lett* 196: 45–48, 1995.

148. Tas PW, Massa PT, Kress HG, Koschel K. Characterization of an $Na^+/K^+/Cl^-$ co-transport in primary cultures of rat astrocytes. *Biochim Biophys Acta* 903: 411–416, 1987.

149. Tazerart S, Vinay L, Brocard F. The persistent sodium current generates pacemaker activities in the central pattern generator for locomotion and regulates the locomotor rhythm. *J Neurosci* 28: 8577–8589, 2008.

150. Thimm J, Mechler A, Lin H, Rhee S, Lal R. Calcium-dependent open/closed conformations and interfacial energy maps of reconstituted hemichannels. *J Biol Chem* 280: 10646–10654, 2005.

151. Trevelyan AJ, Sussillo D, Watson BO, Yuste R. Modular propagation of epileptiform activity: evidence for an inhibitory veto in neocortex. *J Neurosci* 26: 12447–12455, 2006.

152. Tsuruyama K, Hsiao CF, Chandler SH. Participation of a persistent sodium current and calcium-activated nonspecific cationic current to burst generation in trigeminal principal sensory neurons. *J Neurophysiol* 110: 1903–1914, 2013.

153. Uhlhaas PJ, Singer W. Neural synchrony in brain disorders: relevance for cognitive dysfunctions and pathophysiology. *Neuron* 52: 155–168, 2006.

154. Ullrich ND, Voets T, Prenen J, Vennekens R, Talavera K, Droogmans G, Nilius B. Comparison of functional properties of the Ca^{2+}-activated cation channels TRPM4 and TRPM5 from mice. *Cell Calcium* 37: 267–278, 2005.

155. Van Eldik LJ, Zimmer DB. Secretion of S-100 from rat C6 glioma cells. *Brain Res* 436: 367–370, 1987.

156. Vega-Saenz de Miera EC, Rudy B, Sugimori M, Llinas R. Molecular characterization of the sodium channel subunits expressed in mammalian cerebellar Purkinje cells. *Proc Natl Acad Sci USA* 94: 7059–7064, 1997.

157. Verkhratsky A, Steinhauser C. Ion channels in glial cells. *Brain Res Brain Res Rev* 32: 380–412, 2000.

158. Wallen P, Grafe P, Grillner S. Phasic variations of extracellular potassium during fictive swimming in the lamprey spinal cord in vitro. *Acta Physiol Scand* 120: 457–463, 1984.

159. Wang XJ. Neurophysiological and computational principles of cortical rhythms in cognition. *Physiol Rev* 90: 1195–1268, 2010.

160. Westenbroek RE, Bausch SB, Lin RC, Franck JE, Noebels JL, Catterall WA. Upregulation of L-type Ca^{2+} channels in reactive astrocytes after brain injury, hypomyelination, and ischemia. *J Neurosci* 18: 2321–2334, 1998.

161. Xu L, Zeng LH, Wong M. Impaired astrocytic gap junction coupling and potassium buffering in a mouse model of tuberous sclerosis complex. *Neurobiol Disease* 34: 291–299, 2009.

162. Xu W, Lipscombe D. Neuronal Ca(V)1.3alpha(1) L-type channels activate at relatively hyperpolarized membrane potentials and are incompletely inhibited by dihydropyridines. *J Neurosci* 21: 5944–5951, 2001.

163. Zanotti S, Charles A. Extracellular calcium sensing by glial cells: low extracellular calcium induces intracellular calcium release and intercellular signaling. *J Neurochem* 69: 594–602, 1997.

164. Zhang B, Wootton JF, Harris-Warrick RM. Calcium-dependent plateau potentials in a crab stomatogastric ganglion motor neuron. II. Calcium-activated slow inward current. *J Neurophysiol* 74: 1938–1946, 1995.

Jean-Pierre Gossard, Réjean Dubuc and Arlette Kolta (Eds.)
Progress in Brain Research, Vol. 187
ISSN: 0079-6123

CHAPTER 9

Modulation of rhythmogenic properties of trigeminal neurons contributing to the masticatory CPG

Arlette Kolta*, Philippe Morquette, Raphaël Lavoie, Isabel Arsenault and Dorly Verdier

Faculté de médecine dentaire and Groupe de Recherche sur le Système Nerveux Central du FRSQ, Université de Montréal, Succursale Centre-ville, Montreal, Quebec, Canada

Abstract: Increasing evidence suggests that the dorsal part of the principal sensory nucleus of the trigeminal nerve (NVsnpr) contains a significant core of the central pattern generator (CPG) circuitry required for mastication (Tsuboi et al., 2003). Like many trigeminal brainstem neurons, those of NVsnpr are rhythmically active in phase with fictive mastication *in vivo* (Tsuboi et al., 2003) and project directly to the trigeminal motoneurons (Kolta et al., 2000), but in contrast with the others, they are the only neurons with intrinsic bursting abilities (Sandler et al., 1998; Brocard et al., 2006) within the minimal area of the brainstem necessary to produce rhythmic activity in trigeminal nerves (Bourque and Kolta, 2001). Development of bursting in NVsnpr neurons closely follows the development of mastication. It is mediated by a persistent Na^+ current (I_{NaP}) that is expressed only within a certain membrane potential range and that is modulated by the extracellular Ca^{2+} concentration ($[Ca^{2+}]_e$), the lower the concentration, the larger the magnitude of I_{NaP}. Under physiological $[Ca^{2+}]_e$, bursting can also be induced *in vitro* by repetitive electrical stimulation of the trigeminal sensory tract, which projects massively to NVsnpr or by local applications of *N*-methyl-D-aspartic acid. Both types of stimuli also depolarize glial cells recorded in NVsnpr and increase coupling between them. Glial cells play a determinant role in setting $[Ca^{2+}]_e$ and hence are in a key position to influence NVsnpr neuronal firing pattern.

Keywords: Mastication; central pattern generator; rhythmogenesis; I_{NaP}; bursting; calcium; sensory modulation.

* Corresponding author.
Tel.: +1-514-343-7112; Fax: +1-514-343-2111

DOI: 10.1016/S0079-6123(10)87009-8

As everyone knows food intake is essential for life. Ingested food must be broken down in pieces and prepared for digestion. This is done by chewing. Mastication seems like a simple act, but in fact, it requires orchestration of more than 20 oro-facial muscles or muscle compartments and needs to be coordinated with swallowing and respiration. A century ago, (Sherrington, 1917) proposed that mastication was a chain of alternating jaw opening and jaw closing reflexes, even if (Ferrier, 1873) had already shown that it could be induced by stimulating the cerebral cortex in several species of animals. It is only much later, in the early 1970s that Lund and Dellow (1971) showed that the basic pattern of mastication is produced by a brainstem CPG.

Boundaries and components of the CPG

Despite the fact that the brainstem location of the masticatory central pattern generator (CPG) has been identified nearly 40 years ago, its exact boundaries and the elements that form it have not been unequivocally described yet. In the mid-1980s, *in vivo* studies suggested that the essential core of the CPG lies between the rostral poles of the trigeminal (NVmt) and hypoglossal (NXII) motor nuclei. However, it was difficult to ascertain in those studies that the manipulations executed to isolate the masticatory CPG did not also affect the vital and respiratory brainstem centers (Nozaki et al., 1986a,b). Later, transection studies on "en bloc" brainstem preparations showed that rhythmical activity elicited in trigeminal nerves by addition of *N*-methyl-D-aspartic acid (NMDA) to the bath persists as long as a bloc (gray shadow box in Fig. 1) extending from the rostral pole of NVmt to the rostral pole of the facial nucleus and approximately half a millimeter from the lateral border of the brainstem remains intact (Kogo et al., 1996; Tanaka et al., 1999).

This area contains the trigeminal motoneurons embedded in a column of premotor interneurons forming the peritrigeminal area (Peri V) and lateral to which extends the trigeminal sensory complex composed at this level by the trigeminal main sensory nucleus (NVsnpr) and the rostral pole of the spinal nucleus (Fig. 1). Rhythmic activity has been recorded in neurons of all of those nuclei during fictive mastication; that is, mastication elicited by stimulation of the cortical masticatory area in paralyzed and anesthetized animals. Because there is actually no movement and thus no rhythmic sensory feedback, rhythmic firing recorded under these conditions results from activity of rhythmogenic neurons or from inputs received from these rhythmogenic neurons.

Rhythmic outputs of CPGs can result from intrinsic properties of individual neurons ("pacemaker neurons"), from interactions within a network ("network pacemaker"), or a combination of the two (see Chapters 8 and 14). We used an

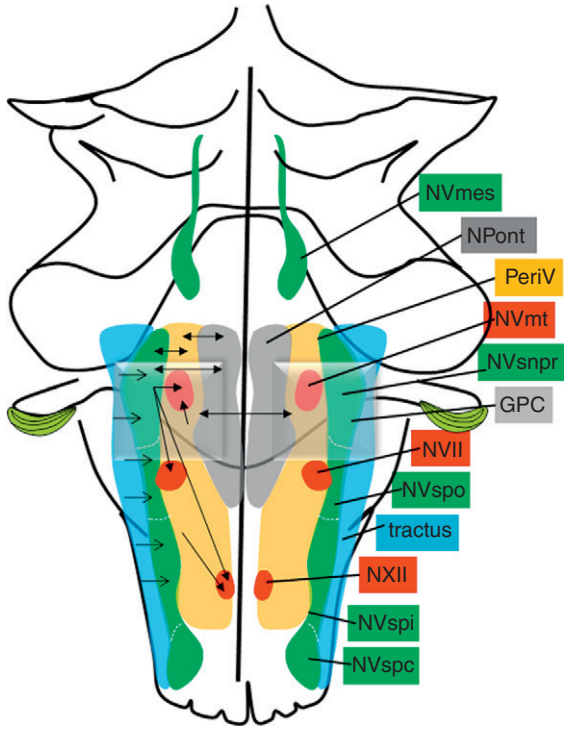

Fig. 1. Schematic representation of the brainstem nuclei involved in oro-facial movements and their connections (arrows). The gray 3D box defines the boundaries of the masticatory CPG.

in vitro slice preparation of rat brainstem to examine the intrinsic properties and synaptic inputs of most groups of neurons within the critical brainstem area essential for mastication, and found that most premotor interneurons of the Peri V could not generate rhythmic activity either intrinsically or through the robust reciprocal connections that they shared (Bourque and Kolta, 2001), except for about 5% of those recorded in the area dorsal and slightly lateral to NVmt, called the supratrigeminal area. However, the dorsal part of NVsnpr immediately adjacent to these few bursting neurons was found to contain a large population of rhythmically firing neurons.

This was a surprise because this nucleus is generally considered as a sensory relay station that faithfully transmits inputs from primary afferents to the thalamus. Sandler et al. (1998) had shown that about half of NVsnpr neurons recorded *in vitro* in slices of the gerbil brainstem have plateau properties that allow them to transform a depolarizing input into bursts which was a puzzling property for neurons with this putative function, and there was anecdotal descriptions (including some of our work) in the literature of projections from NVsnpr to motor nuclei that control the muscles responsible for feeding, the Vth, VIIth, and XIIth motor nuclei (Kolta et al., 2000; Li et al., 1993; Pinganaud et al., 1999; Travers and Norgren, 1983; Yoshida et al., 1998), but there had been no attempt to interpret the functional significance of these data.

Therefore, we decided to investigate the firing of NVsnpr neurons during fictive mastication. A quarter of the neurons recorded throughout the nucleus changed their firing patterns during fictive mastication induced by repetitive stimulation of the left and right cortical masticatory areas and only about a third of these fired rhythmically in phase with trigeminal motoneurons. The others discharged in bursts at more than twice the frequency of trigeminal motoneurons. Most rhythmic masticatory neurons had inputs from muscle spindle afferents and periodontal receptors and were concentrated in the dorsal part, whereas nonmasticatory rhythmical neurons had receptive fields on the lips and face and were spread throughout the nucleus but were denser in the ventral part of NVsnpr. The latter may have been related to whisking. Later, using the expression of c-Fos-like protein as a functional marker of activity, we showed that the activity level increases induced by fictive mastication appear only in dorsal NVsnpr (Athanassiadis et al., 2005).

Development of bursting properties in relation to mastication

On the basis of this evidence, we decided to further investigate the intrinsic properties of NVsnpr neurons in the *in vitro* slice preparation. Under standard control conditions, two-thirds of the population fired tonically upon depolarization, while the others had one or several bursts of action potentials upon depolarization. Bursting occurred almost exclusively in the dorsal part of the nucleus and was maintained and even enhanced under conditions that reduce synaptic transmission (removal of Ca^{2+} from the artificial cerebrospinal fluid [aCSF] used to perfuse the preparation), suggesting that it is an intrinsic property of NVsnpr neurons.

One of the first interesting observations that we made was that these intrinsic bursting properties develop in parallel with mastication. In rats, the transition from suckling to chewing occurs gradually over nearly a week. The first masticatory movements appear around postnatal day 12, and the adult pattern is fully established between postnatal day 18 and day 21 (Westneat and Hall, 1992). It is unclear whether mastication and suckling depend on the same CPG network which evolve during that period or on different CPGs. Both movements involve jaw opening and closing, but in one case, chewing, the power stroke occurs during jaw closure, while in the other it occurs during opening with the tongue moving in peristaltic manner. Over the period of transition from suckling to adult mastication, the membrane properties of

NVsnpr neurons undergo important changes (Brocard et al., 2006); particularly those that determine the ability to generate rhythmic bursting. By postnatal day 10 (P10), some neurons generate one or more bursts at the onset of depolarization (~5%). The frequency of occurrence increases abruptly after P12 (25%) and by P14, about 45% of dorsal NVsnpr cells discharge bursts during sustained depolarization, and 25% of these do this repetitively. In these, bursting frequency is linearly related to injected current. In Ca^{2+}-free aCSF, the proportion of cells expressing recurrent bursting increased at all ages, but displayed the same developmental profile (<15% at P10; ~55% at P10–12; >85% at P16–17). In the same time frame, the proportion of cells showing an afterdepolarization (ADP) after the spike increased in parallel and there was a clear correlation between the presence of ADP and the ability to burst.

Similar age-related changes in membrane properties occur in other brainstem nuclei including the more ventral region of NVsnpr containing whisking-related neurons (Lo and Erzurumlu, 2001), the spinal trigeminal nucleus (Guido et al., 1998), and in several other brainstem regions (Bao et al., 1995; Berger et al., 1996; Nguyen et al., 2004; Núñez-Abades et al., 1993; Tanaka et al., 2003; Tsuzuki et al., 1995).

Mechanisms of rhythmogenesis

Our evidence (see Brocard et al., 2006 and Kolta et al., 2007) suggests that bursting is primarily mediated by a persistent sodium conductance (I_{NaP}), which is also responsible for burst firing in neurons of the pre-Bötzinger complex (Butera et al., 1999; Del Negro et al., 2002, 2005), cultured spinal cord (Darbon et al., 2004), mouse spinal locomotor CPG (Tazerart et al., 2007; Zhong et al., 2007), hippocampus (Azouz et al., 1996; Jinno et al., 2003; Mattia et al., 1997; Su et al., 2001), subthalamic nucleus (Beurrier et al., 2000), neocortex (Brumberg et al., 2000; Franceschetti et al., 1995; Guatteo et al., 1996), and trigeminal primary afferents of the mesencephalic nucleus (Wu et al., 2005). First, bursting persisted in Ca^{2+}-free aCSF and in presence of a Ca^{2+} chelator (1,2-bis (*o*-aminophenoxy)ethane-*N*,*N*,*N*′,*N*′-tetraacetic acid [BAPTA]) injected into recorded cells ruling out involvement of Ca^{2+}-mediated currents. It was not affected by blockers of voltage-activated (tetraethylammonium [TEA]) and Ca^{2+}-activated (apamine and charybdotoxin) K^+ currents, although TEA substantially increased the duration of bursts and charybdotoxin (blocker of BK_{Ca}) increased the amplitude and duration of the ADP facilitating the transition from single spike firing to firing in doublets or triplets. Most importantly, Riluzole, which suppresses I_{NaP} predominately (Urbani and Belluzzi, 2000; Wu et al., 2005), and tetrodotoxin (TTX), inhibited bursts and the underlying plateau potentials. The TTX-sensitive plateau potentials and bursts are only seen within a voltage range that corresponds to the activation and steady-state inactivation voltages typical of I_{NaP} (Crill, 1996) and both the plateau potential and bursting emerge during the second postnatal week, which corresponds with the developmental profile characteristic of I_{NaP} (Alzheimer et al., 1993; Huguenard et al., 1988) and appearance of bursting in other areas of the brain (Franceschetti et al., 1993, 1998; Kriegstein et al., 1987). Finally, lowering the extracellular Ca^{2+} concentration ($[Ca^{2+}]_e$) increases the amplitude of the ADP as well as the proportion of neurons that burst and the duration of TTX-sensitive plateau potentials (Brocard et al., 2006). These results indicate that $[Ca^{2+}]_e$ regulates the firing pattern of NVsnpr neurons by modulating the magnitude of I_{NaP}. A similar relationship has been found in spinal interneurons thought to be part of the locomotor CPG (Tazerart et al., 2008) and several other areas of the central nervous system (Azouz et al., 1996; Li and Hatton, 1996; Su et al., 2001).

To summarize, NVsnpr neurons have intrinsic bursting properties, mediated by I_{NaP}, but expression of these properties depends on factors external to the cell (network properties?). We suggest that the Ca^{2+}-sensitivity of I_{NaP} provides a mean for the system to trigger bursting when

appropriate and to modulate bursting frequency in function of inputs (whether sensory or other). In other words, Ca^{2+}-dependency may be the mechanism that enables sensory and/or cortical feedback to adjust the output pattern.

Pattern variability and sensory modulation of CPGs

By definition, CPGs can generate a rhythmic output in absence of any input. This is not to say that inputs to CPGs do not play an important role. It is well known that sensory feedback is essential to adapt the movement pattern to the prevailing conditions. In absence of cortical or sensory inputs, CPGs produce stereotyped movements that would be identical from cycle to cycle. However, as everyone has experienced before, the form of masticatory movements varies between foods and even within a single masticatory sequence. Cortical input to the masticatory CPG is thought to play an important role in anticipating the pattern of movements required, while sensory inputs provide feedback to adjust the movements to the changes in texture and hardness, error corrections, and to counteract unexpected perturbations. This, of course, is not unique to the masticatory CPG. Many studies in different systems have reported about the importance of sensory feedback in determining different parameters of the movement pattern and phase transition (for review, see Rossignol et al., 1988) but very few have examined the cellular mechanisms at the basis of this interaction between sensory inputs and the rhythm generating neurons. For instance, stretch of pulmonary muscle spindle afferents and diaphragmatic proprioceptors contributes to the termination of inspiration (Speck et al., 1993), while flexing the hip can profoundly alter the locomotor pattern and even block completely the locomotion (Pearson and Rossignol, 1991). In the masticatory system, as the teeth bite into the food, pressure builds within the periodontal ligament and the velocity of closure drops rapidly, causing activation of periodontal receptors (Olsson et al., 1988) and jaw closing muscle spindle afferents (Goodwin and Luschei, 1975). In both cases, this activation is proportional to the food resistance and is determinant for the duration and amplitude of the electromyogram bursts of the jaw closing muscles (Komuro et al., 2001; Lavigne et al., 1987). Coincidently, these are precisely the inputs received by most dorsal NVsnpr neurons that fired rhythmically in phase with trigeminal motoneurons during fictive mastication (Tsuboi et al., 2003). How signals from these afferents interact with the rhythmogenic properties of NVsnpr is still unknown.

Putative cellular mechanisms underlying sensory modulation of bursting in NVsnpr neurons

In *in vivo* animal experimental models, mastication can be elicited by repetitive stimulation of the cortical masticatory area or of sensory nerves. In both cases, stimulation needs to last hundreds of milliseconds before mastication is triggered despite the fact that both types of inputs reach most brainstem trigeminal neurons at short latencies (<10 ms). Similarly, mastication continues several hundreds of milliseconds after cessation of stimulation indicating that a slow process is involved in the command.

This observation led us to propose the functional model described in Fig. 2. We postulated that this prolonged activity of afferent inputs causes a drop in $[Ca^{2+}]_e$ that in turn triggers activation of I_{NaP}. Because of the voltage-dependency of I_{NaP}, this would occur only within a defined membrane potential range; between approximately -60 and -50 mV in our cells. Thus, little afferent activity would cause tonic firing in NVsnpr neurons and a slight depolarization, bringing the cell closer to the activation range of I_{NaP} (stage 1 in Fig. 2). Further afferent activity would cause a small reduction of $[Ca^{2+}]_e$, perhaps causing an inactivation of BK_{Ca}-channels (which have a lower Ca^{2+} affinity) switching the afterhyperpolarization (AHP) in an ADP and hence promoting firing in doublets (stage 2 in Fig. 2). Additional activity of afferents would

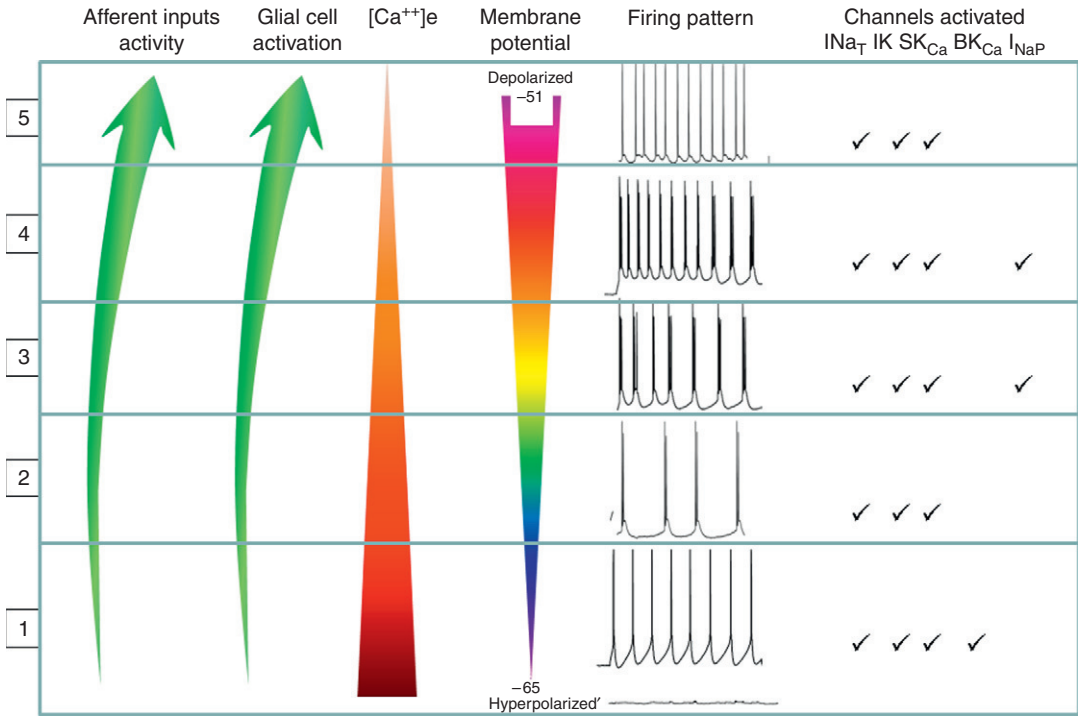

Fig. 2. Functional model of rhythmogenesis in NVsnpr neuron. The model shows the changes in glial cell activation and $[Ca^{2+}]_e$ that could occur as a result of increasing activity in afferent inputs to NVsnpr (going from stages 1 to 5) and the effects that these changes would have on neuronal membrane potential and firing pattern. The right most column shows the ionic channels activated under these different conditions and responsible for the firing pattern represented.

then cause greater Ca^{2+} depletion extracellularly and stronger intracellular depolarization leading to full activation of I_{NaP} and bursting (stage 3 in Fig. 2); bursting frequency being proportional to the depolarization level (stage 4 in Fig. 2). Excessive afferent activity, like would occur if the teeth encountered a hard object for instance, would depolarize the cell above I_{NaP} activation range causing burst termination and reversal to tonic firing (stage 5 in Fig. 2).

According to this model, sustained activation of inputs that normally trigger mastication should elicit rhythmic bursting in NVsnpr neurons. This bursting depends on the cell membrane potential and on the $[Ca^{2+}]_e$.

What are the experimental evidences in support of this model?

As stated above, in *in vitro* slice preparations, bursting is readily observed in NVsnpr neurons when $[Ca^{2+}]_e$ is artificially lowered in the perfusing medium, but we showed in a recent study that under physiological $[Ca^{2+}]_e$ (1.6 mM) repetitive stimulation of the sensory tract containing the fiber terminals of sensory afferents (see arrows in Fig. 1), causes bursting in NVsnpr and synchronization of units (Bernier et al., 2010). Interestingly, the optimal stimulation frequency to elicit bursting was found to be between 40 and 60 Hz, a value close to the natural firing frequency (50 and 60 Hz

during mastication) of the intraoral mechanoreceptors and periodontal receptors which project heavily to dorsal NVsnpr (Appenteng et al., 1982; Trulsson, 2007; Trulsson and Johansson, 2002) and to the optimal stimulation frequency of the cortical masticatory area to elicit mastication *in vivo* (20–100 Hz) (Huang et al., 1989; Lund and Dellow, 1971). Cortical and sensory fibers projecting to NVsnpr are both glutamatergic, so we used local NMDA applications as a mean of mimicking sustained activation of these fibers. In extracellular recordings, local NMDA applications first increased the firing frequency of the recorded units and triggered rhythmic burst firing after a few seconds, when the excitatory effects were wearing off (see Figure 7 of Bernier et al., 2010). NMDA-induced bursting supported by Ca^{2+}-mediated plateau potentials has been described in a number of instances before (Bertrand and Cazalets 2002; Büschges et al., 2000; Gabriel et al. 2008; Hsiao et al. 2002; Zhu et al. 2004). However, the NMDA-induced bursting in NVsnpr neurons probably involves different mechanisms because, in intracellular recordings, it occurs only when hyperpolarizing current is injected into the cell concomitantly to counteract the excessive depolarization produced by NMDA, suggesting a different voltage-dependency from classical NMDA receptors-mediated events. Also, it is insensitive to fluofenic acid (blocker of I_{CAN}) but is readily blocked by Riluzole or TTX.

Thus, the above results suggest that sustained activation of NVsnpr neurons by stimulation of their inputs or application of NMDA elicits bursting. Intense, sustained neuronal activity observed under physiological or pathological conditions has been associated to decreases of $[Ca^{2+}]_e$ in a number of instances (Amzica et al., 2002; Nicholson et al., 1978; Pumain and Heinemann, 1985; Pumain et al., 1983; Somjen, 1980); $[Ca^{2+}]_e$ drops to levels as low as 0.8 mM in the cerebellar cortex of the cat during repetitive local stimulation (Nicholson et al., 1978), 0.1 mM during cortical bursting (Somjen, 1980), and 0.08 mM in rat neocortex after local glutamate application (Amzica et al., 2002). Moreover, bursting in many brain areas is accompanied by drastic drops of $[Ca^{2+}]_e$ (Benninger et al., 1980; Heinnemann et al., 1990; Rusakov and Fine, 2003; for review, see Cohen and Fields, 2004).

Variations of $[Ca^{2+}]_e$ need not to be extreme to induce bursting. In fact, in our hands local extracellular applications of BAPTA triggered bursting in all cells tested ($n=5$) and this bursting was blocked by Riluzole indicating that it was mediated by I_{NaP} (unpublished results).

The next question then is: what causes the $[Ca^{2+}]_e$ drops? Several factors can be responsible for the extracellular Ca^{2+} variations, but implication of glial cells is one of the first that comes to mind given the slow timecourse of the process described above. Glial cells are sensitive to surrounding neuronal activity; they have receptors for many neurotransmitters including glutamate, GABA, acetylcholine, and ATP (for review, see Verkhratsky et al., 1998), and are activated by K^+ released during neuronal firing. Glial processes ensheath synaptic elements (Grosche et al., 1999, 2002; Salpeter, 1987; Spacek, 1985) and evidence is building that glia influences neuronal activity there and at extrasynaptic sites as well by regulating the concentration of several ions (K^+ and Ca^{2+} among others) in the extracellular space and by releasing a number of factors or transmitters such as glutamate, D-serine, ATP, and so on (Auld and Robitaille, 2003). According to a simulation model, activation of a single calcium channel on a glial perisynaptic process could draw nearly all the Ca^{2+} in the synaptic cleft (Smith, 1992). Thus, we propose that glia controls the extracellular levels of Ca^{2+} and by this means plays a role in the onset of bursting. A feature that may be especially important in CPGs is that glial cells form extended networks through which Ca^{2+} waves propagate rapidly via gap junctions. This could provide a way to activate and perhaps eventually synchronize large assemblies of neurons. Bursts would cease with release of Ca^{2+} eventually from neurons and/or glial cells coupled to reduced sensory feedback from softened food.

Such a mechanism would provide an explanation to an observation often made during *in vivo* experiments where mastication stops even when the cortical stimulation goes on.

Preliminary (unpublished) results (Arsenault et al. 2007; Lavoie et al., 2009) indicate that both repetitive stimulation of the sensory fibers and local NMDA applications produce large depolarizations of glial cells recorded in dorsal NVsnpr and dramatically increase coupling between them. Interestingly, glial syncitia formed under these conditions remain confined to dorsal NVsnpr. Finally, addition of carbenoxolone (a blocker of gap junctions) to the bath disrupts NMDA-induced neuronal bursting and we assume that this effect is achieved by an action on glial gap junctions since very little coupling (if any) exists between neurons in this nucleus. Globally, these results point to a possible glial implication.

Conclusion

In summary, NVsnpr neurons can be excited by cortical inputs. They also have sensory inputs from muscle spindle, periodontal, and other intraoral mechanoreceptors, which provide the feedback that is necessary for rapid adaptation of the motor pattern. Most importantly, they are capable of generating bursts within the frequency range of natural mastication, when I_{NaP} is activated. I_{NaP} activation depends on the cell membrane potential and on the $[Ca^{2+}]_e$. This property enables the network to interact with the intrinsic pacemaker properties of the rhythmogenic neurons to elicit rhythmic bursting only under restricted conditions. Glial cells may contribute to this process by controlling $[Ca^{2+}]_e$. In his chapter in this book, Harris-Warrick discusses the necessity of multiple and redundant mechanisms for rhythmogenesis in CPGs that are responsible for vital function. This is clearly the case in the respiratory CPG. We cannot rule out that it may also be the case in the masticatory CPG. However, we also propose that redundancy may not be in the mechanisms as much as in the neuronal population participating to rhythmogenesis. We propose that the rhythmogenic properties reported above are present wherever I_{NaP} is present and will appear in groups of neurons that receive the appropriate level of synchronous input and that are encompassed in an organized glial syncitium. Therefore, the foyer of rhythmogenic neurons may be constantly changing (see also chapter 29) according to the inputs.

It is difficult to conclude this chapter without acknowledging the tremendous contributions of Jim Lund to much of the work and the ideas described above. He is and will remain greatly missed.

Acknowledgment

This work was supported by an operating grant from the CIHR and an infrastructure grant from the FRSQ.

Abbreviations

aCSF	artificial cerebrospinal fluid
ADP	afterdepolarization
AHP	afterhyperpolarization
ATP	adenosine triphosphate
BAPTA	1,2-bis (*o*-aminophenoxy) ethane-*N*,*N*,*N*′,*N*′-tetraacetic acid
BK_{Ca}	big Ca^{2+}-dependent potassium current
$[Ca^{2+}]_e$	extracellular calcium concentration
CPG	central pattern generator
GABA	gamma-aminobutyric acid
I_{CAN}	Ca^{2+}-activated nonspecific cationic current
I_{NaP}	persistent sodium conductance
NMDA	*N*-methyl-D-aspartic acid

NPont	nucleus pontis (caudalis and oralis)
NVmes	trigeminal mesencephalic nucleus
NVmt	trigeminal motor nucleus
NVsnpr	principal sensory nucleus of the trigeminal nerve
NVspc	caudalis area of the spinal nucleus of the trigeminal tract
NVspi	interpolaris area of the spinal nucleus of the trigeminal tract
NVspo	oralis area of the spinal nucleus of the trigeminal tract
NVII	facial nuclei
NXII	hypoglossal motor nuclei
P	postnatal day
Peri V	peritrigeminal area
SK_{Ca}	small Ca^{2+}-dependent potassium currents
TEA	tetraethylammonium
TTX	tetrodotoxin

References

Alzheimer, C., Schwindt, P. C., & Crill, W. E. (1993). Postnatal development of a persistent Na^{+} current in pyramidal neurons from rat sensorimotor cortex. *Journal of Neurophysiology*, *69*, 290–292.

Amzica, F., Massimini, M., & Manfridi, A. (2002). Spatial buffering during slow and paroxysmal sleep oscillations in cortical networks of glial cells in vivo. *The Journal of Neuroscience*, *22*, 1042–1053.

Appenteng, K., Lund, J. P., & Séguin, J. J. (1982). Intraoral mechanoreceptor activity during jaw movement in the anesthetized rabbit. *Journal of Neurophysiology*, *48*, 27–37.

Arsenault, I., Bota, R., Pastor Bernier, A., Lund, J. P., & Kolta, A. (2007). The role of glial cells in repetitive bursting of neurons of the trigeminal main sensory nucleus. Program No. 37. 2007. Neuroscience Meeting Planner. San Diego, CA. Online. *The Society for Neuroscience Abstract*.

Athanassiadis, T., Olsson, K. A., Kolta, A., & Westberg, K. G. (2005). Identification of c-Fos immunoreactive brainstem neurons activated during fictive mastication in the rabbit. *Experimental Brain Research*, *165*, 478–489.

Auld, D. S., & Robitaille, R. (2003). Glial cells and neurotransmission: An inclusive view of synaptic function. *Neuron*, *40*, 389–400.

Azouz, R., Jensen, M. S., & Yaari, Y. (1996). Ionic basis of spike after-depolarization and burst generation in adult rat hippocampal CA1 pyramidal cells. *The Journal of Physiology*, *492*, 211–223.

Bao, H., Bradley, R. M., & Mistretta, C. M. (1995). Development of intrinsic electrophysiological properties in neurons from the gustatory region of rat nucleus of solitary tract. *Brain Research. Developmental Brain Research*, *86*(1–2), 143–154.

Benninger, C., Kadis, J., & Prince, D. A. (1980). Extracellular calcium and potassium changes in hippocampal slices. *Brain Research*, *187*, 165–182.

Berger, A. J., Bayliss, D. A., & Viana, F. (1996). Development of hypoglossal motoneurons. *Journal of Applied Physiology*, *81*(3), 1039–1048.

Bernier, A. P., Arsenault, I., Lund, J. P., & Kolta, A. (2010). Effect of the stimulation of sensory inputs on the firing of neurons of the trigeminal main sensory nucleus in the rat. *Journal of Neurophysiology*, *103*(2), 915–923.

Bertrand, S., & Cazalets, J. R. (2002). The respective contribution of lumbar segments to the generation of locomotion in the isolated spinal cord of newborn rat. *The European Journal of Neuroscience*, *16*, 1741–1750.

Beurrier, C., Bioulac, B., & Hammond, C. (2000). Slowly inactivating sodium current (I_{NaP}) underlies single-spike activity in rat subthalamic neurons. *Journal of Neurophysiology*, *83*, 1951–1957.

Bourque, M. J., & Kolta, A. (2001). Properties and interconnections of trigeminal interneurons of the lateral pontine reticular formation in the rat. *Journal of Neurophysiology*, *86*, 2583–2596.

Brocard, F., Verdier, D., Arsenault, I., Lund, J. P., & Kolta, A. (2006). Emergence of intrinsic bursting in trigeminal sensory neurons parallels the acquisition of mastication in weanling rats. *Journal of Neurophysiology*, *96*, 2410–2424.

Brumberg, J. C., Nowak, L. G., & McCormick, D. A. (2000). Ionic mechanisms underlying repetitive high-frequency burst firing in supragranular cortical neurons. *The Journal of Neuroscience*, *20*, 4829–4843.

Büschges, A., Wikström, M. A., Grillner, S., & El Manira, A. (2000). Roles of high-voltage-activated calcium channel subtypes in a vertebrate spinal locomotor network. *Journal of Neurophysiology*, *84*, 2758–2766.

Butera, R. J., Jr., Rinzel, J., & Smith, J. C. (1999). Models of respiratory rhythm generation in the pre-Botzinger complex. I. Bursting pacemaker neurons. *Journal of Neurophysiology*, *82*, 382–397.

Cohen, J. E., & Fields, R. D. (2004). Extracellular calcium depletion in synaptic transmission. *The Neuroscientist*, *10*, 12–17.

Crill, W. E. (1996). Persistent sodium current in mammalian central neurons. *Annual Review of Physiology*, *58*, 349–362.

Darbon, P., Yvon, C., Legrand, J. C., & Streit, J. (2004). I_{NaP} underlies intrinsic spiking and rhythm generation in

networks of cultured rat spinal cord neurons. *The European Journal of Neuroscience*, *20*, 976–988.

Del Negro, C. A., Koshiya, N., Butera, R. J., & Smith, J. C. (2002). Persistent sodium current, membrane properties and bursting behavior of pre-Botzinger complex inspiratory neurons in vitro. *Journal of Neurophysiology*, *88*, 2242–2250.

Del Negro, C. A., Morgado-Valle, C., Hayes, J. A., Mackay, D. D., Pace, R. W., Crowder, E. A., et al. (2005). Sodium and calcium current-mediated pacemaker neurons and respiratory rhythm generation. *The Journal of Neuroscience*, *25*, 446–453.

Dellow, P. G., & Lund, J. P. (1971). Evidence for central timing of rhythmical mastication. *The Journal of Physiology*, *215*, 1–13.

Ferrier, D. (1873). Experimental researches in cerebral physiology and pathology. *West Riding lunatic Asylum Reports*, *3*, 30–96.

Franceschetti, S., Buzio, S., Sancini, G., Panzica, F., & Avanzini, G. (1993). Expression of intrinsic bursting properties in neurons of maturing sensorimotor cortex. *Neuroscience Letters*, *162*, 25–28.

Franceschetti, S., Guatteo, E., Panzica, F., Sancini, G., Wanke, E., & Avanzini, G. (1995). Ionic mechanisms underlying burst firing in pyramidal neurons: Intracellular study in rat sensorimotor cortex. *Brain Research*, *696*, 127–139.

Franceschetti, S., Sancini, G., Panzica, F., Radici, C., & Avanzini, G. (1998). Postnatal differentiation of firing properties and morphological characteristics in layer V pyramidal neurons of the sensorimotor cortex. *Neuroscience*, *83*, 1013–1024.

Gabriel, J. P., Mahmood, R., Walter, A. M., Kyriakatos, A., Hauptmann, G., Calabrese, R. L., et al. (2008). Locomotor pattern in the adult zebrafish spinal cord in vitro. *Journal of Neurophysiology*, *99*, 37–48.

Goodwin, G. M., & Luschei, E. S. (1975). Discharge of spindle afferents from jaw-closing muscles during chewing in alert monkeys. *Journal of Neurophysiology*, *38*(3), 560–571.

Grosche, J., Kettenmann, H., & Reichenbach, A. (2002). Glial cells form distinct morphological structures to interact with cerebellar neurons. *Journal of Neuroscience Research*, *68*, 138–149.

Grosche, J., Matyash, V., Möller, T., Verkhratsky, A., Reichenbach, A., & Kettenmann, H. (1999). Microdomains for neuron-glia interaction: Parallel fiber signaling to Bergmann glial cells. *Nature Neuroscience*, *2*, 139–143.

Guatteo, E., Franceschetti, S., Bacci, A., Avanzini, G., & Wanke, E. (1996). A TTX-sensitive conductance underlying burst firing in isolated pyramidal neurons from rat neocortex. *Brain Research*, *741*, 1–12.

Guido, W., Günhan-Agar, E., & Erzurumlu, R. S. (1998). Developmental changes in the electrophysiological properties of brain stem trigeminal neurons during pattern (barrelette) formation. *Journal of Neurophysiology*, *79*(3), 1295–1306.

Heinnemann, U., Stabel, J., & Rausche, G. (1990). Activity-dependant ionic changes and neuronal plasticity in rat hippocampus. *Progress in Brain Research*, *83*, 197–214.

Hsiao, C. F., Wu, N., Levine, M. S., & Chandler, S. H. (2002). Development and serotonergic modulation of NMDA bursting in rat trigeminal motoneurons. *Journal of Neurophysiology*, *87*, 1318–1328.

Huang, C. S., Hiraba, H., Murray, G. M., & Sessle, B. J. (1989). Topographical distribution and functional properties of cortically induced rhythmical jaw movements in the monkey (*Macaca fascicularis*). *Journal of Neurophysiology*, *61*, 635–650.

Huguenard, J. R., Hamill, O. P., & Prince, D. A. (1988). Developmental changes in Na^+ conductances in rat neocortical neurons: Appearance of a slowly inactivating component. *Journal of Neurophysiology*, *59*, 778–795.

Jinno, S., Ishizuka, S., & Kosaka, T. (2003). Ionic currents underlying rhythmic bursting of ventral mossy cells in the developing mouse dentate gyrus. *The European Journal of Neuroscience*, *17*, 1338–1354.

Kogo, M., Funk, G. D., & Chandler, S. H. (1996). Rhythmical oral-motor activity recorded in an in vitro brainstem preparation. *Somatosensory & Motor Research*, *13*, 39–48.

Kolta, A., Brocard, F., Verdier, D., & Lund, J. P. (2007). A review of burst generation by trigeminal main sensory neurons. *Archives of Oral Biology*, *52*, 325–328.

Kolta, A., Westberg, K. G., & Lund, J. P. (2000). Identification of brainstem interneurons projecting to the trigeminal motor nucleus and adjacent structures in the rabbit. *Journal of Chemical Neuroanatomy*, *19*, 175–195.

Komuro, A., Morimoto, T., Iwata, K., Inoue, T., Masuda, Y., Kato, T., et al. (2001). Putative feed-forward control of jaw-closing muscle activity during rhythmic jaw movements in the anesthetized rabbit. *Journal of Neurophysiology*, *86* (6), 2834–2844.

Kriegstein, A. R., Suppes, T., & Prince, D. A. (1987). Cellular and synaptic physiology and epileptogenesis of developing rat neocortical neurons in vitro. *Brain Research*, *431*, 161–171.

Lavigne, G., Kim, J. S., Valiquette, C., & Lund, J. P. (1987). Evidence that periodontal pressoreceptors provide positive feedback to jaw closing muscles during mastication. *Journal of Neurophysiology*, *58*(2), 342–358.

Lavoie, R., Arsenault, I., Lund, J. P., Robitaille, R., & Kolta, A. (2009). Régulation of the glial syncitium under conditions that cause neuronal bursting. In: *31st GRSNC Symposium abstr. , Université de Montréal*.

Li, Z., & Hatton, G. I. (1996). Oscillatory bursting of phasically firing rat supraoptic neurones in low-Ca^{2+} medium: Na^+ influx, cytosolic Ca^{2+} and gap junctions. *The Journal of Physiology*, *496*(Pt. 2), 379–394.

Li, Y. Q., Takada, M., & Mizuno, N. (1993). Identification of premotor interneurons which project bilaterally to the trigeminal motor, facial or hypoglossal nuclei: A fluorescent

retrograde double-labeling study in the rat. *Brain Research*, *611*, 160–164.

Lo, F. S., & Erzurumlu, R. S. (2001). Neonatal deafferentation does not alter membrane properties of trigeminal nucleus principalis neurons. *Journal of Neurophysiology*, *85*(3), 1088–1096.

Lund, J. P., & Dellow, P. G. (1971). The influence of interactive stimuli on rhythmical masticatory movements in rabbit. *Archives of Oral Biology*, *16*, 215–223.

Mattia, D., Kawasaki, H., & Avoli, M. (1997). Repetitive firing and oscillatory activity of pyramidal-like bursting neurons in the rat subiculum. *Experimental Brain Research*, *114*, 507–517.

Nguyen, Q. T., Wessel, R., & Kleinfeld, D. (2004). Developmental regulation of active and passive membrane properties in rat vibrissa motoneurones. *The Journal of Physiology*, *556* (Pt. 1), 203–219.

Nicholson, C., ten Bruggencate, G., Stockle, H., & Steinberg, R. (1978). Calcium and potassium changes in extracellular microenvironment of cat cerebellar cortex. *Journal of Neurophysiology*, *41*, 1026–1039.

Nozaki, S., Iriki, A., & Nakamura, Y. (1986a). Localization of central rhythm generator involved in cortically induced rhythmical masticatory jaw-opening movement in the guinea pig. *Journal of Neurophysiology*, *55*(4), 806–825.

Nozaki, S., Iriki, A., & Nakamura, Y. (1986b). Role of corticobulbar projection neurons in cortically induced rhythmical masticatory jaw-opening movement in the guinea pig. *Journal of Neurophysiology*, *55*(4), 826–845.

Núñez-Abades, P. A., Morillo, A. M., & Pásaro, R. J. (1993). Brainstem connections of the rat ventral respiratory subgroups: Afferent projections. *Autonomic Nervous System*, *42*(2), 99–118.

Olsson, K. A., Lund, J. P., Valiquette, C., & Veilleux, D. (1988). Activity during mastication of periodontal mechanosensitive neurons of the trigeminal subnucleus oralis of the rabbit. *Journal of Neurophysiology*, *59*(2), 341–357.

Pearson, K. G., & Rossignol, S. (1991). Fictive motor patterns in chronic spinal cats. *Journal of Neurophysiology*, *66*, 1874–1887.

Pinganaud, G., Bernat, I., Buisseret, P., & Buisseret-Delmas, C. (1999). Trigeminal projections to hypoglossal and facial motor nuclei in the rat. *The Journal of Comparative Neurology*, *415*, 91–104.

Pumain, R., & Heinemann, U. (1985). Stimulus-and amino acid-induced calcium and potassium changes in rat neocortex. *Journal of Neurophysiology*, *53*, 1–16.

Pumain, R., Kurcewicz, I., & Louvel, J. (1983). Fast extracellular calcium transients: Involvement in epileptic processes. *Science*, *222*, 177–179.

Rossignol, S., Lund, J. P., & Drew, T. (1988). The role of sensory inputs in regulating patterns of rhythmical in higher vertebrates. In A. Cohen, S. Rossignol & S. Grillner (Eds.), *Neural control of rhythmic movements in vertebrates* (pp. 201–283). New York: Wiley.

Rusakov, D. A., & Fine, A. (2003). Extracellular Ca^{2+} depletion contributes to fast activity-dependent modulation of synaptic transmission in the brain. *Neuron*, *37*, 287–297.

Salpeter, M. (1987). Vertebarte neuromuscular junctions: morphology, molecular organization, and functional consequences. In M. Salpeter (Ed.), *The vertebrate neuromuscular junction.* New York: 1–54.

Sandler, V. M., Puil, E., & Schwarz, D. W. F. (1998). Intrinsic response properties of bursting neurons in the nucleus principalis trigemini of the gerbil. *Neuroscience*, *83*, 891–904.

Sherrington, C. S. (1917). Reflexes elicitable in the cat from pinna vibrissae and jaws. *The Journal of Physiology*, *51*, 404–431.

Smith, S. J. (1992). Do astrocytes process neural information? *Progress in Brain Research*, *94*, 119–136.

Somjen, G. G. (1980). Stimulus-evoked and seizure-related responses of extracellular calcium activity in spinal cord compared to those in cerebral cortex. *Journal of Neurophysiology*, *44*, 617–632.

Spacek, J. (1985). Three-dimensional analysis of dendritic spines. III. Glial sheath. *Anatomy and Embryology (Berlin)*, *171*, 245–252.

Speck, D. F., Karius, D. R., & Ling, L. (1993). Respiratory afferents and the inhibition of inspiration. In D. F. Speck, M. S. Dekin, W. R. Revelette & D. T. Frazier (Eds.), *Respiratory control: Central and peripheral mechanisms* (pp. 100–103). Lexington: University Press of Kentucky.

Su, H., Alroy, G., Kirson, E. D., & Yaari, Y. (2001). Extracellular calcium modulates persistent sodium current-dependent burst-firing in hippocampal pyramidal neurons. *The Journal of Neuroscience*, *21*, 4173–4182.

Tanaka, S., Kogo, M., Chandler, S. H., & Matsuya, T. (1999). Localization of oral-motor rhythmogenic circuits in the isolated rat brainstem preparation. *Brain Research*, *821*(1), 190–199.

Tanaka, S., Wu, N., Hsaio, C. F., Turman, J., Jr., & Chandler, S. H. (2003). Development of inward rectification and control of membrane excitability in mesencephalic v neurons. *Journal of Neurophysiology*, *89*(3), 1288–1298.

Tazerart, S., Viemari, J. C., Darbon, P., Vinay, L., & Brocard, F. (2007). Contribution of persistent sodium current to locomotor pattern generation in neonatal rats. *Journal of Neurophysiology*, *98*, 613–628.

Tazerart, S., Vinay, L., & Brocard, F. (2008). The persistent sodium current generates pacemaker activities in the central pattern generator for locomotion and regulates the locomotor rhythm. *The Journal of Neuroscience*, *28*(34), 8577–8589.

Travers, J. B., & Norgren, R. (1983). Afferent projections to the oral motor nuclei in the rat. *The Journal of Comparative Neurology*, *220*, 280–298.

Trulsson, M. (2007). Force encoding by human periodontal mechanoreceptors during mastication. *Archives of Oral Biology*, *52*, 357–360.

Trulsson, M., & Johansson, R. S. (2002). Orofacial mechanoreceptors in humans: Encoding characteristics and responses during natural orofacial behaviors. *Behavioural Brain Research*, *135*, 27–33.

Tsuboi, A., Kolta, A., Chen, C. C., & Lund, J. P. (2003). Neurons of the trigeminal main sensory nucleus participate in the generation of rhythmic motor patterns. *The European Journal of Neuroscience*, *17*, 229–238.

Tsuzuki, S., Yoshida, S., Yamamoto, T., & Oka, H. (1995). Developmental changes in the electrophysiological properties of neonatal rat oculomotor neurons studied in vitro. *Neuroscience Research*, *23*(4), 389–397.

Urbani, A., & Belluzzi, O. (2000). Riluzole inhibits the persistent sodium current in mammalian CNS neurons. *The European Journal of Neuroscience*, *12*, 3567–3574.

Verkhratsky, A., Orkand, R. K., & Kettenmann, H. (1998). Glial calcium: Homeostasis and signaling function. *Physiological Reviews*, *78*, 99–141.

Westneat, M. W., & Hall, W. G. (1992). Ontogeny of feeding motor patterns in infant rats: An electromyographic analysis of suckling and chewing. *Behavioral Neuroscience*, *106*, 539–554.

Wu, N., Enomoto, A., Tanaka, S., Hsiao, C. F., Nykamp, D. Q., Izhikevich, E., et al. (2005). Persistent sodium currents in mesencephalic v neurons participate in burst generation and control of membrane excitability. *Journal of Neurophysiology*, *93*, 2710–2722.

Yoshida, A., Hiraga, T., Moritani, M., Chen, K., Takatsuki, Y., Hirose, Y., et al. (1998). Morphologic characteristics of physiologically defined neurons in the cat trigeminal nucleus principalis. *The Journal of Comparative Neurology*, *401*, 308–328.

Zhong, G., Masino, M. A., & Harris-Warrick, R. M. (2007). Persistent sodium currents participate in fictive locomotion generation in neonatal mouse spinal cord. *The Journal of Neuroscience*, *27*, 4507–4518.

Zhu, Z. T., Munhall, A., Shen, K. Z., & Johnson, S. W. (2004). Calcium-dependent subthreshold oscillations determine bursting activity induced by *N*-methyl-D-aspartate in rat subthalamic neurons in vitro. *The European Journal of Neuroscience*, *19*, 1296–1304.

eLIFE elifesciences.org

INSIGHT

OROFACIAL COORDINATION

How do we walk and chew gum at the same time?

A genetic approach has been used to map the neural circuits that control and coordinate the tongue and jaw muscles.

PHILIPPE MORQUETTE AND ARLETTE KOLTA

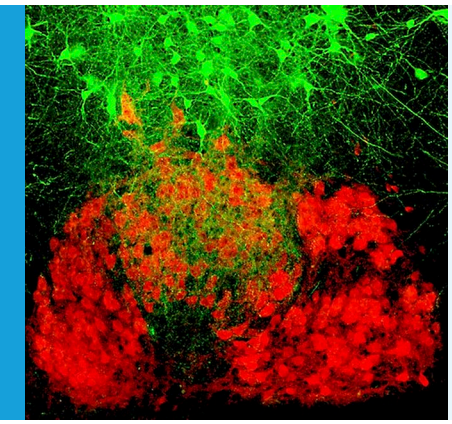

Related research article Stanek E IV, Cheng S, Takatoh J, Han B-X, Wang F. 2014. Monosynaptic premotor circuit tracing reveals neural substrates for oro-motor coordination. *eLife* **3**:e02511. doi: 10.7554/eLife.02511

Image Premotor neurons can project to motoneurons that control the tongue, the jaw muscles or both.

President Lyndon Johnson is reported to have said that Gerald Ford—then a congressman, later the President—was 'so dumb that he can't walk and chew gum at the same time'. What Johnson actually said was somewhat cruder, but his message was the same: the inability to perform two tasks simultaneously is a sign of limited intelligence. Motor coordination does not actually depend on intelligence, but it does not happen automatically. It might seem trivial to coordinate two simple tasks such as walking and chewing, but as we grow older, talking while walking becomes increasingly difficult (***Lundin-Olsson et al., 1997***). And it is even more difficult to simultaneously execute two movements using the same group of muscles, such as talking and chewing for instance.

For decades, neuroscientists have tried to understand how neural circuits are configured so as to allow flexibility and versatility, while also ensuring proper coordination and avoiding conflicts (such as accidentally biting one's tongue while talking or eating). This question was first tackled in the neural circuits responsible for simple rhythmic behaviours (such as breathing, walking or chewing) that are executed automatically. The circuits controlling these movements are called central pattern generators (***Marder and Calabrese, 1996***), and each rhythmic behaviour—and perhaps every muscle—has its own central pattern generator. However, it is not clear how these generators interact in order to coordinate with each other when several different muscles are involved in a specific behaviour, or when a particular muscle is involved in several different behaviours.

Previous work in invertebrate systems suggests that at least two types of neural architectures exist: dedicated circuits and multifunctional circuits. Dedicated circuits generate a specific behaviour and, once activated, they shut off all other circuits that could generate other behaviours using the same muscles. Multifunctional circuits, on the other hand, contain various building blocks and are involved in more than one type of behaviour, although not all building blocks are involved in all behaviours (***Morton and Chiel, 1994***; ***Briggman and Kristan, 2008***).

The operations performed by a neuronal circuit depend on the properties of its constituents (the neurons) and on their pattern of interconnectivity. Motoneurons are the neurons that transmit motor commands from the central nervous system to the muscles. Thus, to understand how a motor circuit operates, one must first identify the premotor neurons that are connected to the motoneurons. However, even the circuits controlling simple rhythmic behaviours in invertebrates

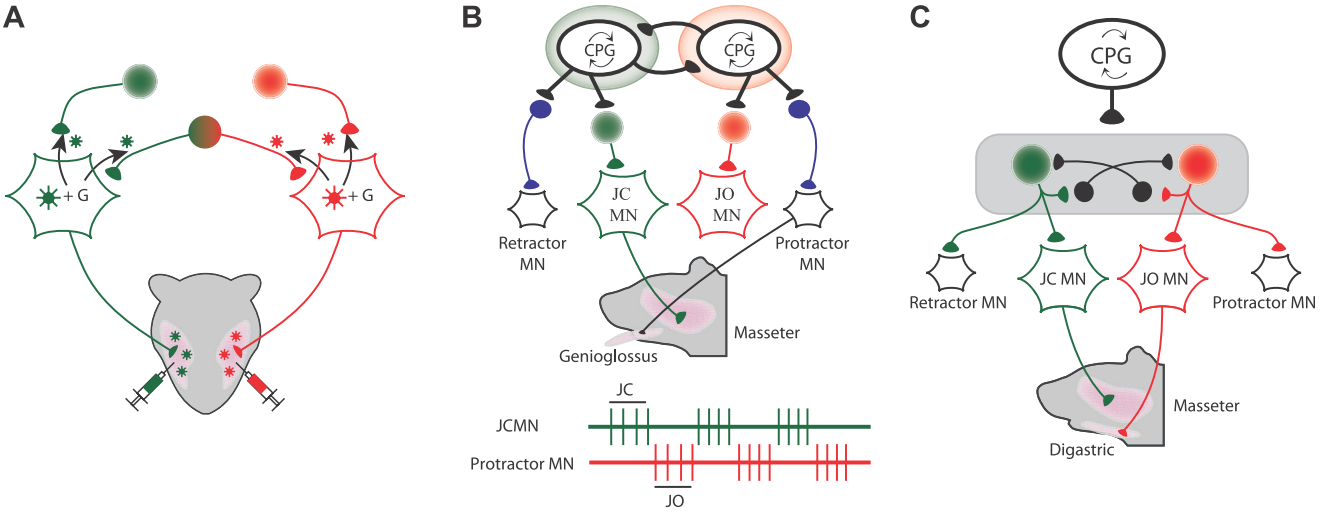

Figure 1. Mapping the neural circuits responsible for orofacial coordination. (**A**) When viruses labelled with green and red fluorescent tags are injected into the left and right muscles that close the jaw, three different sets of premotor neurons can be seen when the fluorescence is imaged: those that project to the motoneurons that drive the muscle on the left (green); those that project to the motoneurons that drive the muscle on the right (red); and those that project to both sets of motoneurons in order to coordinate the movements of the two muscles (green and red). The virus can move across the synapse between the motoneurons and the premotor neurons when it is complemented by a glycoprotein (**G**) that is expressed in the motoneurons of the mice: this movement is indicated by the black arrows. (**B** and **C**) During chewing, the digastric muscles (which open the jaw) and the genioglossus muscle (which protracts the tongue) are active during the jaw opening (JO) phase, while the masseter muscles (which close the jaw) and the muscle that retracts the tongue are both active during the jaw closing (JC) phase. The green and red traces show that the jaw closing motoneurons (JCMN) and the protractor motoneurons (protractor MN) are active at different times. The results of Stanek et al. suggest that orofacial coordination is performed by multifunctional circuits rather than dedicated circuits. In dedicated circuits (**B**), motoneurons do not share their premotor neurons, and those that are active at the same time receive inputs from their central pattern generator (CPG), which inhibits activity of other circuits. In multifunctional circuits (**C**), sets of motoneurons driving different muscles can share their premotor neurons. The same CPG activates premotor neurons that are shared by the motoneurons that are active at the same time, and this same CPG also inhibits (as indicated by the black neurons that end in a black circle) the premotor neurons that project to motoneurons that are active at other times.

turned out to be remarkably complex (***Selverston and Moulins, 1985***), and investigations of the circuits responsible for coordinating more complex behaviours in mammals have been hampered by technical limitations until recently.

Now, in *eLife*, Fan Wang and colleagues at Duke University—including Edward Stanek as first author—report the use of an elegant genetic approach to map the connectivity of the circuits controlling the tongue and jaw muscles in an effort to understand how orofacial movements are coordinated during behaviours such as chewing, swallowing and talking (***Stanek et al., 2014***). They wanted to learn more about the sequence of commands for activating the relevant motoneurons while avoiding problems such as biting your tongue or choking when swallowing.

Stanek et al. used genetic engineering to generate mice that expressed a rabies glycoprotein in all of their motoneurons. They then injected various facial muscles in the mice with a modified rabies virus that contained a fluorescent tag instead of this glycoprotein. The virus entered the motoneurons that drive the muscle and, when complemented by the glycoprotein there, the virus was able to cross the synapse between the motoneurons and the premotor neurons connected to them (***Wickersham et al., 2007***). By sectioning the brainstem and illuminating these sections with a laser to visualize the fluorescence, it was possible to identify the premotor neurons that projected to various groups of motoneurons. Stanek et al. actually used two types of modified virus, one labelled with a red fluorescent tag and one labelled with a green fluorescent tag.

Many of their findings confirmed results obtained with conventional tracing methods, but they also showed that some premotor neurons projected to more than one set of motoneurons. For instance, in one set of experiments they injected the red viruses into the muscle that closes the jaw (the masseter muscle) on one side of the face, and the green viruses into the masseter muscle on the other side of the face (***Figure 1A***). Three different sets of premotor neurons could be seen when the fluorescence was imaged: some premotor neurons projected to the motoneurons that drive the masseter muscle on the

FIGURE CREDIT: PHILIPPE MORQUETTE

left side of the face, others projected to the motoneurons that drive the other masseter muscle, and some premotor neurons projected to both sets of motoneurons. These premotor neurons are responsible for synchronizing the activation of the motoneurons that drive the masseter muscles on different sides of the face

Stanek et al. found similar patterns when they injected viruses into other pairs of muscles. For example, some premotor neurons projected to motoneurons that drive the masseter muscle and also to motoneurons that drive the muscle that retracts the tongue. Similarly, some premotor neurons projected to motoneurons that drive the digastric muscle (which opens the jaw) and also to motoneurons that drive the muscle that protracts the tongue. However, the muscle that protracts the tongue did not share any premotor neurons with the muscle that closes the jaw. Likewise, the muscle that retracts the tongue did not share any premotor neurons with the muscle that opens the jaw. Significantly, however, all these premotor neurons were found in the same areas of the brain, which indicates that they probably receive commands from the same central pattern generator and not from two different central pattern generators. These results argue against purely dedicated circuitry and are more suggestive of a multifunctional scheme (***Figure 1B,C***).

While this study illuminated the anatomical framework for orofacial circuitry, the connectivity of a network only defines the constraints within which it operates; it does not tell us how the network functions. That said, this new technology will open the door to a myriad of studies linking structure to function. Moreover, in addition to fluorescent tags, modified viruses could be used to carry other molecules to specific premotor neurons. These molecules could be used to tell us more about the target neurons: for example, they could tell us when and how the neurons are active. Furthermore, they could be used to modify the activity of the target neurons or to influence gene expression in these neurons (***Osakada et al., 2011***).

Philippe Morquette is in the Groupe de Recherche sur le système Nerveux Central and the Département de Neurosciences, Université de Montréal, Montréal, Canada

[redacted]

Arlette Kolta is in the Groupe de Recherche sur le système Nerveux Central, the Faculté de Médecine Dentaire and the Département de Neurosciences, Université de Montréal, Montréal, Canada

[redacted]

Competing interests: The authors declare that no competing interests exist.

Published 03 June 2014

References

Briggman KL, Kristan WB. 2008. Multifunctional pattern-generating circuits. *Annual Reviews of Neuroscience* **31**:271–294. doi: 10.1146/annurev.neuro.31.060407.125552.

Lundin-Olsson L, Nyberg L, Gustafson Y. 1997. "Stops walking when talking" as a predictor of falls in elderly people. *Lancet* **349**:617. doi: 10.1016/S0140-6736(97)24009-2.

Marder E, Calabrese RL. 1996. Principles of rhythmic motor pattern generation. *Physiological Reviews* **76**:687–717.

Morton DW, Chiel HJ. 1994. Neural architectures for adaptive behavior. *Trends in Neuroscience* **17**:413–420. doi: 10.1016/0166-2236(94)90015-9.

Osakada F, Mori T, Cetin AH, Marshel JH, Virgen B, Callaway EM. 2011. New rabies virus variants for monitoring and manipulating activity and gene expression in defined neural circuits. *Neuron* **71**:617–631. doi: 10.1016/j.neuron.2011.07.005.

Selverston AI, Moulins M. 1985. Oscillatory neural networks. *Annual Reviews of Physiology* **47**:29–48. doi: 10.1146/annurev.ph.47.030185.000333.

Stanek E IV, Cheng S, Takatoh J, Han X-B, Wang F. 2014. Monosynaptic premotor circuit tracing reveals neural substrates for oro-motor coordination. *eLife* **3**:e02511. doi: 10.7554/eLife.02511.

Wickersham IR, Lyon DC, Barnard RJ, Mori T, Finke S, Conzelmann KK, Young JA, Callaway EM. 2007. Monosynaptic restriction of transsynaptic tracing from single, genetically targeted neurons. *Neuron* **53**:639–647. doi: 10.1016/j.neuron.2007.01.033.

Cell Death and Differentiation (2015) 22, 612–625

www.nature.com/cdd

OPEN

REDD2-mediated inhibition of mTOR promotes dendrite retraction induced by axonal injury

B Morquette[1,2,3], P Morquette[1,3], J Agostinone[1,2,3], E Feinstein[4], RA McKinney[5], A Kolta[1,3,6] and A Di Polo*[,1,2,3]

Dendritic defects occur in neurodegenerative diseases accompanied by axonopathy, yet the mechanisms that regulate these pathologic changes are poorly understood. Using Thy1-YFPH mice subjected to optic nerve axotomy, we demonstrate early retraction of retinal ganglion cell (RGC) dendrites and selective loss of mammalian target of rapamycin (mTOR) activity, which precede soma loss. Axonal injury triggered rapid upregulation of the stress-induced protein REDD2 (regulated in development and DNA damage response 2), a potent inhibitor of mTOR. Short interfering RNA-mediated REDD2 knockdown restored mTOR activity and rescued dendritic length, area and branch complexity in a rapamycin-dependent manner. Whole-cell recordings demonstrated that REDD2 depletion leading to mTOR activation in RGCs restored their light response properties. Lastly, we show that REDD2-dependent mTOR activity extended RGC survival following axonal damage. These results indicate that injury-induced stress leads to REDD2 upregulation, mTOR inhibition and dendrite pathology causing neuronal dysfunction and subsequent cell death.
Cell Death and Differentiation (2015) **22,** 612–625; doi:10.1038/cdd.2014.149; published online 26 September 2014

During normal neural development there is selective elimination of dendritic and axonal branches without loss of the neuron itself.[1] This developmental pruning refines neuronal processes and ensures precise connectivity. Most of our current knowledge about structural changes in dendrites stems from studies of dendritic remodeling during development.[2,3] In contrast, little is known about how dendritic arbors are affected by trauma or disease in the adult central nervous system (CNS). Defects in dendritic arborization and connectivity are being recognized as one of the first stages of neurodegeneration. Indeed, dendritic abnormalities and loss of synapses have been reported in neuropsychiatric disorders such as schizophrenia and depression, as well as in neurodegenerative conditions including Alzheimer's disease, stroke and glaucoma.[4,5] Despite the fact that dendritic defects are likely to have devastating consequences on neuronal function and survival, the mechanisms that regulate dendrite degeneration in mature CNS neurons are poorly understood.

Recent studies have identified the mammalian target of rapamycin (mTOR) as a critical component of dendritic tree development.[6–9] A substantial reduction in the number of dendritic branches and arbor shrinkage were observed in developing hippocampal neurons when mTOR was inhibited.[6,7] In addition, mTOR has been recently implicated in the regulation of dendritic spine morphology, synaptogenesis and synaptic plasticity.[10,11] The emerging developmental role of mTOR in the regulation of dendritic dynamics prompted us to put forward the hypothesis that dysregulation of mTOR function might contribute to dendritic pathology in adult neurons following injury.

Many of the signals that impinge upon mTOR activity act through the tuberous sclerosis complex (TSC1/2), a negative regulator of mTOR function. For instance, stress signals such as hypoxia and energy depletion activate TSC1/2 through the REDD (regulated in development and DNA damage response) proteins,[12–14] leading to the loss of mTOR activity. REDD2, a member of this family also known as DDIT4L or RTP801L, is an attractive target because in addition to being a potent mTOR inhibitor, it is implicated in stress responses leading to cell death.[15,16] Although REDD2 is enriched in skeletal muscle and has been shown to inhibit mTOR signaling in response to leucine and stretch,[17] its expression and function in the nervous system is currently unknown.

We used a model of acute optic nerve lesion *in vivo* to ask whether axonal damage had a direct effect on retinal ganglion cell (RGC) dendrite morphology and, if so, to identify the molecular mechanisms that regulate this injury-induced response. Our data demonstrate that axonal damage leads to substantial retraction of RGC dendritic arbors before soma loss. Optic nerve lesion led to selective REDD2 upregulation in RGCs, which coincided with the loss of mTOR activity. Short interfering RNA (siRNA)-mediated knockdown of REDD2

[1]Department of Neuroscience, CHUM Research Center, University of Montreal, Montreal, QC, Canada; [2]University of Montreal Hospital Research Center (CR-CHUM), Montreal, QC, Canada; [3]Groupe de Recherche sur le Système Nerveux Central (GRSNC), University of Montreal, Montreal, QC, Canada; [4]Quark Pharmaceuticals Inc., Research Division, Ness Ziona, Israel; [5]Department of Pharmacology and Therapeutics, McGill University, Montreal, QC, Canada and [6]Department of Stomatology, Faculty of Dentistry, University of Montreal, Montreal, QC, Canada
*Corresponding author: A Di Polo, Department of Neuroscience, CHUM Research Center, University of Montreal, 900 Rue St-Denis, R09.480, Montreal, QC H2X 0A9, Canada. Tel: +1 514 890 8000 ext 31280; Fax: +1 514 412 7936; E-mail: [redacted]

Abbreviations: RGC, retinal ganglion cell; mTOR, mammalian target of rapamycin; mTORC1, mammalian target of rapamycin complex 1; REDD2, regulated in development and DNA damage 2; REDD1, regulated in development and DNA damage 2; siRNA, short interfering RNA; CNS, central nervous system; TSC1/2, tuberose sclerosis complex 1/2; YFP, yellow fluorescent protein; NF-H, neurofilament H; Brn3a, brain-specific homeobox/POU domain protein 3a; p70S6K, p70 ribosomal S6 kinase; S6, ribosomal protein S6; pS6, phosphorylated ribosomal protein S6; TUJ1, tubulin isoform bIII; INL, inner nuclear layer; GCL, ganglion cell layer; Cy3, cyanine 3; HIF-1α, hypoxia-inducible factor-1 alpha; PTEN, phosphatase and tensin homolog; ANOVA, one-way analysis of variance; Hz, hertz

Received 25.6.14; revised 07.8.14; accepted 18.8.14; Edited by N Bazan; published online 26.9.14

restored mTOR function in injured neurons and fully rescued their dendritic arbors, increasing dendritic length, field area and branch complexity. REDD2 depletion also abrogated pathologic RGC hyperexcitability and restored the light response properties of these neurons. Collectively, these data identify the REDD2-mTOR signaling pathway as a critical regulator of dendritic arbor morphology in adult central neurons undergoing axonal damage.

Results

RGC dendritic arbors retract soon after axonal injury and before cell death. To establish whether axonal injury induces structural changes in RGC dendrites, we carried out a detailed analysis of dendritic arbors in transgenic mice that selectively express yellow fluorescent protein (YFP) in RGCs under control of the Thy1 promoter (Thy1-YFPH).[18] In this mouse strain, RGC-specific YFP expression is detected in a small number of RGCs ($<1\%$), thus allowing visualization of individual dendritic arbors without interference from overlapping dendrites in neighboring neurons. A key question is to determine whether dendritic atrophy is a prerequisite or a consequence of RGC soma degeneration. For this purpose, we first established the time course of axotomy-induced RGC loss in Thy1-YFPH mice. Figure 1a shows that at 3 days after complete optic nerve axotomy, the intensity of the YFP label or the number of YFP-positive RGCs did not differ from those in non-injured (intact) retinas (injured: 63 ± 4 RGCs; intact: 66 ± 4 RGCs, mean $\pm$ S.E.M., analysis of variance (ANOVA), $P > 0.05$; Table 1), whereas at 5 days after lesion there was substantial neuronal loss accounting for 35% of the RGC population (injured: 44 ± 3 RGCs, ANOVA, $P < 0.001$). This time course of injury-induced RGC death was confirmed using an antibody against the transcription factor Brn3a, an RGC-specific marker[19] (Figure 1b). Therefore, analysis of dendritic arbors was carried out at 3 days after axotomy, a time when no changes in the intensity or number of YFP-labeled RGCs were observed, and before overt neuronal soma loss.

Fourteen different morphologic RGC subtypes have been identified in the mouse retina,[20,21] all of which are found in Thy1-YFPH transgenic retinas.[21] Neurofilament H (NF-H, SMI-32) is the only marker that labels several structural classes, specifically four subtypes identified by cluster analysis,[21] which encompass a significant portion of the total RGC population (36%: 1213 ± 101 RGCs/mm^2). Therefore, YFP-positive RGCs that colabeled with an antibody against NF-H and had a clearly identifiable axon were selected for dendritic arbor imaging and three-dimensional reconstruction. RGCs located in both central and peripheral retina were included in our analysis and measurements were performed blinded to manipulations. YFP+/NF-H+ RGCs had medium to large monostratified dendritic arbors with smooth dendrites lacking spines, a common feature of adult RGCs[21] (Figures 1c–e). Following axotomy, RGC dendritic arbors were visibly smaller than those in non-injured, intact neurons (Figures 1f and g). Analysis of total dendritic length and total dendritic area demonstrated a reduction of 15% (3707 μm) and 25% (112×10^3 μm^2), respectively, compared with control RGCs (length: 4320 μm; area: 150×10^3 μm^2) (Figures 1h and i and Tables 1 and 2). Sholl analysis, which measures the number of dendrites that cross-concentric circles at increasing distances from the soma, revealed a leftward shift indicating a reduced arbor complexity in axotomized neurons (Figure 1j and Table 2). These changes were not dependent on retinal location or eccentricity. Our results demonstrate that RGC dendritic retraction occurs soon after axonal injury and before cell death *in vivo*.

Selective loss of mTOR activity in injured RGCs. mTOR interacts with intracellular partners to regulate several cellular processes, of which the best characterized is protein synthesis. mTOR phosphorylates the p70 ribosomal S6 kinase (p70S6K) leading to phosphorylation of the ribosomal protein S6, which stimulates mRNA translation rates.[22] Antibodies that recognize phosphorylated S6$^{(Ser240/244)}$ are widely accepted functional readouts of mTOR activity.[23] Therefore, to establish whether RGC dendritic retraction correlates with changes in mTOR activity in these neurons, we examined phospho-S6$^{(Ser240/244)}$ expression in intact and axotomized retinas. Phospho-S6 labeling was detected predominantly in two retinal cell populations, one located in the ganglion cell layer (GCL) and another in the outermost part of the inner nuclear layer (INL) (Figure 2a). Double labeling of phospho-S6 with an antibody against tubulin isoform βIII (TUJ1), a selective marker for RGCs in the retina,[24,25] revealed that adult mouse RGC soma and dendrites are endowed with robust mTOR activity (Figures 2b–i). Phospho-S6 labeling in the INL colocalized with the calcium-binding protein calbindin, a marker for horizontal cells (Figures 2j–l).

A marked decrease in phospho-S6-positive RGCs was observed at 3 days after axotomy, before the onset of cell death, whereas phospho-S6 expression in horizontal cells remained unchanged (Figures 2m and n). Colabeling of axotomized retinas with phospho-S6 and TUJ1 confirmed that phospho-S6 downregulation reflected loss of mTOR activity in RGCs and not RGC loss (Figures 2o–q). Quantification of the number of RGCs that expressed both phospho-S6 and TUJ1 with respect to all TUJ1-positive cells demonstrated that $\sim 50\%$ of RGCs in the intact retina have detectable levels of mTOR activity (Figure 2r and Table 1). Importantly, optic nerve injury led to 40% decrease in the number of RGCs expressing phospho-S6 (Figure 2r). In contrast, the number of horizontal cells expressing both phospho-S6 and calbindin did not change with axotomy (Figure 2s). These data indicate that selective damage to RGC axons leads to the downregulation of mTOR activity in these neurons but not in other retinal cells.

REDD2 is upregulated in injured RGCs. Inhibition of mTOR during stress occurs through stabilization or activation of the TSC1/TSC2 complex. REDD1 and REDD2 likely inhibit mTOR by controlling the release of TSC2 from its association with inhibitory factors, thereby stabilizing the interaction between TSC1 and TSC2.[26] To test the hypothesis that REDD2 might be involved in mTOR inhibition in RGCs, we first examined the expression of REDD2 in intact and axotomized retinas. While low levels of REDD2 were detected in the GCL of non-injured retinas, a marked increase

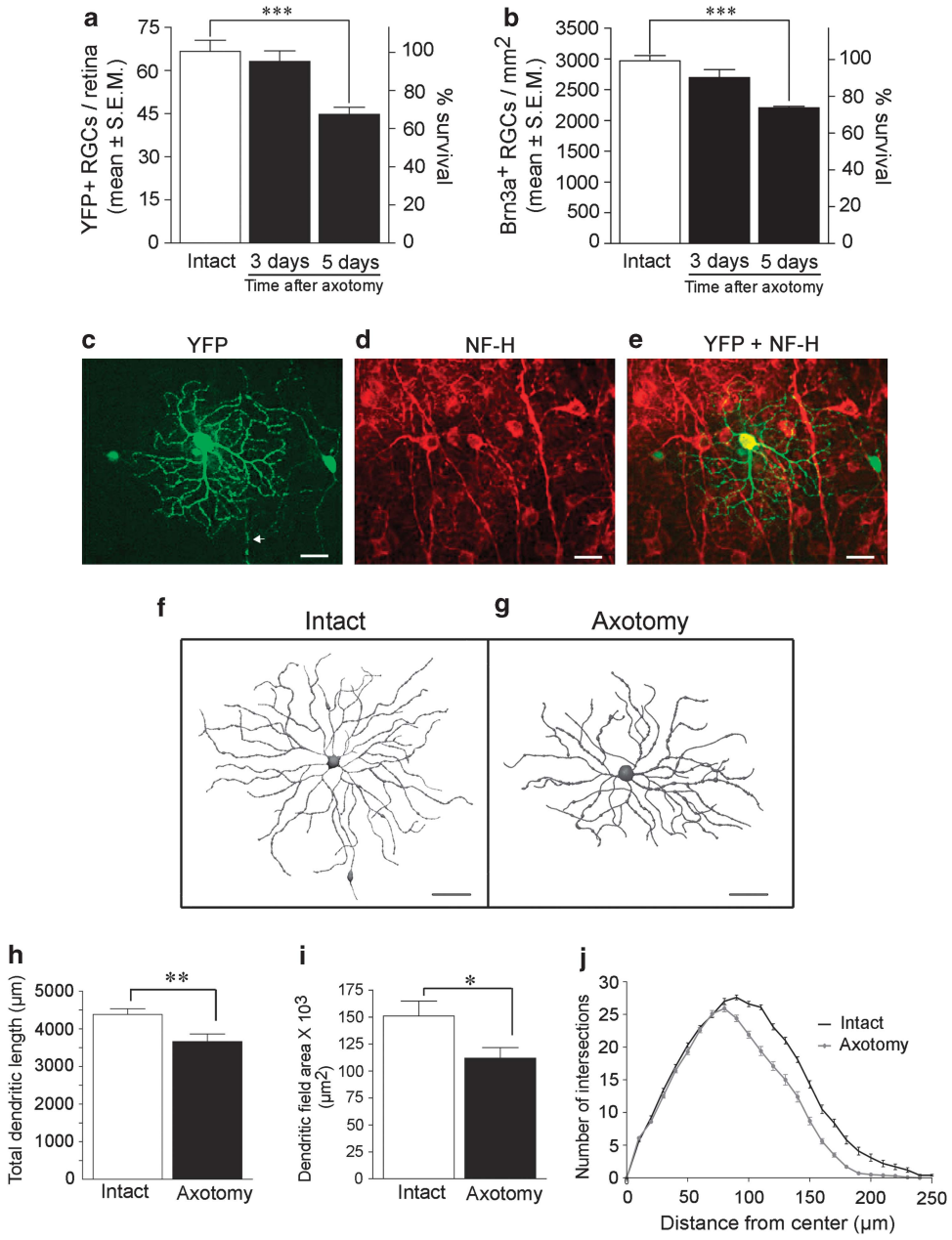

Figure 1 RGC dendritic arbors retract soon after axonal injury and prior to cell death. (**a**) Quantitative analysis of RGC densities showed no significant change in the number of YFP-positive RGCs at 3 days after axotomy, whereas substantial neuronal loss was observed at 5 days after lesion (axotomy 3 days: $n=7$; axotomy 5 days: $n=4$). (**b**) A similar pattern of RGC loss was observed using the RGC-specific marker Brn3a ($n=3$). The density of RGCs in intact, uninjured retinas is shown as reference ($n=11$). Data are expressed as mean ± S.E.M. (ANOVA, ***$P<0.001$, $n=3$–11 mice per group). (**c**–**e**) YFP-positive RGCs that colabeled with an antibody against NF-H and had clearly identifiable axons (arrow) were selected for dendritic arbor imaging and reconstruction. Scale bar: 25 μm. (**f** and **g**) Three days after axotomy, RGCs had visibly smaller dendritic arbors than non-injured, intact neurons (axotomy: $n=21$ cells; intact: $n=17$ cells). Quantitative analysis of dendritic parameters revealed a significant reduction in total dendritic length (**h**), dendritic field area (**i**) and arbor complexity (**j**, Sholl analysis). Values are expressed as mean ± S.E.M. (Student's *t*-test, **$P<0.005$, *$P<0.05$, cells were analyzed from 5 mice per group)

in REDD2-positive labeling was observed at 3 days after axotomy (Figures 3a and b). Colabeling of retinal sections with REDD2 and the RGC-specific marker Brn3a demonstrated that REDD2 expression selectively increases in injured RGCs (Figures 3c–e). REDD2 was also observed in the outer plexiform layer (OPL) and colocalized with horizontal cell proximal dendrites labeled with calbindin (Figures 3a and f–h), but there was no detectable change in REDD2 expression in horizontal cell processes after axonal injury (Figures 3b and f–h). REDD1, a family member that shares 38% homology with REDD2,[27,28] was selectively expressed in the GCL (Figure 3i). Colabeling with the RGC-specific marker Brn3a confirmed that RGCs expressed REDD1 (Figures 3k and l), as reported previously.[29] REDD2 upregulation in damaged RGCs was confirmed by western blot analysis of retinal homogenates as early as 48 h after

Table 1 Number of animals (*N*) used per experiment

Group	Treatment	*N*	Figure no.
RGC survival analysis (YFP)	Intact	11	1a
	Axotomy (3 days)	7	1a
	Axotomy (5 days)	4	1a
RGC survival analysis (Brn3a)	Intact	11	1b
	Axotomy (3 days)	3	1b
	Axotomy (5 days)	3	1b
Immunohistochemistry (NF-H+YFP)	Intact	7	1c–e
Dendritic arbor analysis	Intact	5	1h–j
	Axotomy (3 days)	5	1h–j
Immunohistochemistry (phospho-S6+TUJ1)	Intact	4	2a–i, m, r
	Axotomy (3 days)	4	2a–i, n, o–r
Immunohistochemistry (phospho-S6+calbindin)	Intact	3	2j–l, s
	Axotomy (3 days)	3	2j–l, s
Immunohistochemistry (REDD2, REDD1)	Intact	3	3a
	Axotomy (3 days)	3	3b–k
Western blot analysis (REDD2, REDD1)	Intact	5	3l–n
	Axotomy (2 days)	4	3l–n
	Axotomy (3 days)	4	3l–n
siRNA uptake (siCtl-Cy3+Fluorogold)	Intact+siCtl-Cy3	4	4a–d
Western blot analysis (REDD2, REDD1)	Axotomy+siCtl	4	4e–g
	Axotomy+siREDD2	5	4e–g
Immunohistochemistry (phospho-S6+Brn3a)	Axotomy+siCtl	4	4k–n
	Axotomy+siREDD2	4	4h–j, o
Immunohistochemistry (phospho-S6+calbindin)	Axotomy+siCtl	3	4q
	Axotomy+siREDD2	3	4q
Dendritic arbor analysis	Axotomy+siCtl	5	5a, d–i
	Axotomy+siREDD2	5	5b, d–i
	Axotomy+siREDD2+Rapa	4	5c, d–i
	Intact+siREDD2	5	5d–i
	Intact+rapamycin (Rapa)	5	5d–i
Electrophysiology	Intact	7	6a–h, k, l
	Axotomy	5	6f, g, i, k, l
	Axotomy+siREDD2	5	6f, g, j, k, l
	Axotomy+siCtl	20	N/A
RGC soma analysis	Intact	5	7a
	Axotomy+siCtl	5	7a
	Axotomy+siREDD2	5	7a
RGC survival analysis (Brn3a)	Axotomy (5 days)+siREDD2	4	7b, f
	Axotomy (5 days)+siCtl	3	7c, f
	Axotomy (7 days)+siREDD2	5	7d, f
	Axotomy (7 days)+siCtl	4	7e, f

axotomy (Figures 3m and n). In contrast, the expression of REDD1 did not change after lesion (Figures 3m and o). These results demonstrate selective injury-induced REDD2 upregulation in RGCs.

REDD2 knockdown restores mTOR activity. To establish whether REDD2 upregulation mediated loss of mTOR activity in RGCs, we sought to reduce REDD2 expression by using siRNA followed by analysis of retinal phospho-S6. First, we examined whether siRNA delivered intraocularly was taken up by mouse RGCs. A single intravitreal injection of non-targeting (scrambled) Cy3-tagged control siRNA (siCtl-Cy3) resulted in Cy3 labeling in RGCs as early as 3 h after administration (Figure 4a). The colocalization of Cy3 and the retrograde tracer Fluorogold (FG), following FG application to the superior colliculus, confirmed that siRNA was rapidly taken up by RGCs (Figures 4b–d). Next, we assessed the ability of siRNAs against REDD2 (siREDD2) to knockdown retinal REDD2 protein expression *in vivo*. Western blot analysis of retinal homogenates from eyes that received siREDD2 at the time of axotomy showed a significant reduction of REDD2 protein, whereas non-tagged siCtl had no effect (Figures 4e and f). Importantly, siREDD2 did not reduce the protein levels of REDD1, validating the specificity

Table 2 Dendritic parameters

Group	Treatment	Total dendritic length (μm) (mean ± S.E.M.)	Dendritic field area ($\times 10^3$ μm^2) (mean ± S.E.M.)	Sholl analysis (area under curve) (mean ± S.E.M.)	Number of animals (*N*)	Number of RGCs (*n*)
Intact	—	4391.7 ± 118.0	149.7 ± 10.5	3413.8 ± 128.6	5	17
Intact	siREDD2	4348.4 ± 275.1	170.5 ± 17.5	3138.6 ± 237.7	5	19
Intact	Rapamycin	4225.6 ± 237.1	144.4 ± 20.2	3057.1 ± 241.8	5	17
Axotomy	—	3706.9 ± 190.2	111.8 ± 9.9	2682.0 ± 128.6	5	21
Axotomy	siCtl	3613.6 ± 181.5	108.6 ± 13.8	2565.7 ± 216.4	5	18
Axotomy	siREDD2	4597.5 ± 229.2	163.5 ± 9.7	3713.8 ± 138.5	5	20
Axotomy	siREDD2+Rapamycin	3523.0 ± 185.0	110.8 ± 10.9	2770.0 ± 219.6	4	19

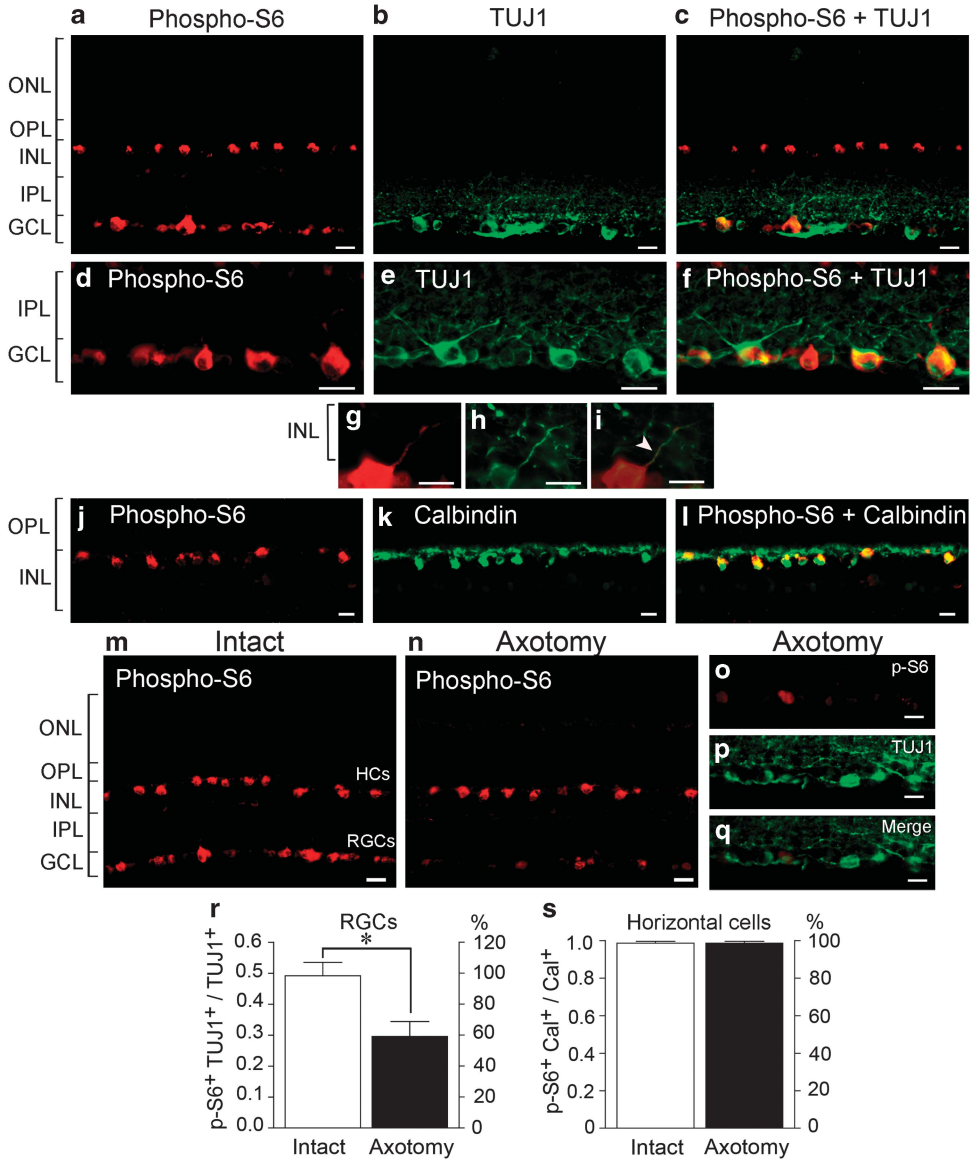

Figure 2 mTOR activity decreases in injured RGCs. (**a**) Phospho-S6 labeling was detected in neurons of the INL and GCL. (**b–i**) Colabeling of phospho-S6 with TUJ1, an RGC-specific marker, revealed mTOR activity in RGC soma and dendrites (arrowhead, **i**). (**j–l**) Phospho-S6 labeling in the INL colocalized with the calcium-binding protein calbindin, a marker for horizontal cells. (**m** and **n**) Loss of phospho-S6 in RGCs was observed at 3 days after axotomy, before the onset of cell death, whereas phospho-S6 expression in horizontal cells remained unchanged. (**o–q**) Phospho-S6 downregulation reflected loss of mTOR activity and not RGC death because these neurons were readily detected with TUJ1. (**r**) RGCs that expressed both phospho-S6 and TUJ1 with respect to all TUJ1-positive cells decreased after injury. (**s**) The number of horizontal cells expressing both phospho-S6 and calbindin did not change with axotomy. Values are expressed as mean ± S.E.M. (Student's *t*-test, $^*P < 0.05$, $n = 3$–4 mice per group). Scale bars: (**a–l** and **o–q**) = 25 μm and (**m** and **n**) = 50 μm. ONL, outer nuclear layer; OPL, outer plexiform layer; IPL, inner plexiform layer; GCL, ganglion cell layer

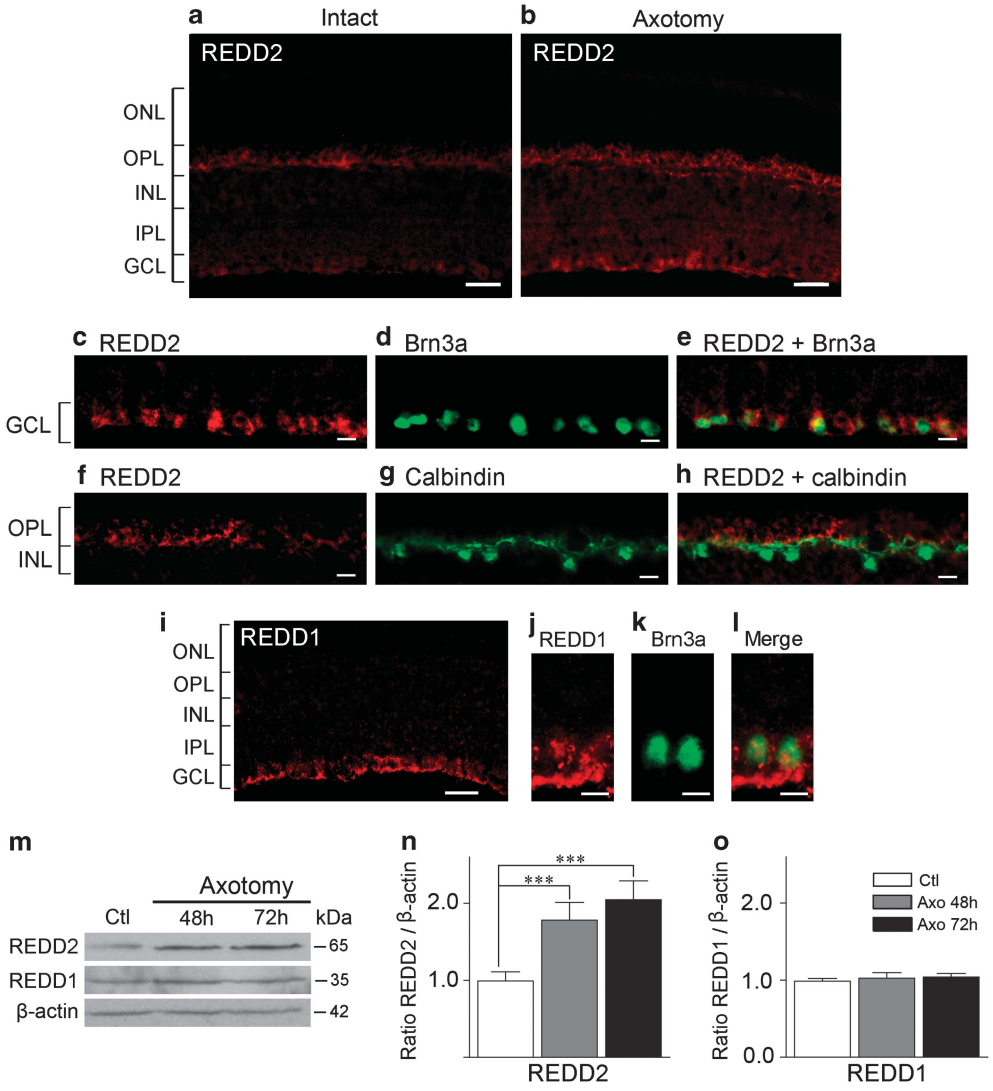

Figure 3 REDD2 is upregulated in injured RGCs. (**a**) Low levels of REDD2 were detected in the GCL of non-injured retinas. (**b**) In contrast, a marked increase in REDD2-positive labeling was observed at 3 days after axotomy. (**c**–**e**) Colabeling with REDD2 and Brn3a demonstrated that REDD2 upregulation in injured RGCs. (**a** and **f**–**h**) REDD2 protein expression in the OPL colocalized with calbindin-positive horizontal cell proximal dendrites. (**i**–**l**) The family member REDD1 was selectively expressed in the GCL, and colabeling with the RGC-specific marker Brn3a confirmed its expression by RGCs. (**m**–**o**) Western blot and densitometric analyses demonstrated that REDD2 was upregulated as early as 48 h after axonal damage, whereas REDD1 remained unchanged. The lower panel represents the same blot as in the upper panels but probed with an antibody that recognizes β-actin used to confirm equal protein loading. Axo 48 h, Axo 72 h: analysis performed at 48 or 72 h, respectively, after axotomy. Values are expressed as mean $\pm$ S.E.M. (ANOVA, $^{***}P < 0.001$, $n = 3$–5 mice per group). Scale bars: (**a** and **b**) = 50 μm and (**c**–**h**) = 25 μm. ONL, outer nuclear layer; OPL, outer plexiform layer; INL, inner nuclear layer; IPL, inner plexiform layer; GCL, ganglion cell layer

of this siRNA (Figures 4e and g). Immunohistochemistry of axotomized retinas confirmed that REDD2 downregulation occurred in RGCs, visualized with Brn3a, following treatment with siREDD2 but not siCtl (Figures 4h–m). We next investigated whether siRNA-mediated knockdown of REDD2 resulted in recovery of mTOR function. Axotomized retinas treated with siREDD2 displayed a larger number of phospho-S6-positive RGCs compared with retinas injected with siCtl (Figures 4n and o). Quantitative analysis demonstrated a 45% increase in the number of axotomized RGCs expressing phospho-S6 in the presence of siREDD2 compared with control retinas (Figure 4p and Table 1), whereas the number of phospho-S6-positive horizontal cells did not change (Figure 4q). These data demonstrate that REDD2 knockdown increases mTOR activity in injured RGCs, and suggests that axotomy-induced REDD2 upregulation leads to the loss of mTOR function in these neurons.

REDD2-dependent increase in mTOR function rescues dendrites. We asked whether siREDD2-induced upregulation of mTOR activity had an effect on dendritic arbor structure after axonal injury. Characterization of neuronal morphology at 3 days after axotomy demonstrated that siREDD2-treated retinas contained RGCs with longer dendrites and more elaborate arbors than control retinas treated with siCtl (Figures 5a and b). Coadministration of siREDD2

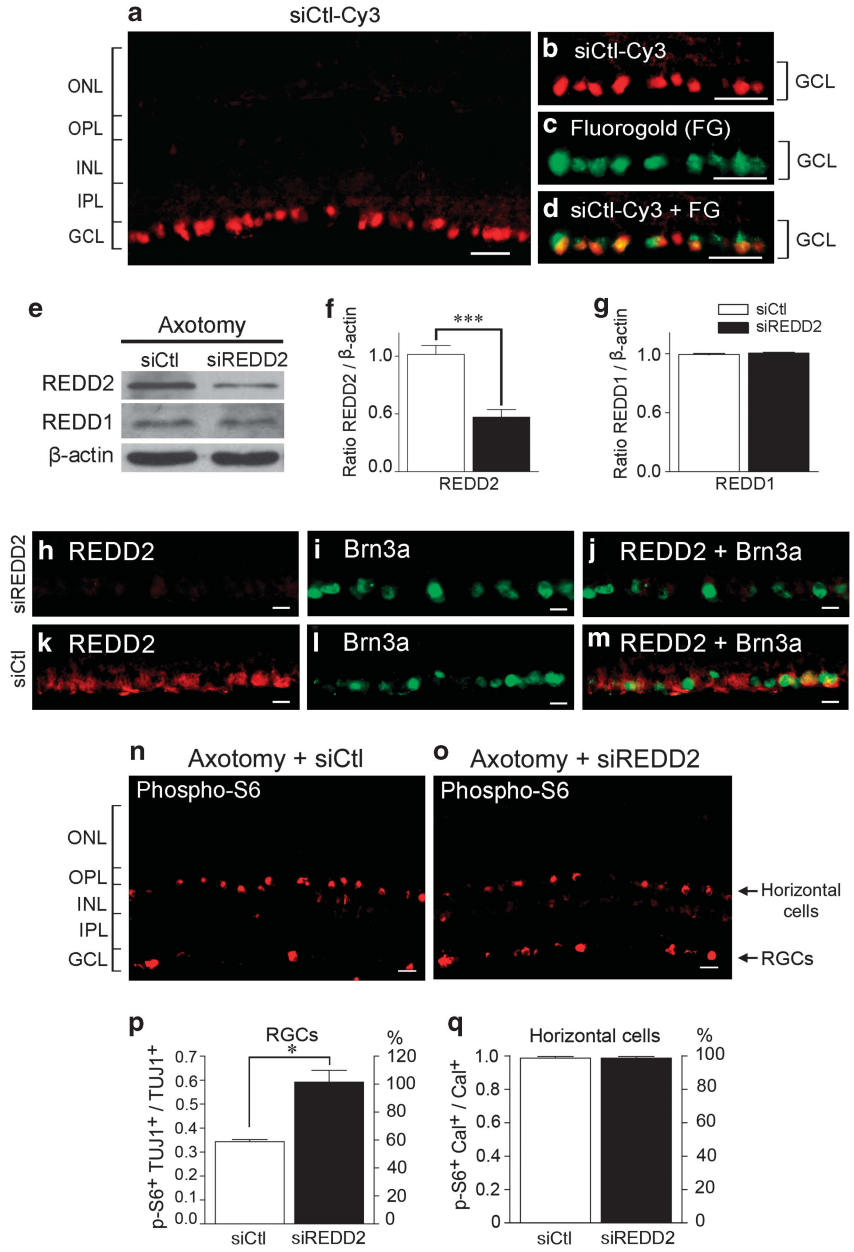

Figure 4 REDD2 knockdown restores mTOR activity. (**a**–**d**) Intravitreal delivery of siCtl-Cy3 resulted in rapid and effective uptake by RGCs, visualized with the retrograde tracer FG. (**e** and **f**) Western blot and densitometric analyses showed that intravitreal delivery of siRNA against REDD2 (siREDD2) led to a reduction of retinal REDD2 protein, while siCtl had no effect (Student's *t*-test, ***$P<0.01$, $n=4$–5 mice per group). (**e** and **g**) siREDD2 did not decrease or increase the protein levels of REDD1, confirming the specificity of the siRNA. The lower panel represents the same blot as in the upper panels but probed with an antibody that recognizes β-actin used to confirm equal protein loading. (**h**–**j**) siRNA-mediated knockdown of REDD2 occurred in RGCs, visualized with Brn3a, but not in retinas treated with siCtl (**k**–**m**). (**n** and **o**) Axotomized retinas treated with siREDD2 had more phospho-S6-positive RGCs compared with siCtl-treated retinas. (**p**) Quantitative analysis demonstrated a 45% increase in the number of TUJ1-positive axotomized RGCs expressing phospho-S6 in the presence of siREDD2 compared with control retinas. The number of phospho-S6-positive horizontal cells did not change (**q**). Values are expressed as mean ± S.E.M. (Student's *t*-test, *$P<0.05$, $n=4$ mice per group). Scale bars: (**a**–**d**) = 50 μm; (**h**–**o**) = 25 μm. ONL, outer nuclear layer; OPL, outer plexiform layer; INL, inner nuclear layer; IPL, inner plexiform layer; GCL, ganglion cell layer

and rapamycin, an inhibitor of the mTOR complex 1 (mTORC1),[30] completely blocked the effect of siREDD2 on dendritic rescue, suggesting that this response was mTORC1-specific (Figure 5c). Quantitative analysis of dendritic arbor parameters revealed that siREDD2 protected 32% of the total dendritic length and 34% of the dendritic field area from injury-induced damage compared with siCtl or a combination of siREDD2 and rapamycin (Figures 5d and f and Table 2). Administration of siREDD2 or rapamycin alone in non-injured, intact retinas did not elicit significant changes in dendritic length or field area (Figures 5e and g). Dendritic arbor reconstruction and measurements were carried out blinded to treatments.

To assess the contribution of proximal and distal dendrites to axotomy-induced changes and the effect of siREDD2, we examined the dendritic length of proximal dendrites (orders 1–3)

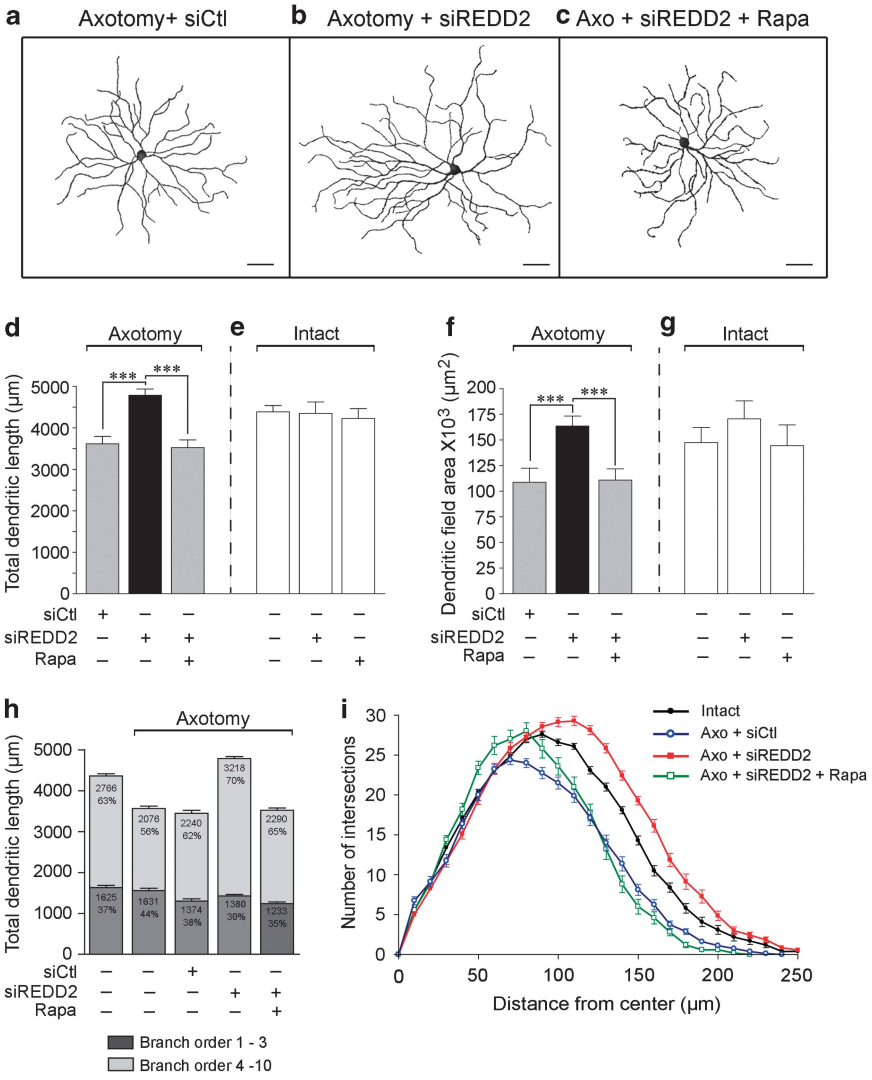

Figure 5 REDD2-dependent increase in mTORC1 function rescues dendritic arbors. (**a** and **b**) siREDD2-treated RGCs ($n=20$ cells) have elaborate arbors with longer dendrites than control neurons treated with siCtl ($n=18$ cells). (**c**) Coadministration of siREDD2 with rapamycin (Rapa, $n=19$ cells), an inhibitor of the mTORC1, blocked the effect of siREDD2 on dendritic morphology (4–5 mice per group). (**d** and **f**) The total dendritic length and field area increased in siREDD2-treated retinas compared with controls treated with siCTL or a combination of siREDD2 and rapamycin. (**e** and **g**) Administration of siREDD2 ($n=19$ cells) or rapamycin alone ($n=17$ cells) did not elicit changes in dendritic length or field area of non-injured (intact) neurons (4–5 mice per group). (**h**) Analysis of the contribution of proximal dendrites (orders 1–3) and distal dendrites (orders 4–10) showed that injury-induced changes and the response to siREDD2 occurred primarily in distal dendrites. (**i**) Sholl analysis revealed an increase in arbor complexity in axotomized siREDD2-treated RGCs compared with cells exposed to siCtl or a combination of siREDD2 and rapamycin. All analyses were performed at 3 days after axotomy. Values are expressed as the mean ± S.E.M. (ANOVA, $^{**}P<0.001$). See Table 2 for all *N* values. Scale bars: (**a**–**c**) = 50 μm, Axo, axotomy

compared with distal dendrites (orders 4–10). This analysis demonstrated that most of the changes occurring after axotomy and following modulation of the REDD2-mTOR pathway take place in distal dendrites (Figure 5h). Furthermore, Sholl analysis revealed a rightward shift indicative of increased arbor complexity in axotomized siREDD2-treated retinas with respect to axotomized retinas treated with siCtl or a combination of siREDD2 and rapamycin (Figure 5i). Increased arbor complexity was more apparent at $>100\,\mu$m from the cell soma, consistent with changes taking place in distal dendritic segments. Intriguingly, the dendritic arbors of injured RGCs that received siREDD2 displayed higher complexity than those in intact, non-injured retinas without treatment (Figure 5i, red curve *versus* black curve; Table 2). siREDD2 administration to intact eyes did not alter dendritic arbor complexity (not shown). These data identify the REDD2–mTORC1 axis as a critical regulator of RGC dendritic arbor morphology in injured neurons, and provide evidence that REDD2-dependent increase in mTORC1 activity rescues RGC dendrites after axotomy.

siREDD2-mediated mTOR activation restores neuronal function. To assess the impact of dendritic arbor rescue on RGC function, we performed whole-cell recordings from single ON-center RGCs at 3 days after axotomy and concurrent intraocular injection of siREDD2 or siCtl at the time of injury. Retinas were placed in the recording chamber with the GCL facing up and visualized with epifluorescence,

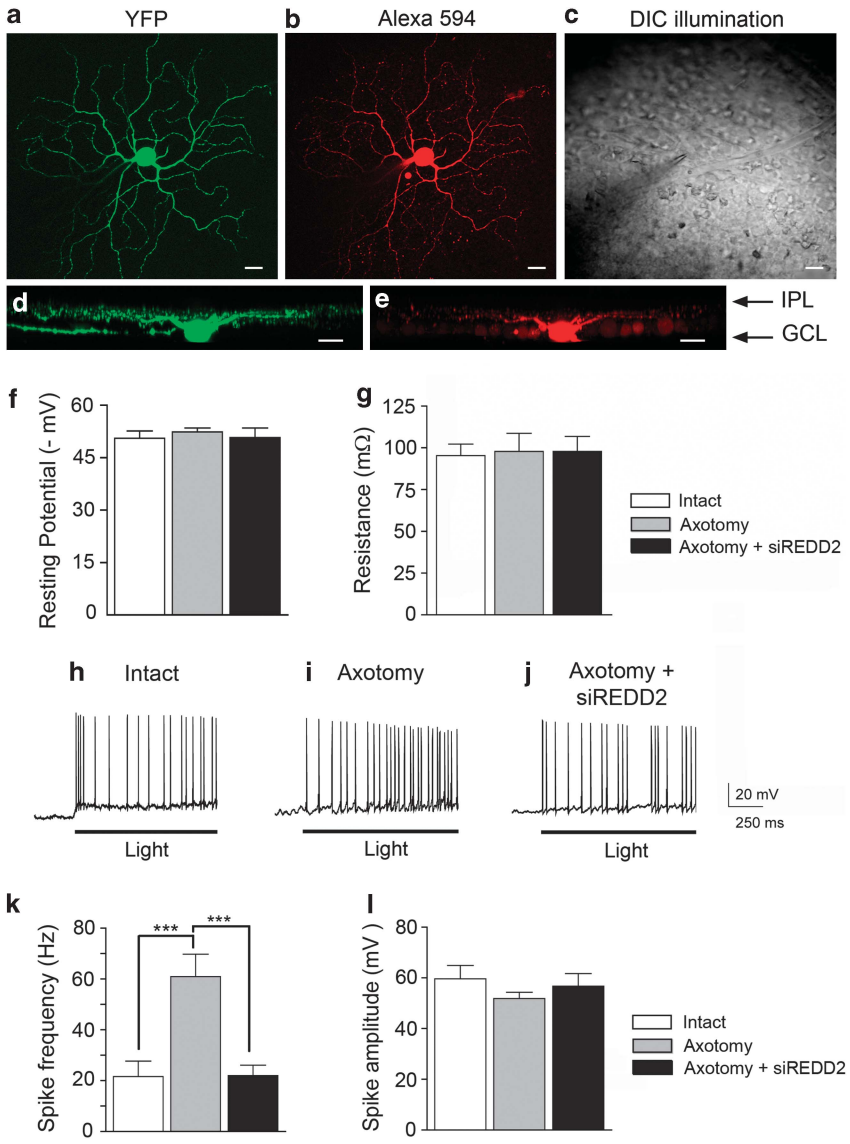

Figure 6 siREDD2-mediated mTOR activation restores RGC function. (**a–c**) Whole-cell recordings were obtained from ON-center YFP-positive RGCs visualized with epifluorescence and infrared differential interference contrast (DIC) optics to position the recording electrode. (**b**, **d** and **e**) The identity of each recorded cell was confirmed following injection of Alexa Fluor 594 through the recording pipette. Analysis of RGC intrinsic properties, including membrane resting potential (**f**) and resistance (**g**), did not reveal significant differences between intact and axotomized neurons with or without siREDD2 treatment. (**h** and **i**) Light stimulation demonstrated an increase in the frequency of action potentials elicited by axotomized RGCs ($n=7$ cells) compared with non-injured controls ($n=7$ cells). (**j** and **k**) siREDD2 treatment restored the light-induced firing frequency to levels similar to those recorded from intact neurons ($n=7$ cells). (**l**) No change in the amplitude of action potentials was observed. Values are expressed as the mean $\pm$ S.E.M. (ANOVA, $^{***}P<0.001$). Cells were recorded from 5 to 7 mice per group. Scale bars: (**a–e**) $=20\,\mu$m

to identify YFP-labeled RGCs, as well as infrared differential interference contrast optics to position the recording electrode. The identity of each recorded cell and its pattern of dendritic arborization in the inner plexiform layer was confirmed *post hoc* following injection of Alexa Fluor 594 through the recording pipette (Figures 6a–e). Analysis of RGC intrinsic properties, including membrane resting potential and resistance, did not reveal significant differences between intact and axotomized neurons with or without siREDD2 treatment (Figures 6f and g). In contrast, light stimulation elicited firing at a much higher frequency in axotomized RGCs compared with non-injured controls (intact: 22 ± 6 Hz; axotomy: 61 ± 9 Hz, mean $\pm$ S.E.M.; Figures 6h and i). Remarkably, siREDD2 treatment restored the light-induced firing frequency in axotomized RGCs to levels similar to those recorded from intact neurons (axotomy +siREDD2: 22 ± 4 Hz; Figures 6j and k and Table 1). No significant change was observed in the amplitude of action potentials (Figure 6l). Intriguingly, attempts to record from axotomized RGCs treated with siCtl or phosphate-buffered saline (PBS) were unsuccessful. These cells had low resting potentials and did not fulfill a minimal criteria for consistency in firing rates (>40 experiments). Taken together, our results indicate that axotomy leads to early RGC hyperexcitability and that siREDD2-mediated rescue of dendritic arbors restores the light response properties of these neurons.

mTOR activation extends neuronal survival. RGC apoptosis after axonal injury has been associated with soma and nuclear shrinkage,[31] and mTOR is known to regulate soma size in neurons.[32] Therefore, we first examined RGC soma size after axotomy and whether it was susceptible to REDD2-dependent mTOR activity. Our data show that there was no significant change in RGC soma size at 3 days after axotomy in the presence or absence of siREDD2 (Figure 7a and Table 1). To determine if siREDD2-mediated rescue of dendritic arbors had an effect on neuronal survival, we examined retinas at 5 and 7 after axotomy. Flat-mounted retinas from eyes treated with siREDD2 at the time of axotomy consistently showed higher densities of Brn3a-labeled RGCs than those treated with siCtl (Figures 7b–e). Quantitative analysis demonstrated that siREDD2 promoted substantial RGC survival relative to siCtl-treated eyes at 5 days (siREDD2: 91% survival, 2700 ± 128 RGCs/mm^2; siCtl: 74%, 2207 ± 22 RGCs/mm^2) and 7 days (siREDD2: 56%, 1675 ± 108 RGCs/mm^2; siCtl: 45%, 1344 ± 27 RGCs/mm^2) after optic nerve injury (Figure 7f and Table 1). Taken together, these data suggest that mTOR-mediated protection of dendritic arbors attenuates RGC loss after axonal damage.

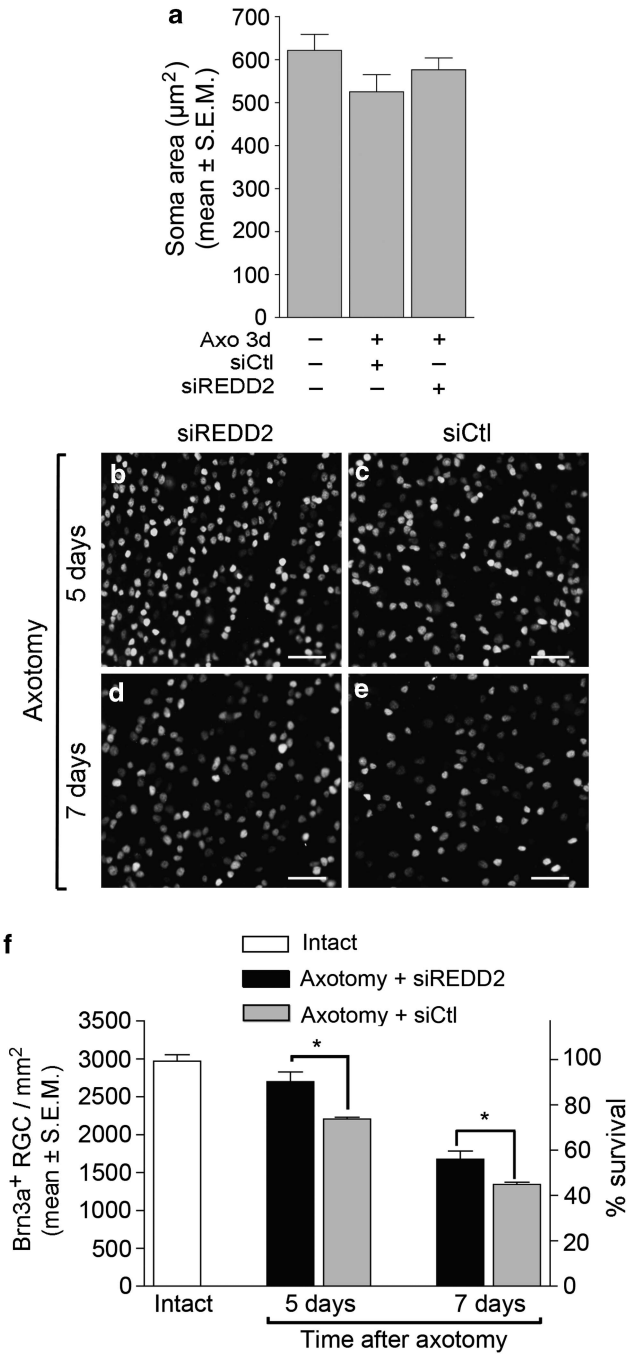

Figure 7 mTOR activation extends neuronal survival. (**a**) No significant change in RGC soma size was found at 3 days after axotomy with or without siREDD2 (Axo alone: $n = 18$ cells; Axo+siREDD2: $n = 20$ cells; intact: $n = 17$ cells; 3–5 mice per group). (**b–e**) Flat-mounted retinas from eyes treated with siREDD2 showed higher densities of Brn3a-labeled RGCs than those treated with siCtl. (**f**) Quantitative analysis demonstrated that siREDD2 promoted substantial RGC survival relative to siCtl-treated eyes at 5 and 7 days after axotomy. Values are expressed as RGC densities (RGCs/mm^2; mean $\pm$ S.E.M., ANOVA, * < 0.05, $n = 3$–5 mice per group). The density of RGCs in intact, uninjured retinas is shown as reference (100% survival). Scale bars: (**b–e**) $= 50\ \mu$m

Discussion

Abnormalities in dendritic structure are a characteristic feature of many brain diseases, yet the molecular mechanisms leading to dendritic pathology in injured neurons are poorly understood. In this regard, the data presented here using the adult mouse visual system support several novel conclusions. First, we show that dendritic retraction occurs rapidly in a substantial population of RGCs, before overt cell death, and as a direct consequence of axonal injury. Second, we demonstrate that damage to RGC axons induces expression of REDD2 coinciding with strong inhibition of mTOR activity in these neurons. Third, we show that REDD2 upregulation underlies the aberrant dendritic phenotype because siRNA-mediated ablation of REDD2 restores mTOR activity and rescues RGC dendritic arbor structure and complexity. Lastly, REDD2 depletion leading to mTOR activation re-establishes the light response properties of injured RGCs and extends their survival. Taken together, these data suggest a novel role for REDD2 in the regulation of dendritic morphology through modulation of mTOR activity after axonal damage.

Dendrites are extremely dynamic during development, expanding and retracting rapidly in response to intrinsic and environmental cues,[33,34] but they become stable by adulthood and display little or no structural changes over extended time periods.[35] The stability of dendritic arbors is believed to be compromised following injury or during neurodegeneration. For example, the selective death of RGCs is a cardinal feature of glaucoma,[36] and shrinkage of RGC dendritic arbors has been observed in primate, cat and rodent models of this disease[37–43] as well as in human glaucomatous retinas.[44] The primary site of damage in glaucoma is believed to be at RGC axons in the optic nerve head.[45] Consistent with this, we show that axotomy triggers rapid dendritic retraction, a finding that is in agreement with early dendritic changes observed after optic nerve crush.[46,47] In spite of the large morphologic diversity of RGC dendritic arbors in the mouse retina,[20,21] few molecular markers for discrete RGC subtypes have been identified and include NF-H, melanopsin and junctional adhesion molecule B.[21,48,49] Among these, only NF-H labels several structural

classes identified by cluster analysis and encompass a substantial RGC population.[21,48] It has been proposed that different RGC subtypes display distinct susceptibilities to injury. In the axotomized feline retina, α cells, which are endowed with large somata and dendritic arbors, undergo a significant decrease in dendritic field size, whereas β cells with medium-sized somata and more compact dendritic trees are less affected.[50] Our results show that NF-H-positive RGCs, which comprise cells with medium- to large-sized dendritic arbors, undergo substantial atrophy after axotomy similar to α cells. A previous study reported dendritic atrophy in NF-H-positive RGCs at 2 months after laser-induced ocular hypertension, a time when there is significant soma and axonal loss, but only in the superior quadrant of hypertensive eyes.[43] We observed dendritic arbor shrinkage in all retinal quadrants that was independent of retinal eccentricity, which may reflect differences between these injury models and also that our analysis was carried out early after axonal injury at a time preceding massive neurodegeneration.

The identification of pathways that contribute to RGC dendritic arbor maintenance is essential to understand the molecular basis of pathologic changes and to identify potential therapeutic targets. Our data suggest that the REDD2-mTORC1 pathway is critical for dendritic stability in adult RGCs. We show that damage to RGC axons leads to cell-specific increase of REDD2, mTORC1 inhibition and dendritic retraction. REDD2 is strongly upregulated by hypoxia, via the hypoxia-inducible factor-1α (HIF-1α),[28] as well as oxidative and osmotic stress.[15,16,51] Optic nerve damage increases HIF-1α and reactive oxygen species in RGCs,[52,53] which may account for the axotomy-induced upregulation of REDD2 reported here. Given that REDD2 is a strong inhibitor of mTOR, we asked whether injury-induced REDD2 upregulation led to mTOR inhibition and dendritic retraction. We show that adult RGCs are endowed with constitutive mTOR activity that is markedly reduced after axotomy, consistent with a study showing reduced mTOR in RGCs following optic nerve crush.[54] Our loss of function experiments using siRNA-mediated REDD2 knockdown demonstrate selective restoration of mTOR activity in injured RGCs accompanied by rescue of dendritic arbors. Moreover, rapamycin administration completely obliterated the effect of REDD2 depletion on dendritic rescue. Our data suggest that REDD2-dependent loss of mTORC1 function underlies RGC dendritic shrinkage, and that mTORC1 is required for the stability of adult RGC dendrites.

Recent work supports a role for mTOR in RGC axon regeneration.[55,56] For example, deletion of the phosphatase and tensin homolog or TSC1, both negative regulators of mTOR, promoted robust RGC axon regeneration along the injured optic nerve tract.[54,57] More recently, Leibinger *et al.*[58] showed that inflammatory stimulation prevented the axotomy-induced decline of mTOR activity in RGCs and demonstrated that mTOR signaling is important to sustain RGCs in an active regenerative state. Further research is required to identify the mTOR-specific targets that contribute to RGC axon regrowth or dendritic stability. A central role of mTOR is to regulate protein translation; thus, it is possible that mTORC1 mediates the translation of structural or signaling proteins in dendrites, to ensure arbor maintenance, and in axons, to promote regeneration. Several molecules that contribute to dendritic arbor stability during development have been identified including the microtubule-associated proteins 1A and 2, integrin $\alpha 3\beta 1$, calcium/calmodulin-dependent protein kinase II, nuclear Dbf2-related kinases and the guanine deaminase cypin.[35] It would be of future interest to assess whether these molecules are translational targets of mTOR and if they are dysregulated in the context of injury in the adult CNS. Alternatively, mTOR may directly regulate protein–protein interactions required for dendritic maintenance. Indeed, mTOR has been shown to enhance the interaction between microtubules and actin-binding proteins required for proper dendritic arbor morphology,[59] suggesting a role beyond that of protein translation.[60]

Our electrophysiologic data demonstrate that, soon after injury, RGCs display increased firing rates characteristic of hyperexcitable neurons. This finding is consistent with a recent study showing a significant increase in RGC spontaneous firing of action potentials in a mouse model of microbead-induced ocular hypertension.[61] This RGC hyperactivity contrasts with reduced spontaneous firing recorded using extracellular multielectrode arrays in a similar glaucoma model in mice,[42] a discrepancy that may reflect differences in methodology and cell sampling. Remarkably, siREDD2 treatment restored firing rates to levels similar to those found in intact, non-injured neurons. Intriguingly, we were not able to obtain whole-cell recordings from axotomized RGCs treated with siCtl. We cannot conclude that siCtl is toxic to cells because we were not able to record from PBS-injected eyes either. Our data rather suggest that the combination of axotomy and intraocular injection has a detrimental effect on the electrophysiologic properties of RGCs, a response that is overcome by siREDD2. The loss of light-triggered responses by RGCs subjected to concomitant axotomy and intravitreal injection suggests that multiple eye injuries impair RGC function, an observation that deserves further investigation. The excitability of a neuron is the result of a balance between several factors including resting potential, input resistance and soma size. The observed dendritic abnormalities reported here were not accompanied by detectable changes in any of these parameters; therefore, it is unlikely that axotomy-induced hyperexcitability and the effect of siREDD2 are the result of changes in intrinsic membrane properties or soma size. Our data suggest that functional deficits most likely derive from injury-induced changes in dendritic integrity and rearrangement of synaptic inputs, with hyperexcitability resulting from an increase in excitatory connections or a decrease in inhibitory synapses. Of interest, mTOR has been previously shown to suppress dendritic translation of the potassium channel Kv1.1,[62] an effect that could increase burst firing and network synchronization.[63,64] More recently, TSC1-mTOR signaling was shown to regulate the balance between excitatory and inhibitory synaptic transmission, which, when defective, led to hippocampal network hyperactivity.[65]

In conclusion, our data support a model in which axonal injury-induced upregulation of the stress-responsive REDD2 leads to mTOR inhibition triggering early dendritic arbor retraction, neuronal dysfunction and subsequent death of adult retinal neurons. Our findings shed light onto a novel

mechanism regulating dendritic pathology, which may be relevant for neurodegenerative diseases including glaucoma.

Materials and Methods

Experimental animals. Animal procedures were performed in accordance with the guidelines of the University of Montreal and the Canadian Council on Animal Care for the use of experimental animals (http://www.ccac.ca). All surgeries were carried out in adult B6.Cg.Tg[Thy1-YFPH]2Jrs/J mice (Jackson Laboratory, Bar Harbor, ME, USA) or wild-type litter mate controls maintained in our animal facility. The number of animals used in each experiment is indicated in Table 1 and in the figure legends.

Axonal injury. Axonal injury was induced by complete transection (axotomy) of the mouse optic nerve leading to apoptotic loss of RGCs.[66] The left optic nerve was transected at 0.5–1 mm from the optic nerve head avoiding damage to the ophthalmic artery. The right eye was never operated on and served as intact control. Fundus examination was performed after axotomy and before the mice were killed to verify the integrity of the retinal circulation after surgery. Animals with compromised blood supply were excluded from the study.

Immunohistochemistry

Flat-mounted retinas: Mice were perfused transcardially with 4% paraformaldehyde (PFA), the eyes were immediately collected and the retinas were carefully dissected out. Retinas were free floated for 30 min in blocking solution: 10% normal goat serum (NGS), 2% Triton X-100 and 0.5% dimethyl sulfoxide (DMSO) in PBS. Retinas were then incubated for 72 h at 4 °C in blocking solution (2% NGS, 2% Triton X-100, 0.5% DMSO) containing each of the following primary antibodies: SMI-32 (NF-H, 10 μg/ml; Sternberger Monoclonals, Baltimore, MD, USA), GFP (4 μg/ml; Sigma-Aldrich, Oakville, ON, Canada) or Brn3a (0.3 μg/ml; Santa Cruz Biotechnologies, Santa Cruz, CA, USA). Retinas were washed and incubated with secondary antibodies: anti-mouse Alexa Fluor 594 (2 μg/ml; Molecular Probes, Eugene, OR, USA), anti-rabbit FITC (1 : 1000; Sigma-Aldrich) or anti-goat Alexa Fluor 594 (2 μg/ml; Molecular Probes). The retinas were washed and flat mounted on glass slides with the RGC layer side up for visualization using a fluorescent microscope (Zeiss AxioSkop 2 Plus; Carl Zeiss Canada, Kirkland, QC, Canada).

Retinal cross-sections: Animals were perfused transcardially with 4% PFA and retinal cryosections (16 μm) were prepared as previously described by us.[67] Some cryosections were prepared from eyes labeled with the retrograde tracer FG (Fluorochrome, Englewood, CO, USA), which was applied to the superior colliculus 1 week before optic nerve axotomy as described by us.[66] Each of the following primary antibodies were added to the retinal sections in blocking solution (3% bovine serum albumin, 0.3% Triton X-100) and incubated overnight at 4 °C: phospho-S6 (Ser 240/244, 1 : 200; Cell Signaling Technology, Boston, MA, USA), βIII-tubulin (TUJ1, 1 : 400; Sigma-Aldrich), calbindin (1 : 200; Swant, Marly, Switzerland), REDD2 (5 μg/ml; Biorbyt, San Francisco, CA, USA), REDD1 (1 μg/ml; ProSci Inc., Poway, CA, USA) or Brn3a (1 μg/ml; Santa Cruz Biotechnologies). The secondary antibodies used were as follows: anti-rabbit Cy3 (1.5 μg/ml; Sigma-Aldrich), anti-mouse FITC (1 : 1000; Sigma-Aldrich), anti-rabbit Alexa Fluor 594 (2 μg/ml; Molecular Probes) or anti-goat Alexa Fluor 488 (2 μg/ml; Molecular Probes). Fluorescent labeling was observed with a Zeiss AxioSkop 2 Plus (Carl Zeiss Canada).

Neuronal survival. Mice were killed by transcardial perfusion with 4% PFA, the retinas were removed and flat mounted with vitreal side up on a glass slide for examination of the GCL. YFP-labeled RGCs were counted within three square areas at distances of 0.25, 0.625 and 1 mm from the optic disc in each of the four retinal quadrants for a total of 12 retinal areas. RGC densities were confirmed using flat-mounted retinas labeled with Brn3a (Santa Cruz Biotechnologies) as described.[68] Fluorescence was examined with a Zeiss Axioskop 2 Plus microscope (Carl Zeiss Canada), and pictures were captured with a CCD video camera (Retiga; Qimaging, Burnaby, BC, Canada) and analyzed with Northern Eclipse software (Empix Imaging, Mississauga, ON, Canada).

Dendritic arbor and soma size analysis. Dendritic arbor reconstruction and measurements were performed blinded to manipulations. High-resolution images of YFP-labeled RGC dendritic arbors were acquired using a Leica SP1 confocal microscope (Leica Microsystems Inc., Concord, ON, Canada). Scans were taken at 0.48 to 0.65 μm intervals along the z axis (x and y = 1024 × 1024 pixels with 4 to 6 images averaged at each focal plane). Reconstruction of the entire RGC dendritic arbor was carried out using the computer-aided filament tracing function of the 3D image analysis software Imaris (Bitplane, South Windsor, CT, USA). The following parameters were measured and analyzed in this study: (i) *total dendritic length*: the sum of the lengths of all dendrites per neuron, (ii) *total dendritic field area*: the area within the contour of the arbor created by drawing a line connecting the outermost tips of the dendrites, (iii) *branch order*: the number of times a dendrite branches, starting with order 1, which corresponds to the primary branch emerging from the soma, (iv) *Scholl analysis*: the number of dendrites that cross concentric circles at increasing distances (10 μm interval) from the soma, and (v) *soma size*: the area within the contour drawn around the RGC soma to outline its shape.

Western blot analysis. Whole fresh retinas were rapidly dissected and homogenized with an electric pestle (Kontes, Vineland, NJ, USA) in ice-cold lysis buffer (20 mM Tris, pH 8.0, 135 mM NaCl, 1% NP-40, 0.1% SDS and 10% glycerol supplemented with protease inhibitors). Protein homogenates were centrifuged at 10 000 r.p.m. for 50 min, and the supernatants were removed and resedimented to yield solubilized extracts. Retinal extracts were resolved on SDS-polyacrylamide gels and transferred to nitrocellulose membranes (Bio-Rad Life Science, Mississauga, ON, Canada). Blots were incubated overnight at 4 °C with each of the following primary antibodies against: REDD2 (0.5 μg/ml; Fitzgerald, Acton, MA, USA), REDD1 (4 μg/ml; Proteintech, Chicago, IL, USA) or β-actin (0.5 μg/ml; Sigma-Aldrich). Membranes were incubated in anti-rabbit or anti-mouse peroxidase-linked secondary antibodies (0.5 μg/ml; Amersham Biosciences, Baie d'Urfé, QC, Canada). Blots were developed with a chemiluminescence reagent (ECL; Amersham Biosciences) and exposed to X-OMAT imaging film (Eastman Kodak, Rochester, NY, USA). Densitometric analysis was performed using Scion Image software (Scion Corporation, Frederick, MD, USA) on scanned autoradiographic films obtained from a series of three independent western blots each carried out using retinal samples from distinct experimental groups.

siRNA and rapamycin delivery. The siRNA molecules against REDD2 and siCtls were designed and provided by Quark Pharmaceuticals Inc. (Research Division, Ness Ziona, Israel). siRNAs were stabilized by alternating 2′O-methylation[69] and were synthesized by BioSpring GmbH (Frankfurt, Germany). The following siRNA sequences for REDD2 were tested with similar results (sense strands): 5′-ACGTGAACTTGGAAATTGA-3′, 5′-CCCAGAGAATTGCCCAAGA-3′ and 5′-TTGGACAGACAGTTCTCCA-3′. siCtls included a non-targeting siCtl: 5′-ACTAAATTACGCGCGATGC-3′ (sense strand), and a siCtl-Cy3: 5′-GUGC CAACCUGAUGCAGCU-3′ (sense strand). Each siRNA (7 μg/μl; total volume: 2 μl) was injected into the vitreous chamber of the left eye using a Hamilton syringe fitted with a 32-gauge glass microneedle. The sclera was exposed and the tip of the needle inserted into the superior ocular hemisphere at a 45° angle through the sclera and retina into the vitreous space using a posterior approach. This route of administration avoids injury to the iris or lens, which can promote RGC survival.[70,71] After the injection, surgical glue (Indermill; Tyco Health Care, Mansfield, MA, USA) was immediately used to seal the site of injection. Rapamycin (LC Laboratories, Woburn, MA, USA) diluted in 5% Tween-80 and 5% polyethylene glycol 400 was administered by intraperitoneal injection (6 mg/kg) at the time of axotomy, and 2 days later, for a total of two treatments. This regimen was selected based on the observation that a single dose of rapamycin (6 mg/kg) fully inhibits mTOR activity for 60 h *in vivo*.[72]

Electrophysiology. Whole-cell recordings were performed on isolated flat-mounted retinas of Thy1-YFPH mice as previously described.[73] Briefly, animals were anesthetized using isoflurane and then killed by decapitation. The killing of the mice and dissections were performed in ambient light, after which retinas were kept in the dark. The eyes were dissected and the retinas were rapidly removed and placed in Ames' solution (Sigma-Aldrich). The vitreous was gently removed and the retinas treated with a collagenase/hyaluronidase mixture (240 and 1000 U/ml, respectively; Worthington Biochemical, Lakewood, NJ, USA) at room temperature for 5–10 min. Retinas were mounted with the vitreal side up and superfused with Ames' solution bubbled with 95% O_2 and 5% CO_2 at room temperature. YFP-positive RGCs were visualized with an epifluorescent microscope, captured with an infrared-sensitive CCD camera and displayed on a video monitor. The camera was mounted on an Olympus FluoView FV 1000 confocal microscope equipped with a ×40 water-immersion objective. Whole-cell recordings were performed using a computer-controlled Multiclamp 700A amplifier and a Digidata 1322A digitizer (Axon Instruments, Downingtown, PA, USA). Patch pipettes (resistance 5–7 MΩ) were

pulled from borosilicate glass capillaries (1.5 mm OD, 1.12 mm ID; World Precision Instruments, Sarasota, FL, USA) on a Sutter P-97 puller (Sutter Instruments, Novato, CA, USA). Intracellular solution contained: 140 mM K-gluconate, 5 mM NaCl, 2 mM $MgCl_2$, 10 mM HEPES, 0.5 mM EGTA, Tris 2 mM ATP, Tris 0.4 mM GTP and Alexa Fluor 594 (15–30 μM; Molecular Probes) (pH 7.2–7.3, 280–300 mOsmol/kg). During recordings, injection of step current from − 250 to 350 pA was carried out to characterize the intrinsic properties of RGCs. An argon laser (488 nm) was used in the line scan mode to provide a linear stimulus moving at the speed of 4 μs per pixel. Data analyses were carried out offline using P-clamp 8 or 9 (Axon Instruments).

Statistical analyses. Data analysis and statistics were performed using the GraphPad Instat software (GraphPad Software Inc., San Diego, CA, USA) by a one-way ANOVA, followed by the Bonferroni or Dunnett's multiple comparison *post hoc* tests, or by a Student's *t*-test as indicated in the legends.

Conflict of Interest

BM, PM, JA, RAM, AK and ADP declare no conflict of interest. EF is Chief Scientific Officer at Quark Pharmaceuticals and owns company's stock options.

Acknowledgements. We thank Drs. TE Kennedy, ES Ruthazer and PP Roux for helpful advice and comments on the manuscript, and Drs. H Kalinski, H Ashush and I Mett (Quark Pharmaceuticals Inc.) for siRNA design and *in vitro* activity testing. This study was supported by grants from the Canadian Institutes of Health Research (to ADP), and the Réseau de Recherche en Santé de la Vision (to ADP). BM is the recipient of a fellowship from the Fonds de recherche du Québec-Santé (FRQS) and the Groupe de Recherche sur le Système Nerveux Central (GRSNC). PM is the recipient of a fellowship from the Réseau de recherche en santé buccodentaire et osseuse. ADP is a Chercheur Boursier National FRQS.

Author contributiions

BM, PM, AK, RAM and ADP designed the experiments. EF designed and characterized the siRNAs used in this study. BM, PM and JA performed the experiments. BM, PM, AK and ADP analyzed data and wrote the manuscript.

1. Luo L, O'Leary DDM. Axon retraction and degeneration in development and disease. *Ann Rev Neurosci* 2005; **28**: 127–156.
2. Cheng P-l, Poo M-m. Early events in axon/dendrite polarization. *Ann Rev Neurosci* 2012; **35**: 181–201.
3. Wong RO, Ghosh A. Activity-dependent regulation of dendritic growth and patterning. *Nat Rev Neurosci* 2002; **3**: 803–812.
4. Lin Y-C, Koleske AJ. Mechanisms of synapse and dendrite maintenance and their disruption in psychiatric and neurodegenerative disorders. *Ann Rev Neurosci* 2010; **33**: 349–378.
5. Liu M, Duggan J, Salt TE, Cordeiro MF. Dendritic changes in visual pathways in glaucoma and other neurodegenerative conditions. *Exp Eye Res* 2011; **92**: 244–250.
6. Jaworski J, Spangler S, Seeburg DP, Hoogenraad CC, Sheng M. Control of dendritic arborization by the phosphoinositide-3'-Kinase–Akt–mammalian target of rapamycin pathway. *J Neurosci* 2005; **25**: 11300–11312.
7. Kumar V, Zhang M-X, Swank MW, Kunz J, Wu G-Y. Regulation of dendritic morphogenesis by Ras–PI3K–Akt–mTOR and Ras–MAPK signaling pathways. *J Neurosci* 2005; **25**: 11288–11299.
8. Gao X, Neufeld TP, Pan D. *Drosophila* PTEN regulates cell growth and proliferation through PI3K-dependent and -independent pathways. *Dev Biol* 2000; **221**: 404–418.
9. Kwon C-H, Luikart BW, Powell CM, Zhou J, Matheny SA, Zhang W *et al.* Pten regulates neuronal arborization and social interaction in mice. *Neuron* 2006; **50**: 377–388.
10. Hoeffer CA, Klann E. mTOR signaling: at the crossroads of plasticity, memory and disease. *Trends Neurosci* 2010; **33**: 67–75.
11. Li N, Lee B, Liu R-J, Banasr M, Dwyer JM, Iwata M *et al.* mTOR-dependent synapse formation underlies the rapid antidepressant effects of NMDA antagonists. *Science* 2010; **329**: 959–964.
12. Brugarolas J, Lei K, Hurley RL, Manning BD, Reiling JH, Hafen E *et al.* Regulation of mTOR function in response to hypoxia by REDD1 and the TSC1/TSC2 tumor suppressor complex. *Genes Dev* 2004; **18**: 2893–2904.
13. Corradetti MN, Inoki K, Guan K-L. The stress-inducted proteins RTP801 and RTP801L are negative regulators of the mammalian target of rapamycin pathway. *J Biol Chem* 2005; **280**: 9769–9772.
14. Sofer A, Lei K, Johannessen CM, Ellisen LW. Regulation of mTOR and cell growth in response to energy stress by REDD1. *Mol Cell Biol* 2005; **25**: 5834–5845.
15. Imen JS, Billiet L, Cuaz-Pérolin C, Michaud N, Rouis M. The regulated in development and DNA damage response 2 (REDD2) gene mediates human monocyte cell death through a reduction in thioredoxin-1 expression. *Free Radic Biol Med* 2009; **46**: 1404–1410.
16. Cuaz-Pérolin C, Furman C, Larigauderie G, Legedz L, Lasselin C, Copin C *et al.* REDD2 gene is upregulated by modified LDL or hypoxia and mediates human macrophage cell death. *Arterioscler Thromb Vasc Biol* 2004; **24**: 1830–1835.
17. Miyazaki M, Esser KA. REDD2 is enriched in skeletal muscle and inhibits mTOR signaling in response to leucine and stretch. *Am J Phys* 2009; **296**: C583–C592.
18. Feng G, Mellor RH, Bernstein M, Keller-Peck C, Nguyen QT, Wallace M *et al.* Imaging neuronal subsets in transgenic mice expressing multiple spectral variants of GFP. *Neuron* 2000; **28**: 41–51.
19. Galindo-Romero C, Avilés-Trigueros M, Jiménez-López M, Valiente-Soriano FJ, Salinas-Navarro M, Nadal-Nicolás F *et al.* Axotomy-induced retinal ganglion cell death in adult mice: quantitative and topographic time course analyses. *Exp Eye Res* 2011; **92**: 377–387.
20. Sun W, Li N, He S. Large-scale morphological survey of mouse retinal ganglion cells. *J Comp Neurol* 2002; **451**: 115–126.
21. Coombs J, van der List D, Wang GY, Chalupa LM. Morphological properties of mouse retinal ganglion cells. *Neuroscience* 2006; **140**: 123–136.
22. Jefferies HBJ, Fumagalli S, Dennis PB, Reinhard C, Pearson RB, Thomas G. Rapamycin suppresses 5[prime]TOP mRNA translation through inhibition of p70s6k. *EMBO J* 1997; **16**: 3693–3704.
23. Ikenoue T, Hong S, Inoki K. Monitoring mammalian target of rapamycin (mTOR) activity. *Methods Enzymol* 2009; **452**: 165–180.
24. Cui Q, Yip HK, Zhao RC, So KF, Harvey AR. Intraocular elevation of cyclic AMP potentiates ciliary neurotrophic factor-induced regeneration of adult rat retinal ganglion cell axons. *Mol Cell Neurosci* 2003; **22**: 49–61.
25. Yin Y, Cui Q, Li Y, Irwin N, Fischer D, Harvey AR *et al.* Macrophage-derived factors stimulate optic nerve regeneration. *J Neurosci* 2003; **23**: 2284–2293.
26. DeYoung MP, Horak P, Sofer A, Sgroi D, Ellisen LW. Hypoxia regulates TSC1/2-mTOR signaling and tumor suppression through REDD1-mediated 14-3-3 shuttling. *Genes Dev* 2008; **22**: 239–251.
27. Reiling JH, Hafen E. The hypoxia-induced paralogs Scylla and Charybdis inhibit growth by down-regulating S6K activity upstream of TSC in *Drosophila*. *Genes Dev* 2004; **18**: 2879–2892.
28. Shoshani T, Faerman A, Mett I, Zelin E, Tenne T, Gorodin S *et al.* Identification of a novel hypoxia-inducible factor 1-responsive gene, RTP801, involved in apoptosis. *Mol Cell Biol* 2002; **22**: 2283–2293.
29. del Olmo-Aguado S, Núñez-Álvarez C, Ji D, Manso AG, Osborne NN. RTP801 immunoreactivity in retinal ganglion cells and its down-regulation in cultured cells protect them from light and cobalt chloride. *Brain Res Bull* 2013; **98**: 132–144.
30. Chung J, Kuo CJ, Crabtree GR, Blenis J. Rapamycin-FKBP specifically blocks growth-dependent activation of and signaling by the 70 kd S6 protein kinases. *Cell* 1992; **69**: 1227–1236.
31. Janssen KT, Mac Nair CE, Dietz JA, Schlamp CL, Nickells RW. Nuclear atrophy of retinal ganglion cells precedes the Bax-dependent stage of apoptosis. *Invest Ophthalmol Vis Sci.* 2013; **54**: 1805–1815.
32. Kwon C-H, Zhu X, Zhang J, Baker SJ. mTor is required for hypertrophy of Pten-deficient neuronal soma *in vivo*. *Proc Natl Acad Sci USA* 2003; **100**: 12923–12928.
33. Wong WT, Wong ROL. Rapid dendritic movements during synapse formation and rearrangement. *Curr Opin Neurobiol* 2000; **10**: 118–124.
34. Cline HT. Dendritic arbor development and synaptogenesis. *Curr Opin Neurobiol* 2001; **11**: 118–126.
35. Koleske AJ. Molecular mechanisms of dendrite stability. *Nat Rev Neurosci* 2013; **14**: 536–550.
36. Almasieh M, Wilson AM, Morquette B, Cueva Vargas JL, Di Polo A. The molecular basis of retinal ganglion cell death in glaucoma. *Prog Ret Eye Res* 2012; **31**: 152–181.
37. Morgan JE, Datta AV, Erichse nJT, Albon J, Boulton ME. Retinal ganglion cell remodelling in experimental glaucoma. *Adv Exp Med Biol* 2006; **572**: 397–402.
38. Shou T, Liu J, Wang W, Zhou Y, Zhao K. Differential dendritic shrinkage of alpha and beta retinal ganglion cells in cats with chronic glaucoma. *Invest Ophthalmol Vis Sci* 2003; **44**: 3005–3010.
39. Weber AJ, Kaufman PL, Hubbard WC. Morphology of single ganglion cells in the glaucomatous primate retina. *Invest Ophthalmol Vis Sci* 1998; **39**: 2304–2320.
40. Li Z-w, Liu S, Weinreb RN, Lindsey JD, Yu M, Liu L *et al.* Tracking dendritic shrinkage of retinal ganglion cells after acute elevation of intraocular pressure. *Invest Ophthalmol Vis Sci* 2011; **52**: 7205–7212.
41. Williams PA, Howell GR, Barbay JM, Braine CE, Sousa GL, John SWM *et al.* Retinal ganglion cell dendritic atrophy in DBA/2J glaucoma. *PLoS One* 2013; **8**: e72282.
42. Della Santina L, Inman DM, Lupien CB, Horner PJ, Wong ROL. Differential progression of structural and functional alterations in distinct retinal ganglion cell types in a mouse model of glaucoma. *J Neurosci* 2013; **33**: 17444–17457.
43. Feng L, Zhao Y, Yoshida M, Chen H, Yang JF, Kim TS *et al.* Sustained ocular hypertension induces dendritic degeneration of mouse retinal ganglion cells that depends on cell type and location. *Invest Ophthalmol Vis Sci* 2013; **54**: 1106–1117.

44. Pavlidis M, Stupp T, Naskar R, Cengiz C, Thanos S. Retinal ganglion cells resistant to advanced glaucoma: A Postmortem Study of Human Retinas with the Carbocyanine Dye DiI. *Invest Ophthalmol Vis Sci* 2003; **44**: 5196–5205.
45. Nickells RW, Howell GR, Soto I, John SWM. Under pressure: cellular and molecular responses during glaucoma, a common neurodegeneration with axonopathy. *Ann Rev Neurosci* 2012; **35**: 153–179.
46. Kalesnykas G, Oglesby EN, Zack DJ, Cone FE, Steinhart MR, Tian J *et al.* Retinal ganglion cell morphology after optic nerve crush and experimental glaucoma. *Invest Ophthalmol Vis Sci* 2012; **53**: 3847–3857.
47. Leung CK-s, Weinreb RN, Li ZW, Liu S, Lindsey JD, Choi N *et al.* Long-term *in vivo* imaging and measurement of dendritic shrinkage of retinal ganglion cells. *Invest Ophthalmol Vis Sci* 2011; **52**: 1539–1547.
48. Lin B, Wang SW, Masland RH. Retinal ganglion cell type, size, and spacing can be specified independent of homotypic dendritic contacts. *Neuron* 2004; **43**: 475–485.
49. Kim I-J, Zhang Y, Yamagata M, Meister M, Sanes JR. Molecular identification of a retinal cell type that responds to upward motion. *Nature* 2008; **452**: 478–482.
50. Weber AJ, Harman CD. BDNF preserves the dendritic morphology of α and β ganglion cells in the cat retina after optic nerve injury. *Invest Ophthalmol Vis Sci* 2008; **49**: 2456–2463.
51. Ortells MC, Morancho B, Drews-Elger K, Viollet B, Laderoute KR, López-Rodríguez C *et al.* Transcriptional regulation of gene expression during osmotic stress responses by the mammalian target of rapamycin. *Nucleic Acids Res* 2012; **40**: 4368–4384.
52. Ergorul C, Ray A, Huang W, Wang D, Ben Y, Cantuti-Castelvetri I *et al.* Hypoxia inducible factor-1α (HIF-1α) and some HIF-1 target genes are elevated in experimental glaucoma. *J Mol Neurosci* 2010; **42**: 183–191.
53. Kanamori A, Catrinescu M-M, Kanamori N, Mears KA, Beaubien R, Levin LA. Superoxide is an associated signal for apoptosis in axonal injury. *Brain* 2010; **133**: 2612–2625.
54. Park KK, Liu K, Hu Y, Smith PD, Wang C, Cai B *et al.* Promoting axon regeneration in the adult CNS by modulation of the PTEN/mTOR pathway. *Science* 2008; **322**: 963–966.
55. Park KK, Liu K, Hu Y, Kanter JL, He Z. PTEN/mTOR and axon regeneration. *Exp Neurol* 2010; **223**: 45–50.
56. Morgan-Warren PJ, Berry M, Ahmed Z, Scott RAH, Logan A. Exploiting mTOR signaling: a novel translatable treatment strategy for traumatic optic neuropathy? *Invest Ophthalmol Vis Sci* 2013; **54**: 6903–6916.
57. Kurimoto T, Yin Y, Omura K, Gilbert H-y, Kim D, Cen L-P *et al.* Long-distance axon regeneration in the mature optic nerve: contributions of oncomodulin, cAMP, and pten gene deletion. *J Neurosci* 2010; **30**: 15654–15663.
58. Leibinger M, Andreadaki A, Fischer D. Role of mTOR in neuroprotection and axon regeneration after inflammatory stimulation. *Neurobiol Dis.* 2012; **46**: 314–324.
59. Swiech L, Blazejczyk M, Urbanska M, Pietruszka P, Dortland BR, Malik AR *et al.* CLIP-170 and IQGAP1 cooperatively regulate dendrite morphology. *J Neurosci* 2011; **31**: 4555–4568.
60. Malik AR, Urbanska M, Macias M, Skalecka A, Jaworski J. Beyond control of protein translation: What we have learned about the non-canonical regulation and function of mammalian target of rapamycin (mTOR). *Biochim Biophys Acta* 2013; **1834**: 1434–1448.
61. Ward NJ, Ho KW, Lambert WS, Weitlauf C, Calkins DJ. Absence of transient receptor potential vanilloid-1 accelerates stress-induced axonopathy in the optic projection. *J Neurosci* 2014; **34**: 3161–3170.
62. Raab-Graham KF, Haddick PCG, Jan YN, Jan LY. Activity- and mTOR-dependent suppression of Kv1.1 channel mRNA translation in dendrites. *Science* 2006; **314**: 144–148.
63. Cudmore RH, Fronzaroli-Molinieres L, Giraud P, Debanne D. Spike-time precision and network synchrony are controlled by the homeostatic regulation of the D-type potassium current. *J Neurosci* 2010; **30**: 12885–12895.
64. Metz AE, Spruston N, Martina M. Dendritic D-type potassium currents inhibit the spike afterdepolarization in rat hippocampal CA1 pyramidal neurons. *J Physiol* 2007; **581**: 175–187.
65. Bateup Helen S, Johnson Caroline A, Denefrio Cassandra L, Saulnier Jessica L, Kornacker K, Sabatini Bernardo L. Excitatory/inhibitory synaptic imbalance leads to hippocampal hyperexcitability in mouse models of tuberous sclerosis. *Neuron* 2013; **78**: 510–522.
66. Lebrun-Julien F, Morquette B, Douillette A, Saragovi HU, Di Polo A. Inhibition of p75NTR in glia potentiates TrkA-mediated survival of injured retinal ganglion cells. *Mol Cell Neurosci* 2009; **40**: 410–420.
67. Lebrun-Julien F, Duplan L, Pernet V, Osswald IK, Sapieha P, Bourgeois P *et al.* Excitotoxic death of retinal neurons *in vivo* occurs via a non-cell-autonomous mechanism. *J Neurosci* 2009; **29**: 5536–5545.
68. Nadal-Nicolás FM, Jiménez-López M, Sobrado-Calvo P, Nieto-López L, Cánovas-Martínez I, Salinas-Navarro M *et al.* Brn3a as a marker of retinal ganglion cells: qualitative and quantitative time course studies in naïve and optic nerve–injured retinas. *Invest Ophthalmol Vis Sci* 2009; **50**: 3860–3868.
69. Czauderna F, Fechtner M, Dames S, Aygun H, Klippel A, Pronk GJ *et al.* Structural variations and stabilising modifications of synthetic siRNAs in mammalian cells. *Nucleic Acids Res* 2003; **31**: 2705–2716.
70. Leon S, Yin Y, Nguyen J, Irwin N, Benowitz LI. Lens injury stimulates axon regeneration in the mature rat optic nerve. *J Neurosci* 2000; **20**: 4615–4626.
71. Mansour-Robaey S, Clarke DB, Wang Y-C, Bray GM, Aguayo AJ. Effects of ocular injury and administration of brain-derived neurotrophic factor on survival and regrowth of axotomized retinal ganglion cells. *Proc Natl Acad Sci USA* 1994; **91**: 1632–1636.
72. Meikle L, Pollizzi K, Egnor A, Kramvis I, Lane H, Sahin M *et al.* Response of a neuronal model of tuberous sclerosis to mammalian target of rapamycin (mTOR) inhibitors: effects on mTORC1 and Akt signaling lead to improved survival and function. *J Neurosci* 2008; **28**: 5422–5432.
73. Schmidt TM, Kofuji P. An isolated retinal preparation to record light response from genetically labeled retinal ganglion cells. *J Vis Exp* 2011; **47**: 2367.